Mohsen M. Baligh
Jacques-Noël Levadoux

Pore Pressure Dissipation After Cone Penetration

MIT Sea Grant
College Program

Massachusetts
Institute of Technology
Cambridge,
Massachusetts 02139

MITSG 80-13

PORE PRESSURE DISSIPATION
AFTER CONE PENETRATION

by

Mohsen M. Baligh

Jacques-Noël Levadoux

Sea Grant College Program
Massachusetts Institute of Technology
Cambridge, Massachusetts 02139

Report No. MITSG 80-13
Index No. 80-313-Cim
April 1980

ABSTRACT

Deep quasi-static cone penetration in saturated soils develops excess pore pressures. This report estimates the consolidation and permeability characteristics of fine grained soils from measurements of the pore pressure decay that takes place after cone penetration is interrupted.

Relatively new conical piezometers with a very rapid response time are described. Linear consolidation analyses are performed to investigate the importance of different factors affecting pore pressure dissipation around cones: initial distribution of excess pore pressures, cone angle and location of the porous stone, soil anisotropy and coupling between pore pressures and total stresses.

A new economical and consistent method for estimating the coefficients of consolidation and permeability is proposed. The method is evaluated by means of extensive dissipation measurements in two clay deposits. The predicted profiles provide good agreement with laboratory data and full scale performance.

FOREWORD

A three-year research program entitled, "In Situ Evaluation of Geotechnical Properties of Marine Sediments," sponsored primarily by the National Oceanic and Atmospheric Administration through its MIT Sea Grant Program, was initiated in July 1978 by the Constructed Facilities Division at MIT. Matching funds for this research were provided by FUGRO, Inc., Consulting Engineers, and by Instituto Tecnologico Venezolano Del Petroleo.

The objective of this research is to provide the geotechnical designer with more reliable methods for estimating in situ properties of marine sediments for foundation design.

The electric (Dutch) cone penetrometer and the conical piezometer probe represent a new generation of in situ testing devices which are particularly valuable offshore, by combining simplicity, consistency, and economy.

Previous efforts at MIT concentrated on:

1. Evaluating the capability of cone penetration in establishing stratification, determining variability, and performing soil identification (Baligh et al, 1980), and
2. Estimating the undrained shear strength of clays (Baligh et al, 1978; Baligh and Vivatrat, 1979).

This report investigates the pore pressure decay that takes place after interrupting cone penetration in order to estimate the coefficients of consolidation and permeability of fine grained soils.

ACKNOWLEDGEMENTS

The authors are indebted to their MIT colleagues who contributed to the success of this research: Charles C. Ladd, Professor; Dr. Robert T. Martin, Senior Research Associate; Dr. Amr Azzouz, Research Associate; Jack Germaine, Research Assistant.

The authors are especially indebted to Dr. A. Azzouz for invaluable help in preparing the final manuscript.

This report describes the results of research done as a part of the MIT Sea Grant College Program with support from the Office of Sea Grant in the National Oceanic and Atmospheric Administration, U.S. Department of Commerce, through grant number NA79AA-D-00101, and from the Massachusetts Institute of Technology. The U.S. Government is authorized to produce and distribute reprints for governmental purposes notwithstanding any copyright notation that may appear herein.

RELATED SEA GRANT REPORTS

MIT/Marine Industry Collegium. RISKS AND COSTS FOR OCEAN STRUCTURES: OPPORTUNITY BRIEF #17. MITSG 79-18. 13 pp. $3.50.

MIT/Marine Industry Collegium. TOWARDS IMPROVED TECHNIQUES FOR PREDICTING SOIL STRENGTH: OPPORTUNITY BRIEF #16. MITSG 79-17. 19 pp. $3.50.

Baligh, Mohsen M., Vitoon Vivatrat and Charles C. Ladd. EXPLORATION AND EVALUATION OF ENGINEERING PROPERTIES FOR FOUNDATION DESIGN OF OFFSHORE STRUCTURES. MITSG 79-8 268 pp. $8.00.

Chryssostomidis, Marjorie. OFFSHORE PETROLEUM ENGINEERING: A BIBLIOGRAPHIC GUIDE TO PUBLICATIONS AND INFORMATION SOURCES. MITSG 78-5. 366 pp. $45.00.

The Sea Grant Marine Resources Information Center maintains an inventory of technical publications. We invite orders and inquiries to:

Marine Resources Information Center
MIT Sea Grant College Program
Massachusetts Institute of Technology
Building E38-302
Cambridge, Massachusetts 02139
(617) 253-5944

TABLE OF CONTENTS

LIST OF TABLES

LIST OF FIGURES

CHAPTER 1

INTRODUCTION

1.1 THE NEED FOR SOIL CLASSIFICATION

Geotechnical engineers classify soils into coarse and fine grained materials for convenience and in order to identify possible foundation problems, select adequate approaches and techniques to evaluate important design parameters and, if needed, plan construction and field monitoring programs. Coarse grained soils consist of gravels and sands and, are generally considered "good" foundation and construction materials with few exceptions e.g. natural deposits of loose uniform sands. Fine grained soils include silts and clays and, deserve more careful consideration by the engineer because of their different and often more adversely complicated behavior. However, the most important characteristic of soils requiring classification of coarse and fine grained materials into separate categories is their very different drainage behavior i.e. their permeabilities. The dominating effect of permeability in geotechnical engineering derives from its very large variation from one soil to another or, for a given soil, depending on its void ratio and possible micro or macrostructure, Fig. 1.1.

Coarse grained soils have a high permeability, $k > 10^{-4}$ cm/sec, quickly dissipate excess pore water pressures and hence reach steady flow conditions very rapidly. Therefore, in most geotechnical problems, the relevant stress-strain-strength behavior of coarse

grained soils corresponds to "drained" conditions and is little affected by the presence of water. Partial or no drainage conditions occur in limited instances e.g. soil dynamics. Particle migration and erosion problems caused by steady fluid flow are important exceptions.

On the other hand, geotechnical problems associated with fine grained soils are intimately related to "excess" pore water pressures (above steady state) that are basically governed by the drainage conditions. Undrained, partially drained or fully drained situations take place depending on the rate of load application, the drainage path (i.e. the linear scale of the problem), the compressibility of the soil and, most importantly, its permeability.

Therefore, estimates of the permeability, k, are essential in geotechnical engineering. The accuracy of these estimates varies with the problem at hand and depends on existing measurement methods.

1.2 COARSE GRAINED SOILS

In most applications, the permeability of gravel is so high ($k > 1$ cm/sec) that accurate estimates of k are rarely needed. In cases where excessive seepage losses from reservoirs are expected or when large volumes of water must be pumped from excavations and cuts, engineering judgement and trial and error methods represent the best available tools.

In sands, reasonable estimates of permeability (10^{-4} cm/sec < k < 1 cm/sec) can be obtained (within an order of magnitude) from correlations with the effective grain size* D_{10} determined from laboratory particle size analyses on disturbed samples (Loudon, 1952; WES, 1956; Mansur and Kaufman, 1962; Ahmad et al, 1975, NAVFAC DM-7, 1971). More accurate estimates of k in natural sand deposits are difficult to obtain by means of direct laboratory measurements because of severe problems associated with "undisturbed" sampling. However, laboratory permeability tests can provide data on the possible ranges of in situ permeability of natural deposits and valuable information when sands are used as construction materials under controlled conditions e.g. in embankments, dams, etc.

In situ permeability tests provide more reliable methods for determining k in the field. Milligan (1975) reviews existing in situ tests, Table 1.1, and describes the accuracy of determining k in sands by "... discrepancies between construction observations of permeability, between bore hole tests in situ and laboratory tests can vary by an order of magnitude. Where the deposits are not uniform and the stratigraphy is erratic, ..., such discrepancies are increased." and concludes that "... existing methods used with discretion and judgement can give workable answers probably to within one order of magnitude." for deposits with $k > 10^{-5}$ cm/sec.

---

*D_{10} is the particle size at which 10% of the soil weight is finer. Because of its correlation to k, the effective grain size D_{10} is probably the most useful parameter (for the designer) obtained from extensive index (and even engineering) tests routinely performed in the laboratory on natural sand deposits.

1.3 FINE GRAINED SOILS

The distinction between silts and clays based on particle size is convenient because silts have generally higher permeabilities ($10^{-7} < k < 10^{-4}$ cm/sec, say) than clays, Fig. 1.1. However, most natural fine grained deposits consist of silt and clay particle sizes and very rarely do "clays" consist of 100% particles less than 2×10^{-3} mm in diameter.

Geotechnical problems of interest involving fine grained soils almost always require consideration of unsteady water flow (or consolidation) before steady conditions are reached. Consolidation rates are governed by the coefficient of consolidation* (c_v or c_h) that depends on soil compressibility (m_v, say) in addition to soil permeability.

1.3.1 Laboratory Tests

In contrast to coarse grained soils, adequate "undisturbed" samples of fine grained soils can be routinely obtained for laboratory testing by means of existing drilling and sampling equipment.** Laboratory tests are designed to minimize interpretation difficulties (caused by the complicated behavior of soils) by imposing well defined boundary conditions leading to simple flow, stress and strain distributions throughout the sample. Good quality laboratory testing can be expensive, time consuming and generally covers a very small fraction of the foundation soil. Most importantly, however, laboratory test results require judgement before application to field situations in order to account

---

*$c_v = k/m_v\gamma_w$, m_v = coefficient of volume change.

**Offshore work requires special precautions; see Baligh and Vivatrat, 1979.

for the differences between the behavior of samples and that of the soil mass in situ. These differences are principally caused by sample disturbance, stress and environmental histories and size effects.

Uniform clays have low coefficients of permeability, k, and consolidation, c_v. However, natural deposits often develop a micro or macrostructure during deposition and their subsequent stress and environmental history. Silt and sand dustings, seams, laminations, clusters or thin layers on bedding planes, in addition to discontinuities in the form of cracks, fissures, slip planes, fractures and passages caused by desiccation, infiltration and organic action can drastically increase the mass permeability and cause significant anisotropy especially if these features are continuous and interconnected. Laboratory measurements of k and c_v in well-structured clays can lead to serious difficulties because

1. Results depend on sample size (Rowe and Barden, 1966; Rowe, 1972).
2. Field values can be underpredicted by several orders of magnitude (Grisak and Cherry, 1975; Grisak, 1975; Rowe, 1972).

Therefore, laboratory measurements of k and c_v on conventional size samples of structured fine grained soils are of doubtful value in predicting field performance.

On the other hand, laboratory tests on relatively unstructured clays can provide acceptable predictions of c_v and k. Using superior sampling and testing equipment and techniques together

with the best understanding of soil behavior and experience in interpreting test results, field values of c_v and k can probably be predicted within a factor of two but can be in error by a factor of 10 (Bishop and Al-Dhahir, 1970). Furthermore, even under these ideal conditions, laboratory tests performed on samples obtained at selected depths will typically show a significant scatter that often prevents good estimates of profiles (variation with depth) to be achieved.

1.3.2 In Situ Tests

In situ tests avoid problems associated with sample size and sample disturbance but lack the simple laboratory testing conditions and hence are more difficult to interpret. Compared to coarse grained soils, in situ tests in fine grained materials require a much longer time to reach steady state conditions* (because of the lower permeability) and can cause significant changes in soil properties (because of the higher compressibility). Theoretically, the longer time required for excess pore pressure dissipation offers the advantage of measuring c_h in addition to k_h (obtained from steady state conditions*). However, from a practical standpoint, the low permeability and high compressibility of fine grained soils represent a major disadvantage because

1. Reliable "large scale" tests used in granular media, e.g., well pumping tests, cannot be applied to fine grained soils, Table 1.1.
2. Performance and interpretation of in situ tests require special equipment and skill and cannot be performed under the severe conditions encountered offshore.

*if any

Available in situ permeability and/or consolidation tests in clays utilize hydraulic piezometers, Table 1.1, of relatively small linear dimension in order to minimize testing time. Piezometers commonly used are installed by 1) sinking a borehole to the required depth, placing a piezometer tip in a pocket of sand and then sealing and back filling (Casagrande, 1946); and 2) pushing a conical piezometer tip into softer soils (Bjerrum and Johannessen, 1961) or into a preformed borehole without the use of a sand pocket. Two types of tests can be performed: 1) Constant head tests where the water pressure in the piezometer is fixed and the discharge is measured; and, 2) Variable head tests where the water pressure in a standpipe is recorded as it equilibrates with time. In each type of test, the piezometer pressure can be raised to cause outflow of water accompanied by swelling or can be lowered to cause inflow of water and soil compression. Outflow tests are more common because they are easier to perform and avoid problems associated with the application of suction.

The major difficulties encountered in conducting in situ tests in fine grained soils are:

1) Disturbance and smear effects due to installation. Piezometer installation invariably causes changes in stresses and properties of the surrounding soils. As in the case of sample disturbance in laboratory testing, the usefulness of the in situ permeability/consolidation test results depends on the severity of these changes.

Installation causes changes in total stresses and distortions (undrained shearing) of the soil surrounding the piezometer and hence develops excess pore pressures that can confuse interpretation of tests performed shortly after installation. Theoretically, piezometers installed by carefully controlled boring can reduce the size of the sheared (disturbed) volume of soil as compared to piezometers installed by pushing but require a very careful monitoring of water pressures in the borehole. Accurate estimates of the waiting time required for installation excess pore pressures to dissipate and the starting of the permeability test is difficult to predict accurately and depends on the size (diameter) of the piezometer, the soil type, the severity of disturbance, etc. Milligan (1975) notes that a period of as much as 20 to 30 days is needed for small diameter tips between installation and testing. After this consolidation period, serious questions remain as to whether soil stresses and properties around the piezometer are comparable to the virgin soil to be tested. Soil stresses after consolidation are difficult to estimate or measure. Experimental observations indicate that significant changes in properties can take place in the so-called smear zone near the piezometer. Accurate estimates of the size and properties of this severely disturbed smear zone are not available. However, rough estimates based on simple spherical solutions (Gibson, 1966) indicate that smear can significantly affect test results and is expected to be more important in clays with well-defined macrostructure i.e. silt layering, silt filled fissures, organic inclusions, etc. (Wilkinson, 1968).

2) Hydraulic fracturing during permeability testing.
An increase in pore pressures beyond a certain fraction of the effective stresses in the soil causes a significant increase in its mass permeability due to soil hydraulic fracture. Therefore, increments of heads imposed during outflow in situ permeability tests must be small and carefully controlled in order to avoid fracturing of the soil and overpredicting its permeability (Bjerrum et al, 1972).

3) Response time and hardware.
Results of in situ permeability tests are very sensitive to the hardware and the testing procedures used. The most important and very difficult task consists of minimizing the flexibility of the system (piezometer tip, leads, measuring devices, etc.) caused by volume compressibility of the different components and, in particular, by the entrapped air in order to reduce the time-lag in measurements (Hvorslev, 1951, Bishop and Henkel, 1962; Whitman et al, 1961; Kallstenius and Wallgren, 1956; Penman, 1961, Bishop et al, 1964, Wilkinson, 1968). Serious additional problems can result from leaks, low permeability piezometers in relatively pervious soils (Gibson, 1966), pressure losses in the leads and, in constant head tests, the difficulties of maintaining accurate constant small pressures for long periods of time.

4) Interpretation of test results.
Gibson (1963) developed an interpretation method for variable head tests conducted by means of a spherical piezometer in an

isotropic soil based on uncoupled* linear closed-form solutions. Results of these spherically symmetric (one-dimensional) solutions are identical to relations obtained earlier by de Jong (1953) who introduced coupling according to Biot's (1941) theory which assumes the soil skeleton behaves as a linear elastic isotropic material. Extensions of these solutions to develop interpretation methods for more realistic conditions of cylindrical piezometers in anisotropic non linear soils can be obtained by existing numerical methods. However, efforts in this direction were apparently curtailed by the non monotonic effective stress loading conditions imposed by variable head tests. Gibson (1963) correctly points out that in falling (or rising) head tests the soil surrounding the piezometer first expands (or contracts), and then contracts (or expands), before excess pore pressures ultimately vanish. Since the compressibility of a clay invariably differs from its swelling characteristics, linear analyses will predict some "average" coefficient of consolidation that is difficult to evaluate. Nonlinear analyses can resolve this problem but interpretation methods based on nonlinear solutions require additional soil parameters to be known a priori and hence add to the uncertainties in interpreting test results. This is, however, generally true in soil mechanics testing where the more realistic the modelling of soil behavior, the more sophisticated (and complicated) the analysis required, and more importantly, the larger the number of soil parameters needed to interpret test results.

---

*i.e., pore pressures are not affected by soil skeleton deformations and hence are independent of total stresses.

Compared to falling head tests, constant head tests are more difficult to conduct* but offer two advantages: a) A steady state is ultimately reached. Theoretically, this means that direct permeability measurements can be obtained without the added complications of consolidation solutions. However, in order to reach a steady state, a very long testing time is often required under difficult field conditions. In practice, measurements are conducted for a few hours and extrapolated to infinite times by means of consolidation solutions. b) Assuming that no significant changes in total stresses occur during a constant head test, no reversals in effective stresses** take place and hence linear solutions can be used with less uncertainties in interpreting test results.

Gibson (1963) developed the necessary linear uncoupled solutions for interpreting constant head tests for spherical piezometers in an isotropic soil. Wilkinson (1968) extended these solutions to the more practical case of a cylindrical piezometer in an anisotropic soil and included non-linear permeability and compressibility relationships. Jezequel and Mieussens (1975), and Al-Dhahir et al (1970) describe useful interpretation details (e.g. plots of test results, etc.) to avoid difficulties and to obtain more reliable predictions. Gibson (1970) suggests the modification of his (1963) theory to include shear-induced pore pressures.

---

*Because of the better controls needed.

**More precisely, reversals in effective stress rates.

Surprisingly, few comprehensive studies were conducted in the USA to evaluate in situ permeability testing in fine grained soils. Most of the published data were obtained in Europe (Bishop and Al-Dhahir, 1970; Al-Dhahir et al, 1970; Rowe, 1968 and 1972; Wilkinson et al, 1970; and Jezequal and Mieussens, 1975) from onshore sites and indicate that:

1) Constant head tests are preferred to variable head tests because of the reduced interpretation uncertainties. However, few variable head tests were thoroughly evaluated (Rowe, 1968).
2) Estimates of the coefficient of consolidation (c_v or c_h) from constant head in situ tests are not very reliable and are sensitive to the test variables, e.g., changes in the stress history of the soil around piezometers due to installation, de-airing, previous test runs, etc.
3) Good estimates of in situ permeability (k_h) can be obtained by extrapolating constant head test results on the basis of linear consolidation solutions. However, it is important to note that, contrary to c_v, direct evaluation of k_h by means of full scale performance data requires estimates of the soil compressibility (m_v, say) and possibly (k_h/k_v) as well. In most cases, laboratory data of m_v and k_h/k_v were used with judgement to achieve good agreement.

Attempts by the authors to evaluate extensive in situ permeability tests in two soft clay deposits using regular piezometers of the Casagrande type (bored) and the Geonor type (pushed) installed and tested according to the standard

U.S. practice, indicated that:

1) Estimates of the coefficients of permeability and consolidation from constant head tests exhibited considerable scatter (two orders of magnitude or more) above that expected due to inherent soil variability.
2) Because of excessive scatter, constant head tests did not prove superior to falling head tests.*
3) Both types of in situ tests added very little useful information to laboratory test results for embankment design.

In conclusion, the successful performance and interpretation of in situ permeability tests in fine grained soils requires considerable skill and experience. The current average U.S. practice of installing piezometers and conducting in situ permeability tests is believed to be well below acceptable levels. This might explain their absence from routine site investigations (even onshore).

1.4 SUMMARY: STATE OF PRACTICE

1. Estimates of the permeability (k) and/or the consolidation characteristics of soils is important in most geotechnical problems.

2. Most practical situations involving coarse grained soils (gravels and sands; $k > 10^{-4}$ cm/sec) impose "drained" conditions.

---

*An approximate theory for cylindrical piezometers had to be developed for falling head tests.

3. The permeability of gravels is often too large ($k > 1$ cm/sec) such that good estimates of k are rarely needed.

4. The permeability of natural sand deposits can be estimated from correlations with the effective grain size, D_{10}, obtained from particle size analyses on disturbed samples. Improved estimates of in situ k cannot usually be obtained from laboratory tests because of limitations of existing sampling capabilities. In situ permeability tests can provide more reliable estimates of k, especially in non uniform deposits, but errors within an order of magnitude are not uncommon. Therefore, considerable judgement and local experience are required in utilizing sand permeability data in practice.

5. Problems of interest involving fine grained soils (silts and clays) cause significant excess pore pressures and hence require estimates of the coefficient of consolidation (c_v or c_h) of the soil.

6. Laboratory measurements of k and c_v in "structured" fine grained soils can be several orders of magnitude lower than field values and thus have a very limited use in designs. In relatively structureless clays, the most experienced engineer using the best laboratory testing equipment and procedures can, at best, predict field values of k and c_v within a factor of two or three. However, the average geotechnical engineer using routine sampling and testing methods can probably estimate k and c_v within a factor of five to ten from laboratory measurements.

7. Reliable in situ tests in fine grained soils are time consuming and require considerable skill and experience above the current average U.S. practice. Under ideal conditions, useful permeability data can be obtained from onshore in situ tests. However, direct measurements of the more important coefficient of consolidation, c_v, are not sufficiently reliable to provide much additional information to laboratory data. Offshore in situ permeability tests do not exist.

1.5 RESEARCH OBJECTIVES

This research is aimed at providing the geotechnical designer with more reliable and economical methods for estimating the in situ consolidation and/or permeability characteristics of fine grained soils. This is achieved by analyzing the pore pressure decay that takes place after interruption of steady penetration by conical piezometer probes having a very rapid response time.

The proposed method is economical and provides consistent* profiles of coefficients of consolidation and permeability. These profiles cannot be obtained by existing laboratory and in situ tests conducted at discrete, widely spaced locations and are especially valuable to:

a) Identify drainage layers in consolidation, excavation, earth pressure and tunneling problems, dewatering and grouting operations; and dam foundations analyses (uplift pressures, erosion and piping),

---

*repeatable

b) perform more accurate consolidation analyses for application in predicting settlement rates, monitoring earth structures, designing preloading surcharge and vertical sand drains, and;

c) aid for decision making in foundation engineering such as selecting adequate dewatering methods and pressure relief, planning of long term instrumentation programs, tunnelling operations, etc...

1.6 REPORT ORGANIZATION

Chapter 2 provides background material. Conical piezometers with a very rapid response time used in this research are described, the difficulties associated with the interpretation of pore pressure decay around cones are discussed and existing methods are reviewed.

Chapter 3 treats excess pore pressures developed during steady cone penetration because they provide the initial distribution required for dissipation studies. The importance of penetration pore pressures on consolidation results is illustrated by means of a parametric one-dimensional study. Penetration pore pressures obtained by the "strain path method" (Baligh, 1975) using soil parameters appropriate to normally consolidated Boston Blue Clay are presented and compared to field measurements in BBC and other clays.

Chapter 4 presents results of two-dimensional linear numerical consolidation analyses around conical probes based on the estimated initial distribution of pore pressures (Chapter 3) in order to evaluate the effects of: the location of the porous stone (on the cone or the shaft behind it), the cone angle, soil anisotropy, coupling, the mesh size, the time increments, and the errors in the estimated initial and hydrostatic (final) pore pressures.

Chapter 5 evaluates simple linear solutions by means of extensive in situ dissipation measurements around cones in BBC; investigates the effects of various practical factors on the reliability of the estimated profiles of the coefficients of consolidation and permeability, e.g., cone angle, porous stone location, degree of dissipation; and compares the estimated coefficients of consolidation and permeability with laboratory measurements and field performance data.

Chapter 6 recommends procedures to estimate the coefficients of consolidation and permeability from dissipation records, applies these procedures to measurements in a varved clay deposit and compares predictions with laboratory test results.

Finally, Chapter 7 summarizes the main conclusions of this study.

METHOD	TECHNIQUE	APPLICATION TO: GRAVEL	SAND	SILT	CLAY	PROBLEMS	METHOD RATING	REFERENCE
(A) Auger hole	Shallow uncased hole in unsaturated material above G.W.L	√	Only where $k > 10^{-5}$ cm/sec	?	–	Difficult to maintain water levels in coarse gravels	Poor	USBR, (1968)
Test Pit	Square OR rectangular test pit (equivalent to circular hole above)	√		?	–		Poor	Lacroix (1960)
(B) Cased borehole (No inserts)	ii) Falling/rising head, Δh in casing measured VS time	√	√	?	–	Borehole must be flushed. Possible fines clog base (falling Δh) Pumping (rising Δh) where W.L. lowered excessively	Fair	Hvorslev (1951)
	iii) Constant head maintained in casing, outflow, Q VS time	√	√	?	–			USBR, (1968)
(C) Cased borehole (Inserts used) i) Sand filter plug ii) Perforated/slotted casing in lowest section iii) Well point placed in hole, casing drawn back	i) Generally falling head, Δh measured VS time only	√	√	?	–	Simple tests only. Cannot be used as boring is advanced	Fair	Hvorslev (1951)
	ii) Variable heads possible	√	√	?	–		Fair to good	
	iii) As for (ii) above	√	√	√	–			
(D) Piezometers/Permeameters (with OR without casing)	i) Suction Bellows apparatus (independent of boring) Inflow ONLY measured VS time	–	? √	√	–	Restricted to fine sands, coarse silts, variable bellows required 'K' range 10^{-4} to 10^{-7} cm/sec	Good (local zones)	Golder, Gass (1963)
	ii) Short Drill (Cementation) (independent of boring) Outflow ONLY measured VS time	√	√	–	–	Carried out in adit OR tunnel		Golder, Gass (1963)
	iii) Piezometer tip pushed into soft deposits/placed in boring, sealed, casing withdrawn/pushed ahead of boring. Constant head, outflow measured VS time Variable heads also possible	–	–	√	√	Possible tip 'smear' when pushed Δu set up in pushing tip. Danger of hydraulic fracture		Gibson (1966) Wilkes (1974) Hvorslev (1950) Bjerrum et al, 1972
(E) Well pumping test	Drawdown in central well monitored in observation wells on, at least, two 90° radial directions.	√	√	√ (?)	–	Screened portion should cover complete stratum tested	Excellent (Mass permeability of foundation material)	Todd (1959)
(F) Test excavation pumping tests)	Monitoring more extensive than (E), during excavation dewatering. (Initial construction stage)	√	√	√ (?)	–	Expensive, but of direct benefit to contractual costing		—

Table 1.1 Existing In Situ Permeability Testing Methods (after Milligan, 1975)

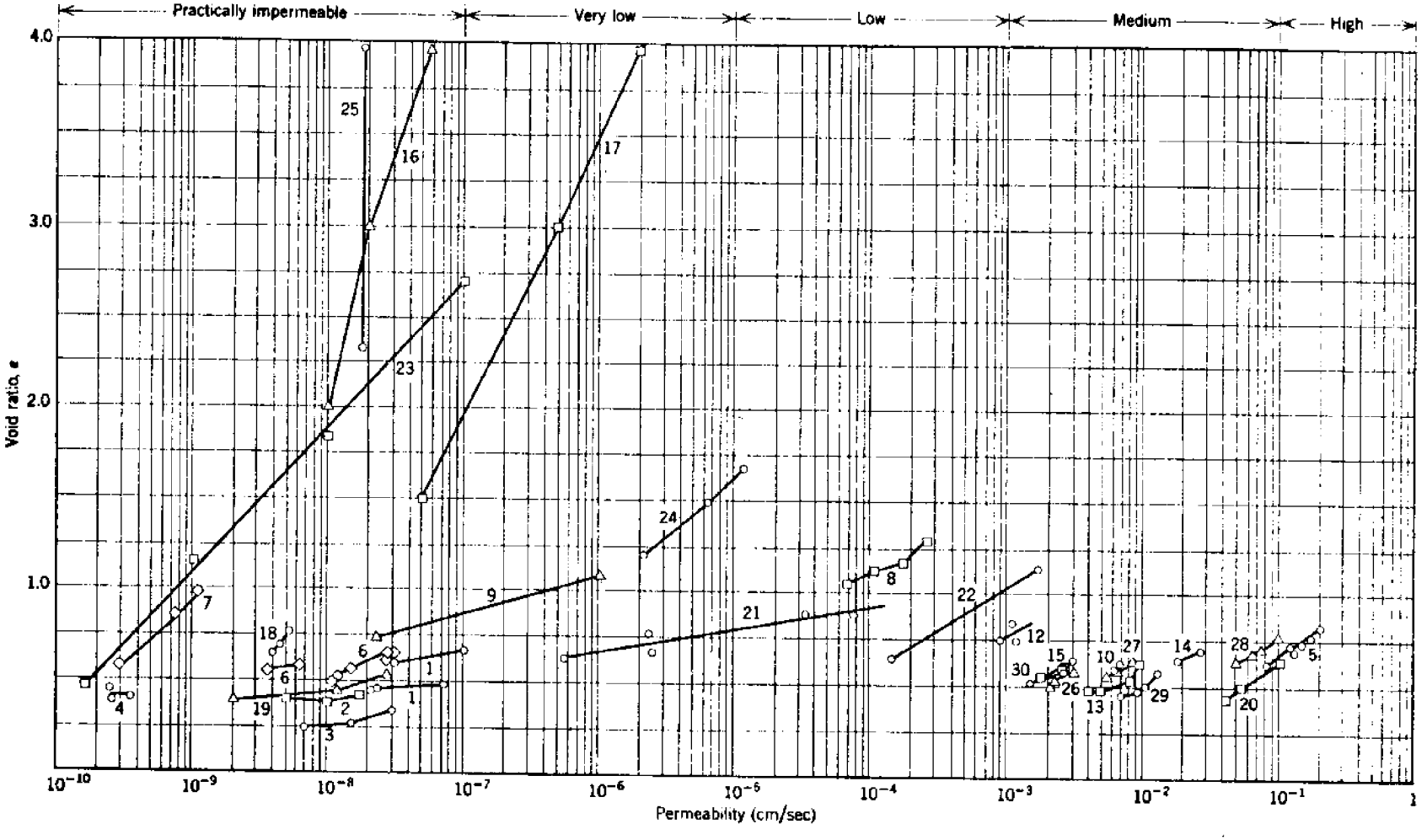

Soil Identification Code

1 Compacted caliche
2 Compacted caliche
3 Silty sand
4 Sandy clay
5 Beach sand
6 Compacted Boston blue clay
7 Vicksburg buckshot clay
8 Sandy clay
9 Silt—Boston
10 Ottawa sand
11 Sand—Gaspee Point
12 Sand—Franklin Falls
13 Sand—Scituate
14 Sand—Plum Island
15 Sand—Fort Peck
16 Silt—Boston
17 Silt—Boston
18 Loess
19 Lean clay
20 Sand—Union Falls
21 Silt—North Carolina
22 Sand from dike
23 Sodium—Boston blue clay
24 Calcium kaolinite
25 Sodium montmorillonite
26–30 Sand (dam filter)

Fig. 1.1 Typical Permeability of Soils (after Lambe and Whitman, 1969)

CHAPTER 2

BACKGROUND

2.1 CONICAL PIEZOMETERS

Conical piezometer probes used in this research were developed by Wissa et al (1975). In the original design, the cone angle was 18° (2δ = 18°) and pore pressures were measured by means of a cylindrical porous stone located at the cone tip, Fig. 2.1. Second generation probes were developed in order to measure the pore pressures along the cone face and at different locations on the shaft (behind the cone) for 2δ = 18° and 60, Fig. 2.1. The pore pressure sensor consists of a high air entry stainless steel porous element hydraulically connected to a pressure transducer contained in a 1.5" (3.8 cm) diameter stainless steel housing. The upper end of the housing screws into a standard A or AW drilling rod used to jack the probe into the soil. Penetration proceeds, in general, by 5 ft increments after which a new pushing rod is installed. The interruption of penetration is often intentionally extended to observe pore pressure decay. The penetration rate* is approximately equal to 2 cm/sec (±50%)**. During

---

*The jacking equipment utilized in pore pressure measurements is attached to a standard drilling rig and is pressure, rather than flow, controlled.

**Tests conducted by M.I.T. to investigate the effect of penetration rate on cone resistance and penetration pore pressures indicate that, in clays, a ±50% change in the "standard" penetration velocity of 2 cm/sec has no detectable effects.

penetration and pore pressure dissipation, the electrical signal is transmitted to the surface by a cable strung through the pushing rods and is recorded continuously on a strip chart recorder as a function of time.

An important feature of these probes compared to existing piezometers is their response time. In order to record a change of pore pressure in the soil, some water flow is required from the soil to the measuring element. A "rigid" system involving well deaired water requires a small volume of displaced water and provides a rapid response. On the other hand, a "flexible" system involving air and requiring large volumes of displaced water creates a time lag in measurements. This time lag is especially significant in penetration and consolidation records and makes the interpretation of pore pressures difficult if at all possible (see Chap. 1).

No accurate measurements of the probe response time was performed by MIT. However, Fig. 2.2 shows the performance of a probe* in a calibration test conducted in the laboratory after the device was left in a saturated clay deposit for about one week. The strip chart on the left represents the water pressure measured through the porous stone when the device is inserted in a pressurized water bath where the pressure is varied rapidly with time. The record to the right is the water pressure as measured by a total stress cell i.e. involving no porous stone. Comparing the two records, the porous element clearly records variations in water pressure taking place within one second

*This proble is built for different purposes but has essentially the same design as the conical probes in Fig. 2.1.

interval. Some sluggish response can be detected for faster changes. This performance is considered acceptable for measurements in clays. Martin (1980) estimates that reasonable measurements in sands require a response time less than 0.1 sec.

Torstensson (1975) developed a piezometer probe, with similar features as the Wissa probe but with a different geometry, Fig. 2.3. M.I.T. did not use the Torstensson probe. Ghionna et al. (1979) present dissipation results in Italian clays using a Torstensson probe where the pore pressure increases for about 1 minute before starting to decrease. Similar results were obtained by Lunne and Lacasse (1980) in Scandinavian clays where they used the same piezometer probe and the same deairing technique.* However, after adopting a deairing technique similar to that used at M.I.T., Lunne and Lacasse observe that: 1) the penetration pore pressures become higher in parts of the deposit, and; 2) the pore pressure starts to decrease as soon as penetration stops.

This emphasizes the importance of adequate deairing of the probe to obtain good quality measurements. It is, therefore, strongly recommended to adopt a deairing technique at least as careful as currently adopted at M.I.T. This method consists of:

a) disassembling the probe, cleaning and thoroughly drying all parts;

---

*The deairing operation is reported as accomplished quickly (≃ 15 minutes) in the field by placing the piezometer probe in a container full of water and connected to a vacuum pump (Lacasse, 1980).

b) placing all parts in a container under a good vacuum (less than 10 millitorrs)* for at least 12 hours;

c) flowing deaired water into the container (still under vacuum), and;

d) assembling the probe under water.

Furthermore, the stone must be prevented from drying by keeping it under water until it is used in the field.

Careful deairing of the piezometer probe is especially important in highly pervious soils (silty sands and sands) and very impervious soils (plastic clays). Pore pressure dissipation in very pervious soils might be faster than the response time of the probe and hence even penetration pore pressures might go undetected. In highly impervious soils, the required inflow of water into the system might be too large to be provided rapidly by the soil.

2.2 TYPICAL RECORDS

2.2.1 Steady Penetration Records

Figure 2.4 shows a typical record of pore pressure measurements at the tip of an 18° conical probe in a Boston Blue Clay (BBC) deposit. When steady penetration starts at a depth of 43.5 ft, say, the pore pressure increases rapidly and reaches the so-called penetration value, u_i, in less than 3 inches. Steady penetration at a rate of about 2 cm/sec

---

*1 Torr = 1 mm of mercury ≈ 0.0013 atm.

continues to a depth of 47 ft (indicated by the arrow) when another push rod is required. The installation of the rod takes 45 sec and the pore pressure during this time decreases due to soil consolidation. Penetration is then resumed and the process repeated. Note the unmistakable sudden decrease in u_i at depths 47.2, 49.3 and 58.6 ft which suggests the presence of dense sandy lenses.

Figure 2.5 shows the cone resistance q_c, and the penetration pore pressure, u_i, obtained from two separate tests 45 ft apart in a deposit consisting of peat, sand and heavily desiccated clay which contains sandy lenses. Individually, q_c and u_i records detect major changes in soil strata, but jointly, they have an excellent potential for soil identification as well. For example, in the peat, q_c is low and u_i is high, whereas in the relatively clean sand, q_c is high and u_i is very close to the hydrostatic values, u_o. Small excess pore pressures during penetration $\Delta u_i (= u_i - u_o)$ were also measured by Schmertmann (1978) when he attempted to assess the liquification potential of sands by means of similar probes.

Baligh et al. (1980) describe the use of steady penetration records for soil profiling.

2.2.2 Dissipation Records

Fig. 2.6 shows typical excess pore pressure dissipation records at the tip of an 18° probe at depths 20, 40, 50 and 68 ft in the same BBC deposit (Figs. 2.4 and 2.5). The measured pore pressure, u, after a time, t, from interrupting steady

penetration decreases from an initial value u_i to a final (hydrostatic) value u_o. Clearly, dissipation of excess pore pressure $\Delta u (= u - u_o)$ takes place slower as the depth increases. This is presumably caused by a decrease in the coefficient of consolidation (and/or permeability) with depth.

It is interesting to note that, at any depth, the initial pore pressure, u_i, for dissipation studies (Fig. 2.6) is the steady penetration pressure (Fig. 2.4) at that depth. The latter varies significantly due to inherent soil variability and hence u_i is difficult to estimate reliably in erratic deposits. Furthermore, the full dissipation of excess pore pressures caused by cone penetration can cause significant delays in the exploration program and, therefore, the final pore pressure, u_o, is more often estimated than measured.

In dissipation studies, it is more meaningful to plot the decay of the excess pore pressure $\Delta u (= u - u_o)$ especially when normalized by its inital value $\Delta u_i (= u_i - u_o)$. Using the same test results presented in Fig. 2.6, a plot of the normalized excess pore pressures, $\bar{u} (= \Delta u / \Delta u_i)$, is shown in Fig. 2.7. During consolidation, $\bar{u}$ decreases* from unity to zero and provides a good measure of the degree of consolidation $(= 1 - \bar{u})$.

Figure 2.7 clearly indicates that dissipation of excess pore pressures becomes much slower with depth in the BBC deposit. At a depth of 20 ft most of the dissipation ($\bar{u} = 0.2$) is completed

---

*In some cases, $\bar{u}$ increases during early stages of consolidation because of soil variability, or due to the special location of the porous stone, but more often indicates poor deairing of the stone.

in 6 seconds whereas at a depth of 68 ft only 30% consolidation ($\bar{u}$ = 0.7) takes place after 100 seconds.

In investigating dissipation results plotted as $\bar{u}$ vs. log t, it is interesting to note that: according to simple linear consolidation analyses based on Terzaghi theory, two soils with the same normalized distribution of initial excess pore pressures (caused by steady penetration) but with different values of the coefficient of consolidation must have parallel (or horizontally shifted) dissipation curves. Furthermore, the amount of horizontal shift required to reach one dissipation curve from another represents the ratio between the coefficient of consolidation for the two soils. This simple rule is quite useful to assess the importance of measurement scatter, evaluate predictions, ...etc. When applied to Fig. 2.7 this rule indicates that:

a) the dissipation curve at a depth of 50 ft can be obtained by shifting the curve at 68 ft by a horizontal distance (to the left) approximately equal to 2 (see scale of log t). This suggests that linear (uncoupled) analyses are applicable at these depths using the same distribution of normalized initial excess pore pressures. Furthermore, the coefficient of consolidation at 50 ft is roughly twice smaller than at 68 ft.

b) the dissipation curve at depth 20 ft cannot be obtained by horizontally shifting the curve at 68 ft (or 50 ft). This indicates that: either the initial distribution of excess pore pressures is different or that linear (uncoupled) analyses are not applicable at shallow depths.

2.3 INTERPRETATION OF DISSIPATION RECORDS

From a practical standpoint, a rational interpretation method of the pore pressure dissipation that takes place after interrupting steady cone penetration should answer two basic questions:* 1) What is the measured soil parameter(s)? e.g. vertical or horizontal coefficient of consolidation and/or permeability; 2) What is the value (magnitude) of this parameter and the range of practical applications** it applies to? Additional questions include 3) How long should dissipation be allowed? i.e. what degree of consolidation is required; 4) What cone angle provides the most reliable results?; 5) Where to measure the pore pressures, on the cone or the shaft behind it? ...etc.

More empirically oriented approaches use engineering judgement to guess the answers to questions 1), 3), 4) and 5), standardize procedures regarding questions 3), 4), 5) and rely on correlations between dissipation measurements, laboratory test results, and foundation performance in the widest possible variety of soil deposits. Empirical approaches in interpreting in situ tests represent the backbone of present geotechnical practice*** and, to some extent, are justified by the very complicated behavior of soils. However, heavy reliance

---

*That face any in situ (or laboratory) test.

**Because of complicated soil behavior rarely does a parameter have the same magnitude for all practical applications, e.g. the appropriate undrained shear strength of a clay for a bearing capacity problem is, in general, different from a retaining wall problem.

***See for example the use of the standard penetration test or the cone penetration test in practice.

on empiricism has serious and far reaching consequences. In particular, new methods and techniques are very difficult to incorporate into practice because of 1) the large effort required to provide convincing empirical evidence, and 2) the dependence of present practice on existing testing methods and techniques.

In this report, a more rational interpretation method is attempted by 1) theoretically investigating the mechanism of dissipation in order to identify and, to the extent possible, evaluate the effect of important factors; 2) developing an adequate model for dissipation on which to base a prediction method; and 3) evaluating the prediction method by means of measurements and foundation performance.

Theoretically, dissipation records are difficult to interpret because of two major factors:

1) The uncertainties associated with the initial excess pore pressure distribution in the soil caused by steady cone penetration. Chapter 3 shows the importance of this distribution; discusses the difficulties encountered in predicting or measuring steady penetration pore pressures; and describes results of significant efforts spent in estimating a reasonable field of excess pore pressures.

2) The complicated aspects of soil behavior as related to soil consolidation around cones. In particular: soil nonlinearities, soil anisotropy, nonhomogeneities caused by soil remolding due to penetration, and time-dependent (creep) behavior.

Additional difficulties in analyses are caused by: 1) The two-dimensional nature of consolidation around a cone. Fluid flow and soil deformations take place in the radial and vertical directions; 2) The high gradients expected near the tip of the cone; 3) The coupling between total stresses and pore pressures during consolidation.

The following sections discuss some of these problems and provide the necessary background for subsequent consolidation analyses.

2.3.1 Linear Consolidation

The analyses required to develop an interpretation method are conceptually different from predicting the response in a particular clay under particular conditions. A useful interpretation method should provide sufficient generality and hence applicability to a wide range of soils. An accurate consolidation analysis that faithfully incorporates soil nonlinearities might provide excellent dissipation predictions around a particular cone in a particular soil. However, this analysis cannot be expected to apply to other deposits because of the significant changes in the nonlinear behavior of different soils due to changes in types, methods of deposition, stress and environmental histories ...etc. Linear analyses provide valuable normalizations and hence cover a wide range of applications.

Linear consolidation studies are generally treated by means of one of two theories: 1) the Terzaghi-Rendulic,* uncoupled or unlinked theory which treats the excess pore pressures independently from the total stresses during consolidation, and; 2) the Biot (1941) coupled or linked theory where the interaction between skeleton and pore water is introduced. Sills (1975) shows that a class of problems exists where both approaches lead to the same governing equation and hence can be treated by uncoupled theories even though total stresses might change during consolidation. These problems include the obvious one-dimensional rectilinear consolidation and the consolidation around spherical and cylindrical cavities in an infinite isotropic linearly elastic medium.

One of the significant features of coupling during consolidation is the so-called Mandel-Cryer effect.** The effect causes an increase in the excess pore pressure at early times which was observed experimentally during consolidation of a spherical sample (Gibson et al., 1963). Schiffman et al. (1969) investigate the plane strain consolidation under a strip footing using Biot's theory and find that significant Mandel-Cryer effects take place under the load and close to the surface. These effects, however, decrease in magnitude when: a) the drainability of the loaded surface decreases, and; b) the drained Poisson's ratio of the material increases. Viggiani (1970) and Davis and Poulos (1970) show that in a wide range of practical problems,

---

*Terzaghi (1923), Rendulic (1936).

**Mandel (1953) and, Cryer (1963).

and except for the occurrence of the Mandel-Cryer effect during the early stages of consolidation, the Terzaghi-Rendulic theory predicts fairly well the excess pore pressure-time relationship provided that the appropriate coefficient of consolidation is used to evaluate the time factor.*

Biot consolidation theory can therefore be considered more correct than the Terzaghi-Rendulic theory because it predicts the Mandel-Cryer effect that has been observed experimentally. However, its use leads to much more complicated computations. In particular, when the finite element method is utilized to solve a two-dimensional consolidation problem, Biot's theory requires 3 degrees of freedom (2 for the displacements and 1 for the pore pressure) at each node whereas the Terzaghi-Rendulic theory requires only one (pore pressure).

2.3.2 Nonlinear Soil Behavior

Terzaghi-Rendulic and Biot theories both assume that the ratio of permeability to compressibility of the soil remains constant during consolidation. In fact, the compressibility of a given clay is a function of its current effective stress level as well as its past stress history (i.e., overconsolidation ratio) whereas its permeability is principally a function of its current void ratio. When the clay is normally consolidated, the compressibility and per-

*The coefficient of consolidation used in Terzaghi-Rendulic equation should be the same as that used in Biot equation.

meability vary in such a way that the coefficient of consolidation remains approximately constant. On the other hand, if an overconsolidated clay is loaded to effective stress levels exceeding its maximum past pressure, large soil nonlinearities arise during consolidation. Consequently, linear solutions are only applicable to small stress increments away from the maximum past pressure. Many researchers have investigated non-linear one-dimensional consolidation. Fuleihan and Ladd (1976) present a comprehensive review of these theories.

Small et al. (1976) propose an incremental finite element formulation to solve the two-dimensional elasto-plastic consolidation of soils by extending Biot's theory. However, in the case of three- and even two-dimensional consolidation problems, solutions are very difficult to obtain because of the large number of soil parameters and the resulting computational difficulties.

Comprehensive non-linear consolidation analyses are thus currently limited to simple geometries and simplified soil behavioral models.

2.3.3 Soil Remolding

Deep steady cone penetration causes very large shearing strains in the soil, especially in the immediate vicinity of the tip. In normally consolidated Boston Blue Clay, these

strains produce a failure zone extending to a radial distance equal to 6.5 times the shaft radius (Levadoux and Baligh, 1980).

When shearing strains are applied to a normally consolidated clay, positive shear-induced pore pressures, Δu_s, develop resulting in a negative mean effective stress change, $\Delta\bar{\sigma}_{oct}$ (= - Δu_s). With regards to clay consolidation, the reduction in mean effective stress at a constant void ratio due to undrained shearing can be viewed as an artificial overconsolidation of the clay. This is illustrated in Fig. 2.8 showing the results of consolidation tests conducted on Atchafalaya Clay* reported by Fuleihan and Ladd (1976). Test A in Fig. 2.8 shows results of a typical oedometer test. Test B consisted of: a) consolidating the clay sample in a Direct Simple Shear apparatus under K_o conditions to a vertical effective stress, $\bar{\sigma}_{vc}$ = 1.0 kg/cm^2; b) conducting an undrained creep test, i.e., applying a constant horizontal shear stress τ_h (equal to 73% of the failure shear stress, $(\tau_h)_{max}$) for more than two days while maintaining the sample volume constant, and; c) reconsolidating the sample to a vertical effective stress, $\bar{\sigma}_{vc}$ = 2.0 kg/cm after relieving the shear stress τ_h. The results in Fig. 2.8 clearly indicate that the initially normally consolidated clay behaves as an overconsolidated clay after being subjected to undrained shearing and creep.**

---

*Atchafalya clay is a soft plastic clay (PI ≈ 75) from south-central Louisiana.

**This behavior might not take place if τ_h is maintained during consolidation or if creep is not allowed.

Figure 2.9 illustrates the effect of overconsolidation on the shear induced pore pressure (normalized with respect to the maximum past pressure), $\Delta u_s/\bar{\sigma}_{vm}$, at different axial strain levels during* $\overline{CK_oU}$ plane strain compressions tests on resedimented Boston Blue Clay. When the clay is initially overconsolidated (OCR = 4, say) undrained shearing generates negative Δu_s and thus the mean effective stress, $\bar{\sigma}_{oct}$, is increased. However, this increase in $\bar{\sigma}_{oct}$ is small compared to $\bar{\sigma}_{vm}$ (< 15%).

In summary, limited experimental data on clay consolidation after undrained shearing suggest that pore pressure dissipation during early stages of consolidation around cones takes place in a recompression mode (as opposed to virgin compression) for both normally consolidated and over-consolidated clays (OCR < 4). More careful testing to simulate the actual soil consolidation around cones requires more complicated stress systems to be imposed on laboratory samples in order to maintain shear stresses during reconsolidation. However, this shearing is expected to vary with time and is difficult to estimate.

2.3.4 Soil Anisotropy

Because of their mode of deposition, natural clays generally exhibit some anisotropy in permeability and in compressibility. The ratio of horizontal to vertical

---

*K_o-consolidated undrained tests with pore pressure measurements.

permeability, k_h/k_v, is difficult to evaluate. Based on limited laboratory data, typical values of k_h/k_v for homogeneous clay deposits (i.e., clays with a uniform stratification) are given by Ladd, 1976:

Nature of Clay	k_h/k_v
1. No evidence of layering	1.2 ± 0.2
2. Slight layering, e.g. sedimentary clays with occasional silt dustings to random lenses	2 - 5
3. Varved clays in Northeastern U.S.	10 ± 5

However, for sedimentary deposits with erratic layers of more pervious soil, the results of tests on samples selected at random locations will generally be misleading. Ladd (1976) recommends to evaluate k_v from laboratory tests and k_h from in situ permeability tests.

Little experimental information exists on the ratio of horizontal to vertical compressibilities. This ratio is, however, believed to be close to unity and, in practice, the compressibility of clays is generally considered isotropic (Mitchell and Gardner, 1975).

Therefore, it appears reasonable to assume that the anisotropic behavior of clays during consolidation is principally caused by anisotropic permeability. Parametric analyses will be presented to determine which permeability (k_v or k_h), if any, governs the consolidation around conical probes.

2.4 EXISTING METHODS

Few attempts have been made to interpret dissipation records around cones because conical piezometers with a sufficiently rapid response have only recently been developed and because of the difficulties of estimating the initial excess pore pressure distribution.

Tortensson (1977) suggests that the pore pressures in the soil caused by steady cone penetration can be estimated by one-dimensional (radial) solutions corresponding to cylindrical and spherical cavities (Soderberg, 1962, Ladanyi, 1963). He assumes the soil to be isotropic, initially subjected to an isotropic state of stress, to behave as an elastic-perfectly plastic material during cavity expansion and utilizes linear uncoupled one-dimensional finite difference consolidation analyses to estimate the normalized excess pore pressure dissipation curves in Fig. 2.10 ($\bar{u}$ vs. log T; $T = ct/R^2$). In order to estimate the coefficient on consolidation, c, Torstensson proposes matching of predictions and measurements at 50% consolidation ($\bar{u} = 0.5$) and hence uses the expression

$$c = \frac{T_{50}}{t_{50}} R^2 \qquad (2.1)$$

where T_{50} is the predicted time factor at $\bar{u} = 0.5$ (Fig. 2.10) for an appropriate value* of E/s_u; t_{50} is the measured time

*E and s_u are "equivalent" Young's modulus and undrained shear strength of the clay, respectively. For undrained shearing E = 3G, where G is the shear modulus.

to achieve 50% consolidation; and R is an "equivalent" radius that simulates the cavity radius.

The use of Torstensson method to estimate the coefficient of consolidation, c, from dissipation records raises serious theoretical and practical problems caused by the severe over-simplifications he introduces.

Practically, given the results in Fig. 2.10, the determination of c requires estimates of: the rigidity index, E/s_u, the equivalent radius, R, and the type of cavity (cylindrical or spherical).

1. The rigidity index E/s_u (= $3G/s_u$)

Soils subjected to undrained shearing exhibit marked non-linearities. Fig. 2.11 shows the variation of the secant shear modulus, G_s, of Boston Blue Clay at different strain levels, γ, as measured by different in situ and laboratory tests. Clearly, the selection of an adequate shear modulus (or E) is very difficult. Estimates of G_s can easily vary by one order of magnitude depending on γ, the overconsolidation ratio, the type of test,...etc. Furthermore, the selection of an appropriate shear strength, s_u, is not an easy task. Table 2.1 shows laboratory test results for six normally consolidated clays determined after consolidating samples under K_o-conditions and shearing under plan strain conditions. Estimated values of s_u in a routine job can easily differ by a factor of 2, especially in view of other uncertainties (e.g., strain rate effects, over-consolidation ratio, strain-softening,...etc.) and the limitations of present testing capabilities.

In summary, significant uncertainties exist in estimating the ratio, E/s_u. A good understanding of the mode and rate of shearing of the clay is necessary before reasonable estimates of E/s_u can be made. The range of E/s_u selected by Torstensson to plot Fig. 2.10 (100 to 500 corresponding to G/s_u = 33 to 165) is probably based on the collective wisdom of the profession at the present time.* However, results in Table 2.1 and Fig. 2.11 indicate that, in BBC, this range corresponds to a "high" straining level of the clay. Based on cavity expansion analyses and comparisons with pressuremeter and other in situ test results, Azzouz et al (1980) estimate that higher values of E/s_u (10 times, say) are more appropriate (see also Chap. 3). This increase in E/s_u causes an increase in the radius of the soil affected by cavity expansion (plastic zone), results in a slower dissipation and hence an increase in the estimated coefficient of consolidation c at 50% consolidation (Eq. 2.1) by about a factor of 3.

2. The cavity type and the quivalent radius R

The geotechnical engineer has to choose between spherical cavity solutions (upper diagram in Fig. 2.10) and cylindrical solutions (lower diagram); and select an appropriate radius R.

---

*Such numbers are often quoted and used in many applications, e.g., Ladd et al (1977); Randolf et al (1978).

This choice is difficult because cavity solutions are one-dimensional whereas cone penetration is two-dimensional, and the geometrical analogy between the two problems is not clear.

For a given clay (E/s_u fixed), spherical cavity solutions predict much faster dissipation (T_{50} smaller) than cylindrical cavities and hence predict smaller values of the coefficient of consolidation c. From Fig. 2.10, the ratio of c estimated by the two methods is about 5.

In selecting an appropriate value of R, two limiting possibilities arise when the Torstensson probe is considered, Fig. 2.3. The first is the radius of the porous stone and the second is the radius of the shaft which is roughly twice as large. Eq. 2.1 indicates that c is proportional to R^2 and hence the estimated coefficient of consolidation will be four times higher if the radius of the shaft is used. When other probe geometries are considered, Fig. 2.1, the selection of R remains a difficult task.

From a theoretical (or rational) standpoint, Torstensson interpretation method does not provide an answer to most questions raised in Section 2.3. In particular, the method fails to provide

1. The necessary insight into the cone penetration mechanism which is essential in understanding and hopefully accounting for soil nonlinearities neglected in consolidation

analyses, e.g. soil straining (remolding), consolidation under variable shearing, creep effects,...etc.

2. The "type" of the estimated coefficient of consolidation c, i.e. horizontal vs. vertical and overconsolidated vs. normally consolidated. Differences between different types of c can reach 20 or 40 times.

3. Guidelines to select an adequate cone angle and to locate the porous stone on the cone.

4. A rational justification for selecting the logarithmic initial excess pore pressure distribution corresponding to cavity expansions in an elastic-perfectly plastic material. Chapter 3 shows that, in one-dimensional consolidation analyses, the initial distribution of excess pore pressures is most important in estimating the value of c. Different initial distributions can easily lead to 5 times higher values of c than the logarithmic distribution assumed by Torstensson.

5. An acceptable argument to select 50% consolidation to estimate c. Ideally, a "good" consolidation analysis should predict the same value of c at all levels of dissipation (degrees of consolidation). On the other hand, <u>any</u> dissipation curve* ($\bar{u}$ vs. log T) will predict some value of c for a given degree of consolidation. Therefore, unless a consistent (the same) value of c is obtained at 20, 50 and 80% consolidation (say), the prediction method cannot be considered adequate.

---

*Even drawn arbitrarily.

2.5 SUMMARY

The evaluation of the consolidation and/or permeability properties of soils is important in a wide variety of geotechnical problems. In concept, this can be achieved by adequately interpreting records of pore pressure dissipation after cone penetration is interrupted provided that the measuring probe has a sufficiently rapid response.

Existing interpretation methods rely on one-dimensional solutions and hence are too simplified to yield reliable results. Acceptable two-dimensional analyses require estimates of the pore pressure distribution in the soil during steady cone penetration and reasonable modelling of the complicated behavior of soils during consolidation around cones.

Type of Soil	Index Properties			$s_u/\bar{\sigma}_{vc}$ (1)		
	w_ℓ (%)	P.I. (%)	L.I. (2)	PSC (3)	DSS (4)	PSE (5)
Portsmouth Clay	35	15	1.8	0.350	0.200	0.155
Haney Sensitive Clay	44	18	0.75	0.296	——	0.211
Boston Blue Clay	41	21	0.81	0.340	0.200	0.190
AGS CH Clay	71	40	——	0.370	0.250	0.220
San Francisco Bay Mud	88	45	1.04	0.370	0.250	0.280
Connecticut Valley Varved Clay	35-65	12-39	1.00	0.280	0.165	0.255

(1) $s_u = q_f = 0.5(\sigma_1 - \sigma_3)_f$ except for DSS where $s_u = (\tau_h)_{max}$

(2) $\text{L.I.} = \dfrac{w_n - w_p}{w_\ell - w_p}$

(3) plane strain compression

(4) direct simple shear

(5) plane strain extension

Table 2.1 Plane strain undrained shear strength of six normally consolidated clays in different modes of failure (data from Ladd et al., 1977; table courtesy of A.S. Azzouz)

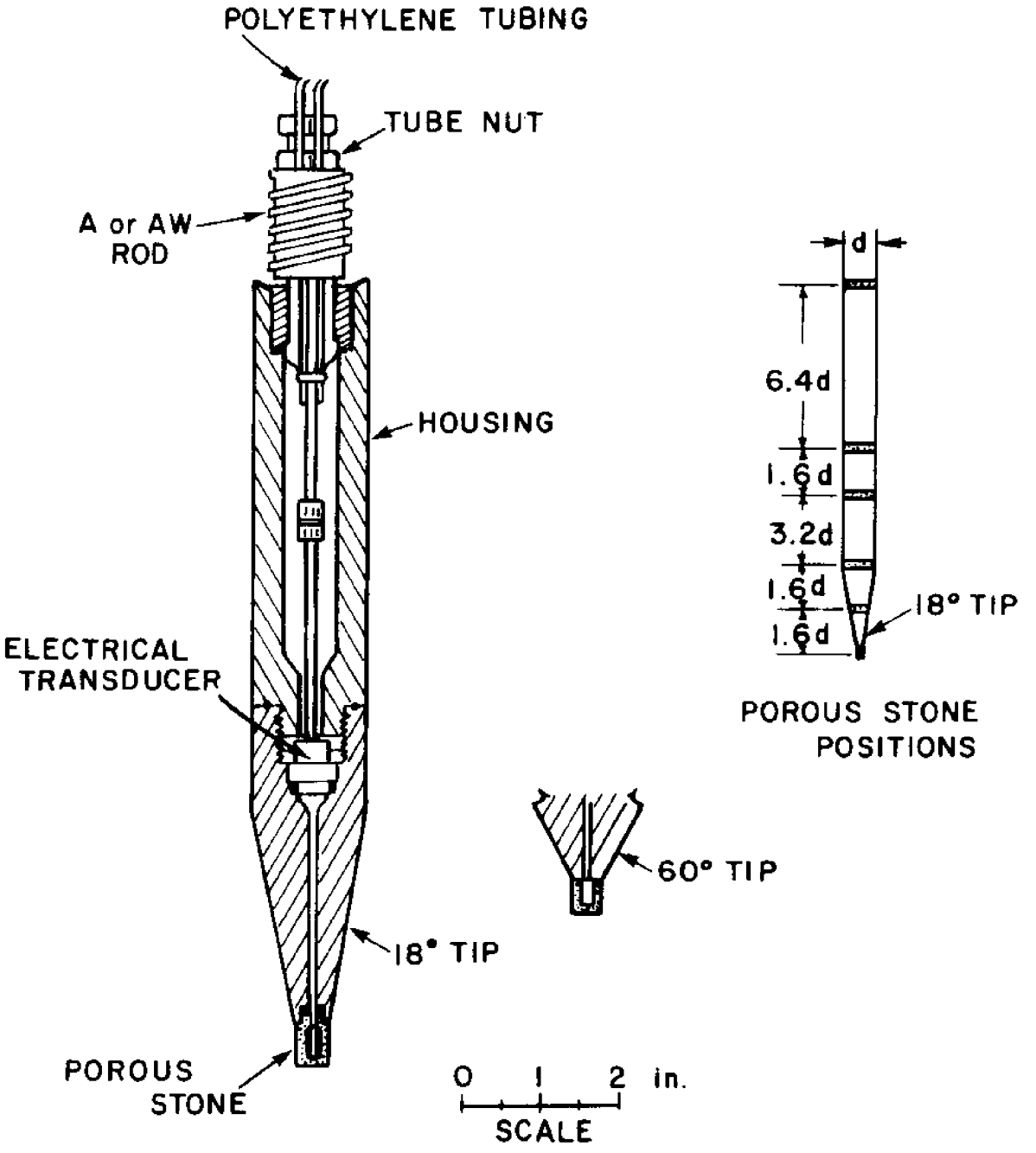

Fig. 2.1 Conical piezometer probes used at MIT (after Wissa et al., 1975; Baligh et al., 1978)

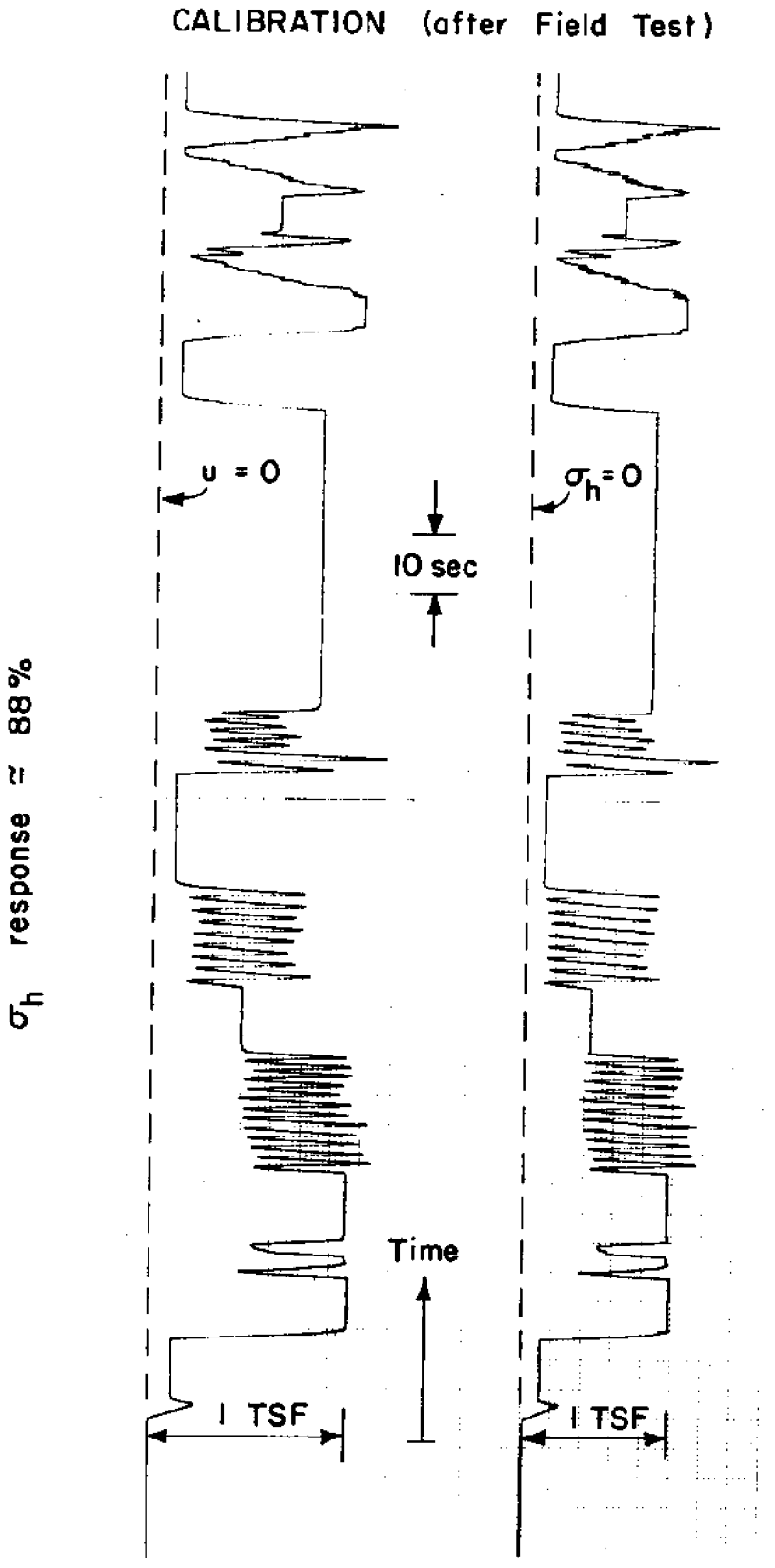

Fig. 2.2 - Piezometer response in a pressurized water bath

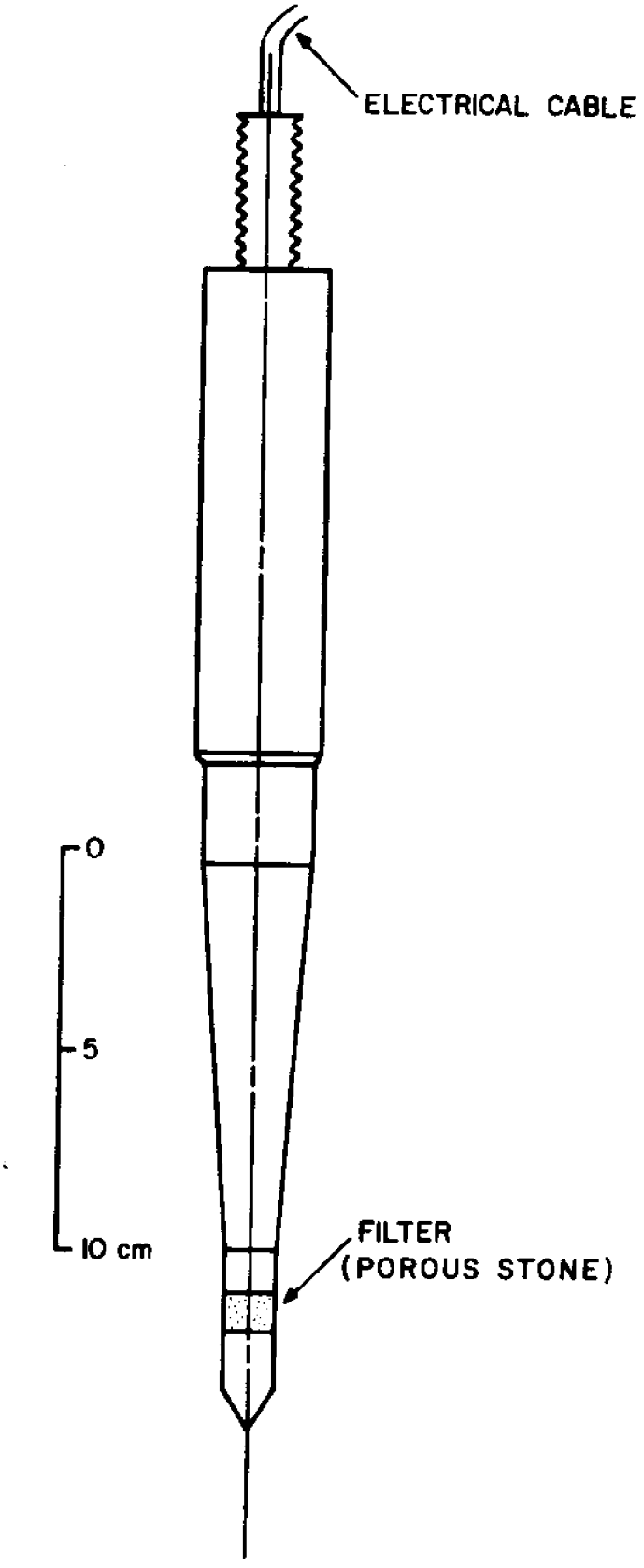

Fig. 2.3 Torstensson's piezometer probe

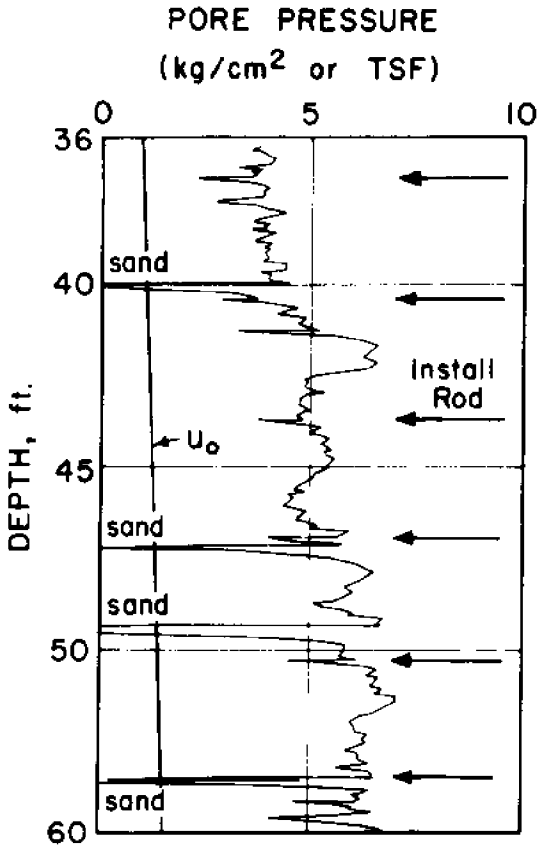

Fig. 2.4 Typical pore pressures recorded at the tip of an 18° conical probe during penetration in clay (from BOSS 79)

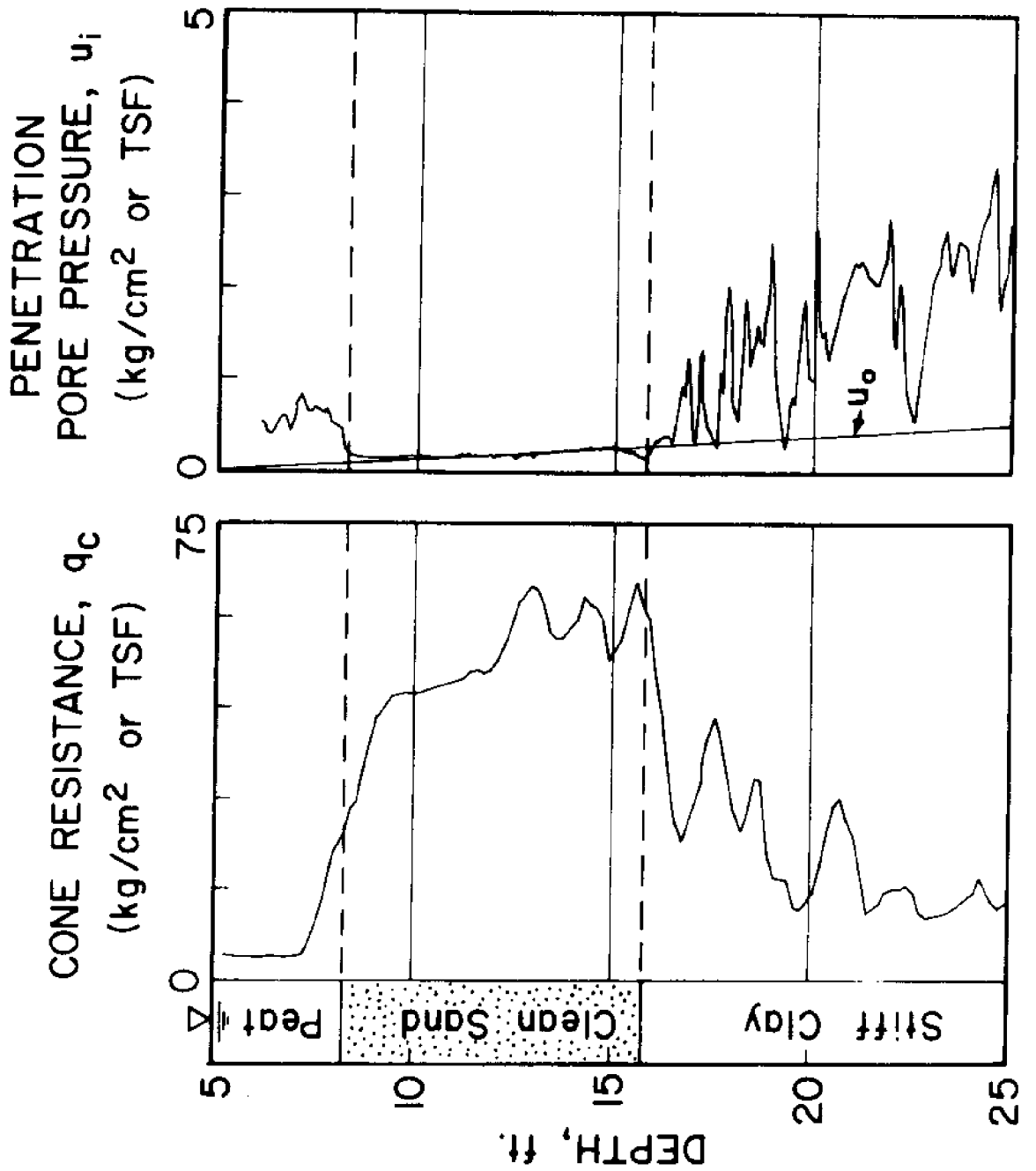

Fig. 2.5 Cone penetration in soil stratification and identification

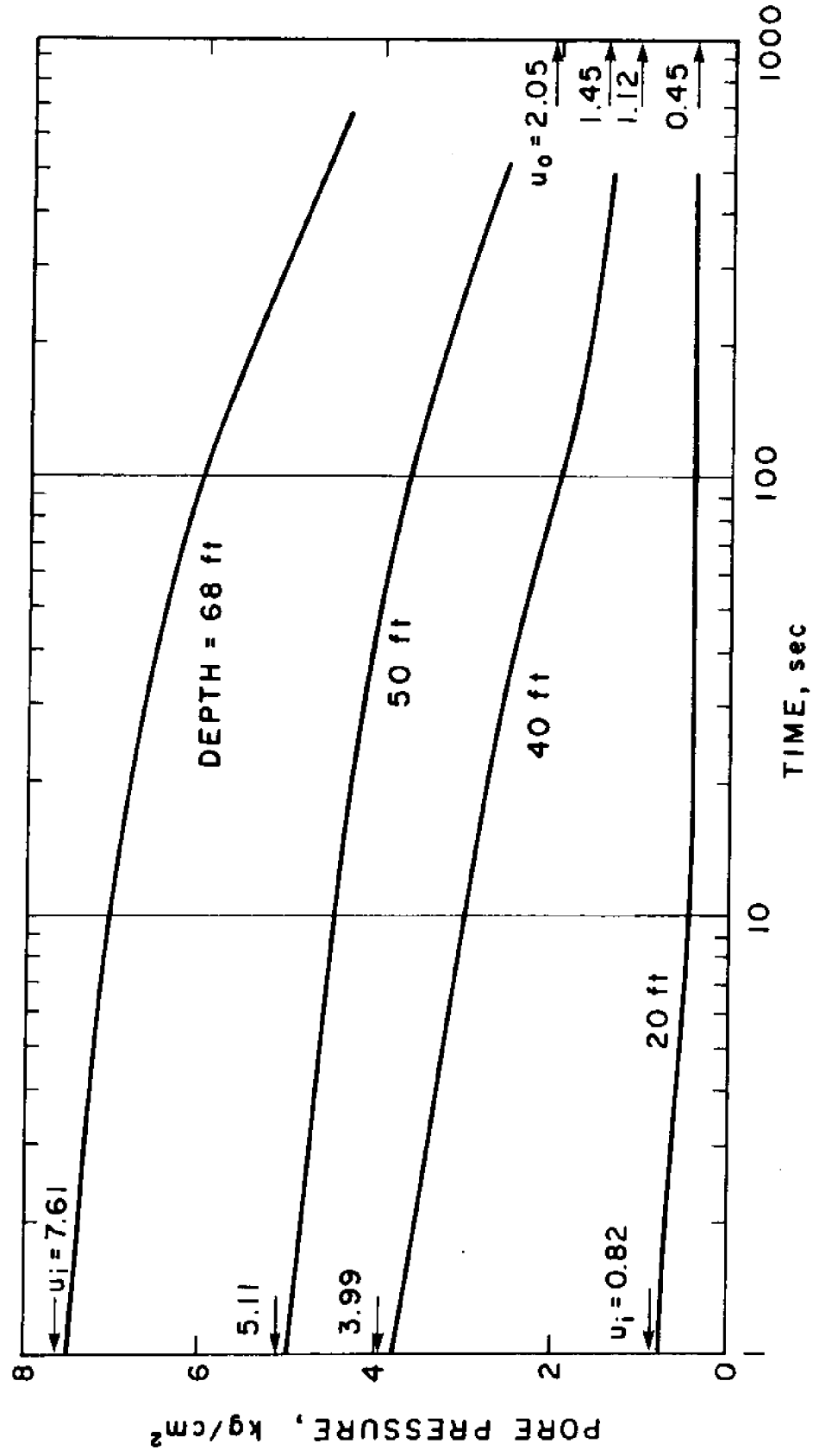

Fig. 2.6 Typical dissipation records after interrupting steady cone penetration in clay

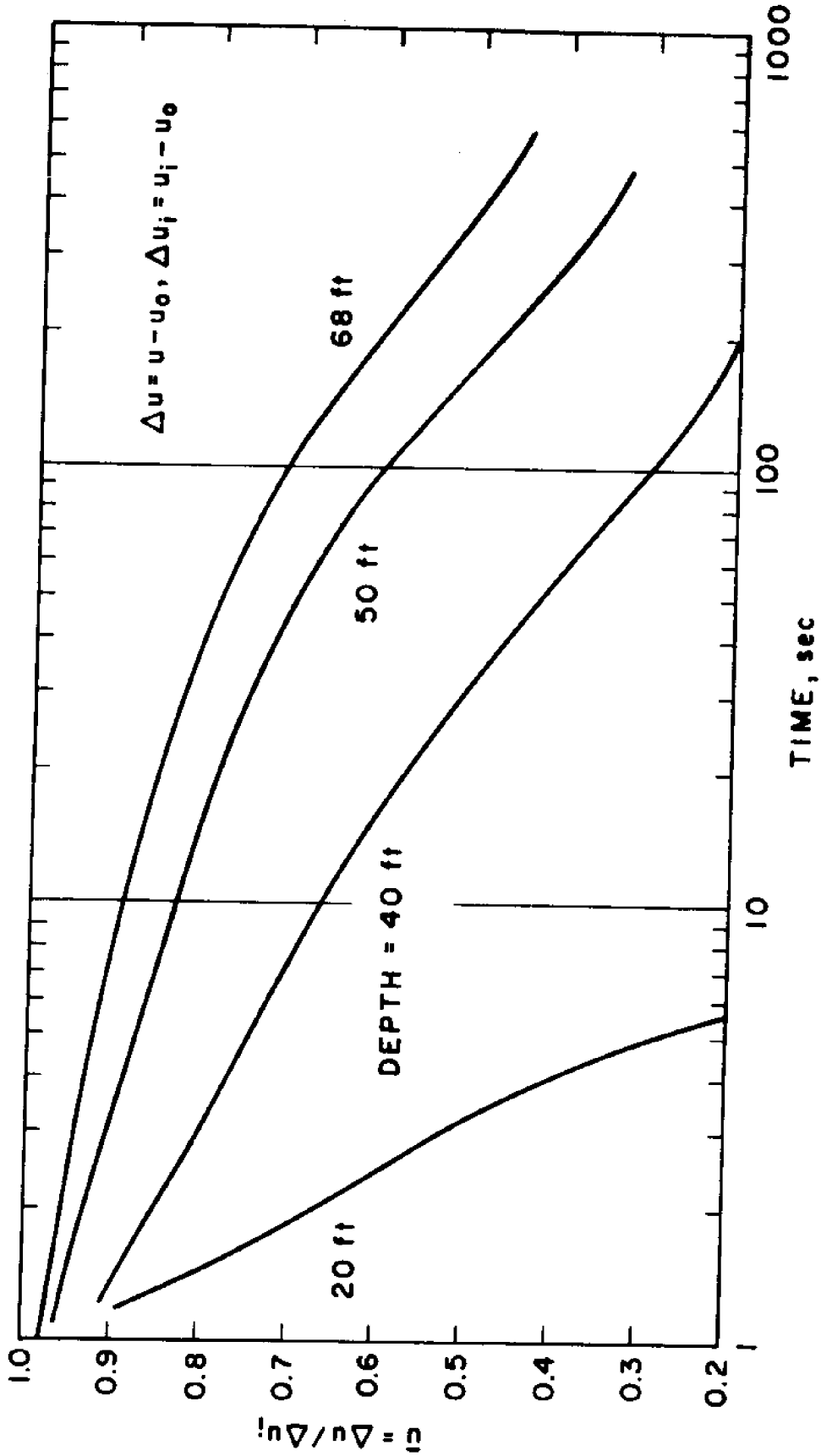

Fig. 2.7 Typical normalized dissipation curves

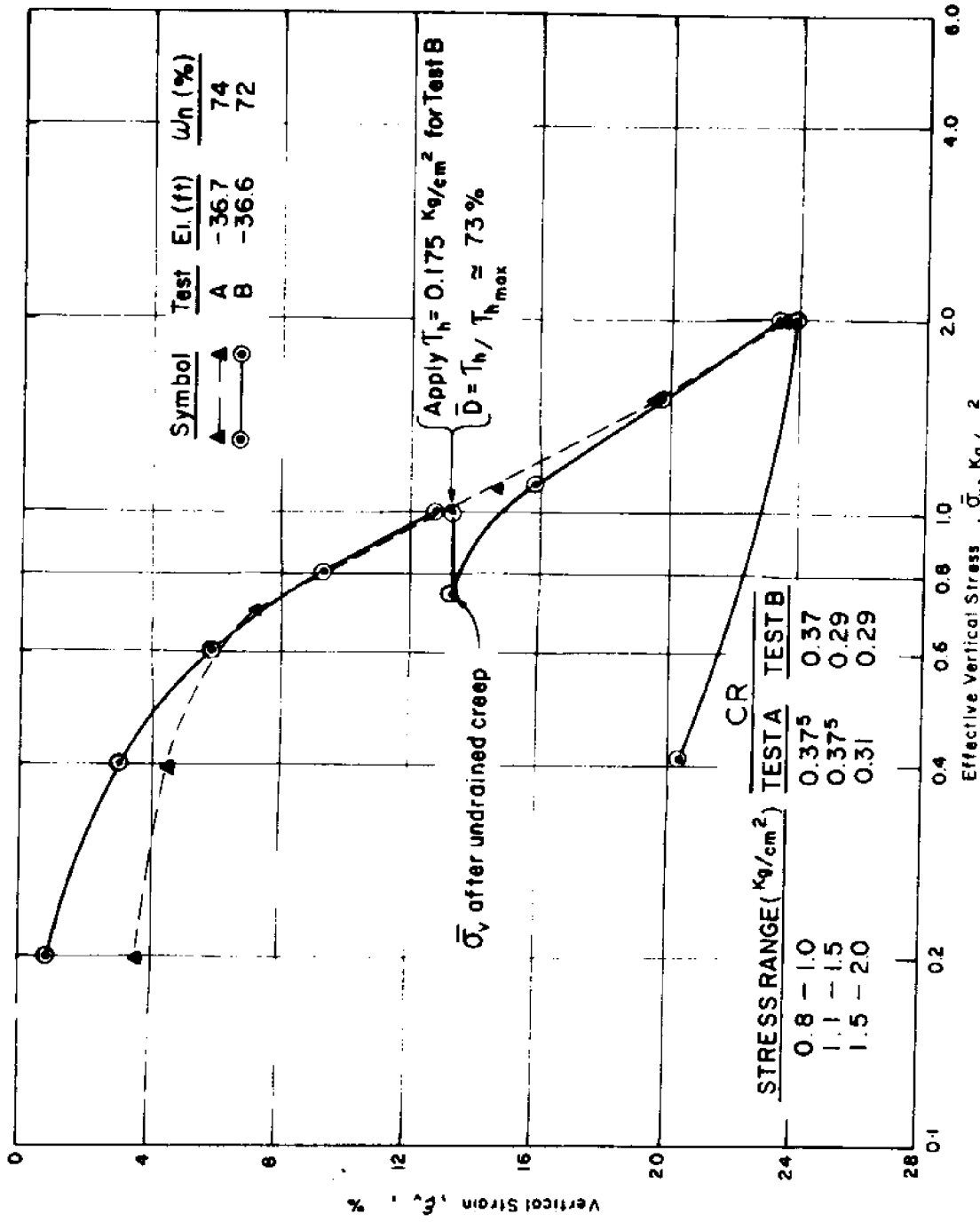

Fig. 2.8 Effect of undrained shear and creep on the compressibility of Atchafalaya clay (from Fuleihan and Ladd, 1976)

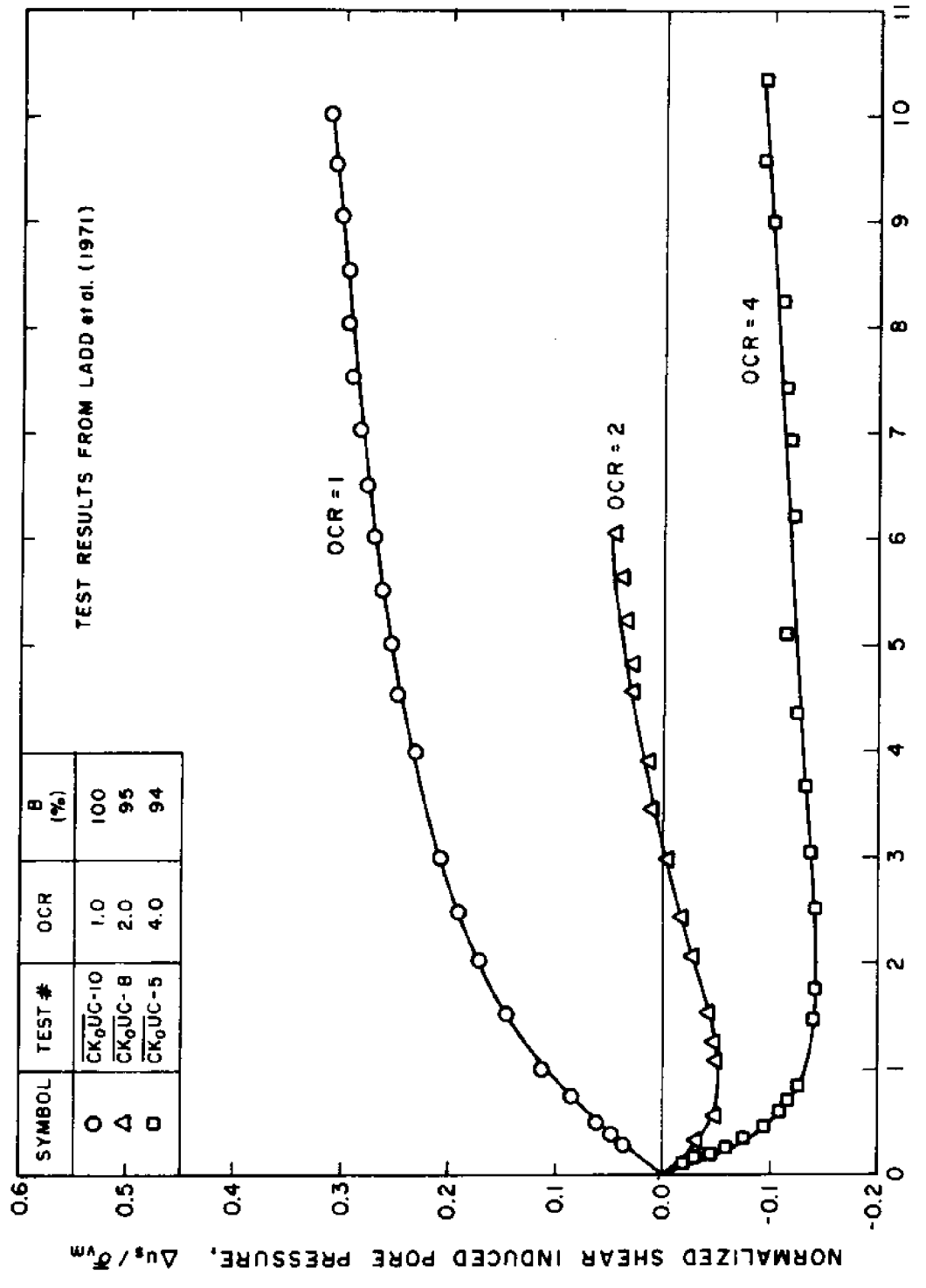

Fig. 2.9 Effect of overconsolidation on the normalized shear induced pore pressure in plane strain compression tests on resedimented Boston Blue Clay

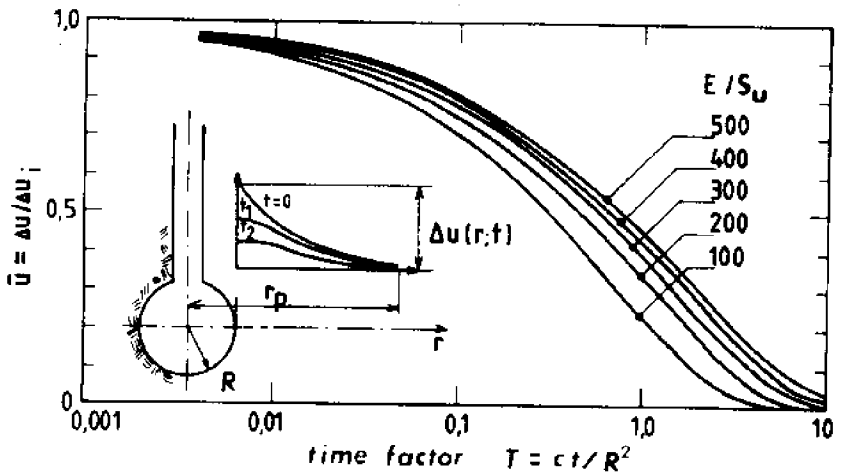

R = radius of pore pressure probe
c = coefficient of consolidation

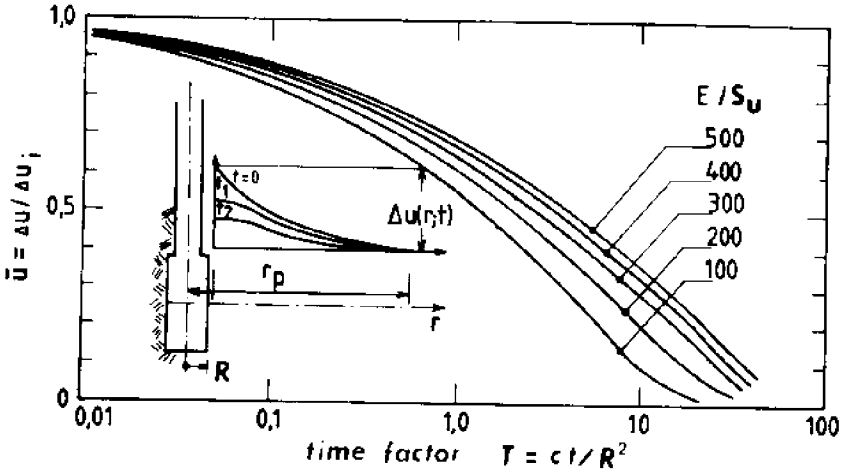

R = radius of pore pressure probe
c = coefficient of consolidation

Fig. 2.10 Pore pressure dissipation around spherical and cylindrical pore pressure probes predicted by Torstensson, 1977

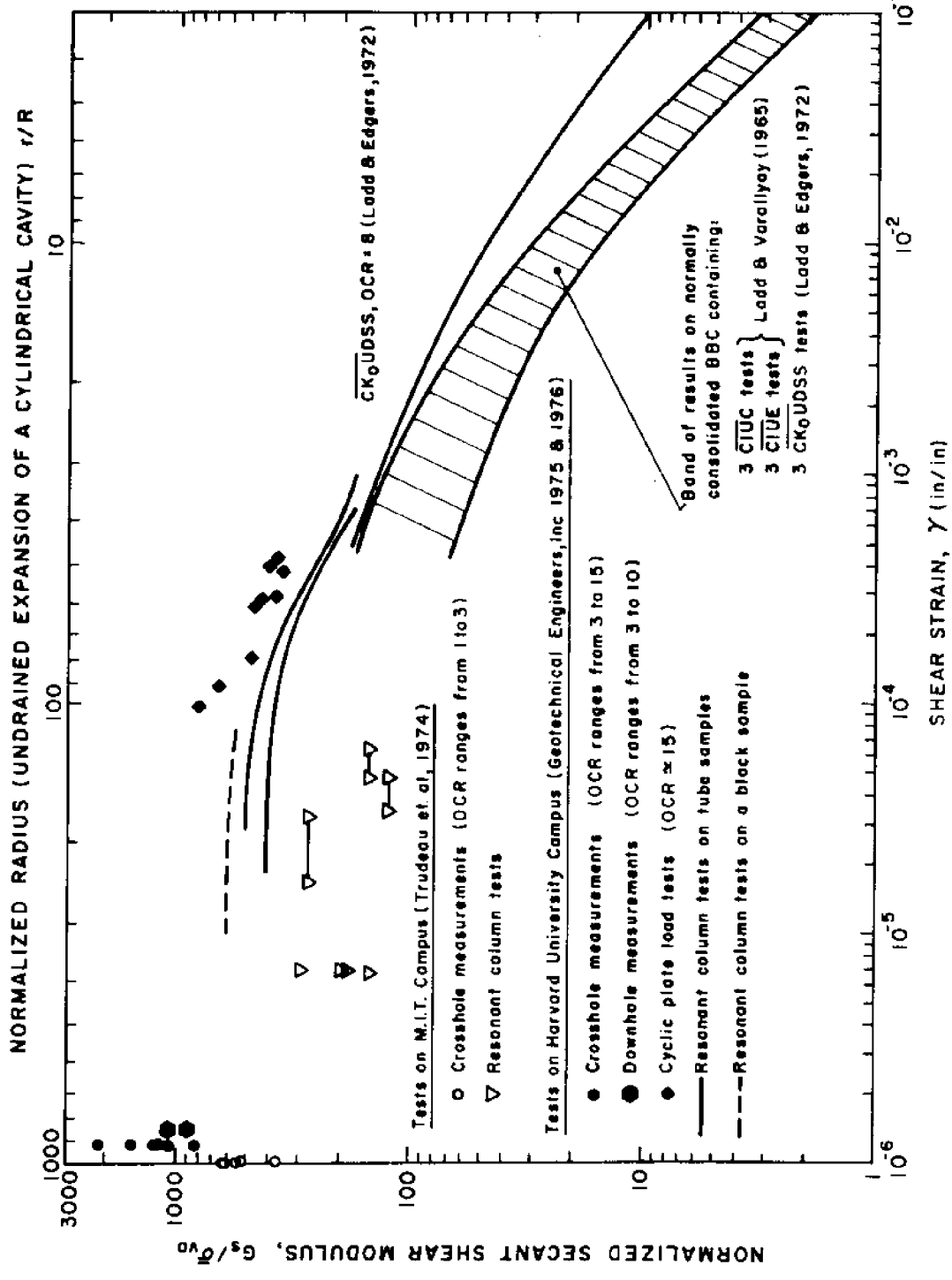

Fig. 2.11 Laboratory and field measurements of the secant shear modulus, G_s, of Boston Blue Clay as a function of strain level (from Azzouz et al., 1980)

CHAPTER 3

INITIAL EXCESS PORE PRESSURES

Steady cone penetration in saturated clays causes undrained shearing and develops excess pore water pressures in the soil. When penetration is interrupted, the initial excess pore pressures governing subsequent dissipation are determined by the pore pressure distribution in the soil during penetration.

3.1 DIFFICULTIES OF ESTIMATING PENETRATION PORE PRESSURES

3.1.1 Theoretical Predictions

The continuous deep penetration of a cone (or pile) in a homogeneous mass represents a two-dimensional steady state problem, i.e., to an observer moving with the cone (or pile), stresses*, strains and deformations in the soil do not change with time. A complete theory of cone penetration should determine stresses*, strains and displacements in the soil to satisfy the boundary conditions corresponding to steady quasi-static penetration and the field equations based on the properties of the soil. However, because soil behavior is complicated and cone penetration involves large strains and high gradients, simplifications are needed.

---

*including pore pressures

Existing theories of cone penetration utilize simple soil models and are based on one of two approaches: 1) Bearing capacity solutions that neglect the steady state aspects of cone penetration: Terzaghi (1943); Meyerhof (1951) and (1961); Mitchell and Dorgunoglu (1973); and, 2) Cavity expansion solutions that neglect the two-dimensional aspects of cone penetration, Table 3.1. Bearing capacity solutions cannot predict the distribution of excess pore pressures during cone penetration. On the other hand, pore pressures estimated by cavity expansion solutions offer some answers but raise serious questions (see Sec. 2.4).

3.1.2 Measurements

Penetration pore pressures can be measured along the face of a penetrating cone and the shaft behind it provided that the response time of the device is sufficiently small (see Chapter 2). However, reliable measurements of pore pressures in the soil at some distance from a penetrating cone (or pile) is a very difficult task* that is often unappreciated by researchers. MIT attempted to measure these pore pressures using conical probes in a Boston Blue Clay deposit.

The testing philosophy was as follows:

1) A probe is pushed to a given depth and left in

---

*even though pore pressures are probably the easiest "stress" that can be measured by existing methods.

place until the pore pressure decay becomes negligible (i.e., until most of the consolidation has taken place).

2) At a lateral distance Δr, a second probe is pushed to a depth approximately 2.5 ft below the first probe while readings of both probes are recorded.

Steps 1) and 2) are then repeated in 5 ft increments by switching the roles of the static and moving probes until the desired maximum depth is reached. Readings obtained from the static probe in tests performed for different values of Δr can thus provide the pore pressure distribution in the soil during cone penetration. Figure 3.1a shows the soil profile* and the testing procedure. Figures 3.1b, c and d show the pore pressure changes Δu_i recorded by the static probe at different depths when the radial spacing between probes, Δr = 2.1, 3.0 and 4.0 ft, respectively. In each figure, Δu_i is plotted vs. the difference in elevation Δz between the two conical tips ($-2.5 < \Delta < 2.5$ ft); negative values of Δz correspond to cases where the static (measuring) probe is below the moving probe.

The results in Fig. 3.1 indicate that:

1) for a given spacing, Δr, and for approximately equal depths, the curves of Δu_i obtained with the two probes

---

*described in more details in Chapter 5.

(playing alternatively the role of the static measuring probe) are very similar. This indicates that the test is repeatable;

2) the results for Δr = 2.1 and 4.0 ft are consistent (Δu_i decreases with increasing Δr). On the other hand, no significant excess pore pressures were recorded for an intermediate spacing Δr = 3.0 ft, thus suggesting that the probes in this test deviated from their intended alignments;

3) the excess pore pressures are significant at Δr = 4.1 ft ($\Delta r/R$ = 30) but show no consistent trend with depth and, most importantly;

4) at all depths and all spacings, Δu_i is negative when Δz is negative (ahead of the moving probe) and becomes positive when Δz is positive (behind the moving probe). This is in agreement with measurements obtained by: (a) Kcizumi and Ito (1967) where the incremental pore pressures measured on a stationary pile at an elevation lower than the pile being pushed ($\Delta z < 0$) are negative ($\Delta u_i < 0$), and; (b) Roy et al (1979) where the pore pressures, during pile driving, monitored by means of an electrical (Geonor) piezometer rigidly connected to the surface, exhibit an identical pattern (Fig. 3.2). However, this contradicts the trend predicted by

simple analyses (such as linear elasticity) where a soil element located below the tip ($\Delta z < 0$) should experience an increase in isotropic stress and, therefore, an increase in pore pressure ($\Delta u_i > 0$). This surprising result can be explained by the interference of the static (measuring) probe with soil deformations. When the moving probe (or pile) is pushed, the static probe cannot accommodate soil deformations and hence causes a relative displacement with respect to the soil where it records the pore pressure. During steady penetration of a conical probe, Levadoux (1980) shows that a soil particle moves monotonically away from the cone axis (in the radial direction), whereas the soil movement in the vertical direction is first downwards and then reverses direction when the cone approximately reaches the elevation of the soil particle. Consequently, the relative displacement between the static (measuring) probe and the surrounding soil induces first tensile and then compressive incremental pore pressures due to the moving probe.

In conclusion, meaningful measurements of pore pressures caused by cone (or pile) penetration are very difficult to conduct because of: a) the interaction between the measuring device and the surrounding soil, and; b) the difficulties in

estimating accurately the relative location of the moving tip with respect to the soil element where pore pressures are measured.

3.2 IMPORTANCE OF INITIAL EXCESS PORE PRESSURES

Since penetration pore pressures are difficult to estimate accurately, it is necessary to identify important factors describing the initial distribution of excess pore pressures and evaluate the effect on dissipation results. This can be indirectly achieved by means of a parametric study of simple one-dimensional consolidation problems.

Levadoux and Baligh (1980) obtained closed form and numerical linear uncoupled consolidation solutions* around impervious spherical and cylindrical cavities in order to study the effect of the following factors on dissipation.

1- The "size" of the soil zone affected by cone penetration. This is conveniently expressed by the parameter $\lambda = r_p/R$; where R is the radius of the cavity**, and r_p is the smallest radius around the cavity where no excess pore pressures develop.

2- The spatial variation of the initial excess pore pressures. Three types of variations with the radius, r, were considered: constant, linear and logarithmic between

---

*according to Terzaghi theory.

**or the radius of the cone shaft, say.

r = R and r = λR, Fig. 3.3

3- The location of boundary drainage. Results were obtained for dissipation in an infinite medium (as in actual situations) and when drainage takes place at r = λR. Comparisons between these two cases provide valuable insights into the effect of the outer soil on dissipation and the importance of the drainage boundary in numerical solutions.

Before discussing the results of these analyses, we note that:

1- In one-dimensional linear problems involving an infinite mass, pore pressure dissipation is controlled by the heat equation and hence solutions can be obtained without consideration of total and/or effective stresses (Sills, 1975). However, the consolidation coefficient differs from Terzaghi's expression.

2- In linear consolidation solutions, dissipation results do not depend on the absolute value (magnitude) of the excess pore pressures. Therefore, it is sufficient to consider the normalized excess pore pressures $\Delta u_i(r)/(\Delta u)_{sh}$ as in Fig. 3.3; where $\Delta u_i(r)$ and $(\Delta u)_{sh}$ are the initial excess pore pressures at a radius r and at the cavity wall (shaft), respectively.

3- When the clay is assumed to be isotropic, incompressible, initially subjected to an isotropic state of stress, elastic (linear prior to yielding) with a shear modulus G,

perfectly-plastic (after yielding) with an undrained shear strength s_u; and when shear-induced pore pressures are neglected, cavity expansion solutions* from a zero radius predict that, for a cylindrical cavity:

$$\lambda = (\frac{G}{s_u})^{1/2}; \quad \Delta u_i(r) = 2s_u \cdot \ln(\frac{\lambda R}{r}) \qquad (3.1)$$

and, for a spherical cavity:

$$\lambda = (\frac{G}{s_u})^{1/3}; \quad \Delta u_i(r) = 4s_u \cdot \ln(\frac{\lambda R}{r}) \qquad (3.2)$$

where $\Delta u_i(r)$ is the excess pore pressure at a radius r. Therefore, the variation of the normalized excess pore pressure $\Delta u_i(r)/(\Delta u)_{sh}$ is given by the logarithmic expression in Fig. 3.3 for both cylindrical and spherical cavities. [Note that $(\Delta u)_{sh} = \Delta u_i(R)$].

Figure 3.4 shows the normalized excess pore pressures, $\Delta u/(\Delta u)_{sh}$ during consolidation around a cylindrical cavity when $\lambda = 20$. We note in Fig. 3.4 that:

1) for a constant initial spatial variation, significant time is required before excess pore pressures at the cavity wall start to decrease;

2) for a logarithmic initial spatial variation**, high

---

*hereafter called elasto-plastic solutions were utilized by Torstensson (1977) and others, Table 3.1

**corresponding to elasto-plastic cavity expansion solutions in a clay with $G/s_u = 400$ or $E/s_u = 1200$, Eq. 3.1

pore pressure gradients occur at the cavity wall and, thus, excess pore pressures at the wall dissipate rapidly, and;

3) for all three types of variation, and at any time factor, $T(=ct/R^2$, where c is the coefficient of consolidation), the soil can be divided into two zones. In the inner zone, pore pressures decrease, whereas in the outer zone, pore pressures increase. The boundary between the two zones (no change in pore pressure at a given time) moves monotonically with time away from the cavity. This indicates that, soil elements close to the wall tend to be constantly subjected to loading (i.e., increase in effective stresses due to decrease in pore pressure). On the other hand, soil elements at a larger distance from the wall are first unloaded and then reloaded (Carter et al., 1978).

Figure 3.5 shows the dissipation curves, $\bar{u}$ vs. log T, at the cavity wall of impervious cylindrical and spherical cavities, in the case of $\lambda = 20$, for different variations of the initial excess pore pressures. The normalized excess pore pressure $\bar{u}$ at the cavity wall is defined as $\Delta u/\Delta u_i$ [Δu_i equals $(\Delta u)_{sh}$ in one dimensional problems]; and, the time factor $T = ct/R^2$; where c is the coefficient of consolidation. The logarithmic variation corresponds to elasto-plastic expansion solutions in a clay with $G/s_u = 400$ for a cylindrical cavity; and; $G/s_u = 8000$ for a spherical cavity. Results in Fig. 3.5

indicate that:

1- for a given initial distribution (λ and variation) dissipation is slightly faster around a spherical cavity (a factor of 1.5 to 2 at 50% dissipation). This appears to contradict results obtained by Torstensson (Fig. 2.10) where the spherical cavity predicts much faster dissipation rates (about 5 times) than the cylindrical cavity. The difference arises because Torstensson does not distinguish between the effects of initial distribution on one hand and, consolidation in radial cylindrical vs. spherical symmetry on the other. Torstensson determines the initial excess pore pressures distribution from elasto-plastic cavity expansion solutions which, for a given clay (i.e., a fixed value of G/s_u), predict a much smaller value of λ for a spherical cavity (see Eqs. 3.1 and 3.2).

2- for a given type of cavity, the initial variation of excess pore pressures in the soil, between $r = R$ and $r = \lambda R$, has an important effect on dissipation, especially at early times. For example, at 50% dissipation: $T_{50} \simeq 7$, 35 and 140 for the logarithmic, linear and constant variations, respectively. Since the time factor T is proportional to the coefficient of consolidation, c, this means that back-figured values of c by the three types of variations are in the ratios of 1:5:20, respectively.

Figures 3.6 and 3.7 show the effects of the size parameter, λ, and the drainage conditions on dissipation curves at the wall of a cylindrical cavity for linear and logarithmic initial distributions, respectively. In both cases, we note that:

1) The effect of λ is significant. Considering a linear variation, Figure 3.6, T_{50} corresponding to $\lambda = 50$ is about seven times larger than $\lambda = 20$. This means that, if the excess pore pressures extend to 50R instead of an assumed value of 20R, the coefficient of consolidation, c, (at 50% dissipation) will be underpredicted by a factor of 7. In case of the logarithmic variation, Figure 3.7, the effect of λ is less pronounced such that the corresponding difference in c is about 3 (instead of 7);
2) Drainage at $r = \lambda R$ instead of ∞ has a negligible effect on dissipation; especially during early consolidation stages. This indicates that consolidation is mainly governed by the soil within a radius λR and is little affected by the outer soil. Furthermore, errors in numerical solutions caused by analyses of finite domains are not very significant, at least in the early stages of dissipation.

In summary, results of simple linear uncoupled one-dimensional consolidation analyses indicate that:

1) Dissipation curves (plotted as $\bar{u}$ vs. log T) are very sensitive to the initial distribution of the normalized excess pore pressures* $\Delta u_i(r)/(\Delta u)_{sh}$ as characterized by:
   a) The extent (or size or radius) of the soil subjected to excess pore pressures compared to the cavity radius, i.e., the parameter λ.
   b) The spatial variation in the soil, e.g., logarithmic, linear, etc.
2) Analyses performed for a given initial distribution (λ and spatial variation) assuming spherical symmetry, lead to slightly faster dissipation than cylindrical symmetry (a factor of 1.5 to 2 in the backfigured coefficient of consolidation at 50% dissipation)
3) Dissipation is mainly controlled by the soil properties within a radius λR and is little affected by the outer soil. Furthermore, the soil near the cavity is predominantly subjected to a decrease in volume (compression or recompression) during dissipation.

---

*Linear solutions are not affected by the absolute value (magnitude) of the excess pore pressure.

3.3 TYPICAL INITIAL DISTRIBUTIONS

The distribution of excess pore pressures around pile shafts is one-dimensional* and is thus relatively simple to investigate. Figure 3.8a shows excess pore pressure measurements due to pile (and model pile) installation in eight clay deposits. The first six cases involve displacement piles whereas cases g and h consist of H piles. In cases a, b, c and d, measurements are conducted in the soil surrounding the pile. In cases c,d,e and f measurements on the pile shaft are available. Important properties of the eight clays are summarized in Figure 3.8a and Table 3.2; and, cover a wide range of soil types. We note in Figure 3.8a that:

1) In a given clay deposit, measurements of pore pressures in the soil surrounding the pile exhibit significant scatter. This is especially clear in cases b and c, and is probably caused by the measurement difficulties discussed earlier in section 3.1.2;

2) Significant excess pore pressures [$\Delta u_i(r) \geq 0.2\ \bar{\sigma}_{vo}$, say] develop within a radius r = 20R (i.e., $\lambda = 20$) around the pile and measurable excess pore pressures extend to r = 50R or even 80R. However, it is difficult to ascertain the effect of probe-soil interaction on these data (see sec. 3.1.2).

---

*In relatively long piles, the only spatial coordinate is the radius r.

3) Little correlation can be established between $\Delta u_i(r)/\bar{\sigma}_{vo}$ and the clay type (as described by the plasticity index PI, say), or its overconsolidation ratio (OCR), or its undrained shear strength (s_u), or its structure or sensisitivity (S_t), or the method of pile installation (driving vs. jacking), or the size or cross section of the pile*, or the depth of measurements (i.e., confining stress).

4) Few data points are available in the vicinity of the pile ($R<r<5R$);

5) In spite of the very different conditions (soil and pile) in cases a, b, c, d, g and h, results between $r = 5R$ and $r = 20R$ fall within a well defined band and suggest that $\lambda \simeq 20R$.

Figure 3.8b shows the band including most of the test data for $r>5R$. A reasonably good fitting of the data between $r = 5R$ and $r = 20R$ can be achieved by either a logarithmic distribution or a linear distribution. Pore pressures beyond $r = 20R$ are small and can probably be neglected in analyses of single piles. Figure 3.5 indicates that the logarithmic and linear distributions of initial excess pore pressures lead to very different dissipation curves such that the backfigured coefficients of consolidation (at 50% dissipation, say) can differ by a factor of five or more. This uncertainty is essentially due to the lack of reliable data near the pile ($R<r<5R$).

---

*For H piles, the radius R was selected as half the pile width, i.e., R = 6".

Noting that the logarithmic initial excess pore pressure distribution is derived by elasto-plastic cylindrical cavity expansion solutions; according to Equation 3.1, the straight line in Figure 3.8b corresponds to a clay with $G/s_u = 400$ and $s_u/\bar{\sigma}_{vo} = 0.68$ (i.e., $G/\bar{\sigma}_{vo} = 272$). This ratio of G/s_u is much higher than estimated by many investigators in analyzing cavity expansion problems* even though $s_u = 0.68\ \bar{\sigma}_{vo}$ is excessively high especially for the soft clays (OCR ≈ 1) in cases a and b. Therefore, special care is needed in selecting the shear modulus, G, for cavity expansion problems, (Figure 2.11). A more realistic soil model than the bilinear elasto-plastic behavior can reduce this difficulty.

In summary, existing measurements of pore pressures in clays due to pile installation indicate that $\lambda = 20$ or more. However, the measurement scatter and the lack of sufficient data near the pile ($R<r<5R$) prevent reliable estimates of the spatial variation of excess pore pressures to be made. Uncertainties in the spatial variation of initial excess pore pressures have an important effect on dissipation results. In the relatively simple problem of consolidation around pile shafts, estimates of the coefficient of consolidation from dissipation rates can easily differ by a factor of 5 depending on the selected initial distribution and the degree of dissipation.

---

*See Fig. 2.10 where Torstensson plots results for G/s_u between 33 and 165.

3.4 PROPOSED PENETRATION PORE PRESSURES

3.4.1 The Strain Path Method

Deep steady cone prenetration in clay is essentially a "strain-controlled" problem where strains and deformations are primarily imposed by kinematic requirements. For this type of problem, Baligh (1975) proposes an approximate method of solution called the "Strain path method". This method is based on concepts similar to the more popular "stress path method" (Lambe, 1967) and consists of four basic steps: a) estimate the initial stresses; b) estimate an approximate strain field satisfying conservation of volume, compatibility and boundary velocity requirements; c) evaluate the deviatoric stresses at a selected number of elements by performing laboratory tests on samples subjected to the same strain paths or, alternatively, by using an appropriate soil behavioral model, and; d) estimate the octahedral (isotropic) stresses by integrating the equilibrium equations.

Table 3.3 compares the strain path method with the stress path method to identify their strong similarities. As indicated in Table 3.3, the strain path method is an approximate method because the estimated stresses will not, in general, satisfy the equilibrium requirements, unless the estimated strain field is identical to the actual one.

3.4.2 The Strain Path Method in Cone Penetration

Figure 3.9 describes the steps for evaluating stresses and pore pressures in the soil due to deep steady cone penetration in saturated clays by means of the strain path method:

1) Estimate a velocity field* satisfying the conservation of volume (or mass) requirement and the boundary conditions.
2) From the velocity field determine the soil deformations by integration along streamlines. Figure 3.10 shows the deformation of a square grid due to steady penetration of a 60° cone as determined by Levadoux and Baligh (1980) after neglecting the shearing resistance of the soil (i.e., assuming the soil to behave as an ideal fluid).
3) Compute the strain rates, $\dot{\varepsilon}_{ij}$, along the streamlines by differentiating the velocities with respect to the spacial coordinates.
4) Integrate the strain rates, $\dot{\varepsilon}_{ij}$, along streamlines to determine the strain path (ε_{ij}) of different soil elements.

---

*The velocity field describes the velocity of soil particles as they move around the cone.

Figure 3.11 shows the deviatoric* strain paths of three soil elements (initially located at r_o/R = 0.2, 0.3 and 1.0 from the axis) due to penetration of a 60° cone (Fig. 3.10). Clearly, the paths are complicated and involve large strains with strain reversals.

5) Estimate the initial stresses, $(\sigma_{ij})_o$, and initial pore pressures, u_o, in the soil prior to cone penetration.

6) Compute the deviatoric stresses, s_{ij}, and the shear-induced pore pressures, Δu_s, along streamlines. Levadoux and Baligh (1980) developed the necessary mathematical models to estimate s_{ij} and Δu_s due to the complicated strain paths imposed by cone penetration taking into consideration the anisotropic inelastic nonlinear behavior of clays. Using soil parameters obtained from laboratory tests on normally consolidated resedimented Boston Blue clay, Levadoux and Baligh (1980) predict: a) The deviatoric stress paths. Fig. 3.12 shows the stress path for an element initially located at a radius r_o = 25R due to steady penetration of a 60° cone. For comparison, the paths corresponding to (idealized) Direct Simple Shear (DSS) and Pressuremeter (PR) modes of shearing are also shown in

*No volumetric straining takes place during undrained shearing of a saturated soil.

Fig. 3.12. Clearly, cone penetration subjects the soil to very complicated stress paths consisting of a combination of triaxial compression, DSS and PR modes. b) The shear induced pore pressures. Fig. 3.13 compares the predicted contours of Δu_s due to penetration of 18° and 60° cones with cylindrical cavity solutions.*

7) (a) From equilibrium considerations, compute the total stresses,** σ_{ij} $(=s_{ij} + \delta_{ij}\ \sigma_{oct})$, given the deviatoric stresses, s_{ij}. This requires the determination of the octahedral stresses, σ_{oct}. Since the assumed strains are not exact, the estimated values of σ_{oct} are approximate because they depend on the integration path, i.e., on the direction where equilibrium is satisfied; radial, axial, etc.

   (b) From s_{ij} and Δu_s, compute the effective stresses, $\bar{\sigma}_{ij}[= (\bar{\sigma}_{ij})_o + \Delta\bar{\sigma}_{ij}\ ;\ \Delta\bar{\sigma}_{ij} = \Delta s_{ij} - \Delta u_s\ \delta_{ij}]$

8) From σ_{oct} and u_s determine the penetration pore pressures u_i $(= u_o + \Delta u_i;\ \Delta u_i = \Delta\sigma_{oct} + \Delta u_s)$

Finally, by estimating the shear stresses at the cone soil interface and integrating tractions along the cone face, the cone resistance, q_c, can be evaluated.

---

*According to the same soil model.

**δ_{ij} = Kronecker delta: = 0 when $i \neq j$; = 1 when $i = j$ and, $\sigma_{oct} = 1/3\ \sigma_{ii}$.

3.4.3 Predictions of Penetration Pore Pressures

Figure 3.14 shows the distribution of excess pore pressures, Δu_i, during penetration of 18° and 60° cones based on soil properties obtained from laboratory tests on resedimented normally consolidated Boston Blue clay. In order to obtain these solutions by the strain path method, displacements and strains were determined by assuming the soil to offer no shearing resistance (i.e., to behave as an ideal fluid, Fig. 3.10 and 3.11) and the octahedral stresses were computed by satisfying equilibrium in the radial direction. Results in Fig. 3.14 indicate that:

1) The excess pore pressures, Δu_i, are significant even at large distances from the cone. These pore pressures are principally due to the increase in octahedral stresses, i.e., the contribution of Δu_s is small (about 20%, see Fig. 3.13).
2) The soil can be divided into two zones: (a) An inner zone where the pore pressure gradients are high and the strains are sufficiently large to cause failure of the soil, and (b) An outer zone where the strains are smaller, the soil is in a pre-peak state* and the excess pore pressures are not significantly dependent on the cone angle. The boundary between

---

*but far from being in an elastic (linear) state as assumed by simple bilinear elasto-plastic models.

the inner and outer zones is roughly given by the contour of the octahedral strain* γ_{oct} = 2% located at a radius approximately equal to 5R.

3) Far behind the cone tip, the excess pore pressures are higher than estimated by cavity expansion solutions** in the outer zone and lower than cavity expansion solutions in the inner zone.

3.4.4 Comparison with Measurements

A detailed discussion of various predictions obtained by applying the strain path method to cone penetration is beyond the scope of this report. However, the method is capable of estimating reasonable distributions of normalized excess pore pressures for conducting linear analyses of dissipation after interrupting cone penetration.

The solid lines in Fig. 3.15 present the same predictions of penetration excess pore pressures,*** Δu_i, at different locations on the face and shaft behind 18° and 60° cones after normalization by the excess pore pressure on the shaft, $\Delta u_{(sh)}$ i.e., $\Delta u_i/\Delta u_{(sh)}$ approaches unity at a sufficiently large distance behind the tip. Fig. 3.15 also shows in situ measurements

---

*$\gamma_{oct} = 1/3[(\varepsilon_r - \varepsilon_\theta)^2 + (\varepsilon_\theta - \varepsilon_z)^2 + (\varepsilon_z - \varepsilon_r)^2 + 6\varepsilon_{rz}]^{1/2}$

γ_{oct} is approximately equal to the radius of Mohr circle of strain.

**Using the same soil model and soil parameters corresponding to normally consolidated BBC.

***As in Fig. 3.14.

of $\Delta u_i/\Delta u_{(sh)}$ conducted in a Boston Blue Clay deposit* at Saugus, Massachusetts. Fig. 3.15 indicates that, even though predictions are based on laboratory test data on resedimented normally consolidated BBC, they provide good agreement with measurements in the natural deposit having overconsolidation ratios OCR = 3, 2 and 1.3. This important result means that linear dissipation analyses can be conducted using the same initial distribution of $\Delta u_i/(\Delta u)_{sh}$ for the entire BBC deposit where OCR $\leq$ 3.

Attempts to extend this result to the upper clay having an OCR>3 were prevented by the large scatter of measured penetration pore pressures, Δu_i, (due to inherent soil variability) as compared to the small average values of Δu_i.

In order to check the predicted penetration pore pressures at some distance from the cone, measurements of u_i in the soil around the cone are required. Such measurements are very difficult to obtain in situ because of: (a) the interference between the measuring device and soil deformations, and; (b) the uncertainties in alignments which can introduce significant errors in the estimated radial distances. Attempts to perform such measurements in BBC by means of two piezometers were unsuccessful, see Sec. 3.1.2.

---

*Discussed in detail in Chapter 5.

Therefore, using the analogy between cone penetration and pile installation, predictions of $\Delta u/(\Delta u)_{sh}$ in the soil are compared with measurements conducted around a cylindrical pile (21.9 cm in diameter) jacked into Champlain Clay (Roy et al., 1979).

The measurements are quite consistent and reliable and, because of the small size of the piezometers (Geonor M-600) compared to the pile,* are hopefully less sensitive to the errors mentioned above (piezometer-soil interaction and alignment). Furthermore, the excess pore pressure measured along the shaft of the pile $(\Delta u)_{sh} \simeq 2\bar{\sigma}_{vo}$ is very close to that measured in BBC behind conical probes, $(\simeq 2.1\bar{\sigma}_{vo})$.

Figure 3.16 compares the predicted radial distribution of excess pore pressure at a sufficiently large distance ($z \simeq 14R$) behind 18° and 60° cones during penetration in normally consolidated BBC to measurements in Champlain Clay. Results in Fig. 3.16 show that:

1) The predicted radial distributions of pore pressures behind 18° and 60° are almost identical;
2) The agreement between predictions and measurements is remarkable, in view of (a) the approximations in the strain path method, (b) the uncertainties in the field measurements (in particular at small radii) and especially, (c) the difference in

*The pile diameter is about 6.5 times that of the piezometer.

behavior between BBC (OCR ≈ 1) used for predictions and the Champlain Clay (OCR ≈ 2) where measurements are made.

Results in Fig. 3.16 are very encouraging since they suggest that the normalized excess pore pressure distribution during pile installation is not very sensitive to soil type or stress history (OCR). This is further supported by the results in Figure 3.8 showing that measurements in Champlain Clay (case d) are not unique but are similar to other clays of different types and stress histories. Results obtained by Azzouz et al., 1980, indicate that, at some distance from the axis, the pore pressures are governed by the shear modulus of the soil at low strain levels. The latter apparently is not very sensitive to OCR* as compared to other factors e.g., soil structure, aging, etc.

In summary, the two-dimensional (axisymmetric) normalized excess pore pressure distribution around cones (or piles) predicted by the strain path method compares very well with field measurements (a) at different locations along the cone for a wide range of overconsolidation ratios ($1.3 < OCR < 3$) and (b) in the radial direction far behind the tip. These distributions appear, therefore, sufficiently accurate to perform dissipation analyses which will hopefully be applicable for a wide variety of clays with $OCR < 3$.

---

*possibly because of the compensating effects of $\Delta\sigma_{oct}$ and Δu_s.

3.5 CONCLUSIONS

1) Measurements of excess pore pressures in the soil due to cone penetration are very difficult to conduct because of (a) the interaction between the measuring device and the soil; and (b) alignment problems.

2) Results of dissipation analyses are sensitive to the initial distribution of the excess pore pressures as characterized by (a) the extent (or size or radius) of the soil subjected to significant excess pore pressures and, (b) the spatial variation of the initial excess pore pressures within this radius.

3) Existing measurements in clays indicate that (a) significant excess pore pressures develop due to pile installation within a radius extending to 20 times the pile radius, (b) uncertainties in the spatial variation of these excess pore pressures due to measurement scatter and the lack of data near the pile can easily lead to a factor of 5 difference in the backfigured coefficient of consolidation from dissipation records.

4) Existing theories cannot predict the distribution of excess pore pressures during cone penetration. Bearing capacity solutions neglect the steady state aspect of cone penetration. Cavity expansion

solutions neglect the two-dimensional nature of cone penetration and, even in the relatively simple problem of estimating pore pressures around pile shafts, require more realistic modelling of soil behavior than presently used* and then, provide questionable results.

5) Linear dissipation analyses are not affected by the absolute value (magnitude) of excess pore pressures Δu_i, and only require estimates of the normalized excess pore pressures, e.g., $\Delta u_i/(\Delta u)_{sh}$ where $(\Delta u)_{sh}$ is the shaft excess pore pressure at a sufficiently large distance behind the cone.

6) Predictions of $\Delta u_i/(\Delta u)_{sh}$ obtained by the strain path method on the basis of laboratory test data on normally consolidated resedimented Boston Blue clay provide good agreement with in situ measurements (a) on the face and the shaft behind 18° and 60° cones in a BBC deposit having $1.3 < OCR < 3$; and (b) in the soil surrounding a jacked pile in Champlain clay.

7) The measurements of pore pressures around the jacked pile in Champlain clay are very similar to a number

---

*e.g., a bilinear elasto-plastic model, say.

of other clays of different types and stress histories. Therefore, it seems possible that the predicted distributions of $\Delta u_i/(\Delta u)_{sh}$ by the strain path method for normally consolidated BBC will prove satisfactory in other clays as well.

8) Finally, linear uncoupled one-dimensional consolidation analyses indicate that (a) dissipation is only affected by the soil where significant initial excess pore pressures develop (i.e., within a radius = 20 times the shaft radius) and (b) this soil is predominantly subjected to a decrease in volume (compression or recompression) during consolidation.

Author	Cavity		Material Model	Initial Stresses	Proposed Applications	Remarks
	Cyl.	Sph.				
Bishop, Hill and Mott (1945)	x	x	Elastic-plastic (Von Mises) strain hardening	Not considered (presumably isotropic)	Metal indentation	Closed form solution; experimental results of copper indentation compare well with theory; use natural strains.
Chadwick (1959)		x	Elastic-perfectly plastic (Tresca)	Isotropic	Cylindrical cavity expansion in soils and metals	Considers both loading (expansion) and unloading (contraction) of a spherical cavity.
Gibson and Anderson (1961)	x		Elastic-perfectly plastic (Tresca)	$\sigma_r = \sigma_\theta$	Interpretation of the pressuremeter test	Closed form solution
Ladanyi (1963)	x	x	Experimental stress and mean effective stress vs. strain curves determined from triaxial test	Isotropic	- Stress distribution around cavities - Bearing capacity of deep foundations - Excess por pressure distribution around driven piles	- Numerical integration of equilibrium equations - Predicts both total stresses and pore pressures.
Butterfield and Bannerjee (1970)	x		Elastic-perfectly plastic (Von Mises)	Isotropic	- Stress and pore pressure distributions around driven piles	- Closed form solution - Consider boundary shear stresses (shaft friction) - Error in equations (do not satisfy the conservation of volume; see Appendix A for correct solution).
Baguelin et al. (1972)	x		General (non linear: stress-strain curve	$\sigma_r = \sigma_\theta$	Pressuremeter test	Provide a method of interpretation of the pressuremeter test (i.e., obtain stress-strain curve from expansion curve).
Ladanyi (1972)	x		General stress-strain curve	$\sigma_r = \sigma_\theta$	Pressuremeter test	Same as above.
Palmer (1972)	x		General stress-strain curve	$\sigma_r = \sigma_\theta$	Pressuremeter test	Same as above.
Vesic (1972)	x	x	Elastic-perfectly plastic	Isotropic	- Ultimate cavity pressure - Evaluation of pressuremeter tests - Evaluation of excess pore pressures due to pile driving	- Considers volume change for drained expansion - Evaluates pore pressures and total stresses for undrained expansion
Prevost and Hoeg (1975)	x		Elastic-plastic (Von Mises) w/ isotropic hardening or softening	Isotropic	Pressuremeter test	- Provide mathematical expressions for the yield function to obtain closed form solution [illegible]
Carter, Randolph and Wroth (1978)	x		Modified cam-clay	K_o condition	Stress distribution along the shaft of a driven pile	Finite element analysis

NOTE: All references consider a) an incompressible isotropic homogeneous non viscous material (unless otherwise indicated)

b) plane strain deformations in the cylindrical cavity expansion with $\Delta\sigma_z = \frac{1}{2}(\Delta\sigma_r + \Delta\sigma_\theta)$

Table 3.1 Summary of existing solutions for cylindrical and spherical cavity expansion

Case	a	b	c	d	e	f	g	h
Reference	Bjerrum and Johannessen (1960)	Lo and Stermac (1965)	Koizumi and Ito (1967)	Roy et al (1979)	Baligh et al (1978)	Airhart et al (1969)	Ismael and Klym (1979)	Soderman and Milligan (1961)
1) Site	Southern Norway	Wallaceburg Ontario, Canada	Otemachi Tokyo, Japan	Saint Alban Quebec, Canada	Saugus Massachusetts, USA	Beaumont Texas, USA	Pickering Ontario, Canada	Big Pic River Canada
2) Soil								
2-a Type and description	Soft Marine clay	Soft to firm silty clay	Very sensitive slightly organic silty clay	Very sensitive Marine soft silty Champlain Clay	Marine illitic Boston Blue Clay	Highly over-consolidated	Firm clayey-sandy silt	Medium to stiff varved silty clay
2-b Plasticity Index (PI)	25	20	60	20	20	40	10	37 clay, 7 silt
2-c Overconsolidation ratio (OCR)	≈ 1	≈ 1	≈ 2.5 [5]	2. 2 to 2.4	1.2 to 4	OCR = 7 [5]	High sand content	OCR = 3 [5]
2-d Undrained Strength (s_u)	2 to 2.5 TSM [1]	2 to 2.5 TSM [1]	3 to 3.5 TSM [2]	1. 2 to 2 [1]	3.5 to 5.5TSM [1]	11 TSM [3]	No OCR & s_u meas.	2.5 to 4.5 TSM
2-e Sensitivity (S_t)	6 to 8 [1]	4 to 6 [1]	v. high	16	6			
3) Pile: 3-a type	Steel Hollow Box	Steel pipe	Steel pipe	Steel pipe	Steel cylinder	Steel pipe	H-pile	H-pile
3-b Cross section	20 x 20 cms	ϕ = 8.9 cm	ϕ = 30 cm	ϕ = 21.9 cm	ϕ = 3.8 cm	ϕ = 40.7 cm	12" x 53 lb.	12" x 53 lb.
3-c Length	= 20 m	15 m	5.5 m	7.5 m	Variable	16.2 m	7.6 m	16.8 to 50.6 m
3-d Installation	Driving	Driving	Jacking	Jacking	Jacking	Driving	Driving	Driving
4) Pore Pressures Measurements								
4-a Device	NGI piezometer	not reported	Cells on piles and piezometers	Glonzl cell on pile & Geonor electric piezometer in soil	Electric Transducer	Pressure Transducer	Gage at surface for pressure on pile and geonor piezometer in soil	Casagrande open tube
4-b Quality	Good		Fair	Very Good	Very Good	Fair	Fair	Questionable
5) Notes	No measurements of u_i close to pile	Significant scatter. Pore pressures still rising after 1hr when second pile was driven	Significant scatter. Comprehensive study [4]	Very repeatable	Very repeatable	Pore pressure still rising after 8 hours. No data on G.W. level.		

(1) Field Vane Test (3) Unconfined Test (5) Estimated

(2) Dutch Cone Test (4) Important uncertainty in $\bar{\sigma}_{vo}$ due to 1.5m excavation. We assume wide excavation and pore pressure equalization. Otherwise $\bar{\sigma}_{vo}$ doubles at depth = 5m.

Table 3.2 Summary of case histories where excess pore pressures were measured during pile installation in clay.

Stress Path Method	Strain Path Method
APPLICATIONS	
Surface Problems	Deep Problems
STEPS	
1. Estimate initial stresses 2. Estimate incremental stresses 3. Perform stress path tests on samples (or use adequate soil model) to obtain strains at selected locations. 4. Estimate deformations by integrating strains	1. Estimate initial stresses 2. Estimate incremental strains 3. Perform strain path tests on samples (or use adequate soil model) to obtain deviatoric stresses at selected locations. 4. Estimate octahedral (isotropic) stresses by integrating equilibrium equations.
APPROXIMATION	
In step 2, stresses are approximate thus leading to strains not satisfying compatibility requirements. i.e., deformations in step 4 depend on strain integration path.	In step 2, strains are approximate thus leading to stresses not satisfying all equilibrium conditions. i.e., octahedral stresses in step 4 depend on equilibrium integration path.

Table 3.3 Comparison of stress path and strain path methods

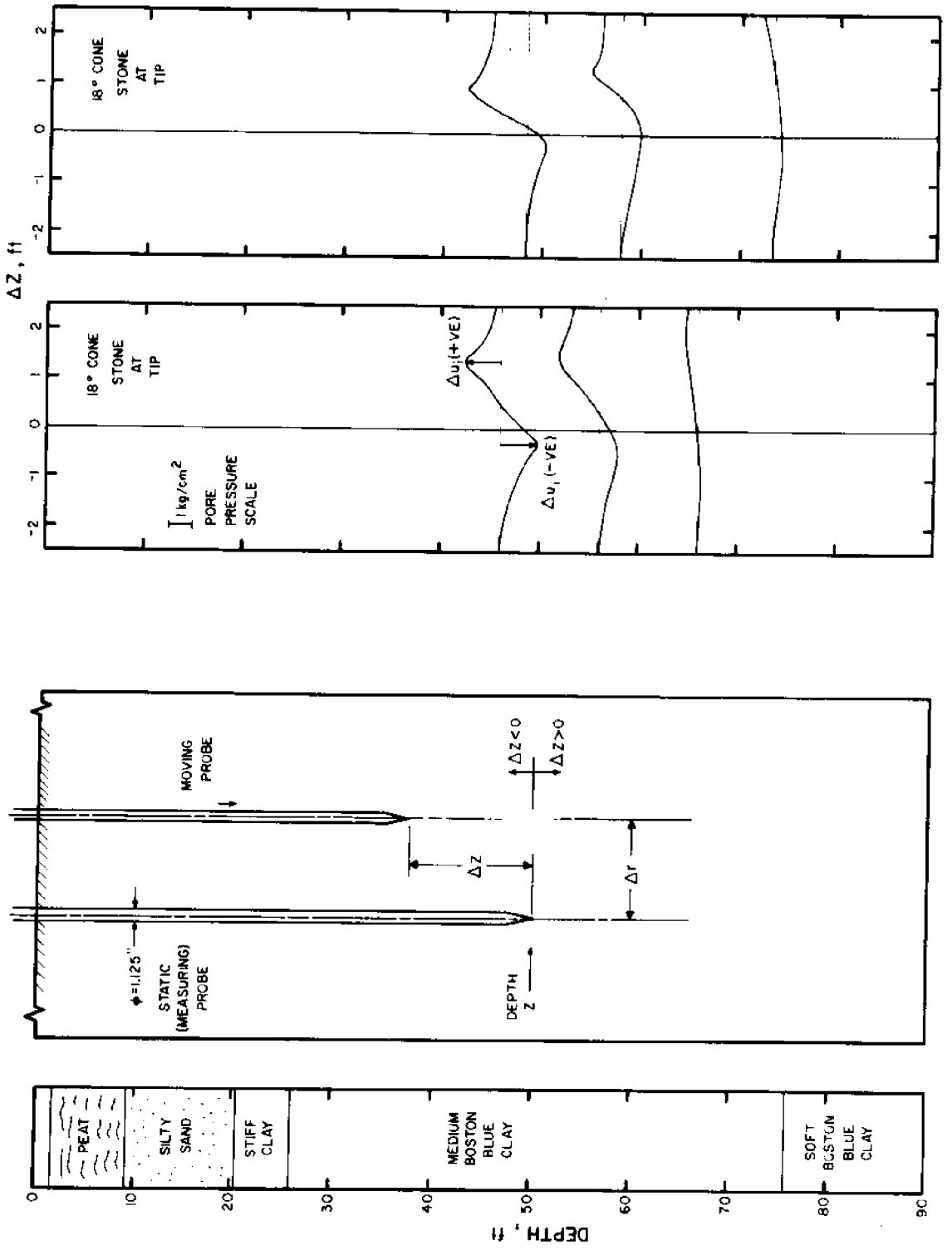

Fig. 3.1 Excess pore pressures during penetration of two adjacent conical probes

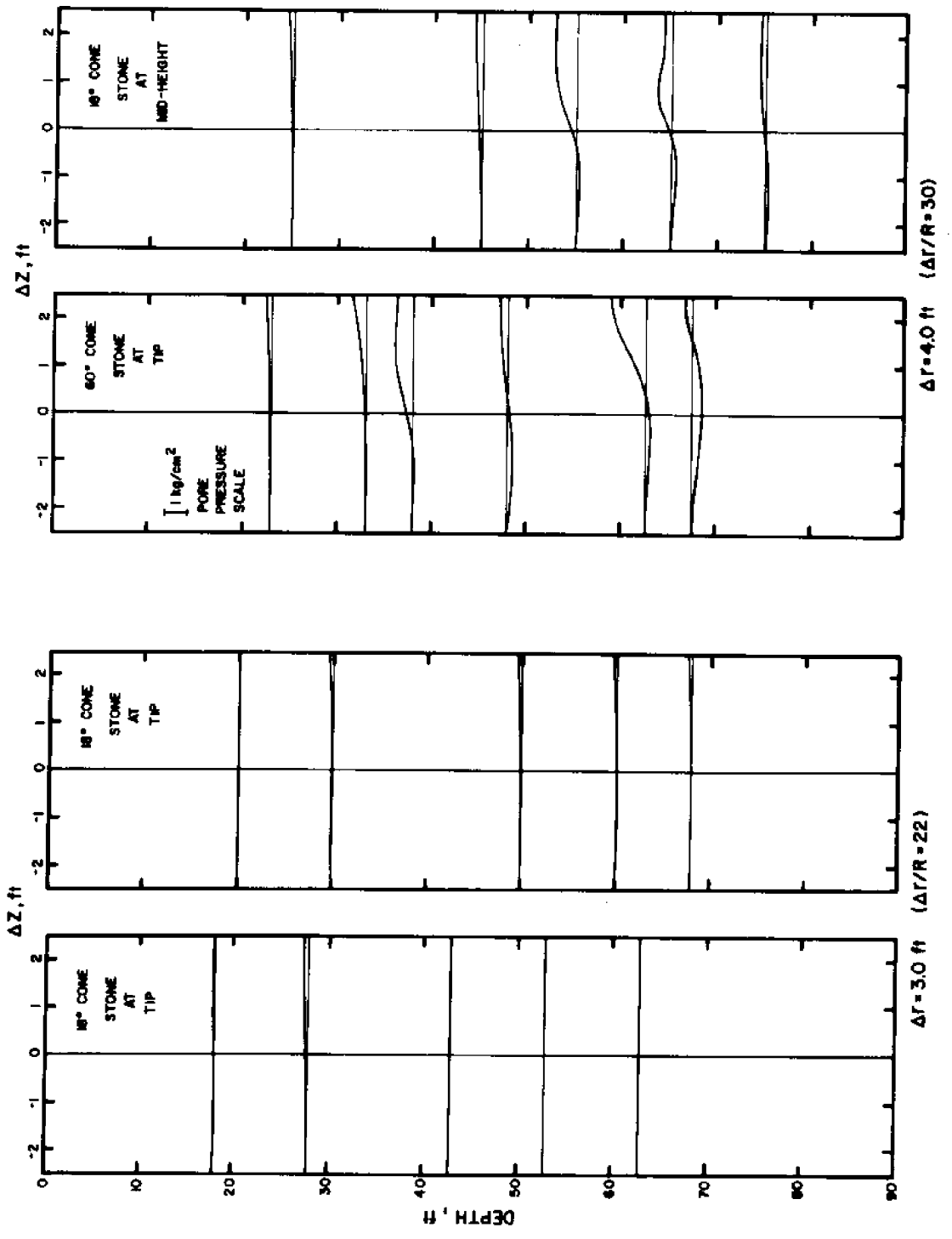

Fig. 3.1 (continued)

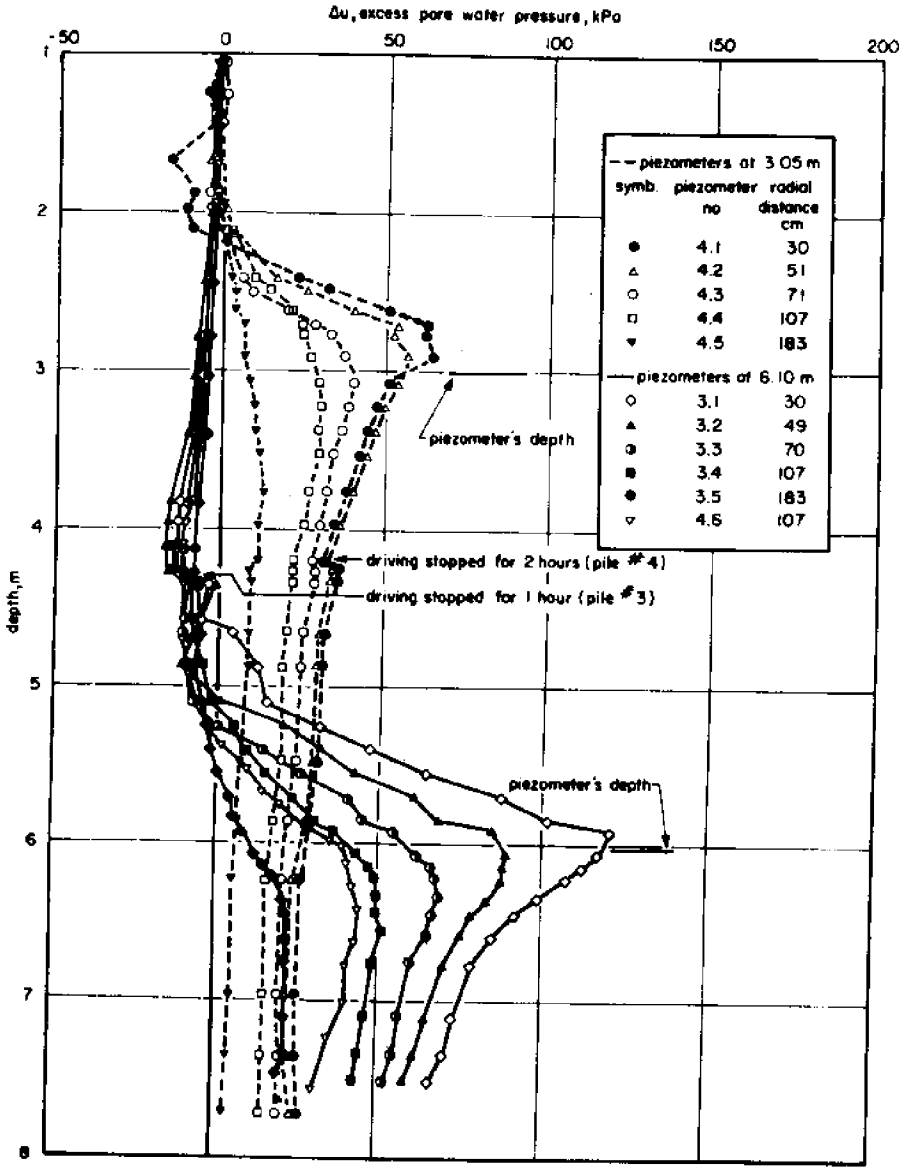

Fig. 3.2 Pore pressures measured during driving in the soil surrounding a pile (after Roy et al., 1979)

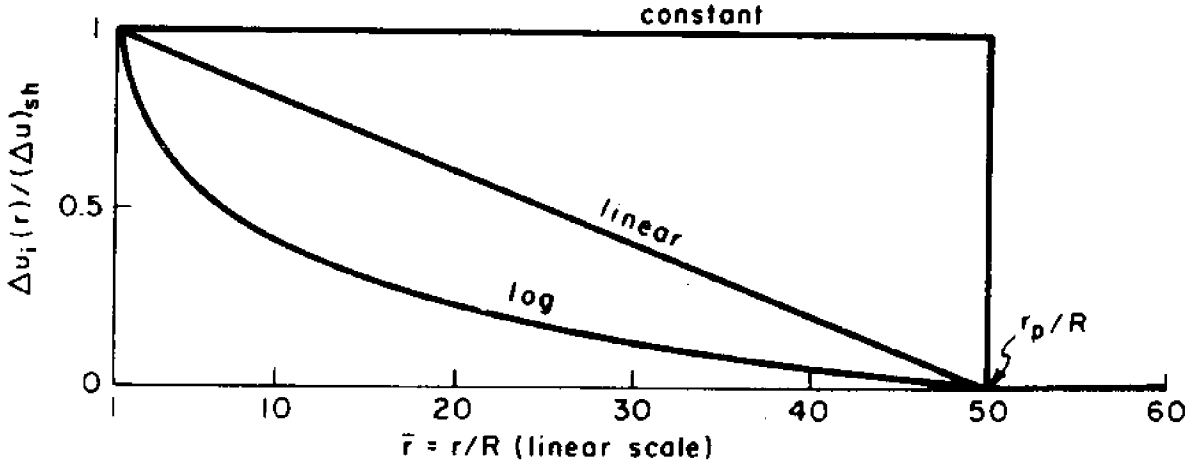

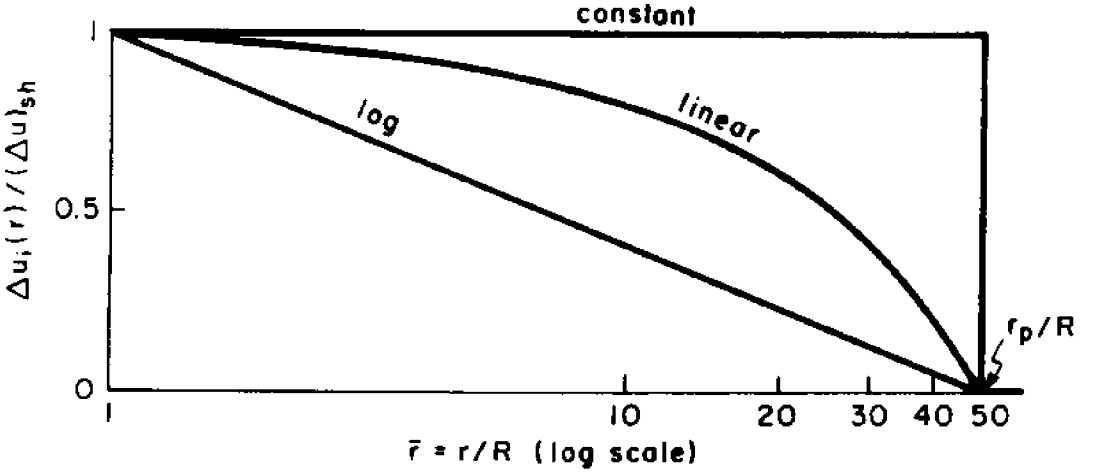

INITIAL NORMALIZED EXCESS PORE PRESSURE DISTRIBUTION	EQUATION	
	$1 < \bar{r} < \lambda$	$\bar{r} > \lambda$
CONSTANT	1	0
LINEAR	$(\lambda - \bar{r})/(\lambda - 1)$	
LOGARITHMIC	$1 - [\ell n(\bar{r})/\ell n(\lambda)]$	

Fig. 3.3 Initial normalized excess pore pressures for one-dimensional consolidation analyses

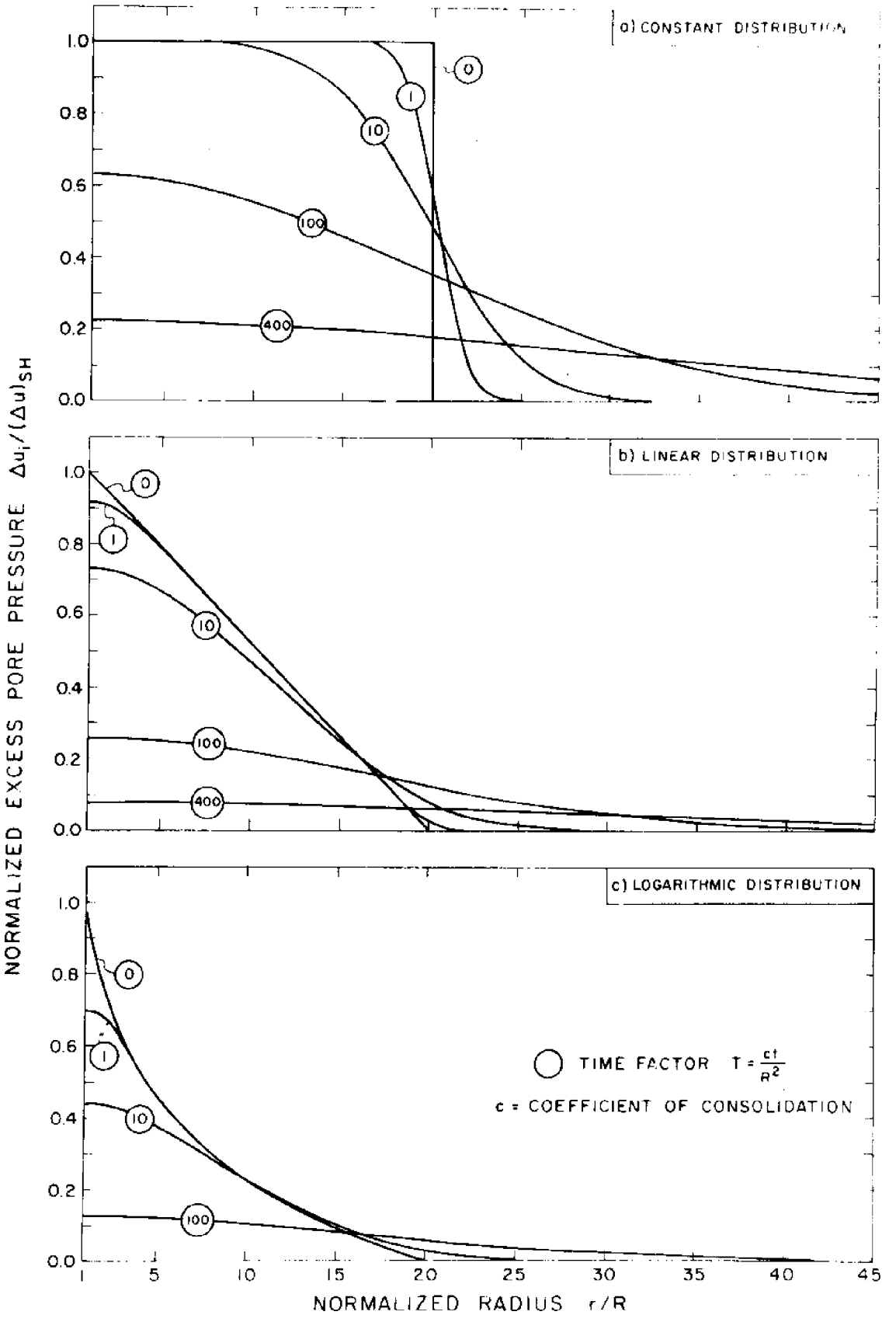

Fig. 3.4 Effect of initial excess pore pressure distribution on dissipation around an impervious cylinder (λ=20)

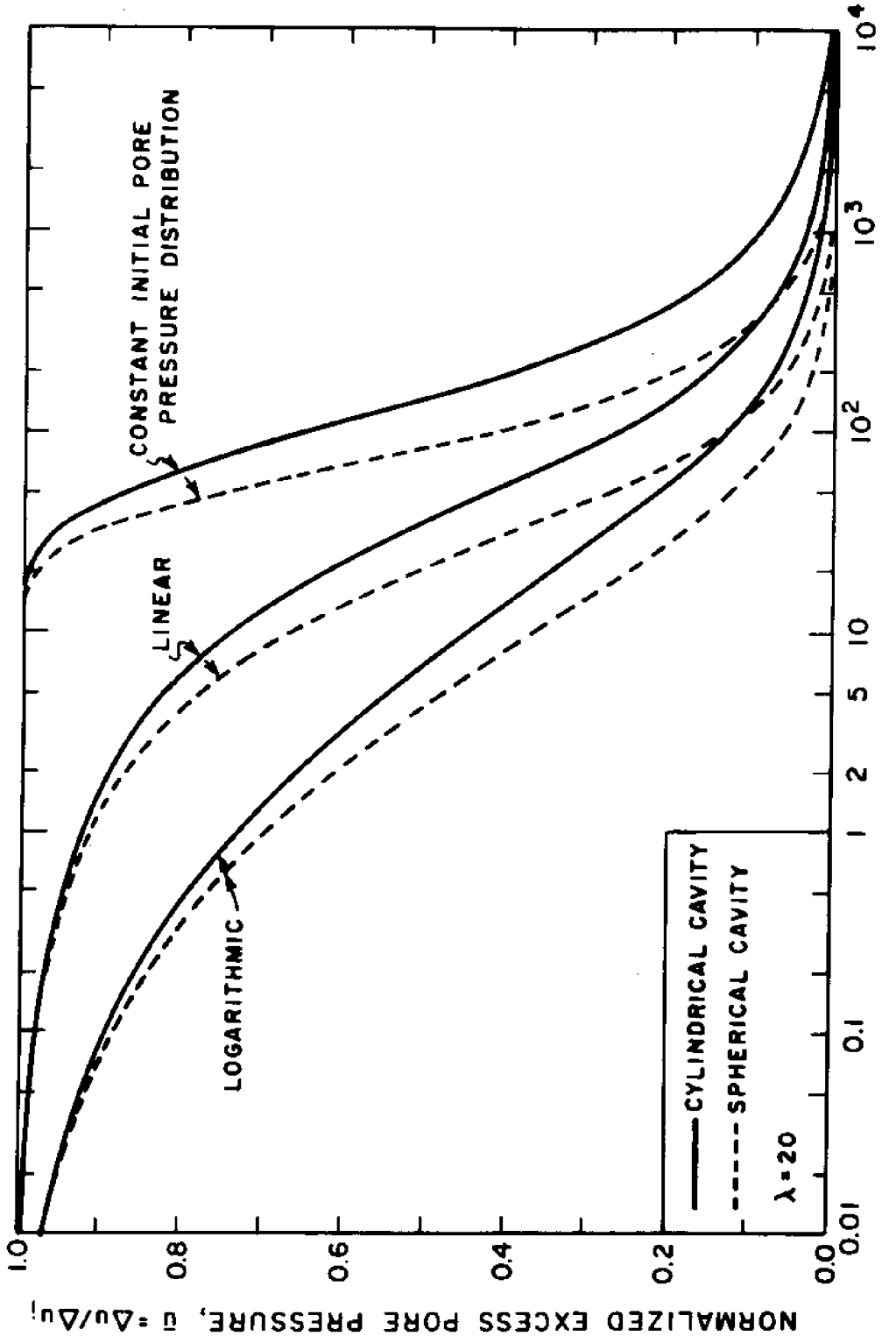

Fig. 3.5 Effect of cavity type and initial distribution of excess pore pressures on dissipation at the cavity wall

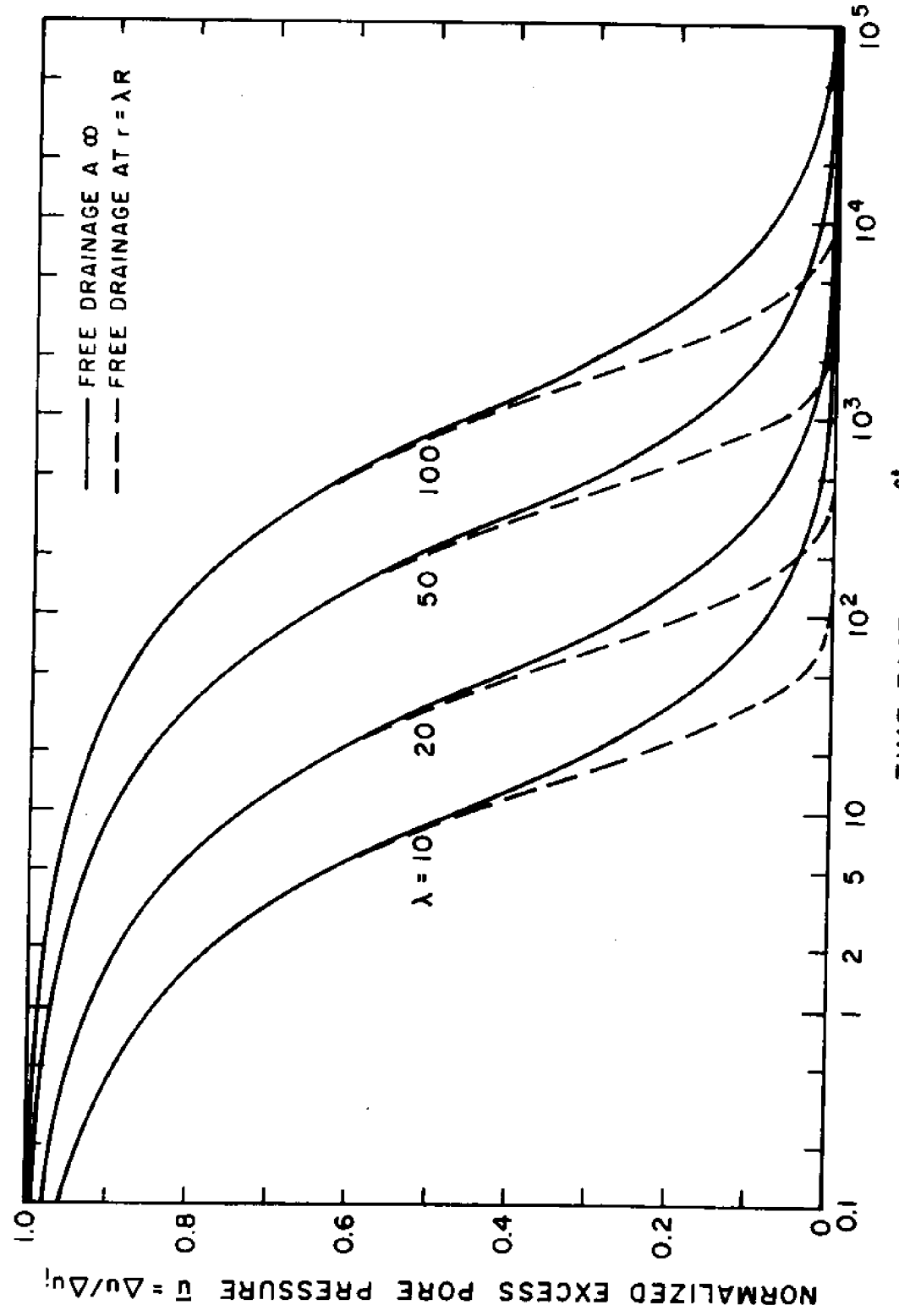

Fig. 3.6 Dissipation curves at the wall of a cylindrical cavity; linear initial pore pressure distribution

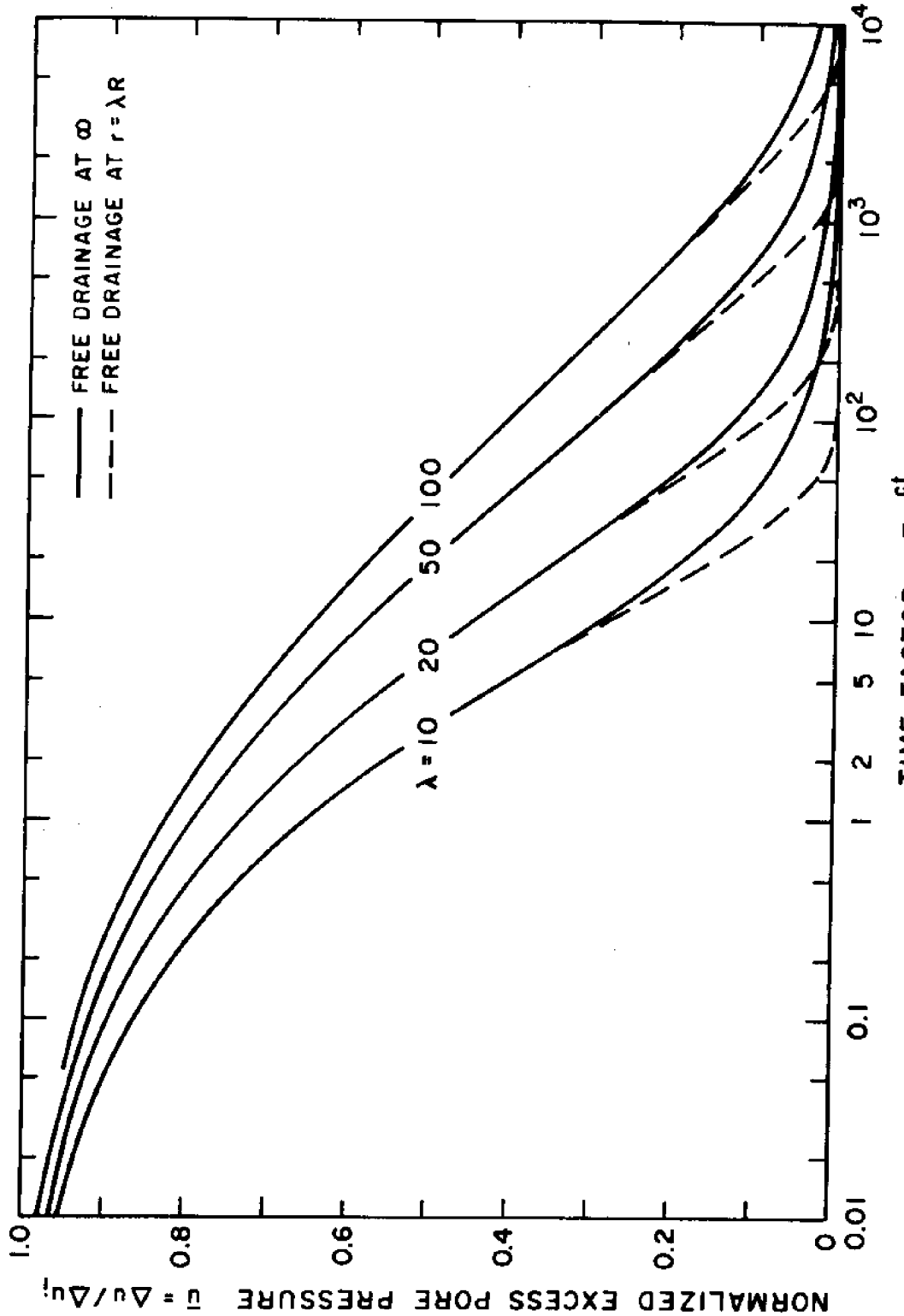

Fig. 3.7 Dissipation curves at the wall of a cylindrical cavity; logarithmic initial pore pressure distribution

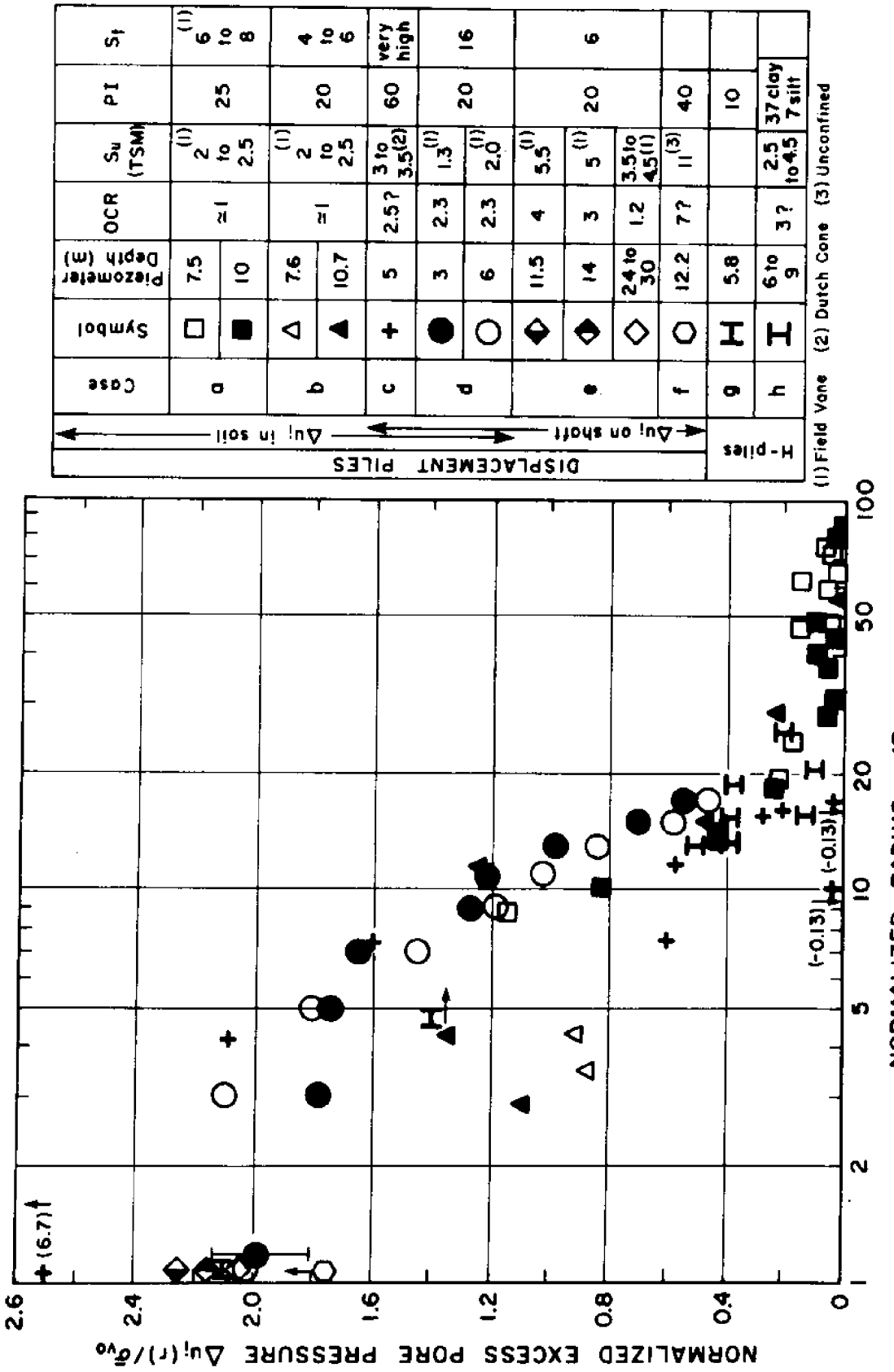

Fig. 3.8a Excess pore pressure measurements due to pile installation in clays - Case histories

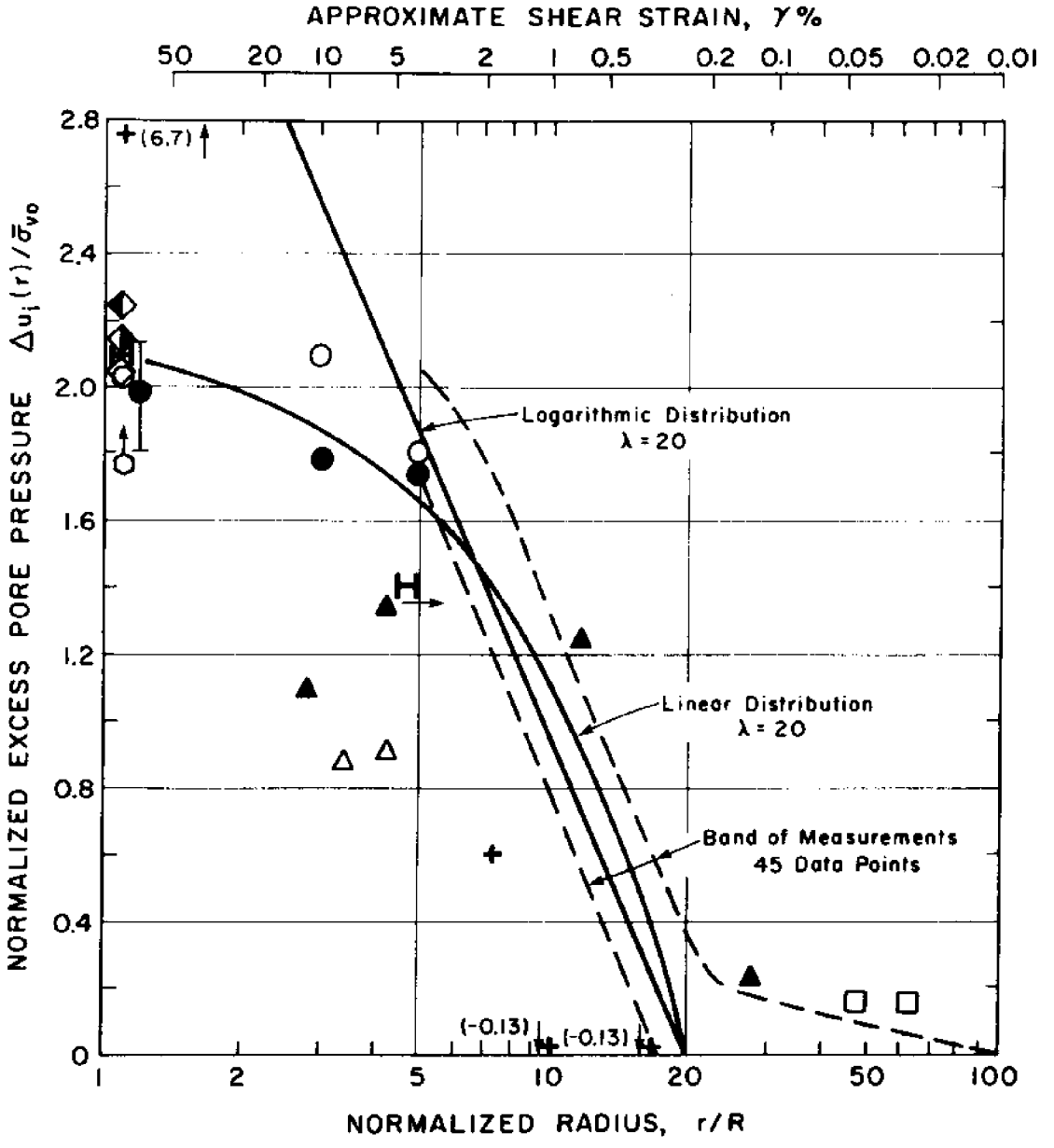

Fig. 3.8b Excess pore pressure measurements due to pile installation in clays - Simplified distributions

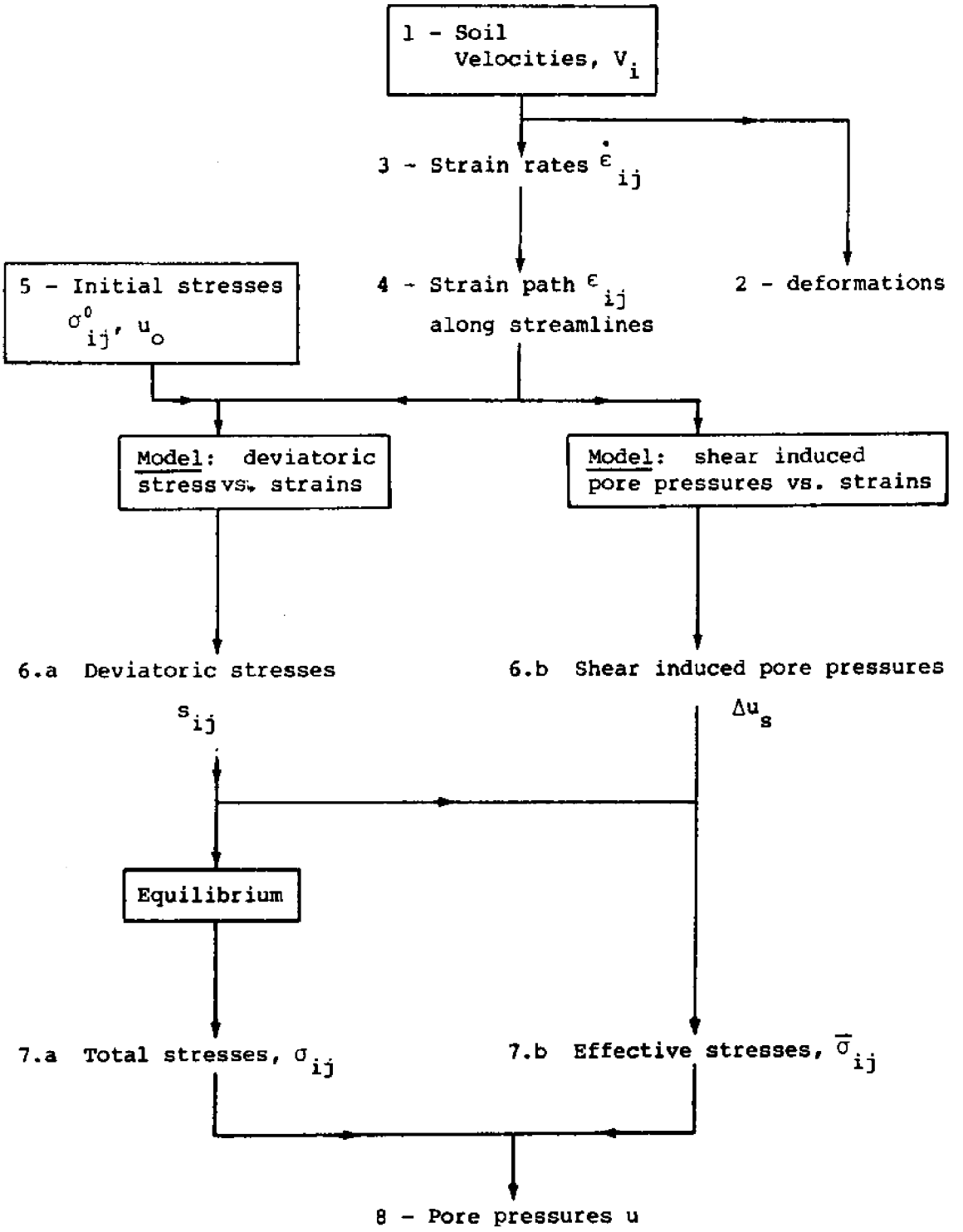

Fig. 3.9 Application of the strain path method to deep steady cone penetration in clays

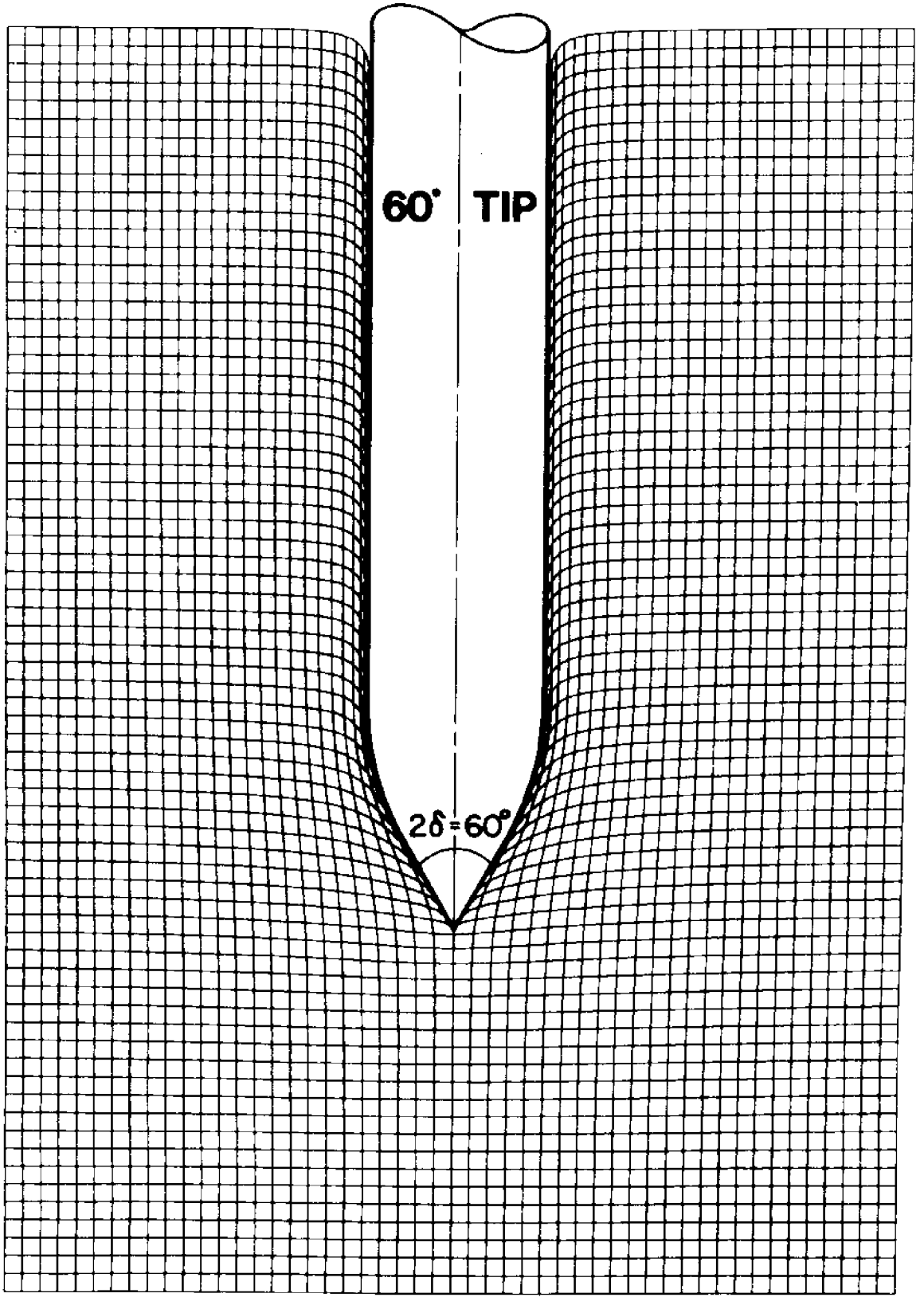

Fig. 3.10 Predicted deformation pattern around a 60° cone assuming no shearing resistance of the soil

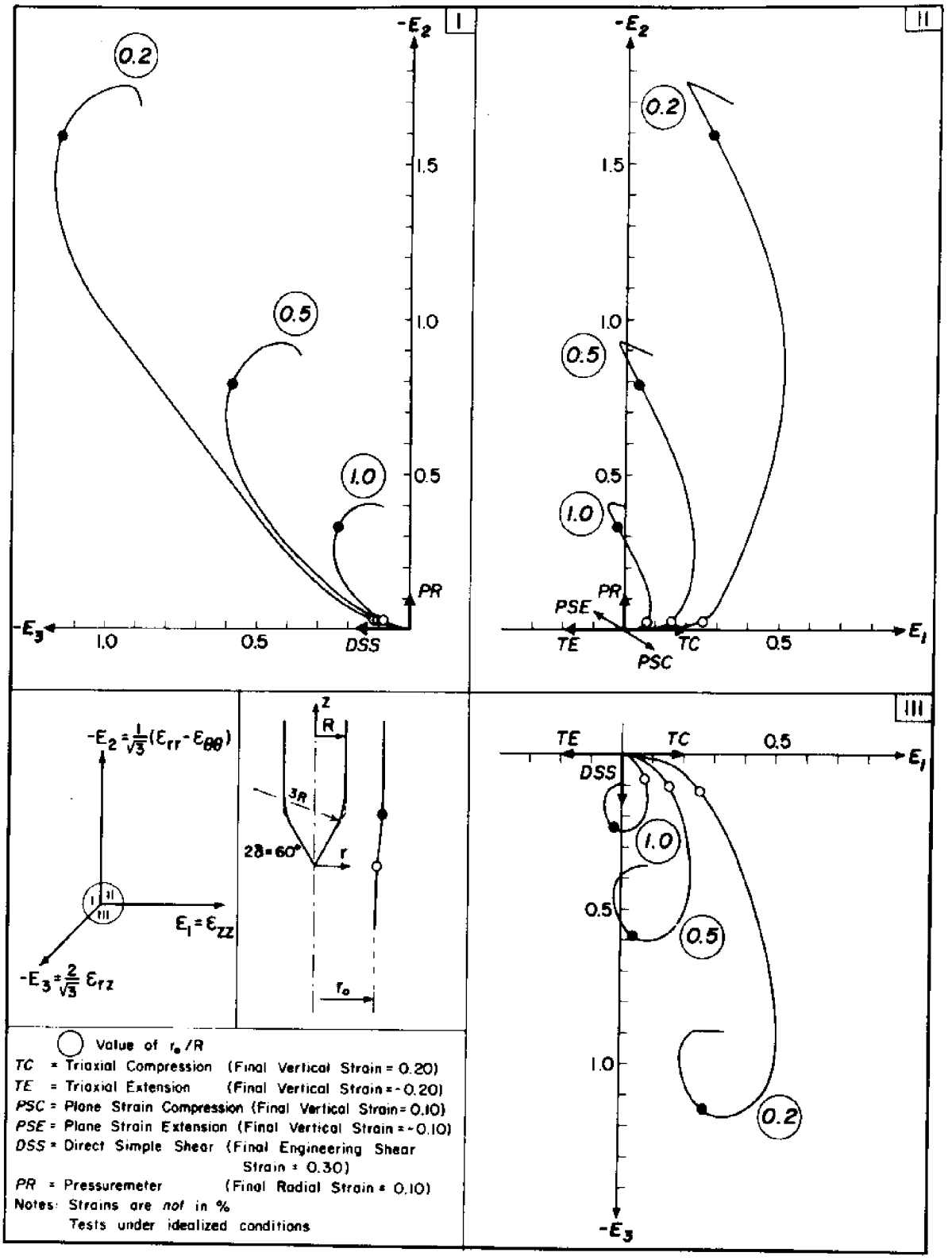

Fig. 3.11 - Strain paths of selected elements during penetration of a 60° cone.

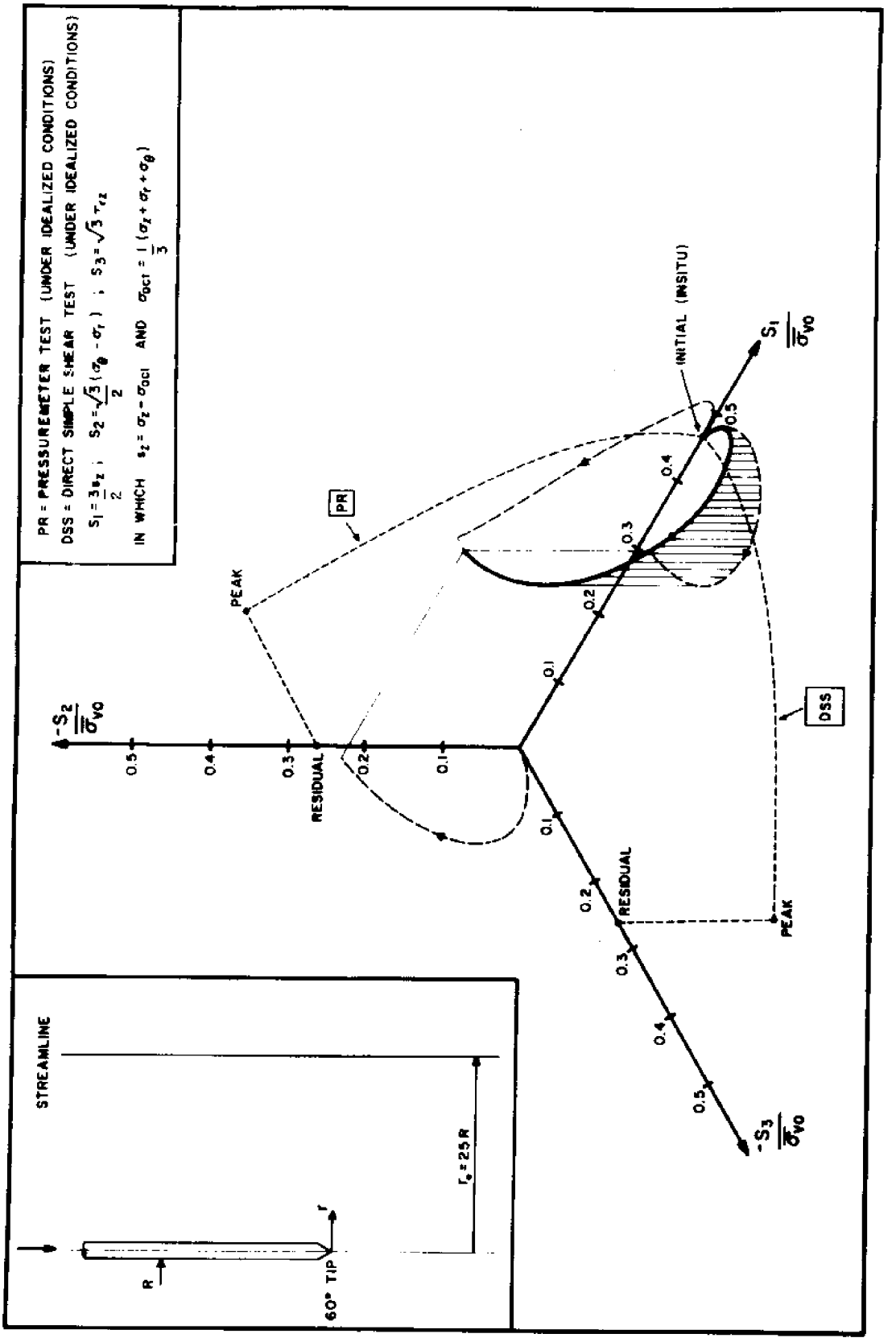

Fig. 3.12 Predicted deviatoric stress path during steady penetration of a 60° cone in normally consolidated Boston Blue Clay

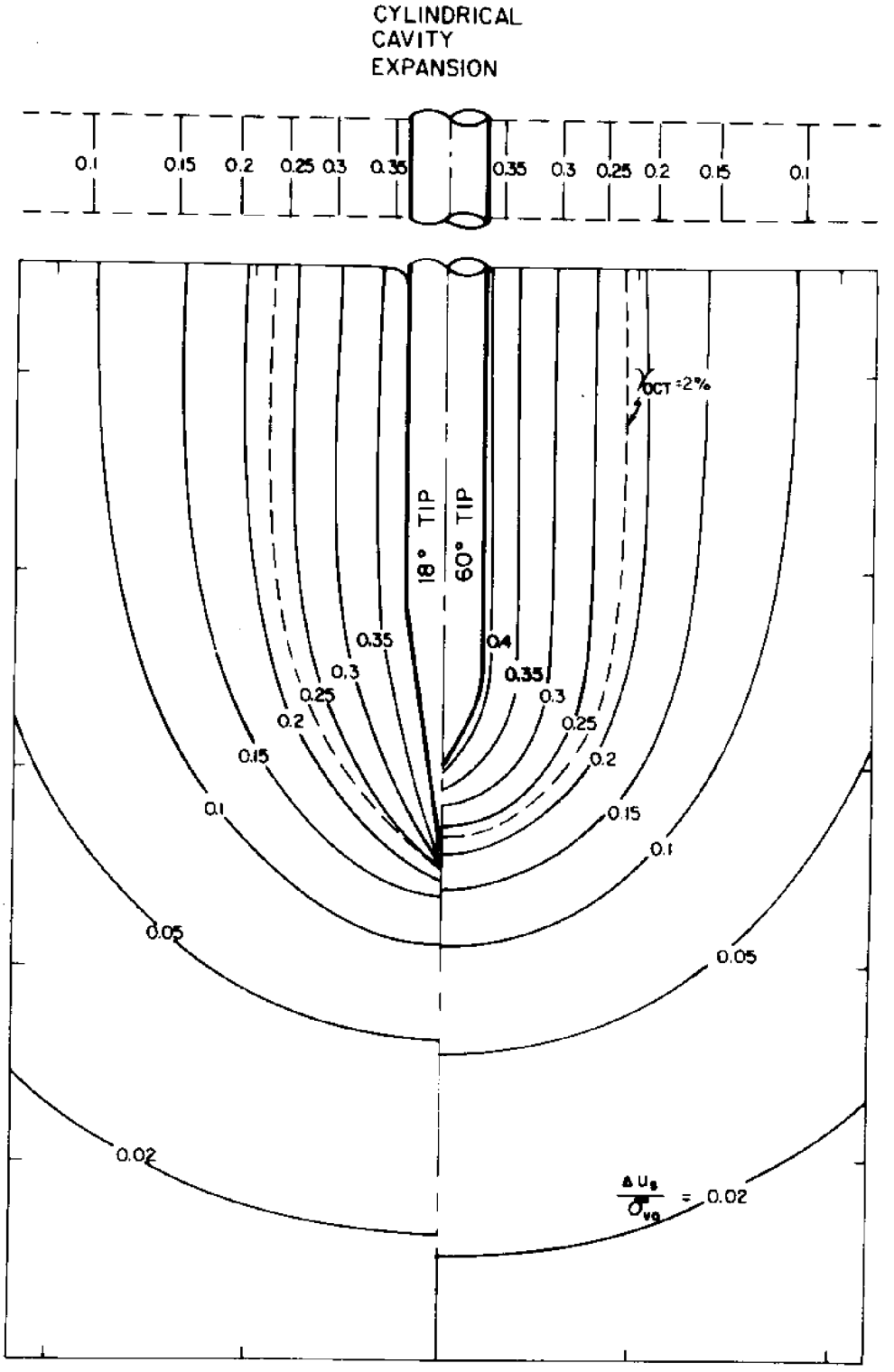

Fig. 3.13 Predicted shear induced pore pressures during steady cone penetration in normally consolidated Boston Blue Clay (18° and 60° tips)

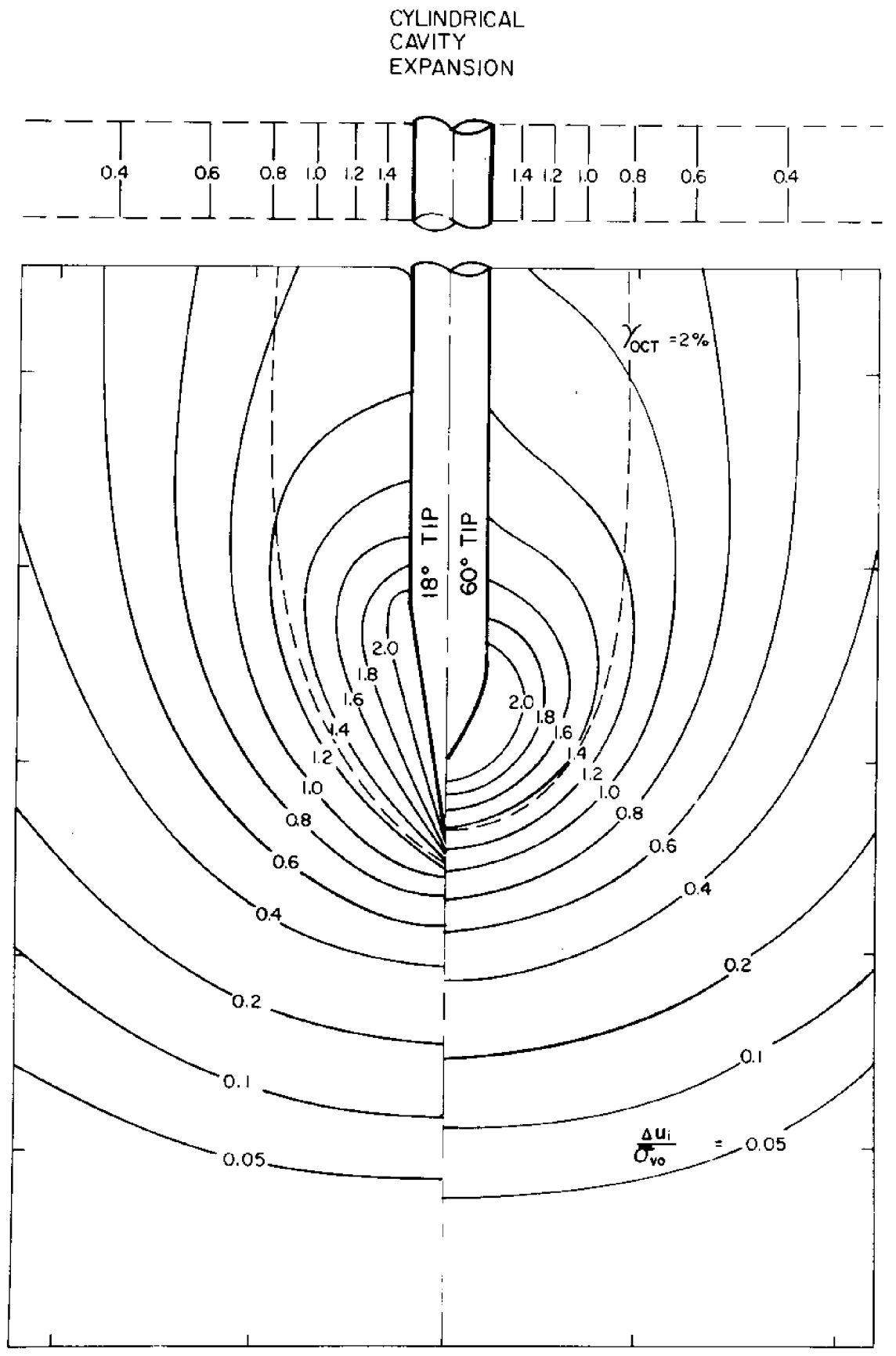

Fig. 3.14 Predicted excess pore pressures during steady cone penetration in normally consolidated Boston Blue Clay (18° and 60° tips)

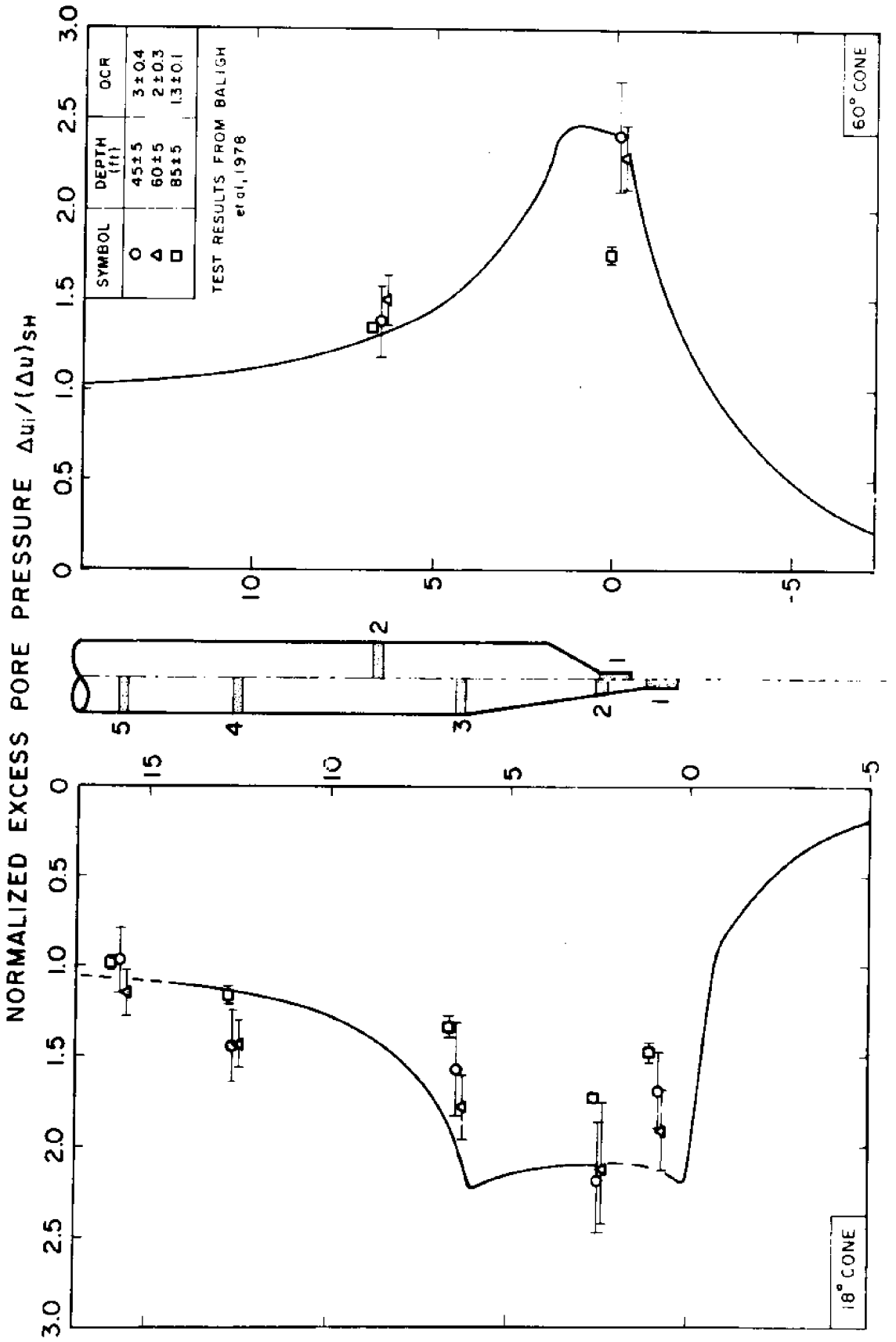

Fig. 3.15 Predicted vs measured normalized excess pore pressures along the face and shaft of 18° and 60° cones during steady penetration in Boston Blue Clay

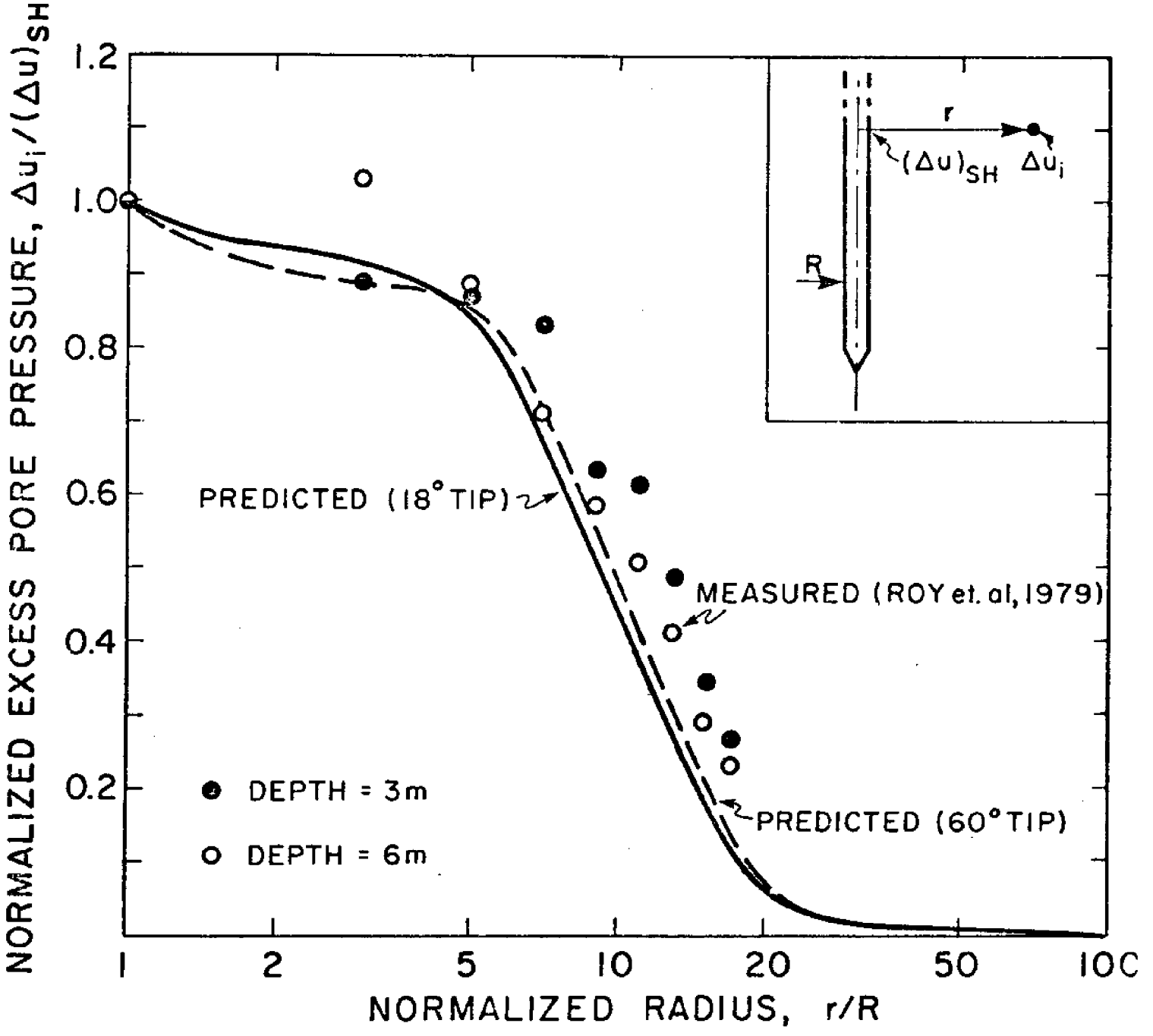

Fig. 3.16 Predicted vs measured distribution of normalized excess pore pressures during penetration in clays

CHAPTER 4

EFFECT OF VARIOUS FACTORS ON PORE PRESSURE DISSIPATION AROUND CONES

4.1 INTRODUCTION

This chapter presents two-dimensional linear consolidation analyses around conical piezometer probes with 18° and 60° tips after steady penetration has been interrupted. The initial distribution of normalized excess pore pressures prior to consolidation is obtained from the steady state penetration solutions in normally consolidated Boston Blue Clay (BBC). Comparisons with field measurements show that the normalized excess pore pressures are reasonably accurate in BBC when the overconsolidation ratio (OCR) is less than 3 and can be acceptable in other clays, Chapter 3.

Isotropic linear uncoupled finite element consolidation analyses are first conducted with a fine mesh to obtain accurate predictions of pore pressure dissipation at various locations on the tip and the shaft of 18° and 60° piezometer probes. The effect of soil anisotropy is evaluated by reducing the vertical coefficient of consolidation, c_v, and comparing the dissipation results around

an 18° piezometer probe with those obtained for the isotropic case. The effects of linear coupling (discussed in Chapter 2) are assessed by comparing dissipation results around an 18° piezometer probe obtained with a) a linear uncoupled finite element program (i.e., based on Terzaghi-Rendulic theory), and; b) a linear coupled finite element program (i.e., based on Biot's theory). Because of the computational limitations of the coupled finite element program, both analyses are performed with a relatively coarse mesh. The effects of finite element mesh are evaluated by comparing the results of uncoupled linear solutions obtained by means of the fine mesh (high resolution) and the coarse mesh (low resolution). Finally, the effects of possible errors* in the estimated penetration pore pressures, u_i, and, static (or initial in situ) pore pressures, u_o, on the predicted dissipation curves are evaluated. These errors are important in developing reliable methods for interpreting dissipation records.

4.2 UNCOUPLED TWO-DIMENSIONAL SOLUTIONS

The analyses presented in this section were conducted with the finite element program ADINAT (Bathe, 1977). This program solves linear (and nonlinear) transient (and

*Due to inherent soil variability or measurement errors.

steady state) heat transfer problems where the temperature θ is governed by the equation:

$$\kappa \nabla^2 \theta = \frac{\partial \theta}{\partial t} \tag{4.1}$$

in which ∇^2 is the Laplacian operator, κ is the diffusivity of the substance* and, t the time.

By simply substituting θ and κ by the pore pressure, u, and the coefficient of consolidation, c, respectively, Eq. 4.1 reduces to the uncoupled Terzaghi-Rendulic equation:

$$c \nabla^2 u = \frac{\partial u}{\partial t} \tag{4.2}$$

Figure 4.1 presents the finite element mesh adopted to analyze the uncoupled linear consolidation around a piezometer probe with an 18° tip angle. The mesh consists of 511 nodal points and 538 elements. It extends between elevations - 30R and + 15 R with respect to the apex of the conical tip (R = shaft radius) and up to a radius r = 100 R away from the symmetry axis. The outside mesh boundary is impervious everywhere except along the cylinder located at r = 100 R where a zero excess pore pressure is maintained at all times.**

---

*See Carslaw and Jaeger, 1959 for further information.

**Chapter 3 indicates that the flow condition at this boundary does not affect the dissipation in the neighborhood of the tip up to very large times.

In order to assess the adequacy of the two-dimensional mesh (Fig. 4.1) and select appropriate time steps, a simple one-dimensional analysis was first conducted. The one-dimensional mesh consisted of 20 rectangular elements connected to 21 pairs of nodes located at the same radii as the upper horizontal row of nodes in the two-dimensional mesh (Fig. 4.1). Figure 4.2 compares the dissipation results at the impervious wall of a cylindrical cavity for a logarithmic initial pore pressure distribution obtained: a) with ADINAT using the one-dimensional mesh described above and the time steps in Table 4.1, and; b) from closed-form solutions, Levadoux and Baligh, 1980. The agreement between numerical and analytical results in Fig. 4.2 is very good especially in view of the large initial pore pressure gradients near the cavity wall due to a logarithmic initial distribution.

Figure 4.3 shows the predicted contours of the excess pore pressures $(\Delta u/\bar{\sigma}_{vo})$ during uncoupled consolidation around an 18° cone in a linear isotropic material obtained with ADINAT (using the mesh in Fig. 4.1 and the time steps in Table 4.1) for selected values of the time factor, T (= ct/R^2 where c is the isotropic coefficient of consolidation, t the time and R the shaft radius). The pore pressures at T = 0 are the same as predicted during steady cone penetration in normally consolidated BBC and presented in Chapter 3.

The results shown in Fig. 4.3 indicate that:

1) the consolidation at early times ($T < 1$, say) is limited to the immediate vicinity of the tip. For example, the contour of $\frac{\Delta u}{\bar{\sigma}_{vo}} = 0.1$ remains virtually unchanged at $T = 1$ compared to its initial location (at $T = 0$).

2) as consolidation proceeds, the contours initially close to the conical tip move closer to the tip where they eventually vanish. This indicates that Δu decreases near the cone. On the other hand, the contours initially far from the tip first move outwards (see, for example, contours of $\frac{\Delta u}{\sigma_{vo}} = 0.01, 0.03$ in Fig. 4.3) and then, at later times (not shown in Fig. 4.3) come back toward the tip where they eventually vanish. This indicates that soil elements close to the tip tend to be subjected to monotonic loading* (i.e., Δu decreases) whereas, those further away are first unloaded (i.e., Δu increases) and then reloaded.** Such results are important in the interpretation of actual dissipation records because soils exhibit a nonlinear behavior with a coefficient of consolidation during loading which is different from unloading.

---

*In terms of effective stresses.

**A similar behavior occurs during the one-dimensional consolidation around a cylindrical cavity, Chapter 3.

Figure 4.4 shows plots of normalized excess pore pressure,* $\bar{u}$, versus time factor, T, at four selected locations** along the tip and the shaft of an 18° piezometer probe during uncoupled consolidation in a linear isotropic material.

We note in Fig. 4.4 that:

1) the time required to achieve a given degree of dissipation, $\bar{u}$, increases for points further away from the apex of the cone;

2) the pore pressure at point 3 (on the shaft, right behind the cone) increases slightly at early times. This is due to the larger initial pore pressures along the cone face (see contours in Fig. 4.3 at T = 0), and;

3) at T = 100, most of the consolidation (82 to 92%) has been achieved ($\bar{u}$ = 18 to 8%) and at T = 1000, consolidation is practically completed ($\bar{u}$ = 1%, say) at all locations.

Analyses identical to those presented above were conducted for the consolidation around a piezometer probe with a 60° tip angle. A finite element mesh very similar to that

---

*$\bar{u} = \Delta u/\Delta u_i$ where, Δu and Δu_i are the current and initial excess pore pressures at the point under study, respectively.

**At the cone apex, mid-cone, cone base and, on the shaft at 10R behind the cone apex (R = shaft radius).

in Fig. 4.1 was used* together with the same time steps (Table 4.1). The predicted contours of excess pore pressure during the uncoupled consolidation around a 60° cone in a linear isotropic material obtained with ADINAT are given in Fig. 4.5. Results in this figure show basically the same trends discussed above for the 18° cone. We note, however, that because of the smaller cone length, the contours around the 60° tip (Fig. 4.5) are more spherical in shape especially at early times.

Figure 4.6 shows plots of the normalized excess pore pressure, $\bar{u}$ (= $\Delta u/\Delta u_i$), versus time factor, T, at four selected locations along the tip and the shaft of a 60° piezometer probe during uncoupled consolidation in a linear isotropic material. We note in Fig. 4.6 that dissipation at locations 1 and 2 are virtually identical and, in fact, are very close to that of point 3. Furthermore, dissipation at location 4 (10 R above the cone apex) behind the two 18° and 60° conical tips (in Figs. 4.4 and 4.6, respectively) are very similar.

One-dimensional (cylindrical) finite difference analyses conducted by Levadoux and Baligh, 1980, using the same initial radial excess pore pressure distributions far behind the 18° and 60° tips give dissipation curves very similar to those at location 4 in Figs. 4.4 and 4.6. However, a logarithmic initial distribution predicted by cylindrical cavity expansion in an elastic perfectly-plastic material leads to different dissipation curves (see, for example, Fig. 3.5).

---

*Nodal points in the tip vicinity were relocated to achieve the new geometry (i.e., 60° tip).

4.3 EFFECT OF ANISOTROPY

Clays typically have a higher horizontal permeability, k_h, than vertical permeability, k_v, and hence a higher coefficient of consolidation in the horizontal direction than in the vertical direction (i.e., $c_h > c_v$). This section investigates the effect of anisotropy on the uncoupled consolidation around an 18° piezometer probe.

The dotted lines in Fig. 4.7 show the contours of excess pore pressure during uncoupled consolidation around an 18° cone in a linear cross-anisotropic material having $c_v = 0.1\ c_h$ as obtained with ADINAT* and where $T = c_h t/R^2$. For comparison, the solid contours denote the results in case of an isotropic soil ($c_v = c_h$) previously presented in Fig. 4.3. Figure 4.7 shows that the effect of decreasing c_v from c_h to $0.1\ c_h$ is very limited especially at early times ($T < 0.1$, provided that the time factor is defined as $T = c_h t/R^2$). This result is particularly important in the interpretation of dissipation records by indicating that c_h controls dissipation, especially at early stages of consolidation.

Figure 4.8 presents another illustration of the effect of soil anisotropy on consolidation by comparing

---

*Using the mesh in Fig. 4.1 and the time steps in Table 4.1.

the normalized excess pore pressure, $\bar{u}$ (= $\Delta u/\Delta u_i$), at four selected locations along the tip and the shaft of an 18° piezometer probe during uncoupled consolidation in a linear isotropic, $c_v = c_h$ (solid lines) and, cross-anisotropic, $c_h = 0.1\ c_h$ (dashed lines), materials.* The results in Fig. 4.8 clearly indicate that c_h governs the consolidation process. A significant decrease in c_v slightly delays the pore pressure dissipation at the locations of interest along the probe.** For example, the normalized time factors, T_{50}, required to reach 50% dissipation (i.e., $\bar{u} = 0.5$) are respectively increased by 20, 34, 36 and 24% at locations 1, 2, 3 and 4 when c_v decreases from c_h to $0.1\ c_h$. These values represent the error in the estimated c_h if, in interpreting dissipation records, soil anisotropy is neglected and results at 50% consolidation are used.

4.4 EFFECT OF LINEAR COUPLING

All solutions presented above were obtained according to the Terzaghi-Rendulic theory neglecting the coupling between total stresses and pore pressures during consolidation. This theory is rigorously applicable to a narrow

---

*Note that in Fig. 4.8 the time factor is controlled by c_h; i.e., $T = c_h t/R^2$.

**A similar conclusion might not hold if c_v is higher than c_h. However, a situation where $c_v > c_h$ is unlikely in practice.

range of problems including one-dimensional consolidation in semi-infinite masses where the soil is assumed to be homogeneous, linear, isotropic and elastic (Sills, 1975).

This section investigates the effect of coupling during consolidation around an 18° piezometer probe in a linear isotropic elastic material. This is achieved by comparing results obtained with the finite element program CONSOL (utilizing Biot theory) to those obtained by ADINAT (utilizing Terzaghi-Rendulic theory).

4.4.1 Finite Element Program CONSOL

Ghaboussi and Wilson (1971 and 1973) propose a finite element formulation for the unsteady saturated fluid flow in a porous isotropic elastic matrix based on Biot's formulation using a Gurtin-type variational principle. For a compressible pore fluid, the constitutive relations can be expressed by the following matrix equation (Ghaboussi and Wilson, 1971):

$$\begin{bmatrix} [K] & [C] \\ [C]^T & -[E]-\tfrac{1}{2}\Delta t[H] \end{bmatrix} \cdot \begin{Bmatrix} \{w_{t+\Delta t}\} \\ \{u_{t+\Delta t}\} \end{Bmatrix} =$$

$$\begin{Bmatrix} \{F_{t+\Delta t}\} \\ -\tfrac{1}{2}\Delta t(\{Q_{t+\Delta t}\} + \{Q_t\}) \end{Bmatrix} + \begin{bmatrix} [O] & [O] \\ [C]^T & -[E] + \tfrac{1}{2}\Delta t[H] \end{bmatrix} \cdot \begin{Bmatrix} \{w_t\} \\ \{u_t\} \end{Bmatrix} \quad \ldots\ldots (4.1)$$

where $[K]$ = skeleton stiffness matrix;

$[E]$ = fluid compressibility matrix;

$[C]$ = coupling matrix;

$[H]$ = permeability matrix;

$\{w_t\}$ = nodal displacement vector at time t;

$\{u_t\}$ = nodal pore pressure vector at time t;

$\{F_t\}$ = externally applied nodal load at time t;

$\{Q_t\}$ = externally applied nodal flow at time t, and;

Δt = time increment.

In this formulation, excess pore pressures, Δu, in the soil due to boundary loading equal the increase in octahedral stress, $\Delta\sigma_{oct}$. Therefore, in order to impose a given distribution of pore pressures at the nodes, $\{u_i\}$, a slight modification of the program was necessary to apply a fictitious set of nodal loads $\{F_i\}$ at time t = 0.

According to Eq. 4.1, the initial response of a system (t = 0) is given by:

$$[K]\ \{w_i\} + [C]\ \{u_i\} = \{F_i\} \qquad (4.2)$$

Neglecting soil deformations* due to an excess pore pressure build-up at t = 0 (i.e., $\{w_i\} = \{0\}$), the fictitious applied nodal force vector $\{F_i\}$ required to simulate a given initial nodal pore pressure vector $\{u_i\}$ at time t = 0 is given by:

---

*Of no consequence to pore pressure solutions of interest in linear problems.

$$\{F_i\} = [C]\ \{u_i\} \tag{4.3}$$

Components of the vector $\{F_i\}$ were therefore obtained by means of the same computer program according to Eq. 4.3 and maintained throughout the solution;* i.e., $\{F_t\} = \{F_i\}$ for any t.

4.4.2 Results of Consolidation Analyses

The finite element program CONSOL requires much larger core storage than ADINAT** and, hence consolidation analyses with CONSOL proved imposssible to carry out with the detailed mesh in Fig. 4.1. Consequently, the coarser mesh shown in Fig. 4.9 was used for the analyses described below (with CONSOL as well as with ADINAT). This mesh consists of 117 nodal points and 96 rectangular elements. It extends between elevations -10 R and 15 R with respect to the apex of the conical tip and up to a radius r = 25 R away from the symmetry axis. The boundary conditions are indicated in Fig. 4.9.

The dotted contours in Fig. 4.10 show the decay of excess pore pressures during coupled isotropic linear consolidation around an 18° cone when the soil is saturated

---

*If effective stresses were also required (and not only their changes) an additional set of nodal forces would be needed to account for the initial nodal displacements and hence satisfy Eq. 4.2.

**Because of a threefold increase in the degrees of freedom (from 1 to 3) and a lesser use of out of core (scratch) storage.

with an incompressible pore fluid as obtained with CONSOL.* The solid contours in Fig. 4.10 denote the uncoupled analyses obtained by ADINAT using the same grid (Fig. 4.9) and identical soil properties, time steps (Table 4.1), etc. The results in Fig. 4.10 indicate that coupling effects are not very significant and are limited to the immediate vicinity of the conical tip.

Figure 4.11 compares plots of normalized excess pore pressures, $\bar{u}$ (= $\Delta u/\Delta u_i$), versus time factor, T, at four locations along the tip and the shaft of an 18° piezometer probe during uncoupled consolidation (solid lines) and coupled consolidation (dashed lines) in a linear isotropic elastic material.

Results in Fig. 4.11 indicate the following effects of linear coupling:

a) as expected (Sills, 1975), the pore pressure at location 4 is practically unaffected by coupling because the one-dimensional cylindrical situation is approached;

b) the coupled dissipation curve at location 3 exhibits Mandel-Cryer effects at early times but comes very close to the uncoupled dissipation curve when $T > 1$ (i.e., $\bar{u} < 0.92$, approximately);

---

*For coupled analyses the results depend on the drained Poisson's ratio $\bar{\nu}$. These analyses were carried out with $\bar{\nu} = 0.25$.

c) coupling causes a faster dissipation at location 2. However, the effect becomes small for $\bar{u} < 0.8$ (about 20% at $\bar{u}=0.5$); and,

d) coupling appears to be especially important at the apex of the cone, location 1*. However, numerical difficulties at this singular point prevent definite conclusions to be reached.

Finally, it is interesting to note the effects of the mesh size on dissipation results obtained by means of ADINAT using a fine mesh (in Fig. 4.1) to those with the coarse mesh (in Fig. 4.9) and shown in Figs. 4.4 and 4.11, respectively:

a) results at location 4 are not affected by the mesh size (they differ by less than 1%) for any time factor T;

b) dissipation at locations 2 and 3 is very slightly affected by the mesh size at large times (when $\bar{u} < 0.5$) but is significantly affected during early stages of consolidation;

c) dissipation at the cone apex. location 1, is strongly affected by the mesh size. For example, the time factor to reach 20% consolidation ($\bar{u} = 0.8$) is $T = 0.065$ for the fine grid and $T = 0.38$ for the

---

*It is important to note that location 1 in consolidation analyses corresponds to the tip of a perfect cone (i.e., a singular point) and does not occur in actual probes.

coarse grid. Therefore, results with the coarse mesh at 20% consolidation overestimate the coefficient of consolidation by a factor of 5.85.

This clearly demonstrates the need for a fine mesh to provide an adequate resolution in the vicinity of the tip where large pore pressure gradients occur especially in the early stages of consolidation.

4.5 EFFECTS OF SOIL VARIABILITY AND/OR ERRORS IN MEASUREMENTS

Dissipation results presented above and subsequently used for estimating the horizontal coefficient of consolidation, c_h, are expressed in terms of the normalized excess pore pressure $\bar{u}$:

$$\bar{u} = \frac{\Delta u}{\Delta u_i} = \frac{u - u_o}{u_i - u_o} \tag{4.4}$$

in which

u = measured pore pressure at time T;

u_o = static pore pressure (i.e., in situ before penetration), and;

u_i = penetration pore pressure (i.e., at T = 0 when penetration is interrupted).

This section investigates the effect of uncertainties in the values of u_o and u_i in order to select reliable methods for estimating c_h.

In practice, the static pore pressure, u_o, should be measured at selected depths by leaving the piezometer probe in the soil long enough to achieve complete soil consolidation. This is, however, a time consuming and expensive task which is often overlooked hence leading to an error δu_o in the estimated static pore pressure, u_o^*, at any depth:

$$u_o^* = u_o + \delta u_o \tag{4.5}$$

where u_o is the "true" (or in situ) static pore pressure.

The apparent normalized excess pore pressure, $\bar{u}^*$, is thus given by:

$$\bar{u}^* = \frac{u - (u_o + \delta u_o)}{u_i - (u_o + \delta u_o)} \tag{4.6}$$

Figure 4.12a shows the effects of the error δu_o on the dissipation at mid-cone of an 18° piezometer probe. The solid line represents the "true" dissipation curve (identical to curve 2 in Fig. 4.4) and the dashed lines represent the "apparent" dissipation curves for $\delta u_o/\Delta u_i$ = 20, 10, -10 and -20% (Δu_i is the "true" initial excess pore pressure at time T = 0). Clearly, the effect of δu_o is more pronounced at late consolidation stages.

On the other hand, errors in the penetration pore pressure, u_i, can occur due to: a) inherent soil variability causing the recorded value u_i^* at the beginning of dissipation to be different from the relevant (average) value u_i, and; b) incomplete deairing of the piezometer or

low permeability of the clay causing a time lag in the measurements. The measured penetration pore pressure, u_i^*, thus becomes:

$$u_i^* = u_i + \delta u_i \tag{4.7}$$

where u_i is the relevant penetration pore pressure.

The apparent normalized excess pore pressure, $\bar{u}^*$, is thus given by:

$$\bar{u}^* = \frac{u - u_o}{(u_i + \delta u_i) - u_o} \tag{4.8}$$

Figure 4.12b shows the effect of δu_i on the dissipation at mid-cone of an 18° piezometer probe. "Apparent" dissipation curves are given for $\delta u_i/\Delta u_i$ = 20, 10, -10 and -20%.

The results in Fig. 4.2 are valuable in providing guidelines for the prediction of the horizontal coefficient of consolidation, c_h, from dissipation measurements:

a) when u_o is reliably measured (i.e., $\delta u_o \simeq 0$), prediction of c_h is best achieved by matching measured and predicted dissipation curves at large times where the effects of δu_i are least significant;

b) when u_i is measured with a high level of confidence (i.e., $\delta u_i \simeq 0$) as indicated by the consistency and uniformity of measurements, prediction of c_h is reliably and economically achieved by early time matching, and;

c) when errors in both u_o and u_i are expected, prediction of c_h at intermediate times (when $\bar{u} = 0.5$, say) appears to represent a reasonable compromise.

4.6 SUMMARY AND CONCLUSIONS

The pore pressure dissipation around conical probes requires two-dimensional numerical analyses in order to interpret dissipation records and hence estimate the coefficient of consolidation of the soil. This chapter presents linear consolidation analyses to investigate the effects of cone angle; the location of the porous stone; the anisotropy of the soil; the size of the mesh (resolution); the coupling between pore pressures and total stresses, and; the uncertainties in the estimated initial and final pore pressures on prediction of dissipation rates.

Results of consolidation analyses indicate that:

1) dissipation at different locations on an 18° cone based on linear uncoupled solutions using a fine finite element mesh (Fig. 4.1) are very different (Fig. 4.4). This emphasizes the need for two-dimensional solutions because one-dimensional consolidation studies cannot detect the effect of porous stone location. Similar analyses for a 60° probe show that the predicted dissipation along the conical tip varies little with location (Fig. 4.6);

2) at a sufficient distance behind the tip dissipation on the shaft is not significantly dependent on the cone angle and is about one to two orders of magnitude slower than dissipation at the tip;

3) a reduction in the vertical coefficient of consolidation, c_v, from c_h to 0.1 c_h causes little delay in the uncoupled pore pressure dissipation at 4 selected locations along the tip and the shaft of an 18° piezometer probe in a linear elastic material* (Fig. 4.8). This suggests that c_h governs consolidation around piezometer probes;

4) the effect of linear coupling between total stresses and pore pressures is reasonably small except at early stages of consolidation especially near the apex of an 18° cone** (Fig. 4.11). This suggests that uncoupled solutions can provide reasonably accurate predictions away from the apex and after sufficient dissipation has taken place;

5) accurate predictions of excess pore pressure dissipation (especially in the vicinity of the conical tip) requires the use of a fine mesh (Fig. 4.1), and;

---

*Provided that the time factor is defined as $T = c_h t/R^2$.

**In analyses, an ideal cone is considered with a singular apex point. This geometry is not encountered in actual probes.

6) errors in the static and penetration pore pressures (u_o and u_i, respectively) can seriously affect the estimated coefficient of consolidation. Matching of measured and predicted dissipation records at small, large and, intermediate degrees of consolidation is recommended if errors in u_o, u_i or both, respectively, are expected.

Time Step ΔT	Time Factor T
0.01	0.01
0.01	0.02
0.01	0.03
0.01	0.04
0.01	0.05
0.01	0.06
0.01	0.07
0.01	0.08
0.01	0.09
0.01	0.1
0.18	0.28
0.18	0.46
0.18	0.64
0.18	0.82
0.18	1.0
1.8	2.8
1.8	4.6
1.8	6.4
1.8	8.2
1.8	10.0
18.0	28.0
18.0	46.0
18.0	64.0
18.0	82.0
18.0	100.0*
180.0	280.0
180.0	460.0
180.0	640.0
180.0	820.0
180.0	1000.0

*Consolidation analyses with the coarse mesh (Fig.11.9) are interrupted at T = 100

Table 4.1 Time steps used in finite element consolidation analyses

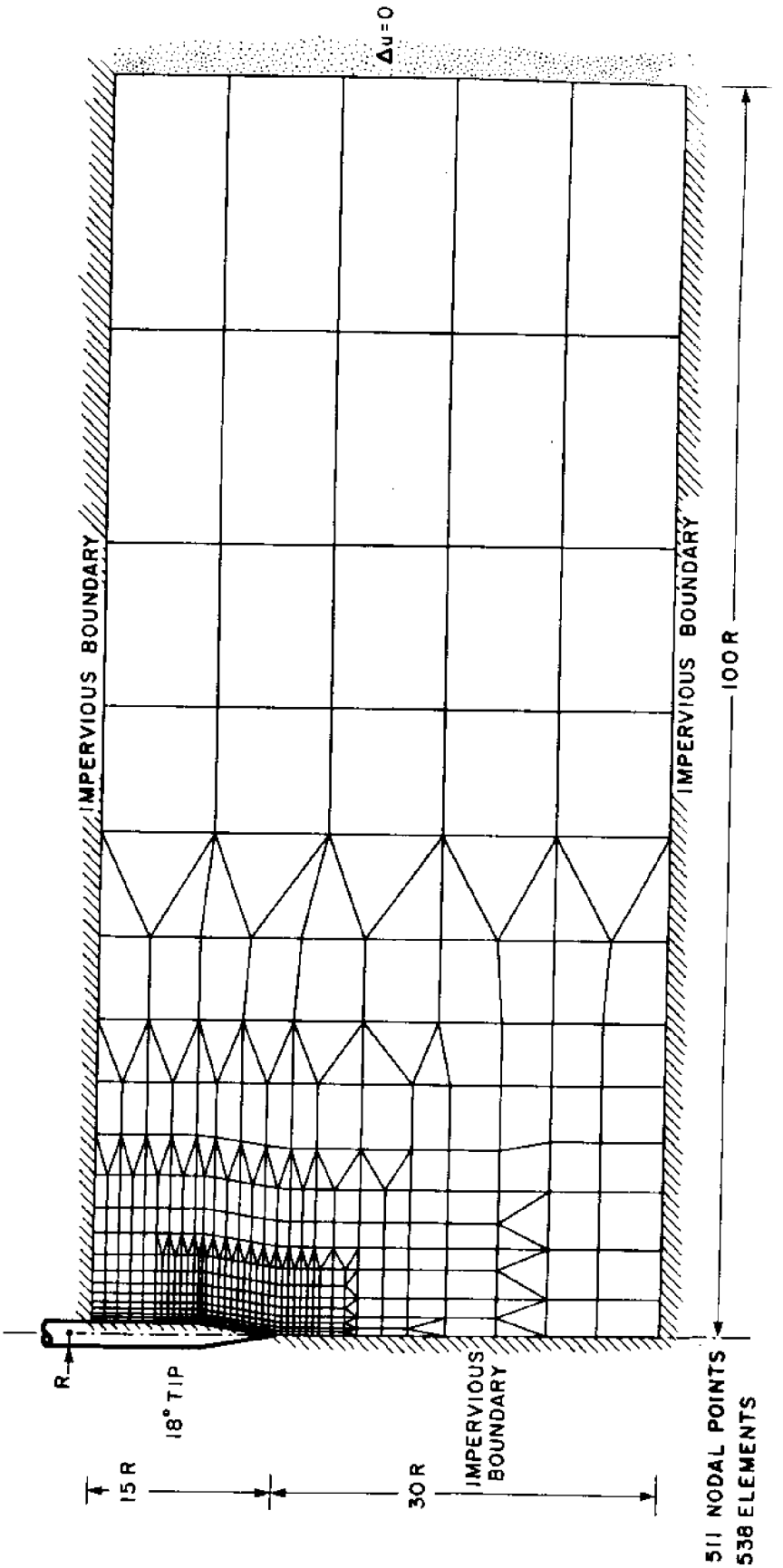

Fig. 4.1 Detailed finite element mesh

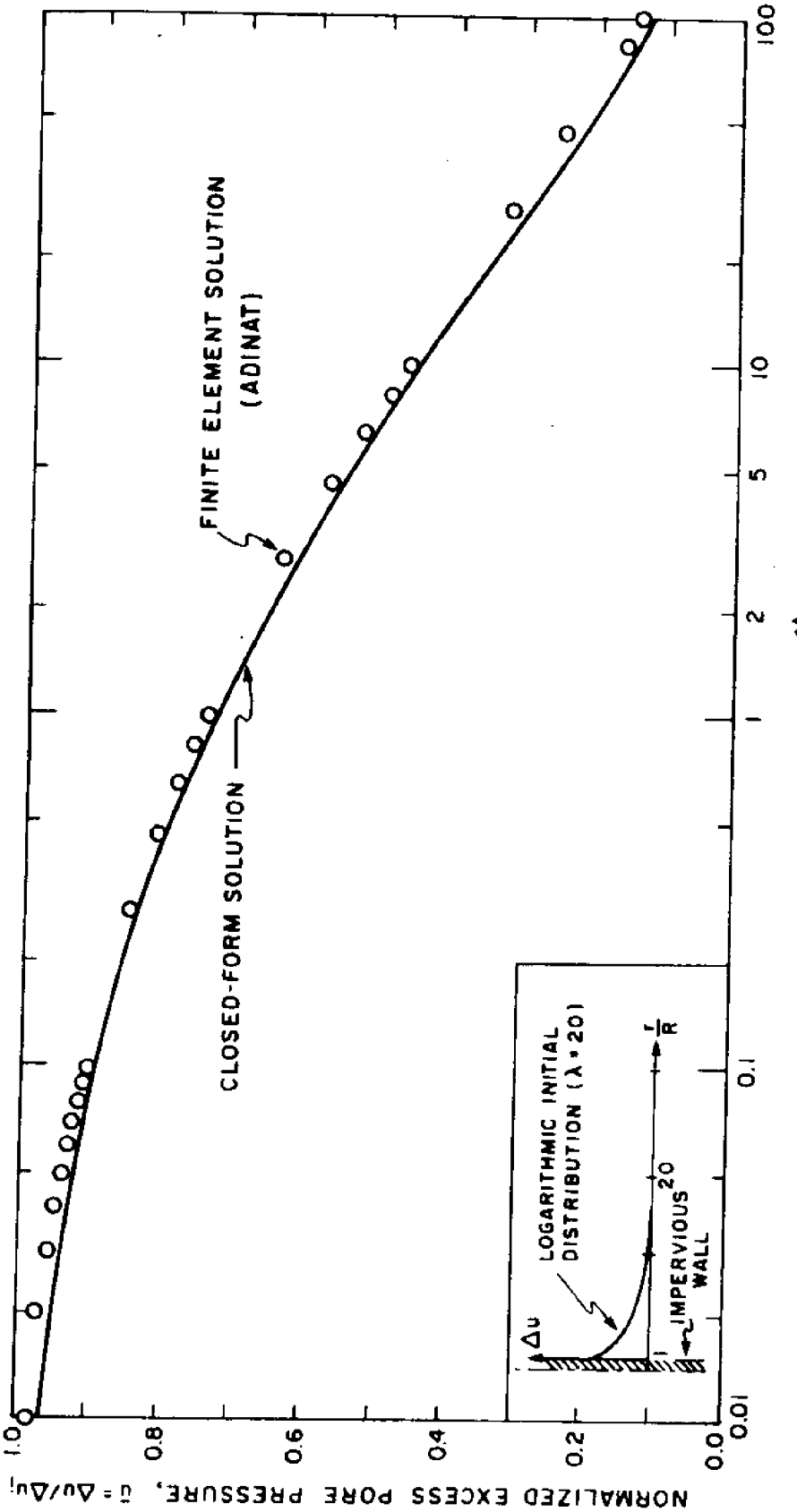

Fig. 4.2 Check on numerical solutions

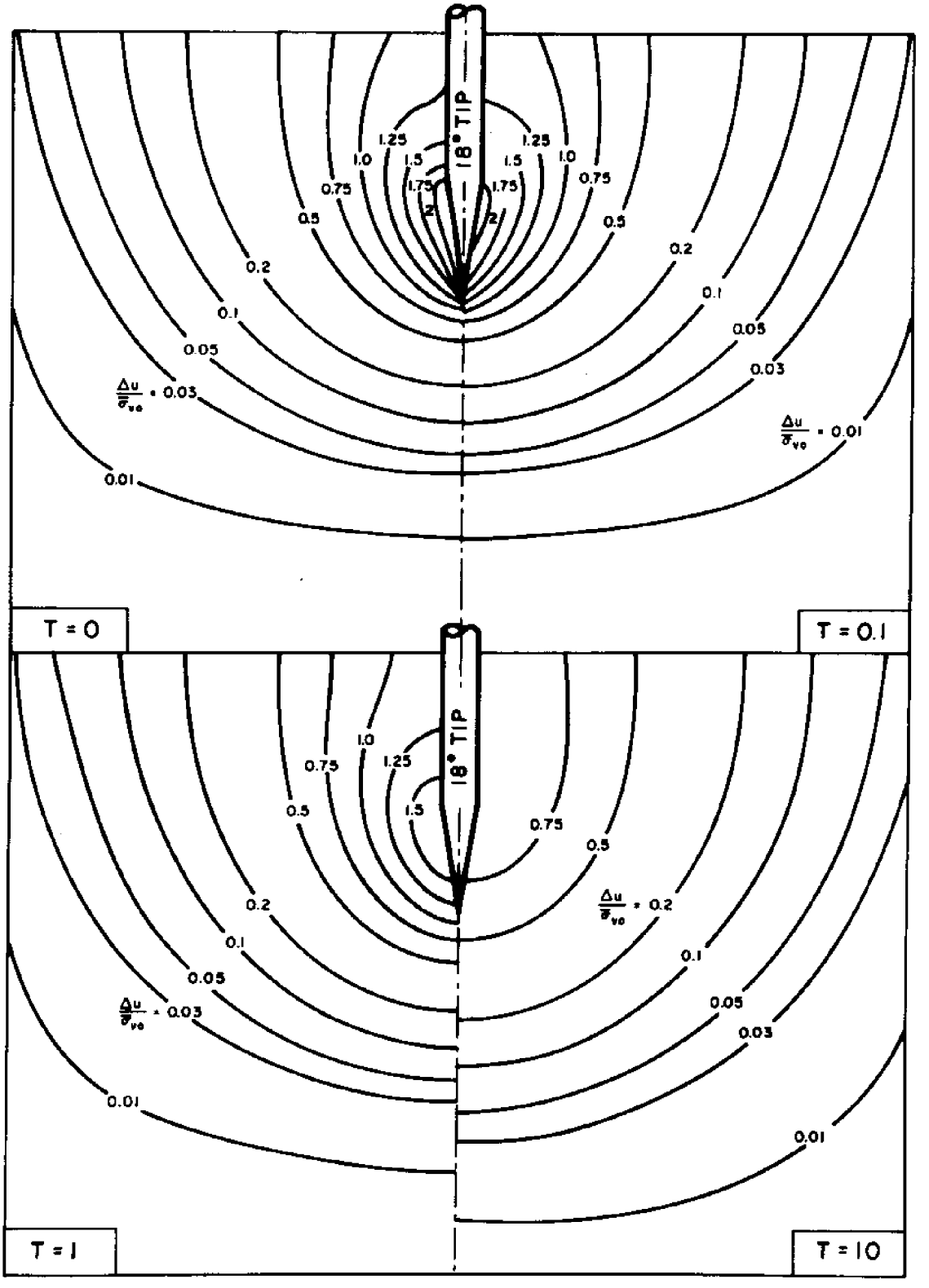

Fig. 4.3 Contours of excess pore pressures during uncoupled consolidation around an 18° cone in a linear isotropic material

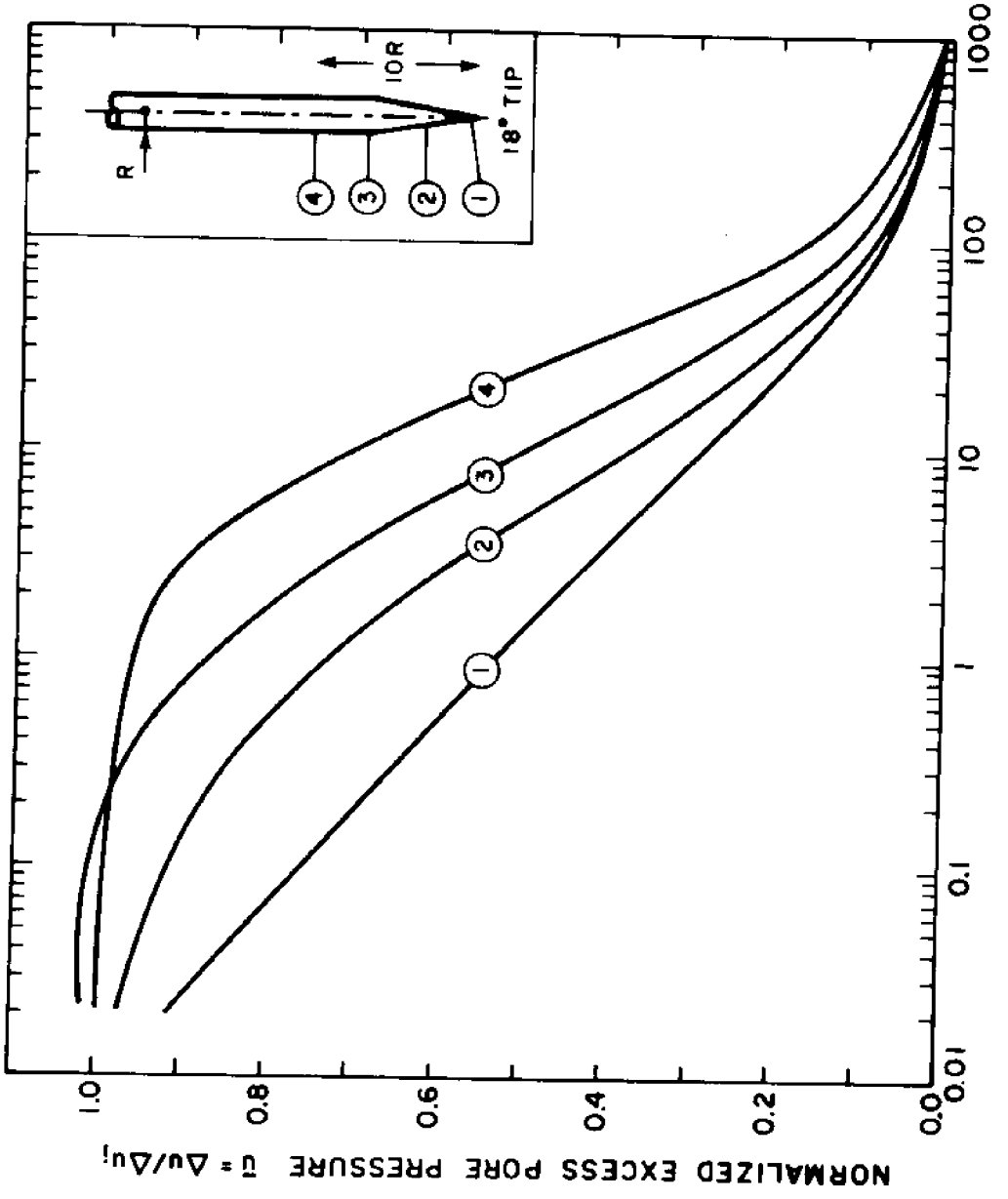

Fig. 4.4 Dissipation curves for an 18° cone according to linear isotropic uncoupled solutions

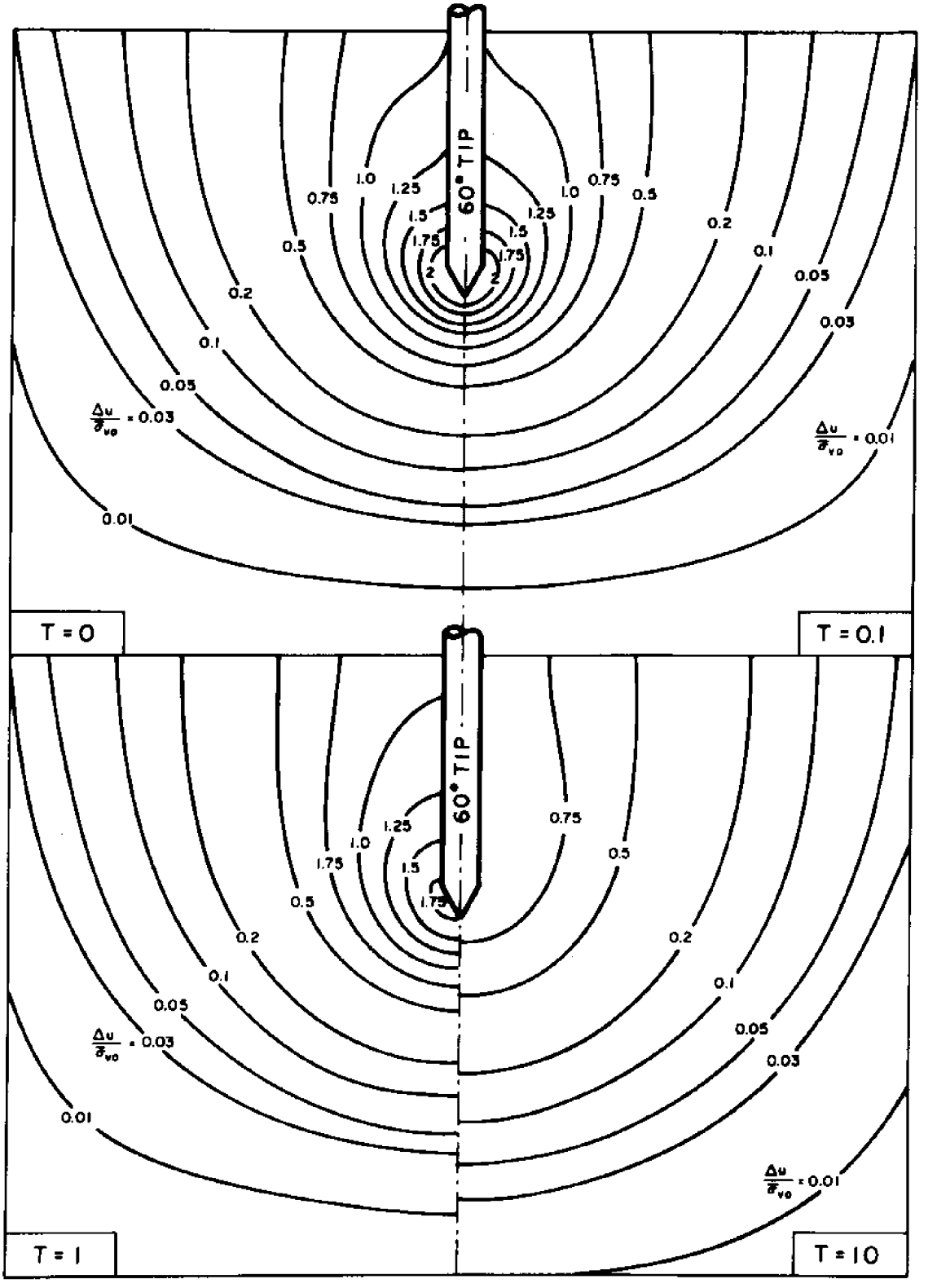

Fig. 4.5 Contours of excess pore pressures during uncoupled consolidation around a 60° cone in a linear isotropic material

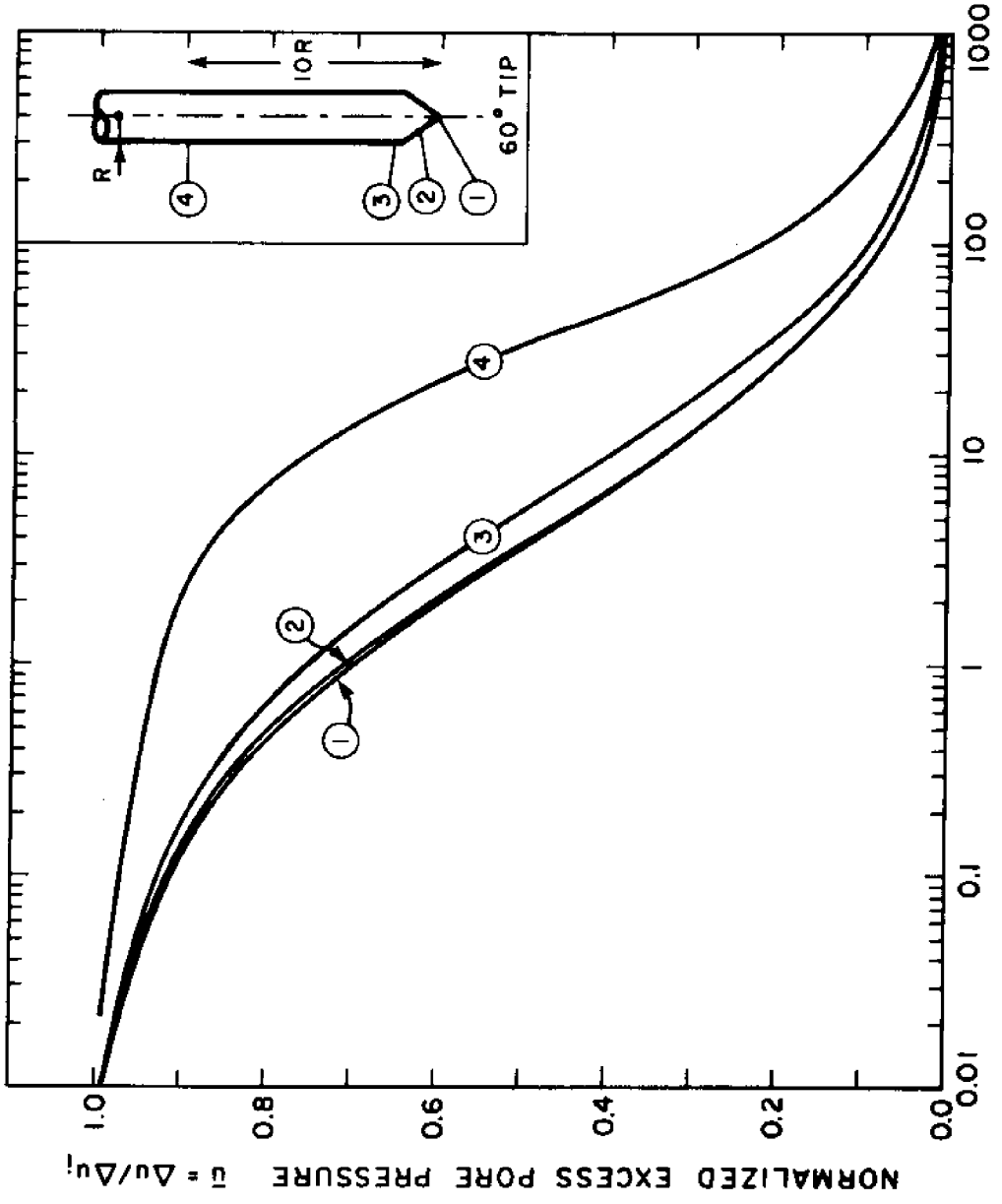

Fig. 4.6 Dissipation curves for a 60° cone according to linear isotropic uncoupled solutions

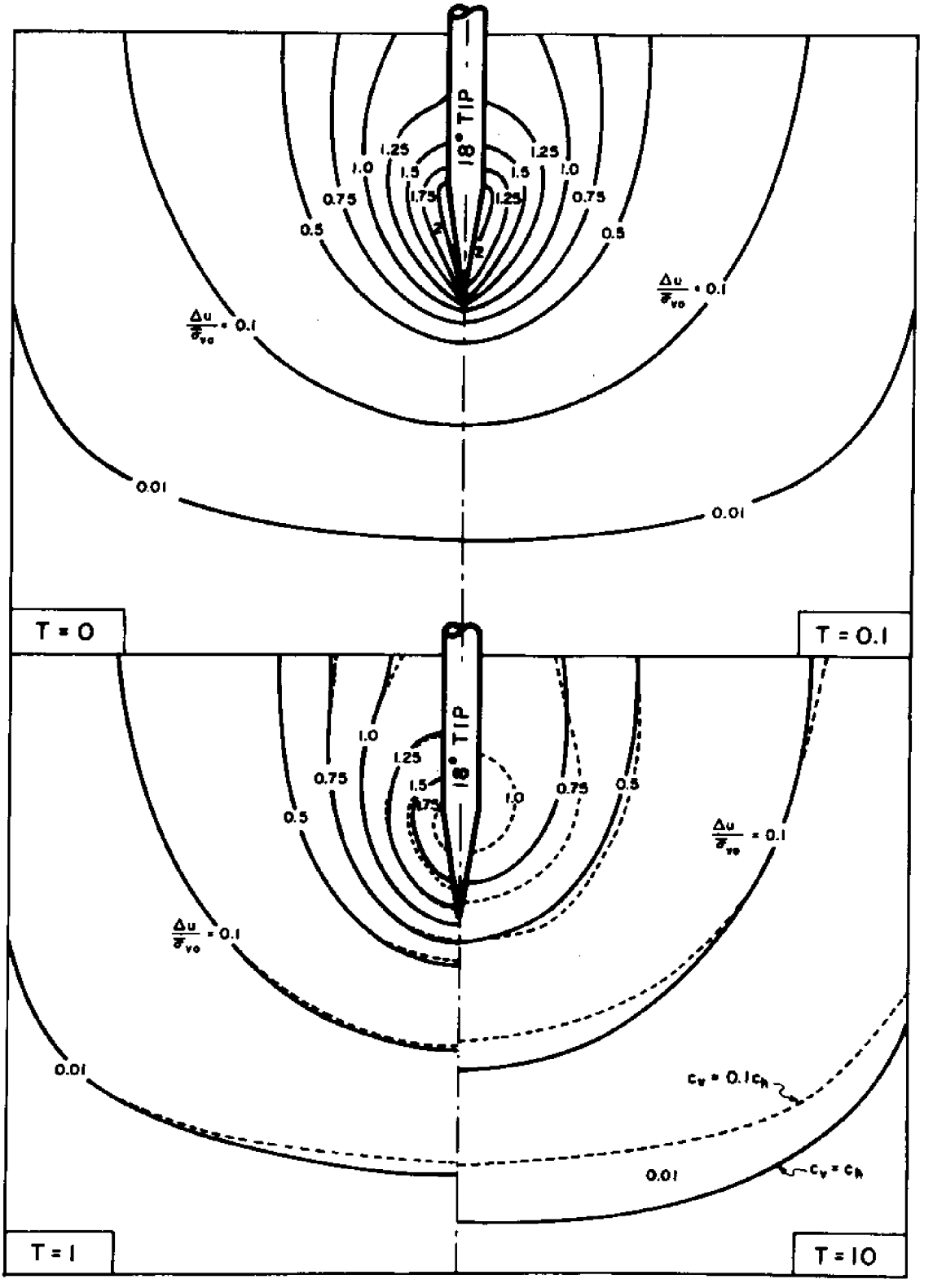

Fig. 4.7 Effect of anisotropy on the contours of excess pore pressures during uncoupled consolidation around an 18° cone ($T = c_h t/R^2$).

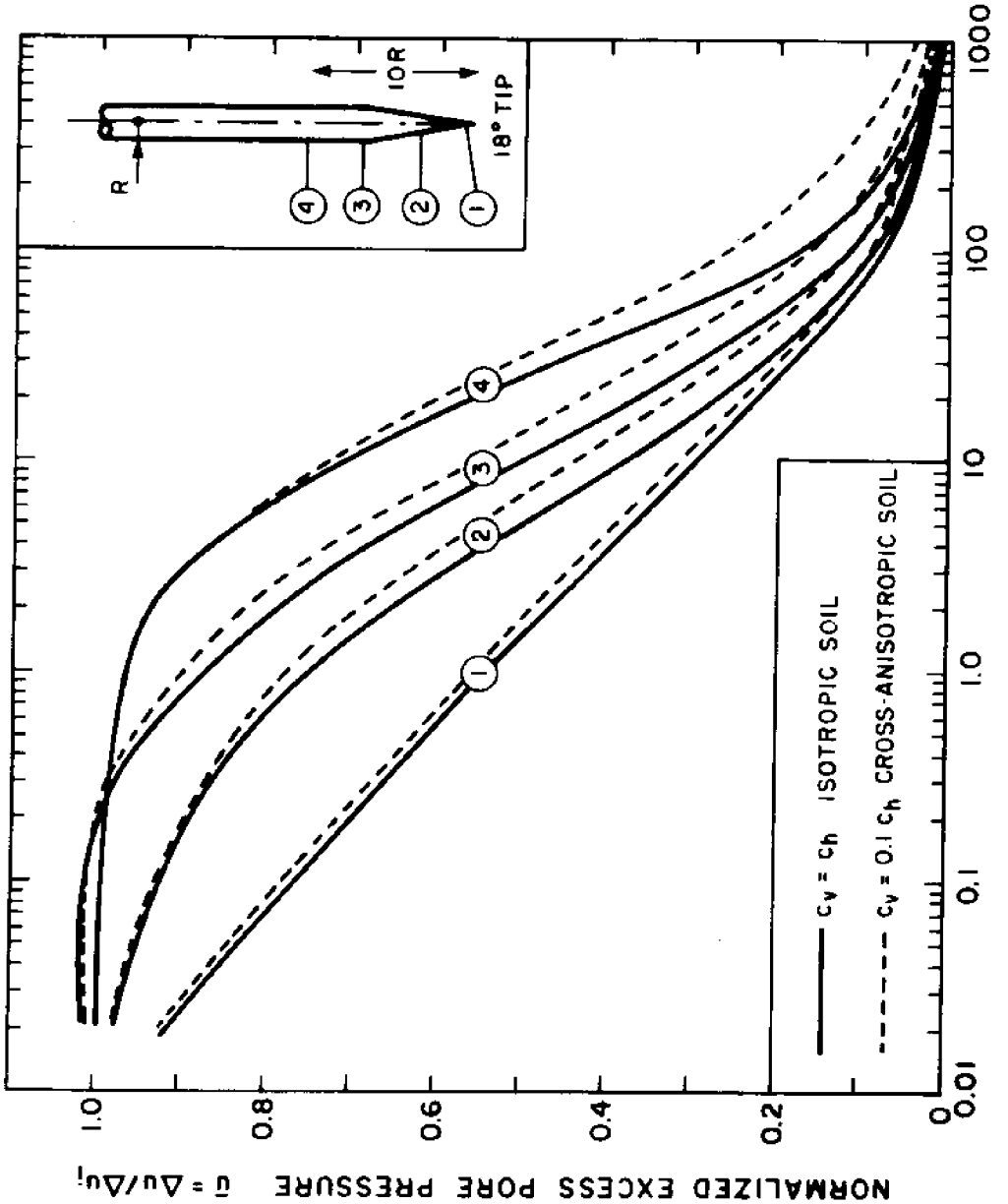

Fig. 4.8 Effect of anisotropy on idssipation curves for an 18° cone (uncoupled linear analysis)

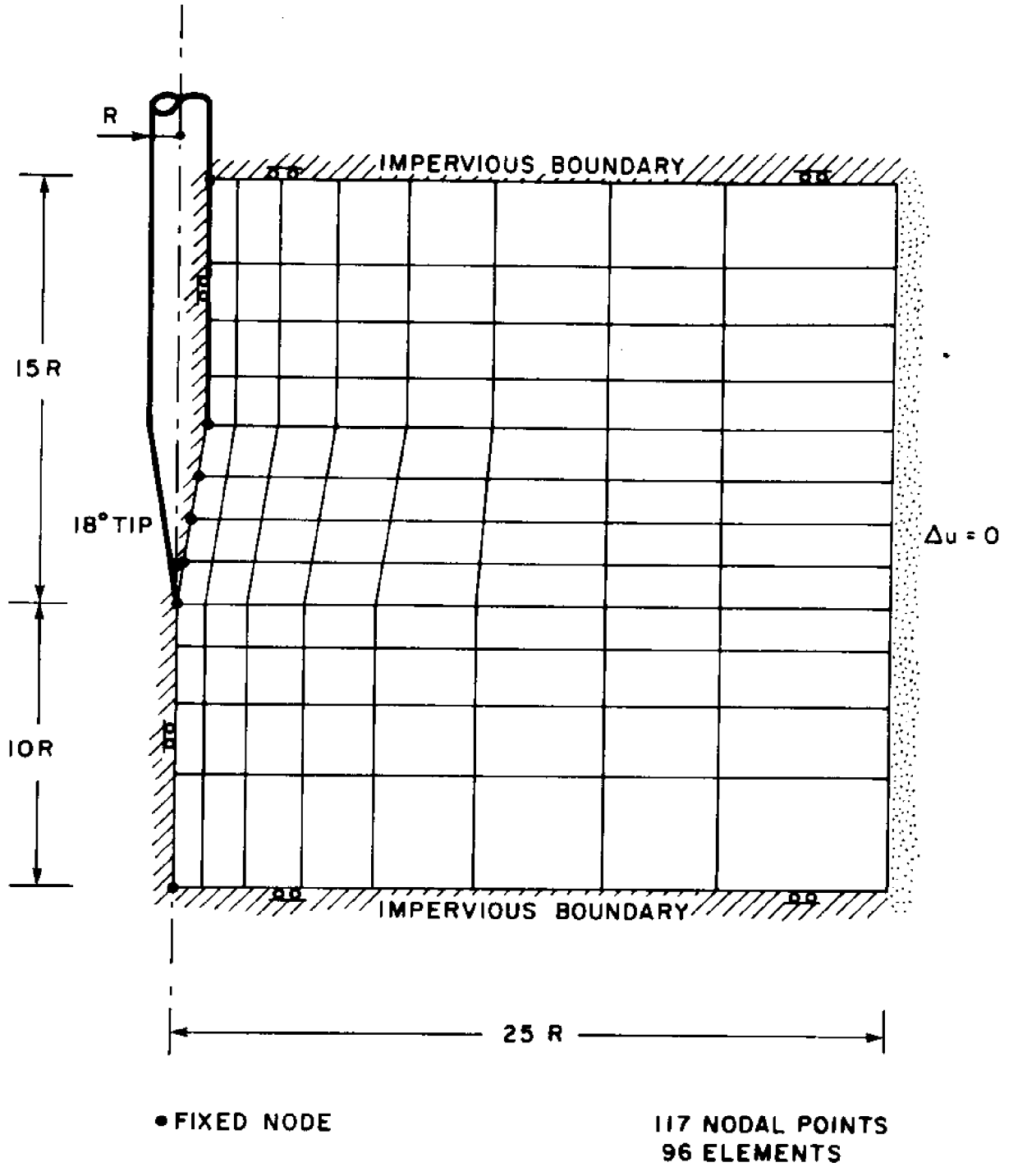

Fig. 4.9 Coarse finite element mesh

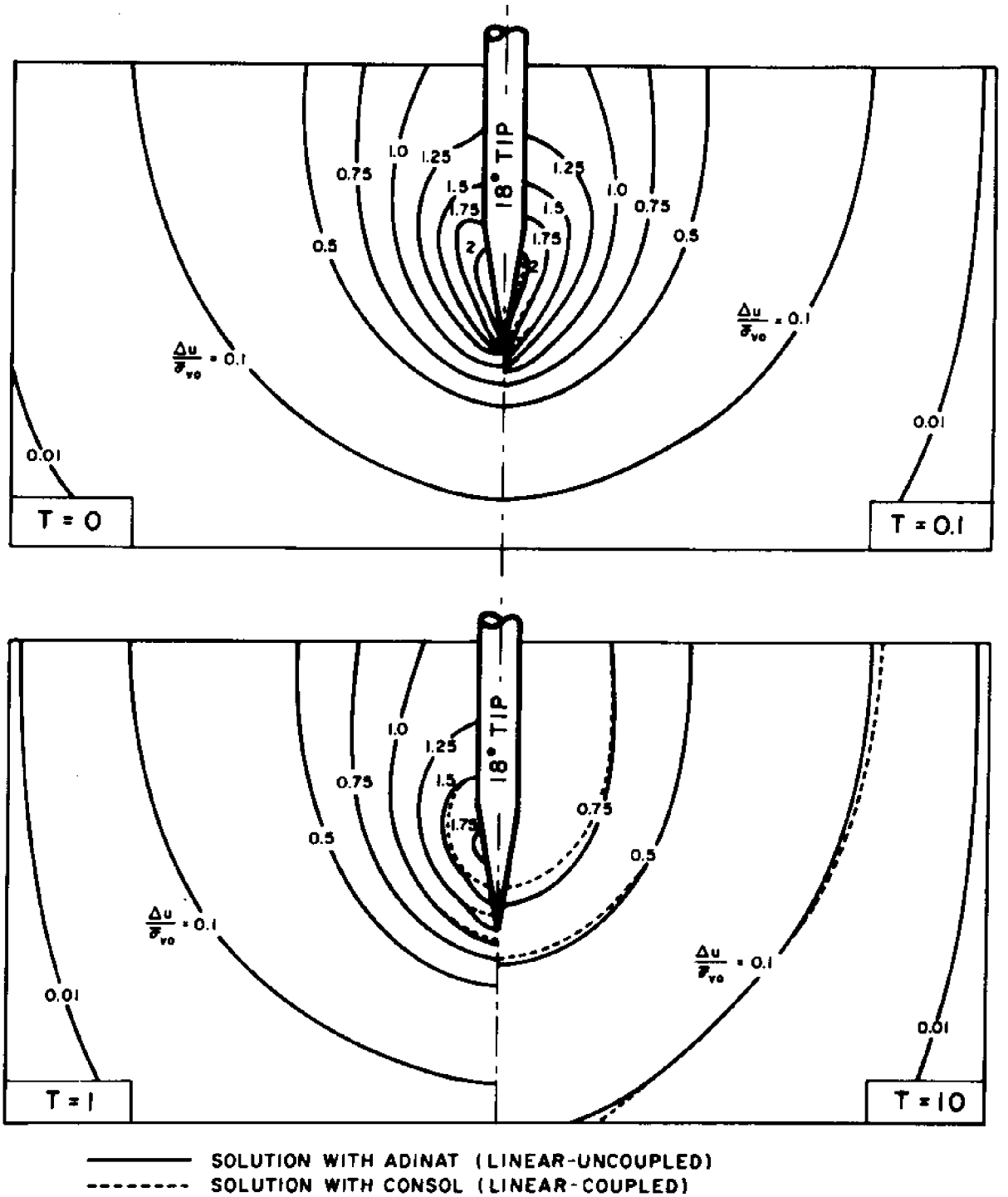

Fig. 4.10 Effect of coupling on the predicted contours of excess pore pressures during isotropic consolidation around an 18° cone

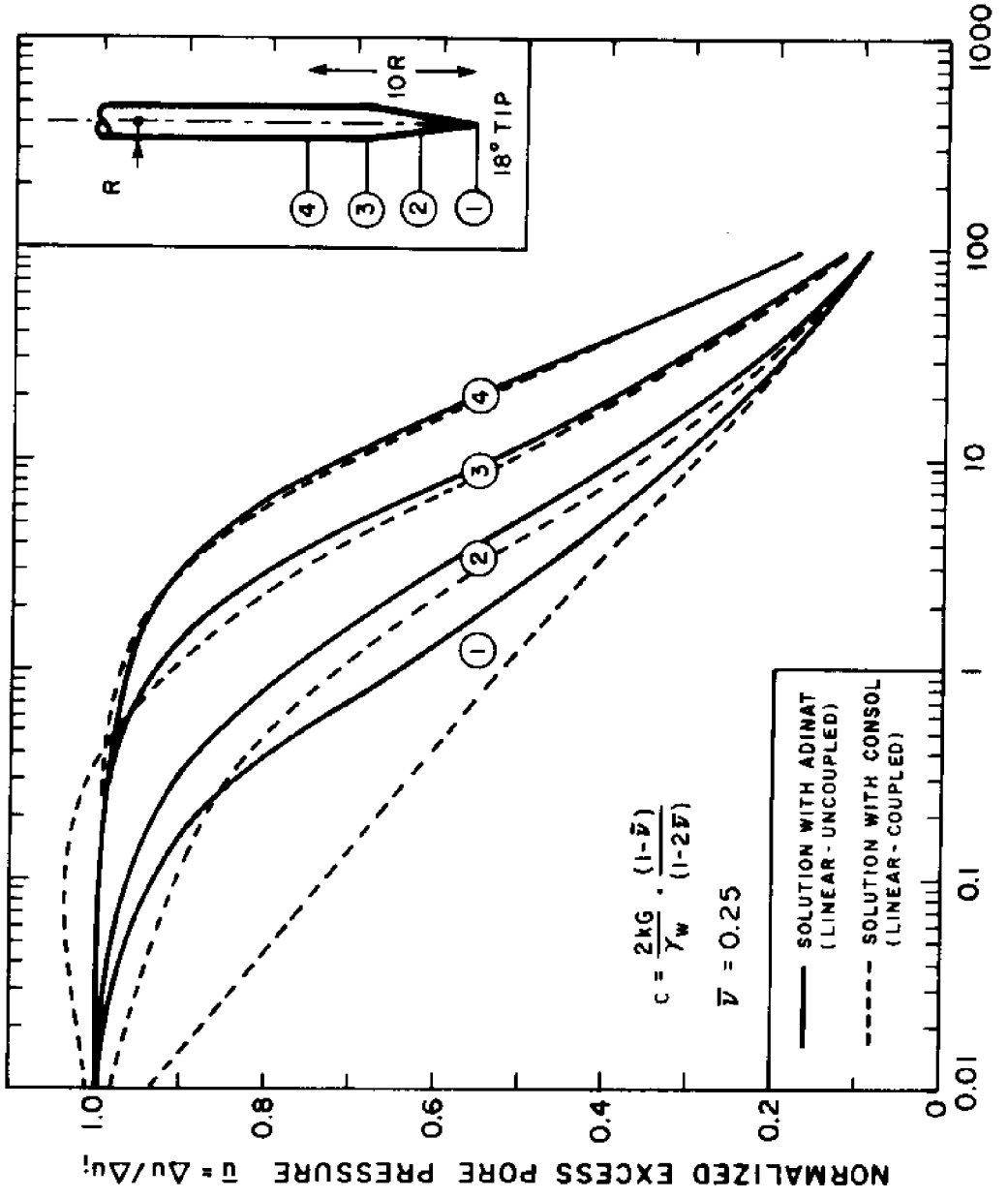

Fig. 4.11 Effect of linear coupling on dissipation curves for an 18° tip (linear isotropic analyses)

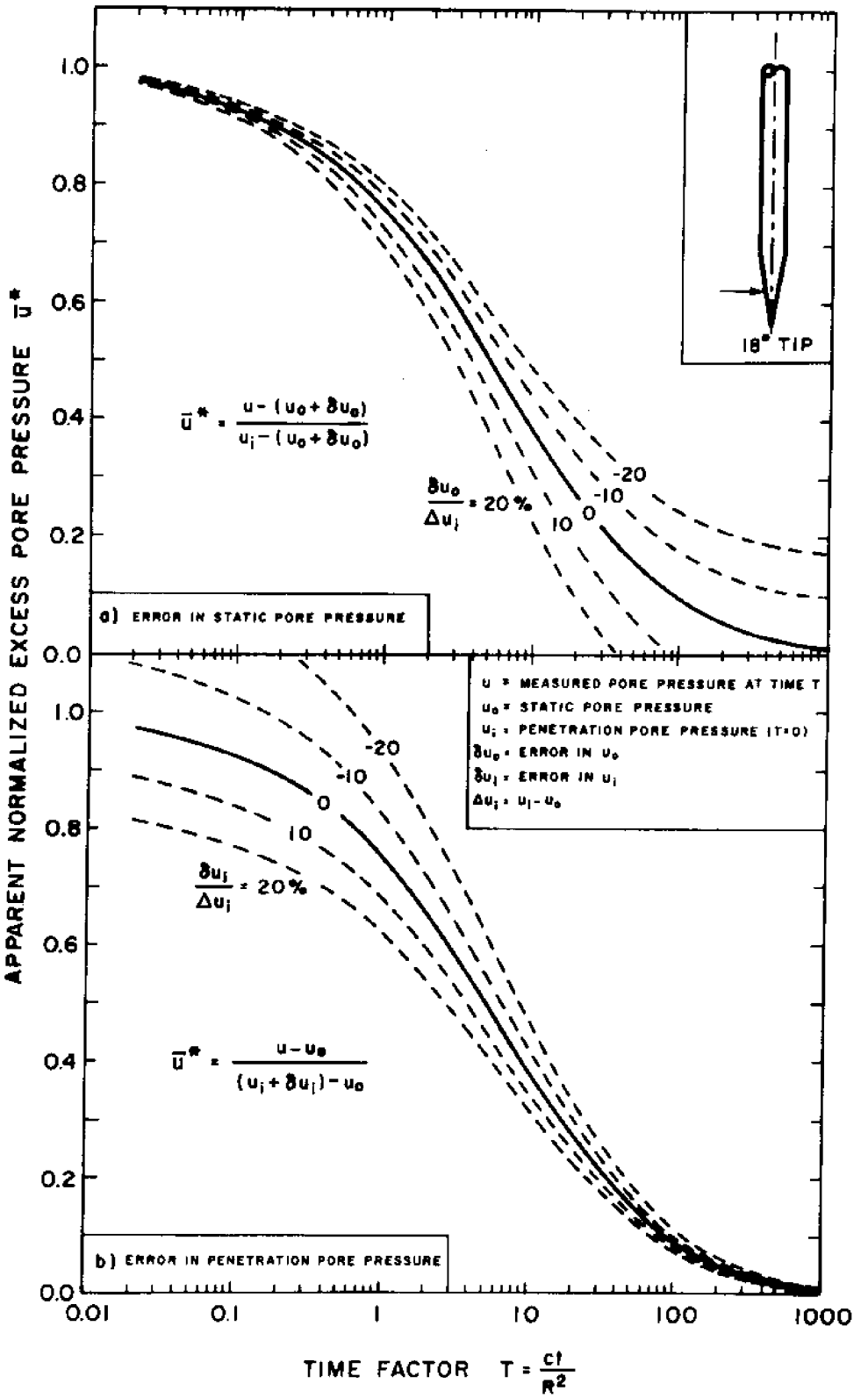

Fig. 4.12 Effect of errors in static and penetration pore pressures on dissipation curves at mid-cone of an 18° piezometer probe

CHAPTER 5

EVALUATION OF DISSIPATION SOLUTIONS IN BOSTON BLUE CLAY

5.1 INTRODUCTION

Linear dissipation solutions obtained in Chapter 4 involve significant simplifications of soil behavior during consolidation* and uncertainties in the initial excess pore pressure distribution**. Simple linear solutions are attractive for applications in different soils, but can cause serious difficulties in interpreting test results for the selection of appropriate engineering parameters for design. Few comprehensive nonlinear analyses were conducted to study consolidation around penetrating objects. Randolf et al. (1978) investigate nonlinear consolidation around pile shafts and conclude that, in this relatively simple one-dimensional problem, pore pressure dissipation is not significantly affected by soil nonlinearities.

---

*By assuming that the soil skeleton is linear and exhibits no time-dependent properties.

**Derived by the strain path method based on properties of normally consolidated Boston Blue Clay.

This chapter has four objectives: a) Evaluate the capability of simple linear solutions in predicting in situ dissipation measurements in Boston Blue clay; b) Investigate the effect of various practical factors on the reliability (repeatability) of the estimated profiles of the coefficients of consolidation and permeability, e.g. cone angle, porous stone location, degree of consolidation (dissipation) required,...etc.; c) Compare the estimated coefficients of consolidation and permeability with laboratory measurements and field performance data; and hence, d) Provide guidelines for the interpretation of dissipation records in practice.

5.2 SITE DESCRIPTION

5.2.1 Geology

The Boston Blue Clay (BBC) was formed during the wane of the late Pleistocene ice age (about 14,000 years ago) under a marine environment in the Boston Basin, probably not very far from the ice margin. The clay deposit overlaid a glacial till which covered the bedrock, and had a typical thickness in excess of 50 to 125 ft depending on the topography of the till. The clay includes numerous lenses of fine sands, isolated sand pockets and occasional stones or pebbles. Subsequent to clay deposition, movements of the earth crust and of the sea level resulted in emergence of the clay above the sea, followed by extensive weathering,

desiccation, and erosion of the upper part of the deposit. This was followed by at least two periods of submergence and deposition, of lesser significance, in which outwash sand, and peat and silt were deposited above the clay. Further geologic details are given by Kenney (1964) and Aldrich (1970).

5.2.2 Soil Conditions at the Test Site

The test site is adjacent to the coastline in Saugus, Mass., 160 to 200 ft (49 to 61 m) to the east of the unfinished Interstate 95 embankment centerline at Station 246, Figs. 5.1 and 5.2. M.I.T. studied this embankment extensively in the last decade by means of laboratory and in situ tests, embankment monitoring during construction, and a planned embankment loading to failure (D'Appolonia et al., 1971; M.I.T., 1975).

Figure 5.3 shows the soil profile at the test site as determined by conventional sampling and laboratory testing methods. The upper 25 ft consist of peat, sand and stiff clay layers which overlie 130 ft of Boston Blue Clay (BBC). The BBC of interest is located between depths 25 and 120 ft. Typically, the visual classification, and index tests (e.g., the natural water content, w_n, the liquid limit, w_ℓ, and plastic limit, w_p) provide little reliable information regarding stratification and variability of the clay.

On the other hand, laboratory estimates of the maximum past pressure, $\bar{\sigma}_{vm}$, by means of conventional oedometer and constant rate of strain consolidation tests clearly indicate that the clay above a depth of 75 ft, approximately, is significantly overconsolidated (i.e., has an OCR = $\bar{\sigma}_{vm}/\bar{\sigma}_{vo}$ well above unity).

5.2.3 Undrained Shear Strength

Figure 5.4.a shows the undrained shear strength, s_u, of the clay determined by means of laboratory tests on 3" ϕ "undisturbed" fixed piston samples. Unconfined (U) and unconsolidated undrained (UU) tests are not significantly different and vary between the wide range given by 0.4 ± 0.2 TSF without a clear trend with depth. Higher quality samples obtained in 1978 give higher strengths and exhibit relatively less scatter because of the reduced effect of sample disturbance.

Figure 5.4a also shows the peak strengths, s_u, obtained by the SHANSEP procedure based on the estimated OCR profile in Fig. 5.3 for K_o-consolidated undrained plane strain compression (PSC) and plane strain extension (PSE) tests (Ladd and Foott, 1974). Direct simple shear and triaxial tests where samples are isotropically and K_o-consolidated generally give s_u between the band provided by PSC and PSE in Fig. 5.4a (except for the K_o-consolidated triaxial extension tests yielding s_u 18% lower than PSE). The SHANSEP profiles in

Fig. 5.4a are smooth and cannot detect soil variability because averaging is required in estimating the profile of $\bar{\sigma}_{vm}$. s_u(PSE) is significantly less than s_u(PSC) and hence indicates the significant strength anisotropy of the clay.

Azzouz and Baligh (1978) backfigured the field strength, s_u(field) required for circular arc stability analyses based on the results of a planned embankment failure that extended to a depth of 75 ft. The profile of s_u(field) above 75 ft is based on their results and below 75 ft is estimated from the SHANSEP strength profiles, Fig. 5.4a.

Figure 5.4.b shows the undrained shear strength, s_u, determined by means of the Geonor Field Vane (FV) at about 3 ft intervals in four holes within 200 ft from the test site where one notes that s_u(FV) is generally between 0.4 and 0.6 TSF throughout the profile. Looking more carefully, two distinct layers can be identified: the first is located below a depth of 75 ft where s_u(FV) exhibits less scatter and increases with depth. The second layer is above 75 ft where s_u(FV) varies between 0.4 and 0.6 TSF with little identifiable trend. This is the more overconsolidated part of the deposit which was probably subjected to significant desiccation.

5.2.4 Cone Penetration Data

Figure 5.5 shows the cone penetration resistance, q_c, obtained by a standard FUGRO 60° cone and the pore pressure, u_i, measured at the tip of an 18° conical piezometer during steady penetration at a rate of 1 to 2 cm/sec in three different holes (each). Since cone penetration is continuous and largely independent of testing procedures and human interference, q_c and u_i provide consistent and reliable data for evaluating stratification and variabiilty of the soil.

As in the case of field vane test results (Fig. 5.4b) and conventional sampling and laboratory testing data (Fig. 5.3), BBC between 25 and 120 ft. can be divided into an upper overconsolidated clay above 75 ft. and a different lower clay. In addition, q_c and u_i indicate that the upper clay can possibly be divided into two sublayers, 25 to 60; and 60 to 75 ft., or even three sublayers, 25 to 40; 40 to 60; and 60 to 75 ft.

5.2.5 In Situ Static Pore Pressures

Figure 5.6 shows estimated values of the total stress, σ_{vo}, and the static pore pressures, u_o, in the soil obtained by leaving conical probes in the ground for sufficient periods of time. Measurements suggest that some artesian pressure exists in the underlying glacial till. For purposes of dissipation calculations, a 10 ft. artesian head in the till was selected.

5.2.6 Pressuremeter Results

Ladd et al. (1979) conducted a comprehensive study of self boring pressuremeter tests in BBC. Fig. 5.7 shows the limit pressure, p_ℓ, obtained at Sta. 246 by means of the French FAFSOR equipment. Amongst all pressuremeter measurements, p_ℓ was most consistent (less scatter) and relatively independent of the testing procedures and the interpretation method. Results in Fig. 5.7 indicate that, regardless of the interpretation method, the variation of p_ℓ with depth in the upper BBC above a depth of 75 ft is different from the lower BBC below 75 ft.

Another interesting aspect of pressuremeter results is the ratio of peak to ultimate* strengths backfigured from FAFSOR tests at Station 246. Fig. 5.8 indicates that: 1) In spite of significant scatter due to testing procedures and different interpretation methods, the lower BBC below 75 ft exhibits a more pronounced strain-softening behavior; and 2) Tests performed by the British CAMKOMETER equipment at Station 263 give basically the same results.

5.2.7 Clay Compressibility

Constant rate of strain tests performed by Germaine (1978) on good quality undisturbed samples at Station 246 indicate different compressibilities in the upper and lower

---

*At relatively large strains.

BBC below 75 ft. Fig. 5.9 shows typical strain* vs. log effective stress plots for two samples recovered from depths 41.5 and 84.5 ft. Clearly, the lower clay exhibits a very sensitive behavior with a collapse in structure once the maximum past pressure is exceeded.

5.3 EVALUATION OF PREDICTIONS: EFFECT OF CONE ANGLE AND POROUS STONE LOCATION

This section attempts to answer two basic questions:

1) Is the initial distribution of excess pore pressures estimated by the strain path method (Chapter 3) adequate for dissipation predictions?

2) Are predictions based on linear uncoupled analyses sufficiently accurate for estimating dissipation rates?

This will be achieved by the following approach:

1) Select a section (layer) of the BBC deposit where dissipation data exhibit no trend with depth. Appendix A shows detailed dissipation measurements indicating that, below a depth of 60 ft (approximately), no depth effect can be detected.

2) Compare dissipation measurements obtained at mid-height of an 18° cone with linear uncoupled solutions in order to estimate a coefficient of consolidation for

---

*Strains are expressed as $e/1+e_o$ for illustration. e_o and e are the initial and present void ratio at any stress level.

this section (below 60 ft). The mid-height of the cone is attractive because (a) Solutions are based on the same cone geometry as actual piezometers. This is not the case for measurements conducted at the tip of a cone. (b) The analytical uncertainties are reasonably small (e.g. low level of linear coupling, pore pressure gradients and numerical instabilities near the cone axis).

3) Using this coefficient of consolidation and the solutions presented in Chapter 4, predict dissipation rates for 18° and 60° cones at different locations on the cone and shaft behind it; and evaluate predictions by comparisons with measurements.

It is important to recall that dissipation is mainly controlled by the horizontal coefficient of consolidation (see Chapter 4) and is believed to impose a reloading mode of drained straining (see Chaps. 2 & 3) in the early dissipation stages.

5.3.1 Dissipation at Mid-Height of an 18° Cone

Figure 5.10 compares measured values of the normalized excess pore pressure, $\bar{u}$ (= $\Delta u/\Delta u_i$) vs. time, with linear uncoupled solutions at mid height of an 18° conical probe (Chapter 4). The shaded band represents the range of six dissipation records below a depth of 60 ft in the BBC deposit at Saugus. No effect of depth could be detected in these records obtained from two holes (test locations).

Results in Fig. 5.10 indicate that:

1) Measurements fall within a narrow band and are bound by linear isotropic uncoupled solutions corresponding to coefficients of consolidation of 0.02 and 0.08 cm^2/sec. Since dissipation is mainly governed by the horizontal coefficient of consolidation, solutions for an anisotropic soil are expected to lead to the same results provided that c_h = 0.02 and 0.08 cm^2/sec, as indicated in Fig. 5.10.

2) For c_h = 0.04 cm^2/sec, good agreement between linear uncoupled predictions and measurements is achieved up to 50% consolidation ($\bar{u}$ = 0.5). At later consolidation stages, actual dissipation appears to take place slightly slower than predicted.

5.3.2 Effect of Stone Location

Using c_h = 0.04 cm^2/sec for the BBC deposit below 60 ft, Fig. 5.11 shows dissipation predictions (heavy lines) at four different locations on an 18° conical probe after substituting the appropriate value of R = 1.91 cm in the expression for the time factor T (= $c_h t/R^2$). The shaded bands represent the range of selected* dissipation records below a depth of 60 ft in the BBC deposit in Saugus, Mass. The selection of dissipation records for this comparison is

---

*Records selected are clearly identified in Appendix A.

performed on the basis of consistency in order to minimize discrepancies due to natural soil variability and, in some cases, to eliminate clearly unacceptable results due to poor deairing of the porous stone.

The results in Fig. 5.11 indicate that:

1) Stone at the cone apex (Fig. 5.11a); the measurement band falls between the predicted dissipation curves at the cone apex and the mid-cone, but remains closer to the latter at most dissipation levels. This result is not surprising since predictions consider a complete conical tip, whereas measurements are conducted with a probe having a cylindrical porous stone at the tip, see Fig. 5.11a and Fig. 2.1.

The dashed (heavy) line in Fig. 5.11a represents the "average" dissipation curve obtained at any time t, by averaging the predicted normalized excess pore pressure, $\bar{u}$, at the cone apex and mid-cone. This semi-empirical "average" dissipation curve shows very good agreement with measurements (especially when $\bar{u} < 0.6$) and will be used subsequently to predict the horizontal coefficient of consolidation, c_h, from dissipation records obtained with the 18° piezometer probe when the porous element is located at the cone tip (Fig. 2.1).

2) Stone at mid-cone; results in Fig. 5.11b are the same as Fig. 5.10 discussed earlier.

3) Stone at the base of the cone (Fig. 5.11c); relatively few experiments were conducted with the porous stone at the base of the cone [One testing location (hole) and 8 depths (dissipation records)] and dissipation was interrupted at relatively small consolidation levels* ($\bar{u} \simeq 0.7$). Nevertheless, records are consistent, plot in a relatively narrow band, and exhibit a slower dissipation rate than predicted.

4) Stone far behind the cone (Fig. 5.11d); pore pressure dissipation far behind the tip is of particular interest because it simulates the condition along pile shafts after driving. The predicted dissipation curve (heavy line) corresponds to solutions obtained at a distance 10 R (R = radius of the shaft) behind the cone apex (location 4 in Fig. 4.4) and is very close to one-dimensional solutions simulating the shaft conditions far behind the tip. The measured dissipation curves are obtained at a distance 16 R behind the tip where a uniform condition along the shaft is closely reached.. Clearly, measurements fall in a narrow band** and take longer to

---

*Dissipation behind the tip requires approximately one log cycle of time more than the tip.

**This does not necessarily imply a small experimental scatter but probably reflects the small number of available records (3 depths).

dissipate than predicted. For example, when $0.7 < \bar{u} < 0.8$, the predicted time to reach a given $\bar{u}$ is approximately 2.5 times less than measured.

5.3.3 Effect of Cone Angle

Figure 5.12 compares predicted and measured normalized excess pore pressure dissipation at the apex of a 60° probe. The predicted (heavy) curve corresponds to linear uncoupled solutions at the apex of the cone (which are very close to mid-cone solutions, Fig. 4.6) and assumes $c_h = 0.04$ cm^2/sec (as in Fig. 5.11). The shaded area represents the range of selected dissipation records below a depth of 60 ft and indicates significant scatter at early stages of consolidation ($t < 1000$ sec, say) when compared to results of the 18° cone (Fig. 5.11). The results in Fig. 5.12 show good agreement between predictions and measurements up to 50% consolidation ($\bar{u} > 0.5$). At later consolidation stages ($\bar{u} < 0.5$) the theory "slightly" overpredicts the dissipation rate as in the case of the 18° cone.

5.3.4 Summary of Comparisons

Predictions of excess pore pressure dissipation based on linear uncoupled solutions lead to good agreement with measurements (at different locations on an 18° cone and at the tip of a 60° cone) at the early stages of consolidation. This suggests that the initial distribution of excess pore

pressures estimated by the strain path method (Chapter 3) is reasonably accurate. On the other hand, predictions at later stages of consolidation tend to overestimate dissipation rates* especially on the shaft behind the 18° cone and the tip of the 60° cone. This discrepancy is believed to result from coupling, nonlinearities, and various levels of soil remolding** around the cone so far neglected in the analysis. The decrease in the (drained volumetric) soil stiffness with the increase in effective stresses during consolidation provides the most reasonable explanation for the delay in measured dissipation rates.

The accuracy achieved by linear uncoupled solutions in estimating c_h (within a factor of 1.5 to 2.5) is believed to provide adequate predictions for most practical purposes, especially in view of other existing methods of determining in situ values of c_h and the scatter of experimental results due to inherent soil variability. More sophisticated analyses would be necessary only if measurements conducted to large degrees of consolidation*** (say $\bar{u} < 0.1$) indicate a more significant deviation from predictions. However, the designer using c_h values estimated

---

*By underestimating the time to reach a given degree of consolidation by a factor of 1.5 to 2.5.

**Leading to a nonuniform c_h in the soil.

***Not performed herein.

from dissipation records by means of linear uncoupled solutions (recommended herein) should bear in mind that these c_h values apply to reloading conditions (after severe shear straining or slight remolding has taken place), might be slightly overestimated if the degree of consolidation achieved is low ($\bar{u} > 0.5$) and are significantly higher than needed to predict foundation performance involving soil consolidation in the normally consolidated range.

Table 5.1 presents the recommended factors to interpret dissipation records obtained by means of 18° probe when the stone is located at the tip and at mid-height; and, for a 60° probe with the stone at the tip. The coefficient of consolidation c_h at a given degree of consolidation is evaluated by dividing the factor R^2T (in Table 5.1) by the measured time necessary to achieve this dissipation level.

5.4 COEFFICIENT OF CONSOLIDATION PROFILES

A major advantage of dissipation tests conducted by means of conical probes is that they are rapidly performed and hence enable profiles of the coefficient of consolidation, c_h, and possibly the coefficient of permeability, k_h vs. depth to be obtained economically. Such profiles are expensive to develop through other in situ or laboratory tests

and are necessary for reliably evaluating the performance of foundations* and many other geotechnical applications (see Chapter 1).

This section investigates the capability of conical probes to establish profiles of c_h (and possibly k_h) in the BBC deposit and, in addition, attempts to answer the following two basic questions:

1. What cone angle and what location of the porous stone provides the most reliable profiles? and,
2. What degree of consolidation (or dissipation time) is necessary to obtain reasonably accurate profiles?

The following c_h profiles are based on the results in Table 5.1 obtained from linear uncoupled dissipation analyses using the initial excess pore pressures derived by the strain path method. These initial distributions were found to provide good agreement with measurements for the BBC deposit below a depth of 45 (±5) ft. having an OCR < 3 (Chapter 3); therefore, predictions of c_h above 45 ft. are not as reliable as the profiles below 45 ft. Finally, adequate theoretical modelling of dissipation can be detected in the following profiles if c_h does not depend on the consolidation level, i.e., the value of $\bar{u}$.

---

*which are, in turn, necessary to evaluate the estimated profile.

5.4.1 18° Piezometer Probe with Measurements at Mid-Cone

Figures 5.13 through 5.17 show the predicted profiles of c_h in BBC (at Saugus, Station 246) obtained by matching solutions and measurements at 20, 40, 50, 60 and, 80% dissipation, i.e. $\bar{u}$ = 0.2, 0.4, 0.5, 0.6 and 0.8, respectively. The solid line in each figure represents a reference line for comparisons which is later shown to provide the best estimate of the c_h profile.*

Results in Figs. 5.13 through 5.17 indicate that:

a) at 20% consolidation, the $(c_h)_{20}$ data in Fig. 5.13 exhibit significant scatter, especially above 40 ft where, at a given depth, c_h can vary within one log cycle. Furthermore, most of the c_h data above 40 ft (to 50 ft) are lower than the reference profile, and, below 40 ft are higher than the reference profile;

b) the scatter is significantly reduced when 40% (Fig. 5.14) and 50% (Fig. 5.15) consolidation are reached. Furthermore, $(c_h)_{40}$ and $(c_h)_{50}$ data are very close and more evenly distributed about the reference profile; and,

c) at high consolidation levels, $(c_h)_{60}$ and $(c_h)_{80}$ (Figs. 5.16 and 5.17) exhibit approximately the same features as $(c_h)_{50}$ but tend to overestimate c_h in the

*At about 50% consolidation.

deposit below 40 (to 50) ft. Note that the number of data points at high consolidation levels is reduced by the long dissipation times required; especially in the lower deposit.

5.4.2 18° Piezometer Probe with Stone at Tip

Figures 5.18 through 5.24 show predicted profiles of c_h in BBC obtained by matching solutions and measurements at 20, 40, 50, 60 and, 80% dissipation. Results indicate that:

a) at 20% dissipation (Fig. 5.18), $(c_h)_{20}$ data exhibit considerable scatter at any depth and are generally smaller than the reference profile. The scatter is consistent with the wide band of measurements in the $\bar{u}$ vs. log t plot at early times (Fig. 5.11a);

b) the experimental scatter is somewhat reduced in the profiles of $(c_h)_{40}$ and $(c_h)_{50}$ (Figs. 5.19 and 5.20) and the predictions are well centered about the reference profile, and;

c) the predicted profiles of $(c_h)_{60}$ and $(c_h)_{80}$ (Figs. 5.21 and 5.22) are very similar to that of $(c_h)_{50}$ but contain much less data points.

5.4.3 60° Piezometer Probe with Stone at Tip

Figures 5.23 through 5.27 show predicted profiles of c_h in BBC obtained by matching predictions and measurements at 20, 40, 50, 60 and 80% dissipation, respectively. Results indicate that:

a) at 20% consolidation (Fig. 5.23), the $(c_h)_{20}$ data exhibit considerable scatter. In the deposit above 40 ft, $(c_h)_{20}$ is significantly higher than the reference profile;

b) at 40% consolidation (Fig. 5.24), the $(c_h)_{40}$ data are much more consistent and plot close to the reference profile;

c) values of $(c_h)_{50}$ exhibit practically no scatter but indicate a slightly lower value of c_h ($\simeq$ 0.03 cm^2/sec) than the reference profile ($c_h \simeq 0.04$ cm^2/sec) for the clay below a depth of 60 ft, and;

c) profiles of $(c_h)_{60}$ and $(c_h)_{80}$ (Figs. 5.26 and 5.27) show the same features as $(c_h)_{50}$ (Fig. 5.25) but contain much less data points.

5.4.4 Summary of c_h(probe) profiles

1 - Estimates of the coefficient of consolidation after 20% consolidation involve significant scatter and are therefore unreliable.

2 - Results obtained after 40,50,60, and 80% consolidation are plotted in Fig. 5.28 for three types of probe:

a) An 18° cone with the porous stone at midheight.

Predictions of c_h(probe) based on linear uncoupled solutions involve moderate scatter and are very close to the reference profile. However, no data are available below 75 ft.

b) An 18° cone with the porous stone at the tip. Predictions of c_h(probe) based on a semi-empirical procedure (see Sec. 5.3.2) are generally close to the reference profile but involve more scatter, especially in the upper clay above 75 ft.

c) A 60° cone with the porous stone at the tip. Predictions of c_h(probe) based on linear uncoupled solutions are close to the reference profile and involve moderate scatter. However, values of c_h(probe) in the lower clay (below 75 ft.) are 25% smaller than the reference profile.

3 - Therefore, it appears reasonable to assume that c_h(probe) is given by the reference profile.

5.5 COMPARISON WITH LABORATORY MEASUREMENTS AND FIELD PERFORMANCE

Figure 5.29 compares the predicted (reference) profile of horizontal coefficient of consolidation, c_h(probe) obtained from dissipation records of conical probes with relevant laboratory and field measurements consisting of:

a) constant rate of strain consolidation (CRSC) tests* conducted by Germaine (1978) on six good quality undisturbed samples recovered between depths 40 ft and 100 ft at the Saugus site. The data from these tests consist of the vertical coefficient of consolidation corresponding to: (1) the normally consolidated range, c_v(NC), after the estimated maximum past pressure has been significantly exceeded; and, (2) the overconsolidated range, c_v(SW), obtained during rebound (swelling) at the corresponding estimated OCR;

b) profiles of c_v (loading) estimated by Davis and Poulos and by Duncan (M.I.T., 1975) on the basis of in situ pore pressure measurements conducted in the foundation clay under the I-95 embankment centerline, about 2000 ft from the cone penetration testing site, since its construction in 1967 and up to 1974.

d) A range of swelling c_v (unloading), back-figured by Bromwell and Lambe (1968) on the basis of in situ pore pressure dissipation measurements in a thick BBC deposit due to a wide excavation for the construction of the Student Center at M.I.T. The soil deposit underlying M.I.T. contains a 50 ft BBC

---

*Wissa et al., 1971

layer with very strong similarities to the BBC below 50 ft at the Saugus site.

Noting that all available lab measurements and field performance data correspond to vertical water flow, the results in Fig. 5.29 indicate that:

(a) c_h(probe) in the lower BBC below 75 ft is virtually identical to the backfigured values of c_v (unloading) obtained by Bromwell and Lambe (1968). This strongly suggests that dissipation predictions by the piezometer probe at 50% consolidation give reasonable field rebound (or reloading) values of c_h and that the lower BBC exhibits little anisotropy.

(b) c_h(probe) is approximately twice higher than swelling laboratory values c_v(SW) in the lower BBC below 75 ft; and, 5 to 8 times higher in the upper clay between 40 and 75 ft. This appears to indicate that the upper clay has a more pronounced anisotropic permeability.

(c) The variation of c_h(probe) with depth shows the same trend as laboratory measurements of c_v(NC). Furthermore, the profile of c_v(NC) is virtually the same as backfigured by Duncan (M.I.T., 1974) for field c_v (loading). However, the magnitude of c_h(probe) is about 40 times higher than c_v (loading) in the

lower clay below 75 ft; and, about 30 ($\pm$10) times in the upper clay between 40 and 75 feet.

In summary, the profile of c_h(probe) determined at 50% dissipation in BBC appears to provide good estimates of the coefficient of consolidation to be used in foundation problems involving unloading and possibly reloading of over consolidated clays above the maximum past pressure. On the other hand, c_h(probe) are significantly higher than values of the coefficient of consolidation required to estimate the pore pressure dissipation rate in foundation clays compressed in the normally consolidated range. The application of c_h(probe) to these problems requires an investigation of the relevant clay compressibility that governs dissipation of excess pore pressures around cones. This is a difficult task involving significant uncertainties but is also necessary to estimate the coefficient of permeability from c_h(probe).

5.6 COEFFICIENT OF PERMEABILITY

5.6.1 Mechanism and Simplifications

Cone penetration in clays causes undrained shearing of the soil under constant volume conditions and hence, in medium to soft clays, reduces the effective stresses. When steady penetration is interrupted and pore pressures start to dissipate, effective stresses increase and the soil decreases in volume. Soil compressibility during dissipation

is very difficult to predict accurately because of the complicated two-dimensional nature of the problem and the variation of soil compressibility during consolidation (i.e. nonlinearity). However, knowing that consolidation starts at an effective stress level lower than previously existed before penetration, suggests that soil compressibility corresponds to a reloading (or recompression) mode, at least in the early stages of consolidation. In this mode, the soil compressibility is low and dissipation takes place rapidly because the coefficient of consolidation is proportional to the ratio of permeability to compressibility. Using one-dimensional consolidation for illustration, this means that the coefficient of consolidation during vertical straining and horizontal water flow, is given by

$$c_h = \frac{k_h}{m_v \gamma_w} \tag{5.1}$$

In a virgin compression mode (normally consolidated clay)

$$m_v(NC) = \frac{CR}{\Delta\bar{\sigma}_v} \log\left(1 + \frac{\Delta\bar{\sigma}_v}{\bar{\sigma}_{vc}}\right) \tag{5.2}$$

and in a recompression mode (overconsolidated)

$$m_v(OC) = \frac{RR}{\Delta\bar{\sigma}_v} \log\left(1 + \frac{\Delta\bar{\sigma}_v}{\bar{\sigma}_{vc}}\right) \tag{5.3}$$

where k_h is the horizontal permeability (cm/sec); m_v is the coefficient of volume change (cm^2/kg); γ_w is the unit weight of water (10^{-3} kg/cm^3); CR and RR are the compression

and recompression ratios* respectively; and, $\bar{\sigma}_{vc}$ and $\Delta\bar{\sigma}_v$ are the vertical effective stress and its increment at any consolidation level, respectively (kg/cm^2)

For small increments of effective stresses (i.e., $\Delta\bar{\sigma}_v/\bar{\sigma}_{vc} \ll 1$). Eqs. (5.2) and (5.3) become

$$m_v(NC) = \frac{CR}{2.3\bar{\sigma}_{vc}}$$

$$m_v(OC) = \frac{RR}{2.3\bar{\sigma}_{vc}} \qquad (5.4)$$

and hence,

$$k_h = \frac{\gamma_w}{2.3\bar{\sigma}_{vc}} \cdot RR \cdot c_h(OC) \qquad (5.5)$$

and; for a fixed value of k_h (small changes in void ratio), we can also write

$$c_h(NC) = \frac{RR}{CR}\ c_h(OC) \qquad (5.6)$$

Eqs. 5.5 and 5.6 provide estimates of the horizontal permeability , k_h, and the normally consolidated coefficient of consolidation, $c_h(NC)$, in terms of the overconsolidated horizontal coefficient of consolidation , $c_h(OC)$, for vertical compression of the clay due to horizontal water flow.

---

*Slope of the vertical strain vs. vertical effective stress

Assuming that early consolidation around cones takes place in a recompression mode, we assume that Eqs 5.5 and 5.6 can be used approximately for dissipation around conical probes when

$$c_h(\text{probe}) = c_h(\text{OC})$$
$$\text{and} \qquad \bar{\sigma}_{vo} = \bar{\sigma}_{vc} \tag{5.7}$$

where $c_h(\text{probe})$ is estimated from dissipation records as discussed previously; and, $\bar{\sigma}_{vo}$ is the vertical effective stress in the soil prior to cone penetration.

Substituting Eqs (5.7) into (5.5) and (5.6) we get

$$k_h(\text{probe}) \simeq \frac{\gamma_w}{2.3\bar{\sigma}_{vo}} \cdot RR(\text{probe}) \cdot c_h(\text{probe}) \tag{5.8}$$

$$c_h(\text{NC}) \simeq \frac{RR(\text{probe})}{CR} c_h(\text{probe}) \tag{5.9}$$

and knowing that $c_v(\text{NC}) = (k_v/k_h) \cdot c_h(\text{NC})$, we can also write

$$c_v(\text{NC}) \simeq \frac{RR(\text{probe})}{CR} \cdot \frac{k_v}{k_h} \cdot c_h(\text{probe}) \tag{5.10}$$

5.6.2 Coefficient of Permeability

Figure 5.30 shows the predicted profile of $k_h(\text{probe})$ based on Eq. 5.8 and the reference $c_h(\text{probe})$ profile* estimated from dissipation studies for selected values of

*basically obtained at 50% dissipation

RR(probe) = 0.5, 1 and 2 x 10^{-2}. Comparing k_h(probe) to the vertical permeability k_v estimated from laboratory CRSC tests we note that:

1. In the lower more uniform BBC below 75 ft, k_h(probe) predicted for RR(probe) = 10^{-2} agree with k_v(lab) = 8.5 ($\pm$1.5)10^{-8}cm/sec.
2. In the upper BBC, between 40 and 75 ft, k_h(probe) obtained for RR(probe) = 10^{-2} underpredicts k_v(lab) by a factor of two (approximately) indicating one or more of the following possibilities.
   a- The upper BBC has a more pronounced anisotropic permeability than the lower clay. This is also suggested by the swelling vertical coefficients of consolidation , c_v(SW), from CRSC tests and discussed earlier (see section 5.5)
   b- The value of RR(probe) in the upper clay is lower than 0.01 (equal to 0.5 x 10^{-2}, say) because of its higher OCR(=3.5 to 1.3) as compared to the lower clay (OCR = 1.3 to 1.2)
   c- The selected c_h(probe) profile (based on results from all probes tested) neglects the reduced permeability of the upper BBC. Some results of 18^{o}-probes suggest this possibility and/or the more erratic nature of this layer (see Figs. 5.14,

5.15, 5.20, and 5.28)

d- More reliable laboratory (or field) permeability measurements are needed, especially the horizontal permeability k_h

In spite of the above uncertainties in selecting adequate values of RR(probe) and the severe simplifications needed to reach Eq. 5.8, the predictions of k_h(probe) are considered very satisfactory especially when compared with other existing in situ permeability testing methods. Figure 5.31 presents "sensitivity" test results performed along the I-95 embankment in Saugus (Recker, 1973). Sensitivity tests basically consist of falling head permeability tests which are conducted to check that field peizometers are functioning adequately. Interpretation of these falling head tests is very questionable, (see Chapter 1 and Bishop et al., 1964) and were conducted by Recker, 1973 after neglecting soil compressibility. Clearly, the amount of scatter (on the order of two log cycles) is unacceptable* for design purposes but the data show a general trend of decreasing permeability with depth.

5.7 DISCUSSION OF CLAY COMPRESSIBILITY DURING DISSIPATION

Ideally, a complete nonlinear analysis of consolidation

*If soil compressibility is introduced in interpreting test data, some reduction of the scatter might be achieved.

around cones should provide appropriate values of the recompression ratio RR(probe) to be used in predictions of k_h(probe) and c_v(NC) in a particular clay.* However, such a sophisticated analysis is not available, and Eqs. 5.8 and 5.10 are based on simplifying assumptions (Eqs. 5.7) and hence, appropriate values of RR(probe) can only be back-figured from measurements (or estimates) of k_h, c_v(NC), k_v, and CR.

5.7.1 The lower BBC below 75 ft.

Eqs. 5.10 and 5.8 are graphically illustrated in the upper and lower parts of Fig. 5.32, respectively. Estimates of RR(probe) can be obtained by two methods. The first (Eq. 5.10) is based on the measured value of $c_v(NC)/c_h(probe)$ and estimates of (k_h/k_v) and CR. The second (Eq. 5.8) is based on the measured value of $k_h/c_h(probe)$ [or $k_v/c_h(probe)$ and k_h/k_v] and an estimate** of the vertical effective stress, $\bar{\sigma}_{vo}$.

At a depth of 90 ft. (27.5 m) in the lower BBC, $c_h(probe) \simeq 40 \times 10^{-3} cm^2/sec$ and laboratory results give $c_v(NC) \simeq 10^{-3} cm^2/sec$ and $k_v \simeq 8.5 \times 10^{-8} cm/sec$. Therefore, $c_v(NC)/c_h(probe)$ and $k_v/c_h(probe)$ equal 0.025 and $2.13 \times 10^{-6} cm^{-1}$ respectively; and are entered in the upper and lower left hand scales of Fig. 5.32. Assuming that CR = 0.4, both consolidation and

---

*Of a given type, stress, and environmental history, etc.

**In Fig. 3.51, $\bar{\sigma}_{vo}$ was computed assuming an effective unit weight $\bar{\gamma} = 0.75 t/m^3 \simeq 47 pcf$.

permeability laboratory test results lead to RR (probe) = 10^{-2} for k_h/k_v=1; and, RR (probe) = 2 x 10^{-2} for k_h/k_v = 2. Clearly, RR (probe) depends on the selected values of CR and k_h/k_v.

a- the compression ratio CR

The selection of an appropriate compression ratio CR in the lower BBC is a difficult task. In CRSC tests, the clay consistently exhibits a structural collapse (see Fig. 5.9) with a very high compression ratio, CR_{max} = 0.7± 0.2, after the maximum past pressure has just been exceeded. At higher pressures, a much reduced compression ration CR_{min} ≈ 0.17 is reached at $\bar{\sigma}_{vc}$ = 5 to 10 kg/cm^2. Therefore, CR = 0.4 selected in Fig. 5.32 appears to be a reasonable average, especially that a decrease in CR causes a decrease in the backfigured value of RR (probe) from consolidation results but does not affect RR (probe) from permeability tests.

b- Anisotropic permeability

Few reliable data exist on k_h/k_v in BBC. Guertin (1967) measured k_h/k_v = 1.7 in laboratory permeability tests and Ladd (1976) recommends k_h/k_v = 1.2 ± 0.2

c- RR (probe)

Since recompression and swelling ratios are generally of the same order, the backfigured values of RR (probe) can be compared to measured swelling ratios SR in CRSC tests:

SR = 2.5 ($\pm$0.4) x 10^{-2} at an OCR = 5; and, SR = 1.7 ($\pm$0.2) x 10^{-2} at an OCR = 2. Increments of effective stresses in the early stages of consolidation around cones are not believed to be large. Therefore, values of SR at an OCR = 2 or less appear reasonable to compare with RR (probe) $\simeq 10^{-2}$ estimated at 50% dissipation.

In conclusion, the above comparisons appear to indicate that the lower BBC below 75 ft. has a very slight anisotropic permeability (i.e. $k_h/k_v \simeq 1$) and a value of RR (probe) $\simeq 10^{-2}$. However, the uncertainties in selecting appropriate values of k_h/k_v and CR; and, the scatter of experimental results cannot eliminate the possibility of RR (probe) being as low as 0.5 x 10^{-2} or as high as 2 x 10^{-2}.

5.7.2 The upper BBC between 40 and 75 ft.

Compared to the lower BBC below 75 ft, the upper BBC has

1- More strength scatter. An analysis of the cone resistance and field vane scatter (Figs. 5.4 and 5.5) indicate a coefficient of variation in strength (= standard deviation/mean) equal to 0.1 $\pm$ 0.05 as compared to 0.05 $\pm$ 0.025 in the lower clay (Baligh and Vivatrat, 1979).

2- A higher OCR $\simeq$ 3.5 to 1.3 as compared to 1.3 to 1.2 in the lower clay, Fig. 5.3.

3- A slightly higher salt concentration in the pore water $\simeq$ 15 gr/litre as compared to 10 to 15 in the lower clay.

4- A slightly lower plasticity index (PI ≃ 19 ± 4% vs. 22 ± 4% in the lower clay); and, a slighly lower liquidity index (LI ≃ 0.8 ± 0.3 vs. 1 ± 0.3 in the lower clay.

5- More "reasonable" peak strengths and stress-strain behavior backfigured from pressuremeter tests. The lower clay has very large peak strengths and very severe strain softening, Fig. 5.8.

6- More "reasonable" compression ratios in CRSC laboratory tests (Fig. 5.9): $CR_{max} = 0.17 \pm 0.03$ and $CR_{min} \simeq 0.14$.

7- Possibly a more pronounced anisotropic permeability, i.e., k_h/k_v is probably about 2 (see sections 5.5 and 5.6.2).

Figure 5.33 shows the backfigured values of RR (probe) at depths 41.5, 52 and 67.5 ft in the upper BBC assuming that $k_h/k_v = 2$ and CR = 0.15. Based on laboratory measurements of the consolidation coefficients c_v(NC), the backfigured values of RR (probe) are 1.5×10^{-2}, 10^{-2} and 0.75×10^{-2}, respectively. On the other hand, based on laboratory estimates of k_v, values of RR (probe) are 0.78×10^{-2}, 0.46×10^{-2} and 1.42×10^{-2} at depths 41.5, 52 and 67.5 ft, respectively.

Therefore, representative values of RR (probe) for the upper BBC seem to be similar to the lower BBC: approximately equal to 10^{-2} and generally in the range between 0.5×10^{-2}

to 2 x 10^{-2}. Swelling ratios for the upper BBC measured in CRSC tests give SR = 2.2 ($\pm$0.4) x 10^{-2} at an OCR = 5; and, SR = 1.6 ($\pm$0.6) x 10^{-2} at an OCR = 2. This provides added evidence that the selected values of k_h/k_v = 2 and CR = 0.15 are reasonable and the recompression of the clay around cones involves relatively "small" increments of effective stresses at the early stages of consolidation.

5.8 DISCUSSION OF PROBE DESIGNS

Table 5.2 describes the advantages and disadvantages of various conical pore pressure probes used by M.I.T. in four clay deposits. Important aspects in this evaluation are: (a) resolution for soil profiling, i.e., detection of small scale soil variability; (b) cost of manufacturing, maintaining (deairing and replacing porous elements) and operating the probe; (c) repeatability and scatter in dissipation results; (d) dissipation time required to achieve various levels of consolidation and to measure the static pore pressure, u_o; (e) reliability and degree of rationality in interpreting results; and, (f) special importance of results to foundation design and the interpretation of cone penetration resistance testing.

Table 5.2 shows that each type of probe provides some attractive features but no single design satisfies all requirements. In particular, some positive features for one

application can represent a disadvantage for another application. For example, the 18° - tip is believed to provide the best resolution for soil profiling, but leads to significant scatter in the pore pressure dissipation at early times.

Therefore, the choice of a probe type must be made after the objectives of the field investigation program have been defined and the most critical parameters clearly identified.

5.9 SUMMARY AND CONCLUSIONS

This chapter investigates the capability of simple linear dissipation solutions in predicting the coefficients of consolidation and permeability in Boston Blue Clay and evaluates the effect of various factors in order to achieve reliable and efficient methods for conducting and interpreting dissipation tests.

(1) Results of linear uncoupled consolidation analyses (Chap. 4), based on the initial distribution of excess pore pressures determined by the strain path method (Chap. 3), are compared to dissipation measurements in the soft (OCR < 2) Boston Blue Clay deposit below 60 ft at the Saugus site. The comparison (Figs. 5.11 and 5.12) indicates that reasonably good dissipation predictions are achieved at four locations on a 18° cone and at the tip of a 60° cone when the horizontal coefficient of consolidation c_h = 0.04 cm^2/sec. Additional results of this comparison show that:

1.1 At early dissipation stages ($\bar{u} \geq 0.8$), measurements fall in a wide band and hence lead to significant uncertainties (scatter) in estimating c_h. This is particularly true when the porous stone is located at the tip of the cone (Figs. 5.11a and 5.12).

1.2 At advanced consolidation stages ($\bar{u} < 0.6$, say) dissipation tends to proceed slower than predicted (Figs. 5.11b, c, d and 5.12). This is believed to result from soil nonlinearities and, in particular, the changes in the (drained) soil compressibility during consolidation.

1.3 The interpretation of dissipation results obtained when the porous stone is located at the tip of an 18° cone requires a semi-empirical procedure because of the difficulty of analyzing the actual cone geometry. In this procedure the degree of consolidation (or $\bar{u}$) is taken as the average of the predicted values at the apex and mid-height of an ideal cone (geometry).

1.4 Dissipation records obtained on the shaft behind an 18° cone plot in a narrow band but exhibit a slightly slower rate of dissipation than predicted (equivalent to a factor of about 2 in c_h, Figs. 5.11c and d). This could reflect inaccuracies in the initial distribution of excess pore pressures and/or nonlinear coupling effects and/or creep effects (neglected in the proposed prediction method) leading to faster dissipation ahead of the cone. More tests conducted (with the porous stone

located on the shaft) to high consolidation levels and tests involving measurements of total stresses on the cone and the shaft behind it are necessary before more definite conclusions can be reached.

(2) Based on these results, the recommended factors for estimating c_h (probe) from dissipation records are summarized (Table 5.1). Profiles of c_h (probe) in the BBC deposit at Saugus are then obtained at different dissipation levels for three types of conical probes: a) an 18° cone with the stone at the tip; b) an 18° cone with the stone at mid-height; and c) a 60° cone with the stone at the tip. Profiles of c_h (probe) are difficult and expensive to develop through other existing in situ and laboratory tests, and are essential for many geotechnical applications. The profiling analysis based on dissipation data indicates that:

2.1 At early dissipation stages ($\bar{u} \geq 0.8$) the scatter of the data is so high that reasonable c_h (probe) profiles cannot be established. The scatter is particularly high when the porous stone is located at the tip of the cone and less severe when the stone is at mid-height.

2.2 All three probes provide consistent c_h (probe) profiles after 50% consolidation ($\pm$10%) involving a very moderate degree of scatter.

2.3 Values of c_h estimated at high levels of consolidation ($\bar{u} = 0.2$) are slightly lower than obtained at 50% dissipation

in the clay below 45 ft.* and higher in the more pervious clay above 45 ft.

(3) The predicted profiles of c_h (probe) after 50% dissipation are then compared with laboratory and field measurements of the vertical coefficient of consolidation, c_v, in BBC (Fig. 5.29). This comparison indicates that:

3.1 The predicted variation of c_h (probe) with depth is consistent with the trends of c_v(NC) measured in the laboratory in the normally consolidated range and the profile of c_v (loading) backfigured by Duncan and by Davis and Poulos (MIT, 1975) on the basis of insitu pore pressure measurements conducted in the foundation clay under the I-95 embankment for a period of 7 years after construction.

3.2 The predicted magnitude of c_h (probe) is: a) very close to c_v (unloading) backfigured by Bromwell and Lambe (1968) on the basis of in situ pore pressure measurements in a very similar BBC deposit due to a wide excation; and, b) much higher (20 to 40 times) than c_v(NC) or c_v (loading) described above.

3.3 Profiles of c_h (probe) can therefore provide good estimates of the coefficient of consolidation to be used in foundation problems involving unloading and possibly reloading of overconsolidated clays above the maximum past pressure. On the other hand, problems involving the compression of clays

---

*Having an OCR < 3 and for which the initial pore pressure distribution, estimated by the strain path method, proved satisfactory (Chap. 8).

in the normally consolidated range require modification of c_h (probe) to account for the difference in clay compressibility during dissipation [as expressed by RR (probe)] and the compression ratio, CR, in the normally consolidated range.

(4) An approximate method for estimating profiles of the horizontal coefficient of permeability k_h (probe) and c_v(NC) from profiles of c_h (probe) is proposed. In spite of significant simplifying assumptions, the predicted profiles of k_h (probe) and c_v(NC) appear very reasonable when compared to laboratory data.

(5) The backfigured compressibility of BBC during dissipation is approximately given by RR (probe) $\approx 10^{-2}$. This confirms that, as expected, the clay in the early stages of dissipation around cones ($\bar{u} > 0.5$) consolidates under relatively "small" increments of effective stresses such that the maximum past pressure is not exceeded.

(6) Finally, a comparison of the advantages of different types of probes (Table 5.2) indicates that the choice of a probe (cone angle and location of porous stone) for a particular job can only be made after the objectives of the investigation program have been defined and the most critical parameters clearly identified.

% Dissipation	$\bar{u}$	Cone Angle - Stone Location					
		18° Tip		18° Mid-cone		60° Tip	
		T*	R^2T^{**} (cm^2)	T*	R^2T^{**} (cm^2)	T*	R^2T^{**} (cm^2)
20	0.8	0.16	0.58	0.52	1.89	0.44	1.60
40	0.6	1.35	4.90	2.6	9.44	1.9	6.90
50	0.5	3.0	10.9	4.7	17.1	3.65	13.2
60	0.4	6.0	21.8	8.2	29.8	6.5	23.6
80	0.2	30.0	109	34	123	27	98

* $T = c_h\, t/R^2$

** R = 0.75 in = 1.91 cm for M.I.T. probes

Table 5.1 Recommended Time Factors for Predicting the Horizontal Coefficient of Consolidation from Dissipation Records

PIEZOMETER TYPE	ADVANTAGES	DISADVANTAGES
18 TIP°	-Very sensitive to local soil variability hence, very good for soil profiling -Fast dissipation hence economical to operate, especially to evaluate the in situ static pore pressures -Inexpensive design	-Stone exposed to bending damage by gravels and other obstructions -Large scatter in dissipation curves at early times and significant scatter at later times -Geometry difficult to include in theoretical analyses hence requires semi-empirical interpretation
60° TIP	-Little scatter in c_h when matching done at intermediate times ($t_{40} < t < t_{60}$, say) -Fast dissipation -Inexpensive design -Rational interpretation despite geometry -Provides insight into penetration mechanisms with dutch cone (same cone angle)	-Stone exposed to bending damage -Large scatter in dissipation curves at early times hence requires at least 40% dissipation to determine c_h.
18° Mid-Height	-Reasonable dissipation time -Reasonable scatter in dissipation curves even at early times -Rational theoretical predictions -Stone well protected from structural damages	-More expensive design (need special porous elements) -Porous stone is easily smeared during penetration in granular materials
18° or 60° With Stone on Shaft	-Close simulation of pile installation hence, useful in pile design -Very little scatter in dissipation curves -Easier to interpret -Appears to provide estimates of c_h closer to normally consolidated values -Excellent protection for the porous stone	-Very long dissipation time (i.e., expensive to operate) -Not very sensitive to small scale soil variability (i.e., tendency to average out pore pressure) -More difficult to keep the stone well drained -More expensive design

NOTES: The conclusions in this table are based on M.I.T. experience in three clay deposits. Different probe designs and/or procedures in other clays might lead to different conclusions.

Table 5.2 Evaluation of different probe designs

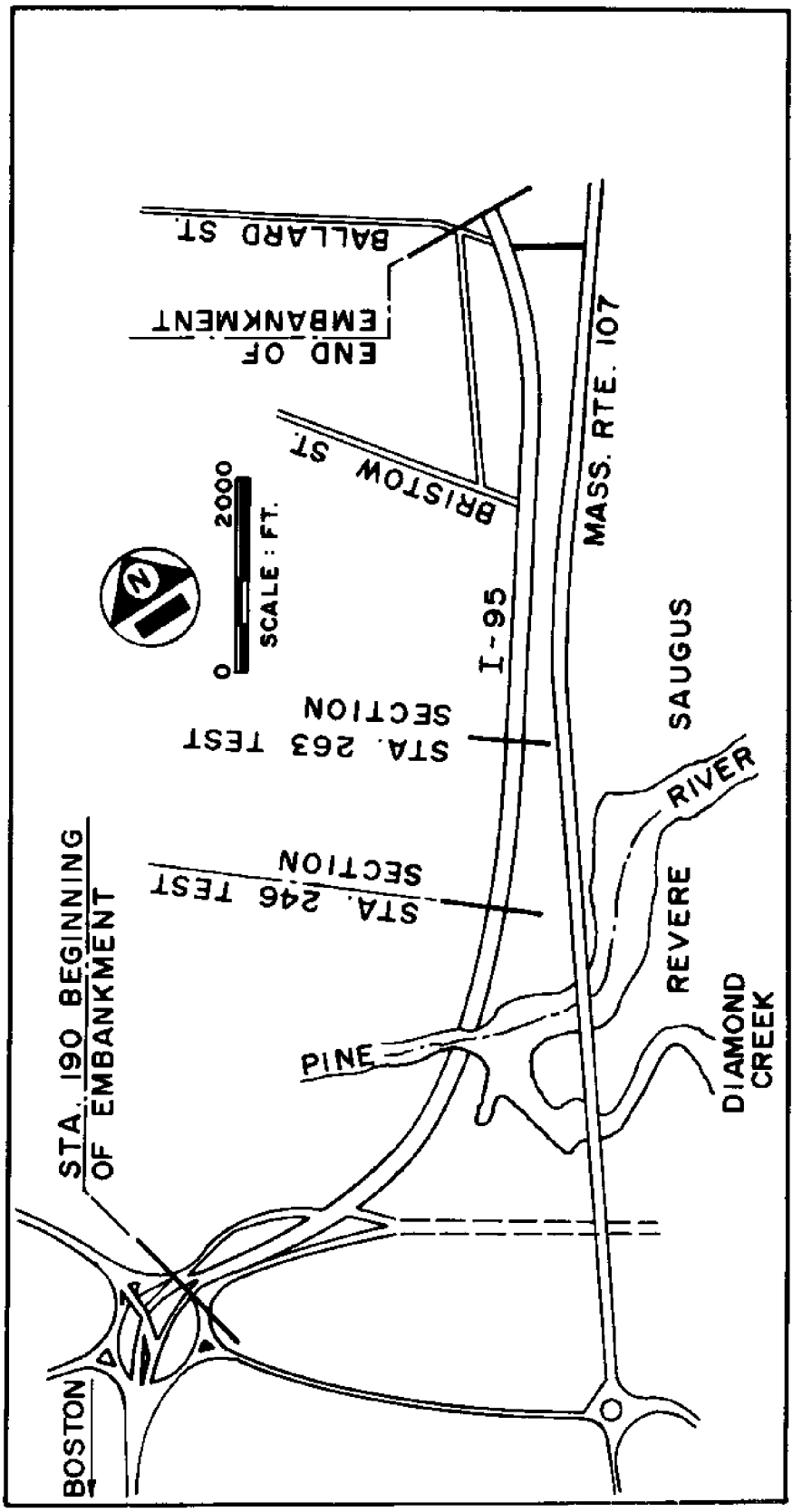

Fig. 5.1 Location map of Saugus I-95 embankment (after Lacasse et al., 1978)

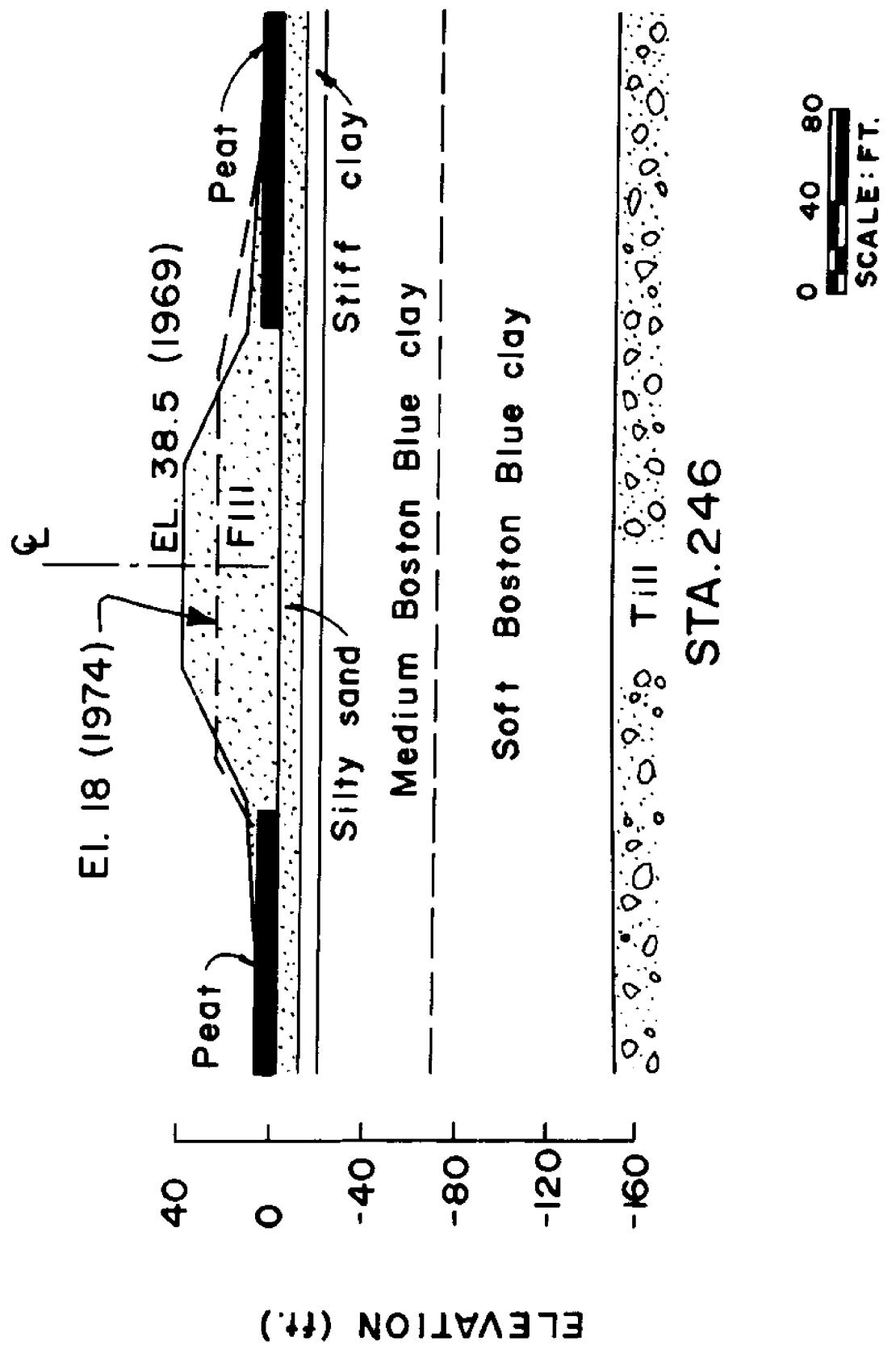

Fig. 5.2 Cross section of Station 246 at Saugus I-95 embankment (after Lacasse et al., 1978)

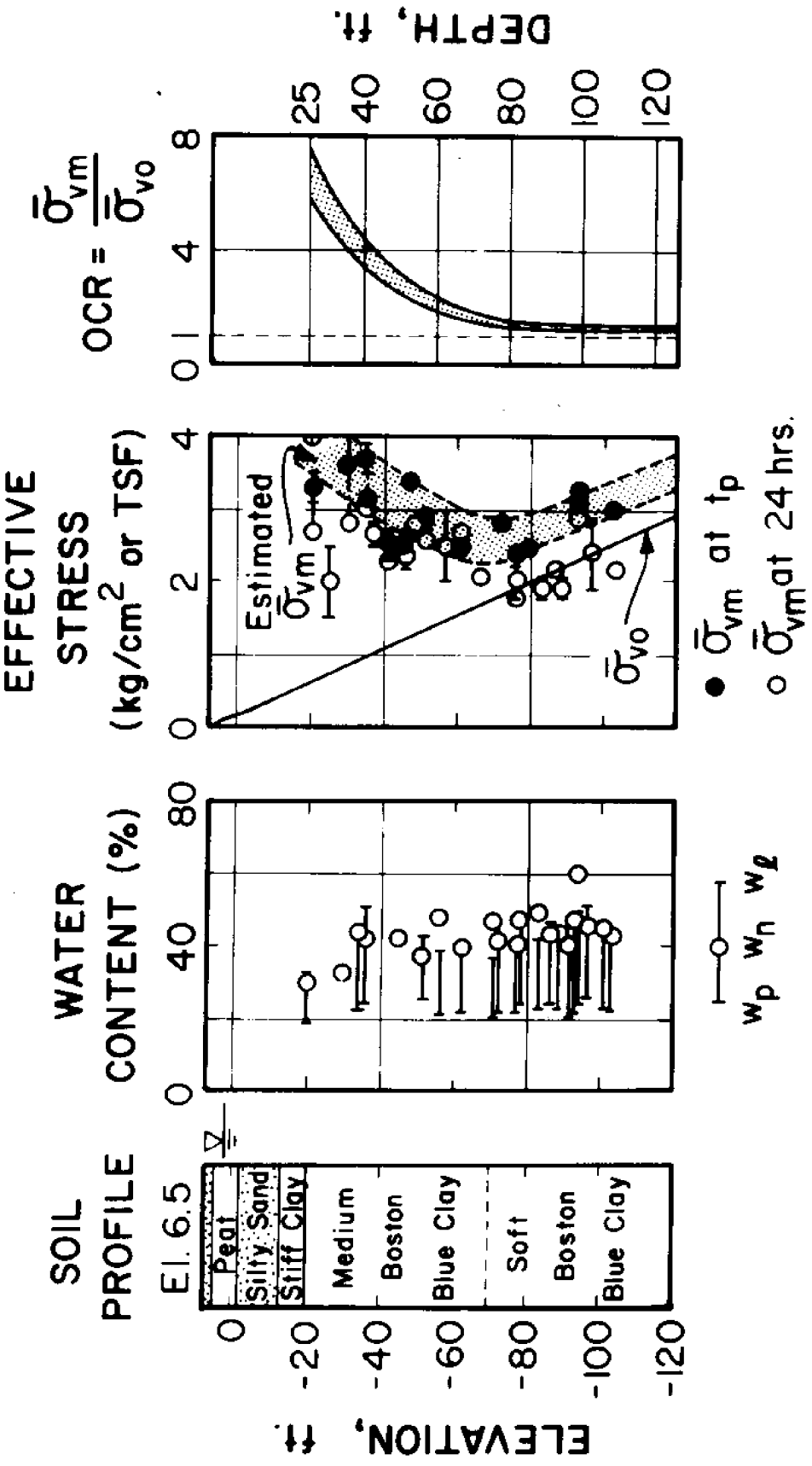

Fig. 5.3 Soil profile, index properties and stress history at the Saugus site (from BOSS 79)

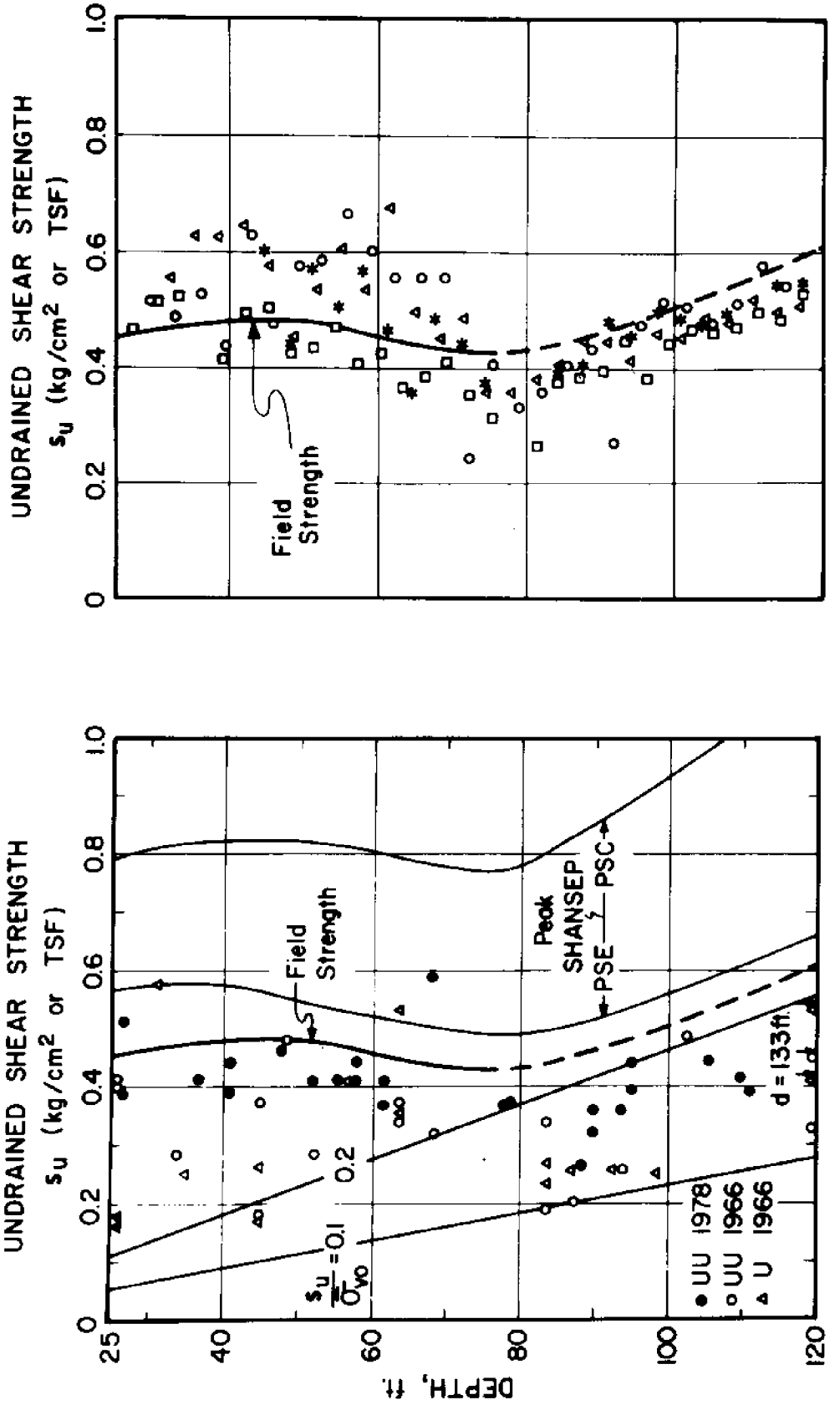

a) Laboratory tests

b) Field vane strength

Fig. 5.4 Undrained shear strengths at the Saugus site (from BOSS 79)

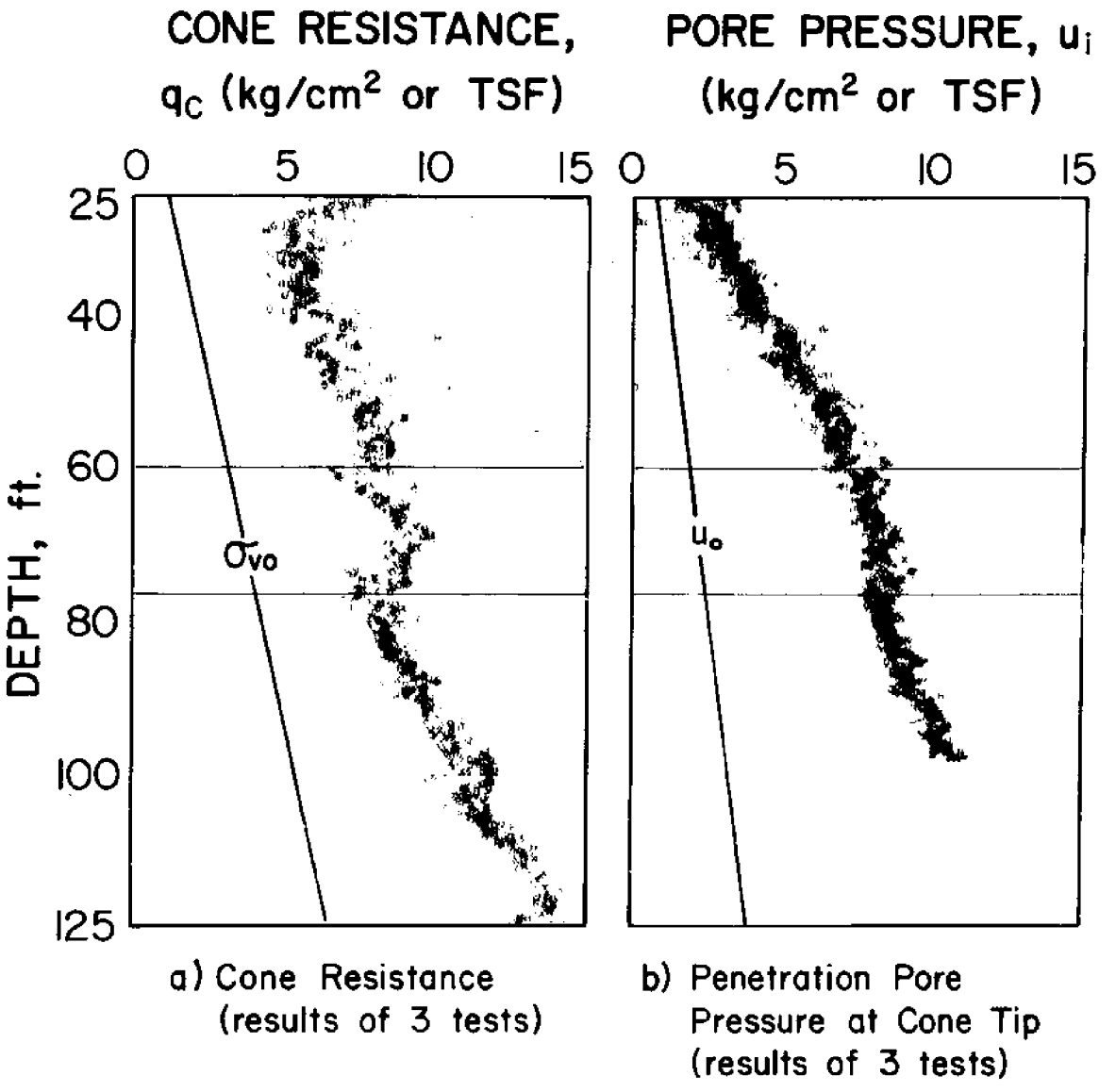

Fig. 5.5 - Cone resistance and penetration pore pressures at the Saugus site

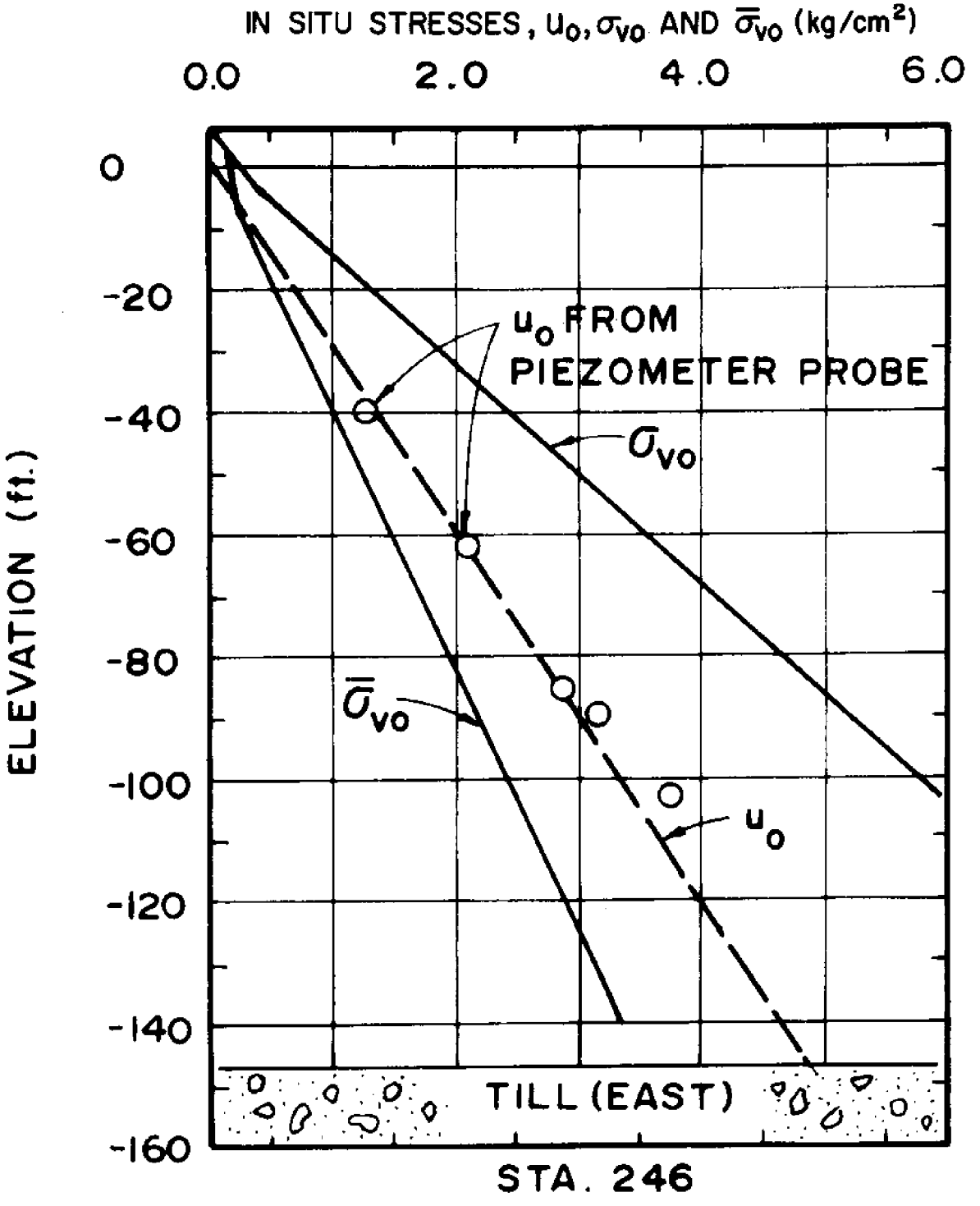

Fig. 5.6 In Situ Stresses at the Saugus site (after Ladd et al., 1979)

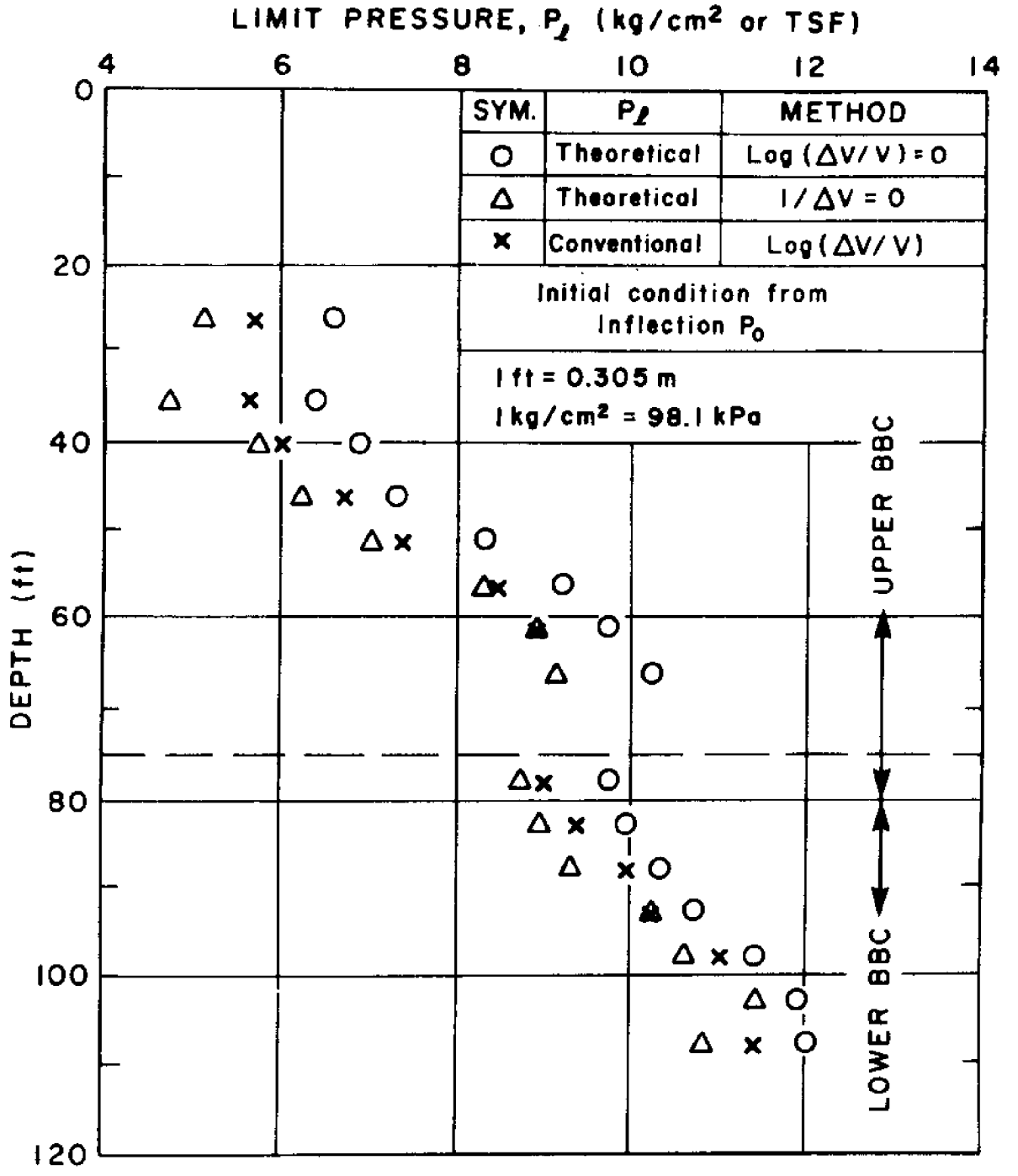

Fig. 5.7 Limit Pressure Measurements at the Saugus Site

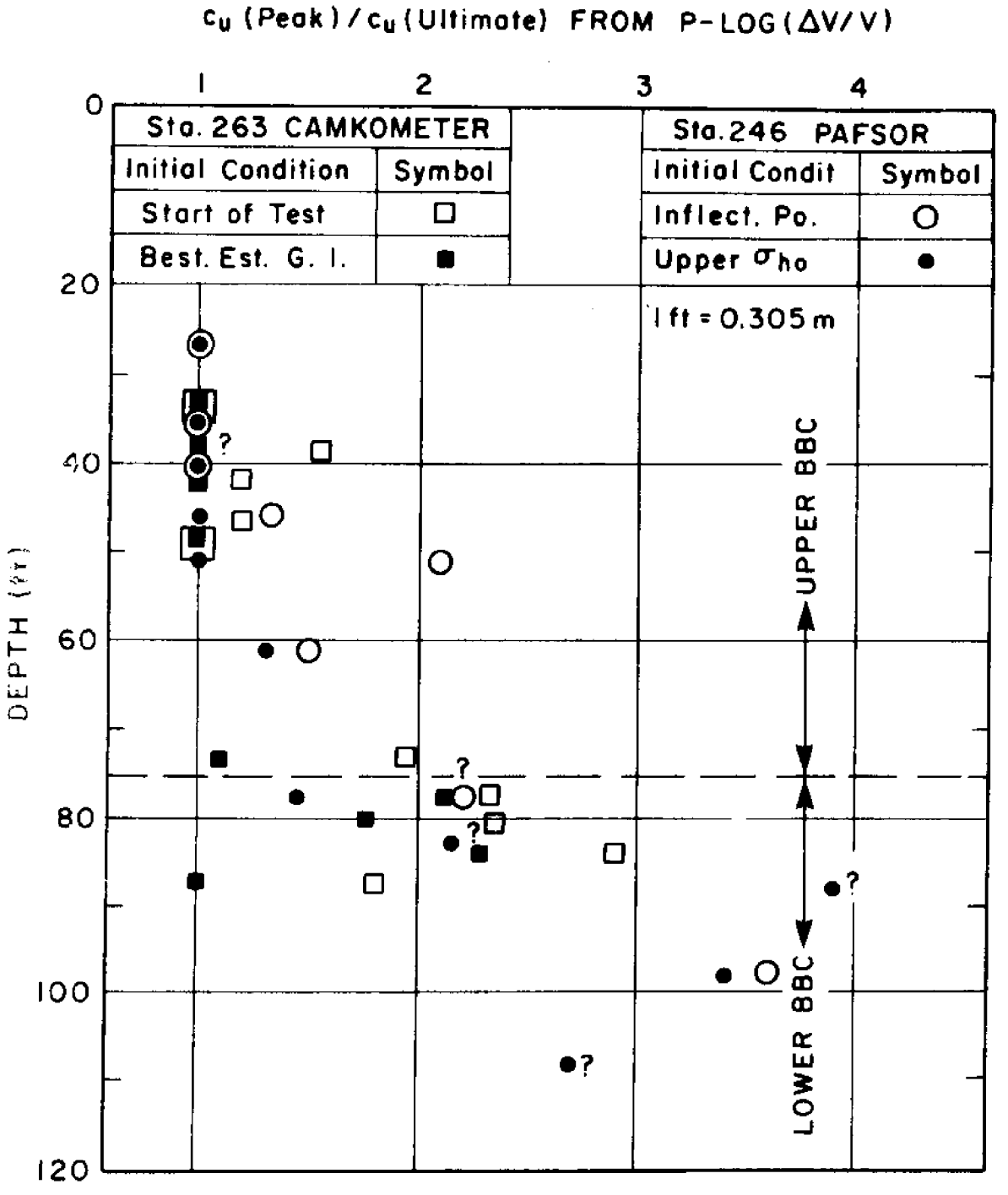

Fig. 5.8 Ratio of Peak to Ultimate Strengths Measured by Pressuremeter at the Saugus Site

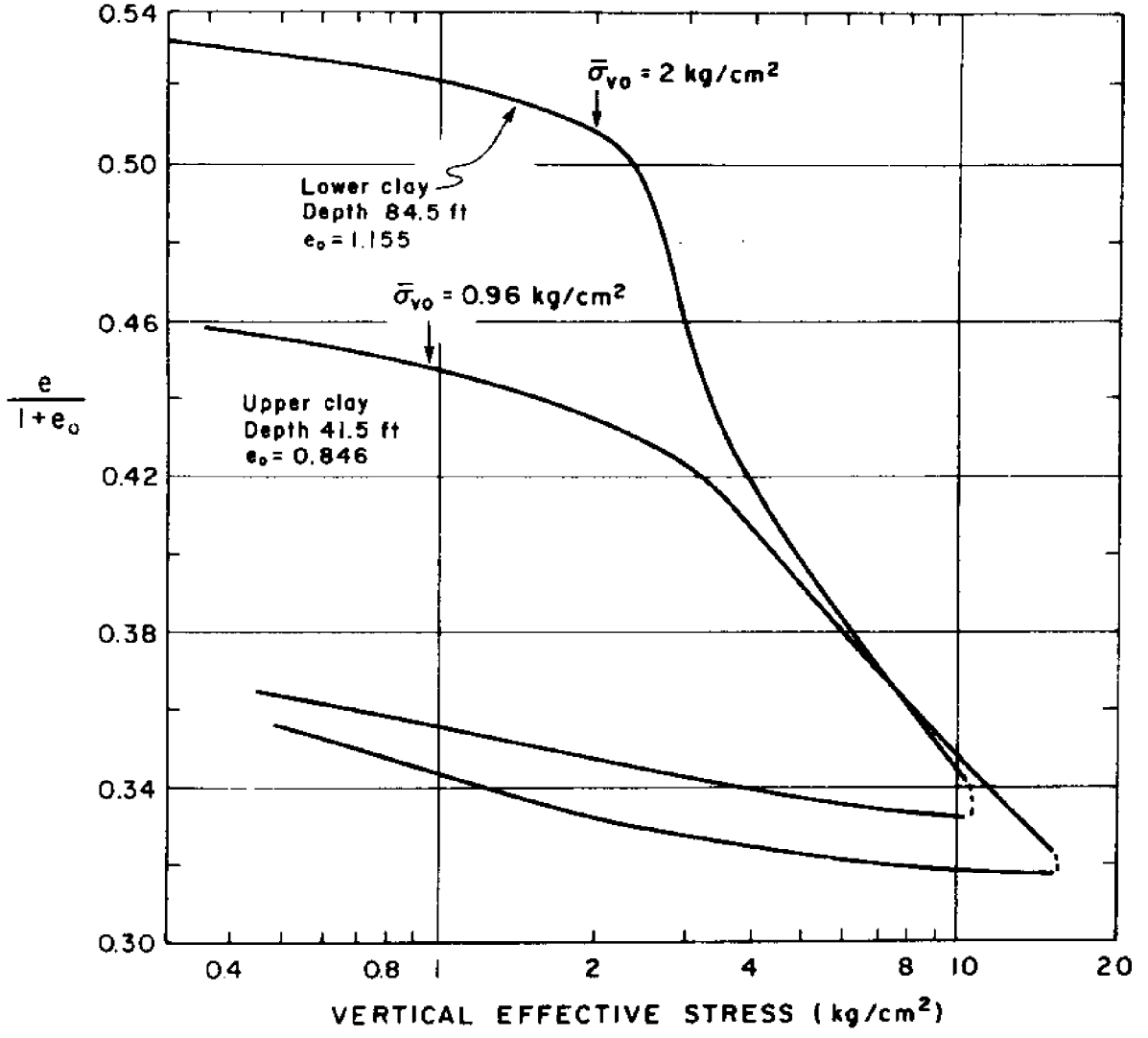

Fig. 5.9 Typical Compressibility of the Upper and Lower Boston Blue Clay at the Saugus Site (CRSC tests)

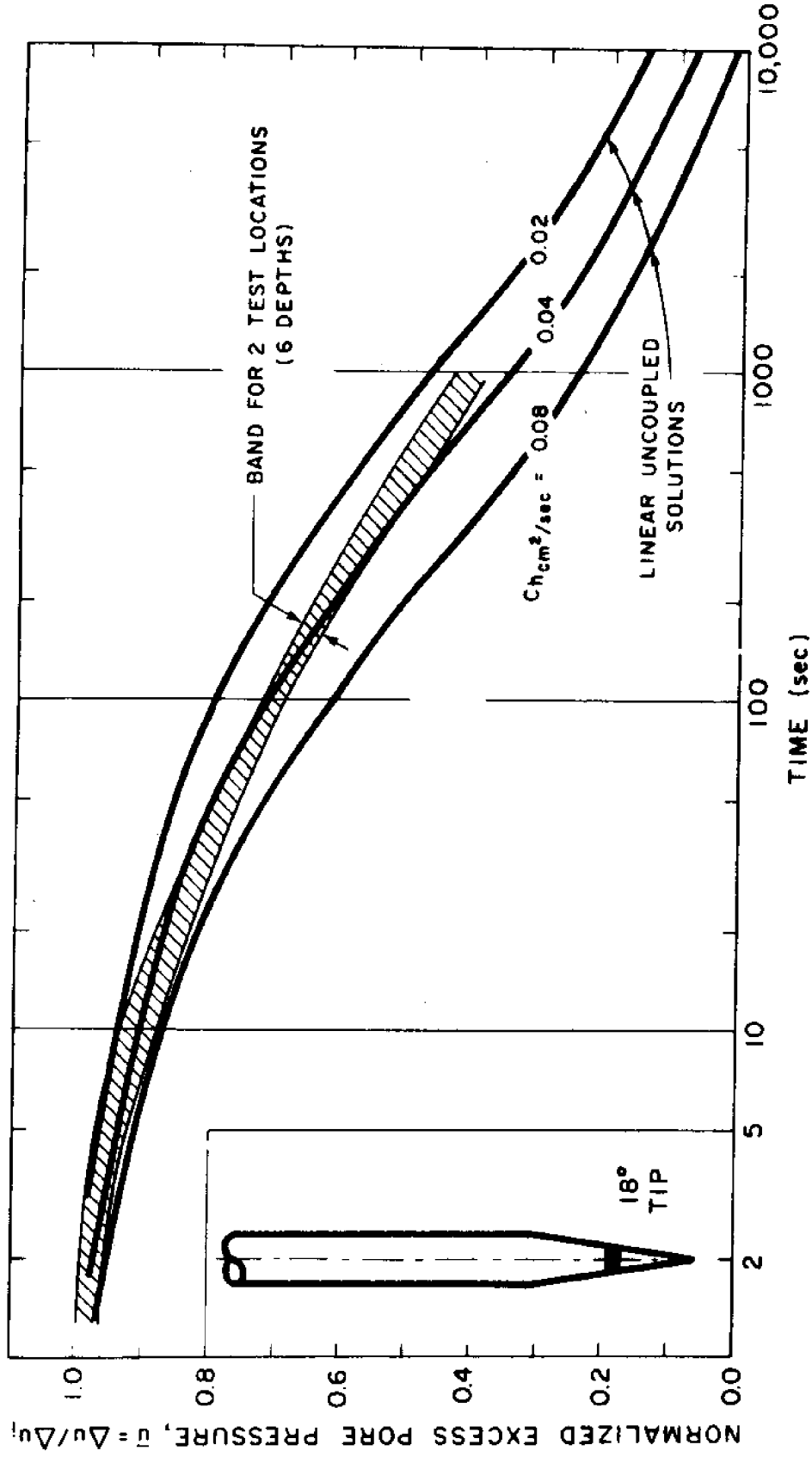

Fig. 5.10 Predicted vs Measured Dissipation Curves at Mid-Height of an 18° Conical Probe Below 60 ft at the Saugus Site

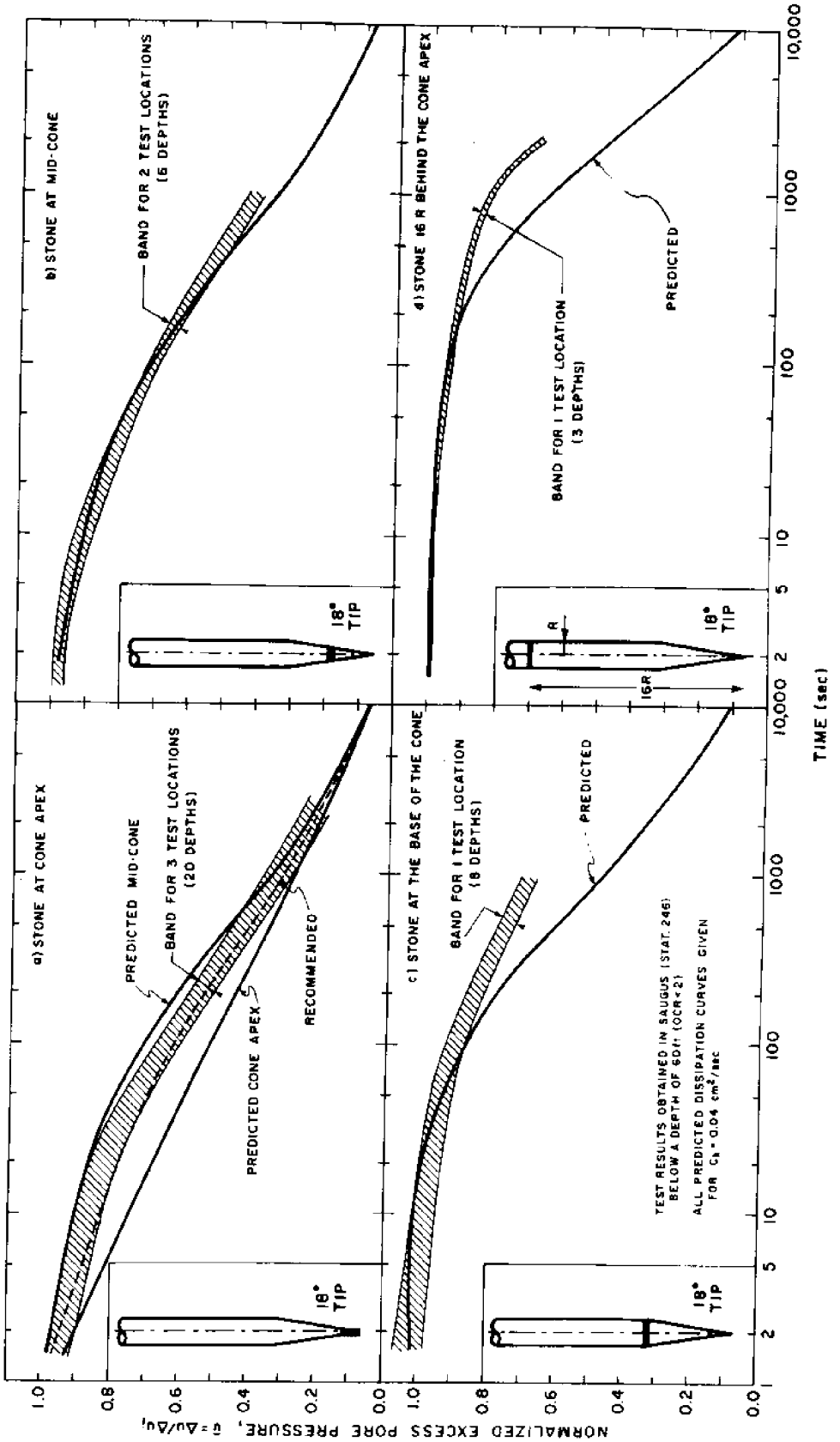

Fig. 5.11 Evaluation of Linear Uncoupled Dissipation Predictions for an 18° Conical Probe in Boston Blue Clay (OCR<2)

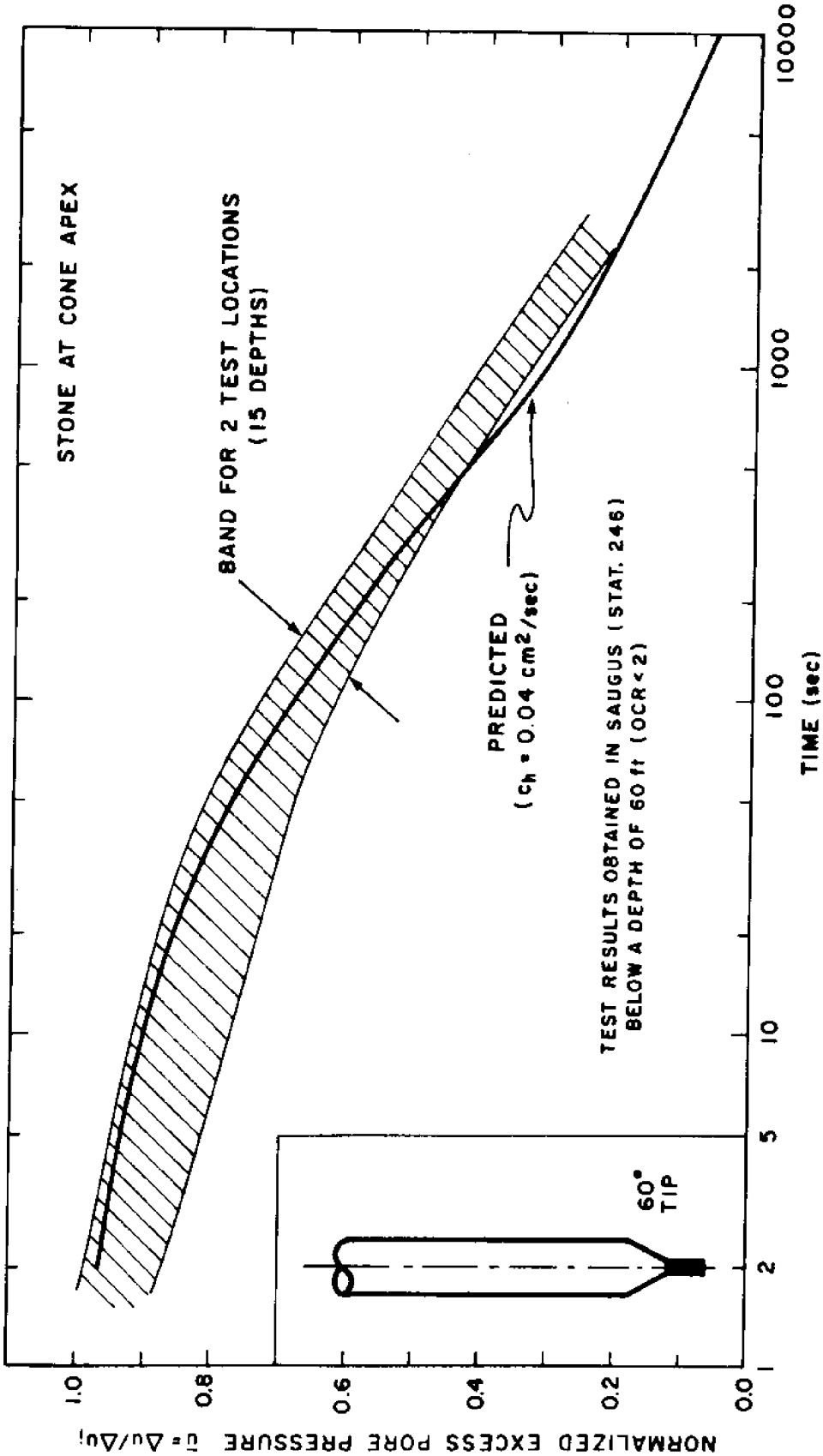

Fig. 5.12 Evaluation of Linear Uncoupled Dissipation Predictions for a 60° Conical Probe in Boston Blue Clay (OCR<2)

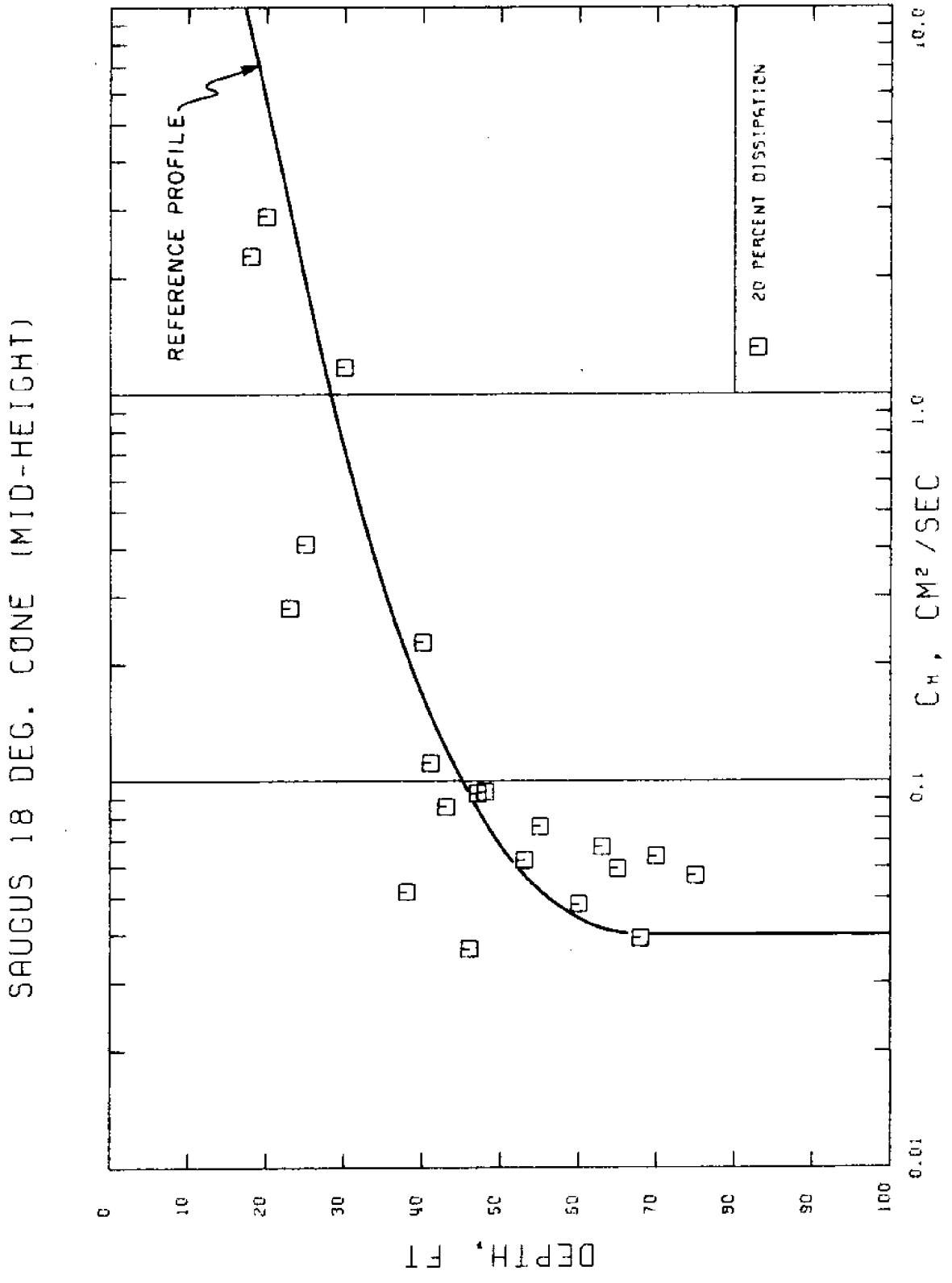

Fig. 5.13 Predicted Profile of c_h in BBC (Saugus, Station 246) 18° Mid-Height, 20% Dissipation

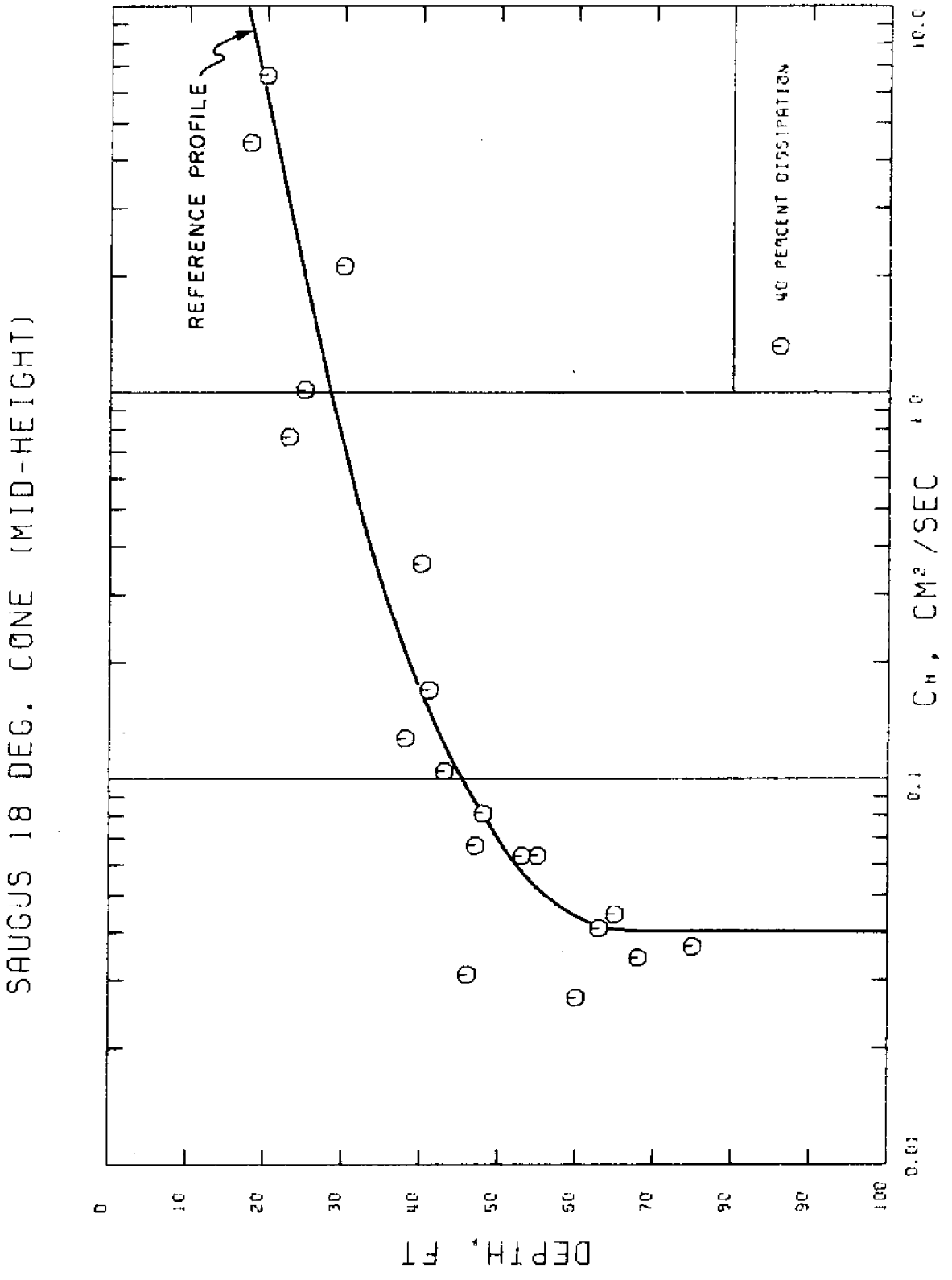

Fig. 5.14 Predicted Profile of c_h in BBC (Saugus, Stat. 246): 18° Mid-Height, 40% Dissipation

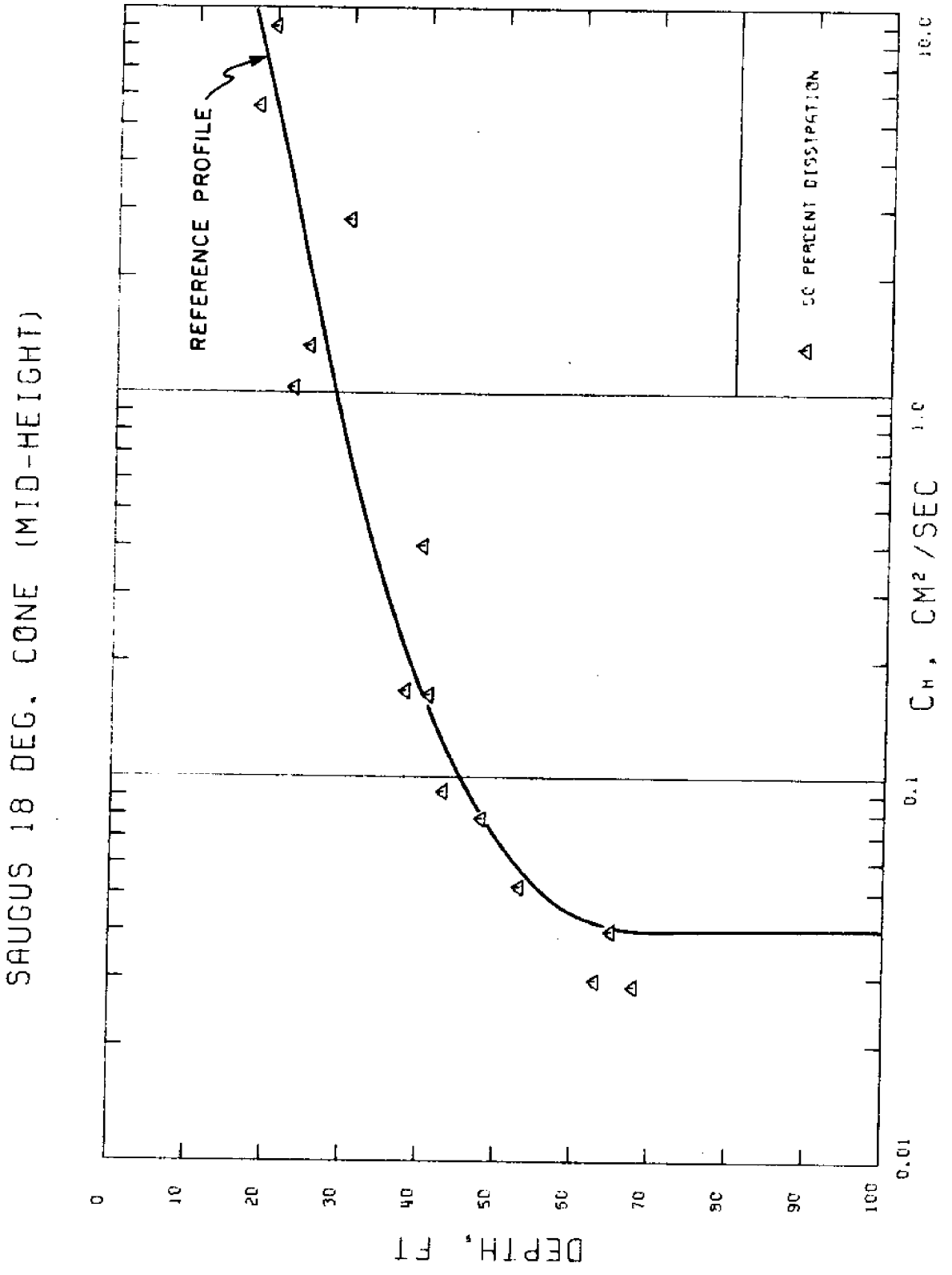

Fig. 5.15 Predicted Profile of c_h in BBC (Saugus Stat. 246): 18° Mid-Height, 50% Dissipation

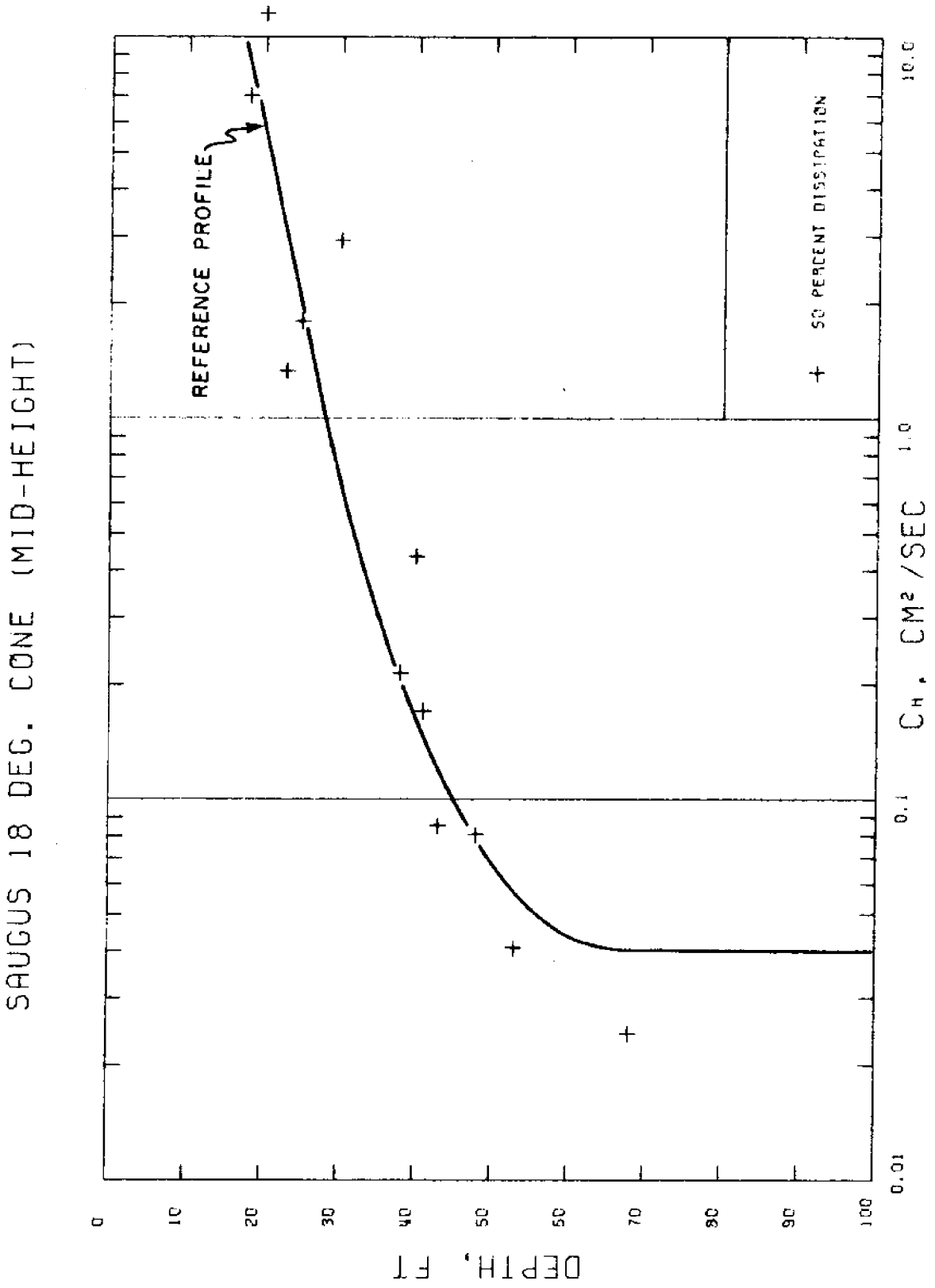

Fig. 5.16 Predicted Profile of c_h in BBC (Saugus, Stat. 246): 18° Mid-Height, 60% Dissipation

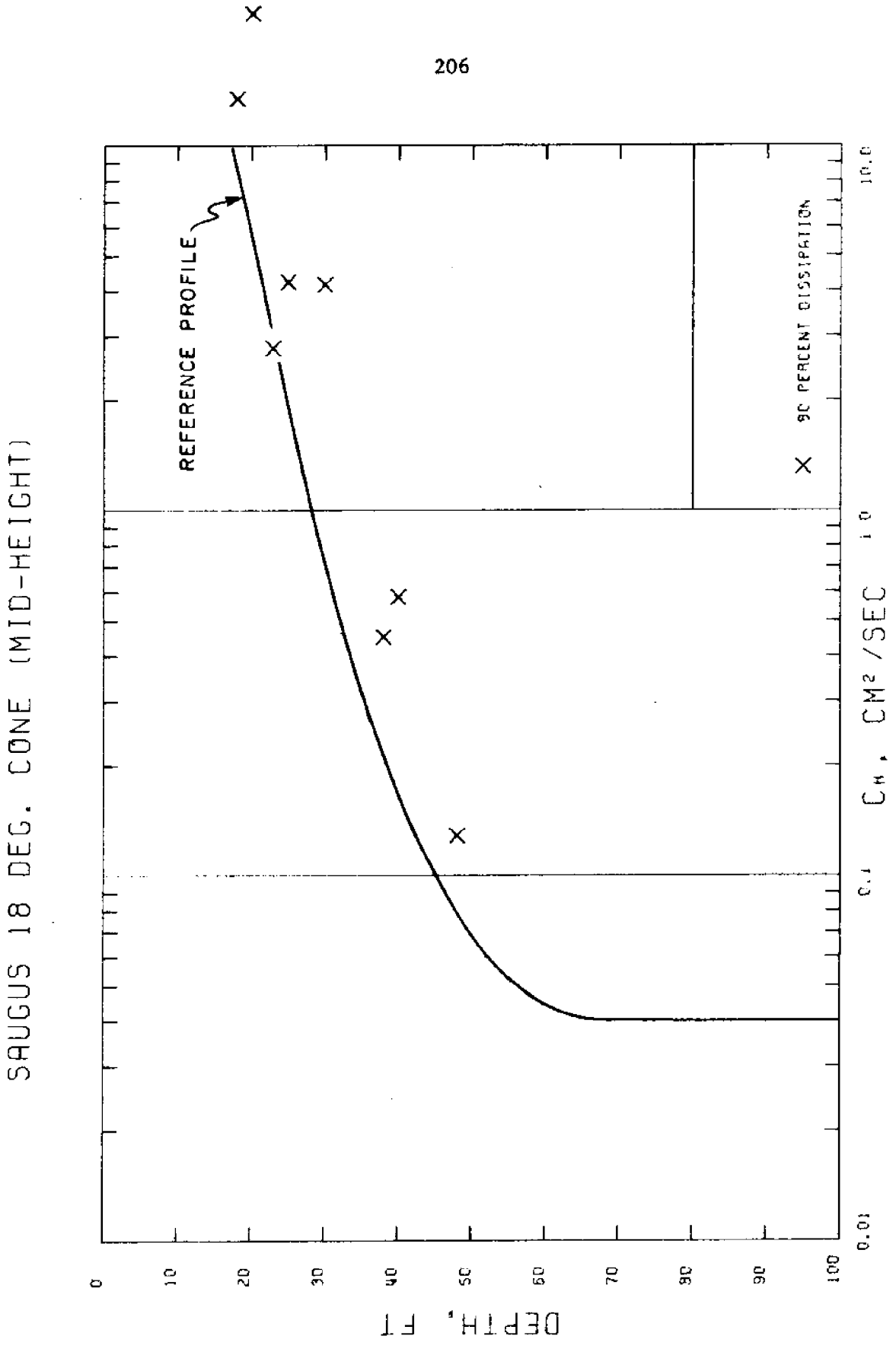

Fig. 5.17 Predicted Profile of c_h in BBC (Saugus, Stat. 246): 18° Mid-Height, 80% Dissipation

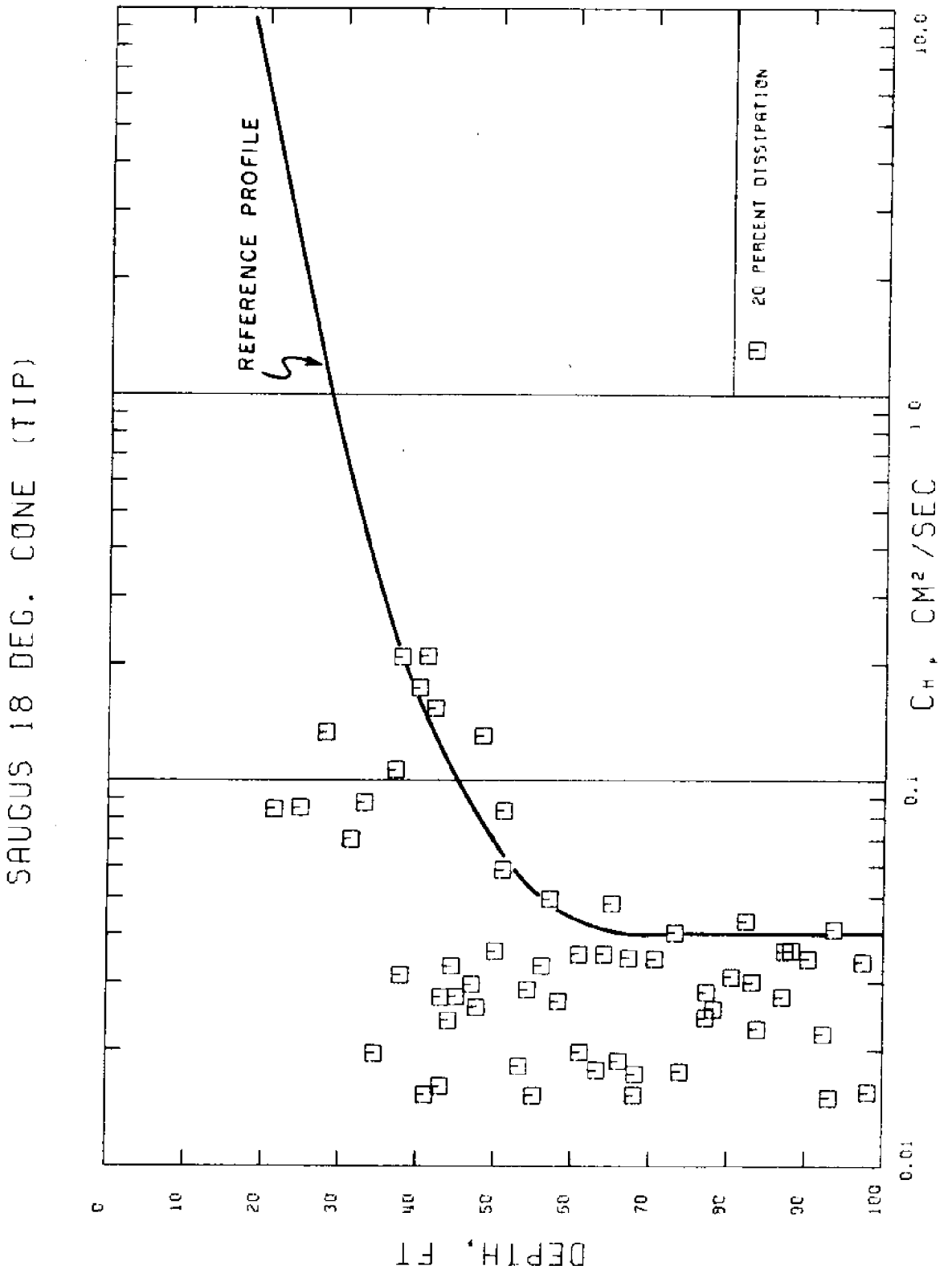

Fig. 5.18 Predicted Profile of c_h in BBC (Saugus, Stat. 246): 18° tip; 20% dissipation

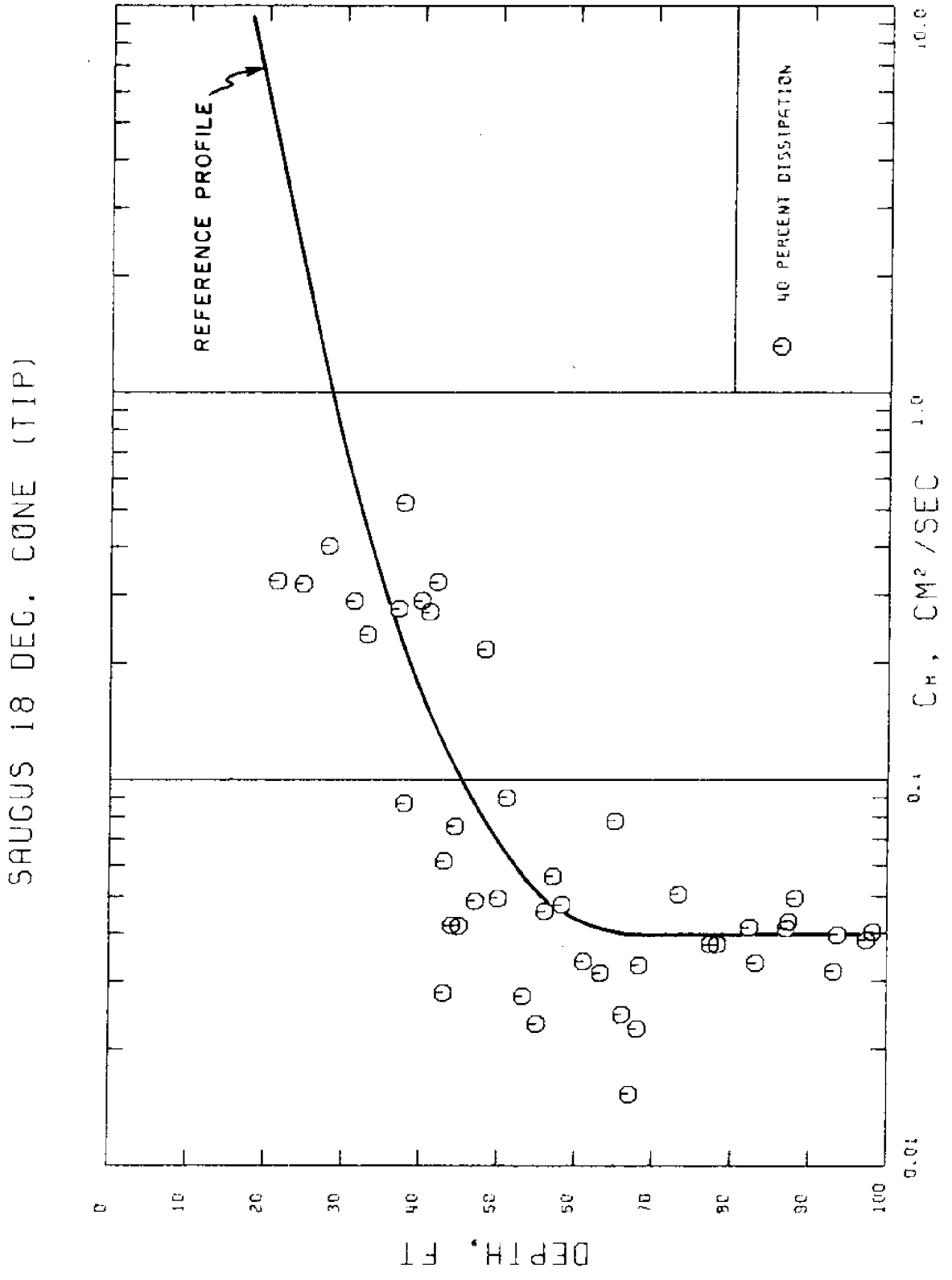

Fig. 5.19 Predicted Profile of c_h in BBC (Saugus, Stat. 246): 18° tip, 40% dissipation

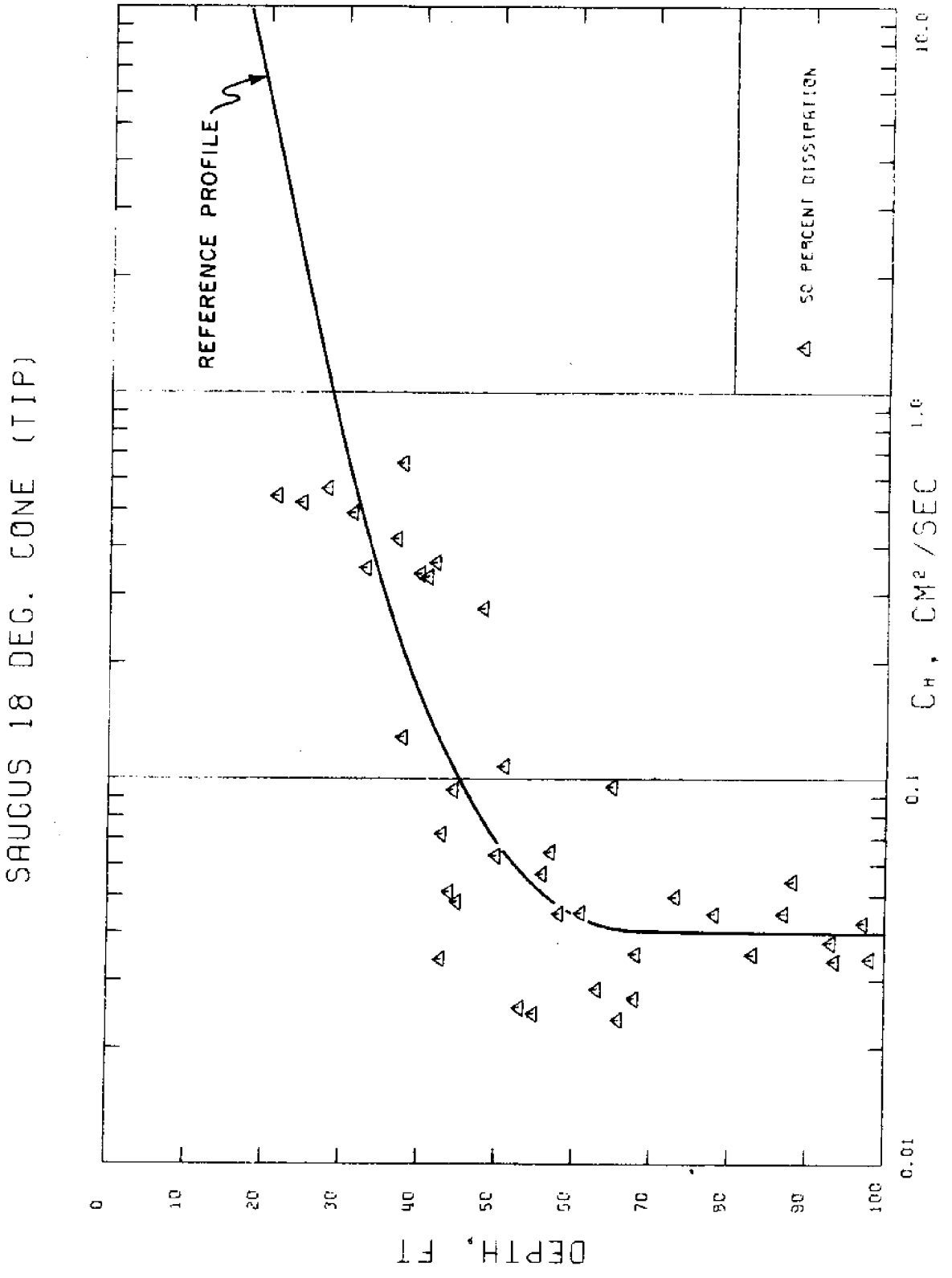

Fig. 5.20 Predicted Profile of c_h in BBC (Saugus Stat. 246): 18° tip; 50% dissipation

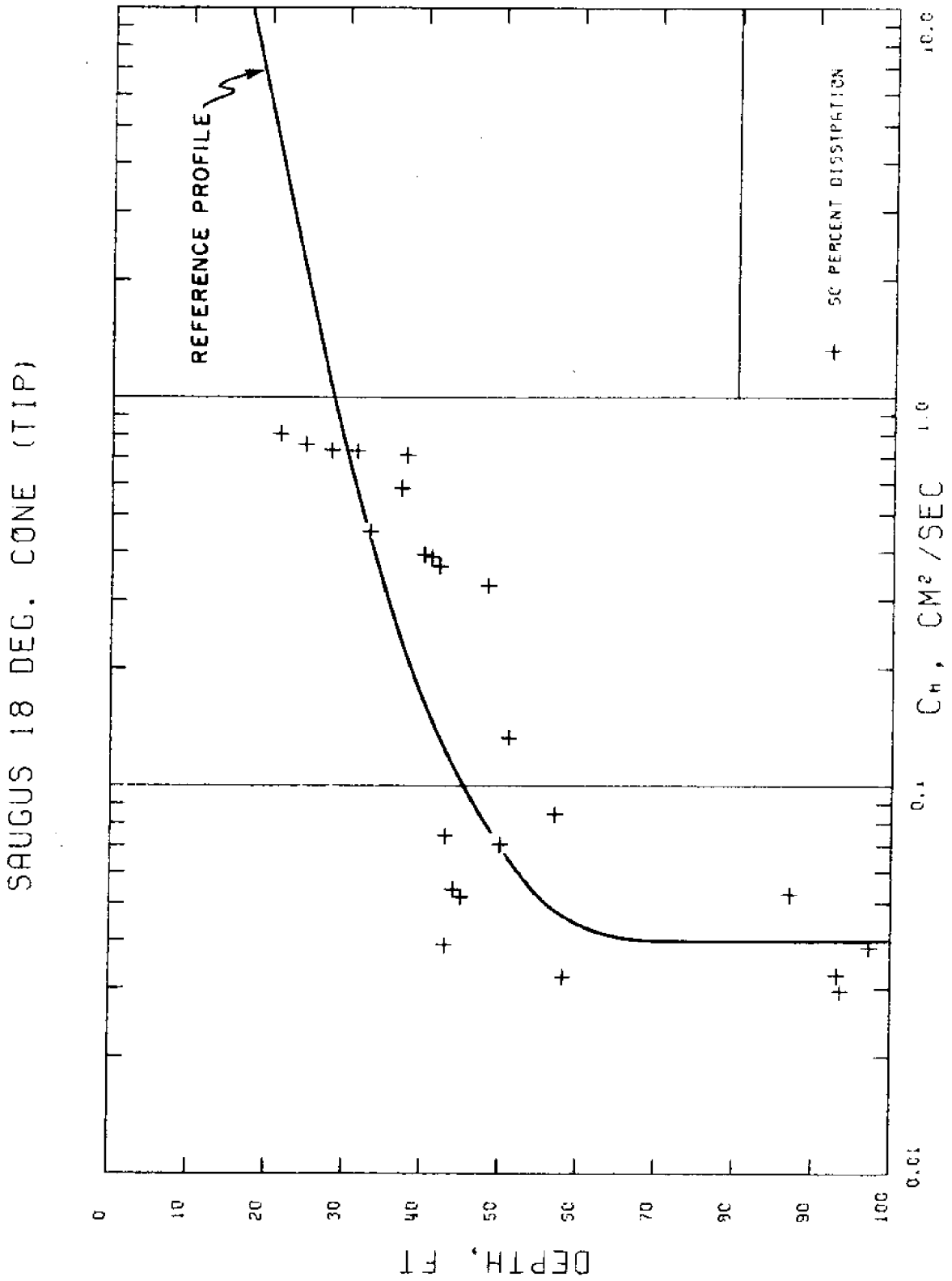

Fig. 5.21 Predicted Profile of c_h in BBC (Saugus, Stat. 246): 18° tip, 60% dissipation

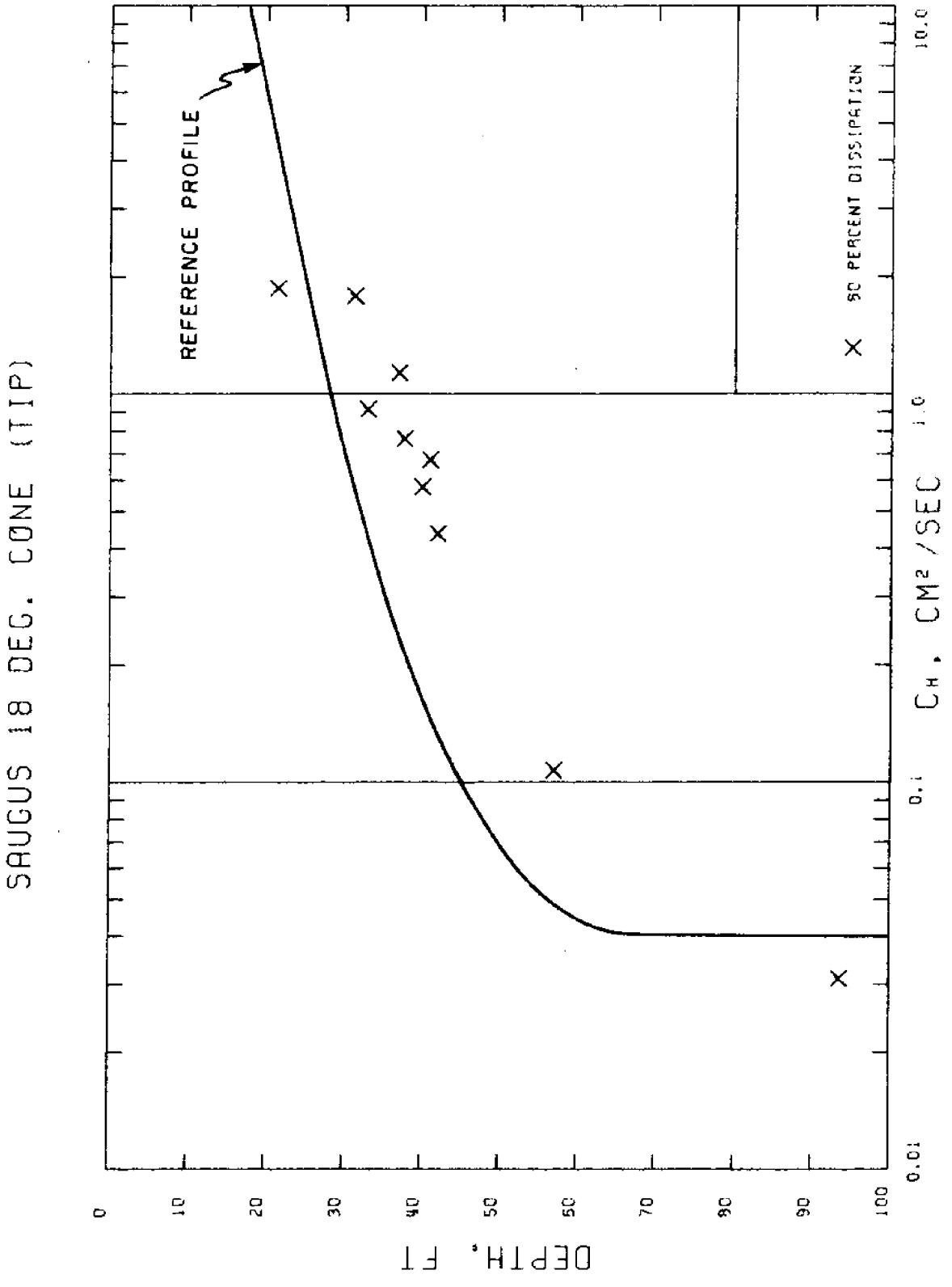

Fig. 5.22 Predicted Profile of c_h in BBC (Saugus Stat. 246): 18° tip, 80% dissipation

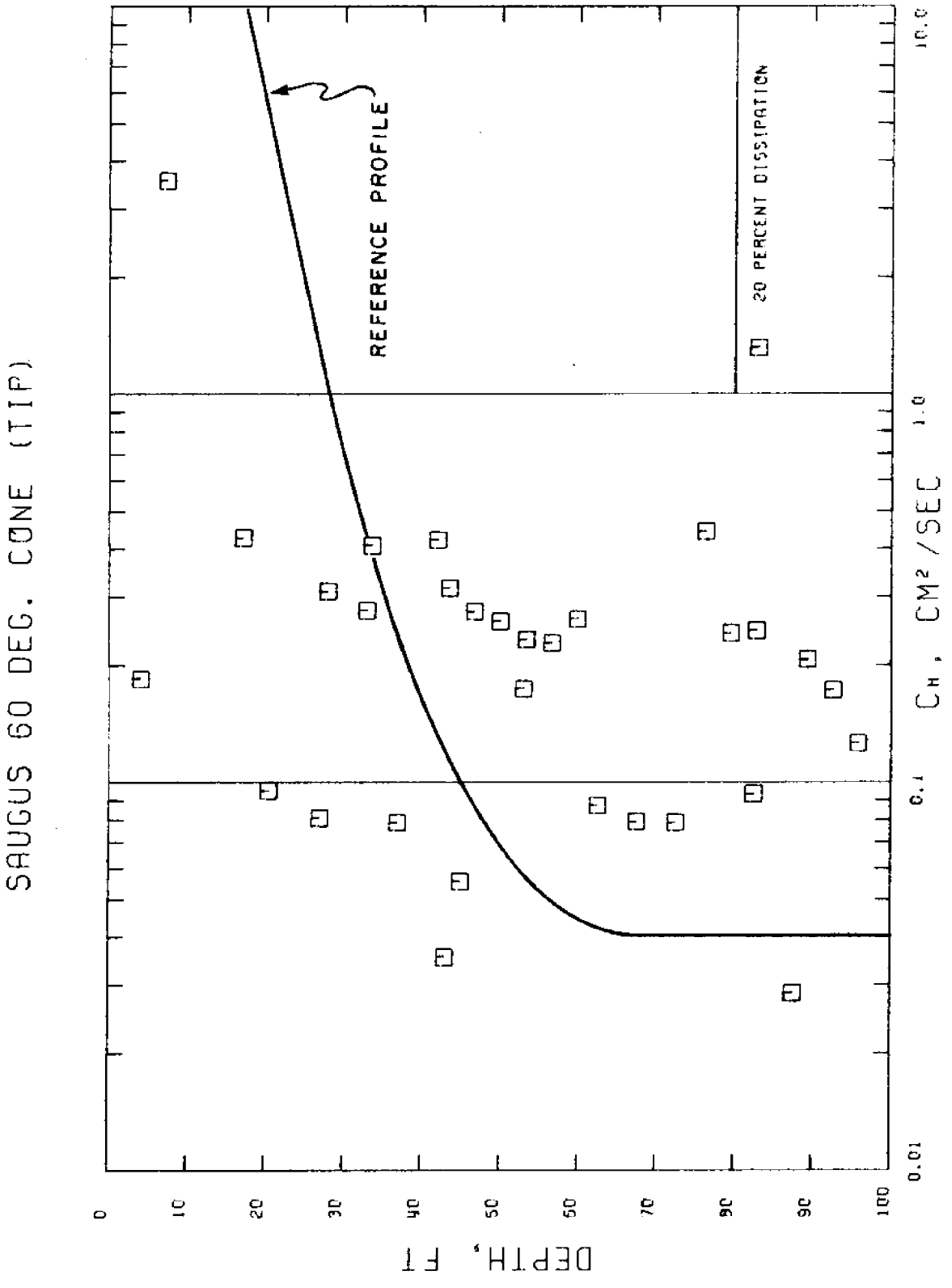

Fig. 5.23 Predicted Profile of c_h in BBC (Saugus, Stat. 246): 60° tip, 20% dissipation

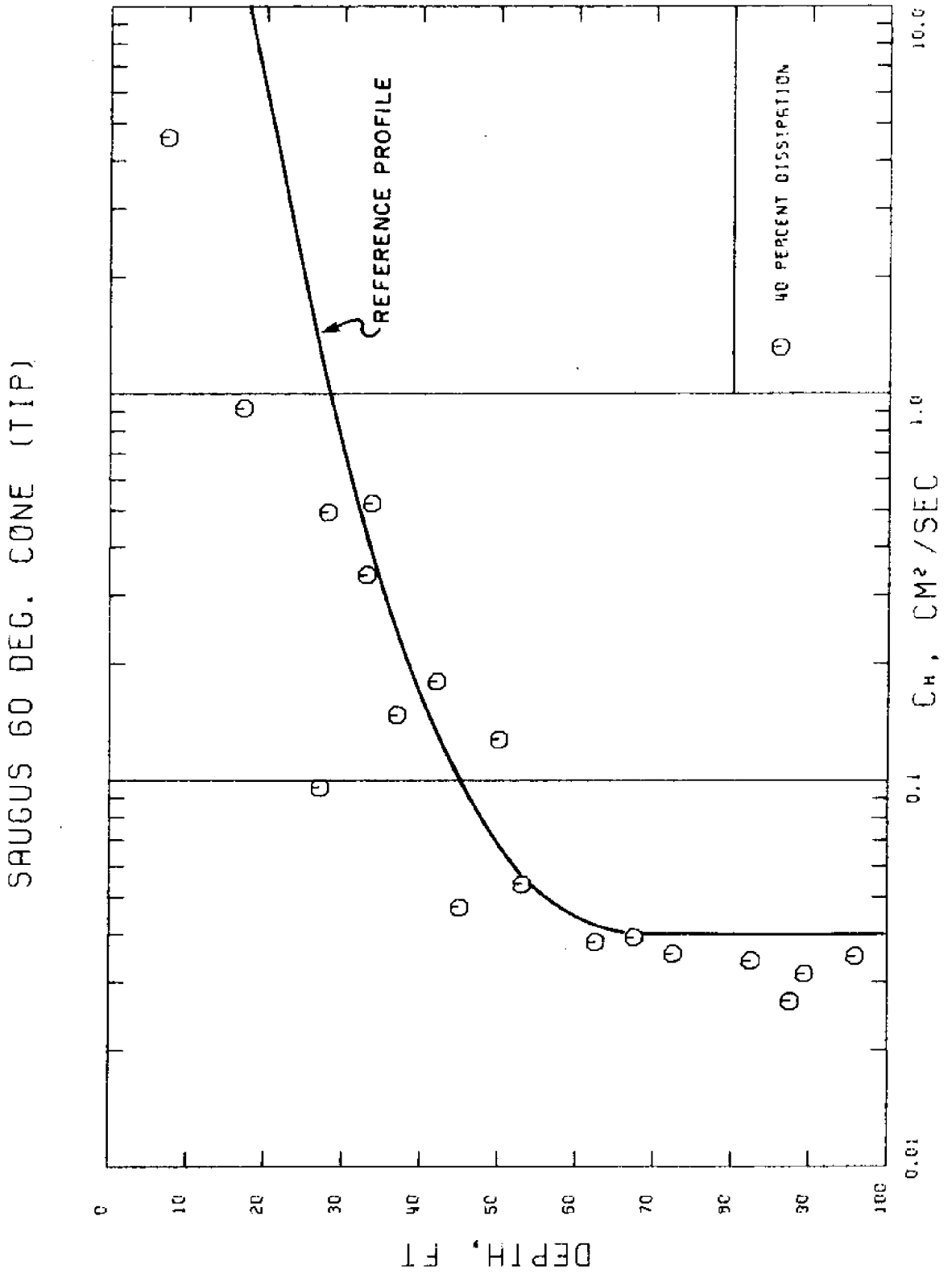

Fig. 5.24 Predicted Profile of c_h in BBC (Saugus, Stat. 246): 60° tip, 40% Dissipation

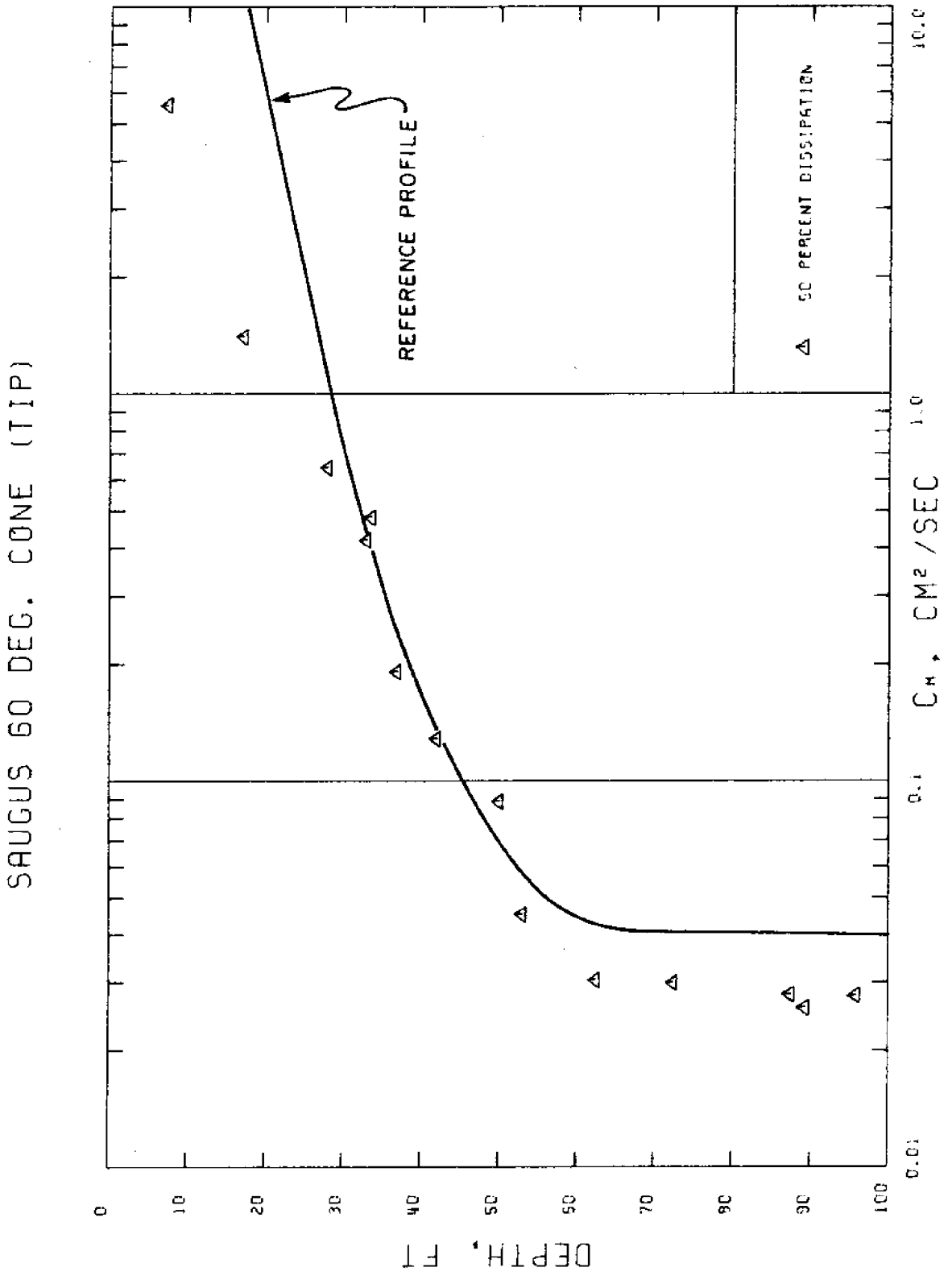

Fig. 5.25 Predicted Profile of c_h in BBC (Saugus, Stat. 246): 60° tip, 50% dissipation

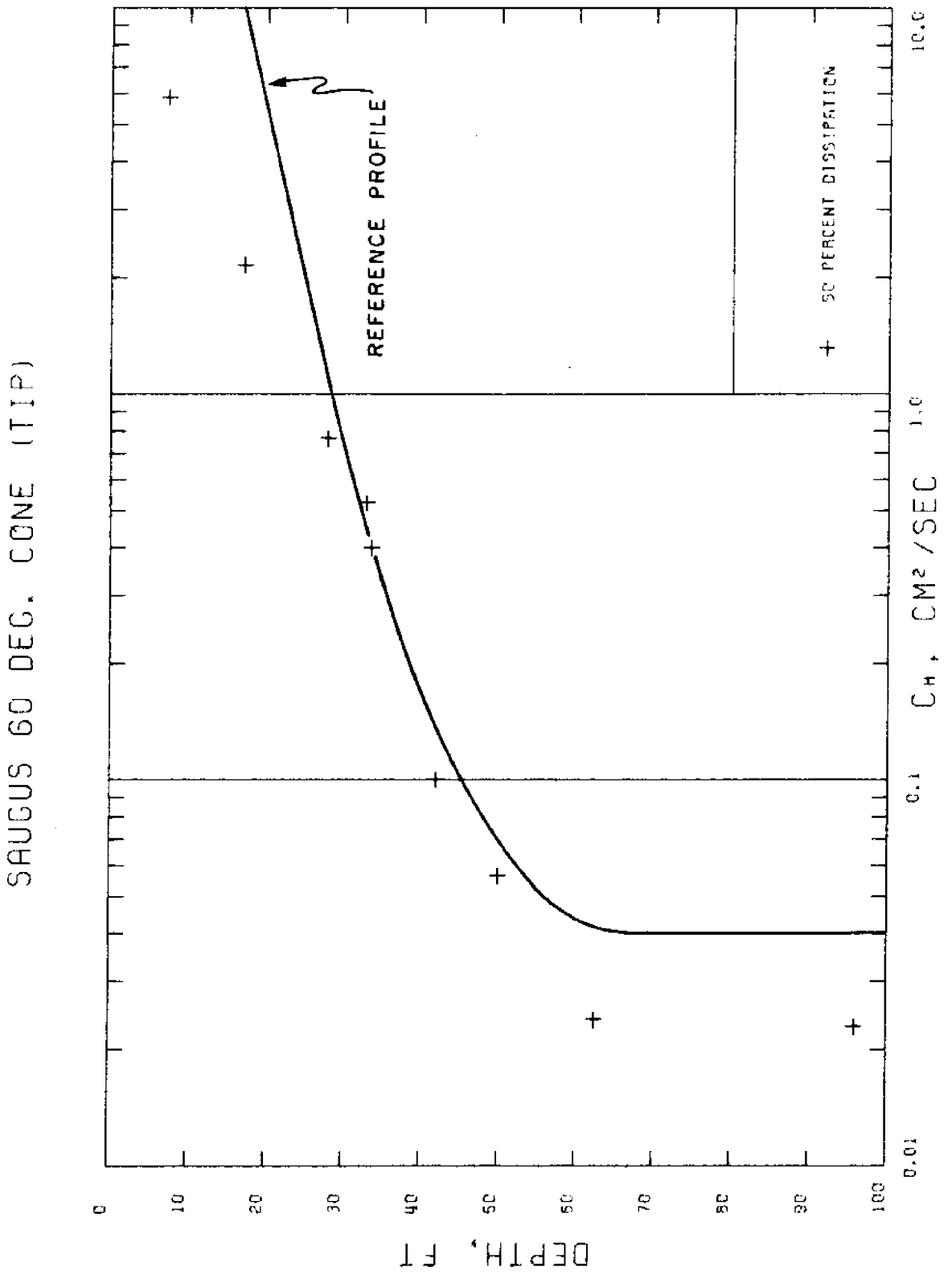

Fig. 5.26 Predicted Profile of c_h in BBC (Saugus, Stat. 246): 60° tip, 60% dissipation

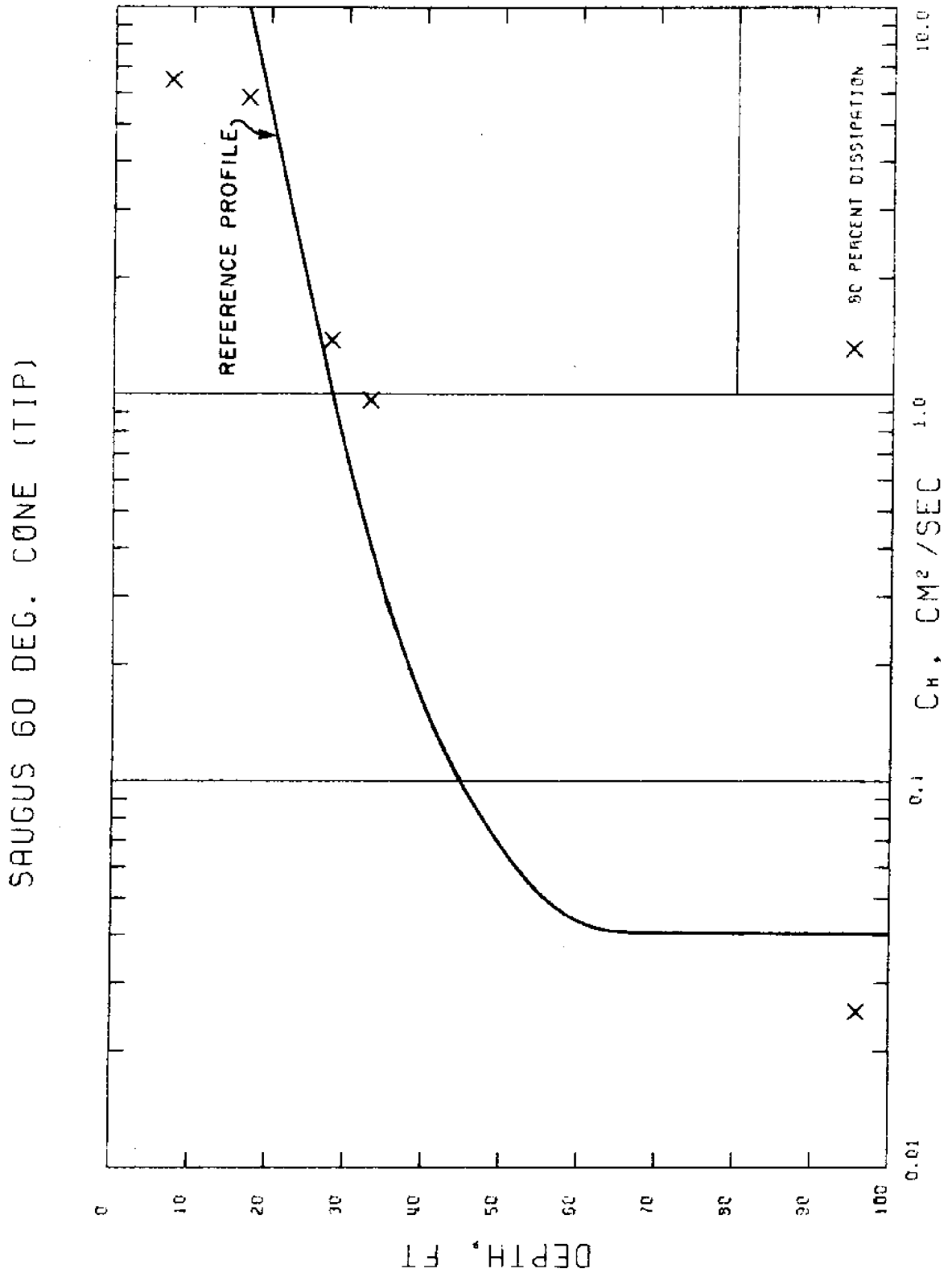

Fig. 5.27 Predicted Profile of c_h in BBC (Saugus, Stat. 246): 60° tip, 80% dissipation

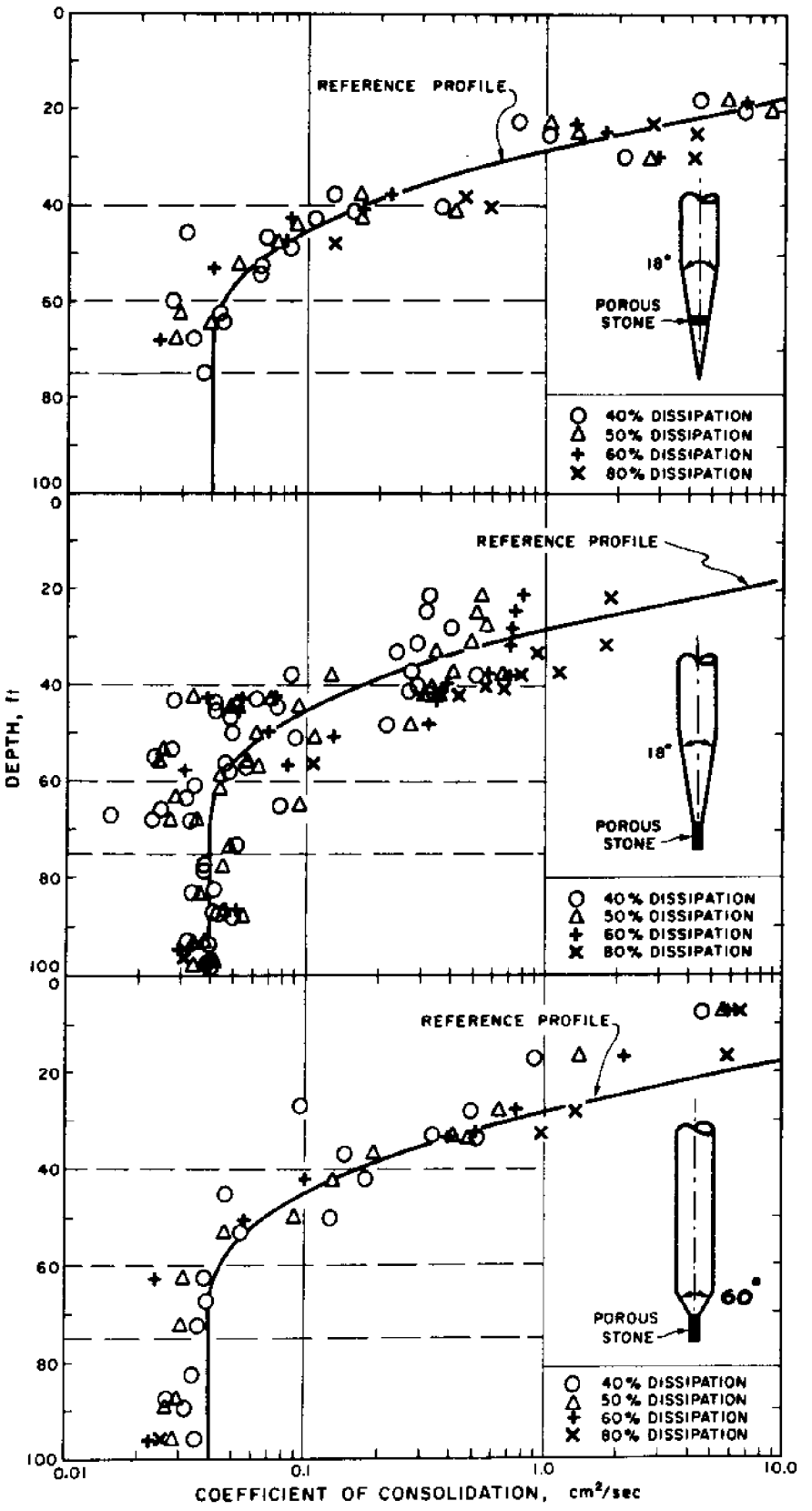

Fig. 5.28 Summary of predicted c_h (probe) profile in Boston Blue Clay, Saugus site

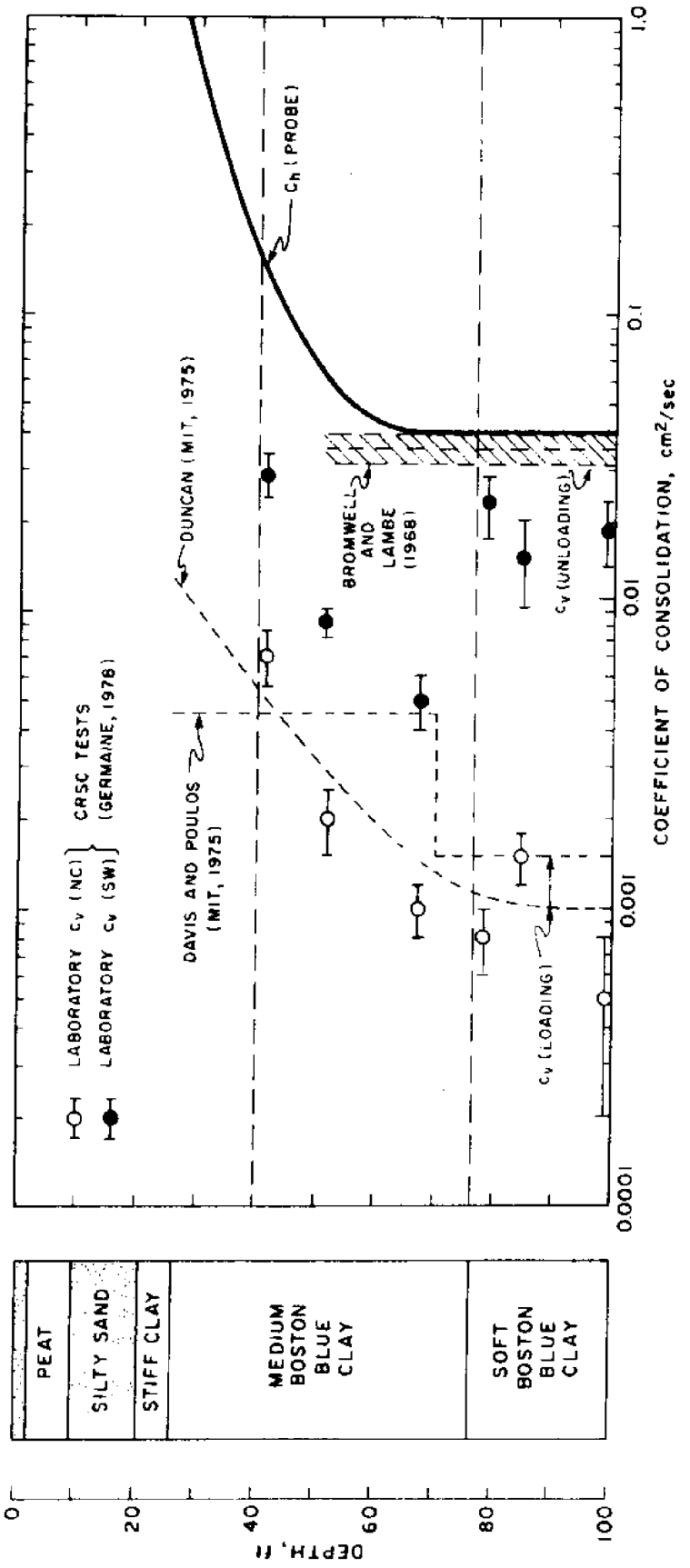

Fig. 5.29 Comparison of Predicted and Measured Coefficients of Consolidation in Boston Blue Clay

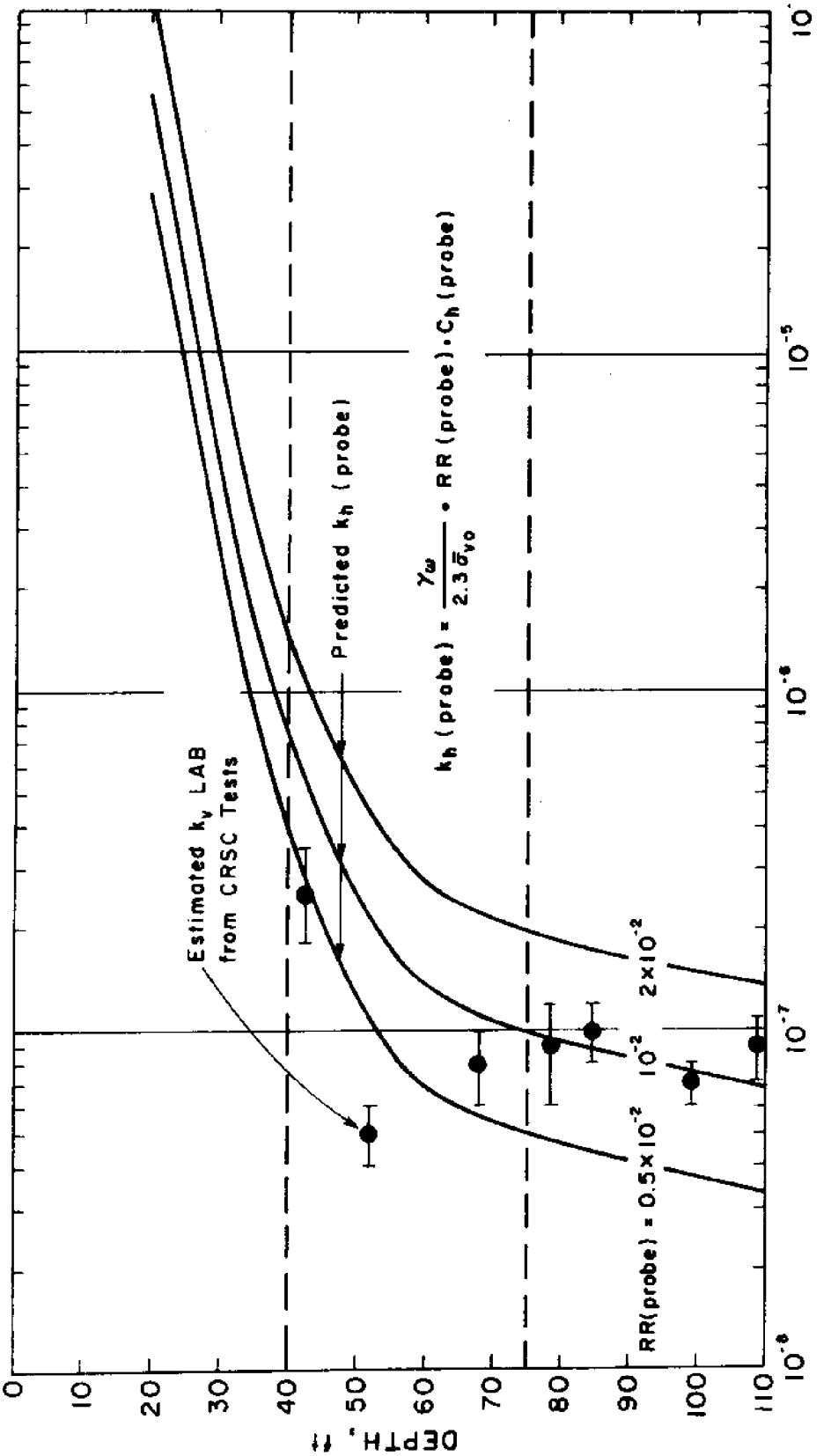

Fig. 5.30 Comparison Between Estimated and Measured Coefficients of Permeability in Boston Blue Clay

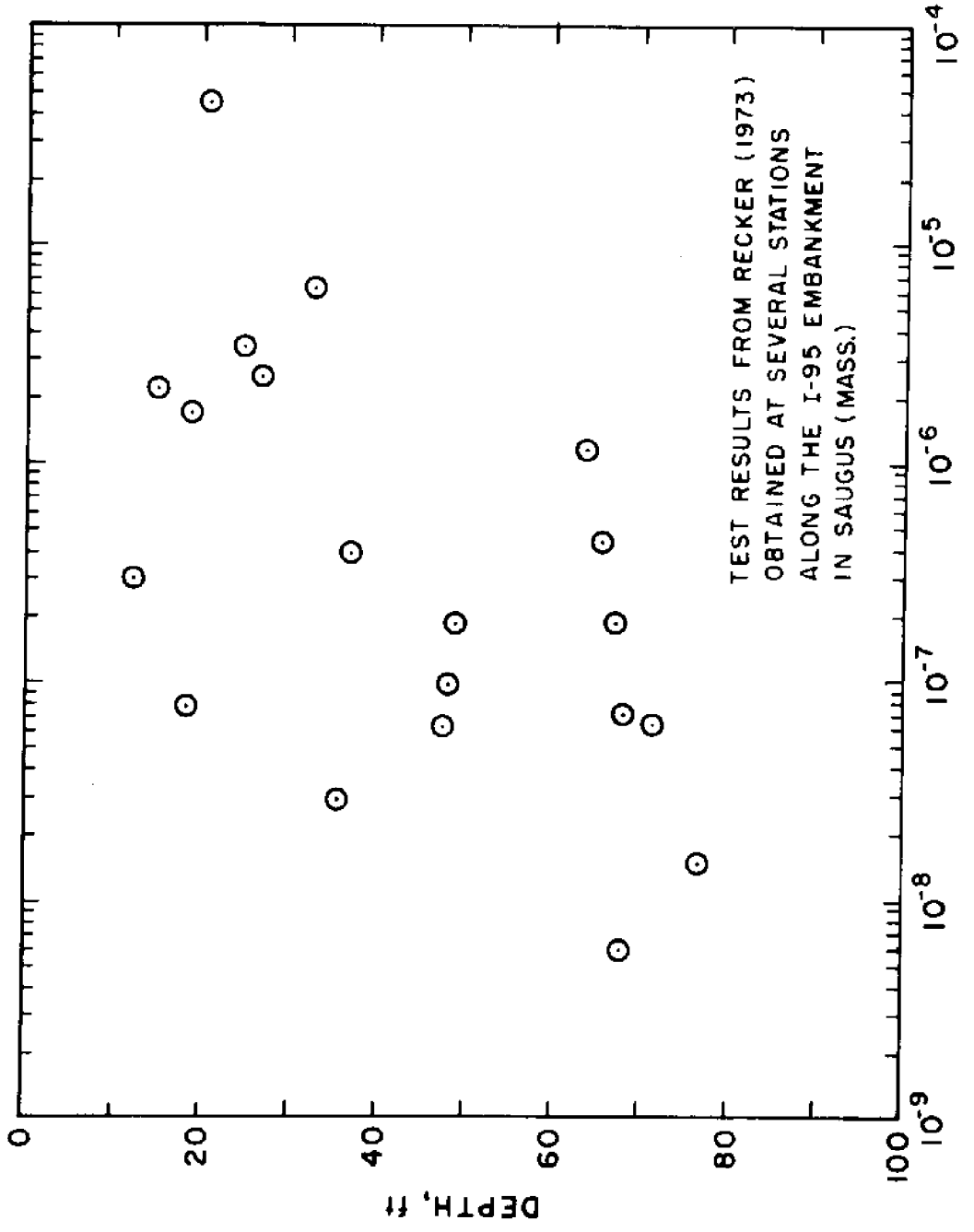

Fig. 5.31 Permeability Data from Sensitivity Tests Along the I-95 Embankment in Saugus (Mass.)

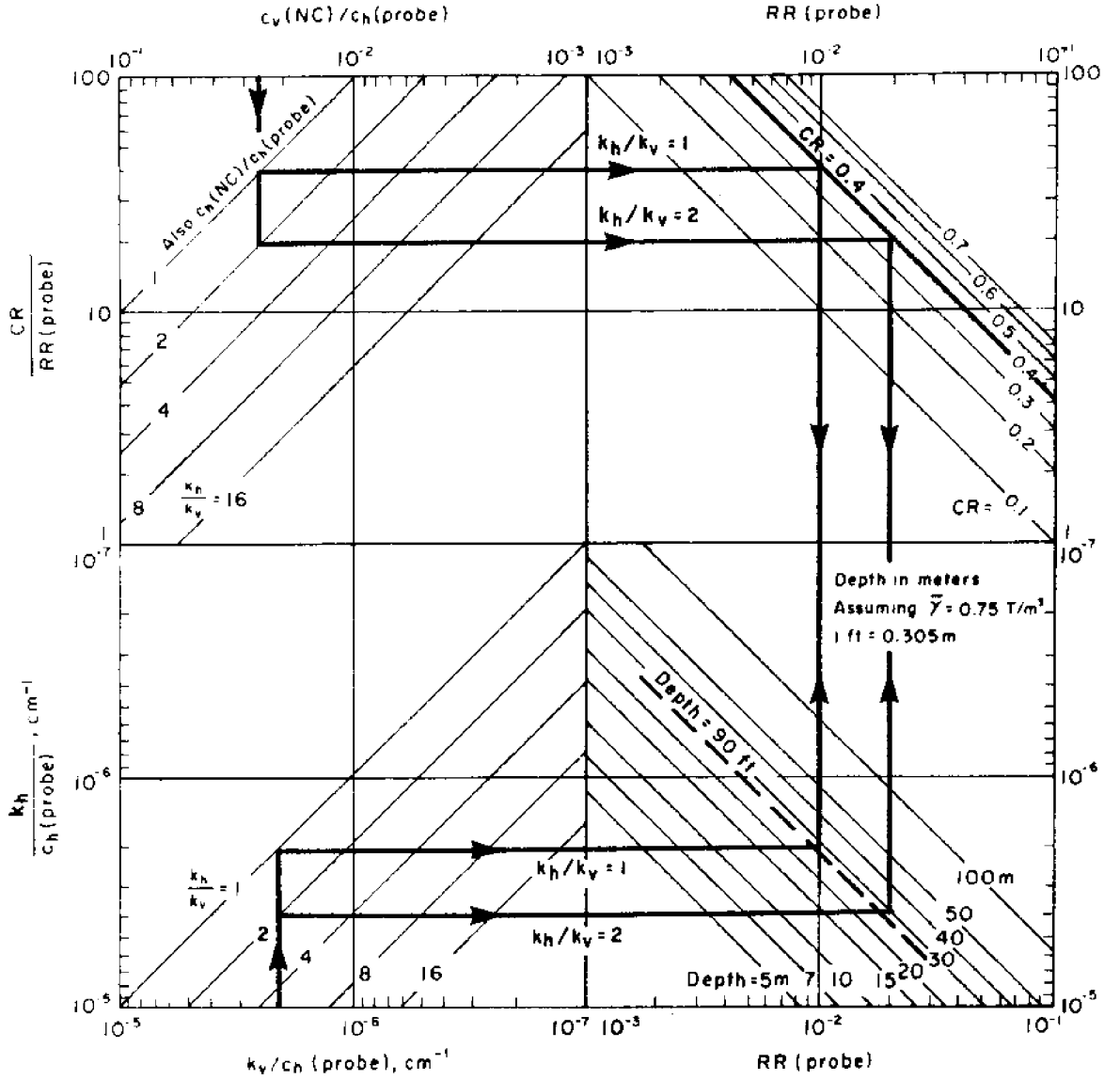

Fig. 5.32 Backfigured compressibility of the lower Boston Blue Clay from dissipation analyses

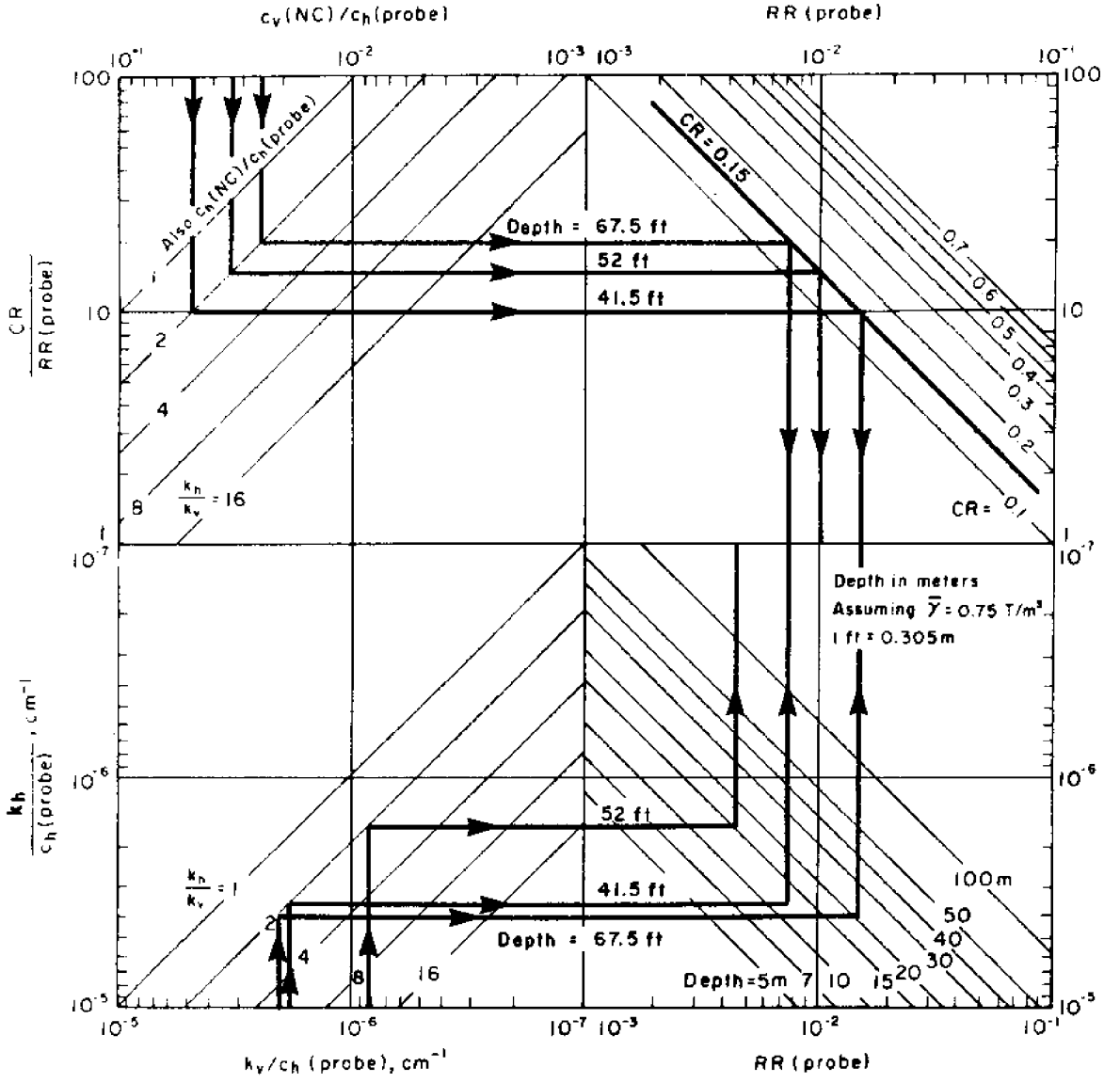

Fig. 5.33 Backfigured compressibility of the upper Boston Blue Clay from dissipation analyses

CHAPTER 6

RECOMMENDED INTERPRETATION METHOD

6.1 INTRODUCTION

This chapter provides recommended procedures to the geotechnical engineer in order to estimate profiles of the coefficients of consolidation and permeability in fine grained saturated soils from dissipation records of pore pressures after interruption of deep steady cone penetration. Important practical aspects related to the preparation, performance and interpretation of dissipation tests are reviewed. The proposed method is then applied to a varved clay deposit and results are compared to existing laboratory data.

6.2 PREDICTION METHOD

The prediction method is based on linear uncoupled consolidation analyses (Chapter 4) using the initial normalized excess pore pressure distribution for normally consolidated Boston Blue Clay (Chapter 3). Results of these analyses are given in Fig. 6.1 and Table 6.1 for three types of probes*: 18°-cone with porous stone at the tip; 18°-cone with the stone at mid-cone; and 60°-cone with the stone at the tip.

---

*The method also applies to probes where the porous stone is located on the piezometer shaft. However, because of the long dissipation time required to reach reasonable dissipation levels, these probes are not practically attractive.

6.2.1 Normalized Dissipation Curves

The first step in the prediction method consists of normalizing dissipation records and plotting $\bar{u}$ vs. log t:

$$\bar{u} = \frac{u-u_o}{u_i-u_o} \tag{6.1}$$

where $\bar{u}$ is the normalized excess pore pressure (at time t), u_o the static (or in situ) pore pressure, u_i the initial (or penetration) pore pressure at t=0 and, u, the pore pressure recorded at time t. In general, the normalized excess pore pressure, $\bar{u}$, decreases monotonically from 1.0 (at t=0) to 0 ($t \to \infty$).

6.2.2 Choice of Records

An important step in predicting reliable profiles is to identify and eliminate unusual dissipation records caused by high soil variability or improper performance of the piezometer probe. This operation requires engineering judgement and some experience. Unusual records are characterized by:

a) A much higher (or much lower) initial pore pressure, u_i, that may be easily detected in a plot of penetration pore pressure versus depth;

b) A fluctuation or an increase in pore pressure (or $\bar{u}$) for a significant period of time (more than 10 sec, say) after penetration stops.

6.2.3 Applicability of Predictions

When dissipation tests are first conducted at a new site, it is important to check that the prediction method is applicable, i.e., check the validity of linear uncoupled analyses and the initial distribution of the normalized excess pore pressure used. This can be achieved graphically by comparing the measured normalized dissipation ($\bar{u}$ vs. log t) curves to the recommended curves of $\bar{u}$ vs. log T ($T=c_h t/R^2$, R=shaft radius) in Fig. 6.1. The measured dissipation curve ($\bar{u}$ vs. log t) is plotted to the same scale of $\bar{u}$ vs. log T and translated horizontally with respect to the predicted curve (while maintaining equality of $\bar{u}$) until the best agreement is achieved. According to linear uncoupled analyses, the horizontal translation reflects changes in c_h whereas the shape of the dissipation curve depends on the initial excess pore pressure distribution around the probe. Therefore, a good agreement between the measured and recommended normalized dissipation curves provides a strong indication* of the applicability of the prediction method to the soil at hand.

---

*Chapter 3 shows that dissipation curves are very sensitive to the initial distribution of excess pore pressures.

6.2.4 Evaluation of c_h(probe)

At a given degree of consolidation, the predicted horizontal coefficient of consolidation c_h(probe) is obtained from the expression

$$c_h(\text{probe}) = \frac{R^2 T}{t} \tag{6.2}$$

where R is the radius of the cone shaft, t is the measured time to reach this degree of consolidation; and, T is the time factor. Table 5.1 provides values of T for different probe types at various degrees of consolidation.

An analytical method* to check the validity of the prediction method consists of determining c_h at different dissipation stages, i.e., different $\bar{u}$. Large differences between c_h at various degrees of consolidation indicate an inadequate initial distribution of excess pore pressure or significant coupling, or creep behavior.

The estimated values of c_h(probe) at 50% dissipation can be used in foundation problems involving horizontal water flow due to unloading or reloading of clays above the maximum past pressure. For problems involving vertical water flow in the overconsolidated range, the vertical

*Equivalent to the graphical method described in Section 6.2.3.

coefficient of consolidation, c_v(probe), can be estimated from the expression:

$$c_v(\text{probe}) = \frac{k_v}{k_h} c_h(\text{probe}) \qquad (6.3)$$

where k_v and k_h are the vertical and horizontal coefficients of permeability, respectively. Reliable estimates of the in situ anisotropy of clays as expressed by the ratio k_h/k_v is difficult to determine in the laboratory because of the effects of sample size sample disturbance,...etc. and is the subject of controversy (Rowe, 1972; Casagrande and Poulos, 1969). In situ tests to determine k_h/k_v are almost non-existent. Table 6.2 provides rough estimates of k_h/k_v for different clays.

6.2.5 Prediction of k_h(probe)

Approximate estimates of the horizontal coefficient of consolidation, k_h(probe), can be obtained from the expression:

$$k_h(\text{probe}) = \frac{\gamma_w}{2.3\bar{\sigma}_{vo}} \cdot RR(\text{probe}) \cdot c_h(\text{probe}) \qquad (6.4)$$

where $\bar{\sigma}_{vo}$ is the initial vertical effective stress (kg/cm^2); γ_w is the unit weight of water ($=10^{-3} kg/cm^3$); and, RR(probe) is the recompression ratio during early stages of consolidation around the probe (50% dissipation, say).

Results in both the upper and lower Boston Blue Clays indicate that:

$$\text{the average } RR(\text{probe}) = 10^{-2} \tag{6.5}$$

$$\text{and generally } 0.5\text{x}10^{-2} < RR(\text{probe}) < 2\text{x}10^{-2} \tag{6.6}$$

6.2.6 Prediction of c_v(NC)

For foundation clays consolidated in the normally consolidated range, estimates of the coefficients of consolidation can be obtained from c_h(probe) by means of the expressions:

$$c_h(\text{NC}) = \frac{RR(\text{probe})}{CR} \cdot c_h(\text{probe}) \tag{6.7}$$

for horizontal water flow, and

$$c_v(\text{NC}) = \frac{RR(\text{probe})}{CR} \cdot \left(\frac{k_v}{k_h}\right) \cdot c_h(\text{probe}) \tag{6.8}$$

for vertical water flow.

The compression ratio CR is the average slope of the strain vs. log effective stress plot in the appropriate effective stress range expected during consolidation of the foundation clay. Values of CR should be obtained from good quality samples carefully tested in the laboratory. Table 6.2 provides rough estimates of CR based on empirical correlations with index properties of various clays.

6.2.7 Assimilation of RR(probe) data in different soils

Figure 6.2 can be used to check estimates of k_h/c_h(probe) and c_v(NC)/c_h(probe) based on Eqs. 6.4 and 6.8, respectively. It can also prove convenient in rapidly assessing the effect of uncertainties in RR(probe), CR, and k_h/k_v. More importantly, however, Fig. 6.2 provides a systematic method of assimilating RR(probe) data in different soils when measurements (or estimates) of k_h, k_v, CR, and c_v(NC) are available (see Figs. 5.31 and 5.32).

6.3 PRACTICAL CONSIDERATIONS

6.3.1 Performance of the Piezometer Probe

One of the essential factors affecting the quality, and hence the reliability of dissipation records is the design and deairing of probes.

A good design must lead to a rigid system capable of providing a very rapid response with a minimum inflow of water into the system. In addition, it should enable the user to easily assemble, disassemble, deair and maintain the probe deaired until in situ tests are performed.

A deairing technique at least as careful as currently adopted at M.I.T. (see Chapter 2) is strongly recommended. Crude deairing in the field is not acceptable. Checking of the response before field testing is important. This can be achieved by moving the probe quickly up and down in a bucket of water. Discard the probe if any sluggish tendency is detected because, in the soil, access to water is more difficult and hence the response will be even slower. A better judgement on response can be made by examining records of pore pressures during cone penetration and their subsequent dissipation.

Improper response leads to the following features in the records: (a) smooth (vs. sharp) changes of pore pressures during penetration; (b) a prolonged rise in pore pressures

after penetration has stopped; and (c) a slow increase in pore pressures when penetration resumes. If one of these features is observed, the test should be stopped and a new piezometer installed.

6.3.2 Static Pore Pressure

The evaluation of the normalized excess pore pressure, $\bar{u}$, requires an estimate of the static (or in situ) pore pressure, u_o, in the soil prior to penetration (Eq. 6.1). The results in Fig. 4.12 show that, an error in the estimated u_o, causes a significant change in the normalized dissipation curve* and thus leads to errors in c_h(probe).

Reliable measurements of u_o can, at best, be performed at selected depths by

a) leaving the piezometer probe in the ground to achieve total dissipation. In clays, this may require days at each depth and hence cause severe delays in exploration and interpretation of results;

b) installing semi-permanent piezometers (such as Casagrande or GEONOR M206) to monitor u_o over extended periods of time without interrupting cone penetration testing, and;

c) recording the pore pressure during penetration in a "clean" sand layer where the penetration pore pressure usually deviates very slightly from u_o (see Fig. 2.5).

---

*The effect is first negligible and then increases with time.

Therefore, estimates of u_o for predicting c_h(probe) require interpolation of measurements at selected depths. The profile of penetration pore pressures can provide valuable information to identify and select key elevations where u_o measurements are more likely to detect "unusual" situations (artesian pressure, under-consolidated clay,...etc.).

6.3.3 Dissipation Time

Steady cone penetration is usually conducted in depth increments determined by the length of the pushing rods (typically 5 ft or 1 m). Installation of a rod takes about one minute when pore pressure dissipation can be routinely recorded at no additional cost to the testing program. In typical onshore testing, an additional minute or two of waiting will not cause serious delays.*

In 3 minutes, lean overconsolidated clays can reach 40 to 60% consolidation and hence provide meaningful results. On the other hand, soft plastic clays might achieve only 10 to 20% consolidation in 3 minutes. Experience in BBC indicates that, at these low dissipation levels, estimates of c_h are not very reliable and involve significant scatter (see Chapter 5). Therefore, longer dissipation times (say 30 min to achieve 50% consolidation) are required in impervious clays at least at selected depths in order to calibrate results obtained at lower consolidation levels.

---

*In offshore work, the movement of the drilling vessel can represent a major problem in obtaining reliable dissipation measurements.

6.4 APPLICATION OF THE PREDICTION METHOD TO A VARVED CLAY DEPOSIT

In 1977, M.I.T. conducted cone penetration and pore pressure measurements in a Connecticut Valley Varved Clay (CVVC) on the campus of the University of Massachusetts in Amherst, Massachusetts*. The soil conditions at the site are presented in Fig. 6.3 as obtained from a typical sampling and laboratory testing program. Fig. 6.4 shows the undrained shear strength of the clay, s_u, as determined by the (Geonor) field vane test and the SHANSEP procedure (Ladd and Foott, 1974). The SHANSEP strengths are based on plane strain compression (PSC) and direct simple shear (DSS) test results and the estimated stress history (OCR = σ_{vm}/σ_{vo}) in Fig. 6.3. Furthermore, Fig. 6.5 presents the cone resistance, q_c, from two standard FUGRO cones (60° angle pushed at 1 to 2 cm/sec.)

Pore pressure measurements were performed at the tip of 60° and 18° cones primarily to determine the pore pressures during cone penetration. Therefore, most of the dissipation records are very short, lasting approximately 1/2 to 1 minute with few exceptions.

This section applies the recommended procedures to estimate c_h(probe) from dissipation records and compares predictions with laboratory data.

---

*Refer to Baligh et al. (1978) for more detailed information on the site.

6.4.1 Static Pore Pressure

The static pore pressures, u_o, at the Amherst site are relatively easy to estimate because of geological consideration and measurements of u_o obtained in the very pervious layers above 15 ft and below 63 ft depth, approximately. By linear interpolation, the static pore pressure, u_o, at a depth z is given by:

$$u_o = 0.0285z + 0.1 \qquad (6.9)$$

in which u_o is in kg/cm^2 and z in feet.

6.4.2 Normalized Dissipation Records

Appendix B presents normalized dissipation plots ($\bar{u}$ vs. log t) obtained at various depths with the 18° and 60° cones (stone at tip). Preliminary examination of these curves shows that dissipation takes place very rapidly above 10-15 ft and below 63 ft, approximately. Tests considered inadequate for estimating c_h(probe) are identified in the summary tables of Appendix B. In these tests, full dissipation takes place in a few seconds and, therefore, cannot be interpreted reliably.

6.4.3 Applicability of the Prediction Method

Figure 6.6 compares measurements at the tip of a 60°-cone conducted at a depth of 37 ft with predictions corresponding to c_h = 0.05, 0.1 and 0.2 cm^2/sec. Clearly, good agreement is achieved for c_h = 0.1 cm^2/sec.

Figure 6.7 shows the same results as Fig. 6.6 In addition, Fig. 6.7 compares measurements at the tip of an 18°-cone conducted at the same depth with predictions based on c_h = 0.1 cm^2/sec. and the recommended curves in Fig. 6.1 (R = 1.91 cm).

Results in Fig. 6.7 indicate that:

a) the measured dissipation curve at the tip of the 18° probe exhibits a slightly steeper slope than the recommended curve, and;

b) the measured dissipation curve at the tip of the 60° probe is slightly oscillating at early times (t < 10 sec) but is very close to the predicted curve at later times.

In conclusion, the overall agreement between measurements and predictions is considered remarkably good* and the recommended method of predicting c_h(probe) can thus be used for CVVC (at least in the same layer where the tests in Fig. 6.7 were conducted, i.e., between depths 15 ft and 63 ft).

6.4.4 Predicted Profile of c_h(probe)

Figures 6.8 and 6.9 present the estimated profiles of c_h(probe) based on measurements of pore pressures obtained with 18° and 60° conical probes (with the stone at the tip) in CVVC. These data include penetration pore pressure, u_i, and profiles of c_h(probe) evaluated according to the recommended method in section 6.2.4.

*In view of the very different behavior of Amherst varved clay compared to Boston Blue Clay for which predictions were developed.

Results in Figs. 6.8 and 6.9 indicate that:

1) Penetration pore pressures, u_i, obtained by the 18° probe (Fig. 6.8) are consistent with the 60° probe (Fig. 6.9) and the cone resistance profiles, q_c (Fig. 6.5);

2) q_c and u_i provide more detailed information on profiling and variability than regular laboratory tests (Fig. 6.3) or field vane tests (Fig. 6.4). In particular, the middle clay between 15 ft and 63 ft is clearly identified as a very uniform layer with minor nonhomogeneities at depths 19, 36 and between 50 to 63 ft;

3) most of the c_h(probe) data are obtained at low dissipation levels (20%). In spite of significant scatter in $(c_h)_{20}$, both 18° and 60° probes identify the middle clay layer [depths 10 (or 15) and 63 ft] as having a much lower consolidation coefficient (about 10 times) than the upper and lower layers;

4) at virtually all depths, $(c_h)_{20}$ is underpredicted* by the 18° probe and overpredicted by the 60° probe. These trends were observed in Boston Blue Clay (Chapter 5) and are compatible with results in Fig. 6.7;

5) at a depth of 37 ft in the middle layer, the difference between c_h evaluated at 40, 50, 60 and 80% dis-

---

*Compared to c_h at higher dissipation levels.

sipation is very small and the values are very close for both probes ($c_h \simeq 0.1$ cm^2/sec). Therefore, values of c_h evaluated at 40% dissipation are considered more reliable than $(c_h)_{20}$;

6) the solid lines in Figs. 6.8 and 6.9 obtained by joining $(c_h)_{40}$ data represent the first estimate of the c_h(probe) profile in this deposit.

7) the c_h(probe) profile is virtually the same for both cones, and;

8) the increase in c_h(probe) between 50 and 63 ft is probably caused by the lack of 40% dissipation data in the clay. Results at 20% dissipation together with q_c and u_i data suggest that the same clay extends to 63 ft where a sharp change in layering occurs.

6.4.5 Comparison of Predicted and Measured Permeabilities

Figure 6.10 presents the predicted horizontal permeability k_h(probe) based on the profile of c_h(probe) estimated at 40% dissipation for the two cones (18° and 60°) according to Eq. 6.4 and using the recommended value of RR(probe)=10^{-2}, Eq. 6.5. Figure 6.10 also shows the results of laboratory measurements of k_h and k_v conducted on 4" cubical samples recovered at three depths (Ladd, 1975).

Clearly, the agreement between k_h(probe) and k_h(Lab) is very good, thus indicating that

1) The recommended value of RR(probe)=10^{-2} back-figured from results in BBC is reasonably applicable to CVVC. The swelling ratio for the middle CVVC at Amherst (between depth 15 and 63 ft) determined from four CRSC tests indicate that: SR=3.5(±0.4)x10^{-2} at an OCR=5; and, SR=1.8(±0.6)x10^{-2} at an OCR=2. This means that CVVC is about 1.5 times more compressible than BBC at an OCR=5 but close to BBC at an OCR=2.

2) Simplifications made to obtain Eq. 6.4 have a minor effect provided that appropriate values of RR(probe) are selected.

3) Since k_v is uniform in this deposit whereas both k_h(lab) and k_h(probe) increase significantly with depth, this confirms that dissipation around conical probes is controlled by horizontal flow (see Chapter 4).

6.4.6 Comparison of Predicted and Measured Coefficients of Consolidation in the Virgin Range

Figure 6.11 presents the predicted values of c_h(NC) and c_v(NC) based on the profile of c_h(probe) according to Eqs. 6.7 and 6.8, respectively. The value of RR(probe)=10^{-2} recommended in Eq. 6.5 was maintained as for k_h predictions. The selected ratios of k_h/k_v were obtained by interpolation (or extrapolation) of laboratory test results (Fig.6.10) and are given in Fig. 6.11. Finally, a reasonable value of the

compression ratio CR=0.2 was selected between CR_{max}= 0.24(±0.04) and CR_{min}=0.19(±0.02) determined from CRSC tests.

Figure 6.11 also shows measurements of c_v(NC) from five CRSC tests with an average of 1.45×10^{-3} cm^2/sec. Comparing the predicted and measured values of c_v(NC), we note that:

1) A very good agreement is achieved in the middle CVVC layer between depths 15 and 63 ft especially in view of the scatter in laboratory test results (This scatter is considered very reasonable compared to typical c_v laboratory data); and hence,

2) The selected values of CR=0.2 and RR(probe)=10^{-2} appear adequate for CVVC.

6.5 SUMMARY AND CONCLUSIONS

This chapter provides recommended methods for predicting the coefficients of consolidation and permeability of saturated fine grained soils from pore pressure dissipation measurements after interrupting deep steady penetration.

The prediction method basically consists of evaluating c_h(probe) by matching measured and predicted dissipation records (Table 6.1). The coefficients of consolidation in the virgin range and the permeability of the soil can then be estimated from c_h(probe).

Guidelines for the practicing engineer are provided in order to: a) identify and eliminate bad records where high soil variability and/or malfunctioning of the probe lead to significant errors in the predictions, and; b) verify the applicability of the prediction method to a new soil.

Important practical aspects of pore pressure dissipation are reviewed and discussed. Special emphasis is made on the deairing and rapid response of the probe, the possible errors in estimating the static (in situ) pore pressure, u_o and, the time required for meaningful dissipation to take place.

The prediction method is then applied to results of dissipation tests in Connecticut Valley Varved Clay (CVVC) at Amherst, Massachusetts. Two sufficiently long dissipation records indicate that predictions apply surprisingly well to CVVC in spite of large differences in behavior from BBC. This is especially important because it means that the prediction method developed for BBC can also be applied to other clays.

Profiles of c_h(probe) estimated according to the proposed method are virtually identical for 18° and 60° cones. Furthermore, c_h(probe) profiles are consistent with measurements of cone resistance and penetration pore pressures.

No (laboratory or field) tests were conducted by M.I.T. to provide direct measurement of the overconsolidated horizontal coefficient of consolidation in CVVC. Therefore, the predicted

values of c_h(probe) cannot, at present, be rigorously evaluated. However, a comparison of k_h(probe) with laboratory measurements of the horizontal permeability indicates very good agreement. Furthermore, the estimates of c_v(NC) from c_h(probe) are very close to laboratory measurements of the coefficient of consolidation in the normally consolidated (virgin) range.

% Dissipation	$\bar{u}$	Cone Angle - Stone Location					
		18° Tip		18° Mid-cone		60° Tip	
		T*	R^2T^{**} (cm^2)	T*	R^2T^{**} (cm^2)	T*	R^2T^{**} (cm^2)
20	0.8	0.16	0.58	0.52	1.89	0.44	1.60
40	0.6	1.35	4.90	2.6	9.44	1.9	6.90
50	0.5	3.0	10.9	4.7	17.1	3.65	13.2
60	0.4	6.0	21.8	8.2	29.8	6.5	23.6
80	0.2	30.0	109	34	123	27	98

* $T = c_h\, t/R^2$

** R = 0.75 in = 1.91 cm for M.I.T. probes

Table 6.1 Recommended Time Factors for Predicting the Horizontal Coefficient of Consolidation from Dissipation Records

1 - Compression Ratio CR (from Ladd, 1973)

$CR = \frac{C_c}{1+e_o}$ = slope of the strain vs. log stress curve

e_o = initial void ratio

C_c = virgin compression index = slop of e vs log stress

ω_L = liquid limit

ω_N = natural water content

$C_c = 0.009\ (\omega_L\% - 10\%)$ Terzaghi and Peck (1967)

$C_c = 0.54\ (e_o - 0.35)$ Nishida (1958)

$C_c = 0.01$ to $0.15\ (\omega_N\%)$ MPMR (1958)

$C_c = 0.6\ (e_o - 1)$ for $e_o < 6$

$= 0.85\ (e_o - 2)$ for $6 < e_o < 14$ Kapp (1966)

2. Anisotropic Permeability of Clays (from Ladd, 1976)

	Nature of Clay	k_n/k_v
1.	No evidence of layering	1.2 ± 0.2
2.	Slight layering, e.g., sedimentary clays with occasional silt dustings to random lenses	2 to 5
3.	Varved clays in north-eastern U.S.	10 ± 5

Table 6.2 Empirical Correlation and Typical Properties of Clays

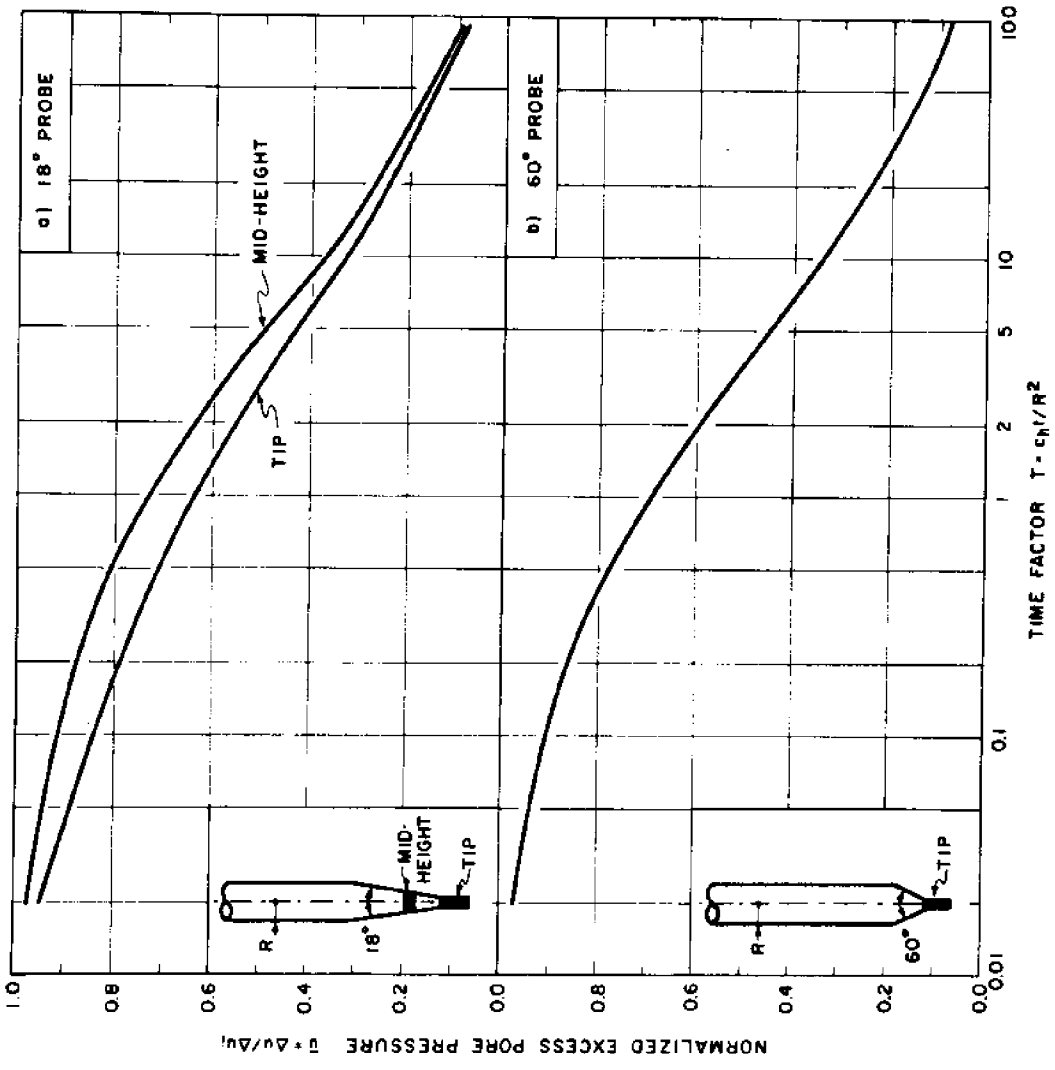

Fig. 6.1 Recommended Dissipation Curves for Predicting c_h (probe)

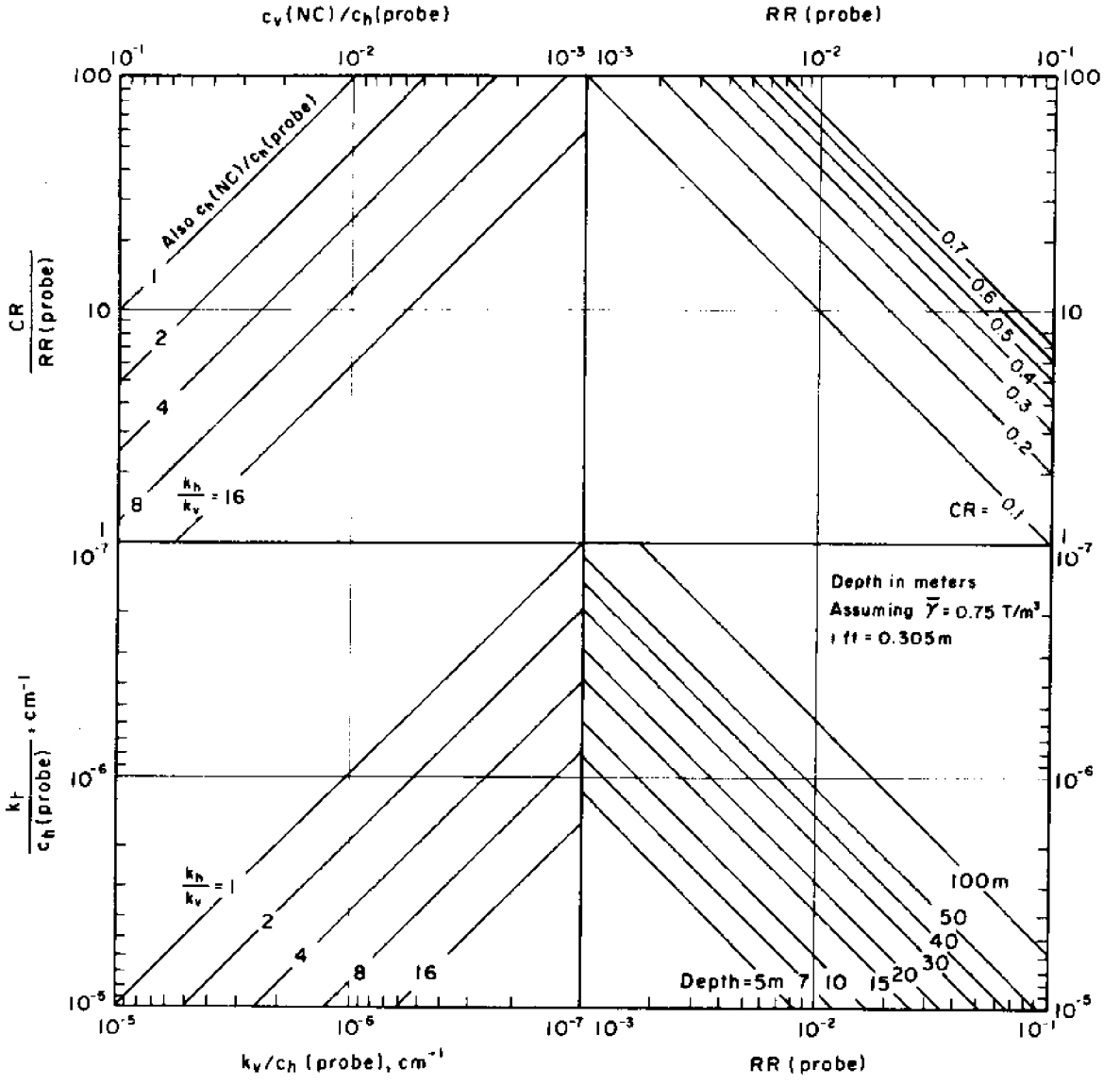

Fig. 6.2 Graphical method of estimating k_h and c_v(NC) from c_h probe

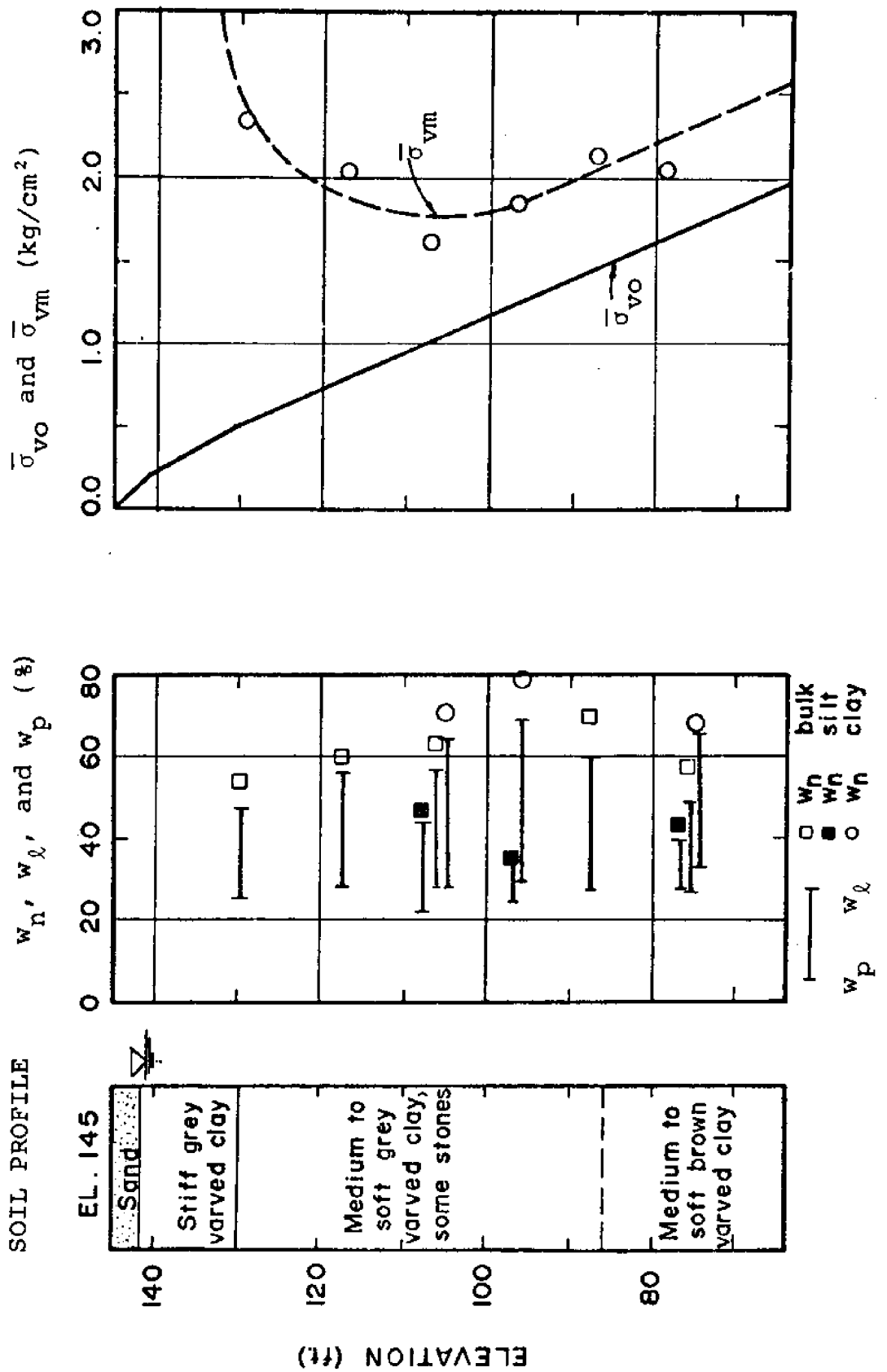

Fig. 6.3 Soil conditions at the Amherst, Mass. testing site (Route 116 bypass and North Hadley Road; data from Ladd, 1975).

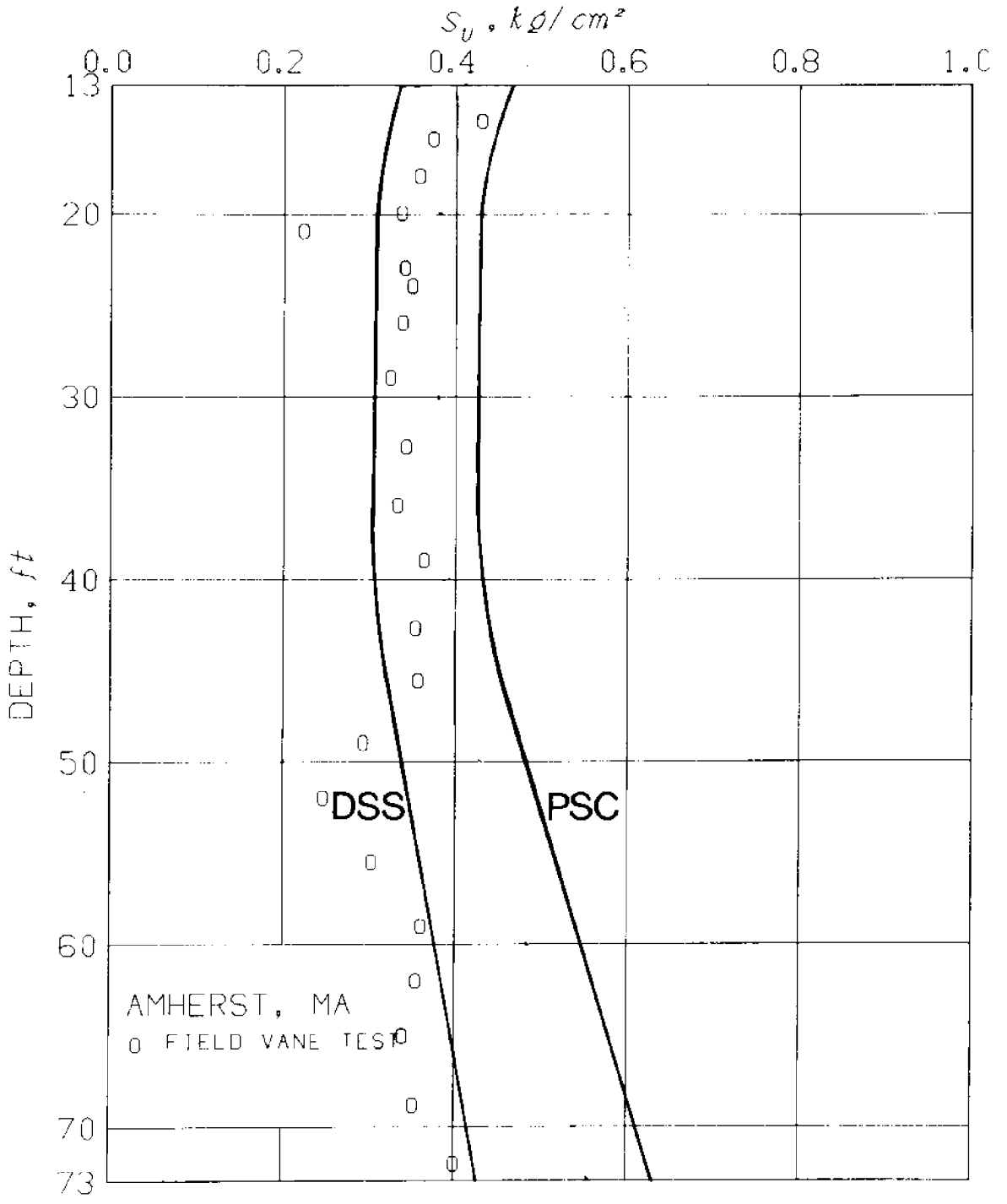

Fig. 6.4 SHANSEP and field vane strength profiles for the Amherst, Mass. testing site (data from Ladd, 1975).

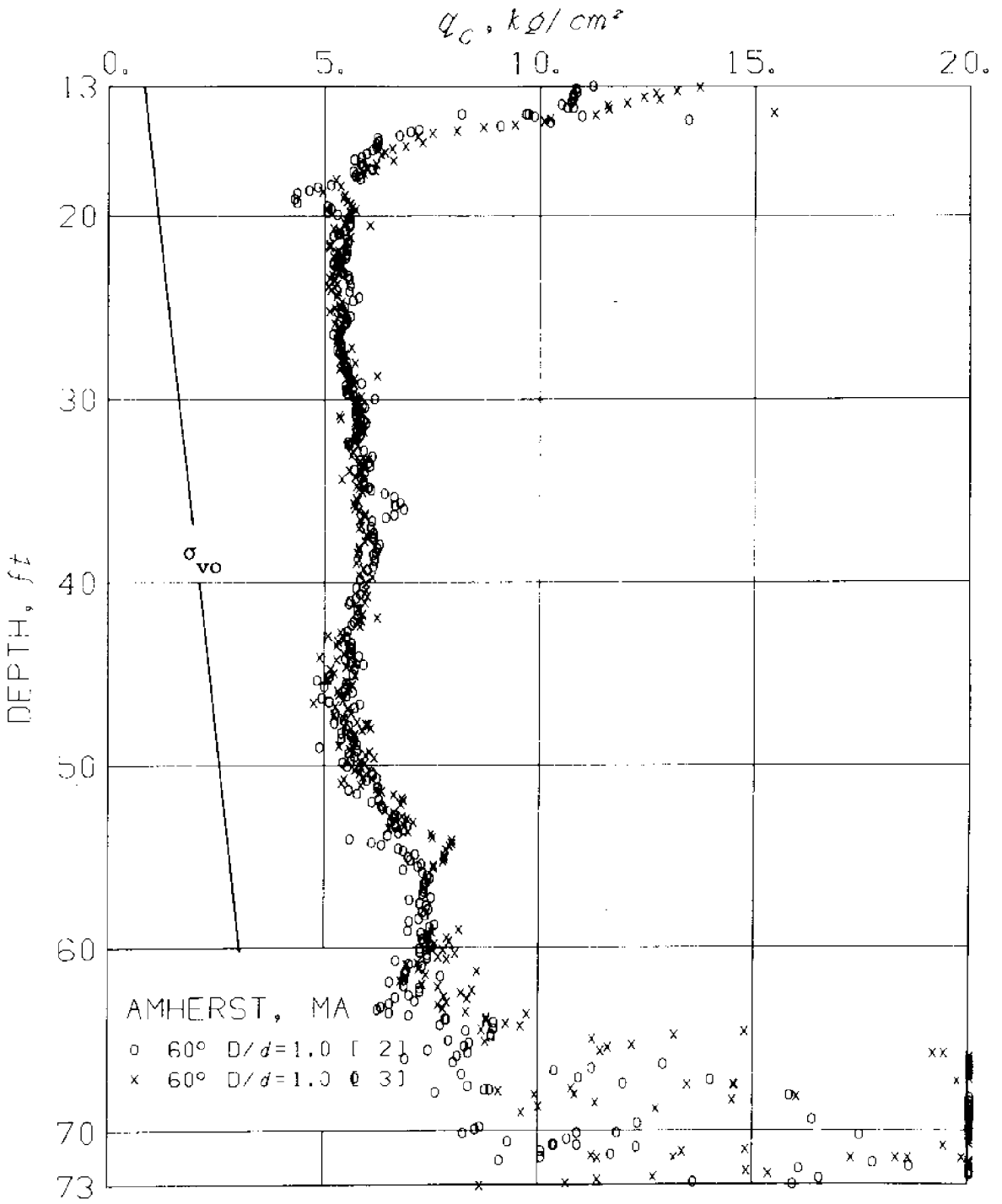

Fig. 6.5 Profile of Cone Resistance, q_c, in Connecticut Valley Varved Clay at Amherst, Mass. (from Baligh et al., 1978)

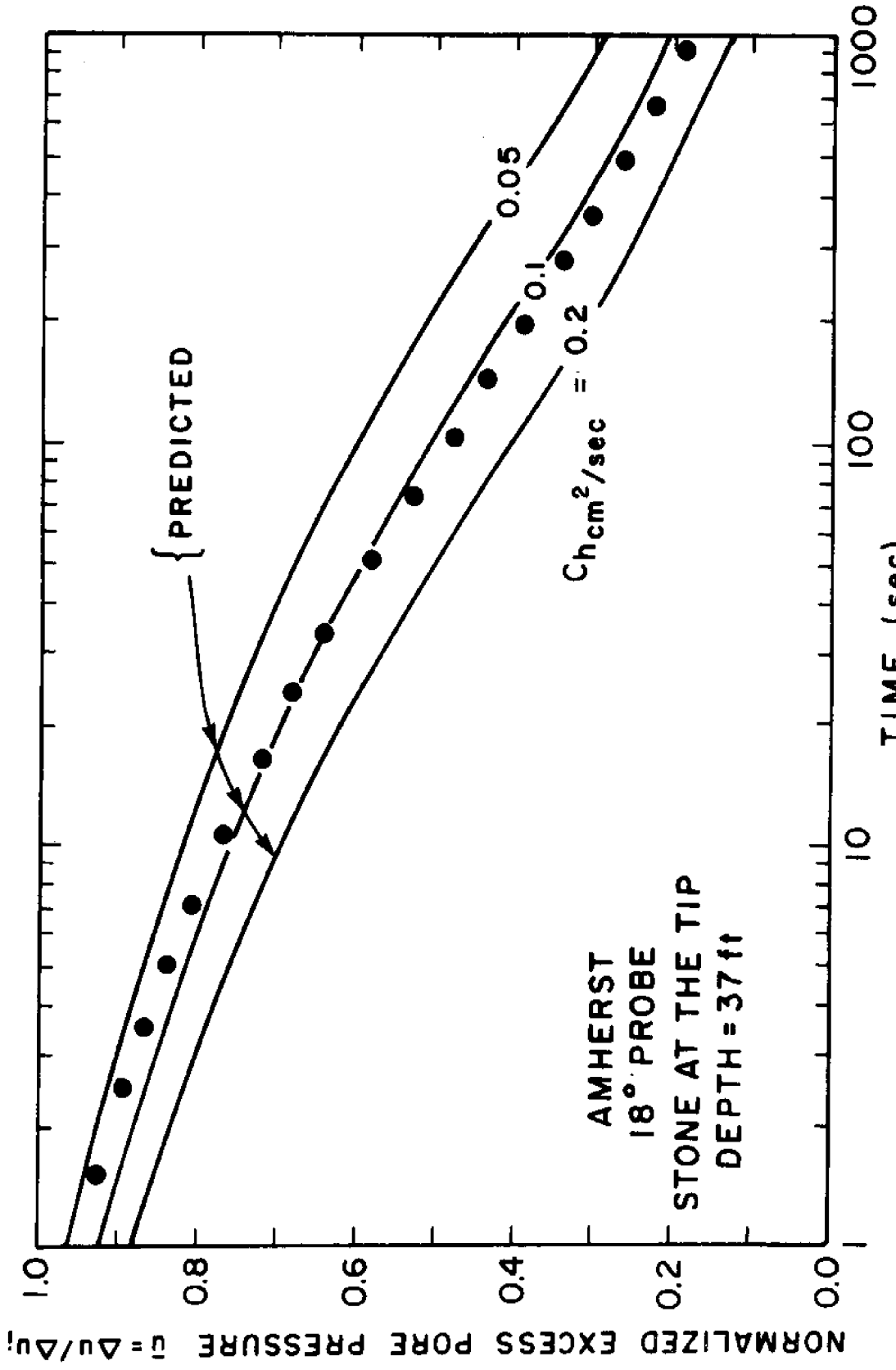

Fig. 6.6 Evaluation of predicted dissipation curves for an 18° cone

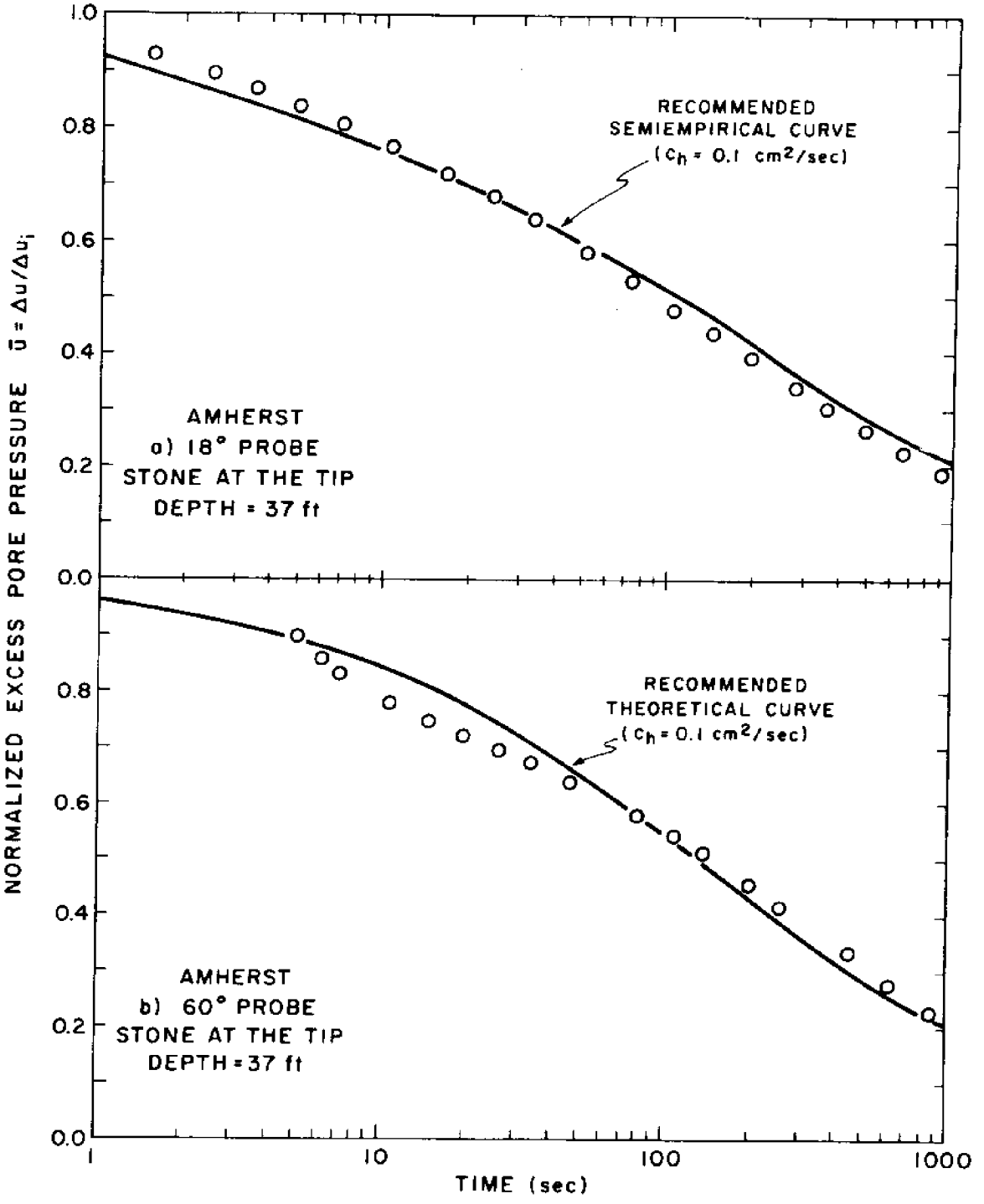

Fig. 6.7 Evaluation of Predicted Dissipation Curves for 18° and 60° cones (assuming c_h = 0.1 cm²/sec)

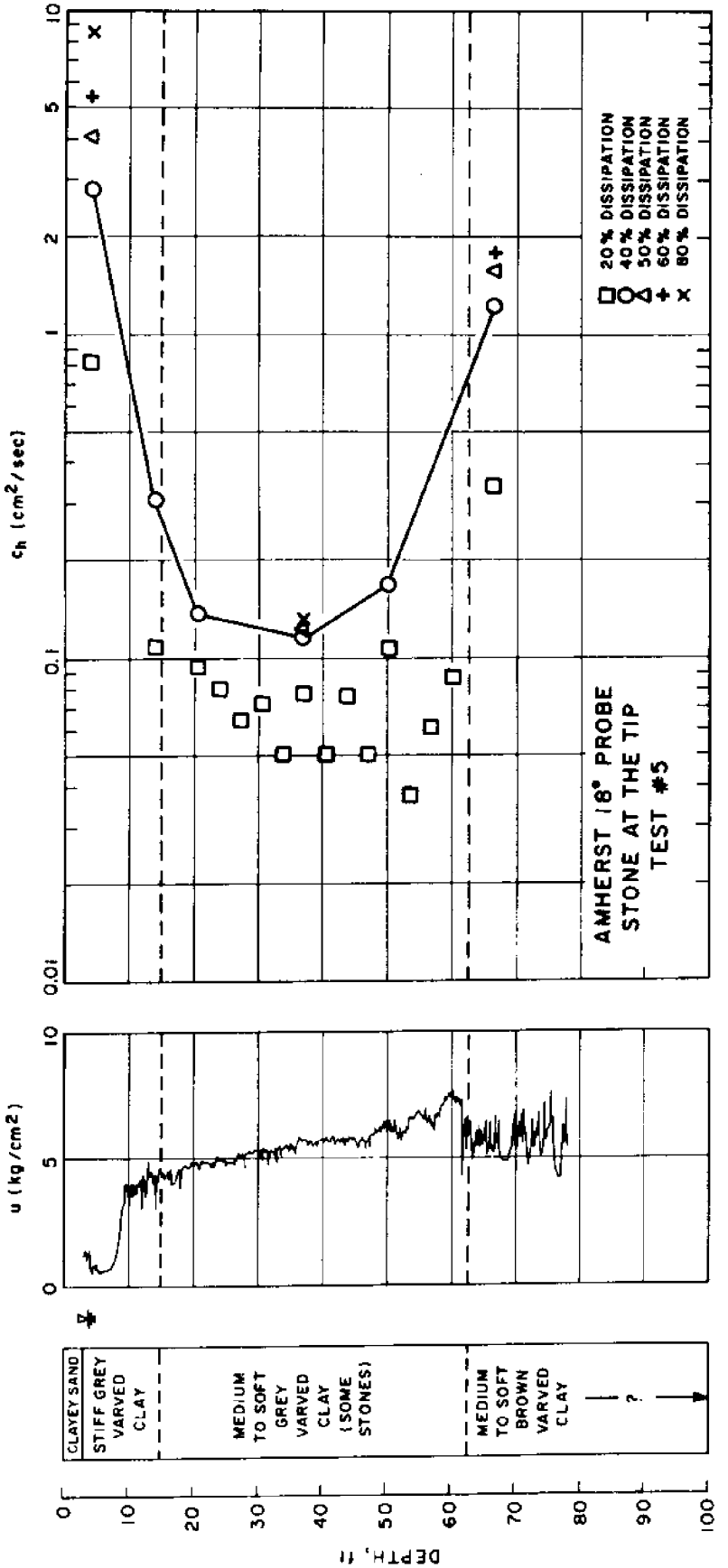

Fig. 6.8 Results of 18° conical probes at the Amherst site

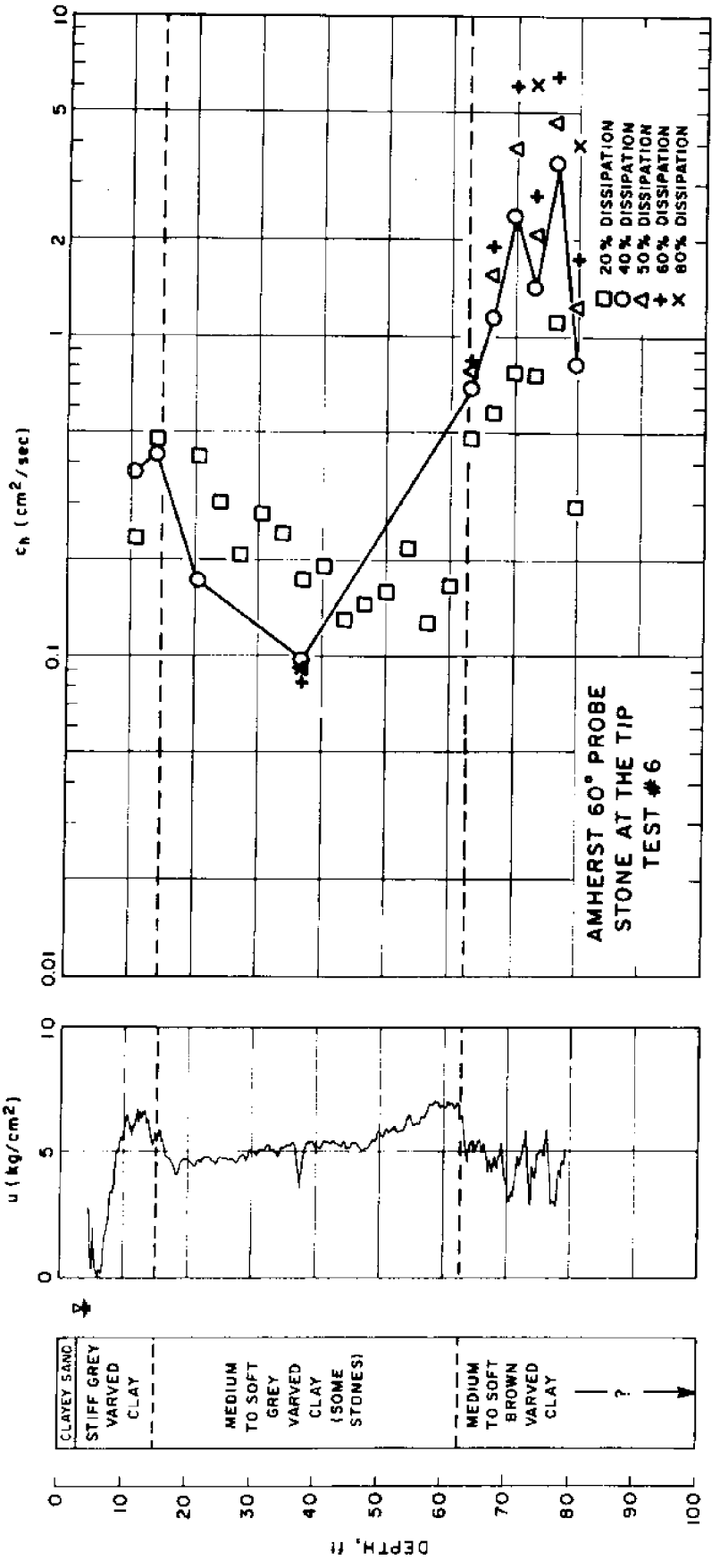

Fig. 6.9 Results of 60° conical probes at the Amherst site

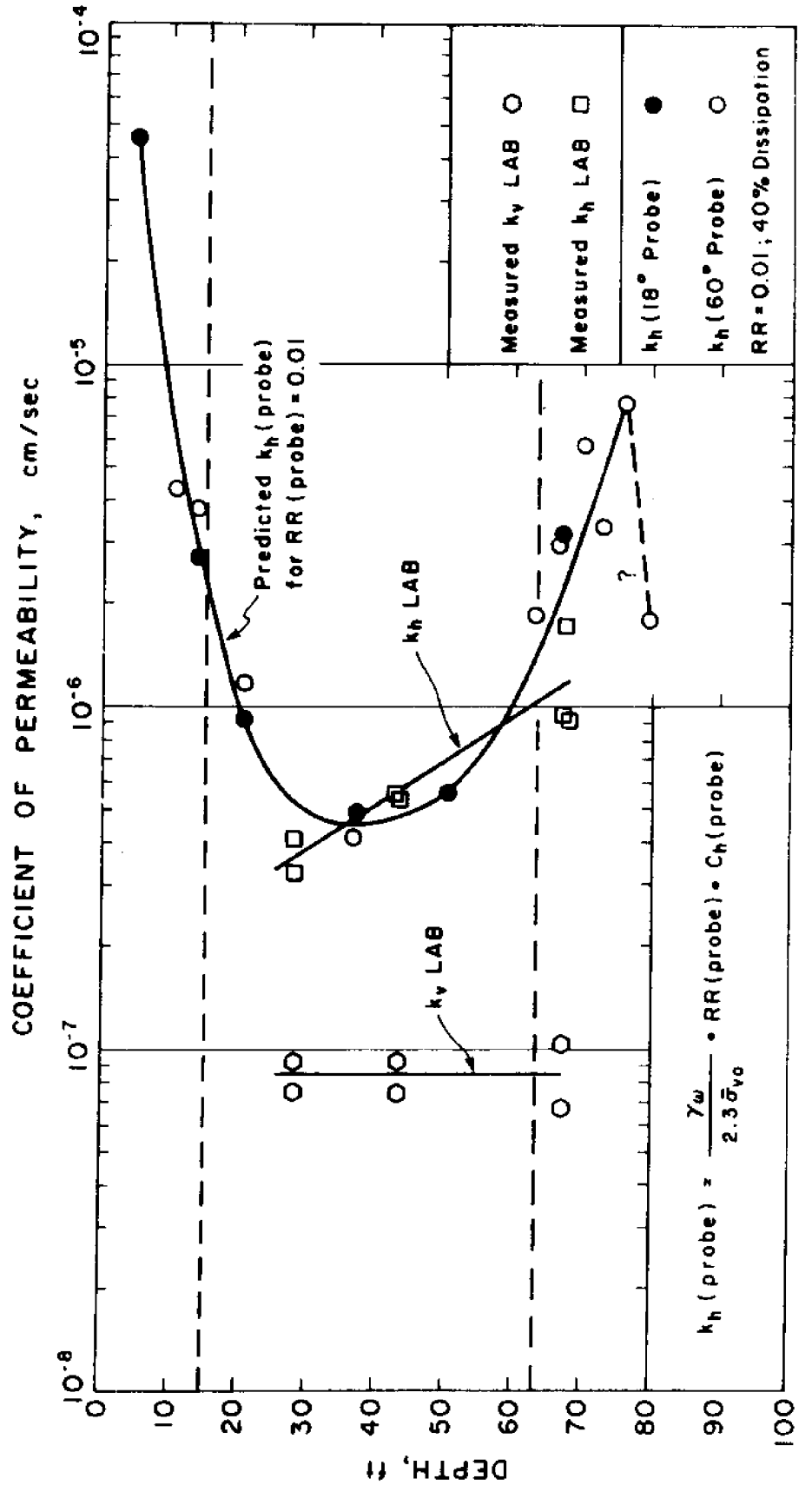

Fig. 6.10 Comparison of Predicted and Measured Coefficients of Permeability at the Amherst Site

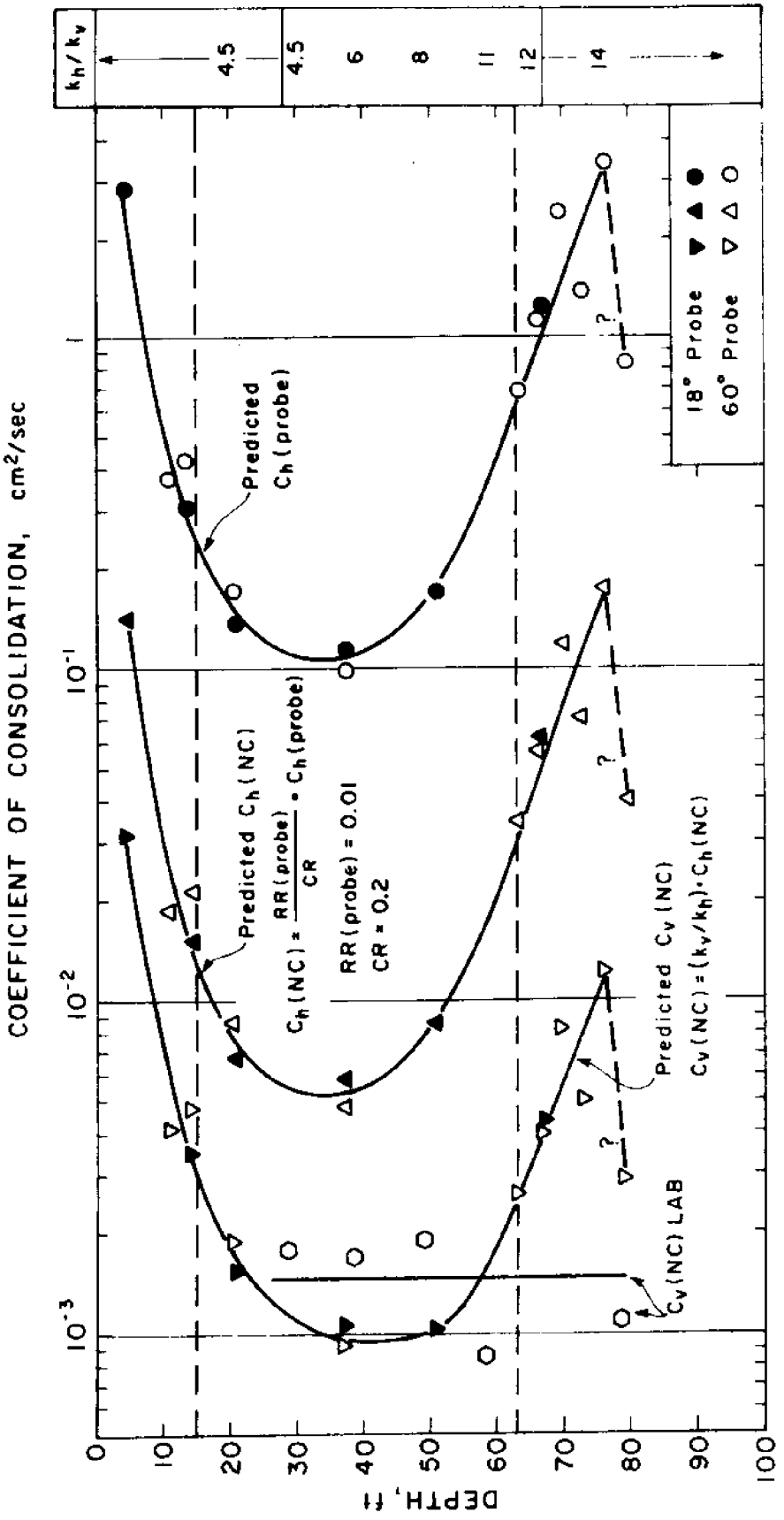

Fig. 6.11 Comparison of Predicted and Measured Coefficients of Consolidation at the Amherst Site

CHAPTER 7

SUMMARY AND CONCLUSIONS

(1) Cone penetration testing provides a superior soil exploration technique to establish stratification, determine variability and perform soil identification; especially if pore pressures generated by cone penetration are measured in addition to cone resistance (Baligh et al., 1980). The technique is particularly well suited for offshore work.

(2) Due to the complicated nature of cone penetration, research is needed to interpret test results and hence estimate engineering properties of the soils for predicting foundation performance and conducting foundation designs. Past research at M.I.T. concentrated on estimating the undrained shear strength of clays (Baligh et al., 1978). This report considers methods of estimating the consolidation and permeability of fine grained soils from the pore pressure decay that takes place after steady cone penetration is interrupted.

(3) Estimates of the consolidation and/or permeability characteristics of natural soil deposits is important in most geotechnical foundation problems (see Sec. 1.5). In on shore work,existing methods rely on laboratory and/or in situ tests.

Offshore, no in situ testing methods are available. The permeability, k, of natural sand deposits can be estimated within an order of magnitude from correlations with grain size measurements conducted in the laboratory or from in situ permeability tests (onshore). Laboratory measurements of k and the coefficient of consolidation, c_v or c_h, in "structured" fine grained soils can be several orders of magnitude lower than field values and thus have limited use in designs. In relatively structureless clays, the most experienced engineer using the best laboratory testing equipment and procedures can, at best, predict field values of k and c_v within a factor of two or three. The average geotechnical engineer using routine sampling and testing methods can probably estimate k and c_v within a factor of five to ten from laboratory measurements. Reliable in situ tests in fine grained soils are time consuming and require considerable skill and experience above the current routine average U.S. practice. Under ideal conditions, useful permeability data can be obtained from in situ tests. However, direct measurements of the more important coefficient of consolidation, c_v, are not sufficiently reliable to provide much additional information to laboratory data.

(4) The coefficients of consolidation and permeability of fine grained soils can be estimated economically onshore and offshore by adequately interpreting the pore pressure dissipation that takes place after cone penetration is inter-

rupted. Important questions related to interpretation include: a) What cone angle provides the most reliable results; b) Where to measure the pore pressures on the cone or the shaft behind it?; c) How long should dissipation take (i.e., what degreee of consolidation is required)?; d) What coefficient of consolidation (vertical, horizontal, etc.) and/or what coefficient of permeability is measured; e) What is the magnitude of the measured parameters; and, for what practical application?

(5) Theoretically, dissipation records are difficult to interpret because of: a) uncertainties in the initial excess pore pressure distribution in the soil caused by steady cone penetration; b) The high-gradients associated with this distribution; c) the two-dimensional nature of consolidation around a cone because fluid flow and soil deformations occur in the horizontal and vertical directions; d) soil anisotropy and nonlinearity; e) coupling between total stresses and pore pressures during consolidation, and; f) uncertainties regarding the level of shearing during consolidation and the creep characteristics of the soil.

Additional practical difficulties include: a) uncertainties in estimating a meaningful initial reading, u_i, of pore pressure before dissipation starts. This is due to

inherent soil variability and is especially important in erratic soils where the penetration pore pressure is highly variable; b) uncertainties in estimating the final (static) pore pressure, u_o, after dissipation, since complete dissipation of excess pore pressures requires very long delays in testing.

(6) Existing solutions for the dissipation of excess pore pressures (around cones and pile shafts) assume cylindrical or spherical symmetry. These one-dimensional solutions are too simplified to yield reliable results for the dissipation around cones. However, they are attractive because of their simplicity and the capabilities they offer to consider more realistic (nonlinear soil) behavior and/or to conduct parametric analyses (in order to identify important factors).

Randolph et al. (1978) evaluate the effects of nonlinearities (due to changes in soil stiffness) on the consolidation around a cylindrical cavity by means of finite element solutions using an elastic perfectly-plastic model and a Cam-Clay model. Results of the analyses indicate that soil nonlinearities might have some effect on effective stresses at the cavity wall depending on the model and soil parameters but have no noticeable effect on pore pressure dissipation.

(7) Linear uncoupled one-dimensional consolidation analyses presented in Chapter 3 indicate that dissipation results are: a) strongly influenced by the initial excess pore pressure distribution, and, b) are controlled by the soil properties in the vicinity of the probe and not the outer soil. Furthermore, the inner soil is predominantly subjected to a decrease in volume during consolidation.

(8) The initial excess pore pressures, Δu_i, caused by steady cone penetration are difficult to predict because of the complicated behavior of soils; the large strains and the complicated strain paths to which the soil is subjected; and, the boundary conditions at the cone-soil interface.

Reliable measurements of, Δu_i, on a penetrating cone (or the shaft behind it) require special care in order to insure a very rapid response time of the measuring probe. Furthermore, meaningful measurements of the pore pressures in the soil surrounding a penetrating cone are very difficult to conduct principally because of the interaction between soil deformations and the measuring probe (See Chapter 3).

(9) Most of the existing methods for modelling cone penetration (and pile installation) utilize one-dimensional cavity expansion solutions that neglect the two-dimensional nature of cone penetration and hence cannot predict the required distribution of initial excess pore pressures.

(10) Deep cone penetration in clays is an axisymmetric two-dimensional steady state problem which is essentially strain-controlled, i.e., strains and deformations in the soil are primarily imposed by kinematic requirements. For this type of problem, Baligh (1975) proposes an approximate method of solution called the "strain path method". Levadoux and Baligh, 1980, apply this method to cone penetration in clays and estimate the normalized excess pore pressures on the basis of laboratory test data on normally consolidated Boston Blue clay. Linear dissipation analyses are not affected by the absolute value (magnitude) of excess pore pressures, Δu_i, and only require estimates of the normalized excess pore pressures $\Delta u_i/(\Delta u)_{sh}$ where $(\Delta u)_{sh}$ is the shaft excess pore pressure at a sufficiently large distance behind the cone.

(11) An evaluation of the normalized excess pore pressure distribution predicted by the strain path method indicates good agreement with in situ pore pressure measurements.

a) Along the face and the shaft behind 18° and 60° cones in a BBC deposit having an overconsolidation ratio $1.3 < OCR < 3$; and,

b) In the soil surrounding a pile jacked into Champlain clay.

(12) The measurements of pore pressures around the jacked pile in Champlain clay are very similar to a number of other clays of different types and stress histories. Therefore, it seems possible that the predicted distributions of $\Delta u_i/(\Delta u)_{sh}$ by the strain path method for normally consolidated BBC can prove satisfactory for dissipation studies in other clays.

(13) Chapter 4 presents linear consolidation analyses to investigate: the effects of cone angle; the location of the porous stone where pore pressures are measured; the anisotropy of the soil; the size of the mesh (resolution); the coupling between pore pressures and total stresses, and; the uncertainties in the estimated initial and final pore pressures on prediction of dissipation rates. Using the normalized excess pore pressure distribution estimated by the strain path method for normally consolidated BBC (Chapter 3), results of these analyses indicate that:

a) dissipation rates are significantly dependent on the location on an 18° cone. Similar analyses for a 60° cone show that the predicted dissipation along the conical face varies little with location.

b) At a sufficient distance behind the cone, dissipation on the shaft is not significantly dependent on the cone angle and is about one to two orders of magnitude slower than dissipation at the tip;

c) a reduction in the vertical coefficient of consolidation, c_v, from c_h to 0.1 c_h causes little delay in the uncoupled pore pressure dissipation at 4 selected locations along the tip and shaft of an 18° piezometer probe provided that the time factor is defined as $T = c_h t/R^2$. This suggests that c_h governs consolidation around piezometer probes;

d) the effect of linear coupling between total stresses and pore pressures is small except at early stages of consolidation especially near the apex of an 18° cone. This suggests that uncoupled solutions can provide reasonably accurate predictions away from the apex and after sufficient dissipation has taken place;

e) accurate prediction of excess pore pressure dissipation requires the use of a fine mesh especially in the vicinity of the conical tip and;

f) errors in the static and penetration pore pressures (u_o and u_i, respectively) can seriously affect the estimated coefficient of consolidation. Matching of measured and predicted dissipation records at small (or large) degrees of consolidation is recommended if errors in u_o (or u_i) are expected.

(14) Chapter 5 evaluates linear uncoupled dissipation predictions by means of pore pressure measurements, at various locations on probes with different cone angles, after deep steady penetration in clay is interrupted. Predictions

based on the initial distribution of excess pore pressures determined by the strain path method for normally consolidated BBC are compared to dissipation measurements in the soft (OCR<2) Boston Blue Clay deposit below 60 ft. at the Saugus site. The comparison indicates that reasonably good dissipation predictions are achieved at four locations on an 18° cone and at the tip of a 60° cone when the horizontal coefficient of consolidation c_h = 0.04 cm^2/sec. Additional results of this comparison show that:

a) At early dissipation levels ($\bar{u} > 0.8$), measurements fall in a wide band and hence lead to significant uncertainties (scatter) in estimating c_h. This is particularly true when the porous stone is located at the tip of the cone.

b) At advanced consolidation stages ($\bar{u} < 0.6$, say) dissipation tends to proceed slower than predicted. This is believed to result from soil nonlinearities and, in particular, the changes in the (drained) soil compressibility during consolidation.

c) The interpretation of dissipation results obtained when the porous stone is located at the tip of an 18° cone requires a semi-empirical procedure because of the difficulty of analyzing the actual cone geometry. In this procedure the degree of consolidation (or $\bar{u}$) is taken as the average of the predicted values at the apex and mid-height of an ideal cone (geometry).

d) Dissipation records obtained on the shaft behind an 18° cone plot in a narrow band but exhibit a slightly slower rate of dissipation than predicted. This could reflect inaccuracies in the initial distribution of excess pore pressures and/or nonlinear coupling effects and/or creep effects (neglected in the proposed prediction method) leading to faster dissipation ahead of the cone. More tests conducted (with the porous stone located on the shaft) to high consolidation levels and tests involving measurements of total stresses on the cone and the shaft behind it are necessary before more definite conclusions can be reached.

(15) Profiles of c_h (probe) in the BBC deposit at Saugus are obtained at different dissipation levels for three types of conical probes: a) an 18° cone with the stone at the tip; b) an 18° cone with the stone at mid-height; and c) a 60° cone with the stone at the tip.

a) At early dissipation stages ($\bar{u} = 0.8$) the scatter of the data is so high that reasonable c_h profiles cannot be established. The scatter is particularly high when the porous stone is located at the tip of the cone and less severe when the stone is at mid-height.

b) All three probes provide consistent c_h (probe) profiles after 50% consolidation ($\pm$ 10%) involving a very moderate degree of scatter.

c) Values of c_h estimated at high levels of consolidation ($\bar{u}$ = 0.2) are slightly lower than obtained at 50% dissipation in the lower clay below 40 ft. and higher in the upper more pervious clay.

(16) A comparison of the predicted profiles of c_h (probe) at 50% dissipation with laboratory and field measurements of the vertical coefficient of consolidation, c_v, in BBC indicates that:

a) The predicted variation of c_h (probe) with depth is consistent with the trends of c_v (NC) measured in the laboratory in the normally consolidated range and the profile of c_v (loading) backfigured by Duncan and by Davis and Poulos (MIT, 1975) on the basis of in situ pore pressure measurements conducted in the foundation clay under the I-95 embankment for a period of 7 years after construction.

b) The predicted magnitude of c_h (probe) is: a) very close to c_v (unloading) backfigured by Bromwell and Lambe (1968) on the basis of in situ pore pressure measurements in a very similar BBC deposit due to a wide excavation; and, b) much higher (20 to 40 times) than c_v (NC) or c_v (loading) described above.

c) Profiles of c_h (probe) can therefore provide good estimates of the coefficient of consolidaiton to be used in foundation problems involving unloading and possibly reloading of overconsolidated clays above the maximum past pressure. On the other hand, problems involving the compression of clays in the normally consolidated range require modification of c_h (probe) to account for the difference in clay compressibility during dissipation [as expressed by RR (probe)] and the compression ratio, CR, in the normally consolidated range.

(17) An approximate method for estimating profiles of the horizontal coefficient of permeability k_h (probe) and c_v (NC) from profiles of c_h (probe) is proposed. In spite of significant simplifying assumptions, the predicted profiles of k_h (probe) and c_v (NC) appear very reasonable when compared to laboratory test data on BBC.

(18) The backfigured compressibility of BBC during dissipation is approximately given by RR (probe) $\simeq 10^{-2}$. This confirms that, as expected, the clay in the early stages of dissipation around cones ($\bar{u} > 0.5$) consolidates under relatively "small" increments of effective stresses such that the maximum past pressure is not exceeded and the clay compressibility is low.

(19) A comparison of the advantages of different types of probes indicates that the choice of a probe (cone angle and location of porous stone) for a particular job can only be made after the objectives of the investigation program have been defined and the most critical parameters clearly identified.

(20) Chapter 6 provides recommended methods for predicting the coefficients of consolidation and permeability of saturated fine grained soils from pore pressure dissipation measurements after interrupting deep steady penetration. The prediction method basically consists of evaluating c_h (probe) by matching measured and predicted dissipation records. The coefficients of consolidation in the virgin range and the permeability of the soil can then be estimated from c_h (probe).

(21) Guidelines for the practicing engineer are provided in order to: a) identify and eliminate bad records where high soil variability and/or malfunctioning of the probe lead to significant errors in the predictions, and; b) verify the applicability of the prediction method to a new soil.

(22) Important practical aspects of pore pressure dissipation are reviewed and discussed. Special emphasis is made on the deairing and rapid response of the probe, the possible errors in estimating the static (in situ) pore pressure, u_o and, the time required for meaningful dissipation to take place.

(23) The prediction method is then applied to results of dissipation tests in Connecticut Valley Varved Clay (CVVC) at Amherst, Massachusetts. Two sufficiently long dissipation records indicate that predictions apply surprisingly well to CVVC in spite of large differences in behavior from BBC. This is especially important because it means that the prediction method developed for BBC can also be applied to other clays.

(24) Profiles of c_h(probe) in CVVC estimated according to the proposed method are virtually identical for 18° and 60° cones. Furthermore, c_h(probe) profiles are consistent with measurements of cone resistance and penetration pore pressures.

(25) No (laboratory or field) tests were conducted by MIT to provide direct measurement of the overconsolidated horizontal coefficient of consolidation in CVVC. Therefore, the predicted values of c_h(probe) cannot be rigorously evaluated. However, a comparison of k_h(probe) with laboratory measurements of the horizontal permeability indicates very good agreement. Furthermore, the estimates of c_v(NC) from c_h(probe) are very close to laboratory measurements of the coefficient of consolidation in the normally consolidated (virgin) range.

REFERENCES

Ahmad, S., Lacroix, Y., and Steinback, J., "Pumping Tests in an Unconfined Aquifer," Proceedings, ASCE Specialty Conference on In Situ Measurements of Soil Properties, Raleigh, N.C., 1975, Vol. I, p. 1.

Airhart, T.P., Coyle, H.M., Hirch, J.T., and Buchanan, S.J., "Piler-Soil Response in a Cohesive Soil," ASTM, STP No. 444, 1969.

Al-Dhahir, Z.A., Kennard, M.F., and Morgenstern, N.R., "Observations on Pore Pressures Beneath the Ash Lagoon Embankments at Fiddler's Ferry Power Station," Proceedings, Conference on In Situ Investigations in Soils and Rocks, British Geotechnical Society London, Paper No. 20, 1970, pp. 265-276.

Aldrich, H.P. Jr., "Back Bay Boston, Part I," BSCE/ASCE Journal, Vol. 57, No. 1, January 1970, pp. 1-33.

Azzouz, A.S. and Baligh, M.M., "Three-Dimensional Stability of Slopes," Research Report R78-8, No. 595, Department of Civil Engineering, MIT, Cambridge, Mass., June 1978.

Azzouz, A.S., Levadoux, J.N., and Baligh, M.M., "Cavity Expansion Approaches in Deep Foundations," Research Report, Department of Civil Engineering, MIT, Cambridge, Mass., 1980 (in preparation).

Baguelin, F., Jezequel, J-F., and LeMehaute, A., "Etude des Pressions Interstitielles Developpees lors de l'Essai Pressiometrique," Proceedings, 8th International Conference on Soil Mechanics and Foundation Engineering, Moscow, Vol. 1.2, 1973, pp. 19-24.

Baligh, M.M., "Theory of Deep Site Static Cone Penetration Resistance," Research Report R75-56, No. 517, Department of Civil Engineering, MIT, Cambridge, Mass., September 1975.

Baligh, M.M., Vivatrat, V., and Ladd, C.C., "Exploration and Evaluation of Engineering Properties for Foundation Design of Offshore Structures," Research Report R78-40, No. 607, Department of Civil Engineering, MIT, Cambridge, Mass., December 1978.

Baligh, M.M. and Vivatrat, V., "In Situ Measurements in a Marine Clay," Proceedings, International Conference on the Behavior of Offshore Structures, Paper 14, 1979, pp. 151-174.

Baligh, M.M., Vivatrat, V., and Ladd, C.C., "Cone Penetration in Soil Profiling," Journal of the Geotechnical Division, ASCE, Vol. 106, April 1980, pp. 447-761

Banerjee, S. and Mitchell, J.K., "In Situ Volume Change Properties by Electro-Osmosis: Theory," Journal of the Geotechnical Division, ASCE, Vol. 106, April 1980, pp. 347-365.

Bathe, K.-J., "ADINAT: A Finite Element Program for Automatic Dynamic Incremental Nonlinear Analysis of Temperatures," Research Report 82448-5, Department of Mechanical Engineering, MIT, Cambridge, Mass., May 1977 (revised, Dec. 1978).

Biot, M.A., "General Theory of Three-Dimensional Consolidation," Journal of Applied Physics, Vol. 12, 1941, pp. 155-164.

Bishop, A.W. and Al-Dhahir, Z.A., "Some Comparisons Between Laboratory Tests, In Situ Tests, and Full Scale Performance, With Special Reference to Permeability and Coefficient of Consolidation," Proceedings, Conference on In Situ Investigations in Soils and Rocks, British Geotechnical Society, London, Paper No. 19, 1970, pp. 251-264.

Bishop, A.W. and Henkel, D.J., "The Measurement of Soil Properties in the Triaxial Test," Arnold, London, 1962.

Bishop, A.W., Kennard, M.F., and Vaughan, P.R., "Developments in the Measurement and Interpretation of Pore Pressures in Earth Dams," Transactions, 8th International Congress on Large Dams, Edinburgh, Vol. 2, 1964, pp. 47-72.

Bishop, R., Hill, R., and Mott, N., "The Theory of Indentation and Hardness Tests," Proceedings, Physical Society, London, Vol. 57, Part 3, No. 321, May 1945, pp. 147-159.

Bjerrum, L. and Johannessen, I., "Pore Pressures Resulting From Driving Piles in Soft Clays," Proceedings, Conference on Pore Pressure and Suction in Soils, London, Butterworths, 1961, pp. 108-111.

Bjerrum, L., Nash, J.K.T.L., Kennard, R.M., and Gibson, R.E., "Hydraulic Fracturing in Field Permeability Testing," Geotechnique, Vol. 22, No. 2, 1972, pp. 319-332.

Bromwell, L.G. and Lambe, T.W., "A Comparison of Laboratory and Field Values of c_v for Boston Blue Clay, Professional Paper P68-3, Soils Publication No. 205, Department of Civil Engineering, MIT, Cambridge, Mass., January 1968.

Butterfield, R. and Bannerjee, P.K., "The Effect of Porewater Pressures on the Ultimate Bearing Capacity of Driven Piles," Proceedings, 2nd Southeast Asian Conference on Soil Engineering, Singapore, June 1970, pp. 385-394.

Carslaw, A.R. and Jaeger, C.J., Conduction of Heat in Solids, Oxford at the Clarendon Press, London, 1959.

Carter, J.P., Randolph, M.F., and Wroth, C.P., "Stress and Pore Pressure Changes in Clay During and After the Expansion of a Cylindrical Cavity," Report No. TR 51, Department of Civil Engineering, University of Cambridge, England, 1978.

Casagranda, A., Piezometers for Pore Pressure Measurements in Clay, Pierce Hall, Harvard Univeristy, Cambridge, Mass., July 1946.

Casagranda, A. and Poulos, S., "On the Effectiveness of Sand Drains," Canadian Geotechnical Journal, Vol. 6, No. 3, 1969, pp. 287-326.

Chadwick, P., "The Quasi-Static Expansion of Spherical Cavity in Metals and Ideal Soils," Quarterly Journal of Mechanics and Applied Mathematics, Vol. 12, Part I, 1959, pp. 52-71.

Cryer, C.W., "A Comparison of the Three-Dimensional Consolidation Theories of Biot and Terzaghi," Quarterly Journal of Mechanics and Applied Mathematics, Vol. 16, Part 4, 1963, pp. 401-412.

D'Appolonia, D.J., Lame, T.W., and Poulos, H.G., "Evaluation of Pore Pressures Beneath an Embankment," Journal of the Soil Mechanics and Foundations Division, ASCE, Vol. 97, No. SM6, 1971, pp. 881-898.

Davis, E.H. and Poulos, H.G., "Discussion of An Analysis of Consolidation Theories by R.L. Schiffman, A.T.F. Chen, and J.C. Jordan," Journal of the Soil Mechanics and Foundations Division, ASCE, Vol. 96, No. SM1, January 1970, pp. 334-336.

DeJong, G.J., "Consolidation Around Pore Pressure Meters," Journal of Applied Physics, Vol. 24, 1953, pp. 922-928.

Fuleihan, N.F. and Ladd, C.C., "Design and Performance of Atchafalaya Flood Control Levees," Research Report R76-24, No. 543, Department of Civil Engineering, MIT, Cambridge, Mass., May 1976.

Germaine, J.T., Unpublished CRSC consolidation results on Boston Blue Clay (Saugus), 1978.

Ghaboussi, J. and Wilson, E.L., "Flow of Compressible Fluid in Porous Elastic Media," UC-SESM Report No. 71-12, Structural Engineering Laboratory, University of California, Berkeley, July 1971.

Ghaboussi, J. and Wilson, E.L., "Flow of Compressible Fluid in Porous Elastic Media," International Journal for Numerical Methods in Engineering, Vol. 5, 1973, pp. 419-442.

Ghionna, V. et al., "Performance of the Self-Boring Pressuremeter in Saturated Cohesive Deposits," Progress Report No. 1, Istituto di Scienza delle Costruzioni, Politecnico di Torino, Joint Research with the Department of Civil Engineering, MIT, Cambridge, Mass., July 1979.

Gibson, R.E., "An Analysis of System Flexibility and its Effect on Time-Lag in Pore Water Pressure Measurements," Geotechnique, Vol. 13, 1963, pp. 1-11.

Gibson, R.E., "A Note on the Constant Head Test to Measure Soil Permeability In Situ, Geotechnique, Vol. 16, 1966, pp. 256-257.

Gibson, R.E., "Discussion on the Interpretation of Constant Head In Situ Field Permeability Tests," Proceedings, Conference on In Situ Investigations in Soils and Rocks, British Geotechnical Society, London, 1970, pp. 297-298.

Gibson, R.E. and Anderson, W.F., "In Situ Measurement of Soil Properties with the Pressuremeter," Civil Engineering and Public Works Review, Vol. 56, No. 658, May 1961, pp. 615-618.

Gibson, R.E., Knight, K., and Taylor, P.W., "A Critical Experiment to Examine Theories of Three-Dimensional Consolidation," Proceedings, European Conference on Soil Mechanics and Foundation Engineering, Wiesbaden, Germany, Vol. 1, 1963, pp. 69-76.

Grisak, G.E., "The Fracture Porosity of Glacial Till," Canadian Journal of Earth Science, Vol. 12, No. 3, 1975.

Grisak, G.E. and Cherry, J.A., "Hydrologic Characteristics and Response of Fractured Till and Clay Confining a Shallow Aquifer," Canadian Geotechnical Journal, Vol. 12, No. 1, 1975.

Guertin, J.D., "Stability and Settlement Analysis of an Embankment on Clay," M.S. Thesis, Department of Civil Engineering, MIT, Cambridge, Mass., 1967.

Hvorslev, M.J., "Time-Lag and Soil Permeability in Ground-Water Observations," Bulletin No. 36, U.S. Waterways Experiment Station, Vicksburg, Miss., 1951.

Ismael, N.F. and Klym, J.W., "Pore-Water Pressure Induced by Pile Driving," Journal of the Geotechnical Division, ASCE, Vol. 105, Nov. 1979, pp. 1349-1354.

Jezequel, J.F. and Mieussens, C., "In Situ Measurement of Coefficients of Permeability and Consolidation of Fine Soils," Proceedings, ASCE Specialty Conference on In Situ Measurement of Soil Properties, Raleigh, N.C., Vol. 1, 1975, pp. 208-224.

Kallstenius, T. and Wallgren, A., "Pore-Water Pressure Measurements in Field Investigations," Proceedings, Royal Swedish Geotechnical Institute, No. 13, 1956.

Kenney, T.C., "Sea Leavel Movements and Geologic Histories of the Post-Glacial Marine Soils at Boston, Nicolet, Ottawa, and Oslo," Geotechnique, Vol. 14, No. 3, 1964, pp. 203-230.

Koizumi, Y. and Ito, K., "Field Tests with Regard to Pile Driving and Bearing Capacity of Piled Foundations," Soils and Foundations, Japan, Vol. 7, No. 3, 1967, pp. 30-53.

Lacasse, S.M., personal communication, 1980.

Ladanyi, B., "Expansion of a Cavity in a Saturated Clay Medium," Journal of the Soil Mechanics and Foundations Division, ASCE, Vol. 89, No. SM4, July 1963, pp. 127-161.

Ladanyi, B., "In-Situ Determination of Undrained Stress-Strain Behavior of Sensitive Clay with the Pressuremeter," Canadian Geotechnical Journal, Vol. 9, No. 3, August 1972, pp. 313-319.

Ladd, C.C., "Foundation Design of Embankments Constructed on Connecticut Valley Varved Clay," Research Report R75-7, No. 343, Department of Civil Engineering, MIT, Cambridge, Mass., June 1975.

Ladd, C.C., "Use of Precompression and Vertical Sand Drains for Stabilization of Foundation Soils," Research Report No. R76-4, No. 541, Department of Civil Engineering, MIT, Cambridge, Mass., June 1976 (revised 1978).

Ladd, C.C. and Foott, R., "New Design Procedure for Stability of Soft Clays," Journal of the Geotechnical Division, ASCE, Vol. 100, July 1974, pp. 763-786.

Ladd, C.C. et al., "Stress-Deformationa and Strength Characteristics," Proceedings, 9th International Conference on Soil Mechanics and Foundations Engineering, Tokyo, Vol. 2, 1977, pp. 421-494.

Ladd, C.C. et al., "Evaluation of Self-Boring Pressuremeter Tests in Boston Blue Clay," Research Report No. R79-4, Department of Civil Engineering, MIT, Cambridge, Mass., 1979.

Lambe, T.W., "The Stress Path Method," Journal of the Soil Mechanics and Foundations Division, ASCE, Vol. 93, November 1967, pp. 309-331.

Lambe, T.W. and Whitman, R.V., Soil Mechanics, John Wiley & Sons, New York, 1969.

Levadoux, J.N., "Pore Pressures due to Cone Penetration," Ph.D. Thesis, Department of Civil Engineering, MIT, Cambridge, Mass., 1980.

Levadoux, J.N. and Baligh, M.M., "Pore Pressures During Cone Penetration in Clays," Research Report, Department of Civil Engineering, MIT, Cambridge, Mass., 1980 (in preparation).

Levadoux, J.N. and Baligh, M.M., "Radial Consolidation in Solutions," Research Report, Department of Civil Engineering, MIT, Cambridge, Mass., 1980 (in preparation).

Lo, K.Y. and Stermac, A.G., "Induced Pore Pressures During Pile-Driving Operations," Proceedings, 6th International Conference on Soil Mechanics and Foundations Engineering, Montreal, Quebec, Vol 2, 1965, pp. 285-289.

Loudon, A.G., "The Computation of Permeability from Simple Soil Tests," Geotechnique, Vol. 3, No. 4, 1952.

Lunne, T. and Lacasse, S.M., "Results of In Situ Self-Boring Pressuremeter Dutch Cone and Piezometer Probe Tests in Norwegian Clays," Norwegian Geotechnical Institute, Internal Report 52155-10, Oslo, 1980.

Mandel, J., "Consolidation des Sols (Etude Mathematique)," Geotechnique, Vol. 3, 1953, pp. 287-299.

Mansur, C.I. and Kaufman, R.I., "Dewatering," Foundation Engineering, Chapter 3, McGraw Hill, New York, 1962.

Martin, R.I, personal communication, 1980.

Meyerhof, G.G., "The Ultimate Bearing Capacity of Foundations," Geotechnique, Vol. II, No. 4, 1951, pp. 301-332.

Meyerhof, G.G., "The Ultimate Bearing Capacity of Wedge-Shaped Foundations," Proceedings, 5th International Conference on Soil Mechanics and Foundation Engineering, Vol. 2, 1961, pp. 103-109.

Milligan, V., "Field Measurement of Permeability in Soil and Rock," Proceedings, ASCE Specialty Conference on In Situ Measurement of Soil Properties, Raleigh, N.C., Vol. 2, 1975, pp. 3-36.

Proceedings, Foundation Deformation Prediction Symposium, MIT, U.S. Department of Transportation, 1975, 2 Vol.

Mitchell, J.K. and Durgunoglu, H.T., "In Situ Strength by Static Cone Penetration Test," Proceedings, 8th International Conference on Soil Mechanics and Foundation Engineering, Moscow, Vol. 1, 1973, pp. 279-286.

Mitchell, J.K. and Gardner, W.S., "In Situ Measurement of Volume Change Characteristics," Proceedings, ASCE Specialty Conference on In Situ Measurement of Soil Properties, Raleigh, N.C., 1975, pp. 279-345.

Mitchell, J.K. and Banerjee, S., "In Situ Volume-Change Properties by Electro-Osmosis: Evaluation," Journal of the Geotechnical Division, ASCE, Vol. 106, April 1980, pp. 367-384.

NAVFAC: DM-7, Naval Facilities Engineering Command Design Manual: Soil Mechanics, Foundations, and Earth Structures, Alexandria, Va., 1971.

Palmer, A.C., "Undrained Plane-Strain Expansion of a Cylindrical Cavity in Clay: A Simple Interpretation of the Pressuremeter Test," Geotechnique, Vol. 22, No. 3, 1972, pp. 451-457.

Penman, A.D.M., "A Study of the Response Time of Various Types of Piezometers," Proceedings, Conference on Pore Pressure and Suction in Soils, London, Butterworth, 1961, pp. 53-58.

Prevost, J.H. and Hoeg, K., "Analysis of Pressuremeter in Strain-Softening Soil," Journal of the Geotechnical Engineering Division, ASCE, Vol. 101, August 1975, pp. 717-732.

Randolph, M.F., Carter, J.P., and Wroth, C.P. "Driven Piles in Clay: Installation, Modelled as the Expansion of a Cylindrical Cavity," Report No. TR 53, Department of Civil Engineering, University of Cambridge, England, 1978.

Randolph, M.F. and Carter, J.P., "Discussion of 'Effects of Driving Subsequent Consolidation on Behavior of Piles,' by C.S. Desai," International Journal for Numerical and Analytical Methods in Geomechanics, Vol. 3, 1979, pp. 213-215.

Randolph, M.F., Steenfelt, J.S., and Wroth, C.P., "The Effect of Pile Type of Design Parameters for Driven Piles," Proceedings, 7th European Conference on Soil Mechanics and Foundation Engineering, Brighton, England, 1979.

Randolph, M.F. and Wroth, C.P., "An Analytical Solution for the Consolidation Around a Driven Pile," Report No. TR 50, Department of Engineering, University of Cambridge, England, 1978.

Recker, K.L., "Measured Deformation and Pore Pressures Under an Embankment on Soft Clay," M.S. Thesis, Department of Civil Engineering, MIT, Cambridge, Mass., 1973.

Rendulic, L., "Poreziffer und Poren Wasserdruck in Tonen," Bauingenieur, Vol. 17, 1936, pp. 559-564.

Rowe, P.W., "The Influence of Geological Features of Clay Deposits in Relate to Site Investigation Practice," Proceedings, Institution of Civil Engineers, Supplement I, 1968, pp. 73-131.

Rowe, P.W., "The Relevance of Soil Fabric to Site Investigation Practice," Geotechnique, Vol. 22, No. 2, 1972, pp. 195-300.

Rowe, P.W. and Bar-en, L., "A New Consolidation Cell," Geotechnique, Vol. 16, June 1966, pp. 162-170.

Roy, M. et al., "Behavior of a Sensitive Clay During Pile Driving," Proceedings, 32nd Canadian Geotechnical Conference, Quebec, Sept. 1979, pp. 4.28-4.49.

Schiffmen, R.L., Chen, A.T.F., and Jordan, J.C., "An Analysis of Consolidation Theories," Journal of the Soil Mechanics and Foundations Division, ASCE, Vol. 95, Jan. 1969, pp. 285-336.

Schmertmann, J.S., "Study of Feasibility of Using Wissa-Type Piezometer Probe to Identify Liquefaction Potential of Saturated Fine Sands," Technical Report S-72-2, Waterways Experiment Station, Vicksburg, Miss., 1978.

Sills, G.C., "Some Conditions Under Which Biot's Equations of Consolidation Reduce to Terzaghi's Equation," Geotechnique, Vol. 25, No. 1, 1975, pp. 129-132.

Small, J.C., Booker, J.R., and Davis, E.H., "Elasto-Plastic Consolidation of Soil," International Journal of Solids and Structures, Vol. 12, 1976, pp. 431-448.

Soderberg, L.O., "Consolidation Theory Applied to Foundation Pile Time Effects," Geotechnique, Vol. 12, 1962, pp. 217-225.

Soderman, L.G. and Milligan, V., "Capacity of Fraction Piles in Varved Clay Increased by Electro-Osmosis," Proceedings, 5th International Conference on Soil Mechanics and Foundation Engineering, Paris, Vol. 2., 1961, pp. 143-147.

Terzaghi, K., "Die Berechnung der Durchlassigheitsziffer des Tones aus dem Verlaug der Hydrodynamischen Spannungsercheinungen," Akademie der Wissenchaften in Win, Sitzungsberichte Mathematish Naturwissenschaftliche Klass, Part IIa, Vol. 132, No. 3/4, 1923, pp. 125-138.

Terzaghi, K., Theoretical Soil Mechanics, John Wiley & Sons, New York, 1943.

Torstensson, B.A., "Pore Pressure Sounding Instrument," Proceedings, ASCE Specialty Conference on In Situ Measurements of Soil Properties, Raleigh, N.C, Vol. II, 1975, pp. 48-54.

Torstensson, B.-A., "The Pore Pressure Probe," Nordiske Geotekniske Møte, Oslo, Paper No. 34, 1977, pp. 34.1-34.15.

Vesic, A.S., "Expansion of Cavities in Infinite Soil Mass," Journal of the Soil Mechanics and Foundations Division, ASCE, Vol. 98, March 1972, pp. 265-290.

Viggiani, C., "Discussion of 'An Analysis of Consolidation Theories,' by R.L. Schiffman, A.T.F. Chen, and J.C. Jordan," Journal of the Soil Mechanics and Foundations Division, ASCE, Vol. 96, January 1970, pp. 331-334.

WES (Waterways Experiment Station), "Investigation of Underseepage and its Control: Lower Mississippi River Levees," TM3-424, Vicksburg, Miss., 1956.

Whitman, R.V., Richardson, A.M., and Healy, A., "Time-Lags in Pore Pressure Measurements," Proceedings, 5th International Conference on Soil Mechanics, Vol. 1, 1961, pp. 407-411.

Wilkinson, W.B., "Constant Head In Situ Permeability Tests in Clay Strata," Geotechnique, Vol. 18, 1968, pp. 172-194.

Wilkinson, W.B. and Rocke, G., "An Assessment of In Situ and Laboratory Tests in Predicting the Pore Pressure in an Earth Dam," Proceedings, Conference on In Situ Investigations in Soils and Rocks, British Geotechnical Society, London, Paper No. 21, 1970, pp. 277-284.

Wissa, A.E.Z., Christian, J.T., Davis, E.H., and Heiberg, S., "Consolidation at Constant Rate of Strain," Journal of the Soil Mechanics and Foundations Division, ASCE, Vol. 97, Oct. 1971, pp. 1393-1412.

Wissa, A.E.Z., Martin, R.T., and Garlanger, J.E., "The Piezo-Probe," Proceedings, ASCE Specialty Conference on In Situ Measurement of Soil Properties, Raleigh, N.C., Vol. I, 1975, pp. 536-545.

APPENDIX A

DISSIPATION DATA IN BOSTON BLUE CLAY: SAUGUS, MASSACHUSETTS

This appendix presents detailed information on the piezometer probe field records conducted by MIT at the I-95 embankment (Station 246) in Saugus, Mass. in 1977 and 1978. Information for each test consists of:

a) A summary table giving pertinent information for each depth: The estimated static (in situ) pore pressure u_o(kg/cm^2), the initial pore pressure u_i(kg/cm^2), the maximum pore pressure measured during dissipation u_{max}(kg/cm^2), the (maximum) duration of the dissipation test TF(sec), the (minimum) normalized excess pore pressure $\bar{u}$ at the end of the dissipation test, and, finally, the estimated coefficient of consolidation c_h(probe) at 20%, 40%, 50%, 60%, and 80% dissipation

b) A profile of penetration pore pressures

c) A profile of c_h predicted at different dissipation levels (20, 40, 50, 60, and 80%)

d) Normalized dissipation curves [$\bar{u} = \Delta u/\Delta u_i$ vs. log(time)] at each testing depth

SITE: SAUGUS DATE: 2/9/77

TEST # 5 CONE ANGLE: 18 DEG. STONE LOCATION: TIP

DEPTH (FT)	U0 (KSC)	UI (KSC)	UMAX (KSC)	TF (SEC)	UBARF	COEF. OF CONS. (CM2/SEC)					COMMENTS	
						CH20	CH40	CH50	CH60	CH80		
21.5	0.499	2.050	2.050	104	0.10	0.084	0.326	0.539	0.807	1.876	FAIR TEST - STEEP CURVE	
24.7	0.608	3.416	3.416	34	0.25	0.085	0.320	0.519	0.756	---	FAIR TEST - STEEP CURVE	
28.0	0.717	2.694	2.694	40	0.35	0.134	0.401	0.568	0.731	---	FAIR TEST - STEEP CURVE	
31.3	0.827	3.175	3.175	61	0.19	0.071	0.289	0.488	0.726	1.786	FAIR TEST - STEEP CURVE	
34.6	0.936	3.202	3.202	39	0.77	0.020	---	---	---	---	GOOD TEST	
37.9	1.045	3.596	3.596	91	0.46	0.031	0.087	0.128	---	---	GOOD TEST	
41.1	1.155	3.730	3.740	85	0.64	0.015	---	---	---	---	FAIR TEST - NO DECAY FOR 4 SEC	
44.4	1.264	5.111	5.111	171	0.44	0.033	0.076	0.094	---	---	VERY GOOD TEST	
47.7	1.374	4.914	4.914	55	0.66	0.026	---	---	---	---	GOOD TEST AFTER 3 SEC	
51.0	1.483	5.498	5.498	45	0.63	0.059	---	---	---	---	GOOD TEST	
54.3	1.592	6.082	6.082	58	0.65	0.029	---	---	---	---	GOOD TEST	
57.6	1.702	0.981	5.459	32	---	---	---	---	---	---	BAD TEST - U START5 BELOW STATIC	
60.8	1.811	6.799	6.799	66	0.69	0.035	---	---	---	---	FAIR TEST - SLOW DISSIPATION	
64.1	1.920	7.046	7.046	36	0.73	0.036	---	---	---	---	GOOD TEST AFTER 3 SEC	←
67.4	2.030	7.790	7.790	79	0.66	0.035	---	---	---	---	VERY GOOD TEST	←
70.7	2.139	8.100	8.100	36	0.74	0.034	---	---	---	---	GOOD TEST AFTER 2 SEC	←
73.9	2.248	8.030	8.030	58	0.74	0.018	---	---	---	---	VERY GOOD TEST	←
77.2	2.358	8.392	8.392	37	0.76	0.024	---	---	---	---	GOOD TEST AFTER 4 SEC	←
80.5	2.467	8.428	8.428	71	0.68	0.031	---	---	---	---	VERY GOOD TEST	←
83.8	2.577	8.379	8.379	55	0.73	0.023	---	---	---	---	VERY GOOD TEST	←
87.1	2.686	8.745	8.745	930	0.29	0.027	0.041	0.045	0.052	---	VERY GOOD TEST	←
90.4	2.795	9.085	9.085	36	0.74	0.035	---	---	---	---	VERY GOOD TEST	←
93.6	2.905	8.621	8.621	8584	0.06	0.041	0.040	0.034	0.029	0.031	VERY GOOD TEST	←

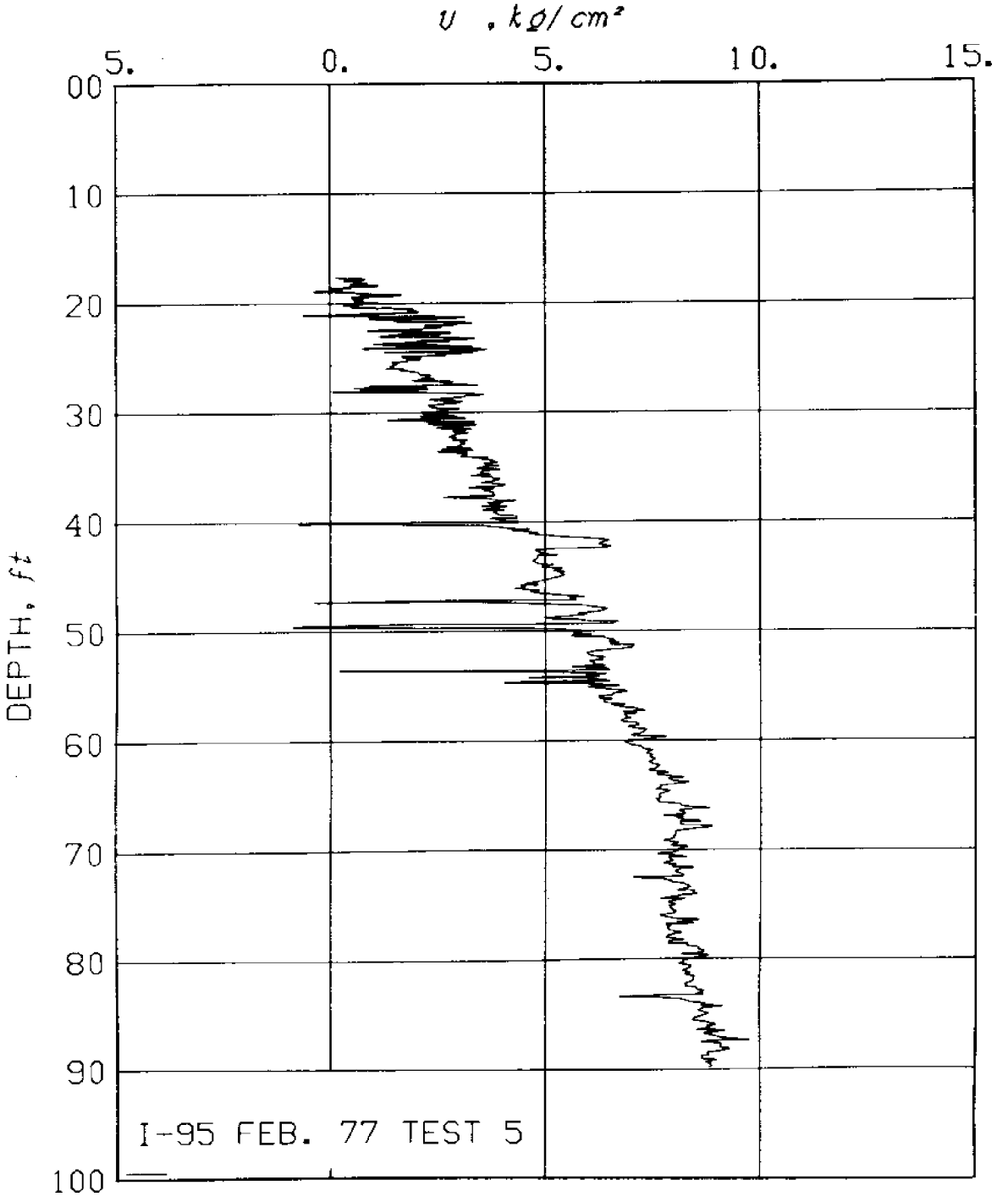
u , kg/cm²
5.
0.
5.
10.
15.
00
10
20
30
40
50
60
70
80
90
100
DEPTH, ft
I-95 FEB. 77 TEST 5

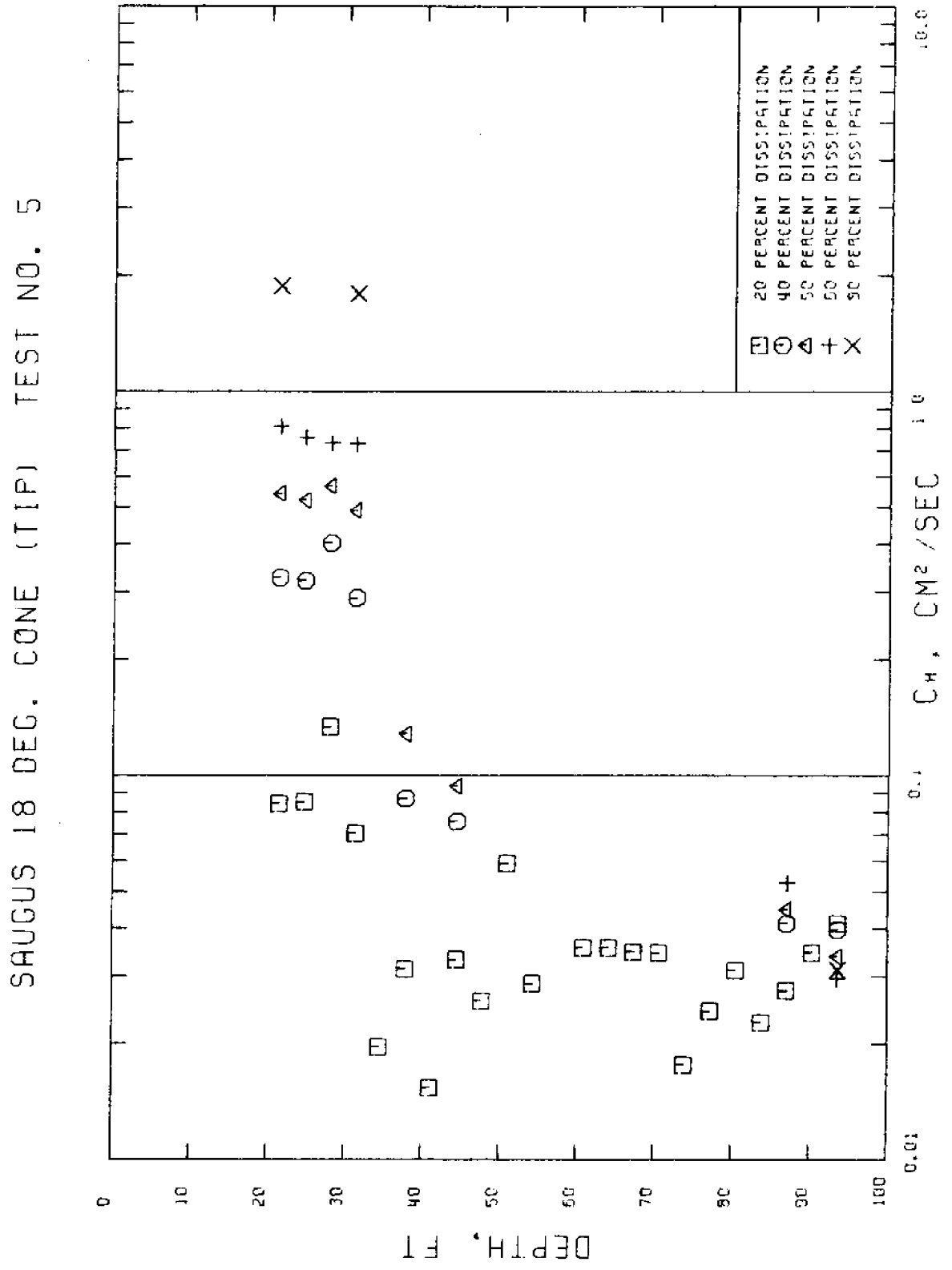
SAUGUS 18 DEC. CONE (TIP) TEST NO. 5
20 PERCENT DISSIPATION
40 PERCENT DISSIPATION
50 PERCENT DISSIPATION
60 PERCENT DISSIPATION
80 PERCENT DISSIPATION
DEPTH, FT
0
10
20
30
40
50
60
70
80
90
100
0.01
0.1
1.0
10.0
C_H, CM^2/SEC

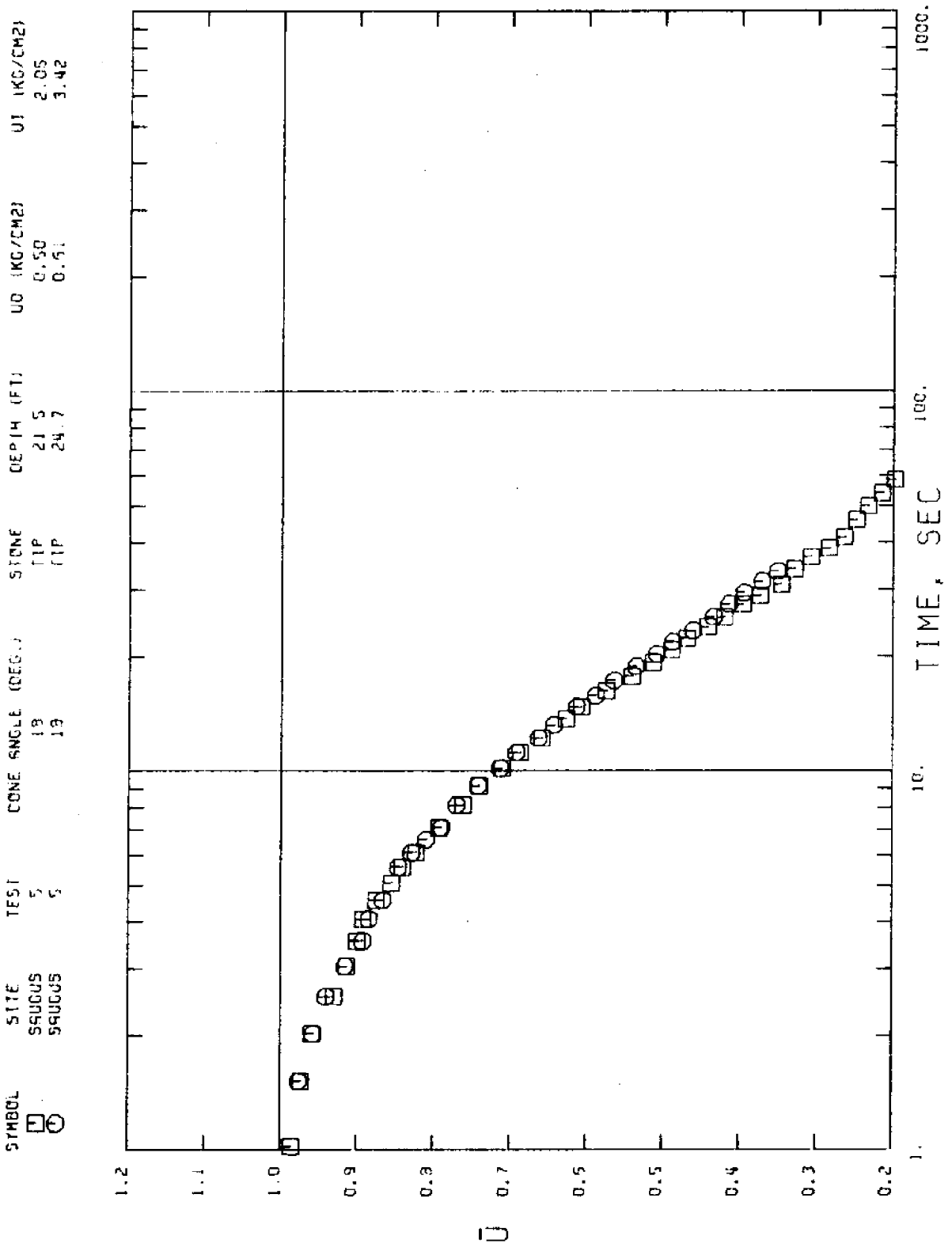
SYMBOL
SITE
TEST
CONE ANGLE (DEG.)
STONE
DEPTH (FT)
UO (KG/CM2)
UI (KG/CM2)
SAUGUS 5 19 TIP 21.5 0.50 2.05
SAUGUS 5 19 TIP 24.7 0.51 3.42
U
TIME, SEC
1.2
1.1
1.0
0.9
0.8
0.7
0.6
0.5
0.4
0.3
0.2
1.
10.
100.
1000.

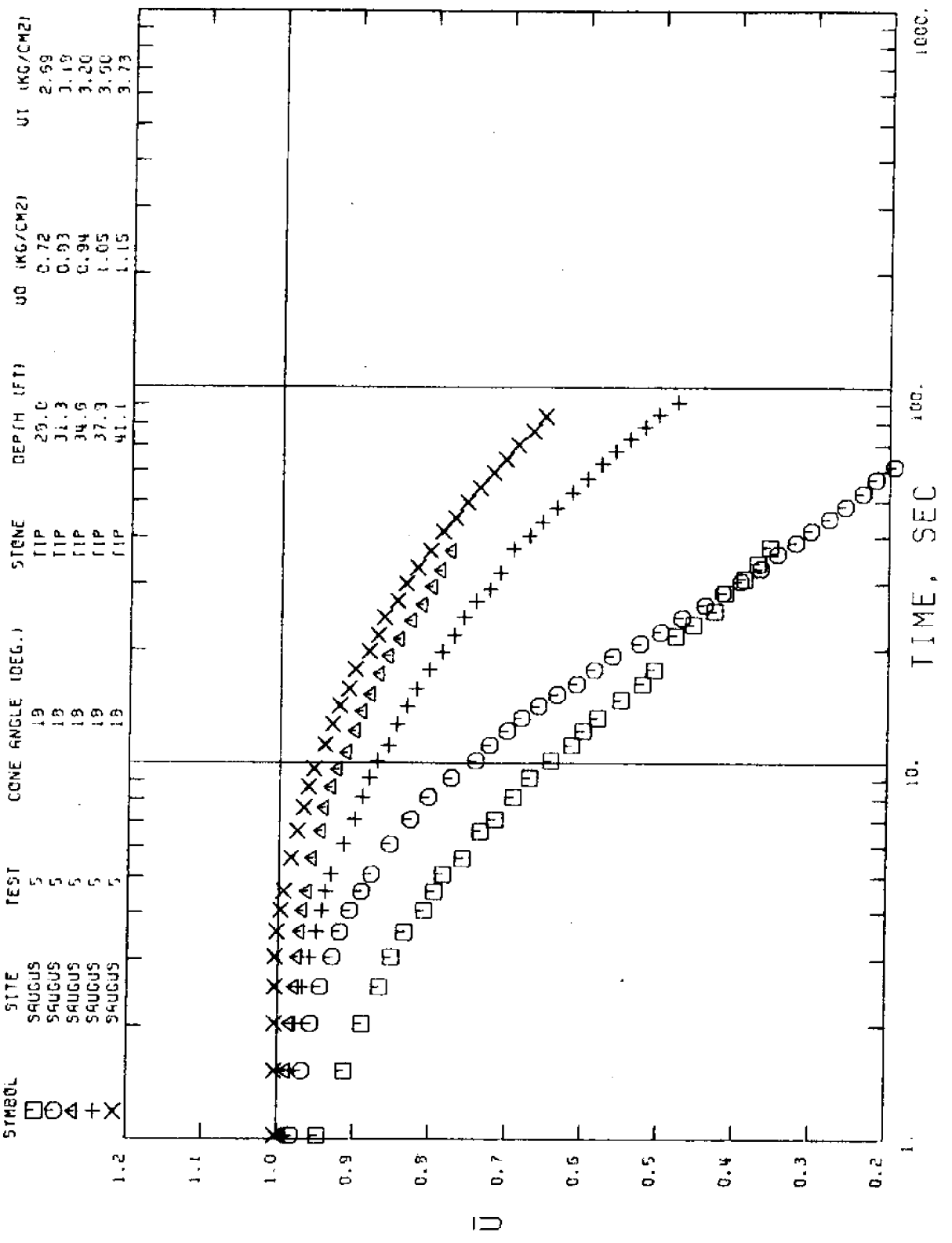
SYMBOL SITE TEST CONE ANGLE (DEG.) STONE DEPTH (FT) UO (KG/CM2) UI (KG/CM2)
SAUGUS 5 19 FIP 25.0 0.72 2.69
SAUGUS 5 19 FIP 31.3 0.93 3.19
SAUGUS 5 19 FIP 34.9 0.94 3.20
SAUGUS 5 19 FIP 37.3 1.05 3.50
SAUGUS 5 19 FIP 41.1 1.15 3.73
U
TIME, SEC
1.2
1.1
1.0
0.9
0.8
0.7
0.6
0.5
0.4
0.3
0.2
1.
10.
100.
1000.

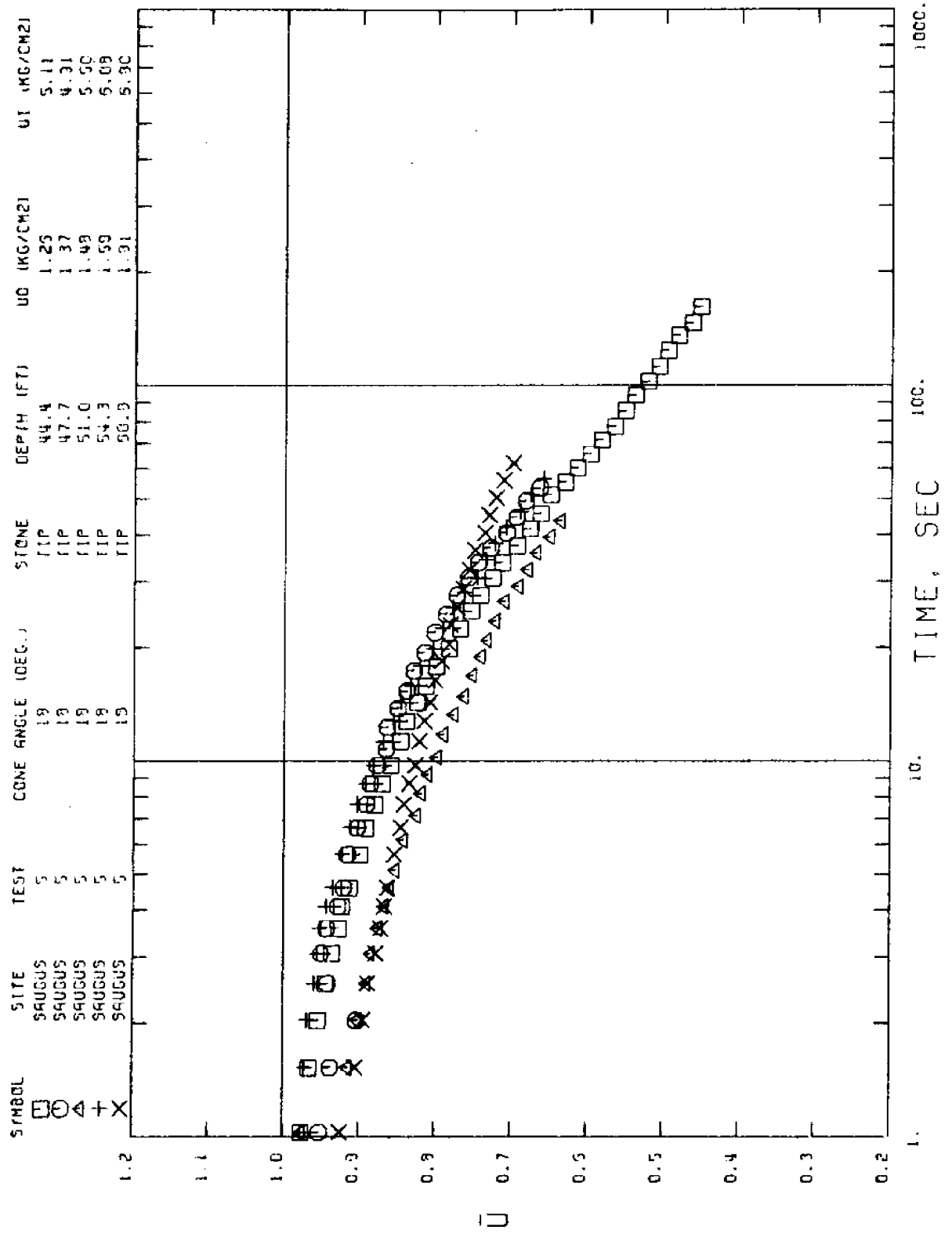
SYMBOL SITE TEST CONE ANGLE (DEG.) STONE DEPTH (FT) UO (KG/CM2) UI (KG/CM2)
SAUGUS 5 19 TIP 44.4 1.25 5.11
SAUGUS 5 19 TIP 47.7 1.37 4.31
SAUGUS 5 19 TIP 51.0 1.49 5.50
SAUGUS 5 19 TIP 54.3 1.59 5.09
SAUGUS 5 19 TIP 58.3 1.91 5.30
TIME, SEC
1.
10.
100.
1000.
1.2
1.0
0.9
0.7
0.5
0.4
0.3
0.2

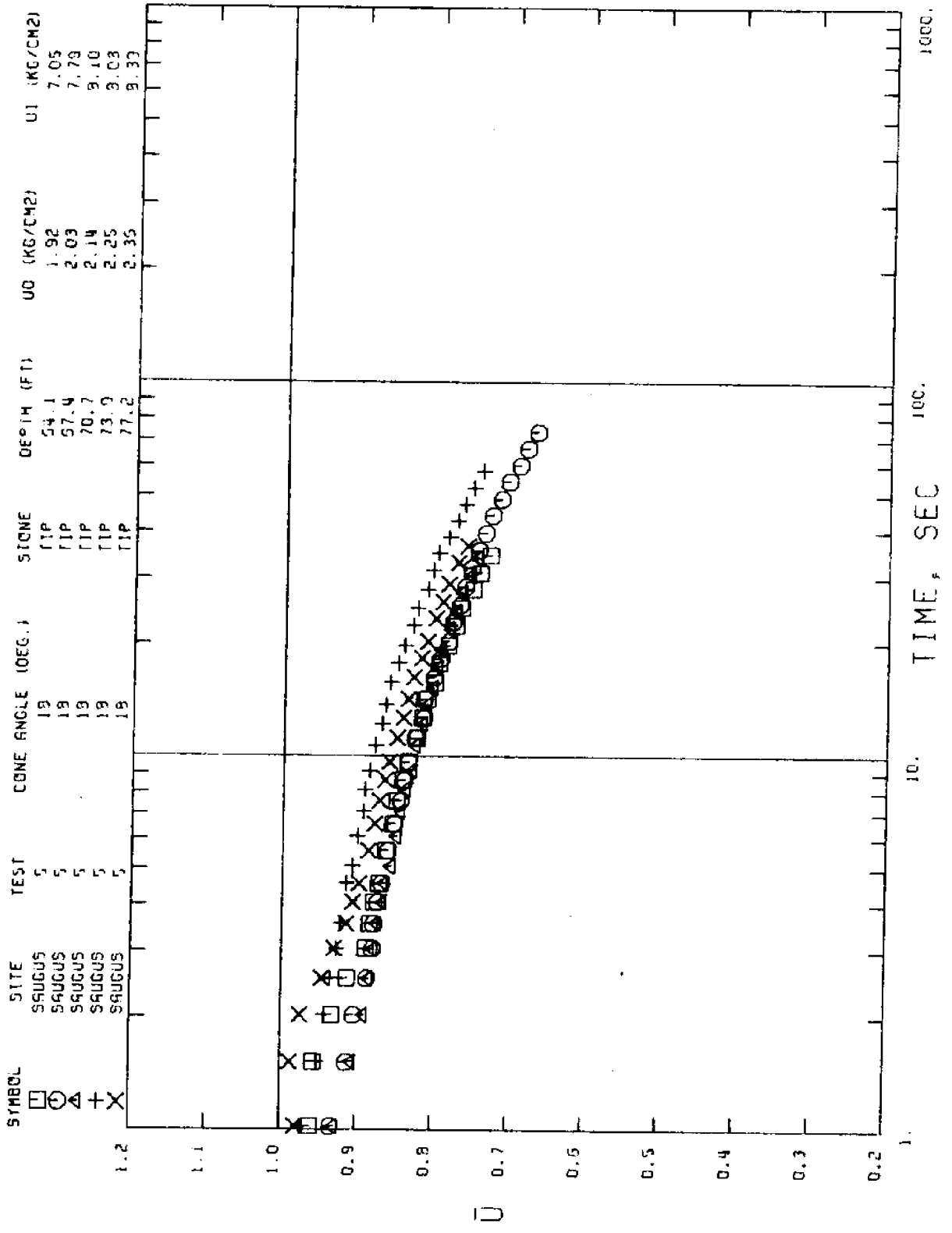
SYMBOL
SITE
TEST
CONE ANGLE (DEG.)
SIGNE
DEPTH (FT)
U0 (KG/CM2)
U1 (KG/CM2)
SAUGUS 5 19 TIP 54.1 1.92 7.05
SAUGUS 5 19 TIP 57.4 2.09 7.79
SAUGUS 5 19 TIP 70.7 2.14 9.10
SAUGUS 5 19 TIP 73.9 2.25 9.03
SAUGUS 5 19 TIP 77.2 2.35 9.33
U
TIME, SEC
1.2
1.1
1.0
0.9
0.8
0.7
0.6
0.5
0.4
0.3
0.2
1.
10.
100.
1000.

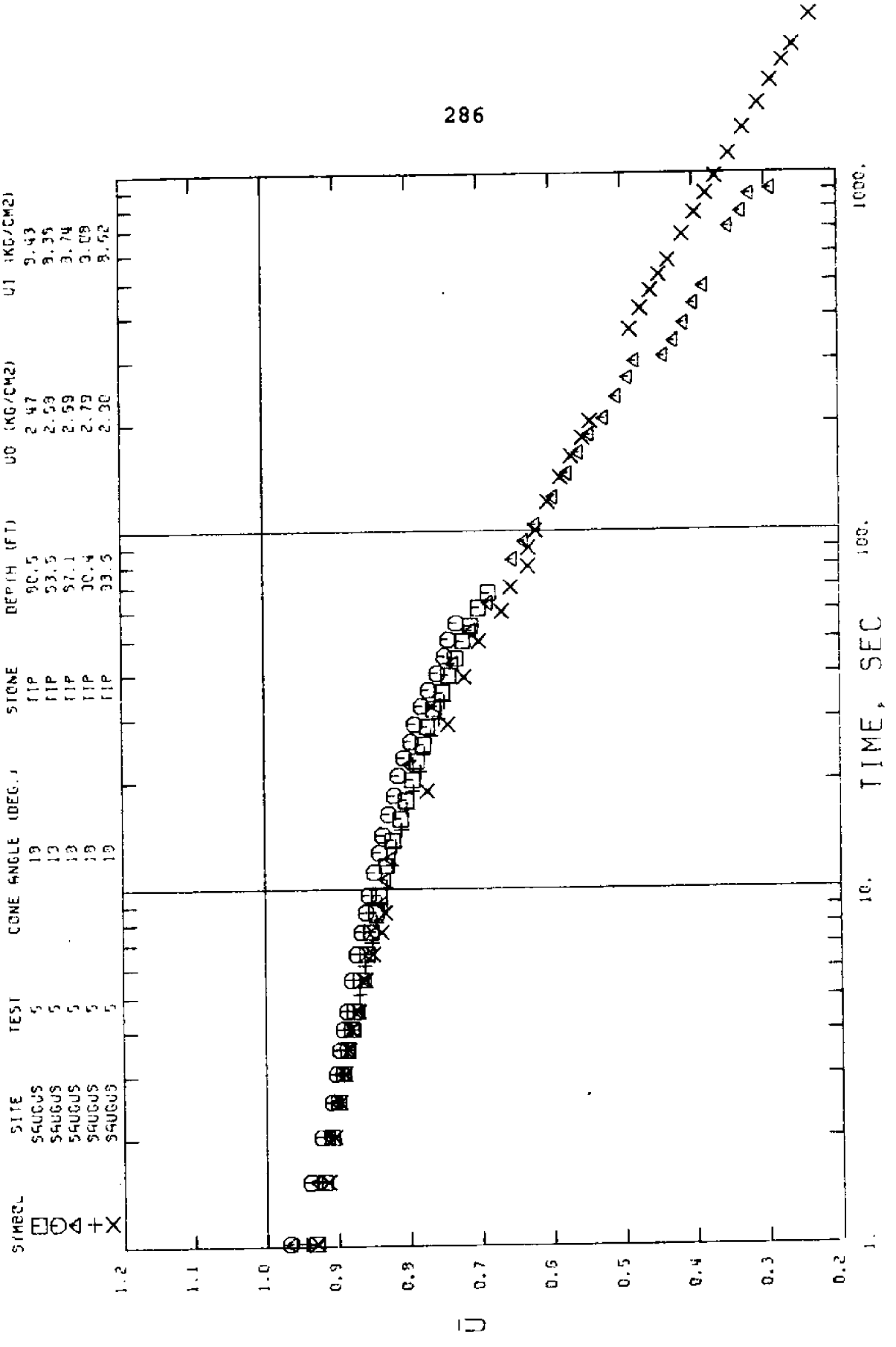
SYMBOL SITE TEST CONE ANGLE (DEG.) STONE DEPTH (FT) U0 (KG/CM2) U1 (KG/CM2)
SAUGUS 5 19 FIP 90.5 2.47 9.43
SAUGUS 5 19 FIP 53.5 2.59 9.35
SAUGUS 5 19 FIP 57.1 2.59 3.74
SAUGUS 5 19 FIP 30.4 2.79 3.09
SAUGUS 5 19 FIP 33.5 2.30 8.52
1.2
1.1
1.0
0.9
0.8
0.7
0.6
0.5
0.4
0.3
0.2
U
1.
10.
100.
1000.
TIME, SEC

SITE: SAUGUS DATE: 2/11/77

TEST # 8 CONE ANGLE: 60 DEG. STONE LOCATION: TIP

DEPTH (FT)	U0 (KSC)	U1 (KSC)	UMAX (KSC)	TF (SEC)	UBARF	COEF. OF CONS. (CM2/SEC) CH20	CH40	CH50	CH60	CH80	COMMENTS
4.1	0.000	1.155	1.155	56	0.67	0.185	---	---	---	---	FAIR TEST
7.4	0.030	0.956	0.956	25	0.17	3.557	4.583	5.594	5.865	6.515	FAIR TEST - STEEP CURVE
10.6	0.137	-0.203	0.179	26	---	---	---	---	---	---	BAD TEST - U STARTS BELOW STATIC
13.9	0.247	-0.380	0.279	35	---	---	---	---	---	---	BAD TEST - U STARTS BELOW STATIC
17.2	0.357	6.303	6.303	28	0.06	0.427	0.917	1.404	2.162	5.855	FAIR TEST - STEEP CURVE
20.5	0.467	3.705	3.705	21	0.75	0.095	---	---	---	---	FAIR TEST
23.8	0.577	5.626	5.626	79	0.51	---	---	---	---	---	BAD TEST - WIGGLING CURVE
27.0	0.683	4.864	4.864	62	0.58	0.081	0.096	---	---	---	GOOD TEST
30.3	0.793	5.935	5.935	192	0.38	---	---	---	---	---	BAD TEST - WIGGLING CURVE
33.6	0.903	5.745	5.745	148	0.28	0.408	0.520	0.481	0.399	---	FAIR TEST
36.9	1.013	4.096	4.096	77	0.47	0.079	0.147	0.191	---	---	FAIR TEST - STEEP CURVE
40.2	1.123	5.672	5.672	23	0.64	---	---	---	---	---	FAIR TEST
43.5	1.233	6.365	6.365	29	0.65	0.317	---	---	---	---	FAIR TEST
46.7	1.340	6.518	6.518	21	0.69	0.275	---	---	---	---	GOOD TEST
50.0	1.450	6.672	6.672	1271	0.25	0.269	0.127	0.089	0.056	---	GOOD TEST
53.3	1.560	7.170	7.170	21	0.71	0.233	---	---	---	---	GOOD TEST
56.6	1.670	7.498	7.498	28	0.70	0.229	---	---	---	---	GOOD TEST
59.9	1.780	8.592	8.592	30	0.69	0.264	---	---	---	---	GOOD TEST
63.1	1.887	7.794	7.794	31	0.80	---	---	---	---	---	FAIR TEST
66.4	1.997	8.729	8.729	17	0.76	---	---	---	---	---	BAD TEST
69.7	2.107	9.121	9.121	32	0.73	---	---	---	---	---	BAD TEST
73.0	2.217	9.315	9.315	37	0.69	---	---	---	---	---	BAD TEST
76.3	2.327	13.444	13.444	24	0.64	0.443	---	---	---	---	GOOD TEST
79.5	2.433	9.646	9.646	34	0.70	0.242	---	---	---	---	FAIR TEST AFTER 5 SEC
82.8	2.543	9.694	9.694	39	0.71	0.247	---	---	---	---	FAIR TEST
86.1	2.653	9.161	9.161	52	0.68	---	---	---	---	---	BAD TEST
89.4	2.763	9.584	9.584	816	0.44	0.207	0.032	0.026	---	---	GOOD TEST AFTER 5 SEC
92.7	2.873	9.831	9.831	43	0.70	0.173	---	---	---	---	GOOD TEST AFTER 5 SEC
95.9	2.980	10.786	10.786	5339	0.16	0.126	0.035	0.028	0.023	0.025	GOOD TEST AFTER 5 SEC

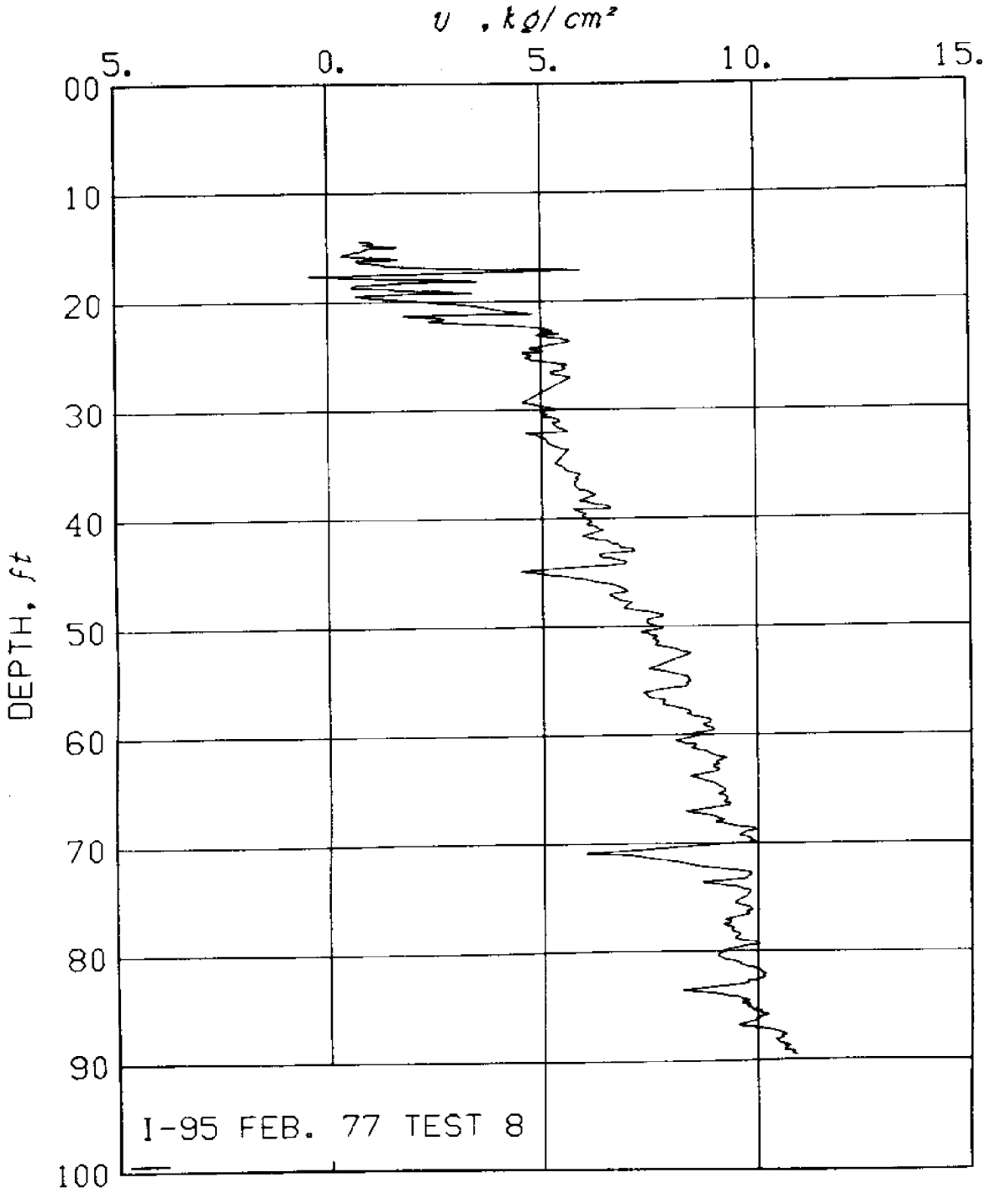
υ , kg/cm²
5.
0.
5.
10.
15.
00
10
20
30
40
50
60
70
80
90
100
DEPTH, ft
I-95 FEB. 77 TEST 8

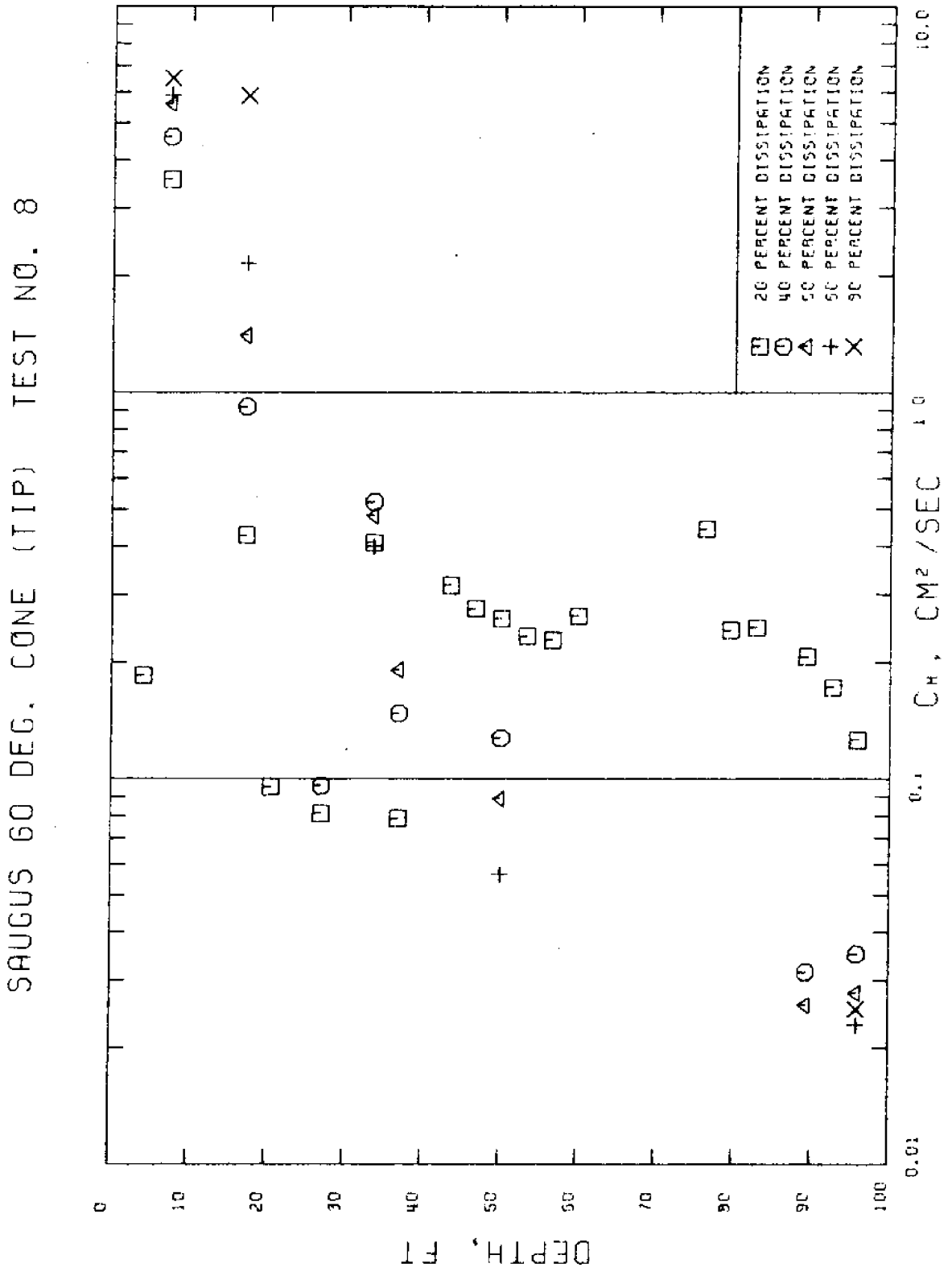
SAUGUS 60 DEG. CONE (TIP) TEST NO. 8
DEPTH, FT
0
10
20
30
40
50
60
70
80
90
100
0.01
0.1
1.0
10.0
C_H, CM^2/SEC
20 PERCENT DISSIPATION
40 PERCENT DISSIPATION
50 PERCENT DISSIPATION
60 PERCENT DISSIPATION
80 PERCENT DISSIPATION

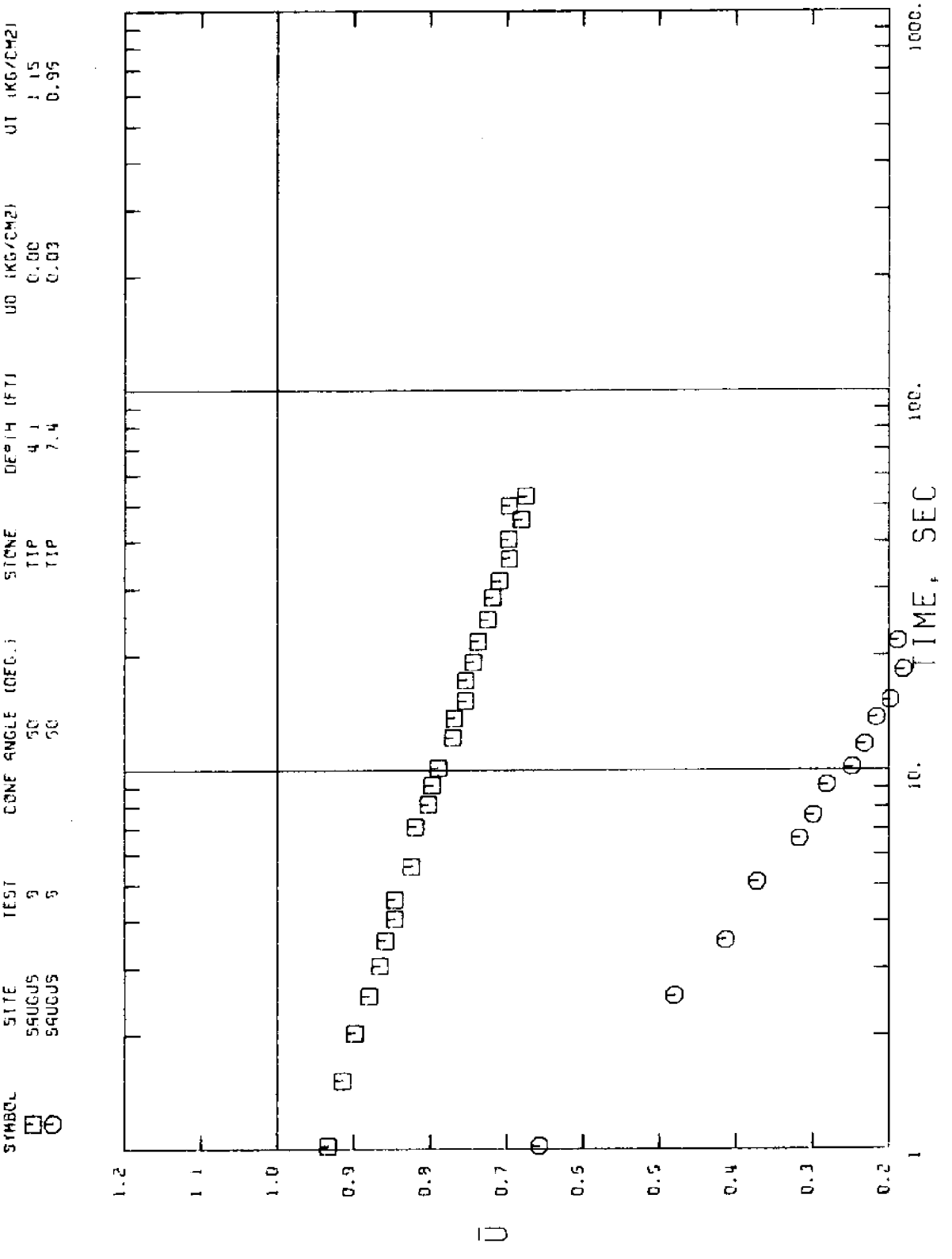
SYMBOL SITE TEST CONE ANGLE (DEG.) STONE DEPTH (FT) UO (KG/CM2) UI (KG/CM2)
SAUGUS 5 60 TIP 41 0.00 1.15
SAUGUS 5 60 TIP 7.4 0.03 0.95
U
TIME, SEC
1.2
1.1
1.0
0.9
0.8
0.7
0.6
0.5
0.4
0.3
0.2
1
10.
100.
1000.

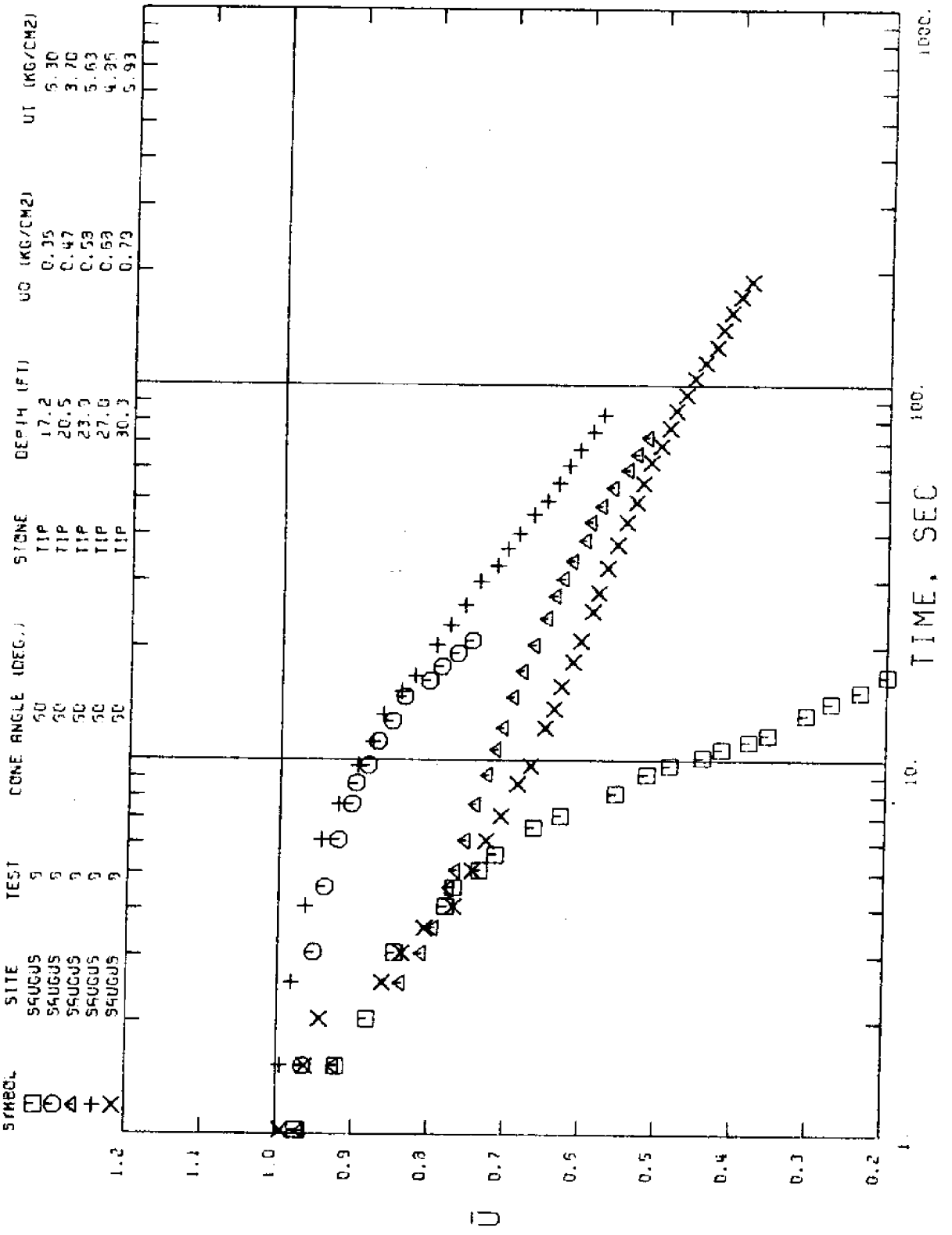
SYMBOL SITE TEST CONE ANGLE (DEG.) STONE DEPTH (FT) UO (KG/CM2) UI (KG/CM2)
SAUGUS 9 60 TIP 17.2 0.35 5.30
SAUGUS 9 60 TIP 20.5 0.47 3.70
SAUGUS 9 60 TIP 23.0 0.53 5.63
SAUGUS 9 60 TIP 27.0 0.69 4.35
SAUGUS 9 60 TIP 30.3 0.79 5.93
U
TIME, SEC
1.
10.
100.
1000.
1.2
1.1
1.0
0.9
0.8
0.7
0.6
0.5
0.4
0.3
0.2

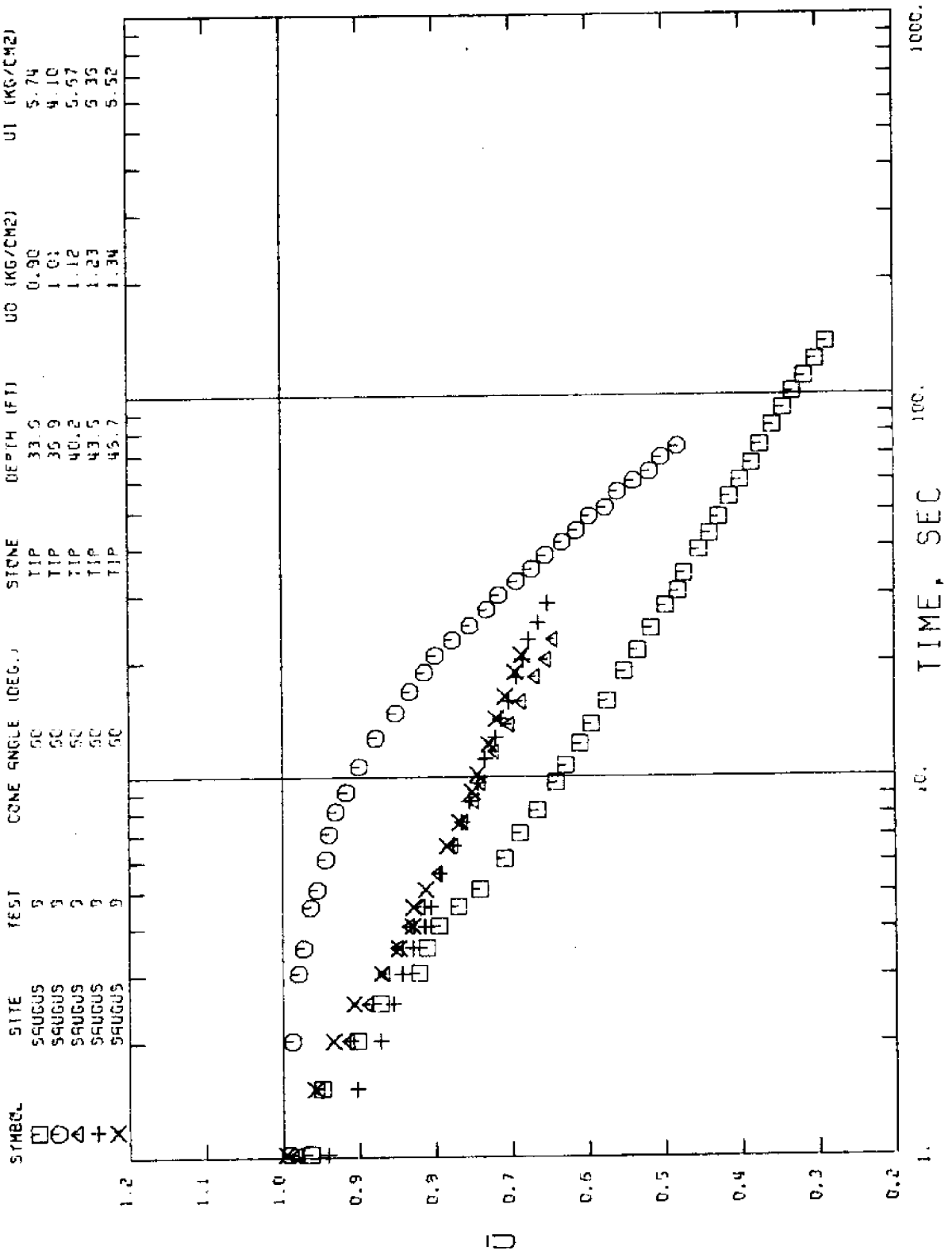
SYMBOL SITE TEST CONE ANGLE (DEG.) STONE DEPTH (FT) U0 (KG/CM2) U1 (KG/CM2)
SAUGUS 5 60 TIP 33.5 0.90 5.74
SAUGUS 5 60 TIP 35.9 1.01 4.10
SAUGUS 5 60 TIP 40.2 1.12 5.57
SAUGUS 5 60 TIP 43.5 1.23 5.35
SAUGUS 5 60 TIP 45.7 1.34 5.52
U
TIME, SEC
1.2
1.1
1.0
0.9
0.8
0.7
0.6
0.5
0.4
0.3
0.2
1.
10.
100.
1000.

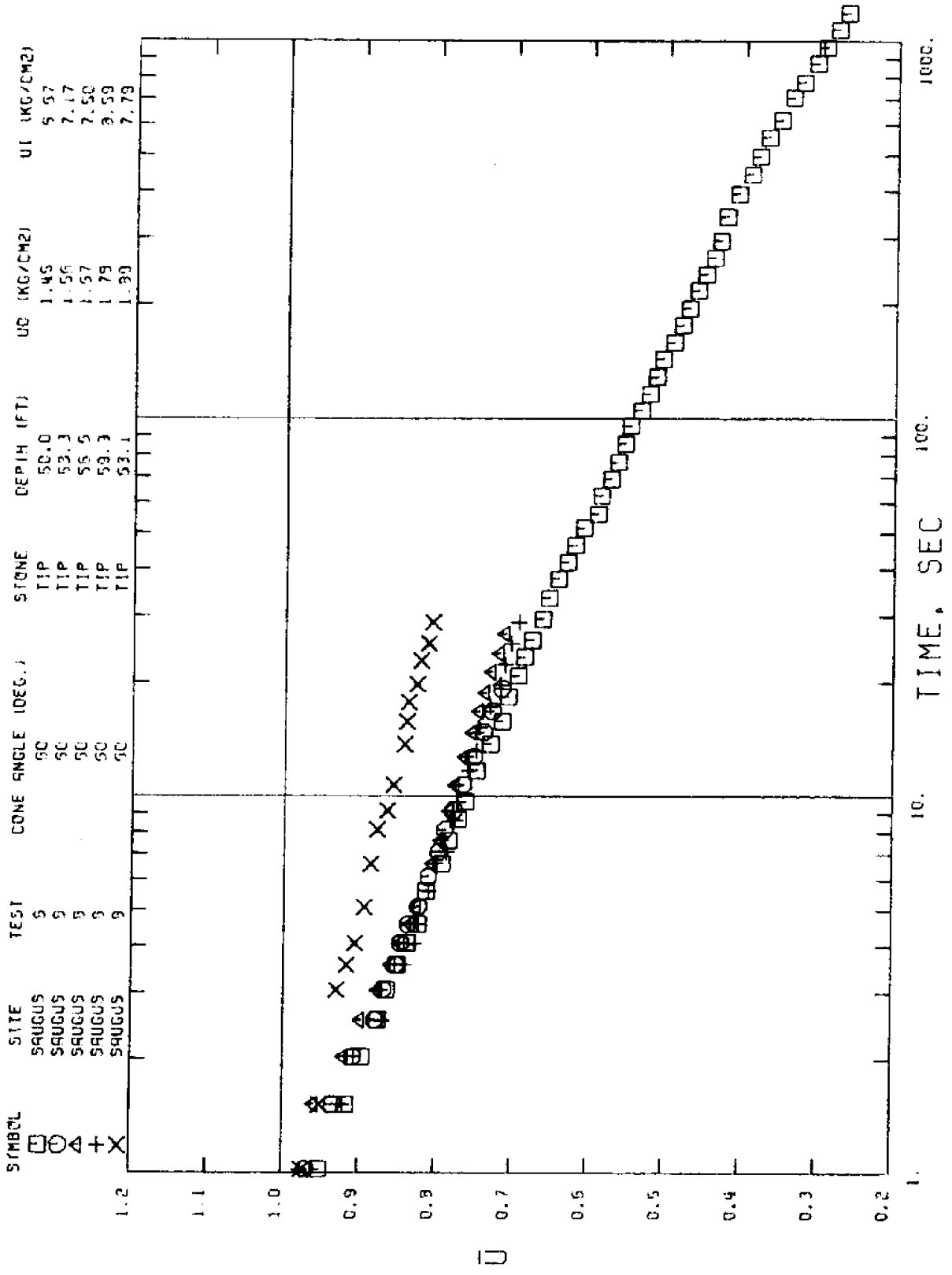
SYMBOL SITE TEST CONE ANGLE (DEG.) STONE DEPTH (FT) UO (KG/CM2) UI (KG/CM2)
SAUGUS 5 60 TIP 50.0 1.45 5.57
SAUGUS 6 60 TIP 53.3 1.56 7.17
SAUGUS 8 60 TIP 56.5 1.57 7.50
SAUGUS 8 60 TIP 58.3 1.79 8.59
SAUGUS 9 60 TIP 53.1 1.39 7.79
U
TIME, SEC
1.
10.
100.
1000.
1.2
1.1
1.0
0.9
0.8
0.7
0.6
0.5
0.4
0.3
0.2

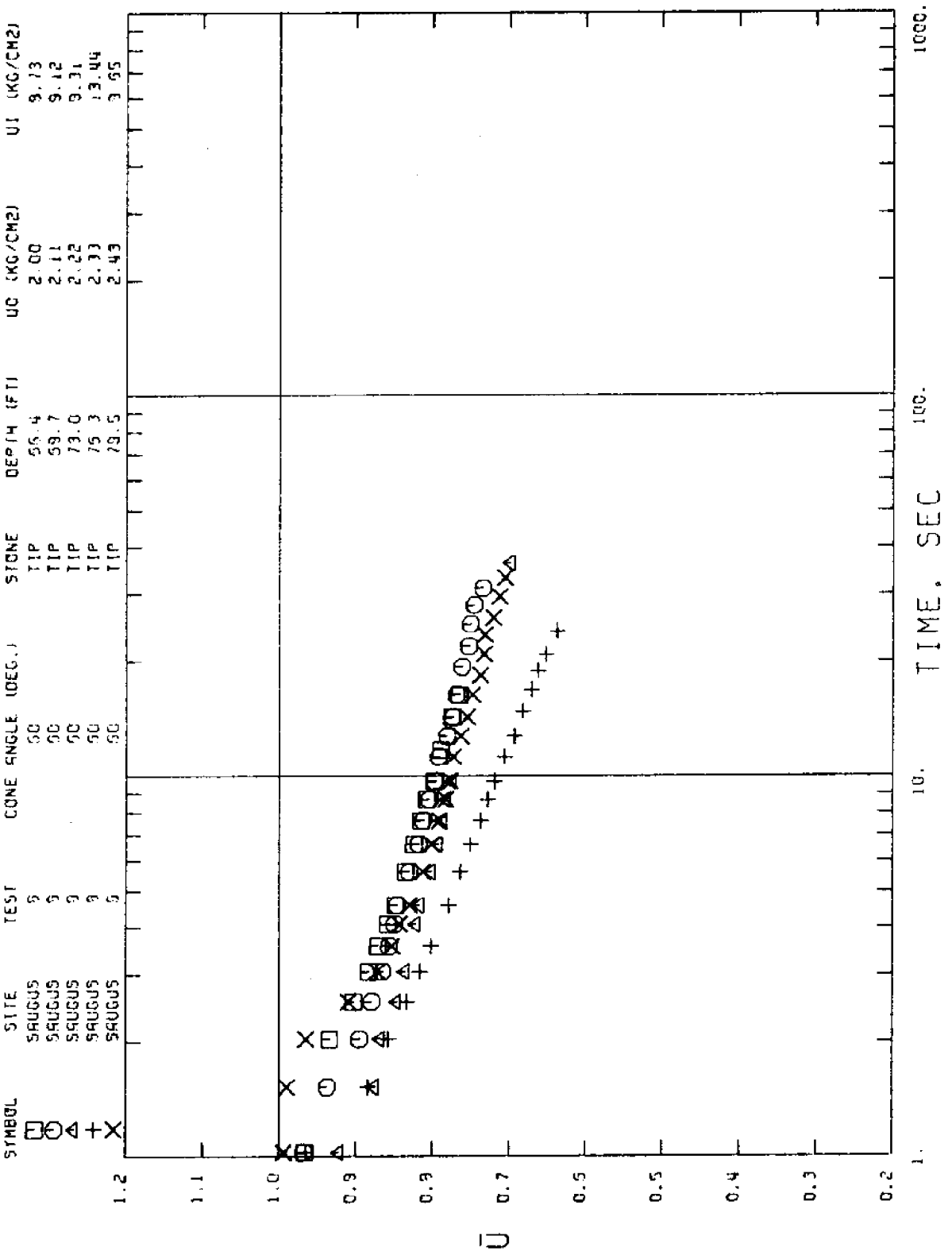
SYMBOL SITE TEST CONE ANGLE (DEG.) STONE DEPTH (FT) UC (KG/CM2) UI (KG/CM2)
SAUGUS 5 60 TIP 55.4 2.00 9.13
SAUGUS 5 60 TIP 59.7 2.11 9.12
SAUGUS 5 60 TIP 73.0 2.22 9.31
SAUGUS 5 60 TIP 75.3 2.33 13.44
SAUGUS 5 60 TIP 79.5 2.43 3.65
U
TIME, SEC
1.
10.
100.
1000.
1.2
1.1
1.0
0.9
0.8
0.7
0.5
0.4
0.3
0.2

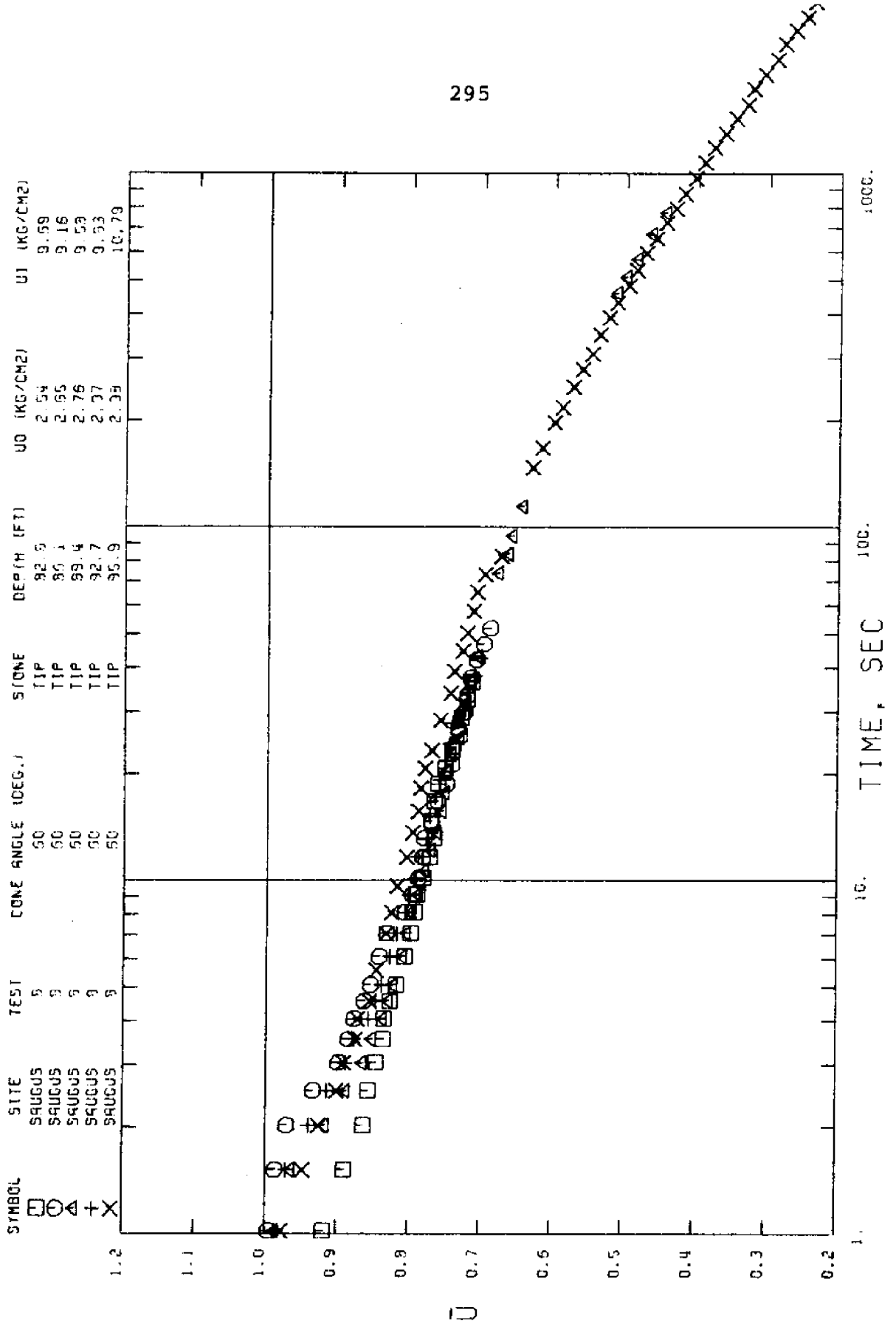
SYMBOL SITE TEST CONE ANGLE (DEG.) STONE DEPTH (FT) U0 (KG/CM2) U1 (KG/CM2)
SAUGUS 5 60 TIP 92.5 2.54 9.69
SAUGUS 5 60 TIP 95.1 2.65 9.16
SAUGUS 5 60 TIP 99.4 2.76 9.53
SAUGUS 5 60 TIP 92.7 2.37 9.53
SAUGUS 5 60 TIP 95.9 2.39 10.79
U
TIME, SEC
1.2
1.1
1.0
0.9
0.8
0.7
0.6
0.5
0.4
0.3
0.2
1.
10.
100.
1000.

SITE: SAUGUS DATE: 6/7/77

TEST # 21 CONE ANGLE: 10 DEG. STONE LOCATION: TIP

DEPTH (FT)	U0 (KSC)	UI (KSC)	UMAX (KSC)	TF (SEC)	UBARF	COEF. OF CONS. (CM2/SEC) CH20	CH40	CH50	CH60	CH80	COMMENTS	
27.0	0.683	2.665	2.866	184	0.16	---	---	---	---	---	BAD TEST - U INCREASES FOR 6 SEC	
32.0	0.850	1.993	2.073	103	0.13	---	---	---	---	---	BAD TEST - U INCREASES FOR 2 SEC	
37.0	1.017	3.978	3.978	220	0.10	0.106	0.276	0.418	0.585	1.134	FAIR TEST - STEEP CURVE	
47.0	1.350	5.084	5.084	153	0.54	0.030	0.048	---	---	---	GOOD TEST	
57.0	1.683	7.916	7.916	1117	0.18	0.049	0.056	0.065	0.084	0.107	GOOD TEST UP TO 150 SEC	
62.3	1.860	7.925	7.925	549	0.29	---	---	---	---	---	BAD TEST - WIGGLING CURVE	
67.3	2.027	8.165	8.165	254	0.45	---	---	---	---	---	BAD TEST - WIGGLING CURVE	
72.3	2.193	8.178	8.178	114	0.62	---	---	---	---	---	BAD TEST - STARTS WITH LARGE DROP	
77.3	2.360	7.363	7.363	147	0.59	0.028	0.037	---	---	---	VERY GOOD TEST	←
82.3	2.527	7.705	7.705	153	0.57	0.043	0.041	---	---	---	VERY GOOD TEST	←
87.3	2.693	8.328	8.328	212	0.51	0.036	0.043	---	---	---	VERY GOOD TEST	←
92.3	2.860	9.539	9.539	149	0.62	0.022	---	---	---	---	VERY GOOD TEST	←
97.3	3.027	9.953	9.953	827	0.38	0.034	0.038	0.042	0.038	---	VERY GOOD TEST	←

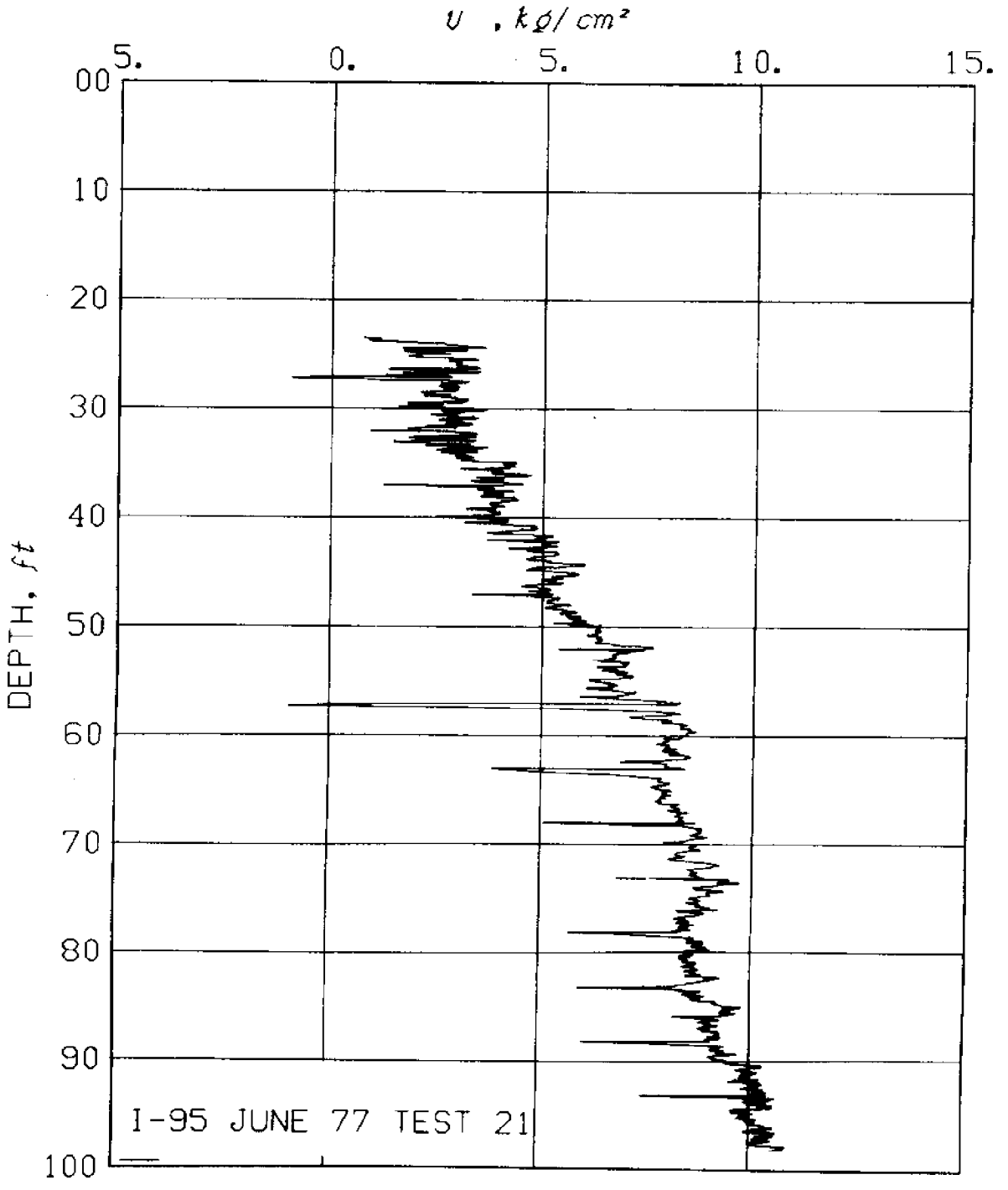
U , kg/cm²
5.
0.
5.
10.
15.
00
10
20
30
40
50
60
70
80
90
100
DEPTH, ft
I-95 JUNE 77 TEST 21

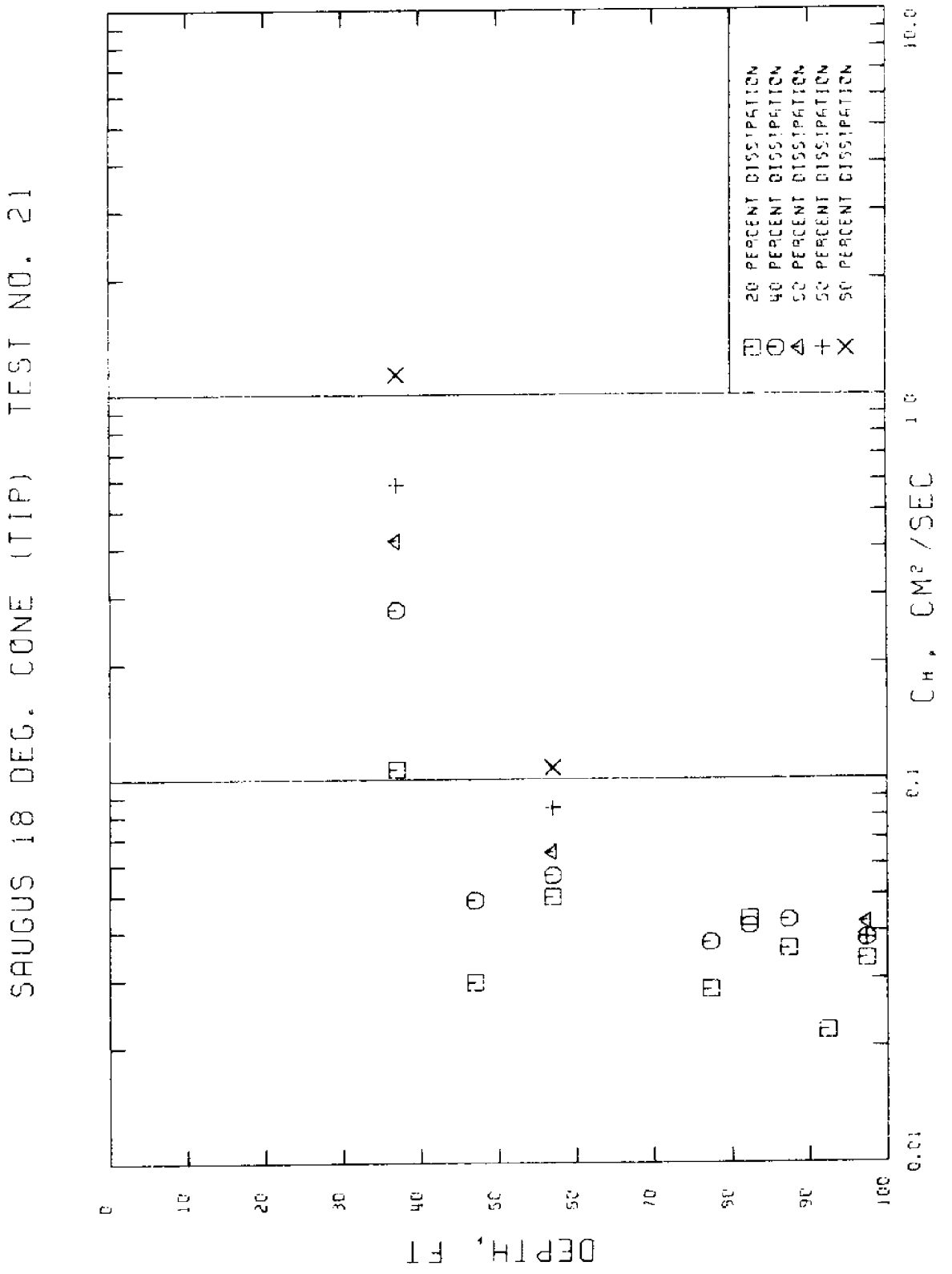
SAUGUS 18 DEG. CONE (TIP) TEST NO. 21
DEPTH, FT
C_H, CM^2/SEC
20 PERCENT DISSIPATION
40 PERCENT DISSIPATION
50 PERCENT DISSIPATION
60 PERCENT DISSIPATION
80 PERCENT DISSIPATION

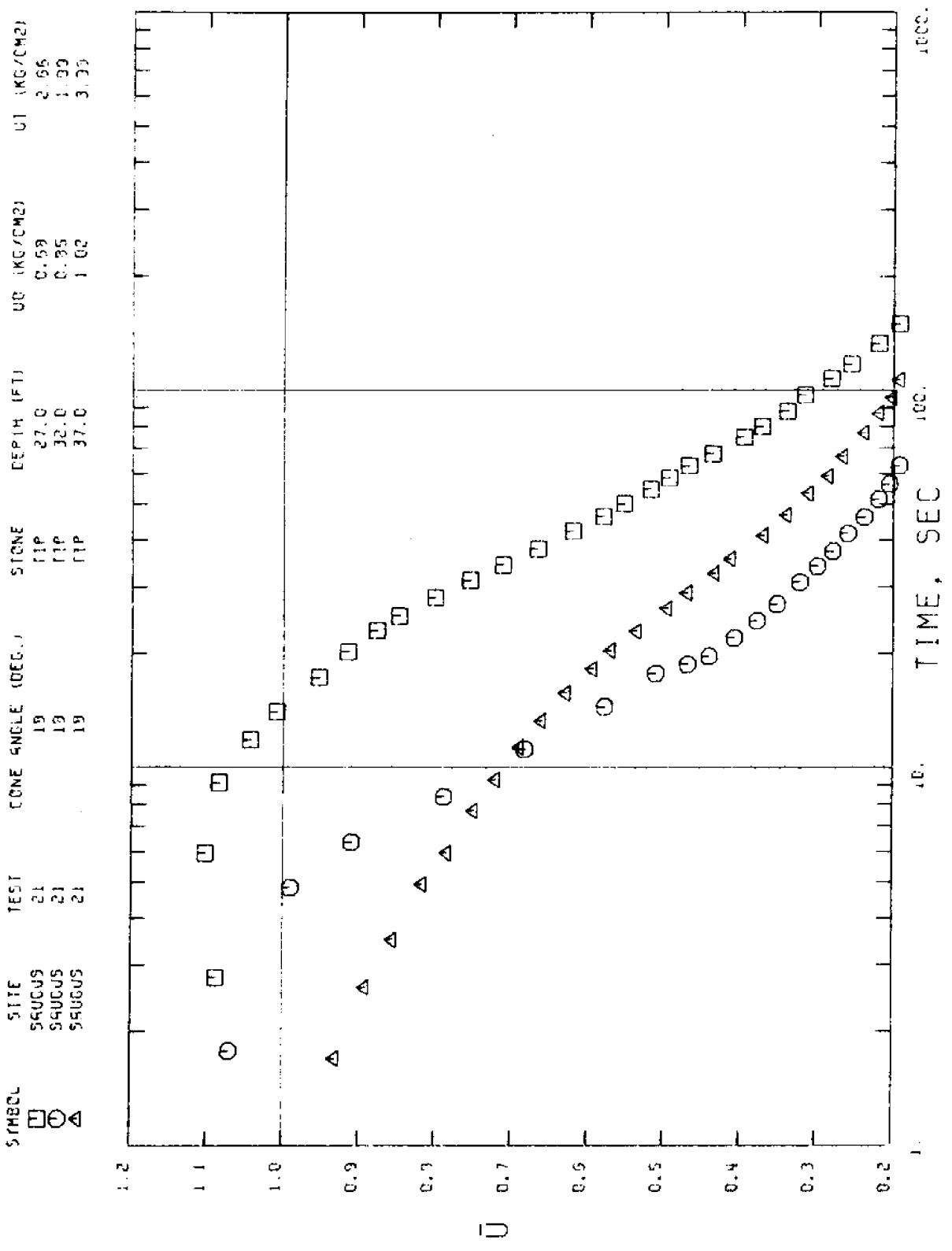
SYMBOL SITE TEST CONE ANGLE (DEG.) STONE DEPTH (FT) U0 (KG/CM2) U1 (KG/CM2)
SQUGUS 21 19 TIP 27.0 0.59 2.66
SQUGUS 21 19 TIP 32.0 0.85 1.99
SQUGUS 21 19 TIP 37.0 1.02 3.35
U
TIME, SEC
1.2
1.1
1.0
0.9
0.8
0.7
0.6
0.5
0.4
0.3
0.2
40.
100.
1000.

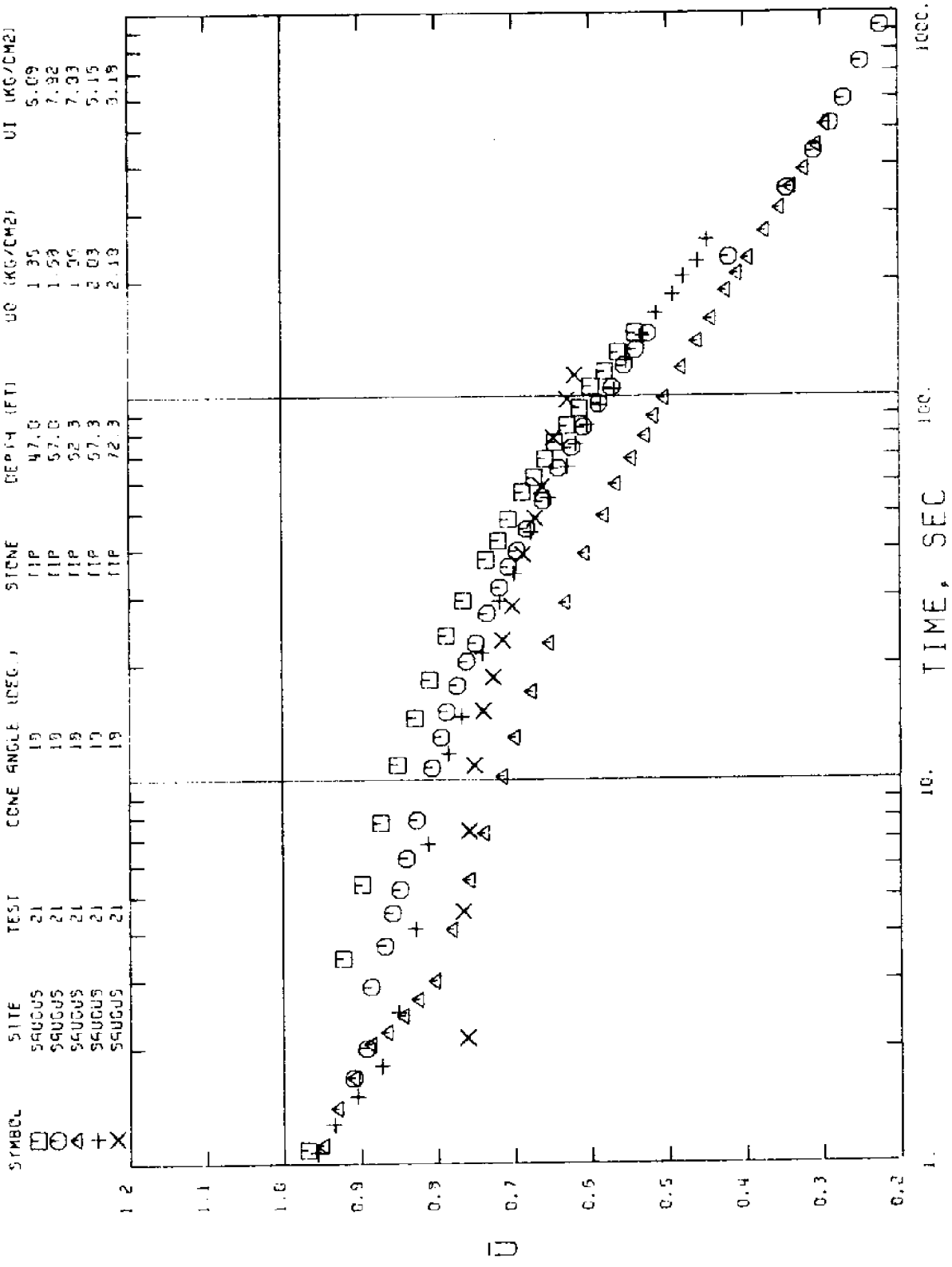
SYMBOL SITE TEST CONE ANGLE (DEG.) STONE DEPTH (FT) UO (KG/CM2) UI (KG/CM2)
SQUGUS 21 19 FIP 47.0 1.35 5.09
SQUGUS 21 19 FIP 52.0 1.58 7.32
SQUGUS 21 19 FIP 52.3 1.95 7.33
SQUGUS 21 19 FIP 57.3 2.03 5.15
SQUGUS 21 19 FIP 72.3 2.19 3.19
TIME, SEC
1000.
100.
10.
1.
1.2
1.1
1.0
0.9
0.8
0.7
0.6
0.5
0.4
0.3
0.2

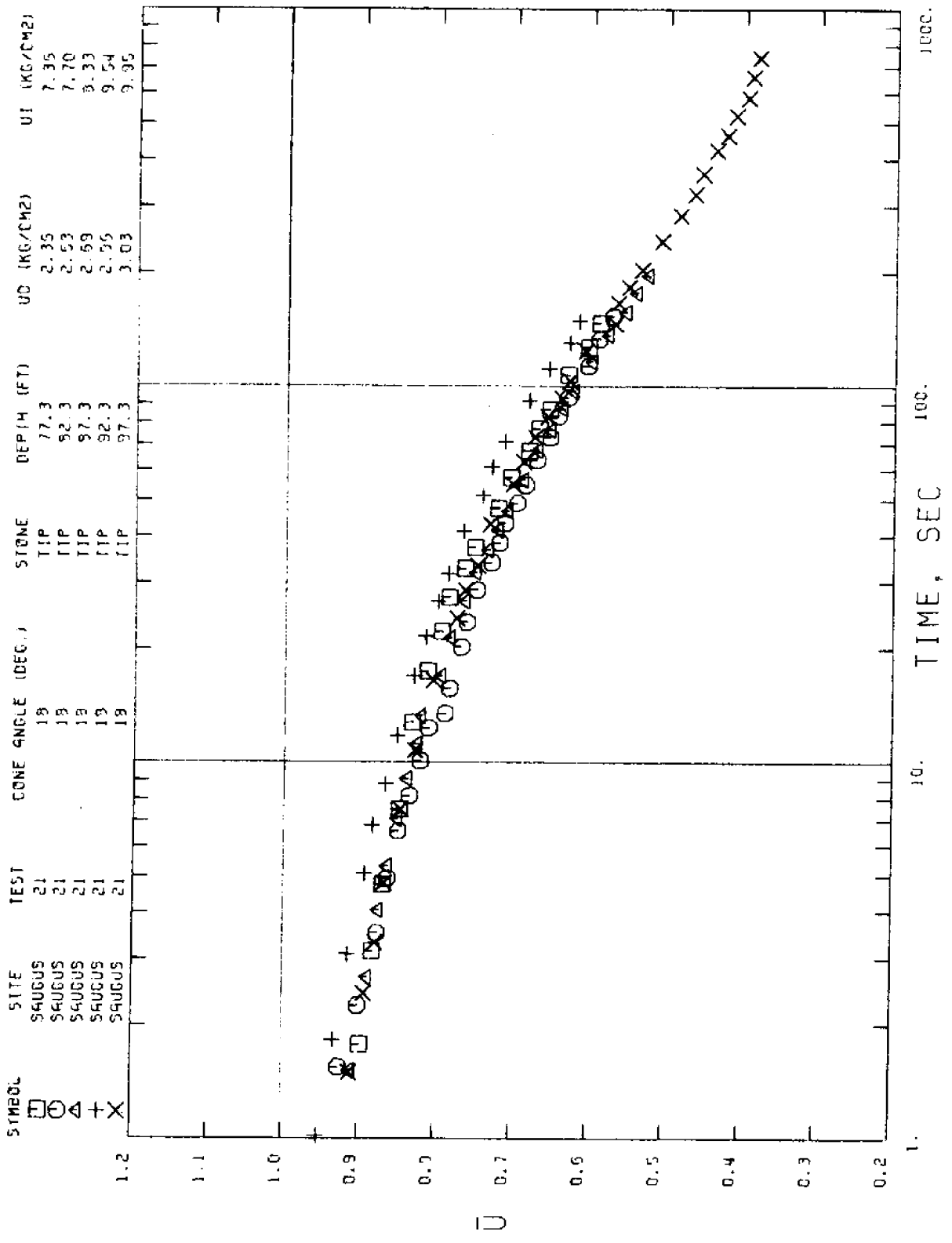
SYMBOL SITE TEST CONE ANGLE (DEG.) STONE DEPTH (FT) UO (KG/CM2) UI (KG/CM2)
SAUGUS 21 19 TIP 77.3 2.35 7.35
SAUGUS 21 19 TIP 82.3 2.53 7.70
SAUGUS 21 19 TIP 87.3 2.69 8.33
SAUGUS 21 19 TIP 92.3 2.56 9.54
SAUGUS 21 19 TIP 97.3 3.03 9.95
U
TIME, SEC
1.2
1.1
1.0
0.9
0.8
0.7
0.6
0.5
0.4
0.3
0.2
1.
10.
100.
1000.

SITE: SAUGUS DATE: 6/8/77

TEST # 23 CONE ANGLE: 18 DEG. STONE LOCATION: CONE BASE

DEPTH (FT)	U0 (KSC)	UI (KSC)	UMAX (KSC)	TF (SEC)	UBARF	COEF. OF CONS. (CM2/SEC) CH20	CH40	CH50	CH60	CH80	COMMENTS
27.5	0.700	2.135	3.645	154	1.08	---	---	---	---	---	BAD TEST
32.5	0.867	3.352	4.369	98	0.85	---	---	---	---	---	BAD TEST
37.5	1.033	4.375	5.169	93	0.96	---	---	---	---	---	BAD TEST
42.5	1.200	4.375	5.018	691	0.57	---	---	---	---	---	BAD TEST
47.5	1.367	5.105	5.730	116	0.96	---	---	---	---	---	BAD TEST
52.5	1.533	6.612	7.146	159	0.85	---	---	---	---	---	FAIR TEST AFTER 15 SEC
57.5	1.700	7.418	7.660	906	0.65	---	---	---	---	---	FAIR TEST - SMALL WIGGLING AT 150 SEC
62.5	1.867	7.155	7.516	136	0.86	---	---	---	---	---	FAIR TEST
67.5	2.033	7.823	8.199	1477	0.62	---	---	---	---	---	GOOD TEST
72.5	2.200	8.468	8.753	160	0.87	---	---	---	---	---	GOOD TEST AFTER 5 SEC
77.5	2.367	8.157	8.157	282	0.78	---	---	---	---	---	GOOD TEST
82.5	2.533	8.052	8.246	140	0.84	---	---	---	---	---	GOOD TEST
87.5	2.700	8.671	8.889	104	0.87	---	---	---	---	---	GOOD TEST AFTER 5 SEC
92.5	2.867	8.827	8.967	147	0.86	---	---	---	---	---	GOOD TEST
97.5	3.033	9.561	9.659	686	0.74	---	---	---	---	---	GOOD TEST

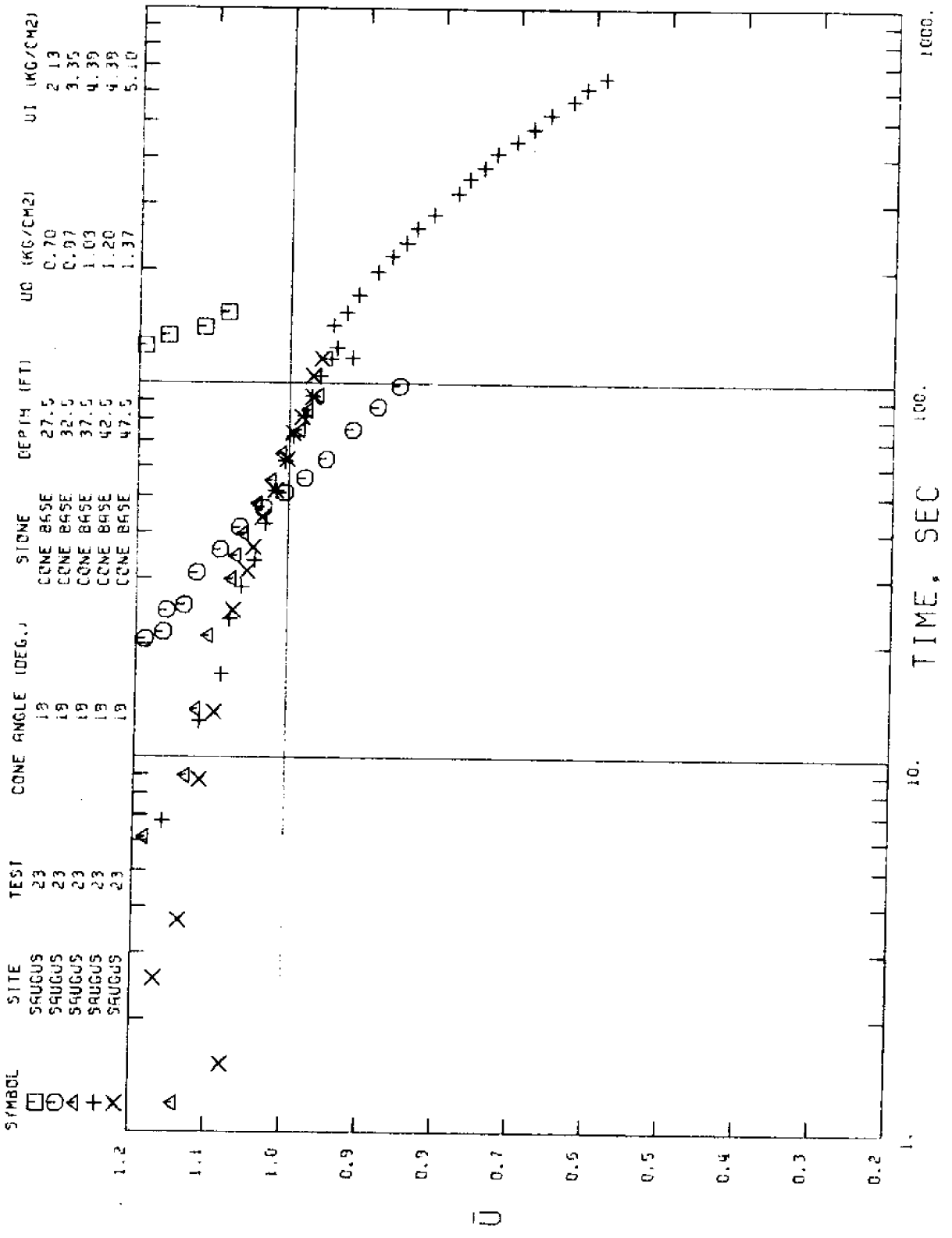
SYMBOL
SITE
TEST
CONE ANGLE (DEG.)
CONE
DEPTH (FT)
UO (KG/CM2)
UI (KG/CM2)
SAUGUS 23 19 CONE BASE 27.5 0.70 2.13
SAUGUS 23 19 CONE BASE 32.5 0.97 3.35
SAUGUS 23 19 CONE BASE 37.5 1.03 4.39
SAUGUS 23 19 CONE BASE 42.5 1.20 4.39
SAUGUS 23 19 CONE BASE 47.5 1.37 5.10
1.2
1.1
1.0
0.9
0.8
0.7
0.6
0.5
0.4
0.3
0.2
1.
10.
100.
1000.
TIME, SEC
U

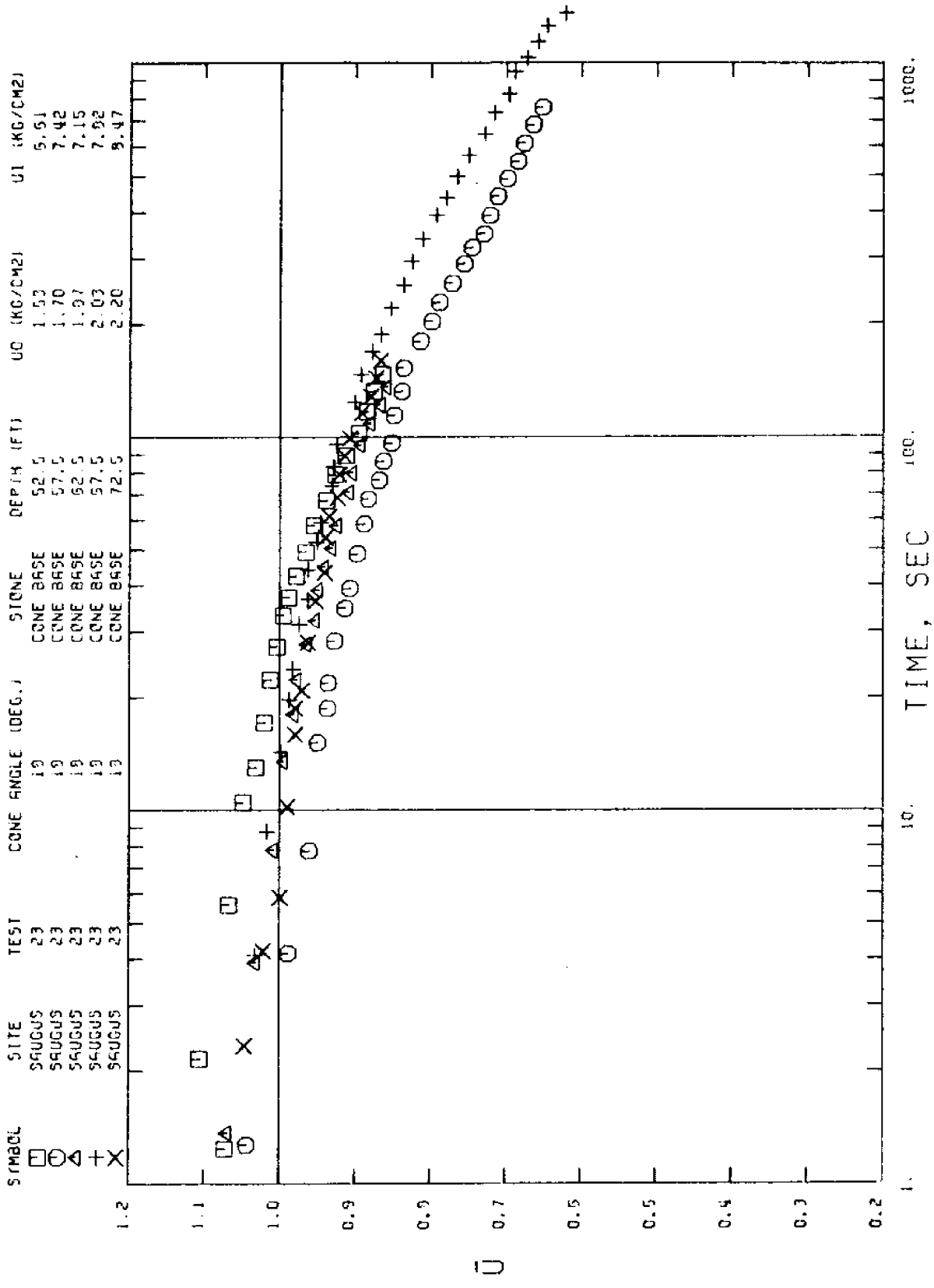
SYMBOL SITE TEST CONE ANGLE (DEG.) SIONE DEPTH (FT) U0 (KG/CM2) U1 (KG/CM2)
SAUGUS 23 10 CONE BASE 52.5 1.53 5.61
SAUGUS 23 10 CONE BASE 57.5 1.70 7.42
SAUGUS 23 10 CONE BASE 62.5 1.97 7.15
SAUGUS 23 10 CONE BASE 67.5 2.03 7.92
SAUGUS 23 10 CONE BASE 72.5 2.20 8.47
U
TIME, SEC
1.
10.
100.
1000.
1.2
1.1
1.0
0.9
0.8
0.7
0.6
0.5
0.4
0.3
0.2

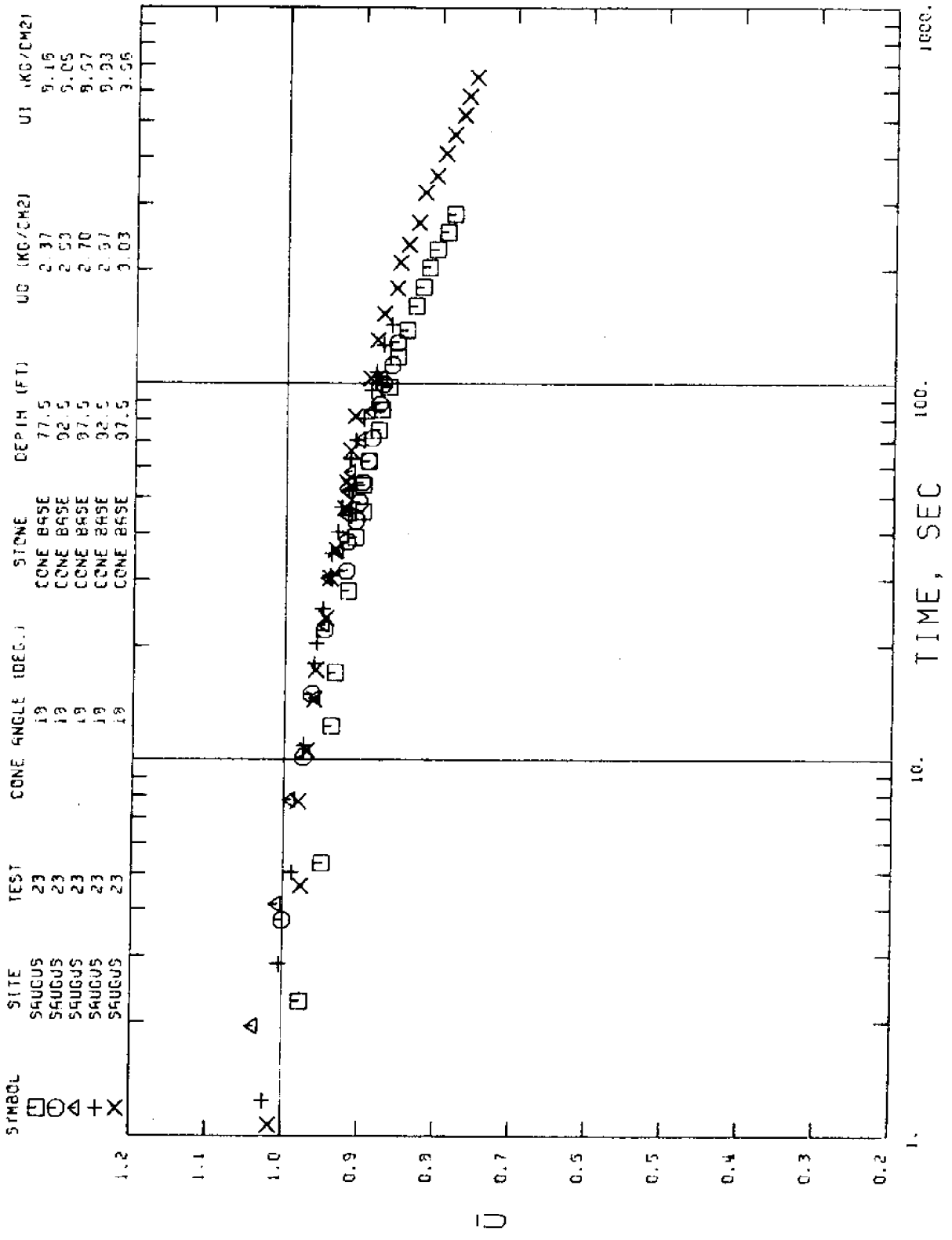
SYMBOL
SITE
TEST
CONE ANGLE (DEG.)
STONE
DEPTH (FT)
UB (KG/CM2)
UI (KG/CM2)
SAUGUS 23 60 CONE BASE 77.5 2.37 5.16
SAUGUS 23 60 CONE BASE 82.5 2.53 5.05
SAUGUS 23 60 CONE BASE 87.5 2.70 8.57
SAUGUS 23 60 CONE BASE 92.5 2.87 9.33
SAUGUS 23 60 CONE BASE 97.5 3.03 3.56
1.2
1.1
1.0
0.9
0.8
0.7
0.6
0.5
0.4
0.3
0.2
U
1.
10.
100.
1000.
TIME, SEC

SITE: SAUGUS DATE: 5/30/77

TEST # 25 CONE ANGLE: 18 DEG. STONE LOCATION: 15.7 R BEHIND CONE APEX

DEPTH (FT)	U0 (KSC)	UI (KSC)	UMAX (KSC)	TF (SEC)	UBARF	COEF. OF CONS. (CM2/SEC)					COMMENTS
						CH20	CH40	CH50	CH60	CH80	
62.5	1.867	5.724	5.724	2030	0.68	---	---	---	---	---	GOOD TEST
87.5	2.033	6.149	6.149	244	0.92	---	---	---	---	---	GOOD TEST
97.5	3.033	7.653	7.653	900	0.86	---	---	---	---	---	GOOD TEST

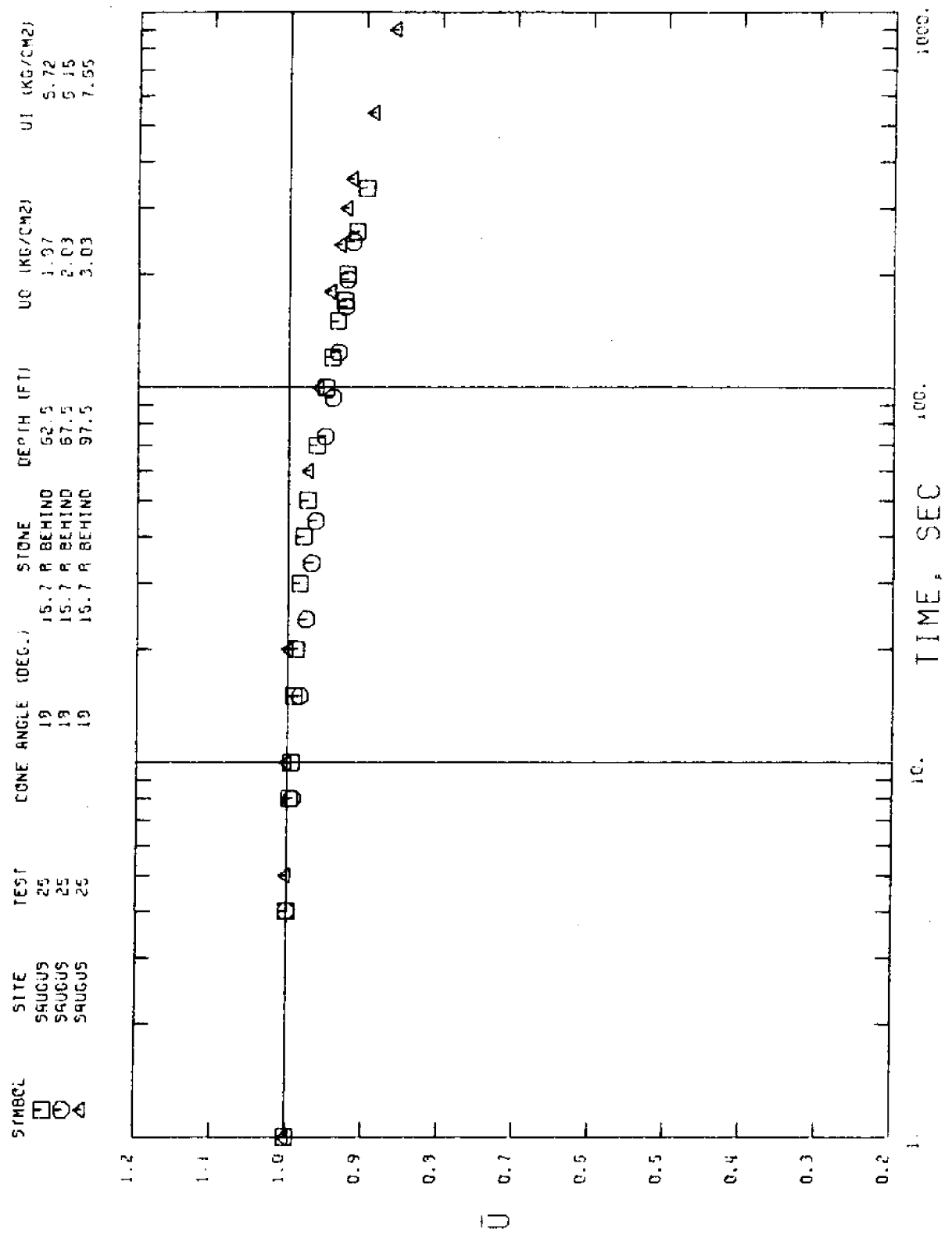
SYMBOL
SITE
TEST
CONE ANGLE (DEG.)
STONE
DEPTH (FT)
UO (KG/CM2)
UI (KG/CM2)
SQUGUS 25 19 15.7 R BEHIND 62.5 1.37 5.72
SQUGUS 25 19 15.7 R BEHIND 67.5 2.03 5.15
SQUGUS 25 19 15.7 R BEHIND 97.5 3.03 7.55
1.2
1.1
1.0
0.9
0.8
0.7
0.6
0.5
0.4
0.3
0.2
U
TIME, SEC

SITE: SAL2US DATE: 6/6/79

TEST # UPP-1 CONE ANGLE: 18 DEG. STONE LOCATION: TIP

DEPTH (FT)	UO (KSC)	UI (KSC)	UMAX (KSC)	TF (SEC)	USARF	COEF. OF CONS. (CM2/SEC) CH20	CH40	CH50	CH60	CH80	COMMENTS
23.0	0.550	-0.217	1.102	394	---	---	---	---	---	---	BAD TEST - U STARTS BELOW STATIC
28.0	0.717	2.088	2.350	491	0.13	---	---	---	---	---	BAD TEST - U INCREASES FOR 10 SEC
33.0	0.883	3.376	3.376	589	0.03	0.089	0.237	0.351	0.450	0.912	FAIR TEST - STEEP CURVE
38.0	1.050	4.239	4.239	531	0.20	---	---	---	---	---	BAD TEST - LARGE INITIAL DROP
43.0	1.217	4.298	4.298	643	0.26	0.027	0.061	0.072	0.074	---	FAIR TEST
46.0	1.317	5.552	5.552	493	0.29	---	---	---	---	---	BAD TEST - LARGE INITIAL DROP
51.0	1.483	5.996	5.996	491	0.25	0.084	0.090	0.108	0.133	---	FAIR TEST
56.0	1.650	6.102	6.102	411	0.41	0.033	0.046	0.057	---	---	FAIR TEST - SLIGHTLY WIGGLING
61.0	1.817	7.122	7.122	491	0.41	0.020	0.034	0.045	---	---	FAIR TEST - SLIGHTLY WIGGLING
66.0	1.983	9.089	9.089	985	0.70	0.001	---	---	---	---	FAIR TEST - SLOW DISSIPATION
71.0	2.150	8.507	8.507	590	0.69	0.004	---	---	---	---	FAIR TEST - SLOW DISSIPATION
76.9	2.347	8.247	8.247	639	0.57	---	---	---	---	---	BAD TEST - LARGE WIGGLING

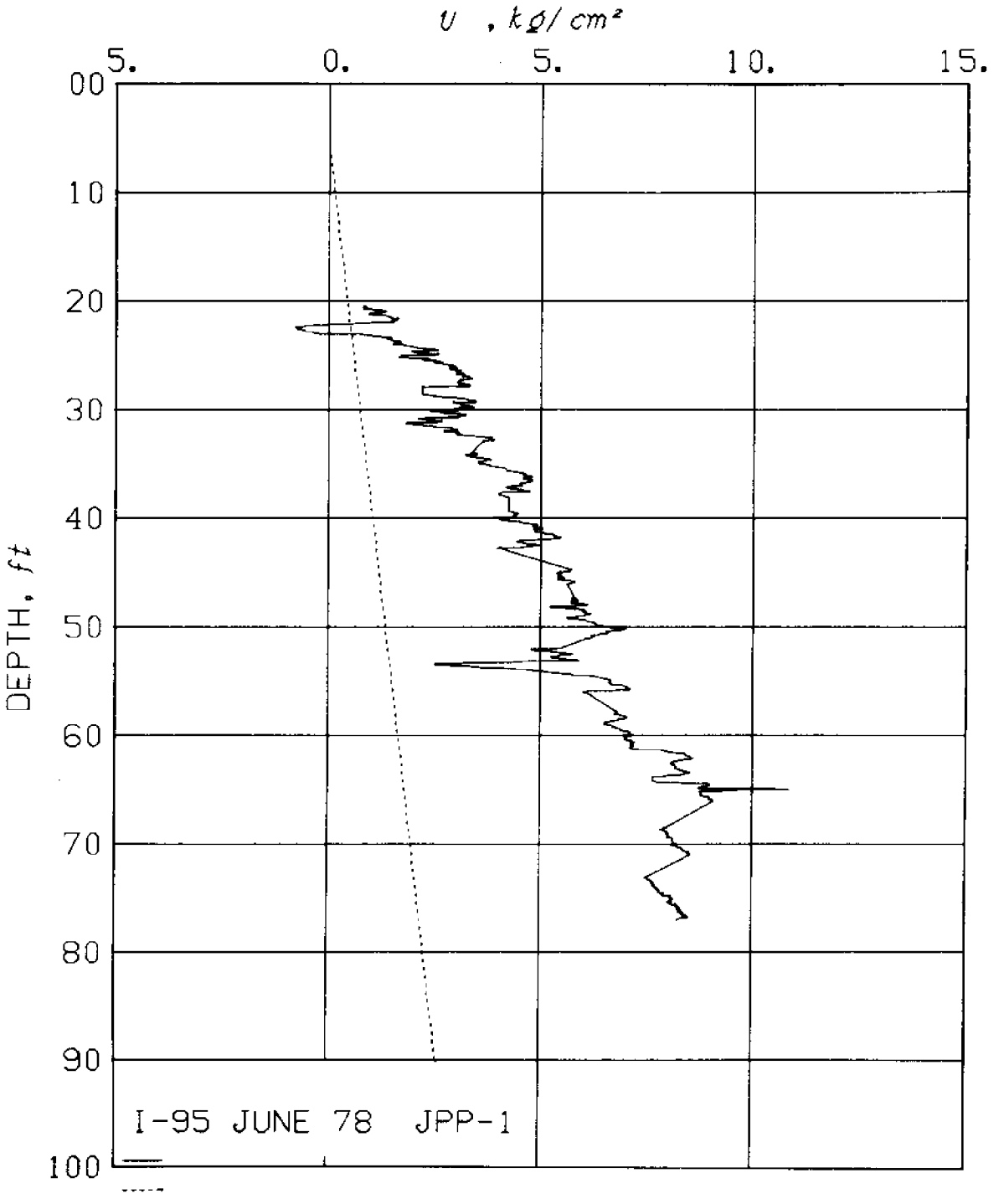
U , kg/cm²
5.
0.
5.
10.
15.
00
10
20
30
40
50
60
70
80
90
100
DEPTH, ft
I-95 JUNE 78 JPP-1

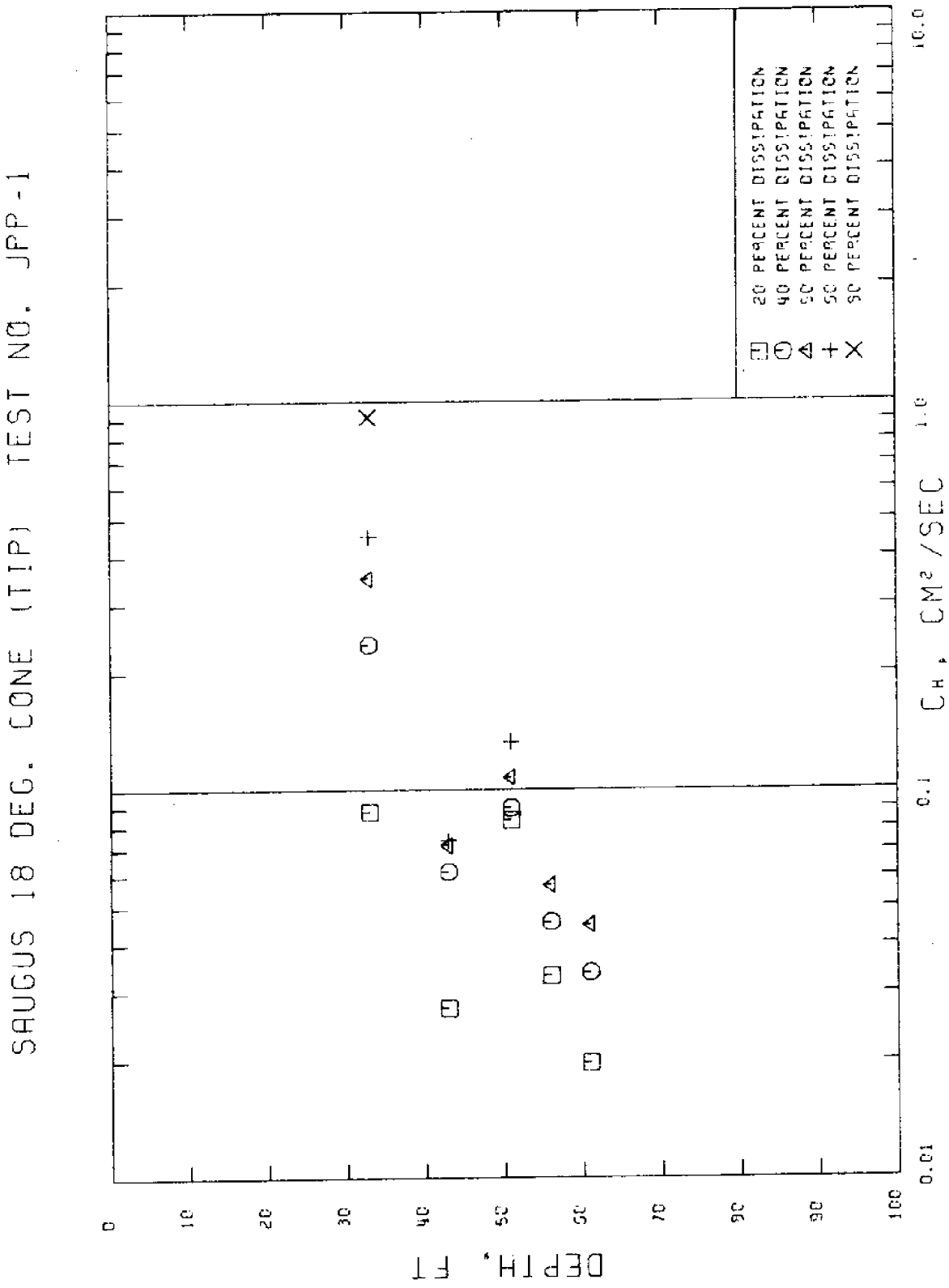
SAUGUS 18 DEG. CONE (TIP) TEST NO. JPP-1
20 PERCENT DISSIPATION
40 PERCENT DISSIPATION
50 PERCENT DISSIPATION
80 PERCENT DISSIPATION
90 PERCENT DISSIPATION
DEPTH, FT
0
10
20
30
40
50
60
70
80
90
100
0.01
0.1
1.0
10.0
CH, CM²/SEC

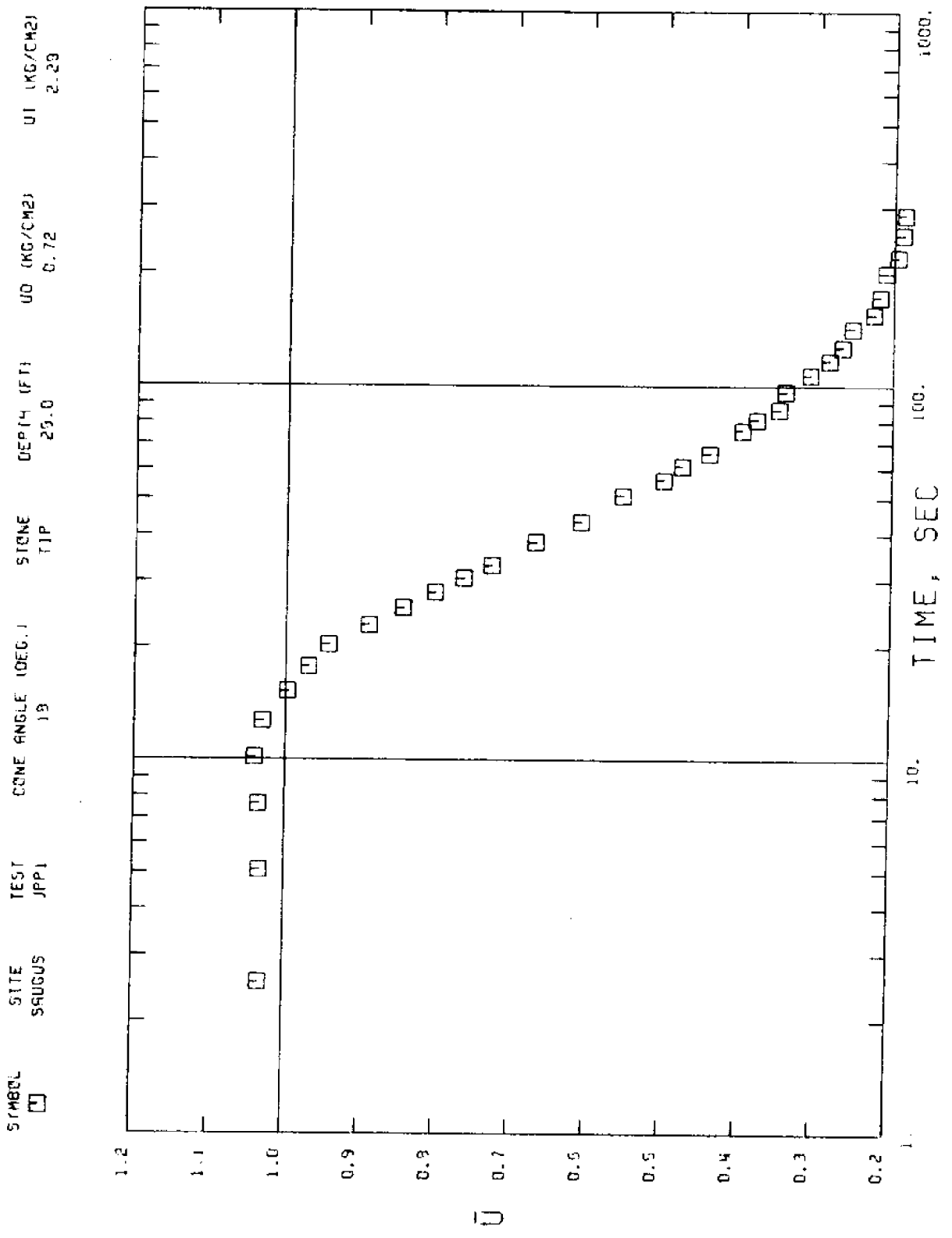
SYMBOL
SITE
SAUGUS
TEST
JPP1
CONE ANGLE (DEG.)
19
STONE
TIP
DEPTH (FT)
25.0
U0 (KG/CM2)
0.72
U1 (KG/CM2)
2.29
U
TIME, SEC
1.2
1.1
1.0
0.9
0.8
0.7
0.6
0.5
0.4
0.3
0.2
10.
100.
1000.

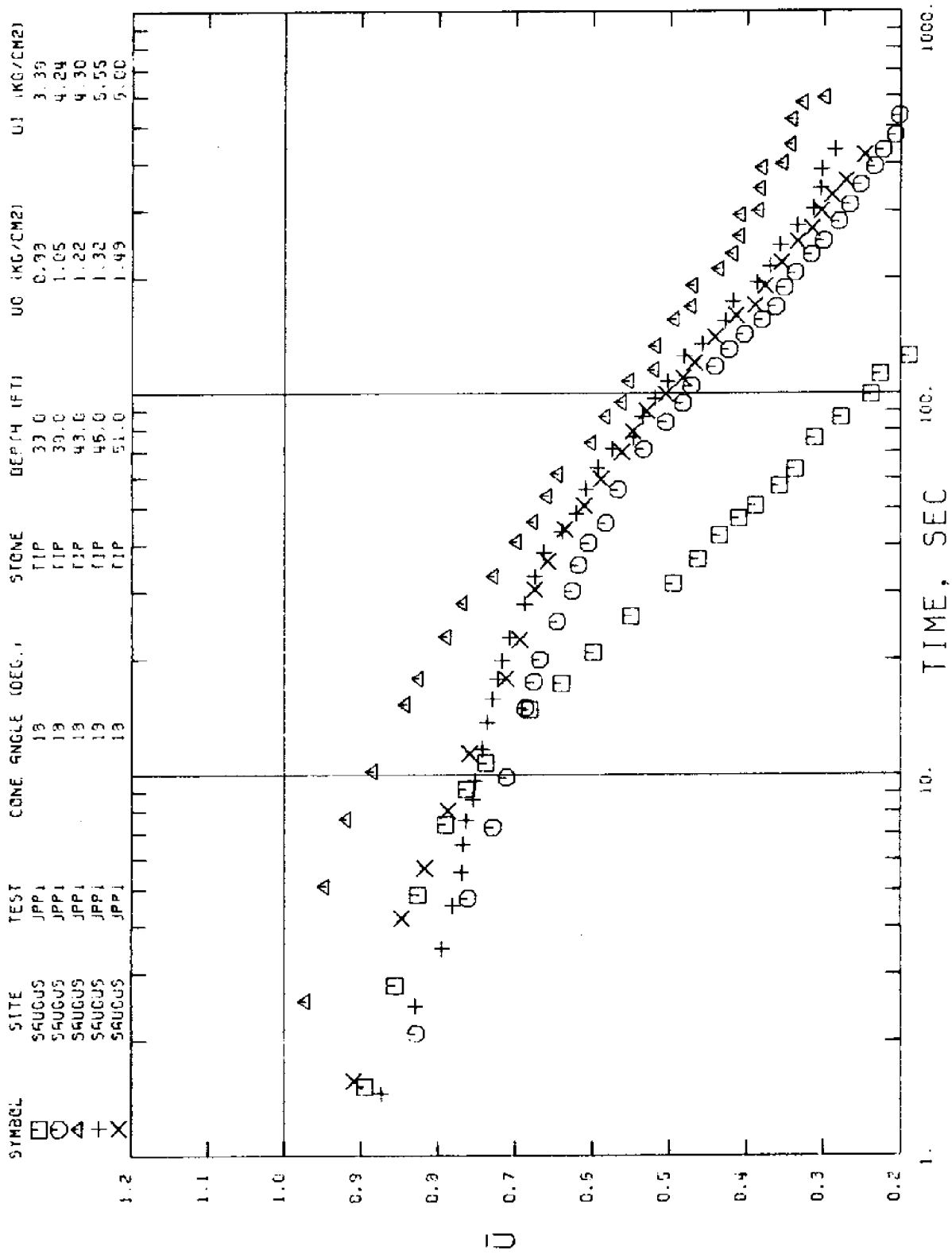
SYMBOL SITE TEST CONE ANGLE (DEG.) STONE DEPTH (FT) UO (KG/CM2) UI (KG/CM2)
SAUGUS JPP1 19 FIP 33.0 0.93 3.39
SAUGUS JPP1 19 FIP 39.0 1.05 4.24
SAUGUS JPP1 19 FIP 43.6 1.22 4.30
SAUGUS JPP1 19 FIP 46.0 1.32 5.55
SAUGUS JPP1 19 FIP 51.0 1.49 5.00
U
TIME, SEC
1.2
1.1
1.0
0.9
0.8
0.7
0.6
0.5
0.4
0.3
0.2
1.
10.
100.
1000.

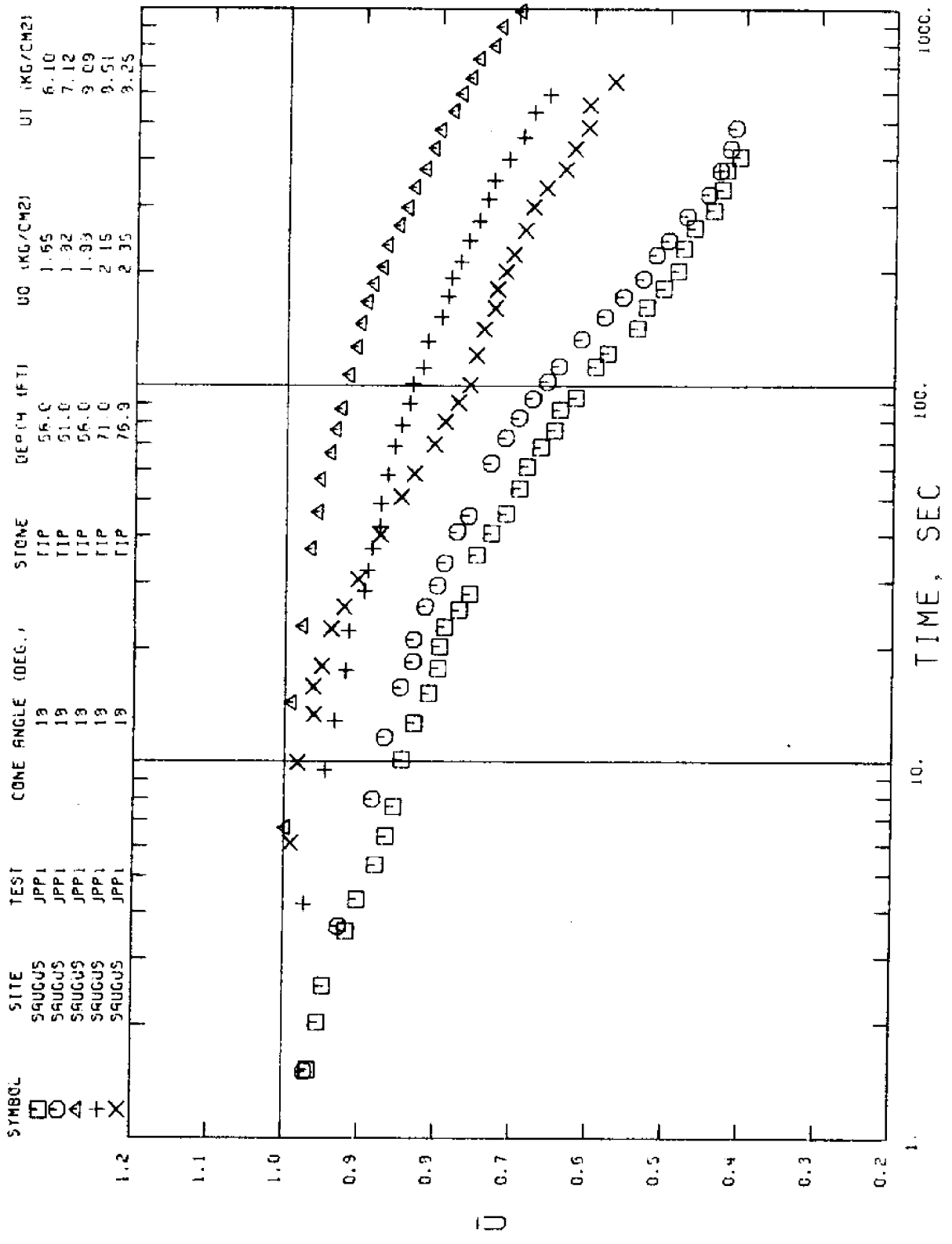
SYMBOL SITE TEST CONE ANGLE (DEG.) STONE DEPTH (FT) UO (KG/CM2) UI (KG/CM2)
SQUGUS JPP1 19 FIP 56.0 1.65 6.10
SQUGUS JPP1 19 FIP 51.0 1.32 7.12
SQUGUS JPP1 19 FIP 56.0 1.39 9.09
SQUGUS JPP1 19 FIP 71.0 2.15 9.51
SQUGUS JPP1 19 FIP 76.9 2.35 9.25
U
TIME, SEC
1.2
1.1
1.0
0.9
0.8
0.7
0.6
0.5
0.4
0.3
0.2
1.
10.
100.
1000.

SITE: SAUGUS DATE: 6/8/78

TEST # UPP-2 CONE ANGLE: 18 DEG. STONE LOCATION: TIP

DEPTH (FT)	U0 (KSC)	U1 (KSC)	UMAX (KSC)	TF (SEC)	UBARF	COEF. OF CONS. (CM2/SEC) CH20	CH40	CH50	CH60	CH80	COMMENTS	
22.7	0.540	2.568	2.568	577	0.04	---	---	---	---	---	FAIR TEST - STEEP CURVE	
27.7	0.707	2.180	2.207	642	0.02	---	---	---	---	---	BAD TEST - NO DECAY FOR 3 SEC	
32.7	0.873	2.081	2.116	414	0.17	---	---	---	---	---	BAD TEST - NO DECAY FOR 4 SEC	
37.7	1.040	3.439	3.439	278	0.14	0.209	0.519	0.657	0.711	0.768	GOOD TEST	
43.2	1.223	5.191	5.191	624	0.34	---	---	---	---	---	BAD TEST - WIGGLING CURVE	
48.2	1.390	5.835	5.835	608	0.24	0.130	0.217	0.275	0.327	---	FAIR TEST UP TO 100 SEC	
53.2	1.557	6.337	6.337	546	0.47	0.018	0.027	0.025	---	---	VERY GOOD TEST	
58.2	1.723	6.499	6.499	758	0.43	0.027	0.047	0.045	0.032	---	VERY GOOD TEST	
63.2	1.890	7.013	7.013	887	0.41	0.018	0.032	0.028	---	---	VERY GOOD TEST	
68.2	2.057	7.400	7.400	437	0.46	0.017	0.033	0.035	---	---	VERY GOOD TEST	
73.2	2.223	7.738	7.738	413	0.44	0.040	0.050	0.049	---	---	GOOD TEST AFTER 9 SEC	
78.2	2.390	8.060	8.060	375	0.47	0.026	0.037	0.045	---	---	VERY GOOD TEST	←
83.2	2.557	8.835	8.835	526	0.44	0.030	0.033	0.035	---	---	VERY GOOD TEST	←
88.2	2.723	9.575	9.575	417	0.40	0.036	0.049	0.054	---	---	VERY GOOD TEST	←
93.2	2.890	9.287	9.287	1469	0.34	0.015	0.032	0.038	0.032	---	VERY GOOD TEST	←
98.2	3.057	10.068	10.068	443	0.48	0.016	0.040	0.034	---	---	VERY GOOD TEST	←

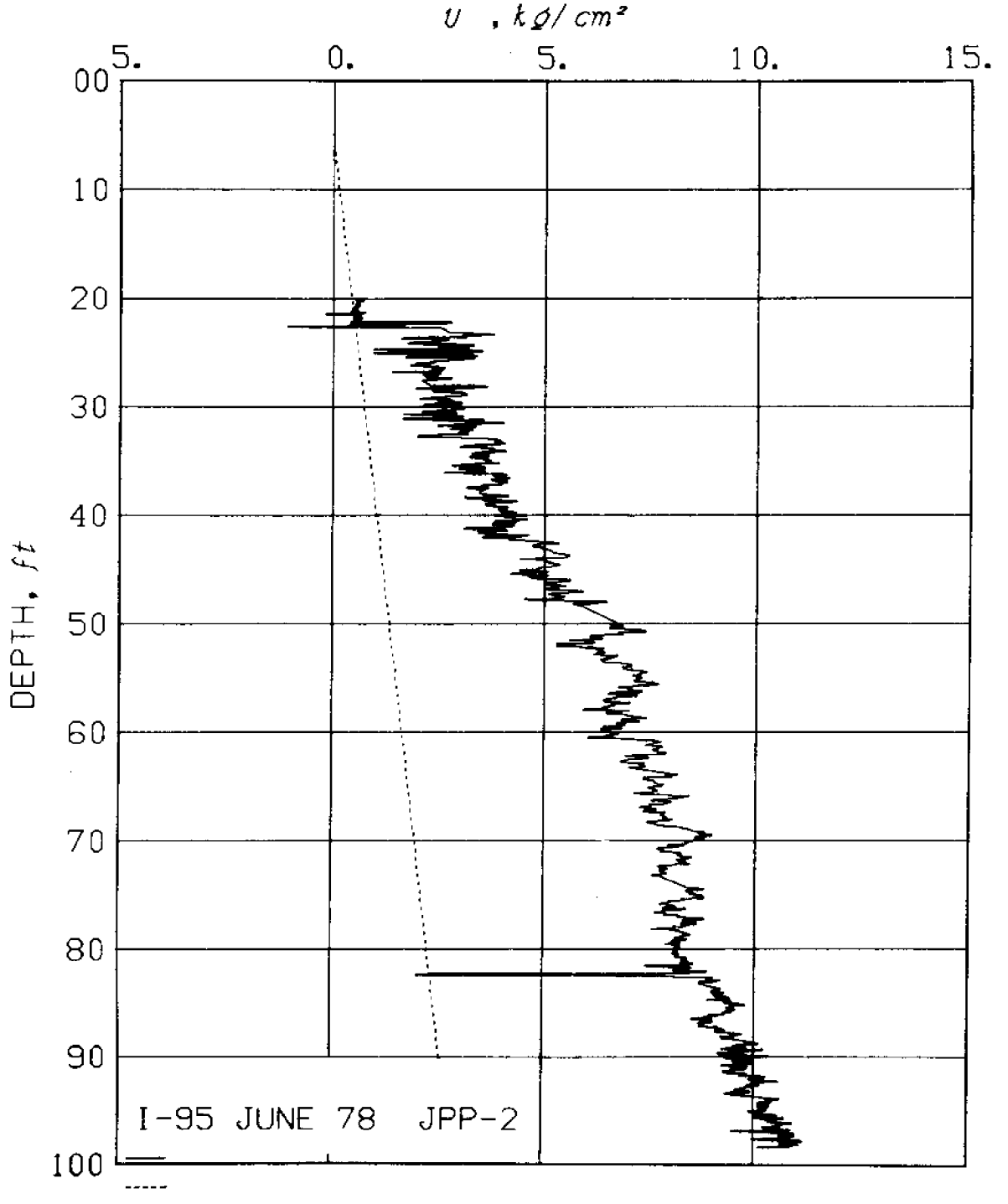
U , kg/cm²
5.
0.
5.
10.
15.
00
10
20
30
40
50
60
70
80
90
100
DEPTH, ft
I-95 JUNE 78 JPP-2

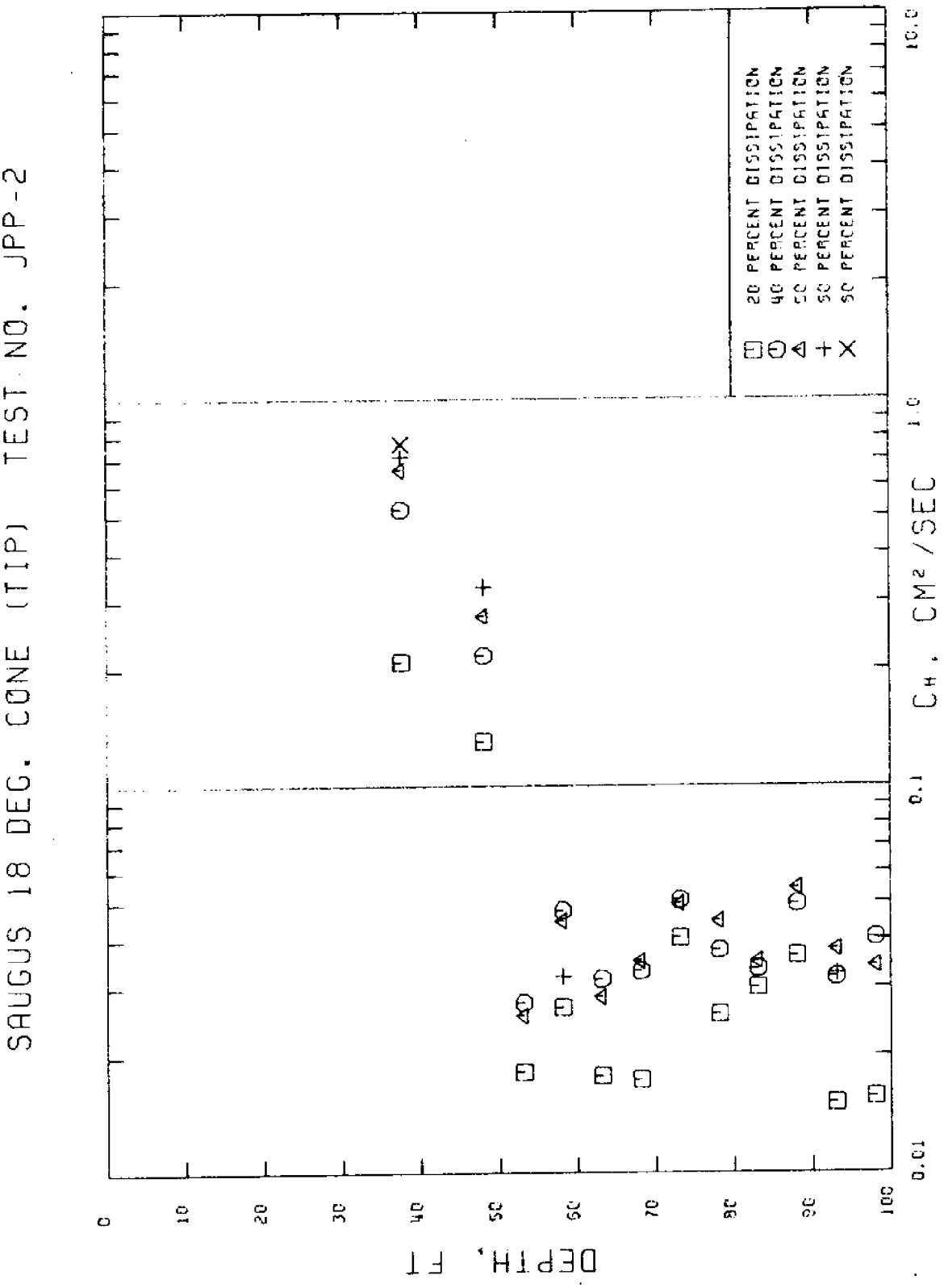
SAUGUS 18 DEG. CONE (TIP) TEST NO. JPP-2
DEPTH, FT
0
10
20
30
40
50
60
70
80
90
100
0.01
0.1
1.0
10.0
C_H, CM^2/SEC
20 PERCENT DISSIPATION
40 PERCENT DISSIPATION
60 PERCENT DISSIPATION
80 PERCENT DISSIPATION
90 PERCENT DISSIPATION

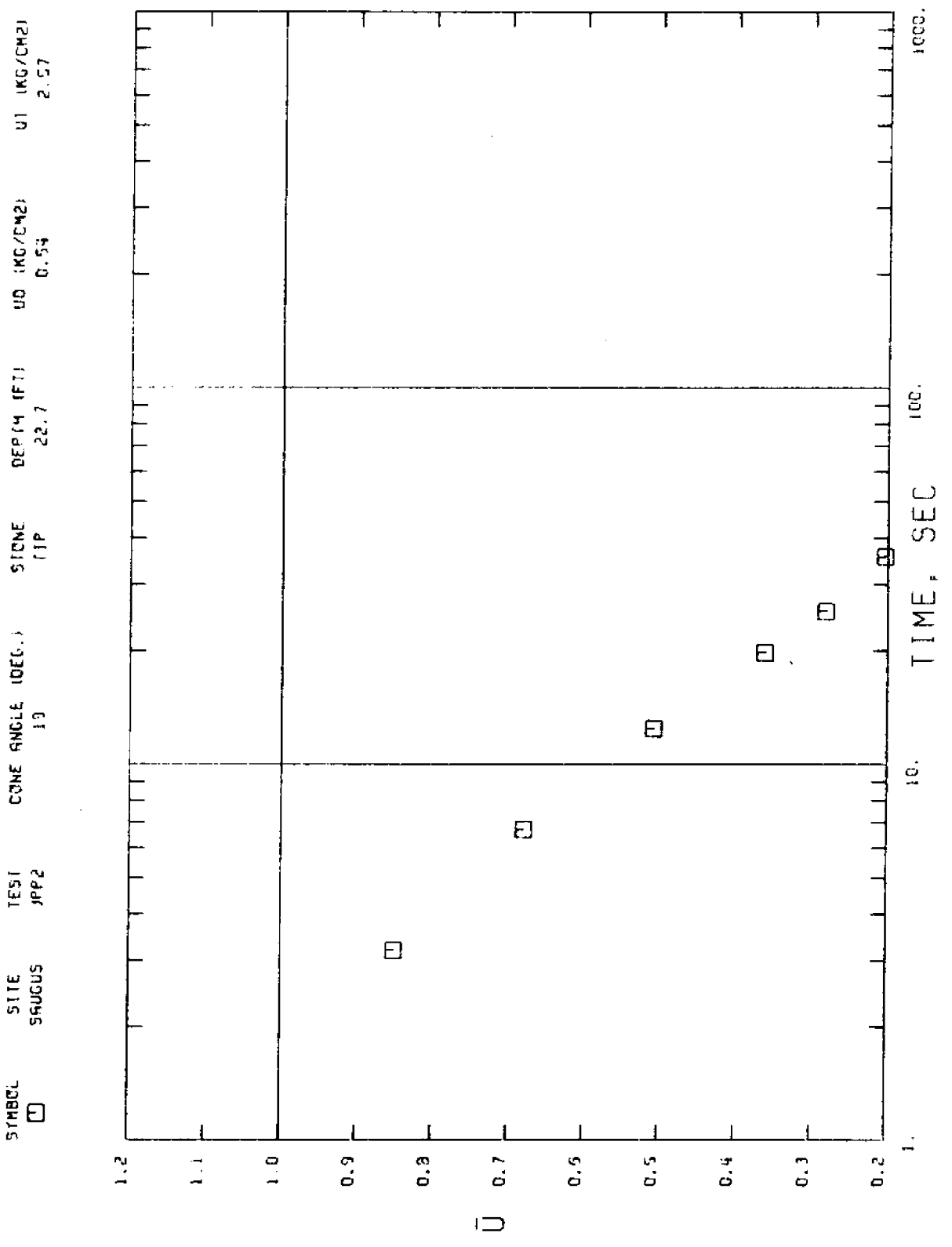
SYMBOL
SITE
SAUGUS
TEST
JPP2
CONE ANGLE (DEG.)
10
STONE
TIP
DEPTH (FT)
22.7
U0 (KG/CM2)
0.54
U1 (KG/CM2)
2.57
1.2
1.1
1.0
0.9
0.8
0.7
0.6
0.5
0.4
0.3
0.2
U
1.
10.
100.
1000.
TIME, SEC

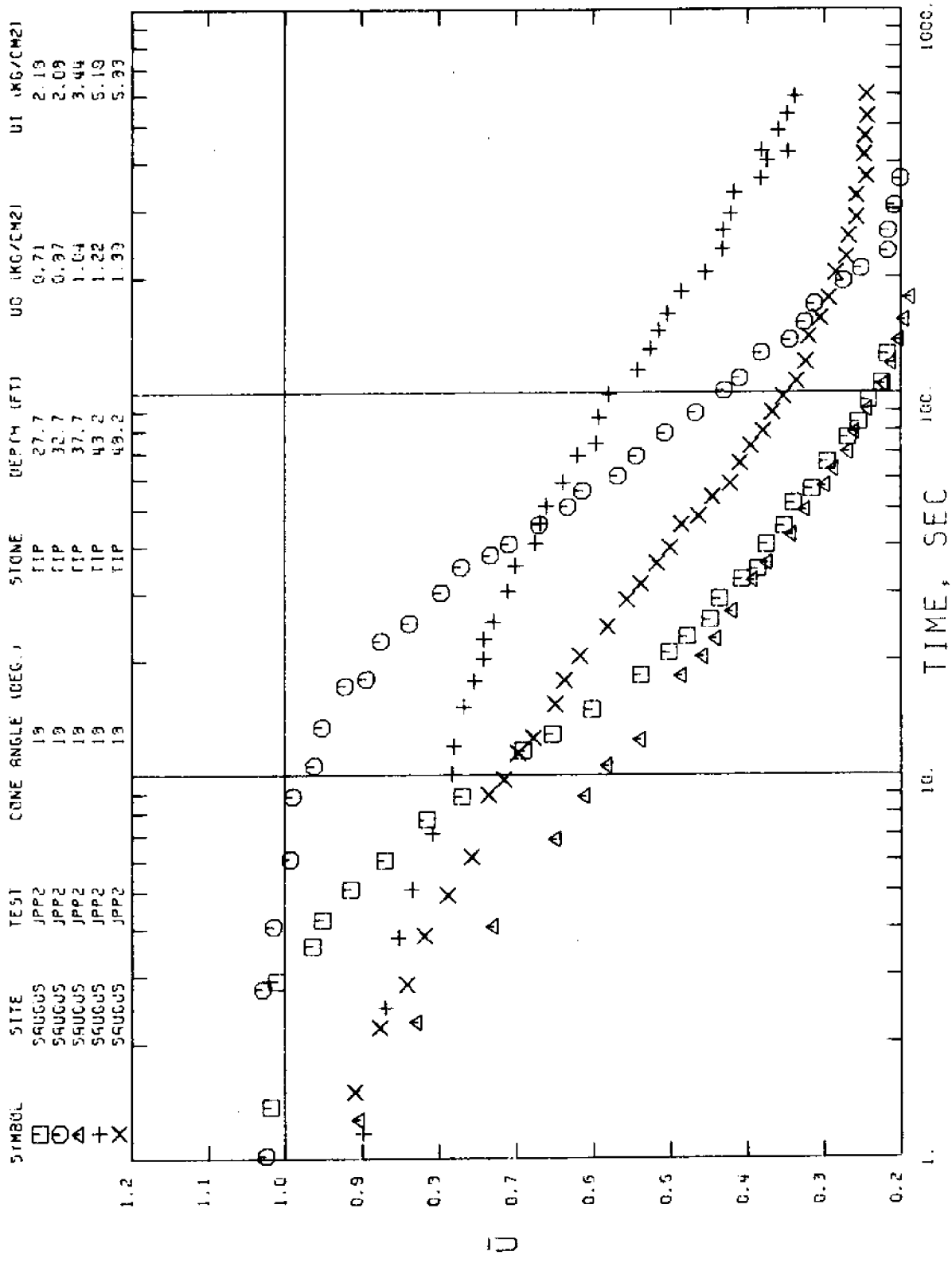
SYMBOL SITE TEST CONE ANGLE (DEG.) STONE DEPTH (FT) UO (KG/CM2) UI (KG/CM2)
SAUGUS JPP2 19 TIP 27.7 0.71 2.18
SAUGUS JPP2 19 TIP 32.7 0.97 2.09
SAUGUS JPP2 19 TIP 37.7 1.04 3.44
SAUGUS JPP2 19 TIP 43.2 1.22 5.18
SAUGUS JPP2 19 TIP 48.2 1.33 5.33
U
TIME, SEC
1.2
1.1
1.0
0.9
0.8
0.7
0.6
0.5
0.4
0.3
0.2
1.
10.
100.
1000.

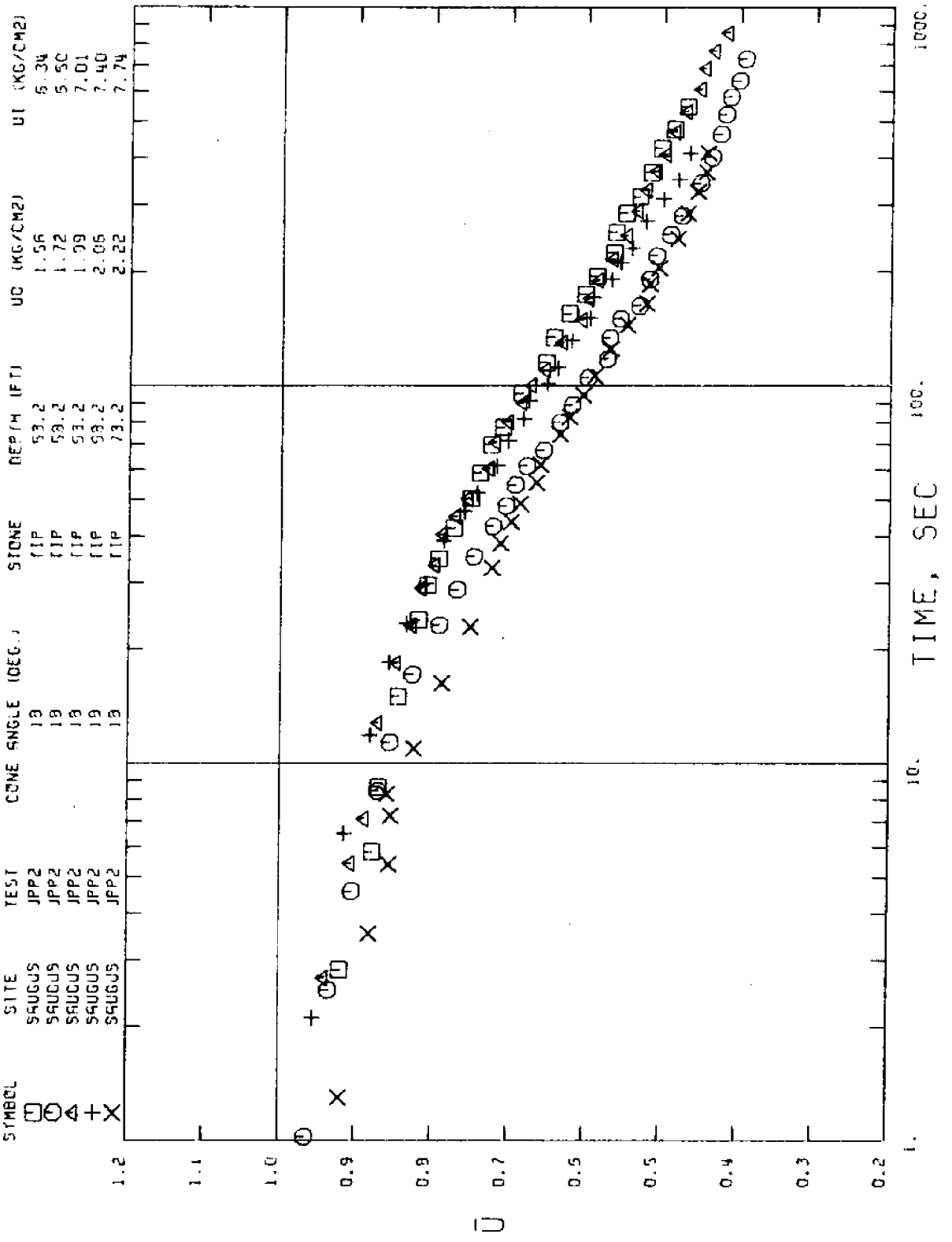
SYMBOL SITE TEST CONE ANGLE (DEG.) SIONE DEPTH (FT) UC (KG/CM2) UI (KG/CM2)
SAUGUS JPP2 19 FIP 53.2 1.56 6.34
SAUGUS JPP2 19 FIP 53.2 1.72 5.50
SAUGUS JPP2 19 FIP 53.2 1.99 7.01
SAUGUS JPP2 19 FIP 53.2 2.06 7.40
SAUGUS JPP2 19 FIP 73.2 2.22 7.74
U
TIME, SEC
1.2
1.1
1.0
0.9
0.8
0.7
0.6
0.5
0.4
0.3
0.2
1.
10.
100.
1000.

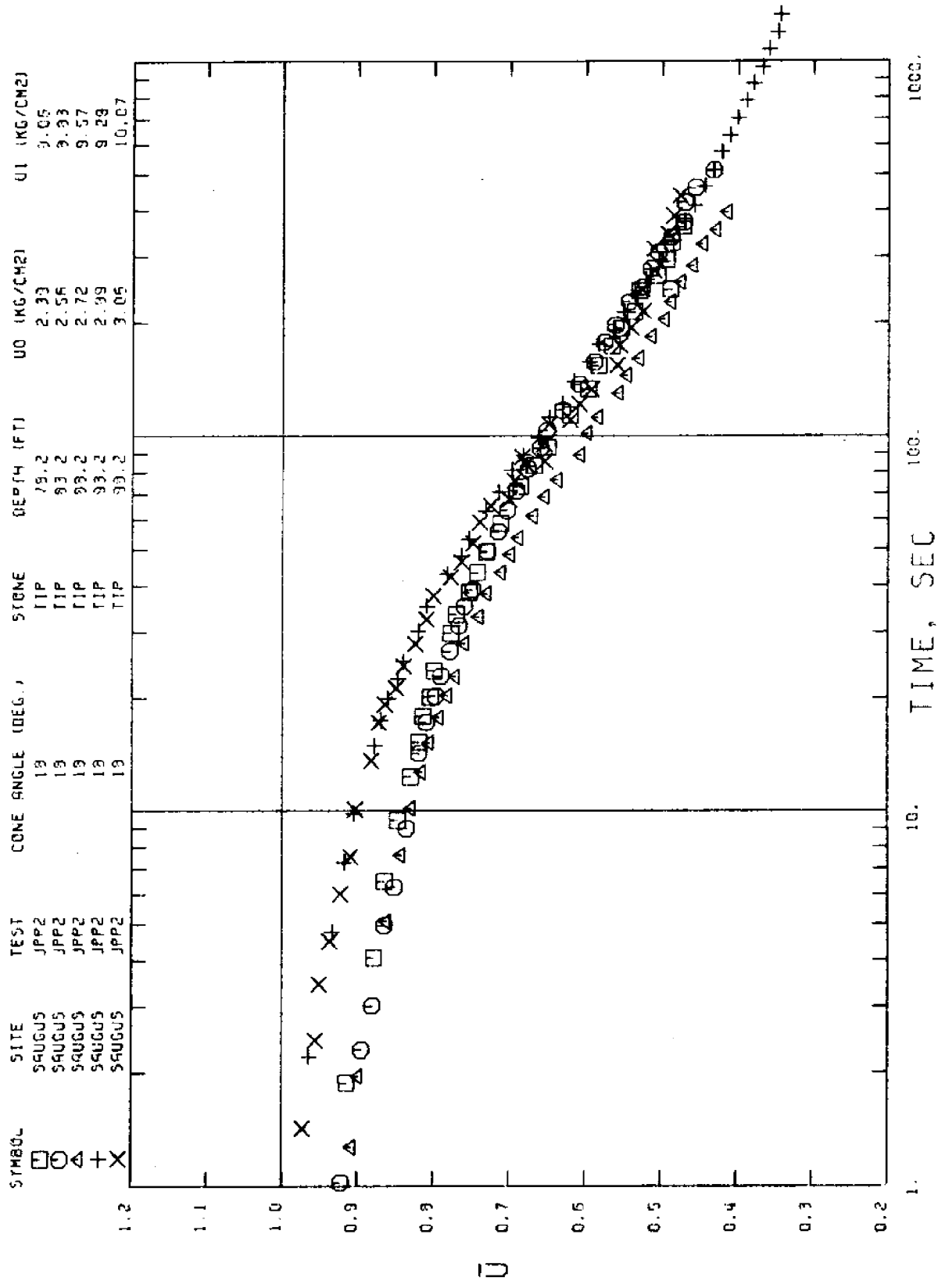
SYMBOL SITE TEST CONE ANGLE (DEG.) STONE DEPTH (FT) U0 (KG/CM2) U1 (KG/CM2)
SAUGUS JPP2 19 TIP 19.2 2.33 3.05
SAUGUS JPP2 19 TIP 83.2 2.56 3.33
SAUGUS JPP2 19 TIP 93.2 2.72 3.57
SAUGUS JPP2 19 TIP 93.2 2.99 3.29
SAUGUS JPP2 19 TIP 93.2 3.05 10.07
U
TIME, SEC
1.
10.
100.
1000.
1.2
1.1
1.0
0.9
0.8
0.7
0.6
0.5
0.4
0.3
0.2

SITE: SAUGUS DATE: 6/12/76

TEST # UPP-3 CONE ANGLE: 60 DEG. STONE LOCATION: TIP

DEPTH (FT)	U0 (KSC)	UI (KSC)	UMAX (KSC)	TF (SEC)	U0/UF	COEF. OF CONS. (CM2/SEC) CH20	CH40	CH50	CH60	CH80	COMMENTS
18.0	0.383	1.697	1.697	94	0.05	---	---	---	---	---	FAIR TEST - VERY STEEP CURVE
28.0	0.717	4.365	4.365	232	0.03	0.311	0.494	0.645	0.768	1.382	FAIR TEST - STEEP CURVE
33.0	0.683	4.388	4.388	486	0.01	0.277	0.340	0.419	0.524	0.965	FAIR TEST - STEEP CURVE
39.0	1.083	4.857	4.857	191	0.44	---	---	---	---	---	BAD TEST UP TO 30 SEC
40.0	1.117	5.516	5.516	234	0.31	---	---	---	---	---	BAD TEST UP TO 30 SEC
41.0	1.150	5.740	5.740	231	0.30	---	---	---	---	---	BAD TEST UP TO 20 SEC
42.0	1.183	5.711	5.711	257	0.39	0.422	0.180	0.129	0.100	---	FAIR TEST
43.0	1.217	5.362	5.362	243	0.66	0.035	---	---	---	---	FAIR TEST - WIGGLING CURVE
44.0	1.250	6.477	6.477	201	0.46	---	---	---	---	---	FAIR TEST - WIGGLING CURVE
45.0	1.283	5.442	5.442	301	0.50	0.056	0.047	---	---	---	FAIR TEST
46.0	1.317	5.424	5.451	282	0.57	---	---	---	---	---	BAD TEST - NO DECAY FOR 10 SEC
47.0	1.350	5.958	6.152	329	0.54	---	---	---	---	---	BAD TEST - U INCREASES FOR 7 SEC
48.0	1.383	5.613	5.700	303	0.65	---	---	---	---	---	BAD TEST U INCREASES FOR 11 SEC
53.0	1.550	8.593	8.593	508	0.44	0.174	0.054	0.045	---	---	GOOD TEST
58.0	1.717	5.518	5.998	954	0.66	---	---	---	---	---	BAD TEST - U INCREASES FOR 26 SEC
62.5	1.867	9.109	9.109	2313	0.29	0.087	0.038	0.031	0.024	---	VERY GOOD TEST ←
67.5	2.033	10.130	10.130	379	0.52	0.079	0.039	---	---	---	VERY GOOD TEST ←
72.5	2.200	9.389	9.389	715	0.43	0.079	0.035	0.030	---	---	VERY GOOD TEST ←
77.5	2.367	7.683	8.219	769	0.56	---	---	---	---	---	BAD TEST - U INCREASES FOR 7 SEC
82.5	2.533	10.010	10.010	316	0.55	0.093	0.034	---	---	---	VERY GOOD TEST ←
87.5	2.700	10.404	10.468	596	0.47	0.029	0.027	0.028	---	---	FAIR TEST AFTER 3 SEC ←

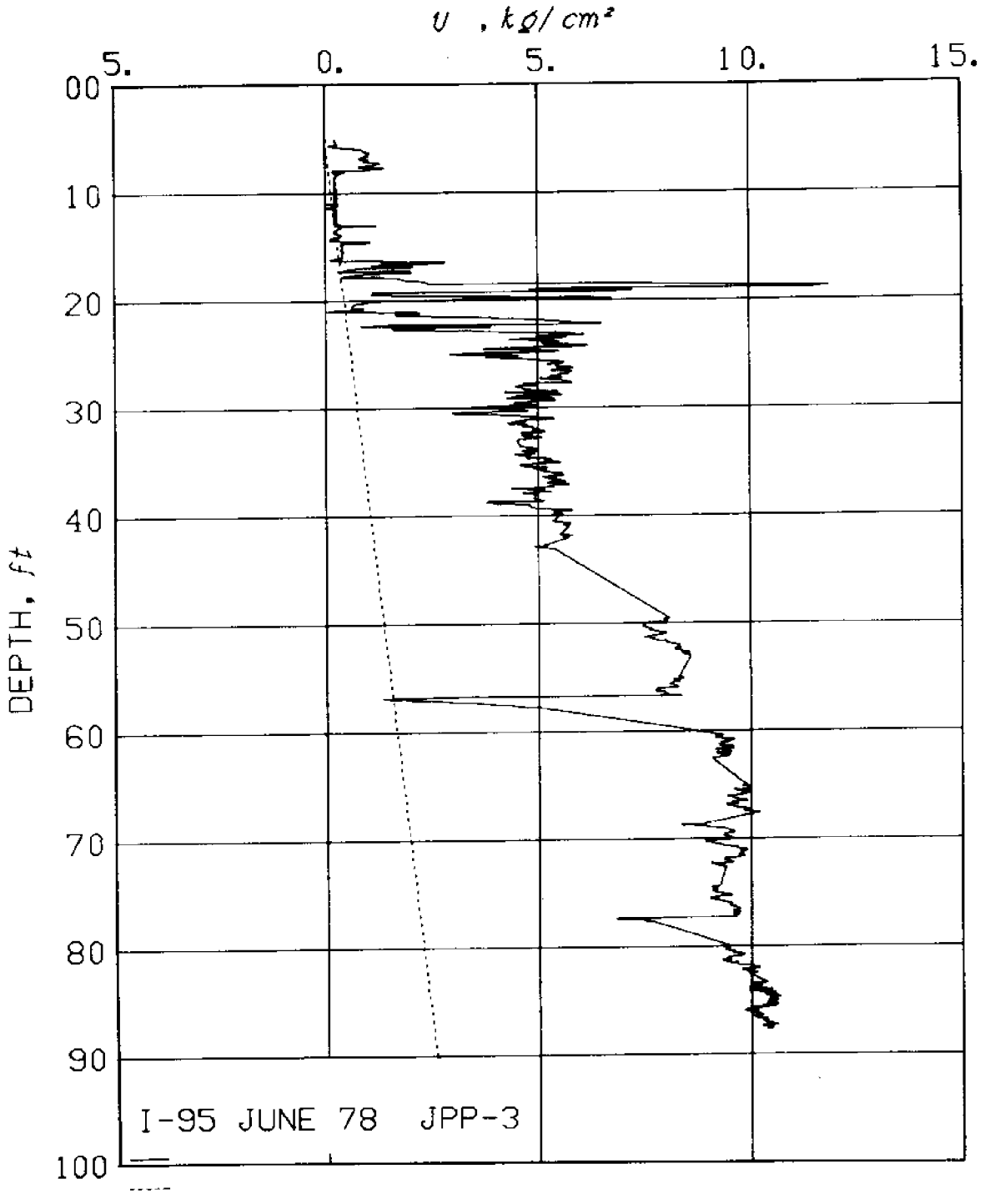
υ , kg/cm²
5.
0.
5.
10.
15.
00
10
20
30
40
50
60
70
80
90
100
DEPTH, ft
I-95 JUNE 78 JPP-3

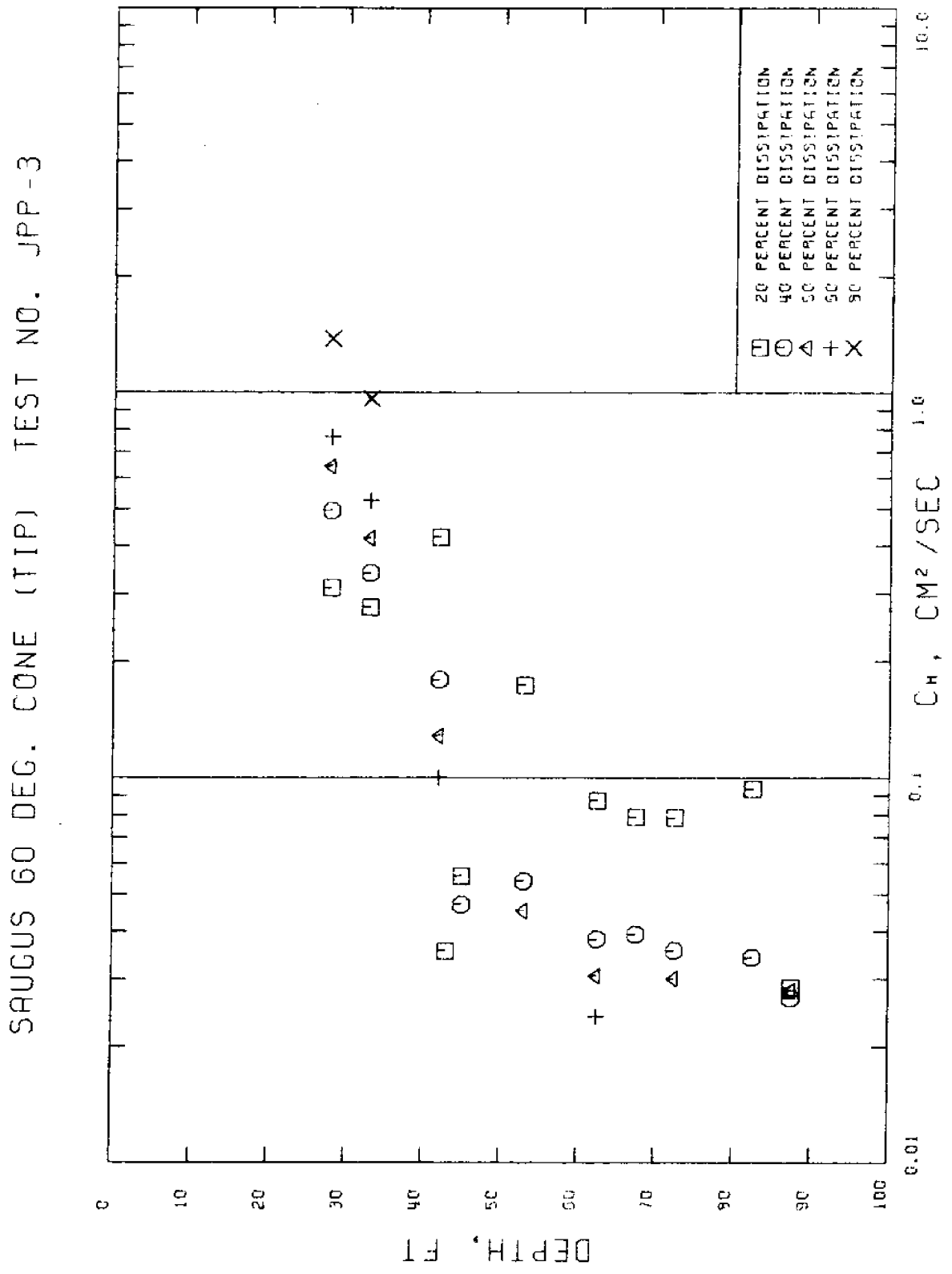
SAUGUS 60 DEG. CONE (TIP) TEST NO. JPP-3
20 PERCENT DISSIPATION
40 PERCENT DISSIPATION
50 PERCENT DISSIPATION
60 PERCENT DISSIPATION
90 PERCENT DISSIPATION
DEPTH, FT
0
10
20
30
40
50
60
70
80
90
100
0.01
0.1
1.0
10.0
C_H, CM^2/SEC

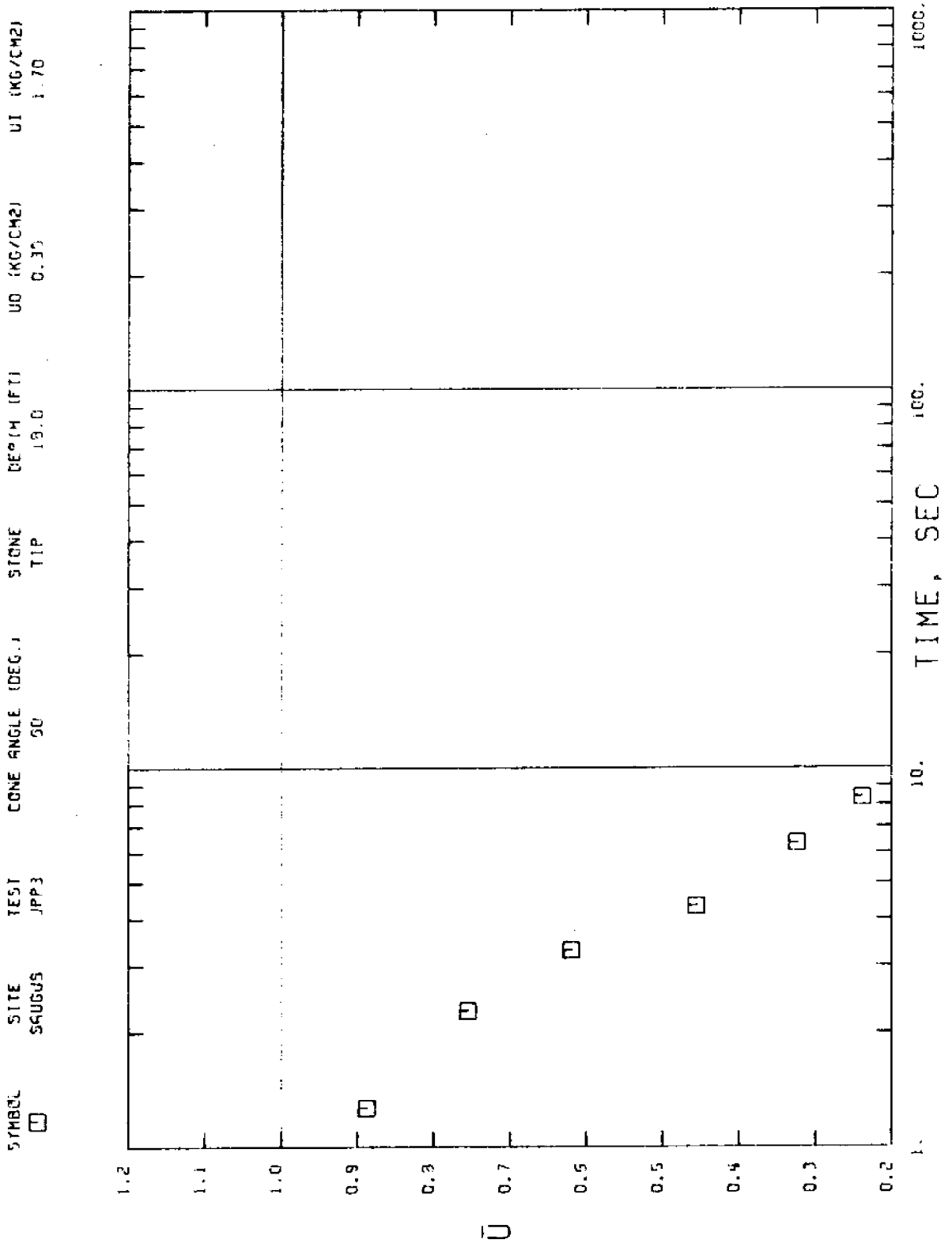
SYMBOL
SITE
SKUGUS
TEST
JPP3
CONE ANGLE (DEG.)
60
STONE
TIP
DEPTH (FT)
10.0
U0 (KG/CM2)
0.35
U1 (KG/CM2)
1.70
1.2
1.1
1.0
0.9
0.8
0.7
0.6
0.5
0.4
0.3
0.2
U
1.
10.
100.
1000.
TIME, SEC

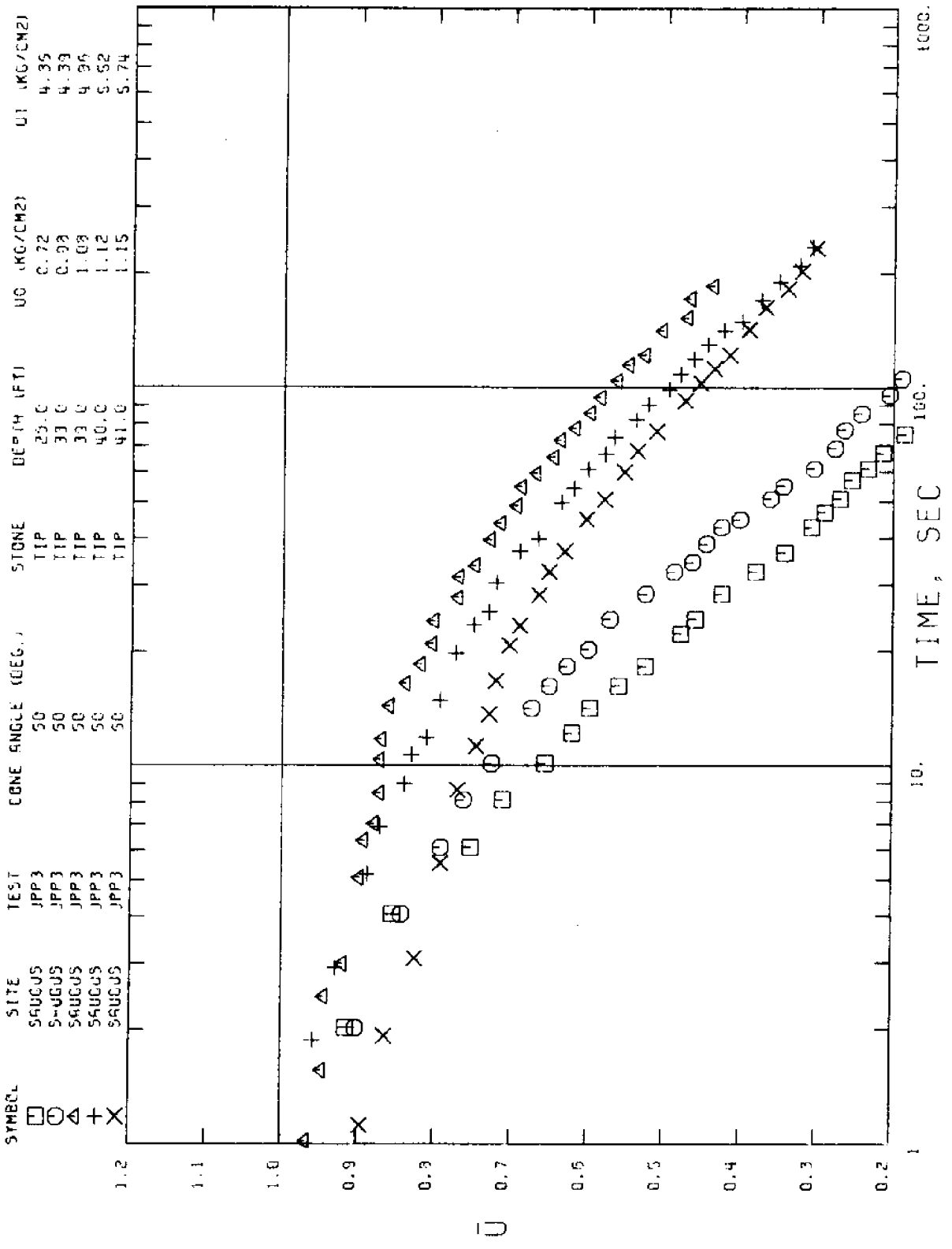
SYMBOL SITE TEST CONE ANGLE (DEG.) STONE DEPTH (FT) U0 (KG/CM2) U1 (KG/CM2)
SAUGUS JPP3 60 TIP 29.0 0.72 4.35
SAUGUS JPP3 60 TIP 33.0 0.93 4.39
SAUGUS JPP3 60 TIP 33.0 1.08 4.96
SAUGUS JPP3 60 TIP 40.0 1.12 5.52
SAUGUS JPP3 60 TIP 41.0 1.15 5.74
U
TIME, SEC
1.2
1.1
1.0
0.9
0.8
0.7
0.6
0.5
0.4
0.3
0.2
1
10.
100.
1000.

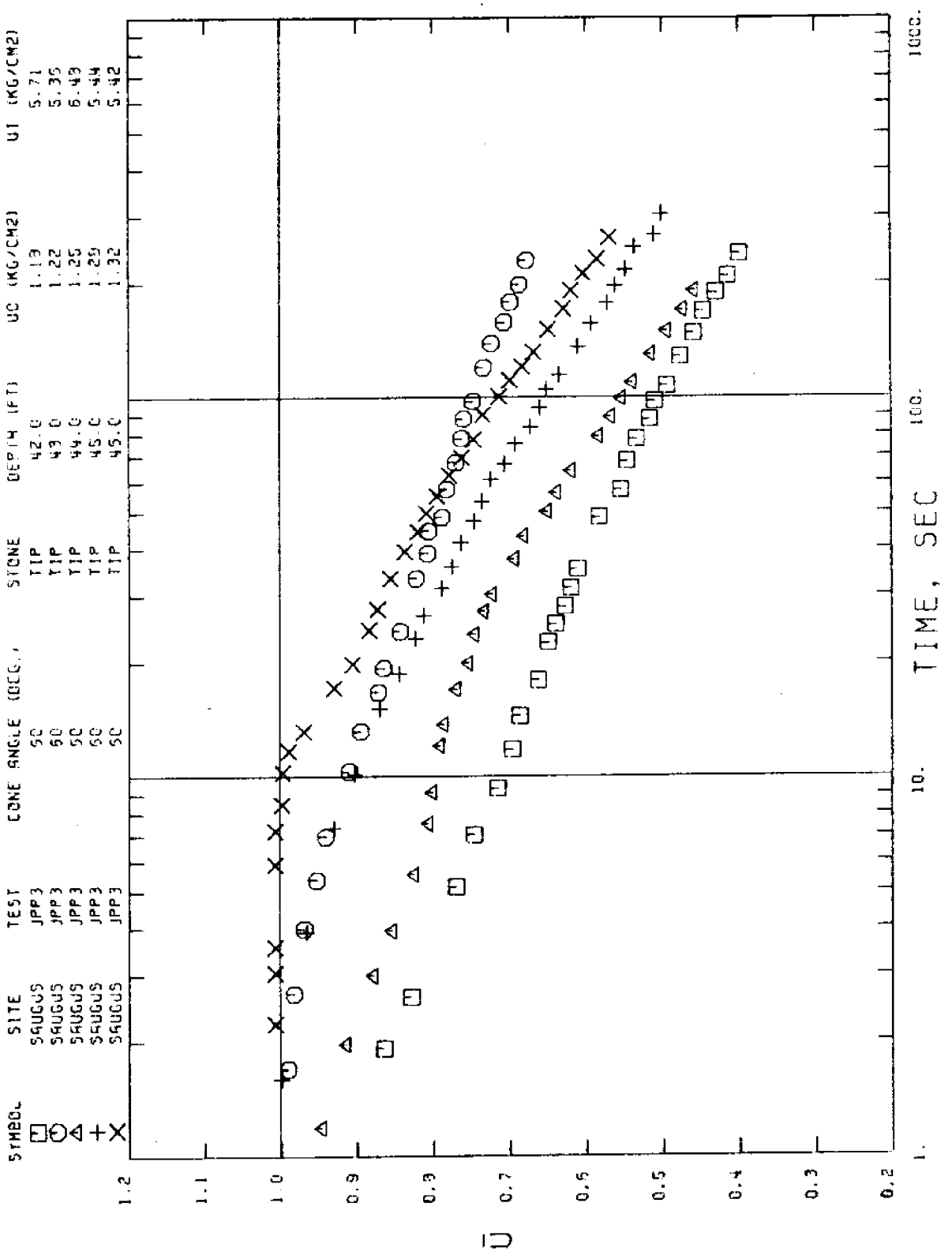
SYMBOL SITE TEST CONE ANGLE (DEG.) STONE DEPTH (FT) UC (KG/CM2) UI (KG/CM2)
SAUGUS JPP3 60 TIP 42.0 1.19 5.71
SAUGUS JPP3 60 TIP 43.0 1.22 5.35
SAUGUS JPP3 60 TIP 44.0 1.25 6.43
SAUGUS JPP3 60 TIP 45.0 1.29 5.44
SAUGUS JPP3 60 TIP 45.0 1.32 5.42
CI
TIME, SEC
1.2
1.1
1.0
0.9
0.8
0.7
0.6
0.5
0.4
0.3
0.2
1.
10.
100.
1000.

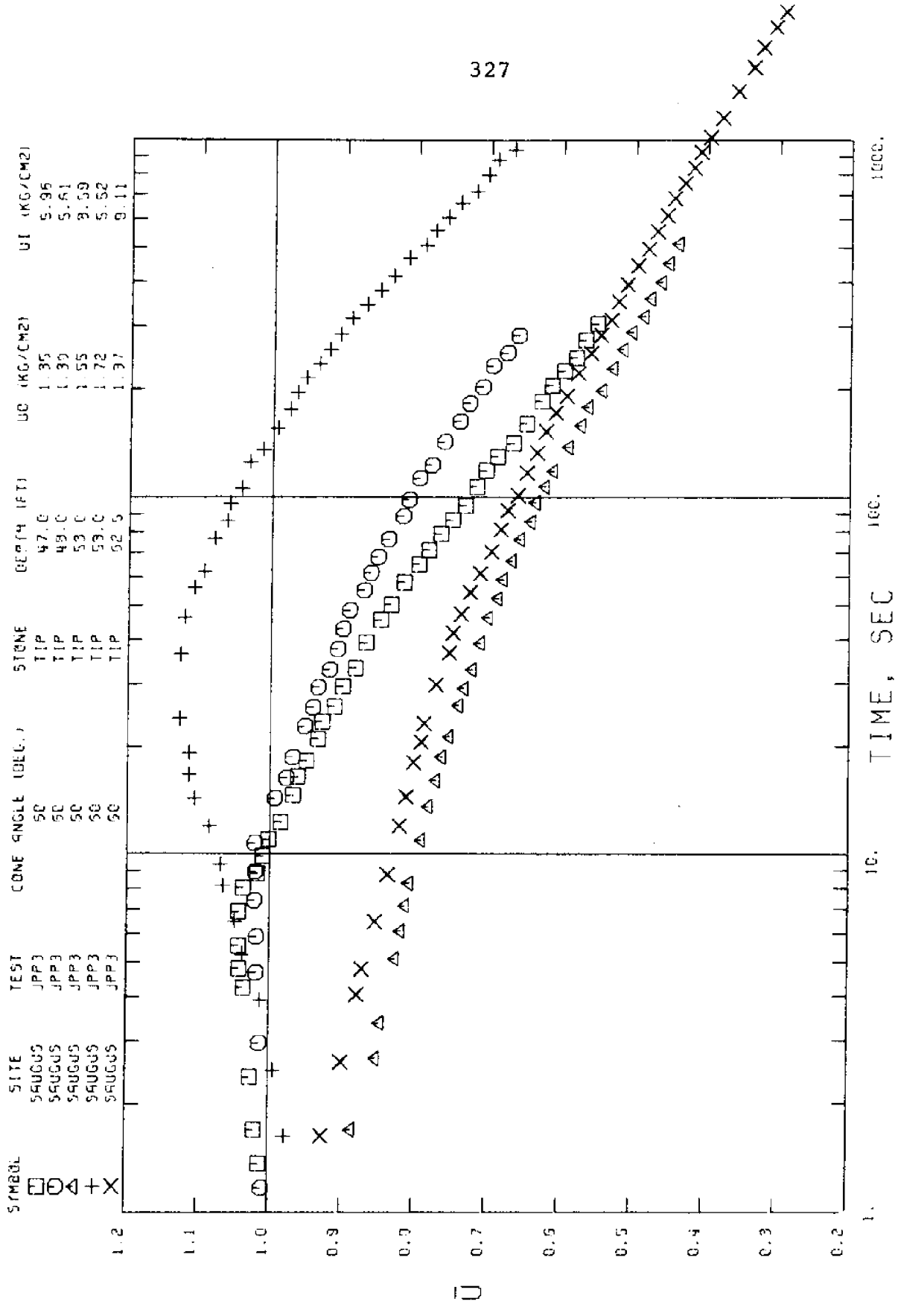
SYMBOL SITE TEST CONE ANGLE (DEG.) STONE DEPTH (FT) UC (KG/CM2) UI (KG/CM2)
SAUGUS JPP3 60 TIP 47.0 1.35 5.96
SAUGUS JPP3 60 TIP 49.0 1.39 5.61
SAUGUS JPP3 60 TIP 53.0 1.55 8.59
SAUGUS JPP3 60 TIP 59.0 1.72 5.52
SAUGUS JPP3 60 TIP 62.5 1.37 8.11
U
TIME, SEC
1.2
1.1
1.0
0.9
0.8
0.7
0.6
0.5
0.4
0.3
0.2
1.
10.
100.
1000.

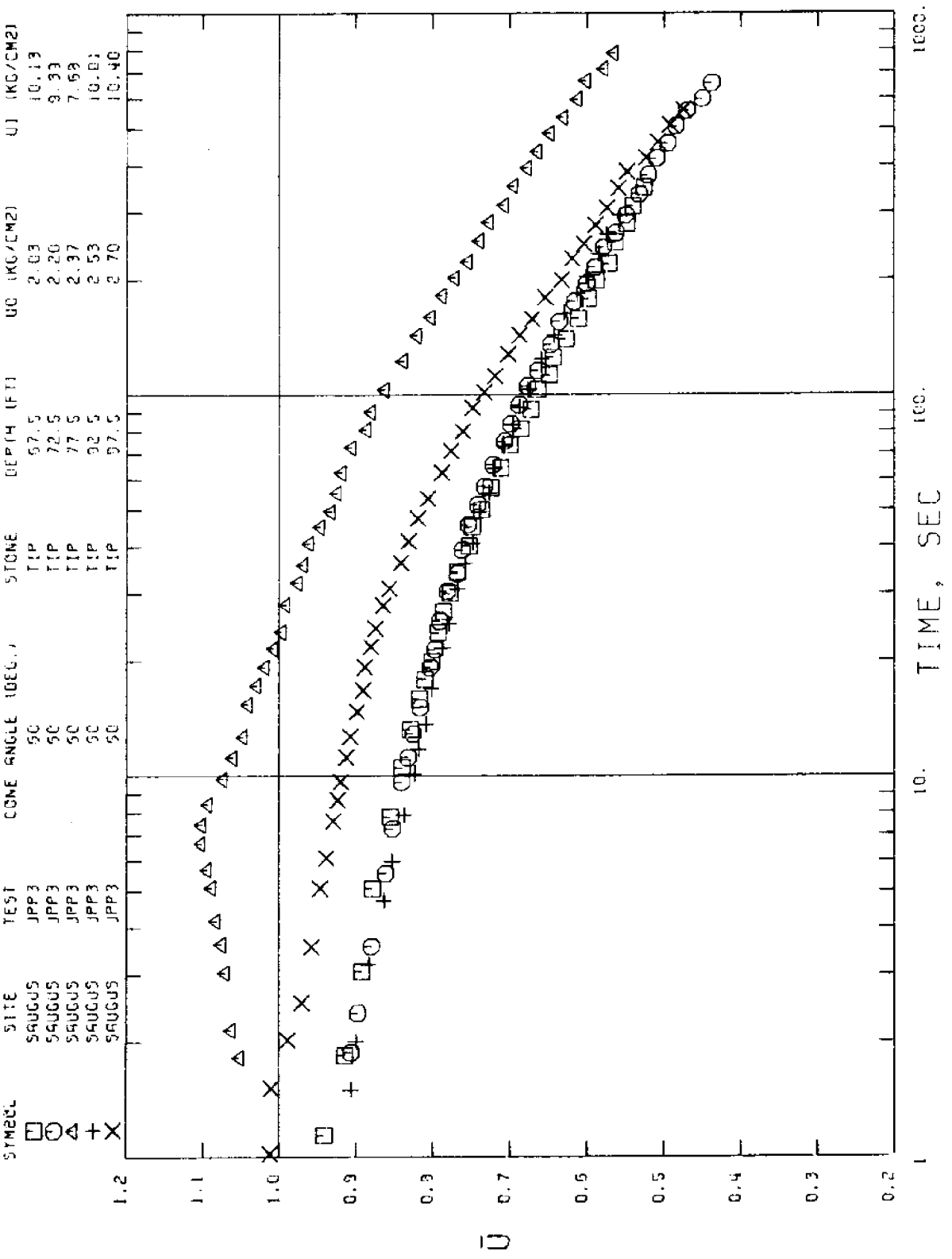
SYMBOL SITE TEST CONE ANGLE (DEG.) STONE DEPTH (FT) UO (KG/CM2) U1 (KG/CM2)
SAUGUS JPP3 60 TIP 57.5 2.03 10.13
SAUGUS JPP3 60 TIP 72.5 2.20 9.33
SAUGUS JPP3 60 TIP 77.5 2.37 7.68
SAUGUS JPP3 60 TIP 82.5 2.53 10.01
SAUGUS JPP3 60 TIP 87.5 2.70 10.40
U
TIME, SEC
1.2
1.1
1.0
0.9
0.8
0.7
0.6
0.5
0.4
0.3
0.2
1
10.
100.
1000.

SITE: SAUGUS DATE: 6/12/78

TEST # JPP-4 CONE ANGLE: 18 DEG. STONE LOCATION: MID-HEIGHT

DEPTH (FT)	UO (KSC)	UI (KSC)	UMAX (KSC)	TF (SEC)	USARF	COEF. OF CONS. (CM2/SEC) CH20	CH40	CH50	CH60	CH80	COMMENTS	
20.0	0.450	0.926	0.926	89	0.0	2.878	6.625	8.899	11.516	22.947	FAIR TEST - STEEP CURVE	
25.0	0.617	2.757	2.757	191	0.0	0.410	1.016	1.320	1.797	4.233	FAIR TEST - STEEP CURVE	
30.0	0.783	3.083	3.083	118	0.05	1.173	2.125	2.808	2.931	4.167	FAIR TEST - STEEP CURVE	
35.0	0.950	4.410	4.537	510	0.27	---	---	---	---	---	BAD TEST - U INCREASES FOR 5 SEC	
40.0	1.117	4.910	4.910	612	0.06	0.229	0.362	0.399	0.435	0.582	FAIR TEST	
41.0	1.150	5.040	5.041	230	0.38	0.111	0.170	0.163	0.171	---	FAIR TEST	
42.0	1.183	4.890	4.890	84	0.61	---	---	---	---	---	BAD TEST AFTER 20 SEC	
45.0	1.283	5.348	5.348	273	0.44	---	---	---	---	---	BAD TEST AFTER 20 SEC	
46.0	1.317	5.243	5.243	391	0.55	0.037	0.031	---	---	---	GOOD TEST	
47.0	1.350	5.685	5.685	220	0.56	0.093	0.067	---	---	---	GOOD TEST - SLIGHTLY WIGGLING	
48.0	1.383	5.770	5.801	328	0.35	---	---	---	---	---	BAD TEST - U CONST. FOR 4 SEC	
49.0	1.417	5.381	5.872	277	0.75	---	---	---	---	---	BAD TEST - U INCREASES FOR 12 SEC	
50.0	1.450	6.423	6.570	335	0.47	---	---	---	---	---	BAD TEST - U INCREASES FOR 6 SEC	
55.0	1.617	7.741	7.741	331	0.51	0.076	0.063	---	---	---	VERY GOOD TEST	
60.0	1.783	7.525	7.525	422	0.58	0.048	0.027	---	---	---	VERY GOOD TEST	←
65.0	1.950	8.634	8.634	558	0.46	0.059	0.045	0.049	---	---	VERY GOOD TEST	←
70.0	2.117	8.205	8.205	273	0.60	0.064	---	---	---	---	VERY GOOD TEST	←
75.0	2.283	8.143	8.143	375	0.55	0.057	0.037	---	---	---	VERY GOOD TEST	←

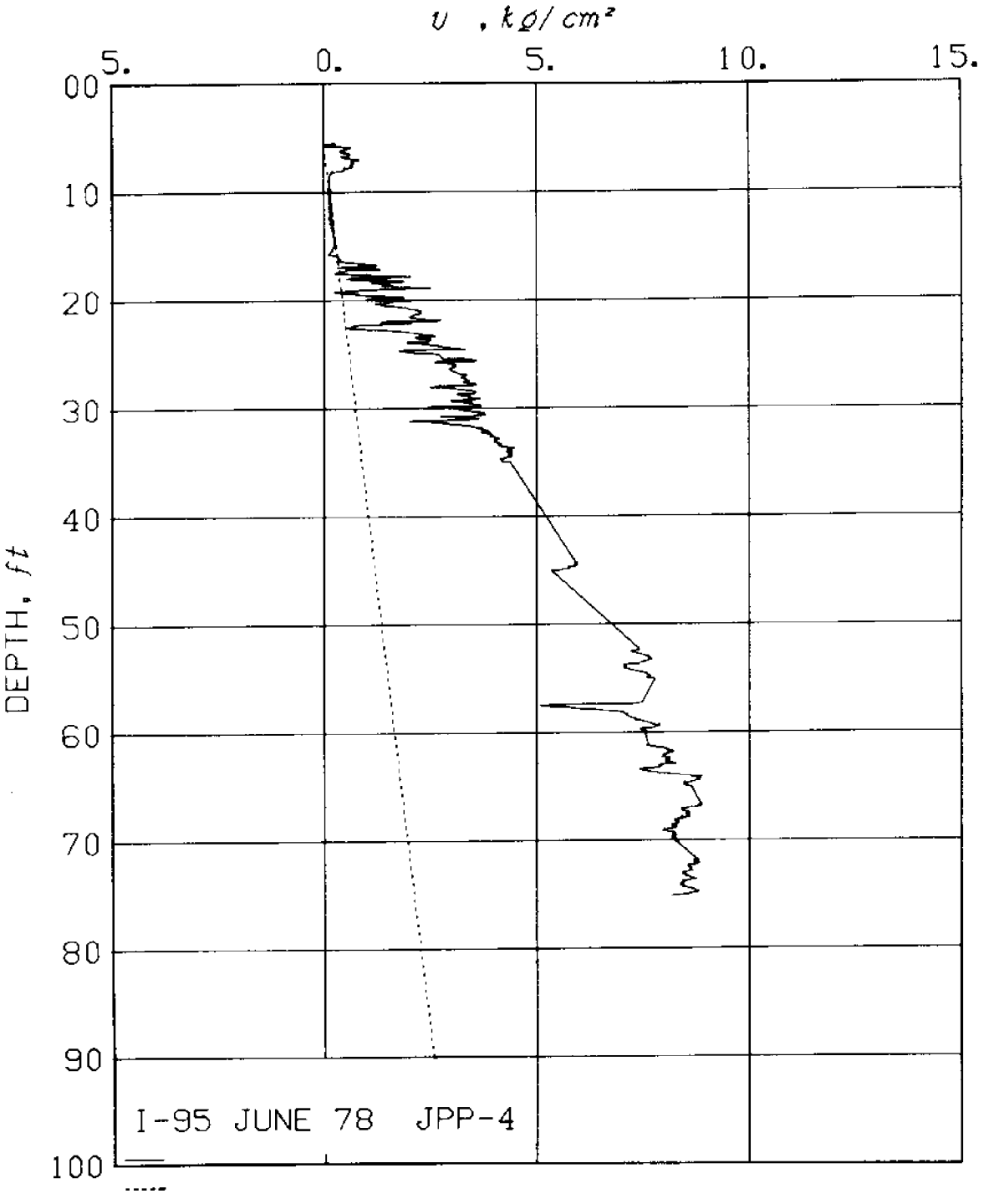
υ , kg/cm²
5.
0.
5.
10.
15.
00
10
20
30
40
50
60
70
80
90
100
DEPTH, ft
I-95 JUNE 78 JPP-4

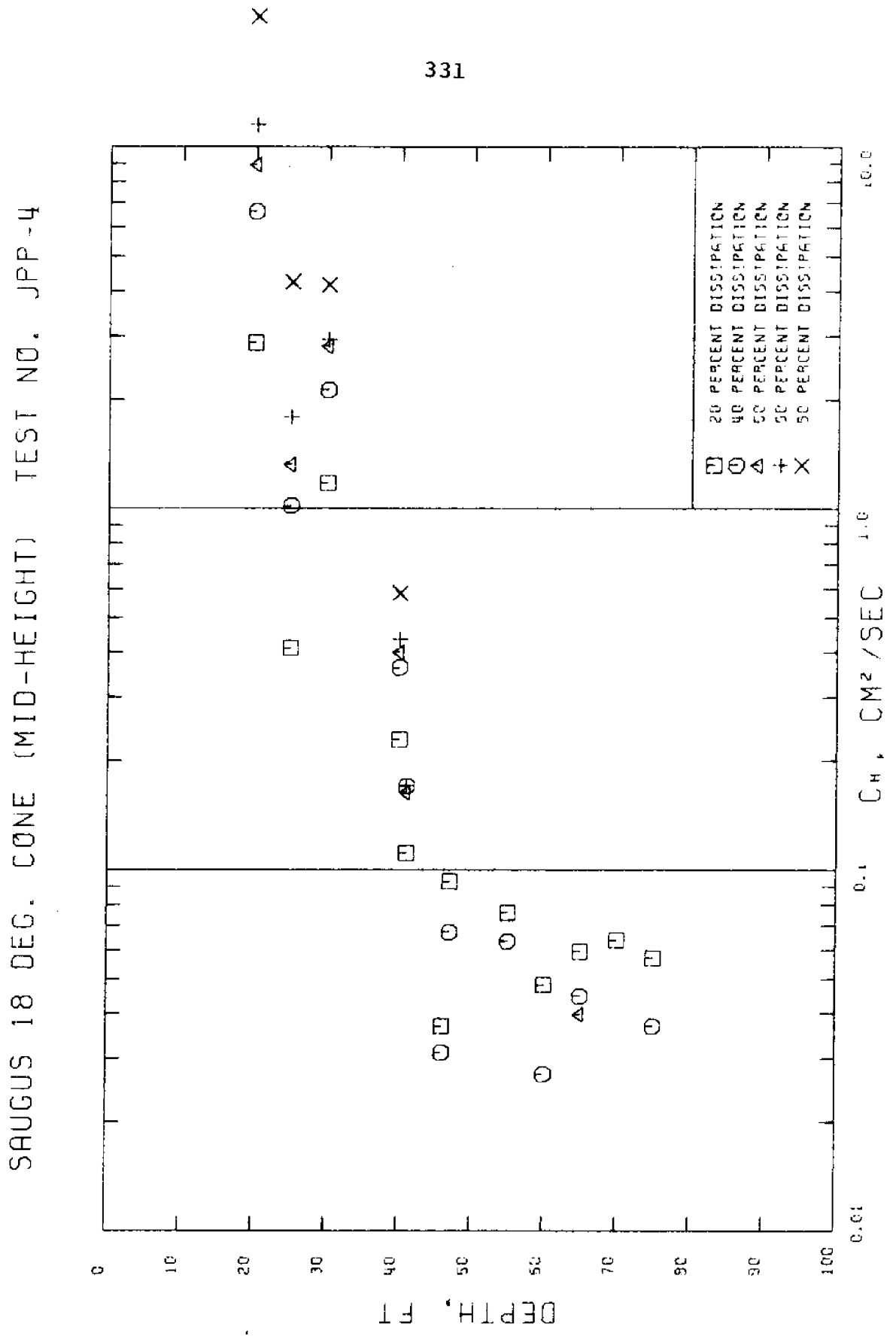
SAUGUS 18 DEG. CONE (MID-HEIGHT) TEST NO. JPP-4
20 PERCENT DISSIPATION
40 PERCENT DISSIPATION
50 PERCENT DISSIPATION
50 PERCENT DISSIPATION
50 PERCENT DISSIPATION
DEPTH, FT
0
10
20
30
40
50
60
70
80
90
100
0.01
0.1
1.0
10.0
C_H, CM^2/SEC

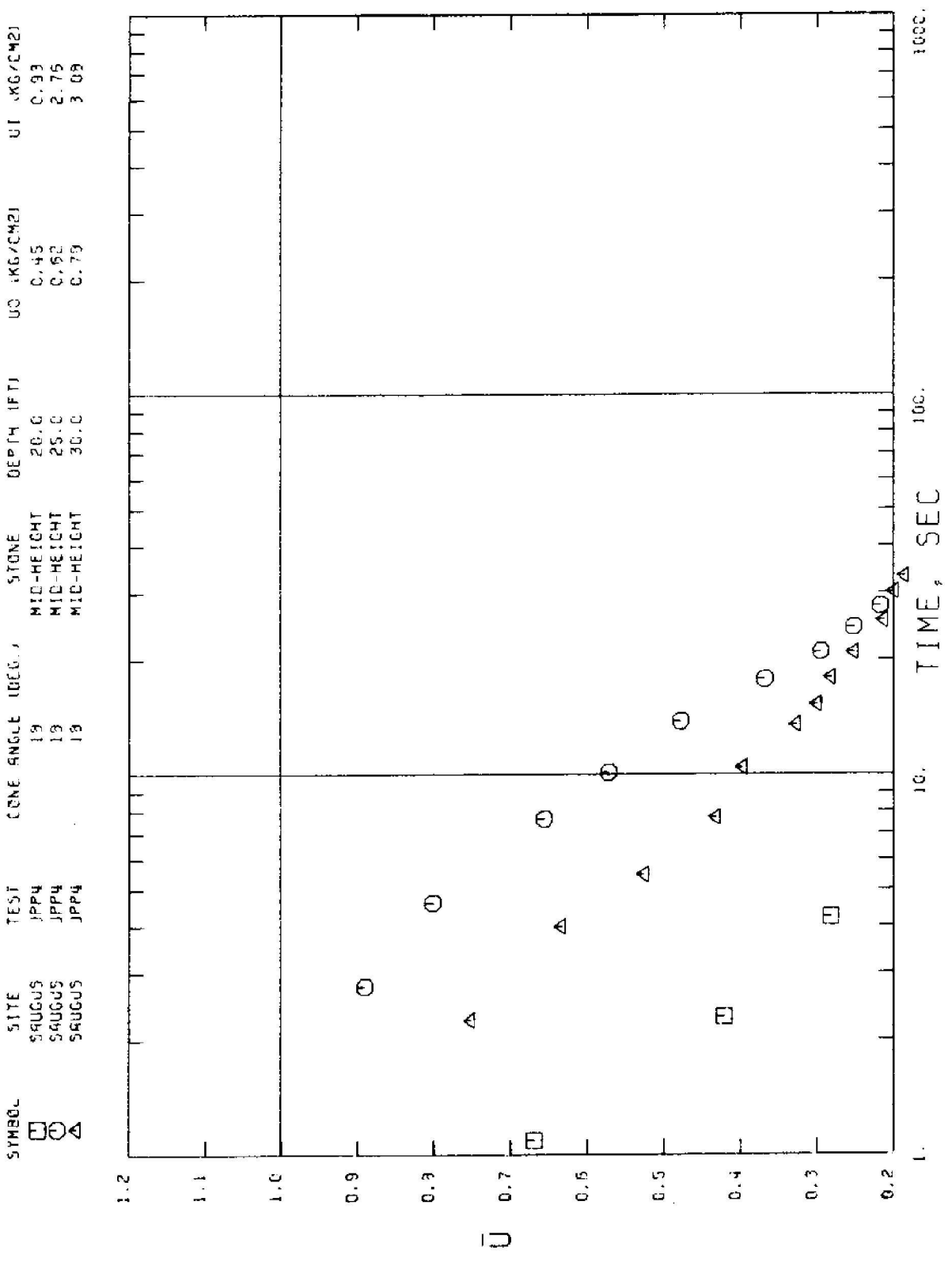
SYMBOL SITE TEST CONE ANGLE (DEG.) STONE DEPTH (FT) UO (KG/CM2) UI (KG/CM2)
SAUGUS JPP4 13 MID-HEIGHT 20.0 0.45 0.93
SAUGUS JPP4 13 MID-HEIGHT 25.0 0.62 2.75
SAUGUS JPP4 13 MID-HEIGHT 30.0 0.79 3.09
U
TIME, SEC
1.2
1.1
1.0
0.9
0.8
0.7
0.6
0.5
0.4
0.3
0.2
1.
10.
100.
1000.

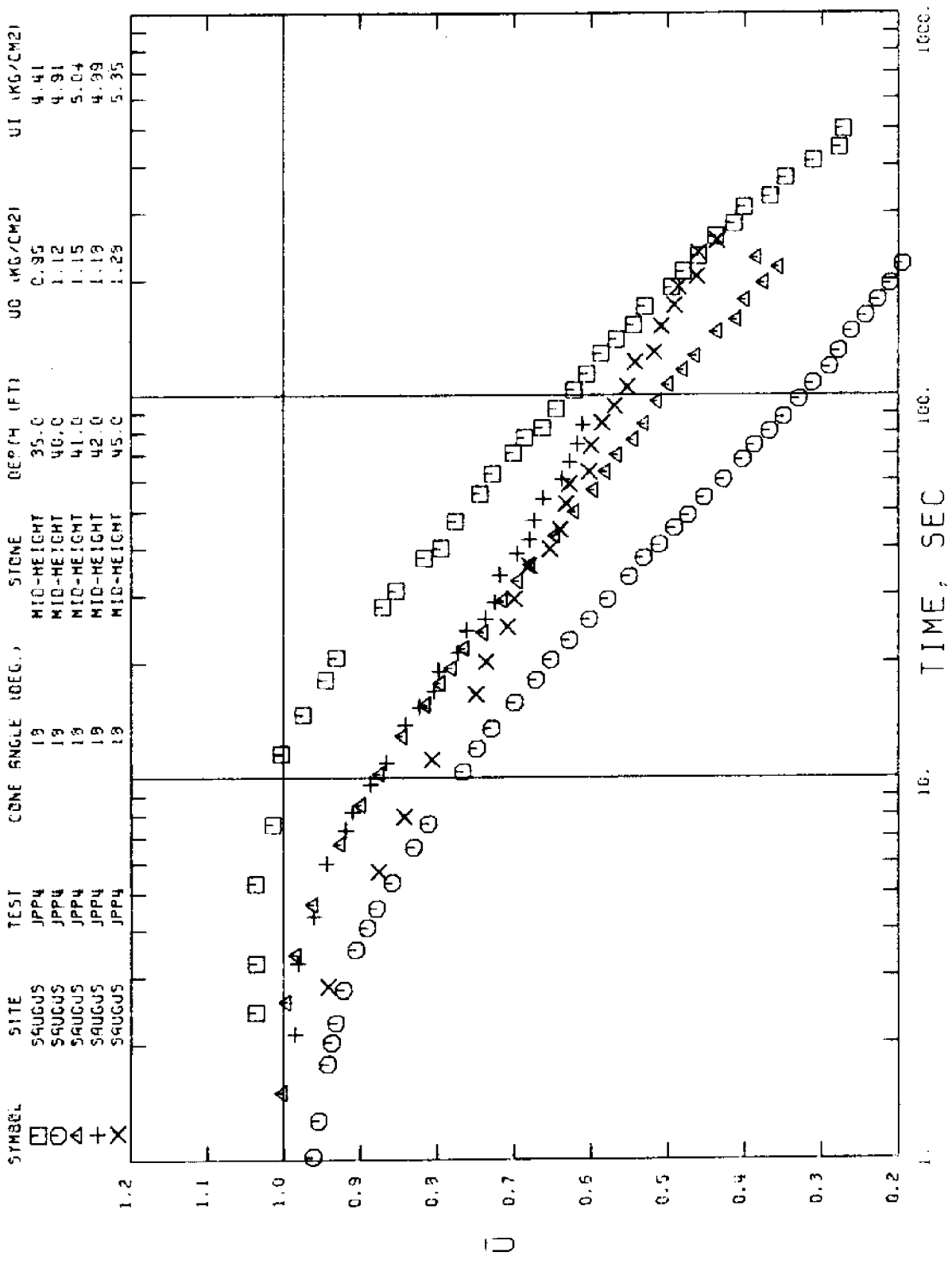
SYMBOL SITE TEST CONE ANGLE (DEG.) STONE DEPTH (FT) UO (KG/CM2) UI (KG/CM2)
SAUGUS JPP4 19 MID-HEIGHT 35.0 0.95 4.41
SAUGUS JPP4 19 MID-HEIGHT 40.0 1.12 4.91
SAUGUS JPP4 19 MID-HEIGHT 41.0 1.15 5.04
SAUGUS JPP4 19 MID-HEIGHT 42.0 1.19 4.99
SAUGUS JPP4 19 MID-HEIGHT 45.0 1.29 5.35
U
TIME, SEC
1.2
1.1
1.0
0.9
0.8
0.7
0.6
0.5
0.4
0.3
0.2
16.
1600.

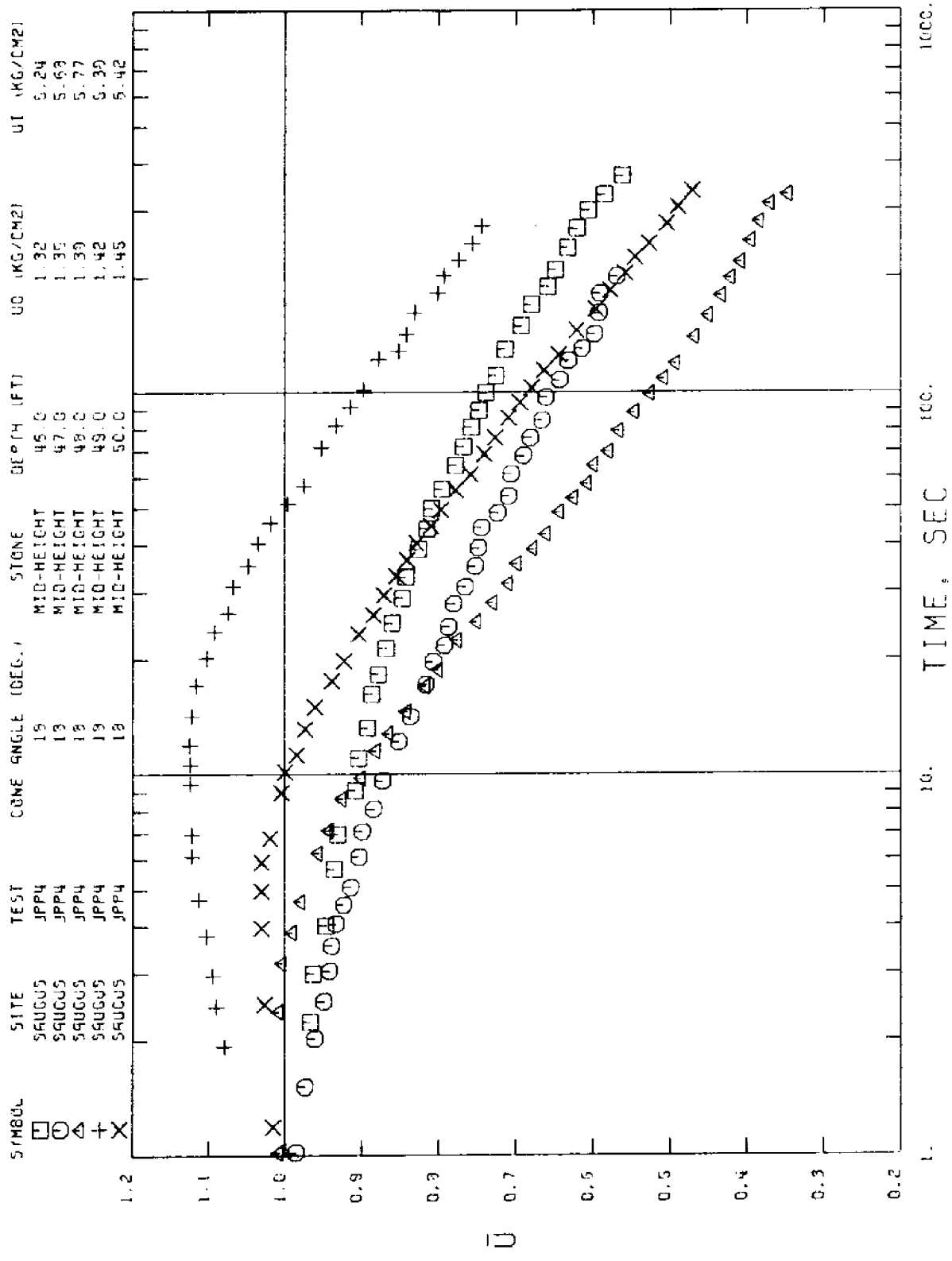
SYMBOL SITE TEST CONE ANGLE (DEG.) STONE DEPTH (FT) UO (KG/CM2) UI (KG/CM2)
SAUGUS JPP4 15 MID-HEIGHT 45.0 1.32 5.24
SAUGUS JPP4 15 MID-HEIGHT 47.0 1.35 5.69
SAUGUS JPP4 15 MID-HEIGHT 48.0 1.39 5.77
SAUGUS JPP4 15 MID-HEIGHT 49.0 1.42 5.39
SAUGUS JPP4 15 MID-HEIGHT 50.0 1.45 5.42
1.2
1.1
1.0
0.9
0.8
0.7
0.6
0.5
0.4
0.3
0.2
U
1.
10.
100.
TIME, SEC

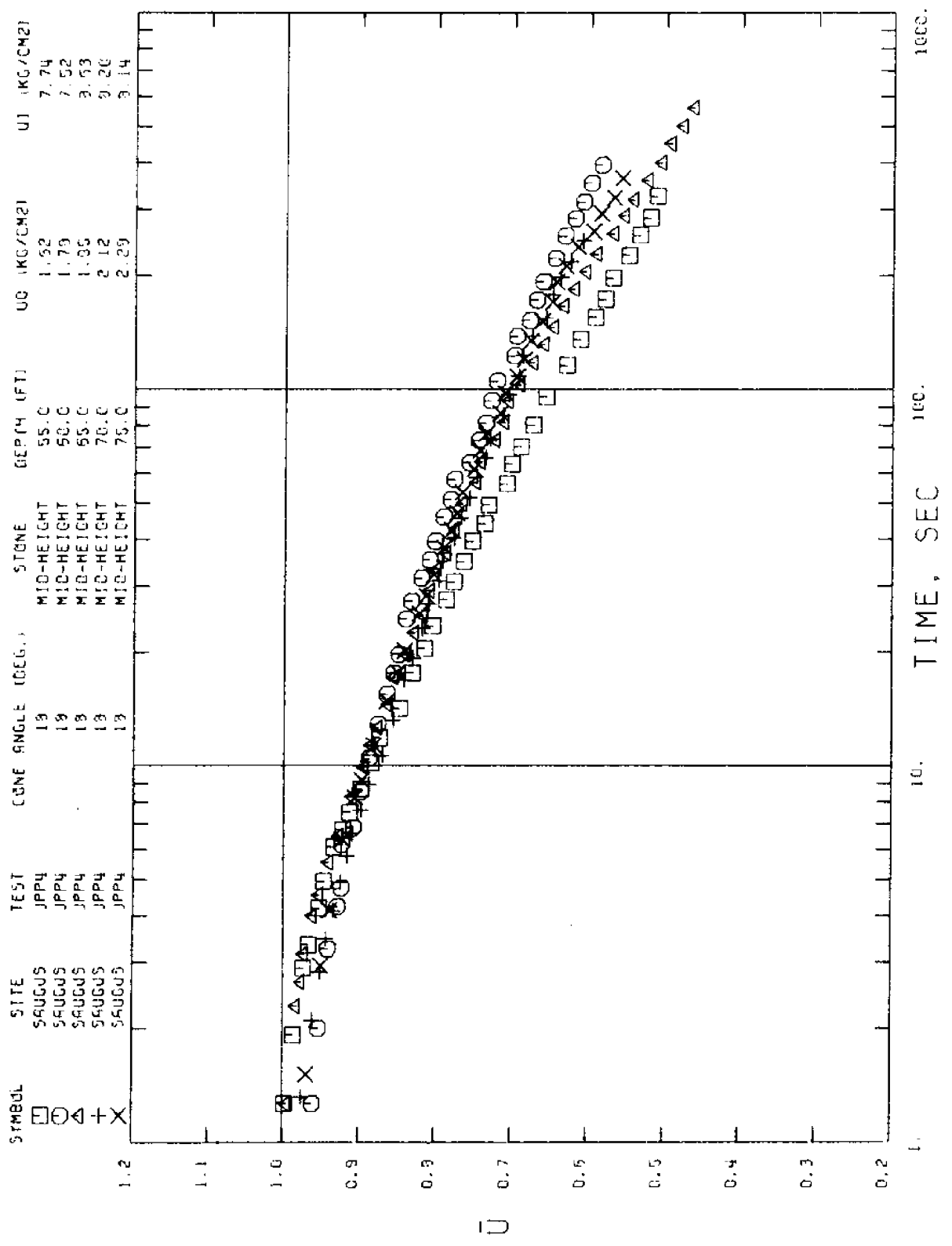
SYMBOL SITE TEST CONE ANGLE (DEG.) STONE DEPTH (FT) UQ (KG/CM2) U1 (KG/CM2)
SAUGUS JPP4 19 MID-HEIGHT 55.0 1.52 7.74
SAUGUS JPP4 19 MID-HEIGHT 60.0 1.79 7.52
SAUGUS JPP4 19 MID-HEIGHT 65.0 1.85 8.53
SAUGUS JPP4 19 MID-HEIGHT 70.0 2.12 9.20
SAUGUS JPP4 19 MID-HEIGHT 75.0 2.29 9.14
U
TIME, SEC
1.2
1.1
1.0
0.9
0.8
0.7
0.6
0.5
0.4
0.3
0.2
10.
100.
1000.

SITE: SAUGUS DATE: 6/15/78

TEST # UPP-5 CONE ANGLE: 18 DEG. STONE LOCATION: MID-HEIGHT

DEPTH (FT)	UO (KSC)	UI (KSC)	UMAX (KSC)	TF (SEC)	UBARF	COEF. OF CONS. (CM2/SEC) CH20	CH40	CH60	CH80		COMMENTS
18.0	0.383	1.303	1.303	89	0.0	2.278	4.436	5.534	7.023	13.429	FAIR TEST - STEEP CURVE
23.0	0.550	1.687	1.687	146	0.04	0.279	0.766	1.029	1.331	2.788	FAIR TEST - STEEP CURVE
28.0	0.717	3.228	3.424	673	0.07	---	---	---	---	---	BAD TEST - U INCREASES FOR 5 SEC
33.0	0.883	1.207	2.152	686	0.0	---	---	---	---	---	BAD TEST - U INCREASES FOR 61 SEC
38.0	1.050	4.181	4.181	907	0.04	0.051	0.127	0.167	0.215	0.452	FAIR TEST - SLOW START
43.0	1.217	5.608	5.608	742	0.20	0.086	0.105	0.092	0.085	---	VERY GOOD TEST
48.0	1.383	5.459	5.459	997	0.19	0.093	0.081	0.078	0.081	0.130	VERY GOOD TEST
53.0	1.550	6.847	6.847	1498	0.30	0.062	0.063	0.052	0.041	---	GOOD TEST UP TO 500 SEC
63.0	1.983	7.838	7.838	1206	0.41	0.068	0.041	0.029	---	---	FAIR TEST - SLOW DISS. AFTER 100 SEC ←
68.0	2.050	8.419	8.419	1256	0.39	0.039	0.034	0.028	0.024	---	VERY GOOD TEST ←

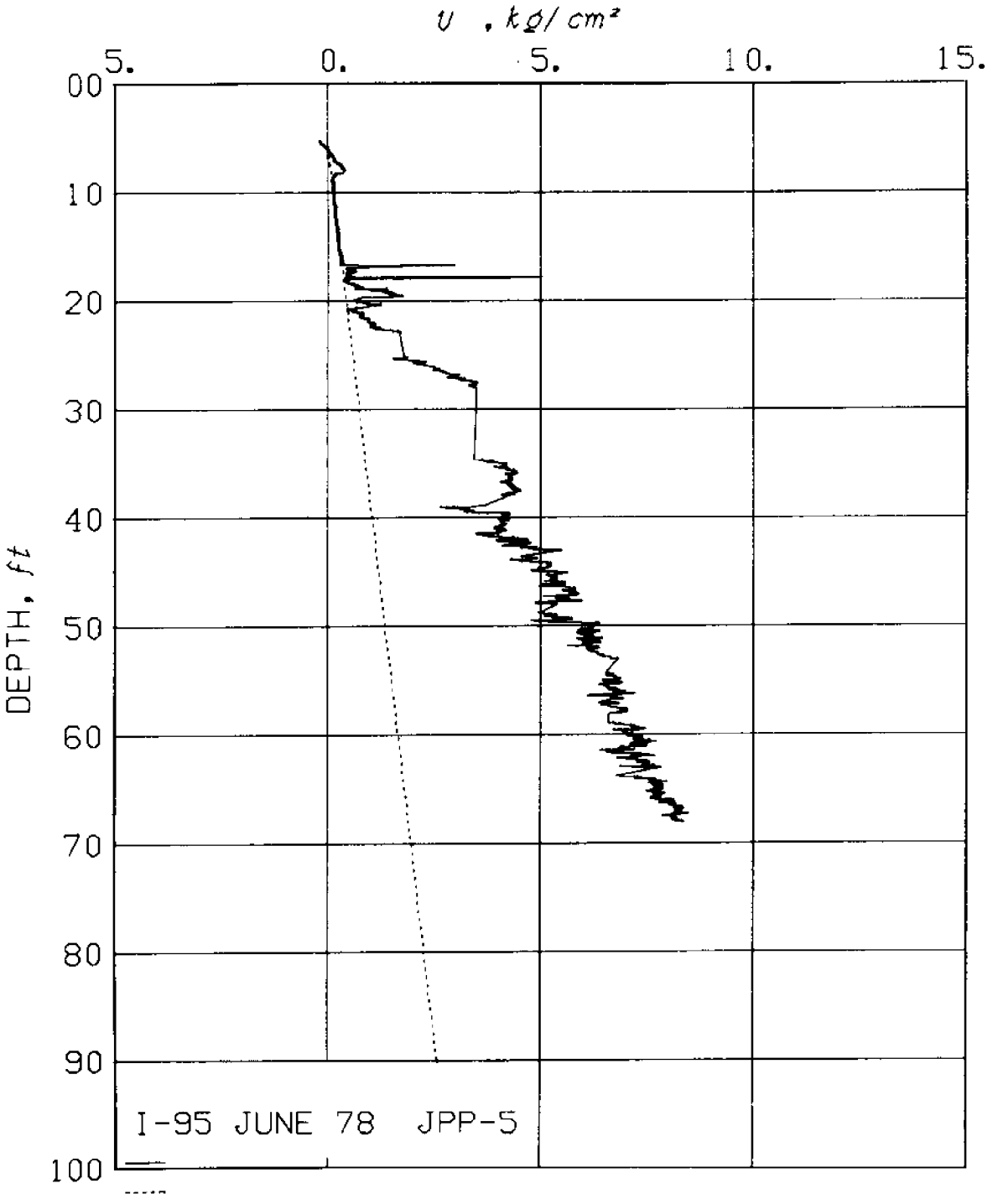
U , kg/cm²
5.
0.
5.
10.
15.
00
10
20
30
40
50
60
70
80
90
100
DEPTH, ft
I-95 JUNE 78 JPP-5

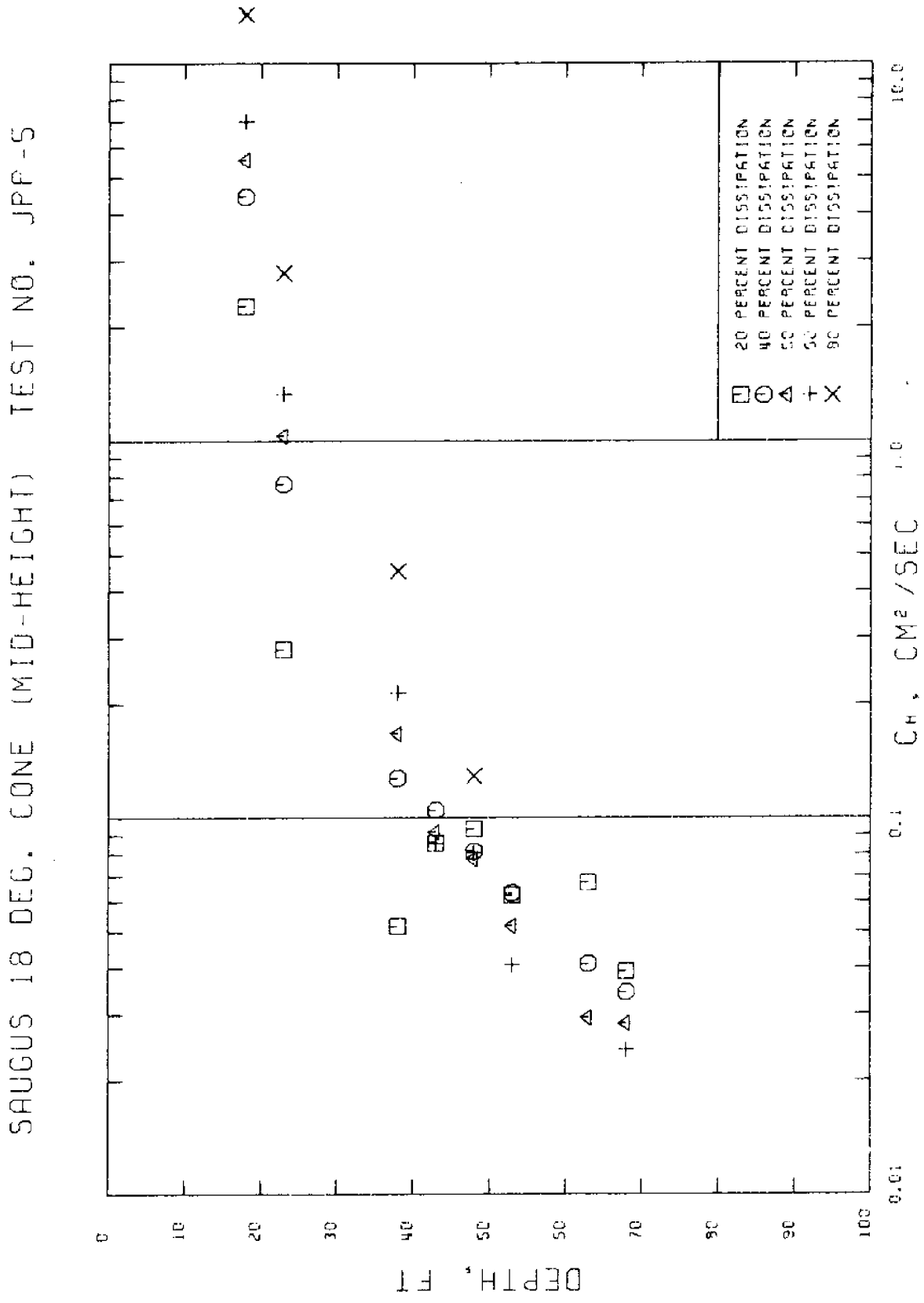
SAUGUS 18 DEG. CONE (MID-HEIGHT) TEST NO. JPP-S
DEPTH, FT
C_H, CM²/SEC
20 PERCENT DISSIPATION
40 PERCENT DISSIPATION
60 PERCENT DISSIPATION
80 PERCENT DISSIPATION
0
10
20
30
40
50
60
70
80
90
100
0.01
0.1
1.0
10.0

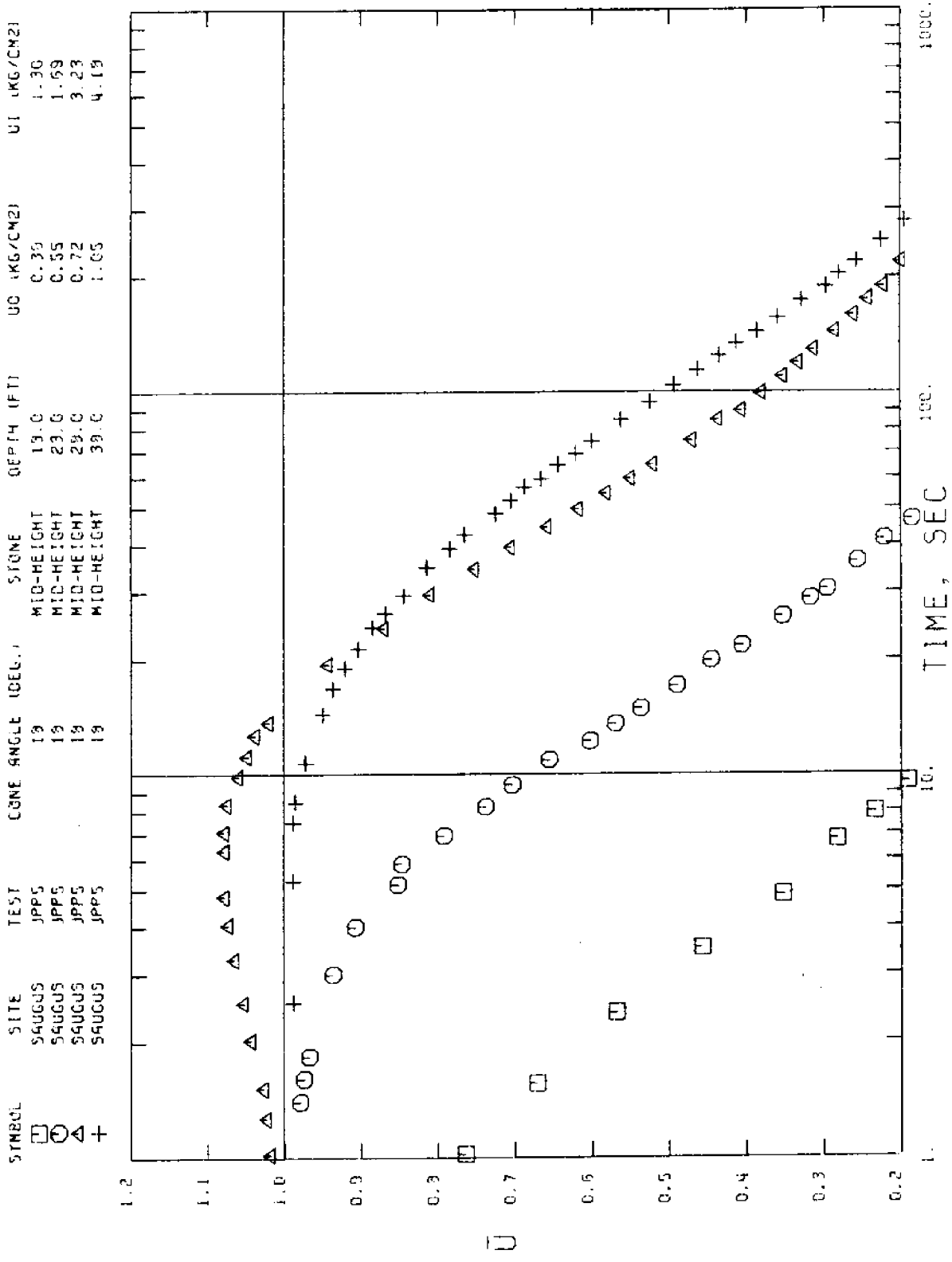
SYMBOL SITE TEST CONE ANGLE (DEG.) STONE DEPTH (FT) UO (KG/CM2) UI (KG/CM2)
SAUGUS JPPS 19 MID-HEIGHT 19.0 0.39 1.30
SAUGUS JPPS 19 MID-HEIGHT 23.0 0.55 1.69
SAUGUS JPPS 19 MID-HEIGHT 29.0 0.72 3.23
SAUGUS JPPS 19 MID-HEIGHT 39.0 1.05 4.19
U
TIME, SEC

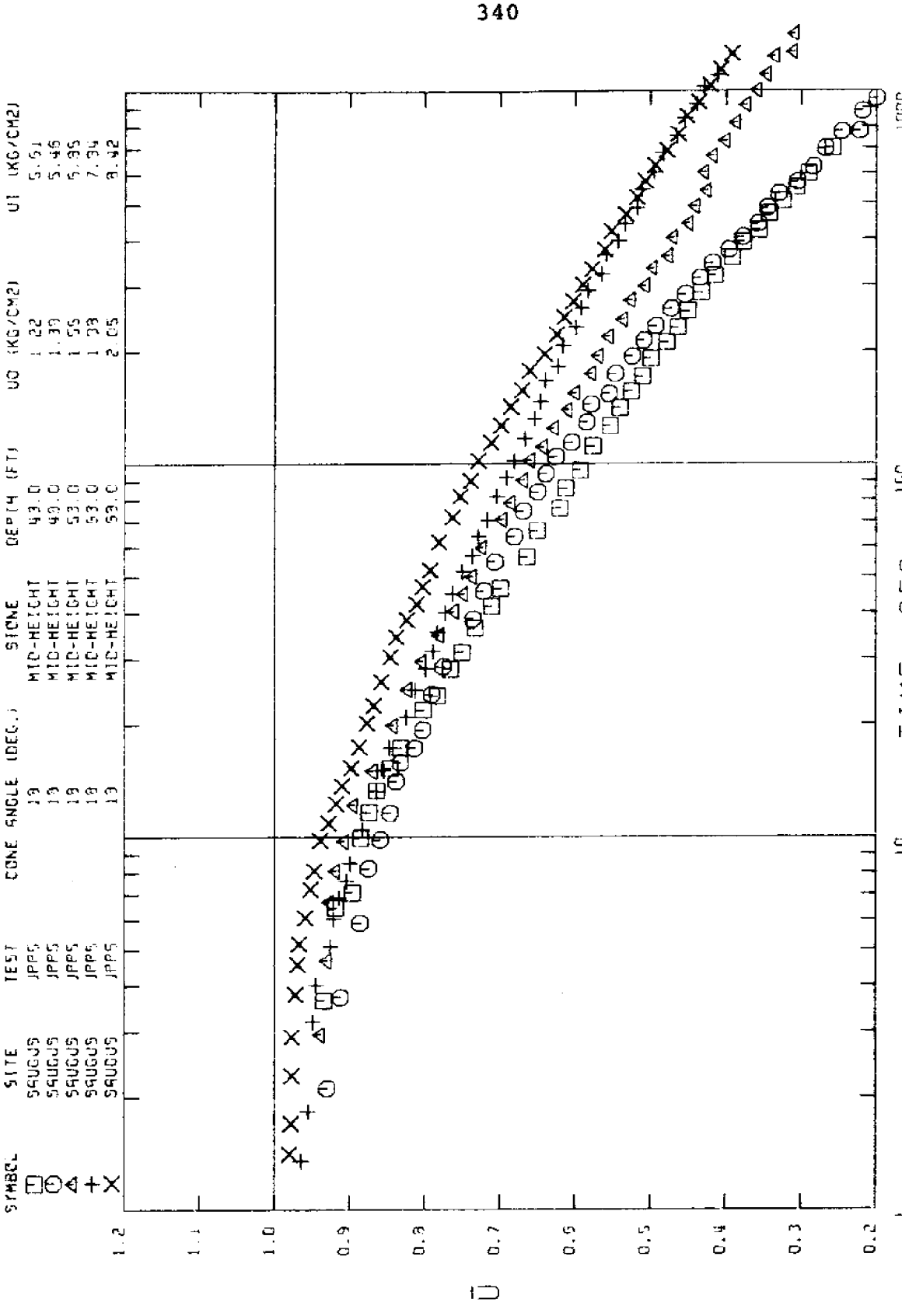
SYMBOL SITE TEST CONE ANGLE (DEG.) STONE DEPTH (FT) UO (KG/CM2) UI (KG/CM2)
SANDS JPPS 19 MID-HEIGHT 43.0 1.22 5.51
SANDS JPPS 19 MID-HEIGHT 48.0 1.39 5.46
SANDS JPPS 19 MID-HEIGHT 53.0 1.55 5.35
SANDS JPPS 19 MID-HEIGHT 53.0 1.38 7.34
SANDS JPPS 19 MID-HEIGHT 58.0 2.05 8.42
U
TIME, SEC
1.2
1.1
1.0
0.9
0.8
0.7
0.6
0.5
0.4
0.3
0.2
1.
10.
100.
1000.

SITE: SAUGUS DATE: 6/16/78

TEST # UPP-6 CONE ANGLE: 18 DEG. STONE LOCATION: TIP

DEPTH (FT)	U0 (KSC)	UI (KSC)	UMAX (KSC)	TF (SEC)	UBARF	COEF. OF CONS. (CM2/SEC) CH20	CH40	CH50	CH60	CH80	COMMENTS
23.0	0.550	-0.695	0.705	323	---	---	---	---	---	---	BAD TEST - U STARTS BELOW STATIC
28.0	0.717	2.246	2.267	408	0.14	---	---	---	---	---	BAD TEST - NO DECAY FOR 15 SEC
30.0	0.783	2.205	2.221	385	0.09	---	---	---	---	---	BAD TEST - NO DECAY FOR 9 SEC
33.0	0.883	2.418	2.425	258	0.04	---	---	---	---	---	BAD TEST - NO DECAY FOR 4 SEC
38.0	1.050	3.478	3.513	597	0.31	---	---	---	---	---	BAD TEST - NO DECAY FOR 20 SEC
43.0	1.217	4.309	4.372	746	0.20	---	---	---	---	---	BAD TEST - NO DECAY FOR 15 SEC
48.0	1.383	5.344	5.345	609	0.35	---	---	---	---	---	BAD TEST - NO DECAY FOR 6 SEC
53.0	1.550	5.647	5.647	646	0.30	---	---	---	---	---	BAD TEST - NO DECAY FOR 6 SEC
58.0	1.717	6.589	6.589	751	0.24	---	---	---	---	---	BAD TEST - CROOKED CURVE
68.0	2.050	7.000	7.000	176	0.49	---	---	---	---	---	FAIR TEST AFTER 10 SEC

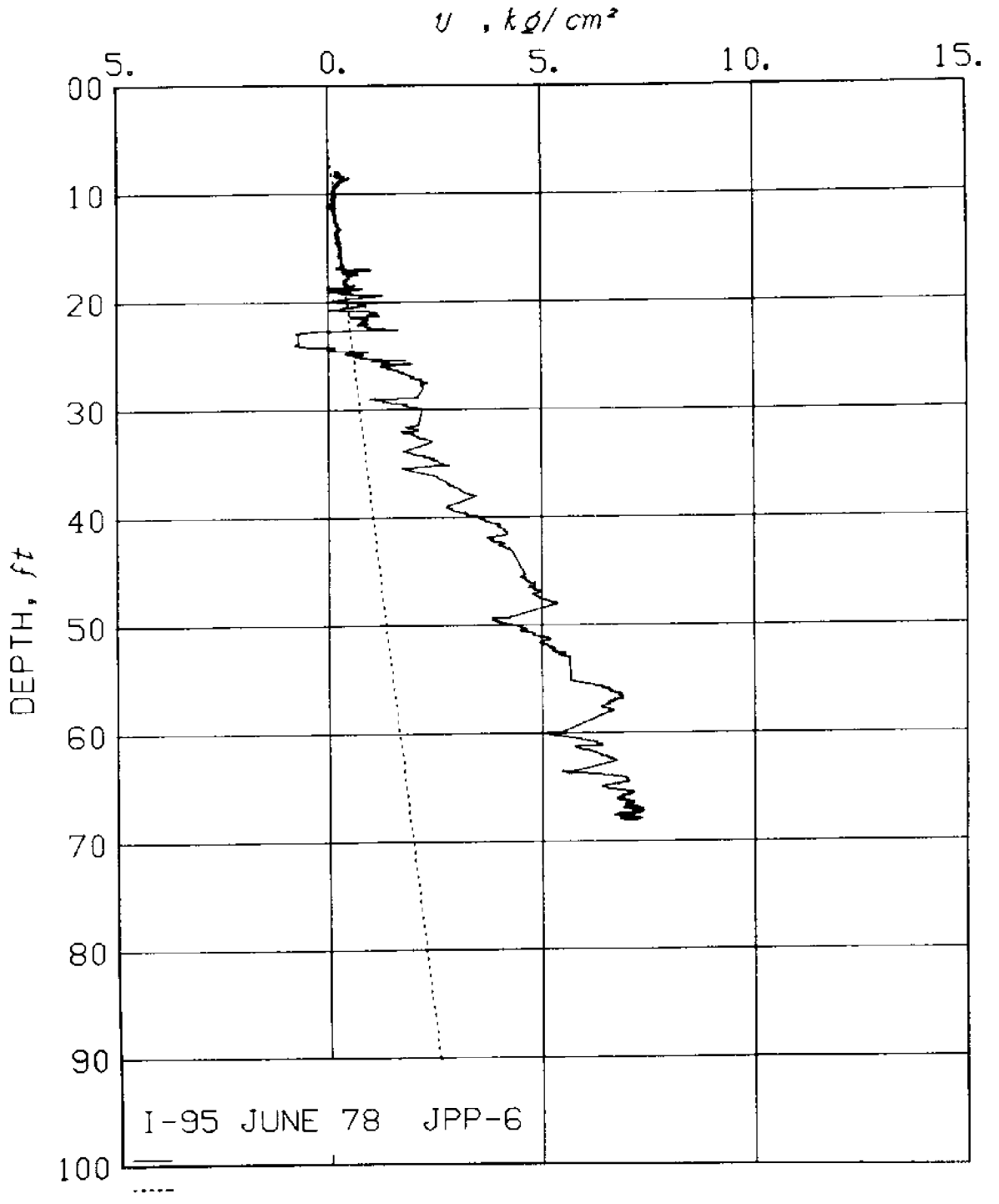
U , kg/cm²
5.
0.
5.
10.
15.
00
10
20
30
40
50
60
70
80
90
100
DEPTH, ft
I-95 JUNE 78 JPP-6

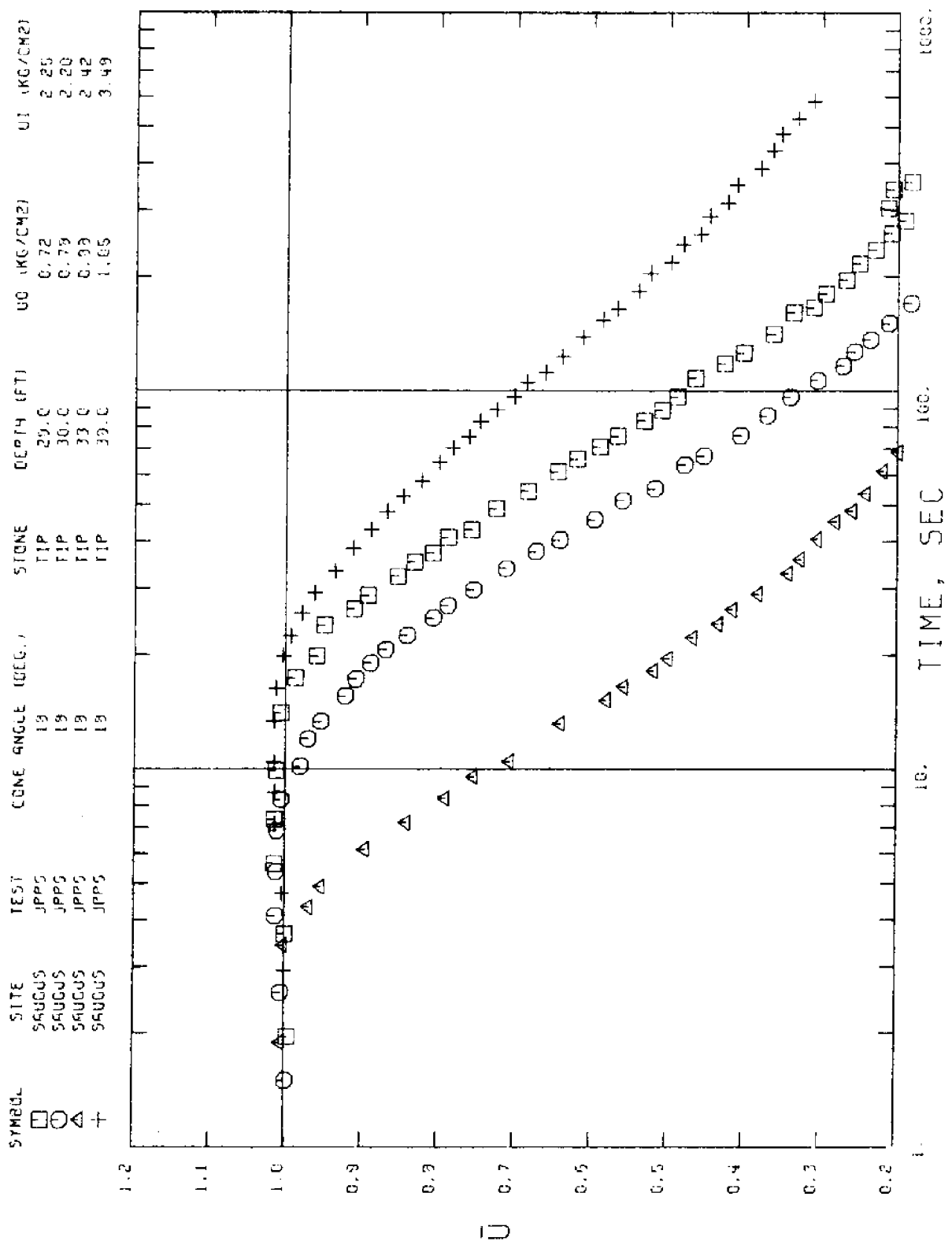
SYMBOL SITE TEST CONE ANGLE (DEG.) STONE DEPTH (FT) U0 (KG/CM2) U1 (KG/CM2)
SAUGUS JPPS 19 FIP 25.0 0.72 2.25
SAUGUS JPPS 19 FIP 30.0 0.79 2.20
SAUGUS JPPS 19 FIP 33.0 0.99 2.42
SAUGUS JPPS 19 FIP 39.0 1.05 3.49
U
TIME, SEC
1.2
1.1
1.0
0.9
0.8
0.7
0.6
0.5
0.4
0.3
0.2
10.
100.
1000.

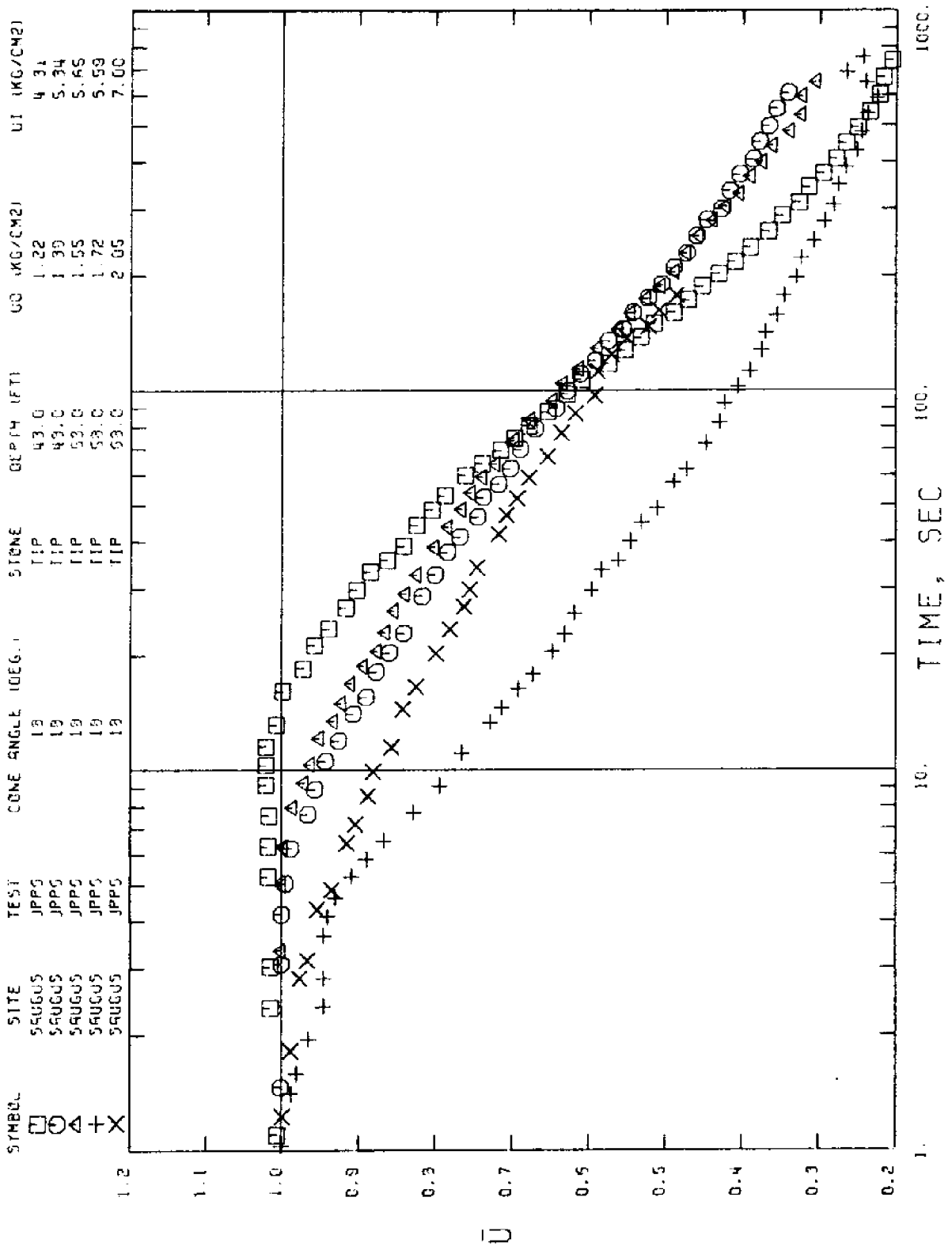
SYMBOL SITE TEST CONE ANGLE (DEG.) STONE DEPTH (FT) GO (KG/CM2) UI (KG/CM2)
SAUGUS JPPS 19 TIP 43.0 1.22 4.31
SAUGUS JPPS 19 TIP 49.0 1.39 5.34
SAUGUS JPPS 19 TIP 52.0 1.55 5.65
SAUGUS JPPS 19 TIP 58.0 1.72 5.59
SAUGUS JPPS 19 TIP 63.0 2.05 7.00
U
TIME, SEC
1.2
1.1
1.0
0.9
0.8
0.7
0.6
0.5
0.4
0.3
0.2
1.
10.
100.
1000.

SITE: SAUGUS DATE: 6/16/78

TEST # UPP-7 CONE ANGLE: 18 DEG. STONE LOCATION: TIP

DEPTH (FT)	U0 (KSC)	UI (KSC)	UMAX (KSC)	TF (SEC)	USARF	COEF. OF CONS. (CM2/SEC) CH20	CH40	CH50	CH60	CH80	COMMENTS
20.0	0.450	0.824	0.824	138	0.0	---	---	---	---	---	FAIR TEST - VERY STEEP CURVE
25.0	0.617	2.415	2.736	364	0.07	---	---	---	---	---	BAD TEST - U INCREASES FOR 8 SEC
30.0	0.783	2.861	2.900	417	0.10	---	---	---	---	---	BAD TEST - U INCREASES FOR 2 SEC
35.0	0.950	3.471	3.471	726	0.16	---	---	---	---	---	FAIR TEST - STEEP CURVE
40.0	1.117	3.988	3.988	620	0.07	0.174	0.290	0.340	0.392	0.576	VERY GOOD TEST
41.0	1.150	4.215	4.215	165	0.19	0.211	0.271	0.333	0.387	0.676	VERY GOOD TEST
42.0	1.183	4.025	4.025	502	0.13	0.154	0.324	0.363	0.366	0.437	VERY GOOD TEST
43.0	1.217	3.931	3.931	727	0.36	0.016	0.028	0.034	0.039	---	VERY GOOD TEST
44.0	1.250	4.255	4.255	560	0.35	0.024	0.042	0.061	0.054	---	VERY GOOD TEST
45.0	1.283	4.378	4.378	680	0.34	0.028	0.042	0.048	0.052	---	VERY GOOD TEST
50.0	1.450	5.109	5.109	475	0.33	0.036	0.049	0.063	0.070	---	VERY GOOD TEST
55.0	1.617	5.998	6.036	515	0.48	0.015	0.023	0.025	---	---	VERY GOOD TEST
60.0	1.783	6.588	6.761	499	0.43	---	---	---	---	---	BAD TEST - U INCREASES FOR 3 SEC
65.0	1.950	7.245	7.245	157	0.45	0.048	0.078	0.095	---	---	VERY GOOD TEST
66.0	1.983	7.157	7.157	478	0.49	0.019	0.025	0.024	---	---	GOOD TEST
67.0	2.017	7.265	7.333	565	0.50	0.010	0.015	---	---	---	FAIR TEST - U INCREASES FOR 2 SEC
68.0	2.050	7.614	7.614	614	0.44	0.015	0.023	0.027	---	---	GOOD TEST

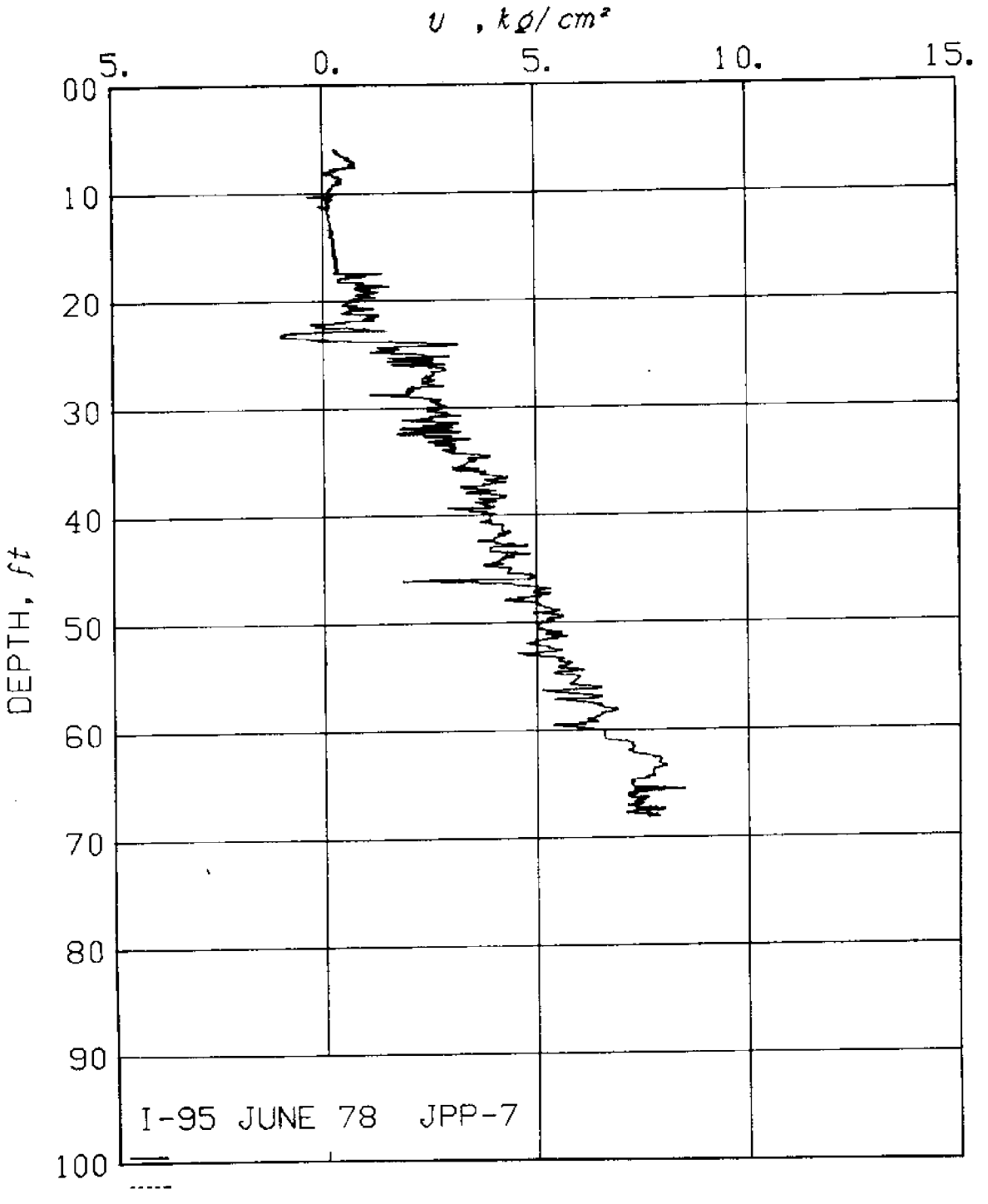
u , kg/cm²
5.
0.
5.
10.
15.
00
10
20
30
40
50
60
70
80
90
100
DEPTH, ft
I-95 JUNE 78 JPP-7

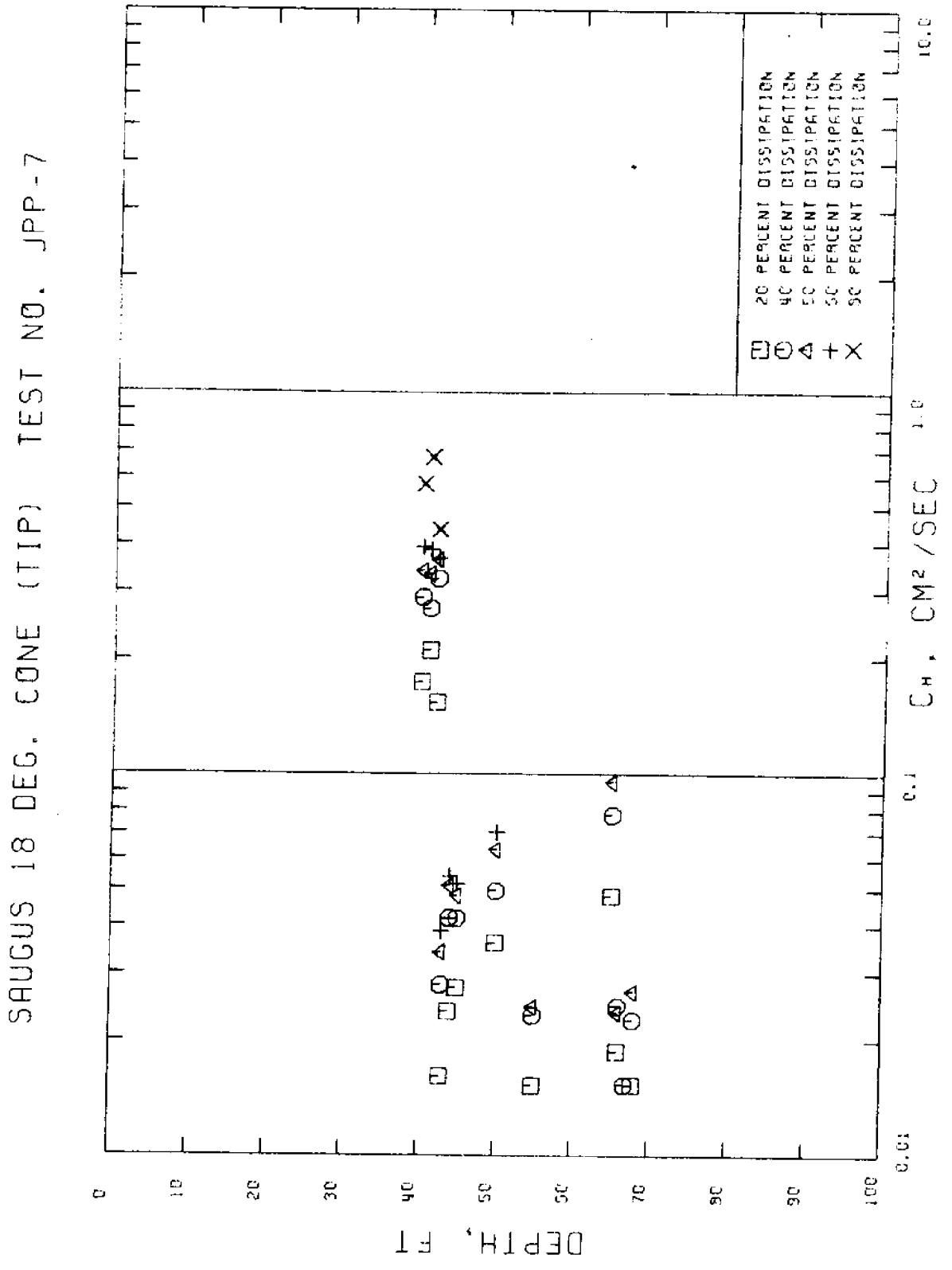
SAUGUS 18 DEG. CONE (TIP) TEST NO. JPP-7
DEPTH, FT
0
10
20
30
40
50
60
70
80
90
100
0.01
0.1
1.0
10.0
C_H, CM^2/SEC
20 PERCENT DISSIPATION
40 PERCENT DISSIPATION
50 PERCENT DISSIPATION
60 PERCENT DISSIPATION
80 PERCENT DISSIPATION

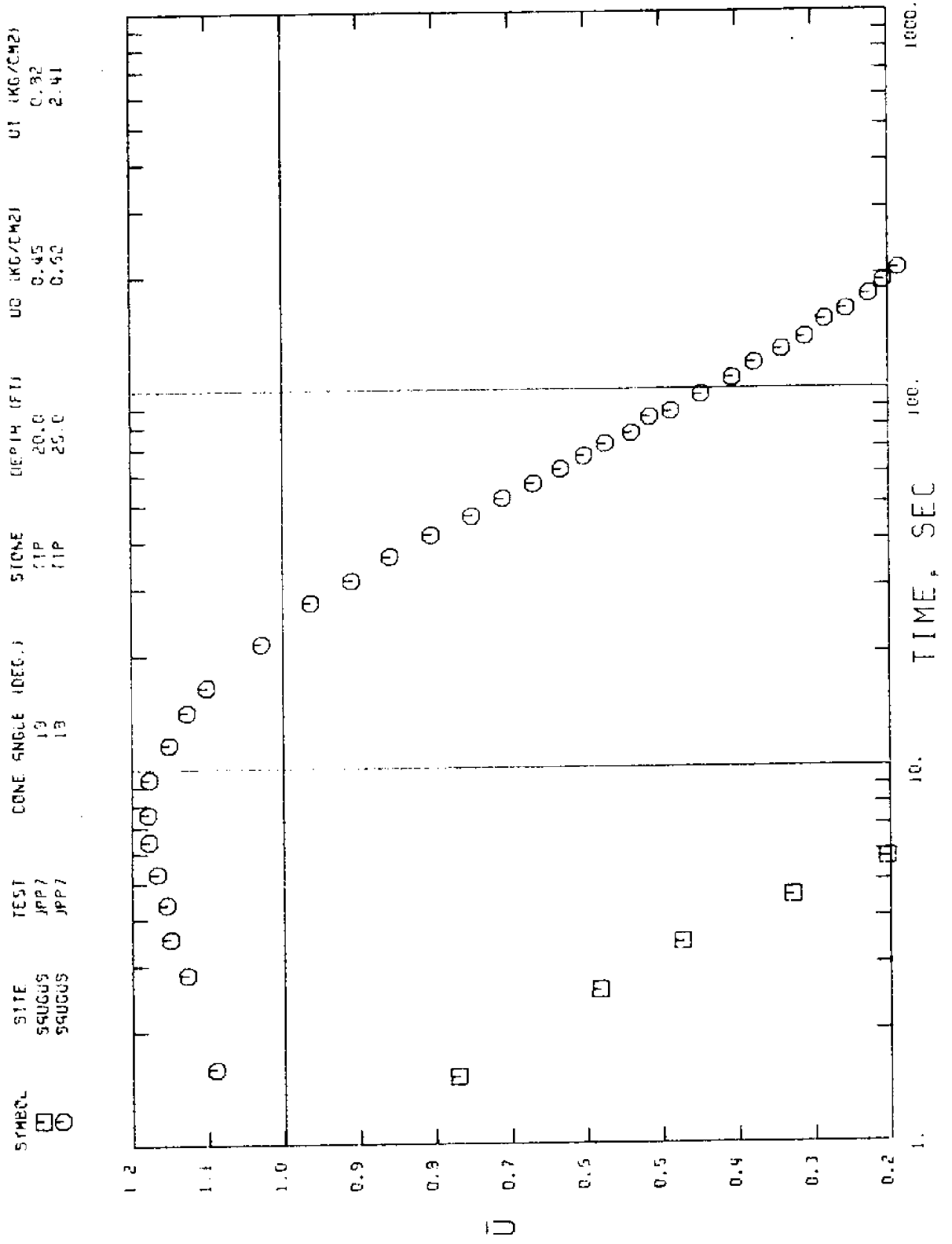
SYMBOL
SITE
TEST
CONE ANGLE (DEG.)
SLEEVE
DEPTH (FT)
U0 (KG/CM2)
U1 (KG/CM2)
SQUGGS JPP7 19 TIP 20.0 0.45 0.32
SQUGGS JPP7 13 TIP 25.0 0.52 2.41
U
TIME, SEC
1.
10.
100.
1000.
0.2
0.3
0.4
0.5
0.6
0.7
0.8
0.9
1.0
1.1
1.2

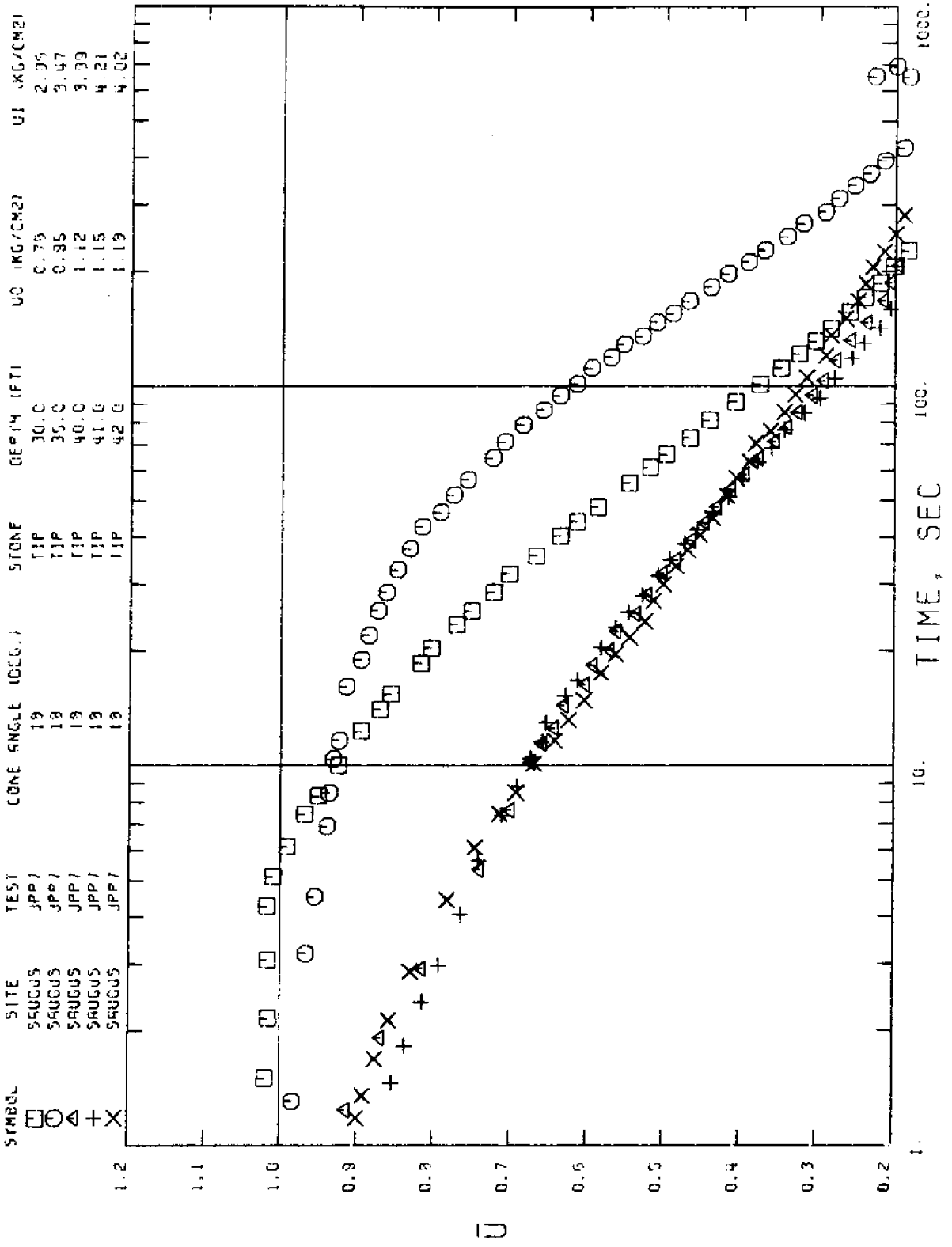
SYMBOL SITE TEST CONE ANGLE (DEG.) STONE DEPTH (FT) U0 (KG/CM2) U1 (KG/CM2)
SAUGUS JPP1 19 TIP 30.0 0.79 2.35
SAUGUS JPP1 19 TIP 35.0 0.95 3.47
SAUGUS JPP1 19 TIP 40.0 1.12 3.39
SAUGUS JPP1 19 TIP 41.0 1.15 4.21
SAUGUS JPP1 19 TIP 42.0 1.19 4.02
U
TIME, SEC

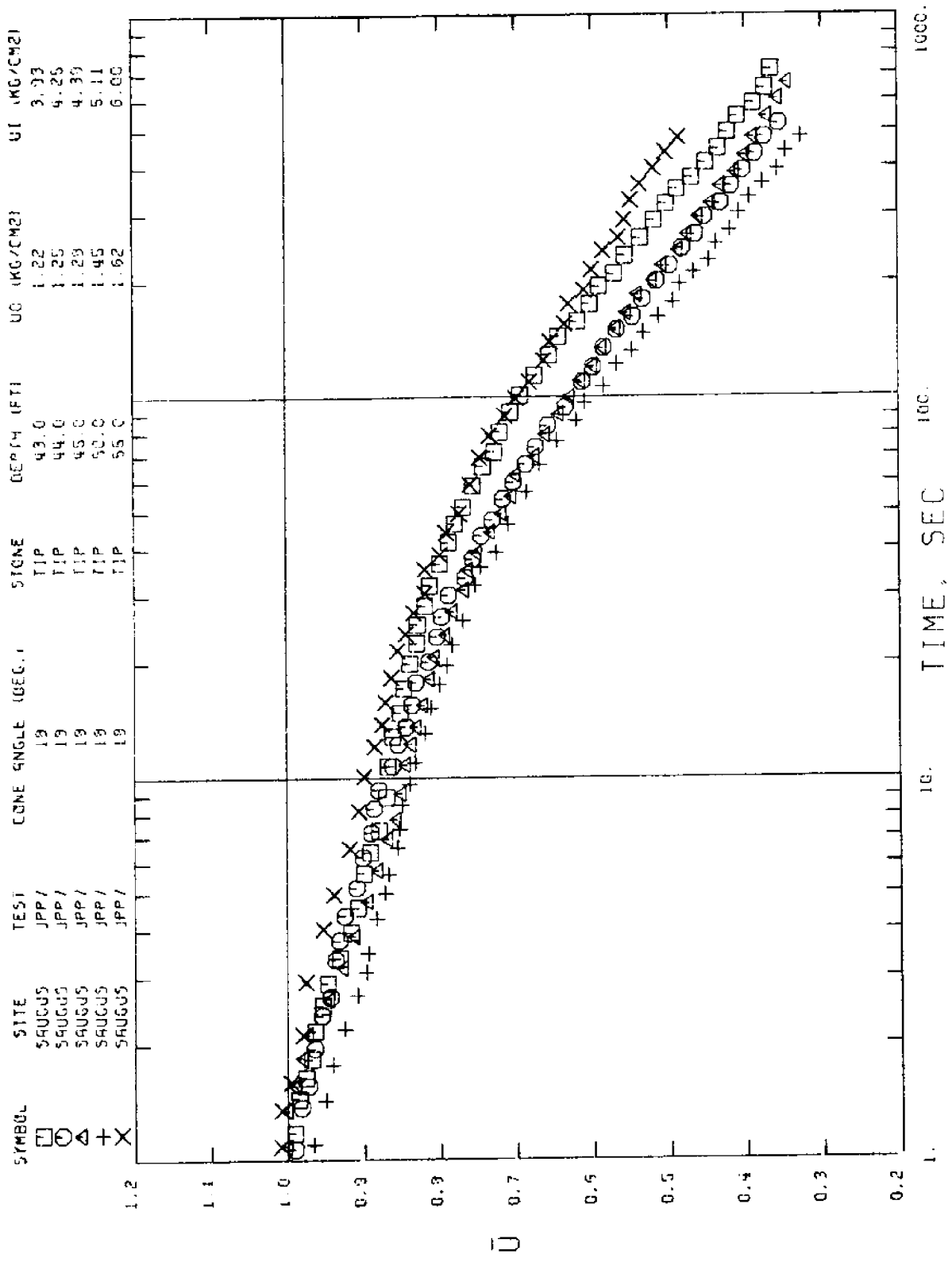
SYMBOL SITE TEST CONE ANGLE (DEG.) SIGNE DEPTH (FT) UO (KG/CM2) UI (KG/CM2)
SAUGUS JPP/ 19 TIP 43.0 1.22 3.03
SAUGUS JPP/ 19 TIP 44.0 1.25 4.25
SAUGUS JPP/ 19 TIP 45.0 1.29 4.39
SAUGUS JPP/ 19 TIP 50.0 1.45 5.11
SAUGUS JPP/ 19 TIP 55.0 1.62 6.00
U
TIME, SEC
1.2
1.1
1.0
0.9
0.8
0.7
0.6
0.5
0.4
0.3
0.2
1.
10.
100.
1000.

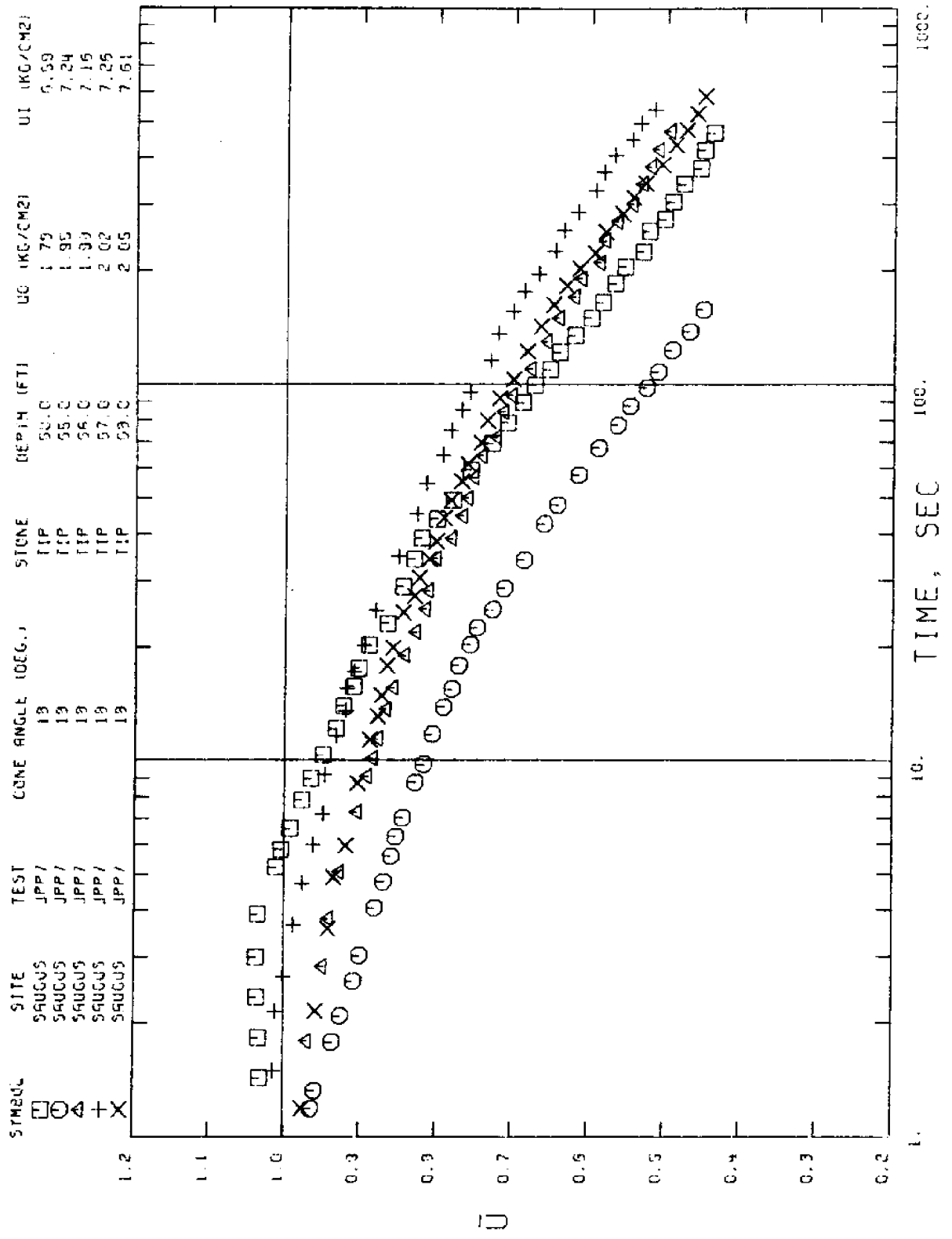
SYMBOL SITE TEST CONE ANGLE (DEG.) STONE DEPTH (FT) UO (KG/CM2) UI (KG/CM2)
SAUGUS JPP/ 13 TIP 54.0 1.75 6.59
SAUGUS JPP/ 13 TIP 55.0 1.95 7.24
SAUGUS JPP/ 13 TIP 56.0 1.90 7.15
SAUGUS JPP/ 13 TIP 57.0 2.02 7.25
SAUGUS JPP/ 13 TIP 58.0 2.05 7.61
U
TIME, SEC

APPENDIX B

DISSIPATION DATA IN CONNECTICUT VALLEY VARVED CLAY: AMHERST, MASSACHUSETTS

This appendix presents detailed information on the piezometer probe field records conducted on the campus of the University of Massachusetts in Amherst, Mass. in 1977. Information for each test consists of:

a) A summary table giving pertinent information for each depth: The estimated static (in situ) pore pressure u_o(kg/cm^2), the initial pore pressure u_i(kg/cm^2), the maximum pore pressure measured during dissipation u_{max}(kg/cm^2), the (maximum) duration of the dissipation test TF(sec), the (minimum) normalized excess pore pressure $\bar{u}$ at the end of the dissipation test, and, finally, the estimated coefficient of consolidation c_h(probe) at 20%, 40%, 50%, 60%, and 80% dissipation

b) A profile of penetration pore pressures

c) A profile of c_h predicted at different dissipation levels (20, 40, 50, 60, and 80%)

d) Normalized dissipation curves [$\bar{u} = \Delta u/\Delta u_i$ vs. log(time)] at each testing depth

SITE: AMHERST DATE: 2/17/77

TEST # 5 CONE ANGLE: 18 DEG. STONE LOCATION: TIP

DEPTH (FT)	U0 (KSC)	UI (KSC)	UMAX (KSC)	TF (SEC)	UBARF	COEF. OF CONS. (CM2/SEC) CH20	CH40	CH50	CH60	CH80	COMMENTS
4.3	0.233	1.019	1.019	27	0.07	0.814	2.800	4.068	5.381	8.594	FAIR TEST - STEEP CURVE
7.5	0.326	-0.594	-0.469	28	---	---	---	---	---	---	BAD TEST - U STARTS BELOW STATIC
10.8	0.419	1.778	2.233	27	0.86	---	---	---	---	---	BAD TEST - U INCREASES FOR 8 SEC
14.1	0.513	3.305	3.305	24	0.51	0.109	0.309	---	---	---	FAIR TEST - STEEP CURVE
17.4	0.606	3.095	3.095	43	0.52	---	---	---	---	---	BAD TEST - WIGGLING
20.6	0.700	3.664	3.664	38	0.59	0.095	0.138	---	---	---	GOOD TEST AFTER 3 SEC
23.9	0.793	3.766	3.766	32	0.62	0.081	---	---	---	---	GOOD TEST AFTER 4 SEC
27.2	0.887	3.754	3.754	26	0.67	0.065	---	---	---	---	GOOD TEST
30.5	0.981	4.107	4.107	44	0.62	0.073	---	---	---	---	GOOD TEST
33.8	1.073	4.259	4.259	30	0.69	0.051	---	---	---	---	VERY GOOD TEST
37.1	1.167	4.344	4.344	6030	0.03	0.078	0.116	0.123	0.120	0.132	VERY GOOD TEST
40.3	1.260	4.316	4.363	57	0.61	0.051	---	---	---	---	GOOD TEST AFTER 4 SEC
43.6	1.353	4.376	4.376	25	0.68	0.076	---	---	---	---	VERY GOOD TEST
46.9	1.447	4.390	4.390	24	0.72	0.080	---	---	---	---	VERY GOOD TEST
50.2	1.540	4.743	4.743	38	0.56	0.107	0.170	---	---	---	VERY GOOD TEST
53.5	1.633	4.541	4.541	23	0.74	0.038	---	---	---	---	FAIR TEST - WIGGLING
56.7	1.727	5.609	5.609	37	0.65	0.061	---	---	---	---	FAIR TEST - WIGGLING
60.0	1.820	5.771	5.771	27	0.64	0.087	---	---	---	---	GOOD TEST
63.3	1.913	3.470	4.403	28	---	---	---	---	---	---	BAD TEST - U INCREASES FOR 8 SEC
66.6	2.007	4.252	4.252	30	0.23	0.341	1.232	1.586	1.811	---	FAIR TEST - STEEP CURVE
69.9	2.100	3.686	3.686	36	0.0	---	---	---	---	---	BAD TEST - DISSIPATION TOO FAST
73.1	2.194	4.829	4.829	32	0.01	---	---	---	---	---	BAD TEST - DISSIPATION TOO FAST
76.4	2.287	4.756	4.756	38	0.05	---	---	---	---	---	BAD TEST - DISSIPATION TOO FAST
79.7	2.380	4.221	4.221	92	0.0	---	---	---	---	---	BAD TEST - DISSIPATION TOO FAST

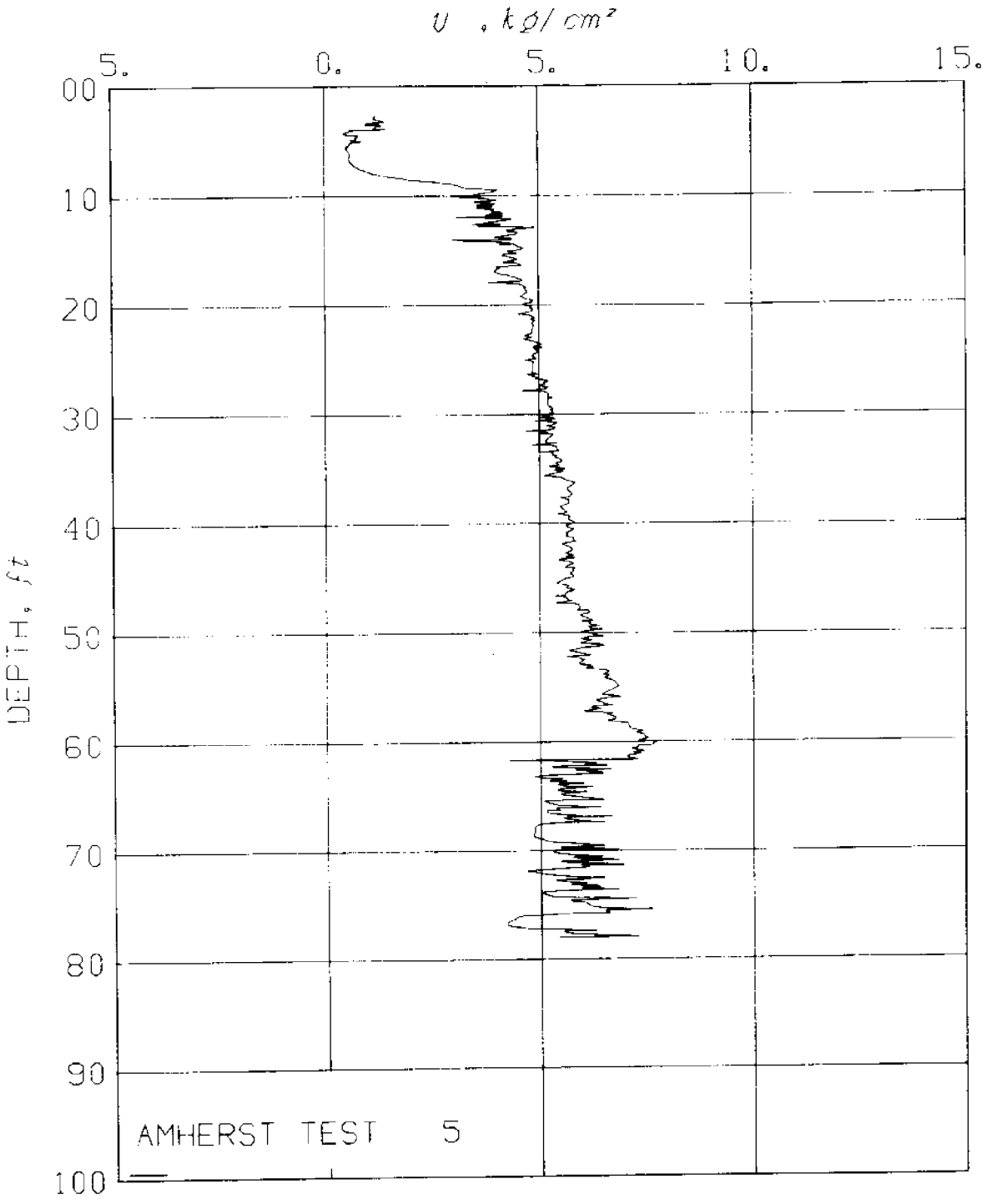
U , kg/cm²
5.
0.
5.
10.
15.
00
10
20
30
40
50
60
70
80
90
100
DEPTH, ft
AMHERST TEST 5

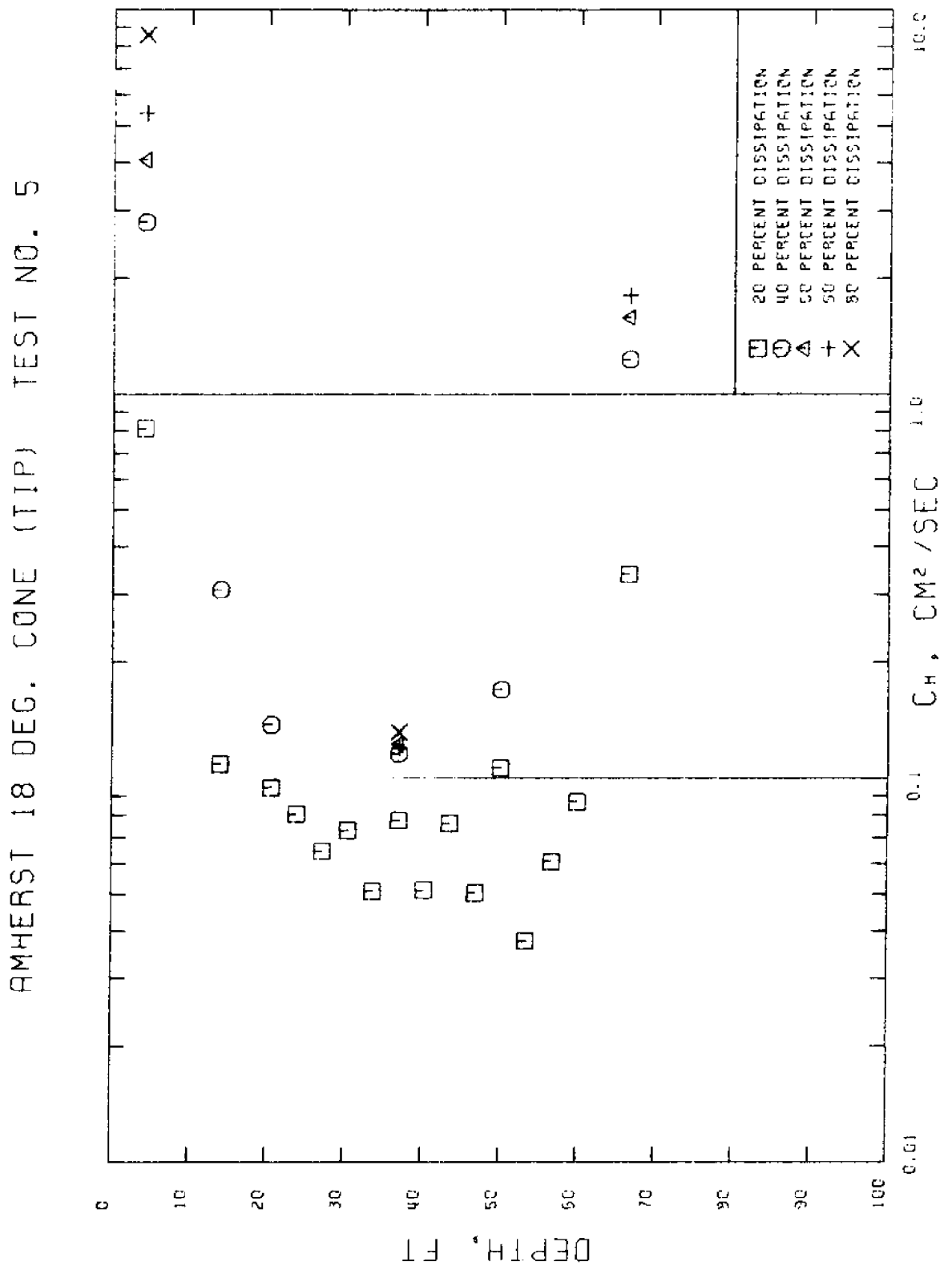
AMHERST 18 DEG. CONE (TIP) TEST NO. 5
20 PERCENT DISSIPATION
40 PERCENT DISSIPATION
50 PERCENT DISSIPATION
60 PERCENT DISSIPATION
80 PERCENT DISSIPATION
DEPTH, FT
0
10
20
30
40
50
60
70
80
90
100
0.01
0.1
1.0
10.0
C_H, CM^2/SEC

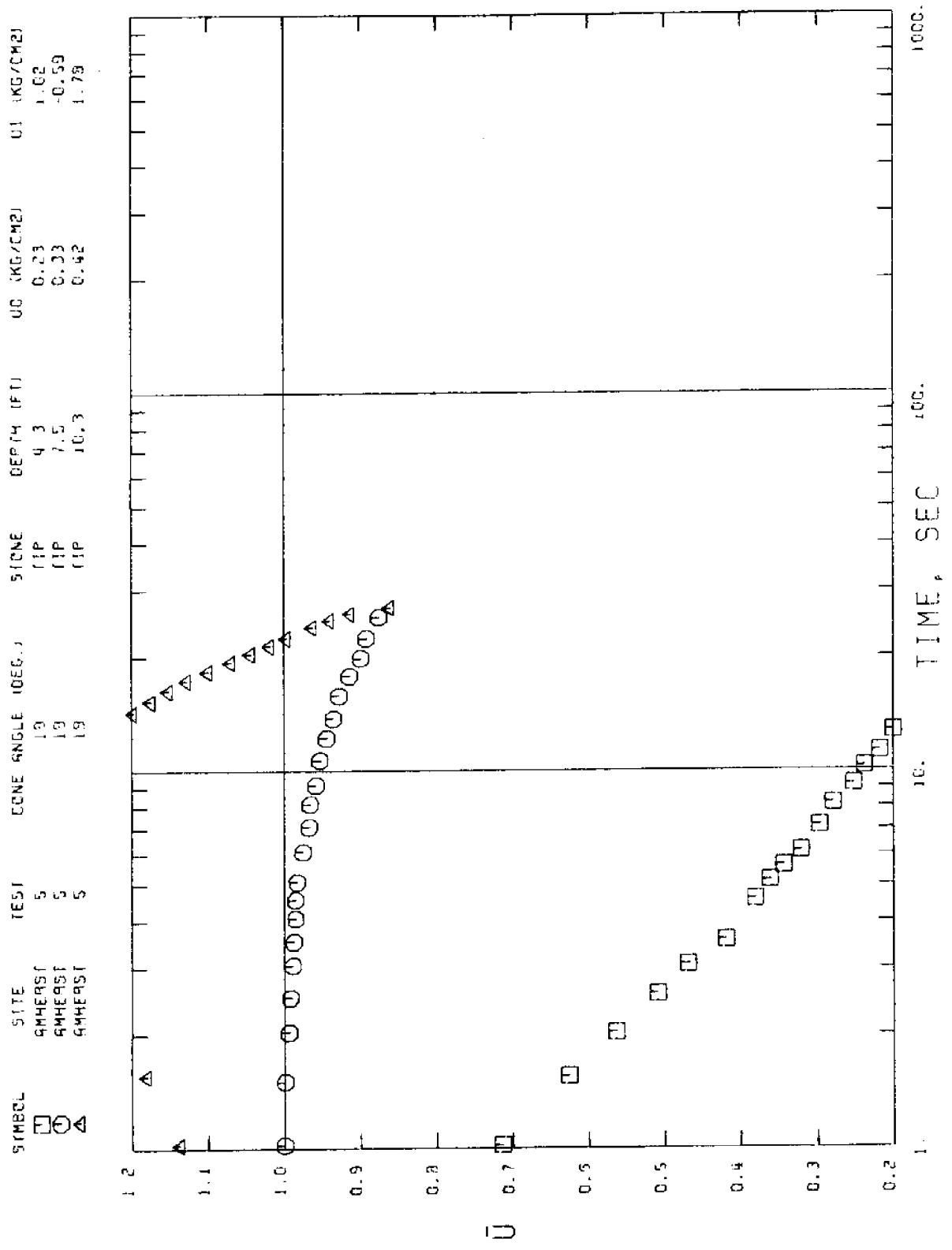
SYMBOL SITE TEST CONE ANGLE (DEG.) SCENE DEPTH (FT) U0 (KG/CM2) U1 (KG/CM2)
GAMBRELL 5 19 TIP 4.3 0.23 1.02
GAMBRELL 5 19 TIP 7.5 0.33 -0.59
GAMBRELL 5 19 TIP 10.3 0.42 1.79
U
TIME, SEC
1.2
1.1
1.0
0.9
0.8
0.7
0.6
0.5
0.4
0.3
0.2
10.
100.
1000.

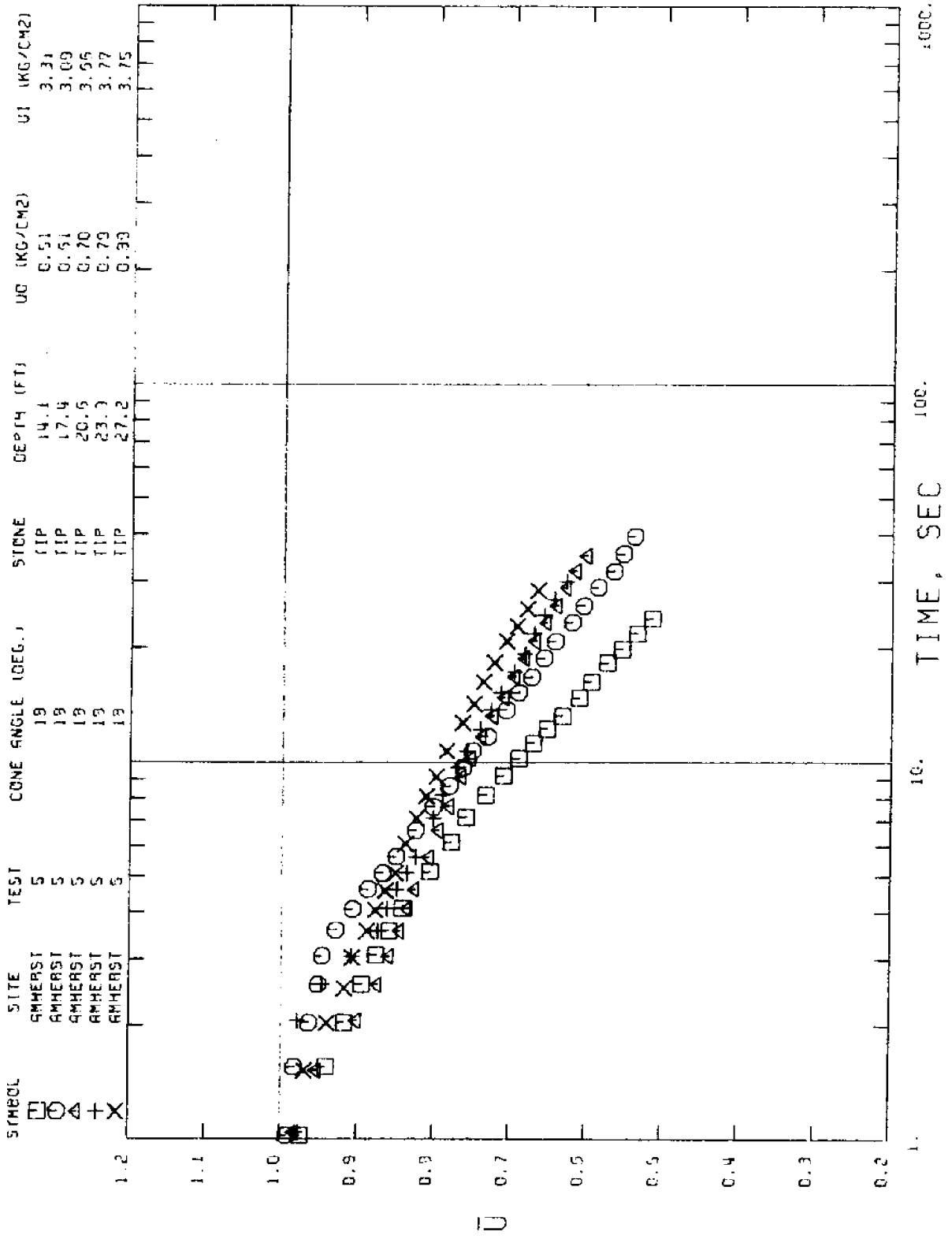
SYMBOL SITE TEST CONE ANGLE (DEG.) STONE DEPTH (FT) U0 (KG/CM2) U1 (KG/CM2)
AMHERST 5 19 TIP 14.1 0.51 3.31
AMHERST 5 19 TIP 17.4 0.51 3.09
AMHERST 5 19 TIP 20.5 0.70 3.55
AMHERST 5 19 TIP 23.3 0.79 3.72
AMHERST 5 19 TIP 27.2 0.93 3.75
U
TIME, SEC
1.2
1.1
1.0
0.9
0.8
0.7
0.6
0.5
0.4
0.3
0.2
1.
10.
100.
1000.

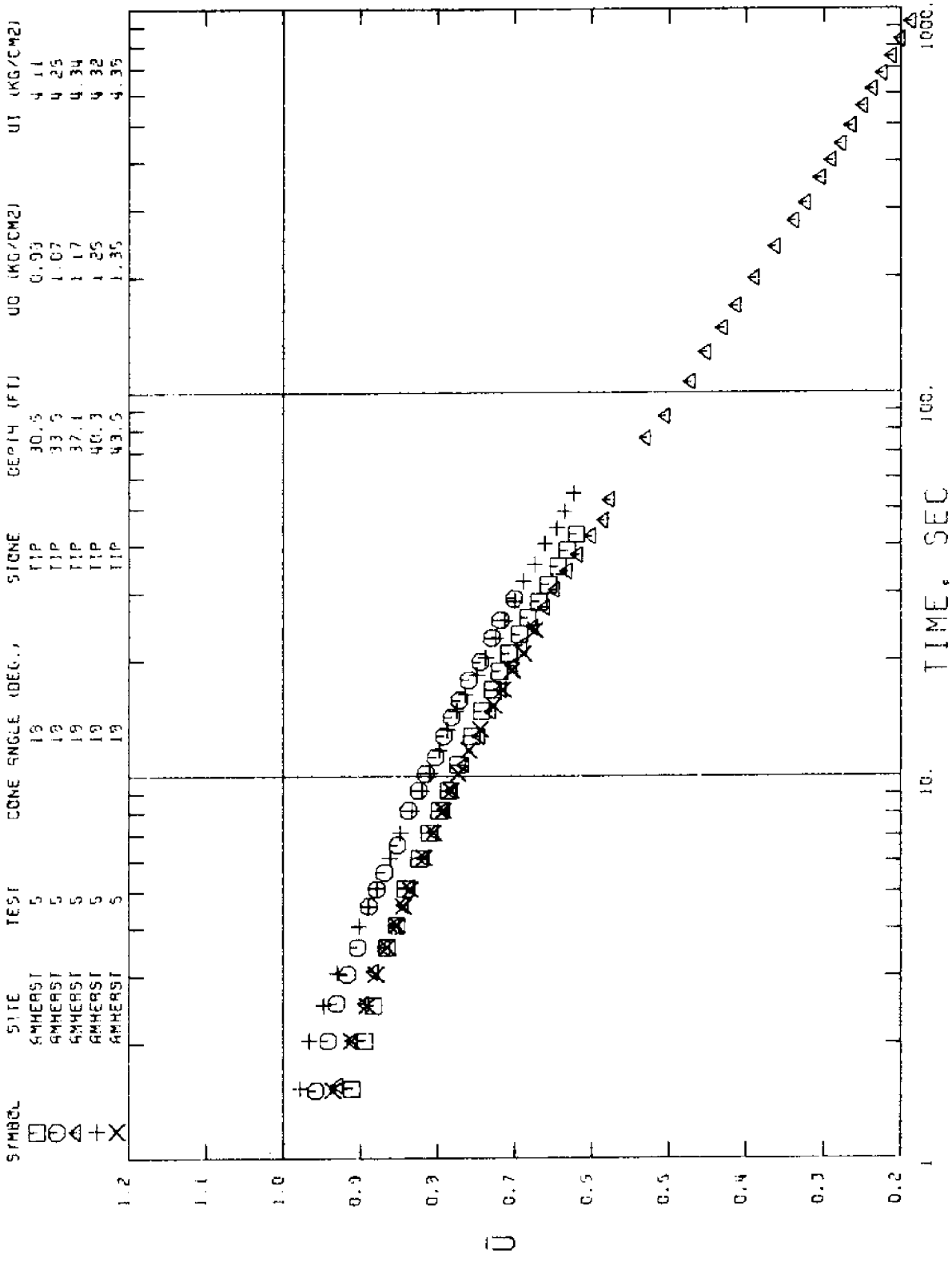
SYMBOL
SITE
TEST
CONE ANGLE (DEG.)
SIGNE
DEPTH (FT)
UO (KG/CM2)
UI (KG/CM2)
AMHERST 5 19 TIP 30.5 0.93 4.11
AMHERST 5 19 TIP 33.5 1.07 4.25
AMHERST 5 19 TIP 37.1 1.17 4.34
AMHERST 5 19 TIP 40.3 1.25 4.32
AMHERST 5 19 TIP 43.5 1.35 4.35
1.2
1.1
1.0
0.9
0.8
0.7
0.6
0.5
0.4
0.3
0.2
Ū
1
10.
100.
1000.
TIME, SEC

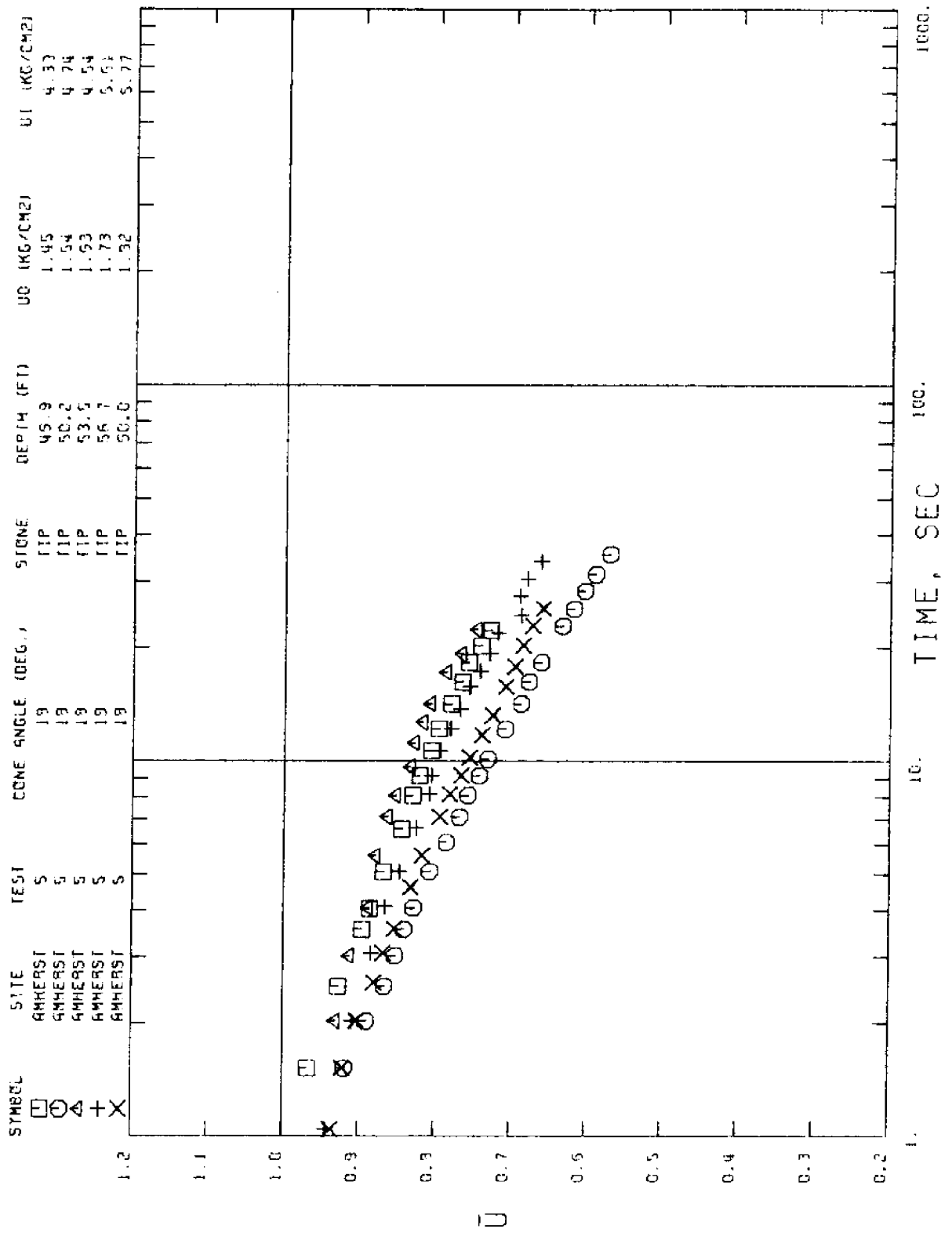
SYMBOL SITE TEST CONE ANGLE (DEG.) SIONE DEPTH (FT) UD (KG/CM2) UI (KG/CM2)
AMHERST S 19 FIP 45.9 1.45 4.33
AMHERST S 19 FIP 50.2 1.54 4.74
AMHERST S 19 FIP 53.5 1.63 4.54
AMHERST S 19 FIP 56.7 1.73 5.51
AMHERST S 19 FIP 50.0 1.82 5.77
U
TIME, SEC
1.2
1.1
1.0
0.9
0.8
0.7
0.6
0.5
0.4
0.3
0.2
1.
10.
100.
1000.

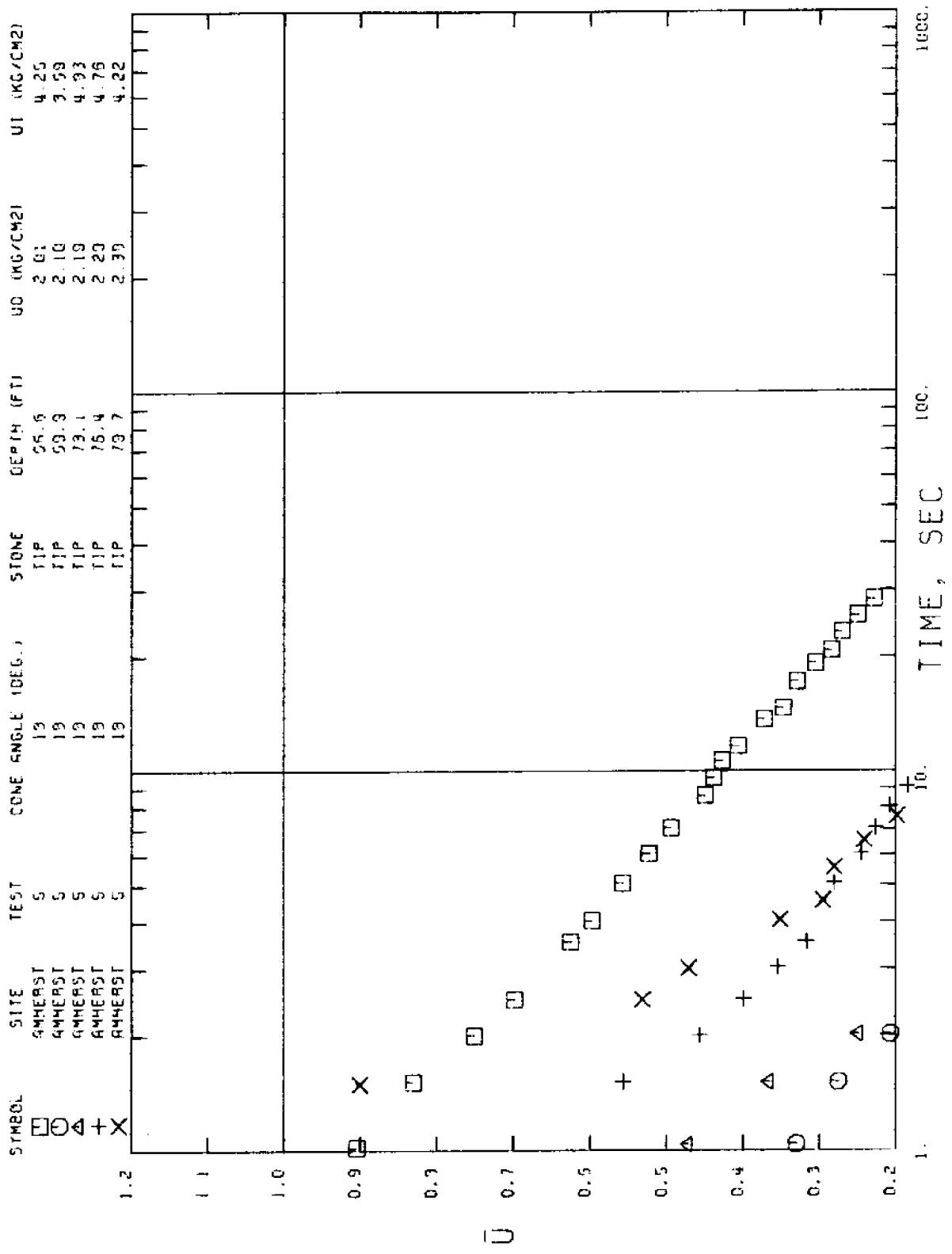
SYMBOL SITE TEST CONE ANGLE (DEG.) STONE DEPTH (FT) UO (KG/CM2) UI (KG/CM2)
AMHERST 5 13 FIP 56.6 2.01 4.25
AMHERST 5 13 FIP 59.3 2.10 3.59
AMHERST 5 13 FIP 73.1 2.19 4.93
AMHERST 5 13 FIP 75.4 2.23 4.76
AMHERST 5 13 FIP 79.7 2.35 4.22
U
TIME, SEC
1.
10.
100.
1000.
1.2
1.1
1.0
0.9
0.8
0.7
0.6
0.5
0.4
0.3
0.2

SITE: AMHERST DATE: 2/17/77

TEST # 6 CONE ANGLE: 60 DEG. STONE LOCATION: TIP

DEPTH (FT)	UO (KSC)	UI (KSC)	UMAX (KSC)	TF (SEC)	UBARF	COEF. OF CONS. (CM2/SEC) CH20	CH40	CH50	CH60	CH80	COMMENTS
10.6	0.415	6.520	6.520	33	0.54	0.233	0.375	---	---	---	FAIR TEST - STEEP CURVE
13.9	0.508	6.258	6.258	27	0.51	0.475	0.426	---	---	---	FAIR TEST
17.2	0.602	4.844	4.844	24	0.63	---	---	---	---	---	BAD TEST
20.5	0.695	4.632	4.632	57	0.57	0.416	0.172	---	---	---	FAIR TEST - SLIGHTLY WIGGLING
23.8	0.788	4.663	4.663	21	0.70	0.301	---	---	---	---	GOOD TEST
27.1	0.882	4.628	4.628	24	0.70	0.207	---	---	---	---	GOOD TEST
30.3	0.975	5.039	5.039	27	0.70	0.277	---	---	---	---	FAIR TEST AFTER 5 SEC
33.6	1.068	5.141	5.141	27	0.67	0.241	---	---	---	---	FAIR TEST - SLIGHTLY WIGGLING
36.9	1.162	5.345	5.345	1707	0.13	0.173	0.098	0.092	0.083	0.092	GOOD TEST AFTER 9 SEC
40.2	1.255	5.224	5.224	25	0.69	0.190	---	---	---	---	GOOD TEST
43.4	1.348	5.262	5.262	25	0.72	0.130	---	---	---	---	GOOD TEST
46.7	1.442	4.945	4.945	19	0.75	0.145	---	---	---	---	GOOD TEST
50.0	1.535	5.779	5.779	28	0.72	0.158	---	---	---	---	GOOD TEST
53.3	1.628	5.838	5.838	21	0.70	0.216	---	---	---	---	GOOD TEST
56.6	1.722	6.318	6.318	27	0.72	0.128	---	---	---	---	FAIR TEST - SLIGHTLY WIGGLING
59.9	1.815	6.828	6.828	26	0.71	0.166	---	---	---	---	GOOD TEST
63.1	1.909	6.309	6.309	42	0.32	0.479	0.687	0.776	0.831	---	FAIR TEST - STEEP CURVE
66.4	2.002	5.345	5.345	21	0.28	0.577	1.144	1.556	1.900	---	FAIR TEST - STEEP CURVE
69.7	2.095	3.983	3.983	35	0.02	0.766	2.366	3.874	6.018	14.120	FAIR TEST - STEEP CURVE
73.0	2.189	5.794	5.794	30	0.08	0.754	1.421	2.099	2.739	6.092	FAIR TEST - STEEP CURVE
76.3	2.282	5.948	5.948	30	0.02	1.104	3.473	4.656	6.466	16.127	FAIR TEST - STEEP CURVE
79.5	2.376	5.064	5.064	148	0.01	0.292	0.815	1.243	1.728	3.976	FAIR TEST - STEEP CURVE

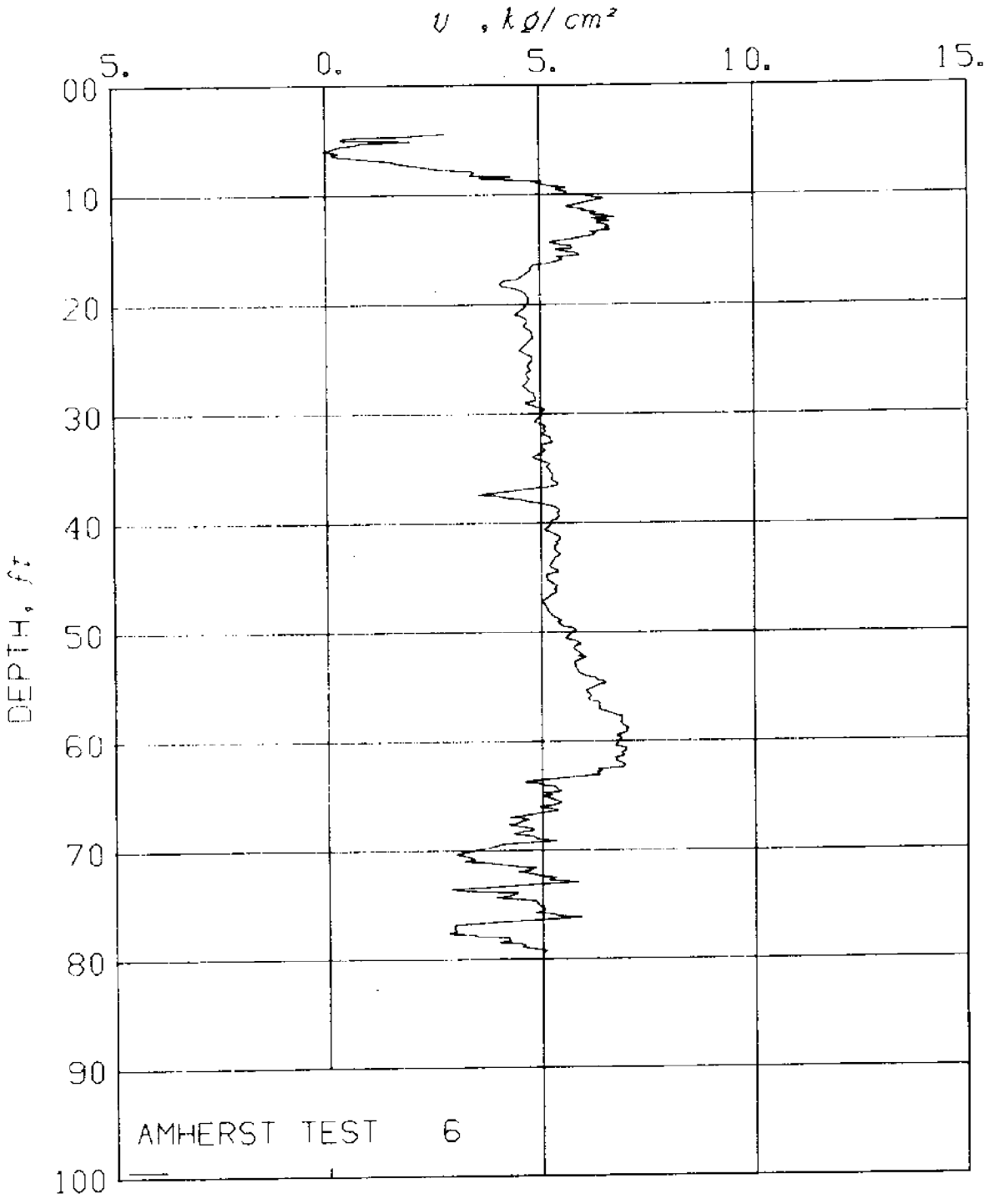
v , kg/cm²
5.
0.
5.
10.
15.
00
10
20
30
40
50
60
70
80
90
100
DEPTH, ft
AMHERST TEST 6

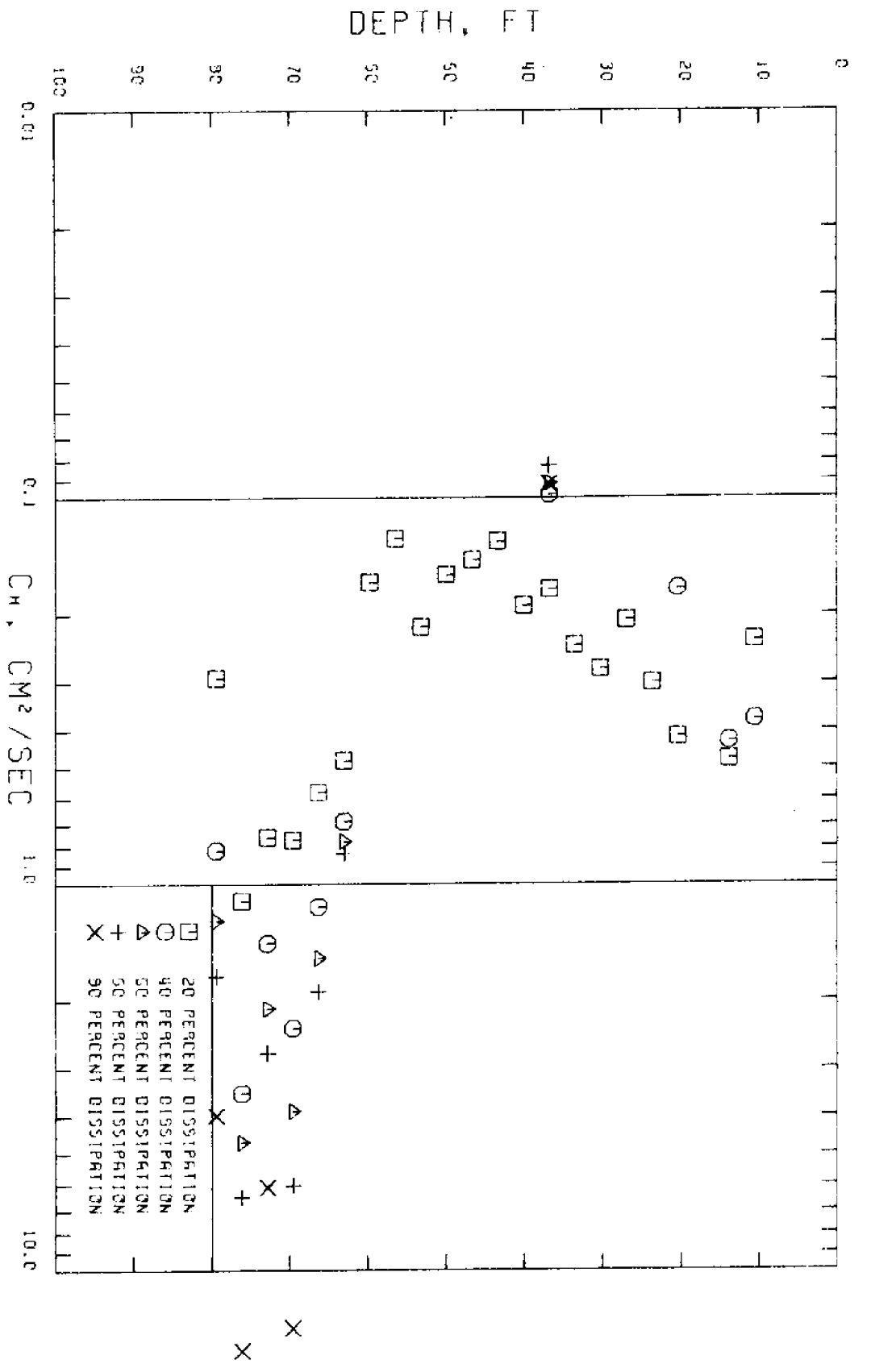
DEPTH, FT
0
10
20
30
40
50
60
70
80
90
100
0.01
0.1
1.0
10.0
C_H, CM²/SEC
20 PERCENT DISSIPATION
40 PERCENT DISSIPATION
50 PERCENT DISSIPATION
60 PERCENT DISSIPATION
AMHERST 60 DEG. CONE (TIP) TEST NO. 6

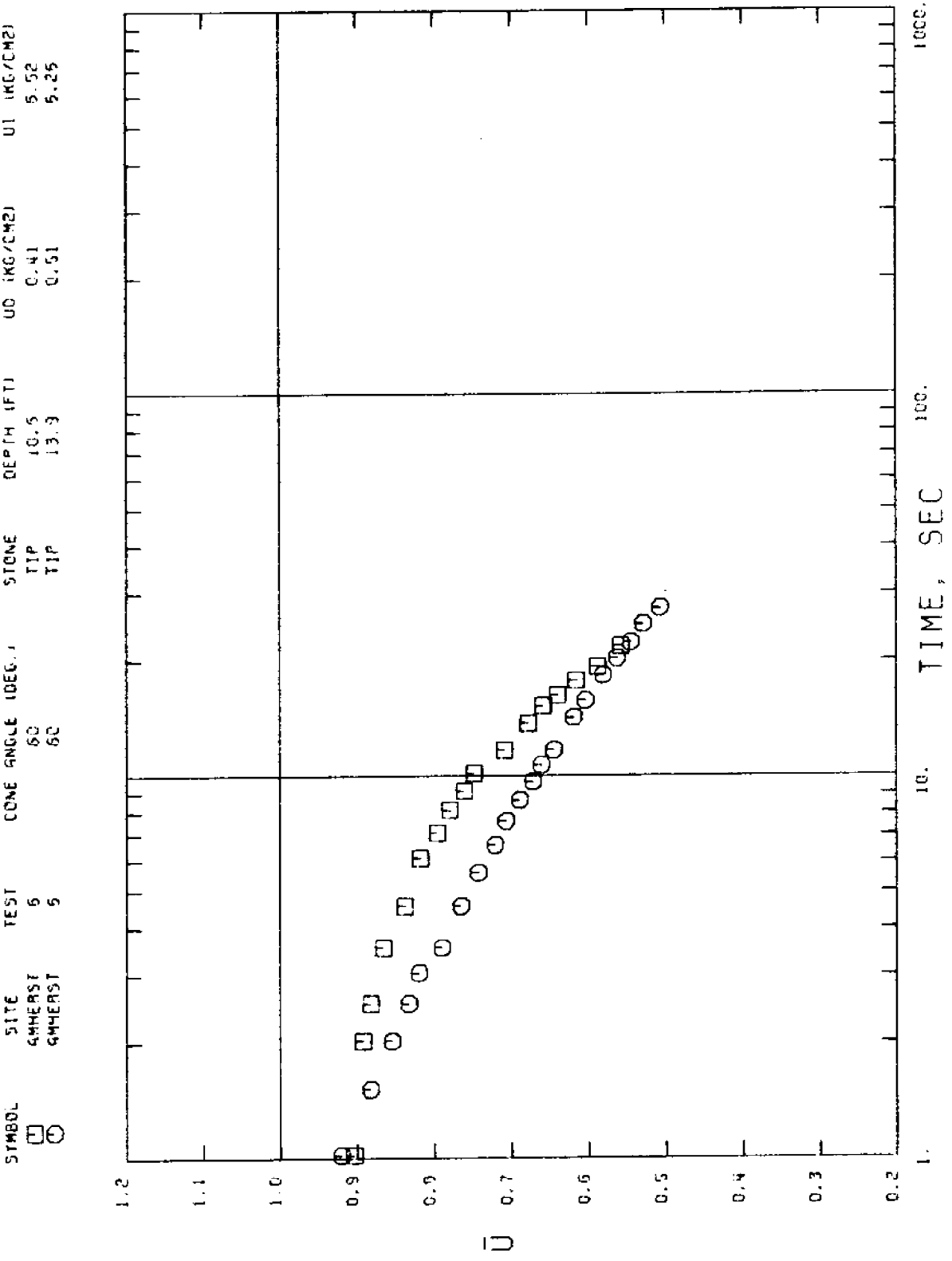
SYMBOL SITE TEST CONE ANGLE (DEG.) STONE DEPTH (FT) UO (KG/CM2) U1 (KG/CM2)
AMHERST 6 60 TIP 10.5 0.41 5.52
AMHERST 5 60 TIP 13.3 0.51 5.25
U
TIME, SEC
1.2
1.1
1.0
0.9
0.8
0.7
0.6
0.5
0.4
0.3
0.2
1.
10.
100.
1000.

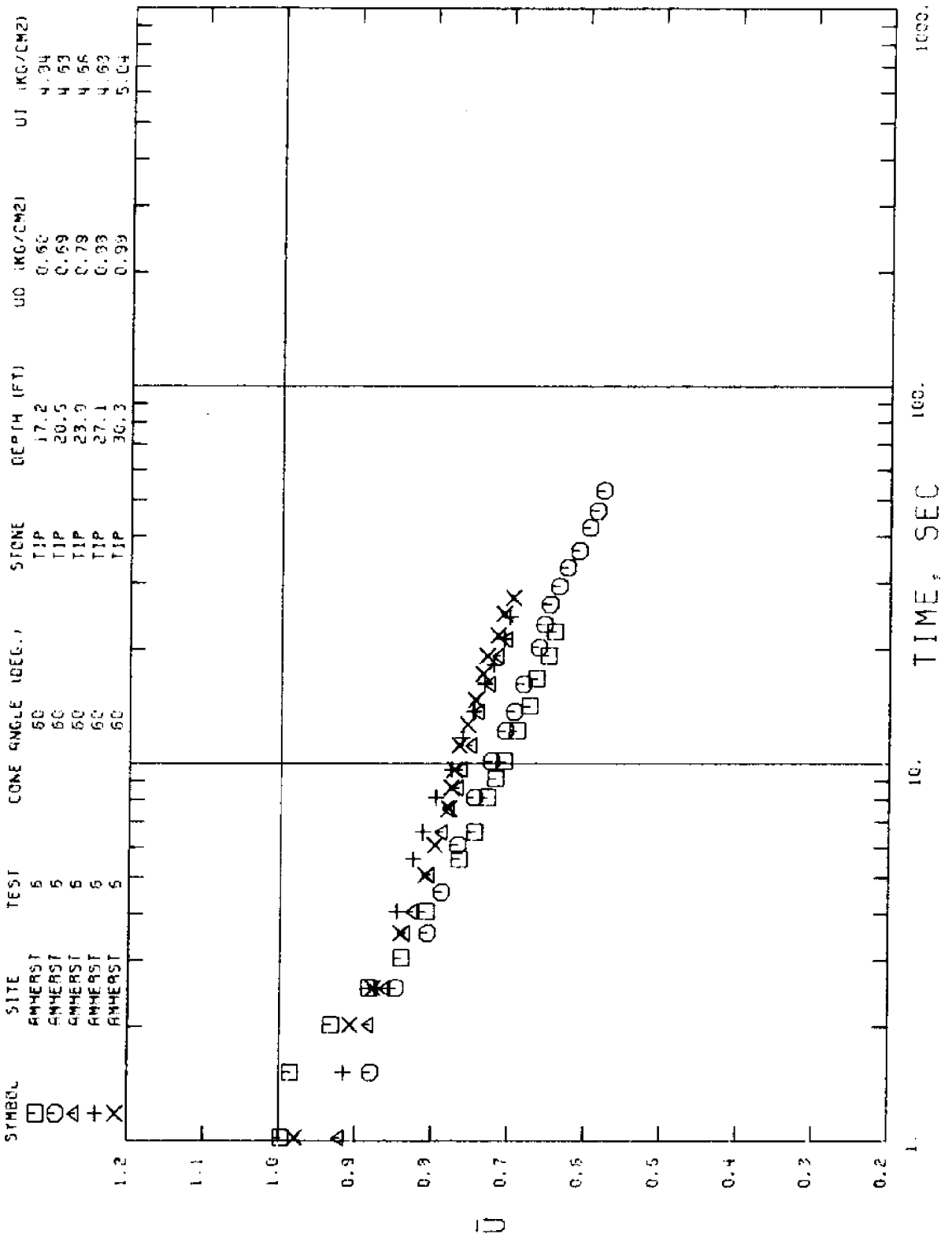
SYMBOL SITE TEST CONE ANGLE (DEG.) STONE DEPTH (FT) UO (KG/CM2) UI (KG/CM2)
AMHERST 6 60 TIP 17.2 0.66 4.34
AMHERST 6 60 TIP 20.5 0.69 4.53
AMHERST 6 60 TIP 23.9 0.79 4.56
AMHERST 6 60 TIP 27.1 0.93 4.63
AMHERST 6 60 TIP 30.3 0.99 5.04
U
TIME, SEC
1.2
1.1
1.0
0.9
0.8
0.7
0.6
0.5
0.4
0.3
0.2
1.
10.
100.
1000.

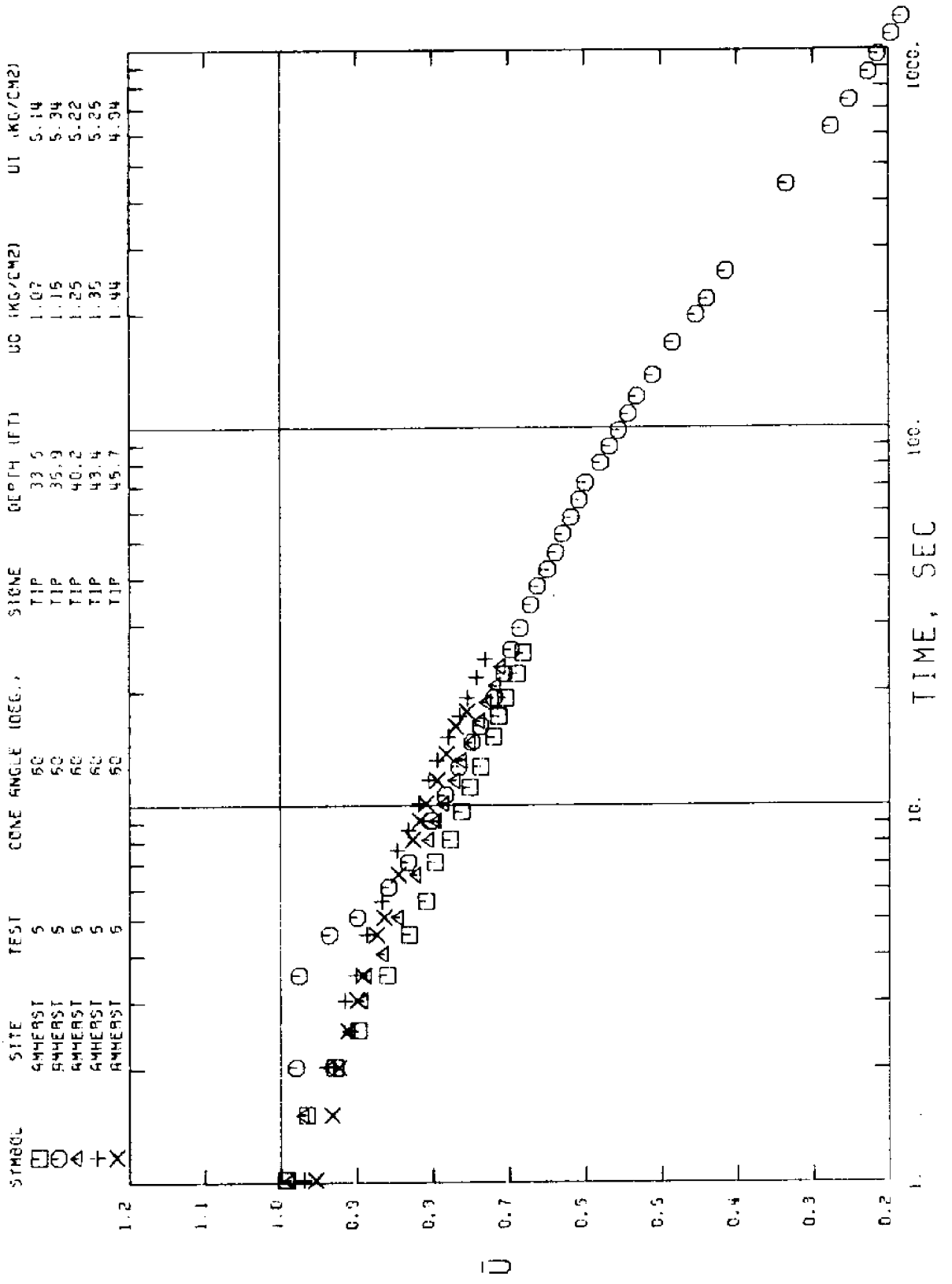
SYMBOL SITE TEST CONE ANGLE (DEG.) SIGNE DEPTH (FT) UC (KG/CM2) UI (KG/CM2)
AMHERST 5 60 TIP 33.5 1.02 5.14
AMHERST 5 60 TIP 36.9 1.15 5.34
AMHERST 6 60 TIP 40.2 1.25 5.22
AMHERST 5 60 TIP 43.4 1.35 5.25
AMHERST 6 60 TIP 45.7 1.44 4.94
1.2
1.1
1.0
0.9
0.8
0.7
0.6
0.5
0.4
0.3
0.2
U
1.
10.
100.
1000.
TIME, SEC

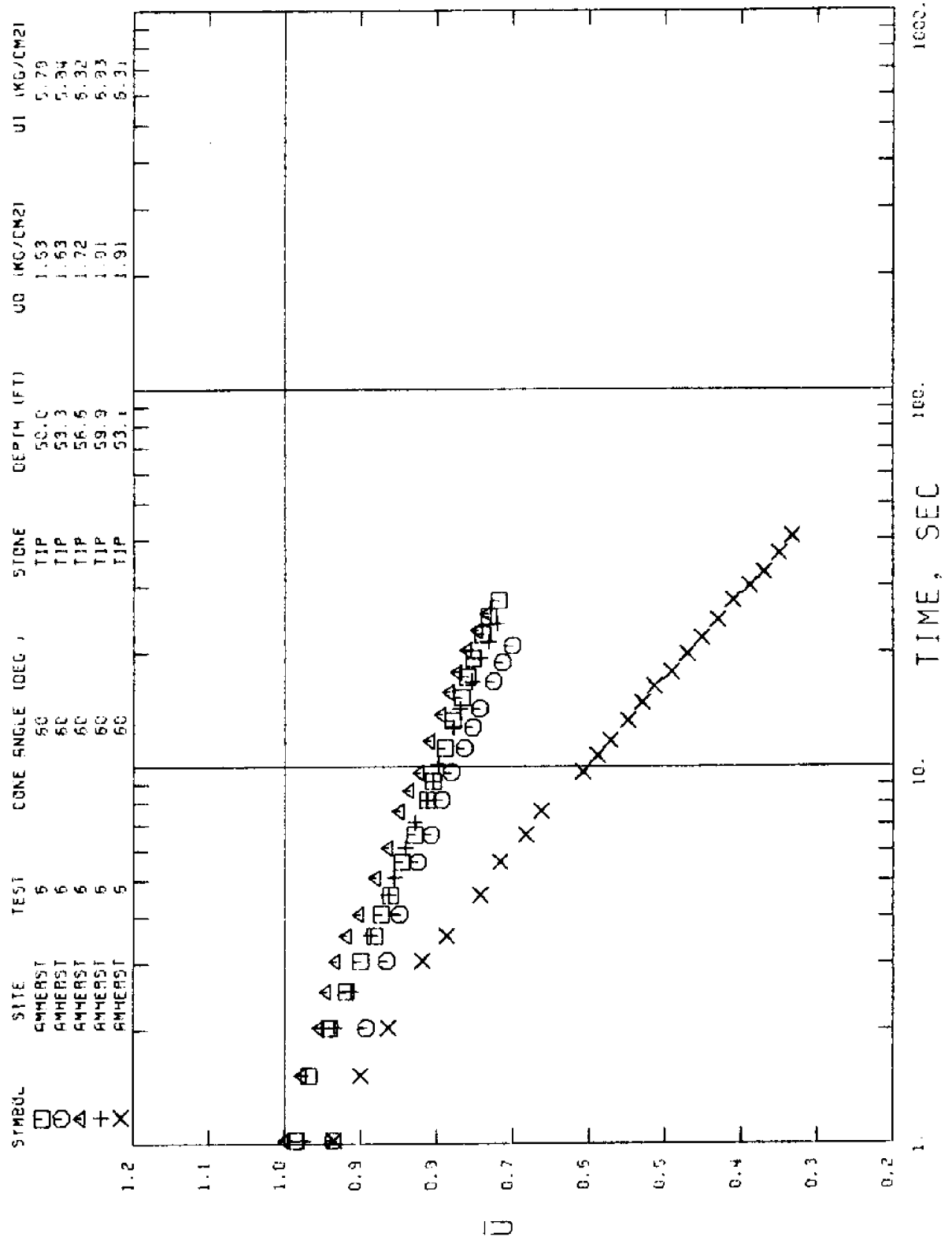
SYMBOL SITE TEST CONE ANGLE (DEG.) STONE DEPTH (FT) UO (KG/CM2) UI (KG/CM2)
AMHERST 5 60 TIP 50.0 1.53 5.29
AMHERST 6 60 TIP 53.3 1.63 5.34
AMHERST 6 60 TIP 56.6 1.72 5.32
AMHERST 6 60 TIP 59.9 1.81 5.33
AMHERST 5 60 TIP 53.1 1.91 5.31
U
TIME, SEC
1.2
1.1
1.0
0.9
0.8
0.7
0.6
0.5
0.4
0.3
0.2
1.
10.
100.
1000.

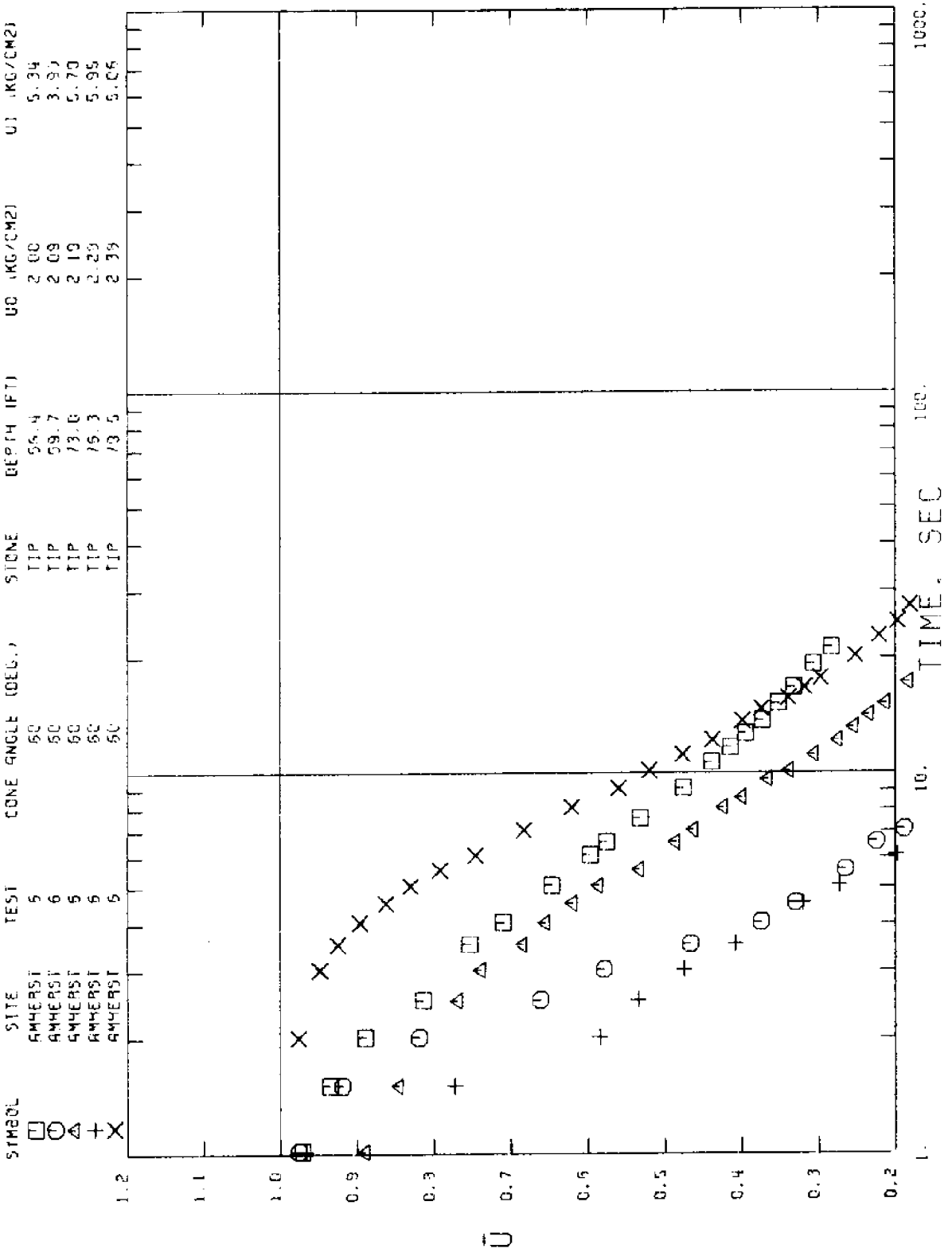
SYMBOL SITE TEST CONE ANGLE (DEG.) STONE DEPTH (FT) U0 (KG/CM2) U1 (KG/CM2)
AMHERST 5 60 TIP 55.4 2.00 5.34
AMHERST 6 60 TIP 59.7 2.09 3.90
AMHERST 5 60 TIP 13.8 2.19 5.70
AMHERST 6 60 TIP 15.3 2.29 5.95
AMHERST 5 60 TIP 13.5 2.39 5.05
U
TIME, SEC
1.2
1.1
1.0
0.9
0.8
0.7
0.6
0.5
0.4
0.3
0.2
1.
10.
100.
1000.